CONF-9603180--

ORNL-6910

FUTURE PROSPECTS OF BARYON INSTABILITY SEARCH IN p-DECAY AND $n \rightarrow \bar{n}$ OSCILLATION EXPERIMENTS

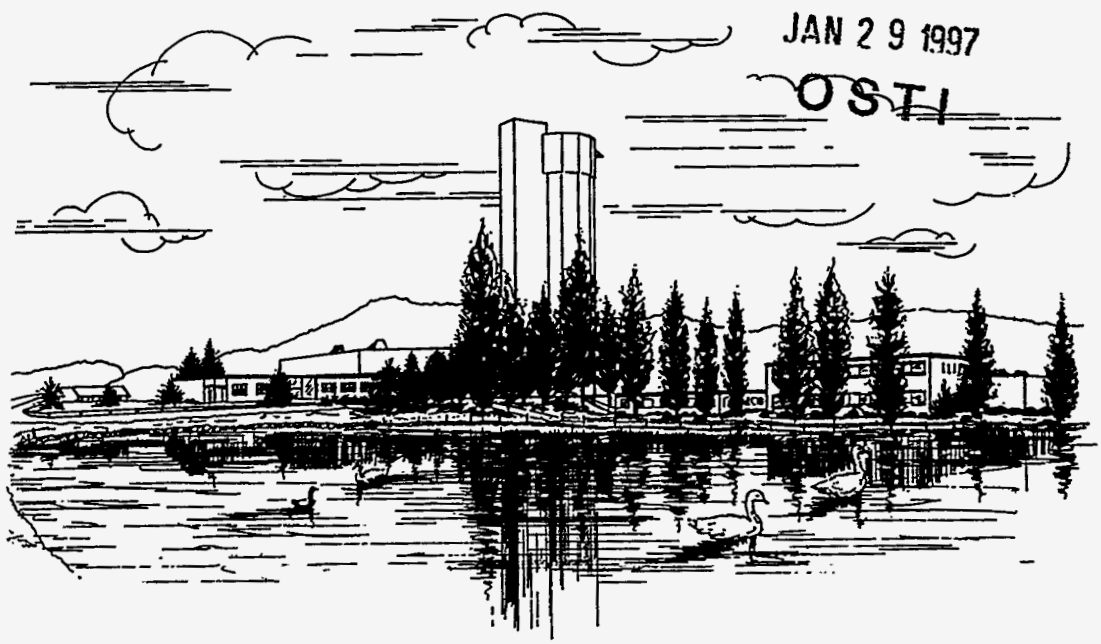

Proceedings of the International Workshop on Future Prospects
of Baryon Instability Search in p-Decay and $n \rightarrow \bar{n}$ Oscillation Experiments
Oak Ridge, Tennessee, U.S.A., March 28-30, 1996

Edited by
S. J. BALL and Y. A. KAMYSHKOV
Oak Ridge National Laboratory
Oak Ridge, Tennessee 37831, U.S.A.

Conference Number: 9603180

Do not Do Analytics on these

Conference 9603180

International workshop on future prospects of baryon instability search in p-decay and n-n oscillation experiments, Oak Ridge, Tennessee, 28-30 Mar 1996

Entered: 06/28/96 Papers : 3 Activities: 0 Energy Meetings:
Changed: 03/18/97 Volumes: 1 Sponsors : 1

Conference Paper 1 of 3

Author : Parker, G. W. Entered : 06/28/96
Report Number: CONF-9603180--1 Changed :
Secondary : Description:
Trac No. SC: : M96012148 Note :

Search for technetium in natural tin metallurgical residues

Conference Paper 2 of 3

Author : Efremenko, Y. Entered : 01/17/97
Report Number: CONF-9603180--2 Changed :
Secondary : Description:
Trac No. SC: : M97001303 Note :

Prospects for baryon instability search with long-lived isotopes

Conference Paper 3 of 3

Author : Kamyshkov, Y. Entered : 01/17/97
Report Number: CONF-9603180--3 Changed :
Secondary : Description:
Trac No. SC: : M97001304 Note :

Prospects for neutron-antineutron transition search

ORNL-6910

FUTURE PROSPECTS OF BARYON INSTABILITY SEARCH IN p-DECAY AND $n \rightarrow \bar{n}$ OSCILLATION EXPERIMENTS

Proceedings of the International Workshop on Future Prospects
of Baryon Instability Search in p-Decay and $n \rightarrow \bar{n}$ Oscillation Experiments
Oak Ridge, Tennessee, U.S.A., March 28-30, 1996

Edited by S. J. Ball and Y. A. Kamyshkov

Published: November 1996

OAK RIDGE NATIONAL LABORATORY
Oak Ridge, Tennessee 37831
managed by
Lockheed Martin Energy Research Corporation
for the
U.S. Department of Energy
under Contract No. DE-AC05-96OR22464

Preface

This workshop is occurring at a most appropriate time for us here at ORNL, as we plan for the facilities which will support our neutron science research into the early part of the next century. In particular, the opportunities for n-$\bar{n}$ experiments need to be explored now as we design these future facilities.

I would remind you that this laboratory has a long tradition in research with neutrons, beginning at its very inception in 1943 with the graphite reactor. Out of that facility came the first accurate measurement of the neutron lifetime, the first medical radioisotopes, the birth of health physics as a discipline, and the field of neutron scattering for which Cliff Schull shared last year's Nobel Prize in physics.

In the years that have followed, there has been a long series of reactors designed and built, for both applied and research needs, culminating in our present facility, the High Flux Isotope Reactor (HFIR).

Our plan to replace HFIR with a more powerful research reactor, the Advance Neutron Source, has not survived the present budget climate emphasizing reducing deficits and balancing the federal budget. Instead, we are now funded for the design of a less costly option, an accelerator driven spallation source, as our next neutron research facility. We are also optimistic that we will be funded for a significant upgrade of our HFIR facility. You will hear more about both of these, including their planned performance specifications, during the course of the workshop.

How well will these facilities be able to address not only neutron science, but also all aspects of baryon instabilities that you will be discussing during this workshop? As we plan for these facilities carrying us into the next century, it is very important to consider all facets of science to which they can contribute. We are most interested to learn what promising possibilities will come from your discussions.

Jim Ball

Oak Ridge, Tennessee
May 1996

Contents

Search for Nucleon Instability *
(Origin and History)

Maurice Goldhaber
Brookhaven National Laboratory **
Upton, N.Y. 11973

Abstract

General considerations governing the search for proton decay – past, present, and future – are discussed.

In attempting to fulfill the task set for me by the Organizing Committee I shall not try to give a definitive history of what I like to call "The Search for Proton Decay", a shorthand term meant to include free and bound protons as well as bound neutrons, which, when free, decay to protons by beta emission. Results from this search, begun more than four decades ago[1], have been reported often. Here, I would like to give a personal perspective which emphasizes general principles that may also have a bearing on many other "searches", chiefly tests of conservation laws, which have since proliferated. I have not sifted through the literature systematically; rather, I have mainly consulted my memory. Thus, my story is far from "definitive", a word which has quite an absolute ring to it, and absolutes, as we have so often learned, should be considered with caution.

Fifty years ago there was a general belief in the existence of absolute conservation laws, including the conservation of baryons. What were usually considered to be absolute conservation laws were deduced either from a well-established theory, from a general principle, from a widely believed "a priori truth", or from just a hunch, but not directly from experiments, which can only yield empirical conservation laws, some later absorbed into theories and then considered "absolute". While an earlier generation of physicists believed in "null experiments", we now like to give upper limits for any value which may be zero, a value which can be approached but not obtained directly from experiment, though it might be deduced from a theory.

The absolute stability of the proton was first postulated in 1929 by Weyl as a hunch, by anology with charge conservation, and then, independently, in 1939 by Stueckelberg and in 1949 by Wigner. These gentlemen may have felt it in their bones that the proton is stable! But an empirical conservation law means only that there is an absence of evidence for non-conservation. Therefore, it is good to remember the old saying: the absence of evidence is

---

* Talk given at the International Workshop on "Future Prospects of Baryon Instability Search in p-Decay and $n - \bar{n}$ Oscillation Experiments" at Oak Ridge, Tennessee, March 28-30, 1996

** Supported by the Department of Energy under contract DE-AC02-76CH0016

not the evidence of absence! If you ask the question: Is the proton stable?, a theory might answer either yes or no, whereas an experiment cannot answer yes. Several theoretical indications favor the answer no. Whenever an experiment cannot, a priori, answer either yes or no, one must beware: small systematic errors, statistical fluctuations or misinterpretations may give a wrong, but "interesting" answer.* When candidates for proton decay were occasionally reported, it was good to remember that the most important fact about a candidate is his background!

If electric charges are absolutely conserved, as the well established gauge theory of electro-magnetism tells us, it would imply, microscopically, that electrons would have to be considered as absolutely stable because there are no known lighter charged particles into which they could decay. Thus, the most stringent tests of charge conservation turned out to be tests of the conservation of the charge of individual electrons or nucleons, as first carried out at Brookhaven in the 1950s and 60s, and later pursued in many places. (For references to early tests, as well as some later ones, see ref. 2, 3, and 4). Okun[3], while emphasizing that charge non-conservation would lead to serious difficulties for QED, nevertheless encourages experimenters to continue such searches.

It is worth noting that if the absolute value of the charge of the electron were not equal to that of the proton, then the charge of its anti-particle, the positron, would differ from the charge of the proton, and charge conservation alone would exclude some proton decays. However, if we assume — compatible with experiments of considerable accuracy — that all the positively charged particles lighter than the proton have charges equal to that of the proton, the possibility of proton decay into lighter particles can be considered (see ref. 2).

While visiting Los Alamos Scientific Laboratory (as it was then called) in the summer of 1954, at a time when the Bondi-Gold-Hoyle theory of continuous creation was much discussed, I asked myself during a walk: If protons can be continuously created, might they not also continuously disappear? Ideas, whether right or not, can beget ideas! The disappearance of a nucleon from a nucleus would usually leave a "hole" behind, equivalent to an excitation energy sufficient to induce nuclear reactions, for example, "spontaneous" fission in ^{232}Th. This allowed a disappearance time $> 10^{20}$ yr to be deduced (see ref. 1). However, it appeared more reasonable to go further and to assume that energy would be conserved in the disappearance of a nucleon, leading to the emission of energetic particles which could be directly detected in a counter. Though baryon number is clearly conserved

* By contrast, in the much (re)searched field of neutrino oscillations, experiment cannot answer no to the question: Do neutrino oscillations exist? Here also, "interesting" answers have occasionally been reported.

in strong, electro-magnetic and weak interactions, it seemed worth testing numerically to what extent it is conserved.

Fred Reines and Clyde Cowan had built a large scintillation counter at Los Alamos to search for atmospheric neutrinos, and we joined forces to look "parasitically" for proton decay. We deduced a mean lifetime $\tau > 10^{21}$ yr for a free proton, and $\tau > 10^{22}$ yr for a bound nucleon, provided at least 100 MeV of the decay energy were deposited in the counter[1]. Over the years, experiments kept greatly extending the limits, both for the disappearance time and for the decay time.

The concept of proton instability entered theoretical considerations slowly. In 1959, Yamaguchi[5] considered the possibility of proton decay induced by superweak interactions. In the seventies, the unification of quarks and leptons, proposed by Pati and Salam[6] and the SU(5) grand unification theory (GUT) proposed by Georgi and Glashow[7], led to predictions for a proton lifetime[8,9] of the order of 10^{30} yr.* Here was the equivalent of a "moon to shoot for", leading to intensified experimental efforts to search for proton decay. Several theorists discussed indications for non-conservation of baryons, though their deductions cannot be directly tested: black holes (Hawking), instantons (t'Hooft), baryon asymmetry in the universe (Sakharov-Weinberg-Yoshimura).

In looking for proton decay, one explicitly assumes that the following four conservation laws hold "absolutely": 1) energy, 2) linear momentum, 3) angular momentum, and 4) electric charge. Since baryons are fermions (with a baryon number $B = 1$), conservation of angular momentum implies that in proton decay an odd number of the only lighter fermions we know, the light leptons, assigned lepton number $L = \pm 1$, would have to be created. Thus, proton decay would also imply non-conservation of leptons.

What are the possible decay modes of the proton? Assuming that the decay products consist only of known particles, and even confining ourselves to two-body decays, there are still a great many potential decay modes. Their number would be reduced if some selection rules governed the decays, e.g. in SU(5) GUT, $B - L = 0$. The Irvine-Michigan-Brookhaven collaboration (IMB), whose membership over the years has gone through many changes, proposed in 1979 to build a water Cherenkov detector, large enough to reach a proton lifetime of $\sim 10^{33}$ yr for some decay modes before background signals from atmospheric neutrinos would compete. The final form of the counter, built in the Fairport salt mine near Cleveland, Ohio, is described in ref. 11, which lists as authors all those who at some time were members of the collaboration. It is difficult to design an experiment equally sensitive to all potential decay modes. Our counter was particularly sensitive to those

* For an alternative exploratory theory which predicts a stable proton, see ref. 10.

involving charged leptons and photons (e.g. $p \to e^+ + \pi^o$ — discussed early as an example of a possible decay mode in ref. 2) with a smaller, but by no means negligible sensitivity for most other decay modes. We took data, starting in 1982, until the demise of the detector in 1991. Water Cherenkov counters permit the study of neutrino interactions "symbiotically" with proton decay which has led to the following results: neutrinos from the supernova 1987A were detected by both Kamiokande and IMB; an anomalous ν_μ/ν_e ratio for atmospheric neutrinos was noticed both by IMB and Kamiokande, and will be further studied by the SuperKamiokande-U.S. collaboration; solar neutrinos were recorded by Kamiokande.

A theory predicts so-called partial lifetimes, i.e. lifetimes for particular branches; for lifetimes too long for exponential decay to be observed directly, experiments measure partial lifetimes only. The SU(5) GUT assumes, for example, that the two u quarks in the proton can virtually change into a lepton-quark which can, in turn, decay into $\overline{d} + e^+$, conserving $B - L$ and leading some of the time to the decay $p \to e^+ + \pi^o$. This is predicted to be a favored branch, for which the partial lifetime was estimated by Marciano to be $4.5 \times 10^{29\pm1.7}$ yr (see ref. 12). The IMB experiment reached a limit $> 8.5 \times 10^{32}$ yr for this branch; combining this result with the limits obtained by Kamiokande and Fréjus, we obtain a limit $> 1.2 \times 10^{33}$ yr, thus disproving the SU(5) GUT.* But SU(5) GUT also meets with other difficulties: with better knowledge of the interaction constants, extrapolation to high energies did not lead to a common intersection at a grand unified mass, which may, however, be achieved in a supersymmetric theory. For example, following Marciano[13], who estimates that the grand unified mass would be $\sim 10^{16}$ GeV for the supersymmetric SU(5) GUT, predicts (in round numbers) a lifetime of $\sim 10^{35\pm2}$ yr for the $e^+ + \pi^o$ branch. For some values of the parameters of the heavy Higgs scalars and their supersymmetric partners, the branch $p \to K^+ + \overline{\nu}$ is predicted to become dominant.

A more exotic possibility is given in ref. 12, inspired by analogy with t'Hooft's instanton ideas, and experimentally testable up to lifetimes not exceeding 10^{30} yr by many orders of magnitude: three nucleons in a nucleus might decay into three leptons, one from each generation, (plus pions).

Limits on $n - \overline{n}$ oscillations were deduced for neutrons bound in the oxygen of water Cherenkov counters, where the energy released in anti-neutron annihilation would be easily detected. Theoretical estimates suggest a comparable limit for the oscillation time obtained directly for free neutrons. The theories are discussed at this workshop, together with a dissenting view.

---

* The calculation of the partial lifetime tacitly assumes that the forces between the two u quarks are given by QCD. If a short-range repulsive force also existed, a longer lifetime would result.

Yuri Kamyskow emphasizes in his communication, that both types of experiments, free and bound neutrons, need pursuing: there are conceivable circumstances where they might give different results.

To continue the search for proton decay to much longer lifetimes, experimenters have to increase the effective ton-years of observation, as well as reduce the importance of the background from atmospheric neutrinos, for example, by improving energy and momentum resolution, as we shall learn from talks by Jim Stone on SuperKamiokande, and Larry Sulak on a next-generation search for proton decay. Though the proton's lifetime is not expected to be appreciatively changed when nucleons are bound[14], the Fermi motion and the interaction of the hadrons emitted smears the signals, making it harder to distinguish them from those due to atmospheric neutrinos. In principle, counters containing liquid H_2 or CH_4 would be better choices than water, but their use would confront us with considerable practical difficulties.

How long will the search for proton decay continue? It may end with a bang if proton decay is actually found, but with a whimper if a considerable gap remains between a lifetime accessible to experiment and one predicted by a generally accepted theory. Such a theory would only be convincing if it made other predictions, successfully tested experimentally. One possible end to the search might come if the grand unified mass predicted by such a theory turned out to be close, or equal, to the Planck mass.

[1]F. Reines, C.L. Cowan Jr. and M. Goldhaber, Phys. Rev. **96**, 1157 (1954).

[2]G. Feinberg and M. Goldhaber, Proc. Natl. Acad. Sci. **45**, 1301 (1959) and Sci. Am. **209**, 36 (1963).

[3]L.B. Okun, Comments on Nucl. Part. Phys., Part A, **XIX**, No. 3, 99 (1989).

[4]E.B. Norman, J.N. Bahcall and M. Goldhaber, Phys. Rev. D **53**, 4086 (1996)

[5]Y. Yamaguchi, Progress in Theor. Phys. **22**, 373 (1959).

[6]J.C. Pati and A. Salam, Phys. Rev. Lett. **31**, 661 (1973) and Phys. Rev. D **8**, 1240 (1973).

[7]H. Georgi and S.L. Glashow, Phys Rev. Lett. **32**, 438 (1974).

[8]H. Georgi, H. Quinn and S. Weinberg, Phys. Rev. Lett. **33**, 451 (1974).

[9]A.J. Buras, J. Ellis, M.K. Gaillard and D.V. Nanopoulos, Nucl. Phys. B **135**, 66 (1978).

[10]D.J. Castaño and S.P. Martin, Phys. Rev. Lett. B **340**, 67 (1993).

[11]R. Becker-Szendy, R.M. Bionta, C.B. Bratton, D. Casper, R. Claus, B. Cortez, S.T. Dye, S. Errede, G.W. Foster, W. Gajewski, K. Ganezer, M. Goldhaber, T.J. Haines, P.G. Halverson, E. Hazen, T.W. Jones, D. Kielczewska, W.R. Kropp, J.G. Learned, J.M. LoSecco, S. Matsuno, J. Matthews, G. McGrath, C. McGrew, R. Miller, M.S. Mudan, H.S. Park, L. Price, F. Reines, J. Schultz, S. Seidel, D. Sinclair, H.W. Sobel, J.L. Stone,

L.R. Sulak, R. Svoboda, G. Thornton, J.C. Van der Velde, and C. Wuest, Nucl. Instr. Methods A **324**, 363-382 (1993).

[12]M. Goldhaber and W. Marciano, Comm. Nucl. Part. Phys. **16**, 23 (1986).

[13]W.J. Marciano, Proc. of the XXI SLAC Summer Institute on Particle Physics, 35 (1993).

[14]C.B. Dover, M. Goldhaber, T.L. Trueman and L.L. Chau, Phys. Rev. D **24**, 2886 (1981).

Baryon Non-Conservation in Unified Theories, in the Light of Supersymmetry and Superstrings [1]

Jogesh C. Pati

Department of Physics
University of Maryland
College Park, MD 20742

Abstract

The first part of this talk presents the general complexion of baryon and lepton number non-conservation that may arise in the context of quark-lepton unification, and emphasizes the importance of searching for both $(B-L)$-conserving proton decay modes–i.e. $p \to \bar{\nu}K^+, \mu^+K^o$, and $e^+\pi^o$ etc.–as well as $(B-L)$-violating transitions–i.e. $p \to e^-\pi^+\pi^+, n-\bar{n}$-oscillation and neutrinoless double beta decay.

The second part presents the status of grand unification with and without supersymmetry and spells out the characteristic proton decay modes, which if seen, will clearly show supersymmetry. The *main theme* of this talk, that follows next, pertains to two issues: (i) the need to remove the mismatch between MSSM and string-unifications; and especially (ii) the need to resolve naturally the problem of rapid proton decay, that generically arises in SUSY unification. Seeking for a natural solution to this second problem, it is noted that SUSY GUTS, including SUSY SO(10) and E_6, can at best accommodate proton-stability by a suitable choice of the Higgs-multiplets and discrete symmetries, but not really explain it, because they do not possess the desired symmetries to suppress both $d=4$ and $d=5$ proton-decay operators. By contrast, following a recent work, I argue that a class of string-solutions, possessing three families, does possess the desired symmetries, which naturally safeguard proton-stability from all potential dangers. They also permit neutrinos to have desired light masses. This shows that, believing in supersymmetry, *superstring is needed just to understand why the proton is so stable.* Some implications of the new symmetries, in particular the fact that they still lead to observable rates for proton-decay in the same context in which the mismatches between MSSM and string-unification are removed, are noted.

[1]Research supported by NSF grant No. PHY-9119745. Invited talk, presented at the Oak Ridge International Workshop on "Baryon Instability", March, 1996. Email: pati@umdhep.umd.edu

1 Introduction

Non-conservation of baryon and lepton numbers, in particular proton decaying into leptons, is one of the hallmarks of grand unification [1,2,3]. In this context, other forms of baryon and lepton non-conservation could be permitted as well – such as neutrinoless double beta decay and neutron-anti-neutron oscillation [4]. Unfortunately, experimental searches for any of these processes have not yet produced a positive result [5,6,7]. Nevertheless, it is known that some form of violation of baryon and/or lepton number must have occurred in the early universe to account for the observed excess of baryons over anti-baryons [8,9], which is in fact crucial to the origin of life. In addition, as discussed below, violation of at least lepton number is strongly suggested by recent neutrino-oscillation experiments [10], which indicate non-vanishing but light masses for the neutrinos. From a purely theoretical viewpoint, to be presented in the following, it turns out that for a number of grand unified as well as superstring-derived models, observation of proton decay, into modes such as $\bar{\nu}_\mu K^+$ and/or $e^+\pi^o$, should be within the reach of current and forthcoming experimental facilities.

It thus seems most encouraging and timely that SuperKamiokande, with the capability to improve the sensitivity of previous facilities - with respect to searches for both proton decay and neutrino-oscillations – by more than an order of magnitude, has just been turned on; and new facilities like SNO and ICARUS, as well as those designed to search for neutrino-less double beta decay and $n-\bar{n}$ oscillations with improved sensitivity are expected to be available in the near future.

On the theoretical front, the original motivation for a unity of the fundamental forces and that for questioning baryon and lepton-number conservation laws in the context of such unification ideas [1,2,3] have remained unaltered. But the perspective with regard to both issues has changed significantly over the last two-and-a-half decades, owing to the introduction of the ideas of supersymmetry [11] and superstrings [12]. In particular, supersymmetry, which seems to be an essential ingredient for higher unification (see discussion in Sec. 5) poses the problem of rapid proton decay. This is because, in accord with the standard model gauge symmetry $SU(2)_L \times U(1)_Y \times SU(3)^C$, a supersymmetric theory in general permits, in contast to non-supersymmetric ones, dimension 4 and dimension 5 operators which violate baryon and lepton numbers [13]. Thus, unless these operators are suppressed to the extent needed (see discussions later), they pose

the danger of unacceptably rapid proton decay. It turns out that obtaining a natural solution to this problem gets even harder if one wishes to obtain at the same time non-vanishing but light masses for the neutrinos ($\leq$ few eV)[10].

Bearing these issues in mind, I will first present here a brief summary of the status of non-supersymmetric and supersymmetric grand unificiation, and next a current perspective on baryon- and lepton-number conservation laws in the light of the ideas of supersymmetry and superstrings. In this latter part, following a recent work by me [14], I will also present a natural solution to the problem of rapid proton decay in the context of supersymmetry. *It turns out that the solution in question needs certain symmetries which can not arise within conventional grand unification symmetries including E_6, but they do arise within superstring-derived three-family solutions.* These symmetries play an *essential role* in safeguarding proton-stability from all potential dangers, to the extent desired, and simultaneously permit neutrinos to have light masses of a nature that is relevant to current experiments. *This in turn provides a strong motivation for symmetries of string-origin.* The extra symmetries in question lead to extra $Z'-$ bosons, whose currents bear the hallmark of string theories. It turns out that there is an interesting correlation between the masses of the $Z'-$ bosons and observability of proton decay.

In section 2, I present the need for $B-L$ violation and that for $SU(4)$-color. In section 3, general complexion of (B,L) violations and the characteristic mass-scales associated with different processes are listed, and in Section 4, the main ideas as regards physics beyond the standard model are presented. Section 5 provides the current status of grand unification in the context of supersymmetry and raises the issue of compatibility between MSSM and string-unification. Certain attempts to achieve this compatibility are presented. In section 6, I present the problem of $d=4$ and $d=5$ proton-decay operators and propose a solution that naturally safeguards proton-stability from all potential dangers. Some concluding remarks are presented in Section 7.

2 $B-L$ Violation and $SU(4)$-Color

As stated above, the observed excess of baryons over anti-baryons implies that some form of violation of B and/or L must have occurred in the early universe[8,9]. Such an excess could arise through (B,L) violating processes which either conserve $B-L$, or violate it. Kuzmin, Rubakov and Shaposnikov pointed out, however, that any excess

generated through $(B-L)$-conserving processes at very early moments of the universe (corresponding to temperatures $\gg 1TeV$, i.e. $t \ll 10^{-12}sec$) is erased subsequently by purely electroweak effects[15]. At the same time, generating baryon-excess through electroweak effects alone does not seem to be adequate to account for the observed baryon-asymmetry[15]. These considerations suggest that baryogenesis must have its origin (at least in part) in processes which violate $B-L$.

There is yet an *independent motivation* for violation of $B-L$ which stems from considerations of neutrino masses. The reason is as follows. The simplest explanation for non-vanishing but light masses for the neutrinos[10] arises in the context of left-right symmetric gauge theories[16] and the so-called see-saw mechanism[17]. The minimal nonabelian version of a left-right symmetric gauge theory is provided by the symmetry[1]

$$\mathcal{G}_{224} = SU(2)_L \times SU(2)_R \times SU(4)^C \tag{1}$$

which ensures (i) quantization of electric charge, (ii) quark-lepton unification (through $SU(4)$-color), as well as (iii) parity-conservation[16], at a basic level. Any such theory containing either $SU(2)_L \times SU(2)_R$ or $SU(4)^C$ necessarily implies the existence of right-handed neutrinos (ν_R^i), accompanying the left-hand ones (ν_L^i). The see-saw mechanism[17] assigns *heavy Majorana masses* ($M_R^i \gg 1TeV$) to the right-handed neutrinos, though not to the left-handed ones. This involves a breaking of left-right symmetry and thus parity spontaneously at a high scale[16]. Now, the Majorana masses for the $\nu_R's$, in conjunction with the standard Dirac masses m_D^i, naturally yield very light masses ($\ll m_D^i$) for the known neutrinos:

$$m(\nu_L^i) \sim (m_D^i)^2/M_R^i \quad (i = e, \mu, \tau) \tag{2}$$

Noting that the Dirac mass m_D^i of the ith neutrino is expected to be comparable to the mass of the ith up-quark (barring QCD renormalization effects), it turns out that these masses for the $\nu_L's$ have just the right pattern to be relevant to the neutrino-oscillation experiments[9,18] and to ν_τ being hot dark matter, with

$$m(\nu_L^i) \sim (10^{-8})eV,\ 3\times 10^{-3}eV,\ 1-10eV)\ \ (i = e, \mu, \tau) \tag{3}$$

if $M_R^i \sim 10^{12}$ GeV, within a factor of 10 [19]. Heavy Majorana masses for $\nu_R's$, however, needs spontaneous violation of lepton number L (with $\Delta B = 0$) and therefore of $B-L$

at a heavy intermediate scale.

We thus see that both baryogenesis and neutrino masses suggest the need for microscopic violation of $B-L$. One can argue that spontaneous violation of $B-L$ becomes obligatory in theories in which it is gauged. This is because, in these theories, there is a massless spin-1 particle coupled to $B-L$. Such a particle would be inconsistent with the results of Eötvos-type experiments [20], unless it acquires mass spontaneously. Thereby, the associated charge, in this case $B-L$, must be violated spontaneously [1]. Now, the simplest symmetry that gauges $B-L$ is $SU(4)$-color, which unifies quarks and leptons by using the idea that lepton number is the fourth color [1]. In short, (B,L)-violation, is an integral feature of any theory containing $SU(4)$-color. By contrast, $SU(5)$ [2] does not contain $B-L$ as a generator, and thus need not violate $B-L$, because, in this case, $B-L$ can only be a global symmetry.

These considerations thus suggest that our very existence, requiring baryogenesis and therefore violation of $B-L$, bears the footprints of certain unification ideas - in particular that of quark-lepton unification through a symmetry-like $SU(4)$-color.

3 General Complexion of (B,L)-Violating Processes and Effective Mass Scales

The (B,L) violating processes which conserve $B-L$ primarily involve only proton decaying into an *anti-lepton* plus mesons: e.g. $p \to e^+\pi^o, p \to \mu^+K^o, p \to \bar{\nu}K^+, p \to \bar{\nu}\pi^+$ etc. Once one permits violation of $B-L$, however, a whole new set of processes can in general occur. These include: (i) a nucleon decaying into a *lepton* plus mesons - i.e. $p \to e^-\pi^+\pi^+$ and $n \to e^-\pi^+$ etc., or proton decaying into a lepton + lepton + antiplepton + mesons - e.g. $p \to e^-e^+\nu\pi^+$, (iii) Majorana masses for the neutrinos, (iv) neutrinoless double beta decay and (v) $n-\bar{n}$ oscillation.

Now, Majorana masses for the right handed neutrinos, that are needed for the see-saw mechanism [17], can arise by introducing the pair of Higgs multiplets Δ_L and Δ_R which transform as (3,1,10) and (1,3,10) of $\mathcal{G}_{224}$ or equivalently a single Higgs multiplet 126 of SO(10) [21], which contains Δ_L and $\bar{\Delta}_R$. (An alternative choice of Higgs multiplets will be presented later.) Parameters of the Higgs sector can be arranged such that the minimum of the potential induces a large VeV $<\Delta_R>=v_R>>1$ TeV, while $<\Delta_L>\approx 0$ [22]. In the presence of the Yukawa coupling $h_M(\nu_R{}^TC^{-1}\nu_R\Delta_R+\nu_L{}^TC^{-1}\nu_L\Delta_L)+hc$,

such a VeV would induce a heavy Majorana mass for ν_R. As mentioned before, this, in conjunction with the familiar Dirac mass, yields a very light Majorana mass for ν_L, (see eq. (2)). The VeV of Δ_R would also break $\mathcal{G}_{224}$ into the standard model symmetry $SU(2)_L \times U(1)_Y \times SU(3)^C$. In this way, $< \Delta_R >$ breaks lepton number L and $(B-L)$, each by two units. It also breaks parity and quark-lepton unification.

A specific set of diagrams which utilize $< \Delta_R > \neq 0$ and/or Majorana masses for the neutrinos and thereby induce some of the (B-L) violating processes mentioned above are shown in figs. 1, 2, and 3. The amplitudes for these processes would, of course, depend upon the effective Yukawa, quartic and gauge couplings entering into the respective vertices, as well as on the masses of the intermediate particles - i.e. those of Δ_R, the color-triplets and color-octets ξ_3 and ξ_8, as well as W_R and ν_R - which enter into figs. 1, 2, and 3. Now, in minimal symmetry-breaking schemes of left-right symmetric grand unification models, such as those based on one- (or two-step)- breaking of SO(10), the masses of these intermediate particles typically turn out to be either superheavy $\sim 10^{15}$ GeV, or at least medium heavy $\sim 10^{12} GeV$)[23]. In this case, it is easy to verify that the rates of all these (B, L)-violating processes would be far too small to be observable. For example, even if effective Yukawa and quartic couplings are of order one, the amplitudes for $qqq \rightarrow l + (q\bar{q})$ (Fig. 2a) and $qqq \rightarrow \bar{q}\bar{q}\bar{q}$ (Fig. 3) would be of order $(1/M_{\text{eff}}^5) \leq (\frac{1}{10^{12} GeV})^5 \leq 10^{-60} GeV^{-5}$, where as one would need these amplitudes to be greater than or of order of $10^{-30} GeV^{-5}$ - i.e. $M_{\text{eff}} \leq 10^6 GeV$ (say), for the corresponding processes to have observable rates. Roughly, a similar conclusion can be drawn from a general operator analysis, based on construction of effective invariant operators[24] and dimensional estimate. The results of such estimates for the effective mass-scales that would be necessary for the various (B, L)-violating processes to have observable rates are shown in Table I.

It needs to be said that while minimal symmetry-breaking schemes for SO(10) typically lead to effective mass-scales which are considerably larger than those shown in Table I and thus rates that are considerably smaller than what would be observable, there exist viable models of the Higgs system, some involving supersymmetry and thereby at least technically natural fine tuning, where relatively low effective mass-scales of the type shown in Table I and, therefore, observable rates for $n - \bar{n}$ oscillation [25] and/or proton decaying into lepton plus mesons are obtained [26].

Thus, I believe that, from a broader theoretical perspective, and also because of the

	Processes	Selection Rules	Eff. Mass Scale
I.	$p \to e^+\pi^o, \bar{\nu}\pi^+$ $n \to e^+\pi^-$ $p \to \bar{\nu}_\mu K^+, \mu^+ K^o$	$\Delta B = \Delta L = -1$ $\Delta(B-L) = 0$	$\sim 10^{15} GeV$
II.	$p \to e^-\pi^+\pi^+,$ $n \to e^-\pi^+$ $p \to e^-e^+\nu\pi^+,$ $n \to e^-e^+\nu$	$\Delta B = -\Delta L = -1$ $\Delta(B-L) = -2$ $\Delta(B+L) = 0$	$\sim 10^{5} GeV$
III.	$p \to e^-\nu\nu\pi^+\pi^+$ $n \to e^-\nu\nu\pi^+$	$\Delta B = -\frac{\Delta L}{3} = -1$ $\Delta(B-L) = -4$	$\sim 10^{5} GeV$
IV.	$p \to e^+\bar{\nu}\bar{\nu}$	$\Delta B = \frac{\Delta L}{3} = -1$ $\Delta(B-L) = +2$	$\sim 10^{4.5} GeV$
V.	$n - \bar{n}$	$\Delta B = 2, \Delta L = 0$	$\sim 10^{5} GeV$
VI.	$nn \to ppe^-e^-$	$\Delta B = 0, \Delta L = 2$	$\sim 10^{4.5} GeV$

Table 1: Effective Mass-Scales based on operator analysis and dimensional estimates for the corresponding processes to have observable rates.

great significance of a positive result, if it should show, experimental searches for both $(B-L)$–conserving, as well as the $(B-L)$–violating processes shown in Table I, are strongly motivated.

To discuss these issues specifically in the context of grand unification and supersymmetry, I will first present briefly in the next section the motivations for certain theoretical ideas involving physics beyond the standard model, and then discuss grand unificaiton with supersymmetry in the following section.

4 Going Beyond the Standard Model

The standard model of particle physics has brought a good deal of synthesis in our understanding of the basic forces of nature and has turned out to be brilliantly successful in terms of its agreement with experiments. Yet, as recognized for some time, it falls short as a fundamental theory because it introduces some 19 parameters. And it does not explain (i) the coexistence of the two kinds of matter: quarks *and* leptons; (ii) the coexistence of the electroweak *and* the QCD forces with their hierarchical strengths $g_1 \ll g_2 \ll g_3$, as observed at low energies; (iii) quantization of electric charge; (iv) family-replication; (v) inter and intrafamily mass-hierarchies; and (vi) the origin of diverse mass scales that span over more than 27 orders of magnitude from M_{Planck} to m_W to m_e to

m_ν. There are in addition the two most basic questions: (vii) how does gravity fit into the whole scheme, especially in the context of a good quantum theory?, and (viii) why is the cosmological constant so small or zero?

These issues constitute at present some of the major puzzles of particle physics and provide motivations for contemplating new physics beyond the standard model which should shed light on them. The ideas which have been proposed over the last two-and-a-half decades and which do show promise to resolve at least some of these puzzles include the following hypotheses:

(1) **Grand Unification:** The hypothesis of grand unification [1,2,3], which proposes an underlying unity of the fundamental particles and their forces, appears attractive because it explains at once (i) the quantization of electric charge, (ii) the existence of quarks *and* leptons with $Q_e = -Q_p$, and (iii) the existence of the strong, the electromagnetic and the weak forces with $g_3 \gg g_2 \gg g_1$ at low energies. These are among the puzzles listed above and grand unification resolves all three. By itself, it does not address, however, the remaining puzzles listed above, including the issues of family replication and origin of mass-hierarchies.

(2) **Supersymmetry:** This is the symmetry that relates fermions to bosons [11]. As a local symmetry, it is attractive because it implies the existence of gravity. It has the additional virtue that it helps maintain a large hierarchy in mass-ratios such as $(m_\phi/M_U) \sim 10^{-14}$ and $(m_\phi/M_{pl}) \sim 10^{-17}$, without the need for fine tuning, provided, however, such ratios are put in by hand. Thus it provides a technical resolution of the gauge hierarchy problem, *but by itself does not explain the origin of the large hierarchies.*

(3) **Preonic Substructures with Supersymmetry:** The idea [27,28] that quarks, leptons and Higgs bosons are composites of a *common* set of constituents called "preons," which possess supersymmetry, is still unconventional. On the negative side, the preonic approach needs a few unproven, though not implausible, dynamical assumptions as regards the preferred direction of symmetry breaking and saturation of the composite spectrum [28]. On the positive side, it has the advantage that it is far more economical in field-content and especially in parameters than the conventional grand unification models, because it has no elementary Higgs boson. Second, and most important, utilizing primarily the symmetries of the theory (rather than detailed dynamics) and the forbiddeness of SUSY-breaking, in the absence of gravity, the preonic approach provides simple explanations for the desired protection of composite quark-lepton masses and

at the same time for the origins of family-replication, inter-family mass-hierarchy and diverse mass scales [27]. It also provides several testable predictions. For this reason, I still keep an open mind about the preonic approach. To maintain a focus, however, I will assume in the rest of this talk that quarks, leptons and Higgs bosons are elementary.

(4) **Superstrings:** Last but not least, the idea of superstrings [12] proposes that the elementary entities are not truly pointlike but are extended stringlike objects with sizes $\sim (M_{Planck})^{-1} \sim 10^{-33}$ cm. These theories (which may ultimately be just one) appear to be most promising in providing a unified theory of all matter (spins 0, 1/2, 1, 3/2, 2, ...) and of all the forces of nature including gravity. Furthermore, by smoothing out singularities, they seem capable of yielding a well-behaved quantum theory of gravity. In principle, assuming that quarks, leptons and Higgs bosons are elementary, a suitable superstring theory could also account for the origin of the three families and the Higgs bosons at the string unification scale, as well as explain all the parameters of the standard model. But in practice, this has not happened as yet. Some general stumbling blocks of string theories are associated with the problems of (i) a choice of the ground state (the vacuum) from among the many solutions and (ii) understanding supersymmetry breaking.

These provide in a nutshell motivations for physics beyond the standard model, which, as it turns out, has strong implications for non-conservation of baryon and lepton numbers. The ideas listed above are, of course, not mutually exclusive. In fact the superstring theories already comprise the idea of local supersymmetry and the central idea of grand unification. In the following, I first recall the status of conventional grand unification with supersymmetry and then discuss the issue of (B, L)-nonconservation in the context of these ideas.

5 Grand Unification and Supersymmetry

5.1 The Need for SUSY

It has been known for some time that the dedicated proton decay searches at the IMB and Kamiokande detectors[5] and more recently the precision measurements of the standard model coupling constants (in particular $sin^2\theta_W$) at LEP[29] put severe constraints on the idea of grand unification. Owing to these constraints, the non-supersymmetric minimal $SU(5)$, and for similar reasons, the one-step breaking minimal non-supersymmetric

$SO(10)$-model as well, are now excluded.[30] For example, minimal non-SUSY $SU(5)$ predicts: (i) $\Gamma(p \to e^+\pi^o)^{-1} < 6 \times 10^{31} yr$ and (ii) $sin^2\theta_W(m_Z))\ |_{\bar{MS}} = .214 \pm .004$, where as current experimental data show: (i) $\Gamma(p \to e^+\pi^o)_{expt}{}^{-1} > 6 \times 10^{32} yr$[5] and (ii) $sin^2\theta_W(m_Z)_{expt}{}^{LEP} = .2313 \pm .0003$[29,30]. The disagreement with respect to $sin^2\theta_W$ is reflected most clearly by the fact that the three gauge couplings (g_1, g_2 and g_3), extrapolated from below, fail to meet by a fairly wide margin in the context of minimal non-supersymmetric $SU(5)$ (see Fig. 4).

But the situation changes dramatically if one assumes that the standard model is replaced by the minimal supersymmetric standard model (MSSM), above a threshold of about $1TeV$. In this case, the three gauge couplings are found to meet[31,32], at least approximately, provided $\alpha_3(m_Z)$ is not too low (see figs. 4 and 5 and discussions below). Their scale of meeting is given by

$$M_X \approx 2 \times 10^{16} \quad \text{(MSSM or SUSYSU(5))} \tag{4}$$

M_X may be interpreted as the scale where a supersymmetric GUT (like minimal SUSY SU(5) or SO(10)) breaks spontaneously into the supersymmetric standard model gauge symmetry $SU(2)_L \times U(1) \times SU(3)^c$. Both because a straightforward meeting of the three gauge couplings (in accord with LEP data) is possible only provided SUSY is assumed, and also because SUSY provides at least a technical resolution of the gauge-hierarchy problem by preserving the input small ratio of (m_W/M_X) in spite of quantum corrections, SUSY has emerged as an essential ingredient for higher unification.

With $M_X \sim 2 \times 10^{16} GeV$ and thus lepto-quark gauge boson masses $\sim 10^{16} GeV$, as opposed to $2 \times 10^{14} GeV$ for non-SUSY $SU(5)$, the dimension-6 gauge boson-mediated proton-decay amplitude of order $g^2/{M_X}^2$ would lead to proton lifetime of order $10^{37\pm1}$ years. This is too long to allow observable proton decay. For SUSY grand unification, there are,however, new contributions to proton-decay possibly from dimension 4 and necessarily from dimension 5 operators [13]. These latter arise due to exchange of color-triplet (anti-triplet) Higgsinos, which lie in the $5(\bar{5})$ of SU(5), or in the 10 of SO(10). Since they are damped by just one power of the color-triplet Higgsino mass m_{HC}, these new contributions would lead to extra rapid proton decay, unless M_{HC} is sufficiently heavy. For example, for SUSY SU(5) (with low $tan\beta \leq 2.5$), the experimental limit ($\geq 10^{32}$ yrs) on $\Gamma(p \to \bar{\nu}_\mu K^+)^{-1}$ is met provided [33].

$$m_{HC} \geq 2 \times 10^{16} GeV. \tag{5}$$

It is interesting that the requirement of coupling-unification for SUSY SU(5) puts an upper limit on m_{HC} of about 2.4×1^{16} GeV [33], which is barely compatible with the lower limit given above (eq.(5)).

5.2 SUSY GUT and Proton Decay Modes

Leaving out for a moment the issue of how to ensure naturally such a large mass for the triplet, while its doublet partner is light ($\leq 1TeV$) (I will return to this issue in Sec. 6), if one takes the attitude that the $d = 4$ operators are forbidden by a discrete symmetry or R-parity (see discussions later), and that the parameters and/or the Higgs-spectrum and the couplings for SUSY SU(5) or SUSY SO(10) can be arranged so that the triplet is appropriately heavy [34], as noted above, proton decay would occur primarily through the $d = 5$ operators (rather than $d = 6$), with an observable rate $\sim (10^{32} - 10^{34} yrs)^{-1}$, which would be induced by the exchange of color-triplet Higgsinos. These bring a new complexion to proton decay modes.

Owing to symmetry of the bosonic components, the effective $d = 5$ operators of the form QQQL/M in the superpotential must involve at least two different families [35]. As a result, the non-vanishing operators relevant for proton decay, which arise effectively through exchange of color triplets, are of the form: (a) $(\phi_{u,t,c})\phi_{di}\phi_s\phi_{\nu_\mu}$ and (b) $\phi_u\phi_{di}(\phi_{t,c})\phi_\mu^-$. These give rise to $d = 5$ interactions which are quadratic in both fermion and boson operatos. They need to be dressed by wino or gluino-exchange loops to yield effective four-fermion proton-decay interactions of the form $qqql$. Operators of class (a) lead to decay modes such as (see figs. 6)

$$p \rightarrow \bar{\nu}_\mu K^+, \quad n \rightarrow \bar{\nu}_\mu K^o \tag{6}$$

and also (see fig. 7)

$$p \rightarrow \bar{\nu}_\mu \pi^+ \; and \; n \rightarrow \bar{\nu}_\mu \pi^o, etc. \tag{7}$$

which arise primarily through wino-exchange loops. Those of class (b) give rise, through both wino and gluino-exchange, to charged antilepton decay modes (see fig. 8):

$$p \rightarrow \mu^+ K^o, \quad p \rightarrow \mu^+ \pi^o, etc. \tag{8}$$

Note that these do not include the canonical $p \rightarrow e^+\pi^o$-mode, which is induced, in $SUSYSU(5)$ or minimal $SUSYSO(10)$, primarily by the exchange of heavy gauge

bosons ($\sim 10^{16} GeV$) and thus strongly suppressed. Given the quark masses and the relevant mixing angles, it turns out that one typically expects the rate of $p \to \bar{\nu}_\mu K^+$-mode to be larger than that of both $p \to \bar{\nu}_\mu \pi^+$-mode, by about a factor of 2-10, and of $p \to \mu^+ K^o$-mode by as much as two to three orders of magnitude, and similarly for neutron-decay [35,36,33]. However, given the large top mass, which leads to large $\tilde{t} - \tilde{u}$ mixing through renormalization group corrections, it turns out that contribution from gluino-exchange can be quite important, especially for large $\tan\beta \geq 40$ (such large $\tan\beta$ is permitted for SUSY SO(10) though not for SUSY SU(5)). In this case, $p \to \mu^+ K^o$ can compete favorably and perhaps even dominate over the $p \to \bar{\nu}_\mu K^+$-mode [37]. In either case, we see that *one characteristic signal of SUSY GUT is that strange particle decay modes – i.e. $p \to \bar{\nu}_\mu K^+$ and/or $p \to \mu^+ K^o$ – are at least prominent, and under some circumstances dominant* [35]. There are regions in SUSY parameter space, pertaining to the masses of the SUSY particles, the mass of the color-triplets and $\tan\beta$, for which the non-strange modes involving anti-leptons of the muon-family – i.e. $p \to \bar{\nu}_\mu \pi^+$ and possibly $p \to \mu^+ \pi^o$ – can be prominent or even dominant [36], but those involving antileptons of the first family – in particular the $p \to e^+ \pi^o$ mode – are strongly suppressed. These latter are, however, the dominant modes in non-SUSY GUTS, like minimal non-$SUSYSU(5)$ and non-$SUSYSO(10)$.

Thus observation of strange particle decay modes of the nucleon, like $\bar{\nu} K^+$ or $\mu^+ K^o$, as the dominant or at least prominent modes, would clearly be a strong signal in favor of supersymmetry. Furthermore, observation of certain non-strange decay modes of the proton like $\bar{\nu}_\mu \pi^+$ or $\mu^+ \pi^o$, as opposed to $e^+ \pi^o$, as prominent modes, should also be a strong hint for the dominance of $d = 5$ operators and thus for supersymmetry.

For the sake of completeness, it should be added, however, that there exist SUSY non-GUT models, for which even the $e^+ \pi^o$-mode can be prominent or even dominant. That is the case, for example, for the supersymmetric flipped $SU(5) \times U(1)'$-model [38], for which the mass of the relevant leptoquark gauge boson, determined by the point of meeting of only α_3 and α_2 (though not $\alpha_1{}'$), can be much lower than 10^{16} GeV. As a result the gauge-boson mediated $d = 6$-operator, which would lead to $e^+ \pi^o$ as the dominant mode, can be the primary source of proton decay and is likely to yield lifetimes of order $10^{32} - 10^{34}$ yrs. The $e^+ \pi^o$-mode can also arise as a prominent or dominant mode through effective $d = 4$ operators, which may be induced in string-derived solutions through higher dimensional operators ($d > 5$) utilizing VEVs of appropriate fields (see

discussions in Sec. 6). Thus, observation of $e^+\pi^o$ as a prominent or dominant decay mode of the proton would certainly disfavor familiar SUSY GUTS, like $SUSYSU(5)$ or $SUSYSO(10)$, but it would be perfectly compatible with the dominance of *induced* $d = 4$ operators, as mentioned above, or with the flipped $SU(5)$ -model, and therefore with supersymmetry.

These points, as well as some related ones raised in the previous section, show that *low-energy* studies of *selection-rules* for (B, L) non-conservation, pertaining to proton decay modes as well as $n - \bar{n}$ oscillation, including a study of whether strange versus non-strange decay modes of the nucleon are prominent; can provide us with much information on possible new physics at very short distances, spanning from $(100TeV)^{-1}$ to $(10^{17}GeV)^{-1}$. I now return to the question of unification of couplings in MSSM.

5.3 MSSM-Unification and α_3

Before entering into the question of doublet-triplet spliting and a natural suppression of the $d = 4$ and $d = 5$ proton decay operators, it would be useful to probe into the accuracy with which the three couplings meet and discuss the issue of a matching between MSSM and string-unifications. Minimal SUSY SU(5) predicts $\sin^2\theta_w(m_Z)\mid_{\bar{M}S} = .2334 \pm .0036$, by using reasonable range of masses for the SUSY particles, and more importantly a value of $\alpha_3(m_Z) = .12 \pm .01$ as an input[29,30,31], where the error bar in α_3 is more generous than that allowed by the present world average data (see below). Note that the predicted value of $sin^2\theta_W$ would agree with the observed one of $sin^2\theta_W(m_Z)_{expt} = .2313 \pm .0003$[29], only provided $\alpha_3(m_Z)$, is *considerably higher than .12*, which is what is reflected clearly by Fig. 5b (taken from Ref. [29]), if we demand a meeting of the three couplings.

This may be seen more succinctly by using the more accurately determined value of $sin^2\theta_W(m_Z) = .2313 \pm .0003$ as an input and thereby getting $\alpha_3(m_Z)$ as an output[29, 32]. If one ignores possible corrections from GUT-threshold and Planck-scale physics, it turns out that in this case one needs $\alpha_3(m_Z) > .127$ to achieve coupling-unification within MSSM, assuming $m_{\tilde{q}} \sim 1TeV$ and $m_{1/2} < 500GeV$. Such high values of $\alpha_3(m_Z) \geq .125$ (say) are, however, incompatible with its world-average value [39],

$$\alpha_3(m_Z) = .117 \pm .005 \qquad (9)$$

which is based on high as well as low-energy determinations of α_3. The former is based

on LEP-data and the latter on the analysis involving $J/\psi, \Upsilon$, deep inelastic scattering and lattice-calculations.

To summarize the situation with regard to coupling-unification, we see that MSSM, which may be embedded in SUSY SU(5) or SUSY SO(10), fares far better than non-SUSY GUT as regards achieving unification of the three gauge couplings. There does seem to be some discrepancy, however, between the predicted and the world-average values of α_3, which, if genuine, would imply that the three couplings do not quite meet at a point in the context of MSSM. The discrepancy may be resolved through large corrections to the predicted α_3 (as much as about $-.006$) which may arise from GUT-threshold and Planck-scale physics. Alternatively, the discrepancy may have its origin in *new physics, beyond MSSM*, which may manifest at relatively low or intermediate scale. At this stage, not knowing precisely the GUT-threshold and Planck-scale corrections, *it seems to me that one can not discard MSSM, nor can one accept it necessarily as the whole truth, representing the correct effective theory below the GUT-scale.* It turns out that a resolution of this issue gets merged into a still bigger one pertaining to a matching between MSSM and string-unifications, which in turn has implications on the precise nature of (B,L)-nonservation. I therefore discuss next the issue of this matching of unification from the two ends and the problem of low α_3.

5.4 The Problem of Unification-Mismatch and Some Solutions

Achieving a complete unity of the fundamental forces together with an understanding of the origin of the three families and their hierarchical masses is among the major challenges still confronting particle physics. Conventional grand unification, despite all the merits noted in preceding sections, falls short in this regard in that owing to the arbitrariness in the Higgs sector, it does not even unify the Higgs exchange force, not to mention gravity. Superstring theory is the only theory we know that seems capable of removing these shortcomings. It thus seems imperative that the low energy data extrapolated to high energies be compatible with string unification.

It is, however, known [40,41] that while the three gauge couplings, extrapolated in the context of the minimal supersymmetric standard model (MSSM) meet, at least aproximately[32], provided $\alpha_3(m_Z)$ is not too low (as discussed above), their scale of meeting, $M_X \approx 2 \times 10^{16}\ GeV$, is nearly 20 times smaller than the expected (one–loop

level) string–unification scale [42] of $M_{\rm st} \simeq g_{\rm st} \times (5.2 \times 10^{17}\ GeV) \simeq 3.6 \times 10^{17}\ GeV$.

Babu and I recently noted that very likely there is a second mismatch concerning the value of the unified gauge coupling α_X at M_X [43]. Subject to the assumption of the MSSM spectrum, extrapolation of the low energy data yields a rather low value of $\alpha_X \approx 0.04$[32], for which perturbative physics should work well near M_X. On the other hand, it is known [44] that non–perturbative physics ought to be important for a string theory near the string scale, in order that it may help choose the true vacuum and fix the moduli and the dilaton VEVs. The need to stabilize the dilaton in particular would suggest that the value of the unified coupling at $M_{\rm st}$ in four dimensions should be considerably larger than 0.04 [45]. At the same time, α_{st} should not be too large, because, if $\alpha_{\rm st} \gg 1$, the corresponding theory should be equivalent by string duality [46] to a certain weakly coupled theory that would still suffer from the dilaton runaway problem [47]. Furthermore, $\alpha_{\rm st}$ at $M_{\rm st}$ should not probably be as large as even unity, or else, the one–loop string unification relations for the gauge couplings [42] would cease to hold near $M_{\rm st}$ (e.g. in this case, the string threshold corrections are expected to be too large) and the observed (approximate) meeting of the three couplings would have to be viewed as an accident. *In balance, therefore, the preceding discussions suggest that an intermediate value of the string coupling* $\alpha_{\rm st} \sim .15 - .25(say)$ *at* $M_{\rm st}$ *in four dimensions, which might be large enough to stabilize the dilaton, but not so large as to disturb significantly the coupling unification relations, is perhaps the more desired value* [43]. In short, the desired unification of the gauge couplings may well be *semi-perturbative*, rather than perturbative, in character. It is thus a challenge to find a suitable variant or alternative to MSSM which removes the mismatch not only with regard to the meeting point M_X, but also with regard to the value of α_X, as mentioned above.

A third relevant issue noted in the last section is that the world average value of $\alpha_3(m_Z) = 0.117 \pm 0.005$ [39] seems to be low compared to its value that is needed for MSSM unification. I note briefly a few alternative suggestions which have been proposed to address these issues, pertaining to removing the mismatch between MSSM and string-unifications.

Matching Through String-Duality: One suggestion in this regard is due to Witten [48]. Using the equivalence of the strongly coupled heterotic $SO(32)$ and the $E_8 \times E_8$ superstring theorie s in $D = 10$, respectively to the weakly coupled $D = 10$

Type I and an M–theory, he observed that the 4-dimensional gauge coupling and M_{st} can both be small, as suggested by MSSM extrapolation of the low energy data, without making the Newton's constant unacceptably large. While this observation opens up a new perspective on string unification, its precise use to make $\alpha_{st} \approx 0.04$ at M_{st} would seem to run into the dilaton runaway problem as in fact noted in Ref. [48].

Matching Through SUSY GUT: A second way in which the mismatch between M_X and M_{st} could be resolved is if superstrings yield an intact grand unification symmetry like $SU(5)$ or $SO(10)$ with the right spectrum – i.e., three chiral families and a suitable Higgs system including an adjoint Higgs at M_{st} [49], and if this symmetry would break spontaneously at $M_X \approx (1/20 \text{ to } 1/50)M_{st}$ to the standard model symmetry. However, as yet, there is no realistic (or close-to realistic) string–derived GUT model [49]. Furthermore, for such solutions, there is the likely problem of doublet-triplet splitting and rapid proton decay (see discussions later).

Matching Through Intermediate Scale Matter: A third alternative is based on string–derived standard model–like gauge groups. It attributes the mismatch between M_X and M_{st} to the existence of new matter with intermediate scale masses ($\sim 10^9 - 10^{13}$ GeV), which may emerge from strings [50]. Such a resolution is in principle possible, but it would rely on the delicate balance between the shifts in the three couplings and on the existence of very heavy new matter which in practice cannot be directly tested by experiments. Also, within such alternatives, as well as those based on non–standard hypercharge normalization [51] and/or large string–scale threshold effects [52], α_X typically remains small (~ 0.04), which is not compatible with the need for a larger α_X, as suggested above.

Matching Through ESSM – An Example of Semi-Perturbative Unification: Babu and I recently noted [43] that all three issues raised above – i.e. (i) understanding fermion mass-hierarchy, (ii) finding a suitable alternative to MSSM which would be compatible with string-unification, and (iii) accommodating low $\alpha_3(m_Z)$ can have a *common resolution* through a certain variant of the MSSM spectrum, which was proposed some time ago [27]. The variant spectrum extends the MSSM spectrum by adding to it two light vector-like families $Q_{L,R} = (U, D, N, E)_{L,R}$ and $Q'_{L,R} = (U', D', N', E')_{L,R}$, two Higgs singlets ($H_S$ and H_λ) and their SUSY partners, all as light as about 1 TeV and as heavy as about 100 TeV [53]. We refer to this variant as the Extended Supersymmetric Standard Model (ESSM). The combined sets $(Q_L|\overline{Q'_R})$ and $(\overline{Q_R}|Q'_L)$ transform as **16**

and $\overline{\mathbf{16}}$ of $SO(10)$ respectively. Barring addition of singlets, one can argue that ESSM is in fact *the only extension* of the MSSM, containing complete families of quarks and leptons, that is permitted by measurements of the oblique electroweak parameters and N_ν on the one hand, and renormalization group analysis on the other hand [43]. While the derivation of such a spectrum in string theories, is not yet in hand, it is worth noting that the emergence of pairs of $\mathbf{27}+\overline{\mathbf{27}}$ of E_6 or $\mathbf{16}+\overline{\mathbf{16}}$ of $SO(10)$ in addition to chiral multiplets is rather generic in string theories [54,55].

Babu and I performed a two-loop renormalization-group analysis for the running of the three gauge couplings for ESSM. In this analysis, we included the contributions of the Yukawa couplings of the two vector-like families with themselves and with the three chiral families. Such a pattern of Yukawa coupling, which leads to a see-saw mass-matrix for the 3 chiral and two vector-like families, is motivated by the inter-family mass-hierarchy [27,56]. All the relevant (unknown) Yukawa couplings were assumed to have their fixed point values at the electroweak scale, so that the analysis is essentially parameter-free, except for the input gauge couplings and the variation in the ESSM–spectrum. Remarkably enough, we found that the three gauge couplings $\alpha_{1,2,3}$ meet, even perfectly for many cases, for a fairly wide variation in the ESSM spectrum. A typical case of this meeting is shown in Fig. 9. The corresponding values of α_X, M_X and $\alpha_3(m_Z)\mid_{\bar{M}S}$, with vector-like quarks having masses $m_Q \approx 1.5-2TeV$, are found to be [43]:

$$\alpha_X \approx .2-.25,\ M_X \approx 10^{17}GeV,\ \alpha_3(m_Z)_{\bar{M}S} \approx .112-.118 \qquad (10)$$

Raising m_Q to $10-50\ TeV$ would lower α_X to about .18 - .16, and M_X by about a factor of 2, leaving α_3 in the range shown above.

Thus we see that ESSM leads to coupling–unification, with an intermediate value of α_X, and a lower value of $\alpha_3(m_Z)$ than that needed for MSSM unification, just as desired. The resulting $M_X \sim 10^{17}\ GeV$, though higher than the MSSM value, is still lower than the one–loop string–unification scale of Ref.[42], which, for $\alpha_X \approx 0.2$, yields $M_{\rm st} \approx 6\times 10^{17}\ GeV$. Considering the proximity of $M_X \sim 10^{17}\ GeV$ to the expected string scale of $(5-8)\times 10^{17}\ GeV$, however, it would seem that contributions from the infinite tower of heavy string-states, which have been neglected in the running of α_i's, quantum gravity and three and higher-loop effects [57] may well play an important role, especially for intermediate $\alpha_X \approx .2$, in bridging the relatively small gap between M_X

and M_{st}.

As a general comment, with an intermediate unified coupling ($\alpha_X \sim .2$), the increased, though not overwhelming, importance of three and higher loop-effects, compared to the case of MSSM, cannot of course be avoided. Yet, for such a case, the three gauge couplings are still fairly weak ($< .15$, say) for most of the region of extrapolation – i.e. for $Q < 10^{15.5}$ GeV (say) (see Ref. [43]). As a result, perturbation theory is still fairly reliable, all the way up to M_X, and the benefits of calculability are not lost for this case, in contrast to the case of a non-perturbative unification [58]. Thus, ESSM presents a good example of semi-perturbative unification, that is viable, and also seems desirable, if one wishes to stabilize the dilaton without losing the benefits of coupling-unification [43]. The main reason for devoting some discussion to these issues is that intermediate $\alpha_X \sim .16 - .2$ turns out to be crucial to ensure observable rate for proton decay in the same context in which rapid proton decay is prevented. This is what I discuss next.

6 The puzzle of proton–stability in Supersymmetry

In this section, I first outline the problem of the unsafe $d = 4$ as well as the color-triplet mediated and/or gravity-linked $d = 5$ proton decay operators, and then, following a recent paper by me [14], present a solution which suppresses these unsafe operators naturally, so as to ensure proton–stability, in accord with observation. The solution highlights the need for certain symmetries which cannot arise in conventional grand unification, but which do arise in string theories.

6.1 The Problem and Attempted Solutions in SUSY GUTS

As mentioned before, in accord with the standard model gauge symmetry $SU(2)_L \times U(1)_Y \times SU(3)^C$, a supersymmetric theory in general permits, in contrast to non-supersymmetric ones, dimension 4 and dimension 5 operators which violate baryon and lepton numbers [13]. Using standard notations, the operators in question which may arise in the superpotential are as follows:

$$\begin{aligned} W &= [\eta_1 \overline{U}\,\overline{D}\,\overline{D} + \eta_2 Q L \overline{D} + \eta_3 L L \overline{E}] \\ &+ [\lambda_1 Q Q Q L + \lambda_2 \overline{U}\,\overline{U}\,\overline{D}\,\overline{E} + \lambda_3 L L H_2 H_2]/M. \end{aligned} \tag{11}$$

Here, generation, $SU(2)_L$ and $SU(3)^C$ indices are suppressed. M denotes a characteristic mass scale. The first two terms of $d = 4$, jointly, as well as the $d = 5$ terms of strengths λ_1 and λ_2, individually, induce $\Delta(B-L) = 0$ proton decay with amplitudes $\sim \eta_1\eta_2/m_{\tilde{q}}^2$ and $(\lambda_{1,2}/M)(\delta)$ respectively, where δ represents a loop-factor. Experimental limits on proton lifetime turns out to impose the constraints: $\eta_1\eta_2 \leq 10^{-24}$ and $(\lambda_{1,2}/M) \leq 10^{-25}$ GeV^{-1} [59]. Thus, even if $M \sim M_{string} \sim 10^{18}$ GeV, we must have $\lambda_{1,2} \leq 10^{-7}$, so that proton lifetime will be in accord with experimental limits.

Renormalizable, supersymmetric standard-like and $SU(5)$ [60] models can be constructed so as to avoid, *by choice*, the $d = 4$ operators (i.e. the $\eta_{1,2,3}$-terms) by imposing a discrete or a multiplicative R-parity symmetry: $R \equiv (-1)^{3(B-L)}$, or more naturally, by gauging $B - L$, as in $\mathcal{G}_{224} \equiv SU(2)_L \times SU(2)_R \times SU(4)^C$ or $SO(10)$. Such resolutions, however, do not in general suffice if we permit higher dimensional operators and intermediate scale VEVs of fields which violate $(B - L)$ and R-parity (see below). Besides, $B - L$ can not provide any protection against the $d = 5$ operators given by the λ_1 and λ_2 - terms, which conserve $B - L$. These operators are, however, expected to be present in any theory linked with gravity, e.g. a superstring theory, unless they are forbidden by some new symmetry.

As mentioned in Section 5, for SUSY grand unification models, there is the additional problem that the exchange of color-triplet Higgsinos which occur as partners of electroweak doublets (as in $\mathbf{5} + \overline{\mathbf{5}}$ of $SU(5)$) induce $d = 5$ proton-decay operators [13]. Thus, allowing for suppression of λ_1 and λ_2 (by about 10^{-8}) due to the smallness of the relevant Yukawa couplings, the color-triplets still need to be superheavy ($\geq 10^{17}$ GeV) to ensure proton-stability [59], while their doublet partners must be light (≤ 1 TeV). This is the *generic problem of doublet-triplet splitting* that faces all SUSY GUTS. Basically, four types of solutions to this problem have been proposed in the context of SUSY grand unification. They are as follows:

(i) The Case of Extreme Fine Tuning: In this case, utilizing cubic coupling in the superpotential of the form $W = A\overline{5}_{H'} \cdot < 24_H > \cdot 5_H + B\overline{5}_{H'} \cdot < 1_H > .5_H$, one can assign masses to the triplets and the doublets in $\overline{5}$ and 5 of $SU(5)$ through the VEVs of both 24_H (which is traceless) and 1_H. By arranging these two contributions to add for the triplets, but to almost cancel for the doublets, *to one part in* 10^{14}, one can keep the doublets appropriately light, and the triplets superheavy[60]. This case, however, needs extreme fine tuning.

(ii) The Missing Partner Mechanism [61]: In this case, by introducing suitable large-size Higgs multiplets, such as $50_H + \overline{50}_H + 75_H$, in addition to $5_H + \overline{5}_H$ of $SU(5)$, and allowing couplings of the form $W = C\,5_H \cdot \overline{50}_H \cdot < 75_H > + D\,\overline{5}_H \cdot 50_H < 75_H >$, one can give superheavy masses to the triplets (anti-triplets) in $5(\overline{5})$ by pairing them with anti-triplets (triplets) in $\overline{50}(50)$. But there do not exist doublets in $50(\overline{50})$ to pair up with the doublets in $5(\overline{5})$, which therefore can remain light, provided a direct superheavy $5 \cdot \overline{5}$ mass-term is prevented.

(iii) The Dimopoulos-Wilczek Mechanism [62]: Utilizing the fact that the VEV of 45_H of $SO(10)$ does not have to be traceless (unlike that of 24_H of $SU(5)$), one can give mass to color-triplets and not to doublets in the 10 of $SO(10)$, by arranging the VEV of 45_H to be proportional to diag (x, x, x, o, o), and introducing a coupling of the form $\lambda 10_{H1} \cdot 45_H \cdot 10_{H2}$ in W. Two $10's$ are needed owing to the anti-symmetry of 45. Because of two $10's$, this coupling would leave two pairs of electroweak doublets massless. One must, however, make one of these pairs superheavy, by introducing a term like $M\,10_{H2} \cdot 10_{H2}$ in W, so as not to spoil the successful prediction of $sin^2\theta_W$ of SUSY GUT. In addition, one must also ensure that only 10_{H1} but not 10_{H2} couple to the light quarks and leptons, so as to prevent rapid proton decay. All of these can be achieved by imposing suitable discrete symmeries. There is, however, still some question as to whether the triplets can be sufficiently heavy $(\geq 10^{17})GeV)$ without conflicting with unification of the gauge couplings. One can avoid this issue altogether and ensure a strong suppression of color-triplet mediated proton decay, provided one introduces additional 45's and 10 of SO(10) (see e.g. Babu and Barr, Ref. [62]).

(iv) The Case of Higgses as Pseudogoldstone Bosons [63]. A new line of approach, though not a complete model, has been proposed recently, in which suitable choice of discrete symmetries lead to accidental global symmetries of the Higgs-potential, which are broken explicitly by the Yukawa couplings of the model. The associated pseudogoldstone bosons are identified with the Higgs doublets. While this idea has some nice features, because it proposes to use only adjoint and fundamental representations for the Higgs scalars, the full consistencey of this idea in the context of a complete model in realizing electroweak-scale masses for the Higgs-doublets, and a desirable pattern of masses for the fermions, remains to be shown. Furthermore, in this case, one needs to make heavy use of discrete symmetries to (a) ensure the accidental global symmetry of the Higgs-potential, (b) obtain a desired pattern of masses for the fermions, and (c) suppress

undesirable flavor-changing neutral currents. Thus, the prospect of a natural origin of this class of models (i.e. of all the necessary discrete symmetries) from an underlying theory, like a string theory, is far from clear. Furthermore, the question of a natural suppression of the $d = 4$ -operators and of the gravity-linked $d = 5$ operators, of course, still remains open even in the context of this class of models.

In summary, solutions to the problem of doublet-triplet splitting needing either unnatural fine-tuning as in SUSY $SU(5)$ [60], or suitable *choice* of large number and/or large size Higgs multiplets and/or choice of discrete symmetries as in SUSY $SO(10)$ [62], missing-partner [61] and psuedogoldstone models [63], are technically feasible. *They, however, do not seem to be compelling by any means because they have been invented for the sole purpose of suppressing proton-decay, without a deeper reason for their origin.* Furthermore, such solutions are not easy to realize, and to date have not been realized, in *string-derived* grand unified theories [49].

These considerations show that, in the context of supersymmetry, the extraordinary stability of the proton is a major puzzle. *The question in fact arises: Why does the proton have a lifetime exceeding* 10^{39} *sec, rather than the apparently natural value (for supersymmetry) of less than 1 sec?* As such, the known longevity of the proton deserves a natural explanation. Rather than being merely accommodated, it ought to emerge as a *compelling feature*, owing to symmetries of the underlying theory, which should forbid, or adequately supress, the unsafe $d = 4$ as well as $d = 5$ operators in Eq. (11). As discussed below, the task of finding such symmetries becomes even harder, if one wishes to assign non-vanishing light masses ($\leq$ few eV) to neutrinos. Following Ref. 14, I will present in this section, a class of solutions within supersymmetric theories, which *(a) naturally* ensure proton-stability, to the extent desired, and *(b)* simultaneously permit neutrinos to acquire light masses, of a nature that is relevant to current experiments [10,18]. These solutions need <u>either</u> I_{3R} and $B - L$ as *separate* gauge symmetries, as well as *one extra abelian symmetry* that lies beyond even E_6 [21]; <u>or</u> the weak hypercharge Y $(= I_{3R} + (B - L)/2)$ accompanied by *two extra symmetries* beyond those of E_6. The interesting point is that while the extra symmetries in question can not arise within conventional grand unification models, including E_6, they do arise within a class of string-derived three generation solutions. This in turn provides *a strong motivation* for symmetries of string-origin. The extra symmetries lead to extra Z'-bosons, whose currents would bear the hallmark of string theories. It turns out that there is an interesting correlation

between the masses of the Z'-bosons and observability of proton decay.

6.2 The need for symmetries beyond $SO(10)$ and E_6:

In what follows, I assume that operators (with d $\geq$ 4), scaled by appropriate powers of Planck or string-scale mass, exist in the effective superpotential of any theory which is linked to gravity, like a superstring theory [12,64], unless they are forbidden by the symmetries of the effective theory. For reasons discussed above, the class of theories – string-derived or not – which contains $B-L$, as in $\mathcal{G}_{2311} \equiv SU(2)_L \times SU(3)^C \times U(1)_{I_{3R}} \times U(1)_{B-L}$, as a symmetry, the $d = 4$ operators in Eq.(11) are naturally forbidden. They can *in general* appear however through non-renormalizable operators if there exist VEVs of fields which violate $B - L$. This is where neutrino-masses become relevant. As discussed in Sec. 2, the familiar see-saw mechanism [17] that provides the simplest reason for known neutrinos ν_L^i's to be so light, assigns *heavy Majorana masses* M_R^i to the right-handed neutrinos ν_R^i, which in turn need spontaneous violation of $B - L$ at a heavy intermediate scale.

If $B - L$ is violated by the VEV of a field by two units, an effective R-parity would still survive [65], which would forbid the $d = 4$ operators. That is precisely the case for the multiplet 126 of $SO(10)$ or $(1, 3, \overline{10})$ of $\mathcal{G}_{224}$, which have commonly been used to give Majorana masses to ν_R's. Recent works show, however, that 126 and very likely $(1, 3, \overline{10})$, as well, are hard – perhaps impossible – to obtain in string theories [66]. We, therefore, assume that this constraint holds. It will become clear, however, that as long as we demand safety from both $d = 4$ *and* $d = 5$ operators, our conclusion as regards the need for symmetries beyond E_6, would hold even if we give up this assumption.

Without 126 of Higgs, ν_R's can still acquire heavy Majorana masses utilizing product of VEVs of sneutrino-like fields $\widetilde{\overline{N_R}}$ and $\widetilde{N'_L}$, which belong to 16_H and $\overline{16}_H$ respectively. (as in Ref. [54], see also [55].) In this case, an effective operator of the form $16 \cdot 16 \cdot \overline{16}_H . \overline{16}_H / M$ in W, that is allowed by $SO(10)$, would induce a Majorana mass $(\overline{\nu}_R C^{-1} \overline{\nu}_R^T)(\langle \widetilde{N'_L} \rangle \langle \widetilde{N'_L} \rangle / M) + hc$ of magnitude $M_R \sim 10^{12.5}$ GeV, as desired, for $\langle \widetilde{N'_L} \rangle \sim 10^{15.5}$ GeV and $M \sim 10^{18}$ GeV. [67] However, consistent with $SO(10)$ symmetry and therefore its subgroups, one can have an effective $d = 5$ operator in the superpotential $16^a \cdot 16^b \cdot 16^c \cdot 16_H / M$. This would induce the terms $\overline{U}_R \overline{D}_R \overline{D}_R \langle \widetilde{\overline{N_R}} \rangle / M$ and $QL\overline{D} \langle \widetilde{\overline{N_R}} \rangle / M$ in W (see Eq.(11)) with strengths $\sim \langle \widetilde{\overline{N_R}} \rangle / M \sim 10^{15.5}/10^{18} \sim 10^{-2.5}$,

Operators	I_{3R}	$B-L$	Y	Q_ψ	Q_T
$\overline{U}\,\overline{D}\,\overline{D}, QL\overline{D}$	1/2	-1	0	3	4
$LL\overline{E}$	1/2	-1	0	3	4
$QQQL/M$	0	0	0	4	4
$\overline{U}\,\overline{U}\,\overline{D}\,\overline{E}/M$	0	0	0	4	4
LLH_2H_2/M	1	-2	0	-2	0
$\widetilde{\overline{N_R}}$	-1/2	1	0	1	0
(H_1, H_2)	(-1/2, 1/2)	0	(-1/2, 1/2)	-2	-2
χ	0	0	0	4	4

Table 2:

which would lead to unacceptably short proton lifetime $\sim 10^{-6}$ yrs. We thus see that, without having the 126 or $(1,3,\overline{10})$ of Higgs, $B-L$ *and therefore* $SO(10)$ *does not suffice to suppress even the* $d=4$ *- operators adequately while giving appropriate masses to neutrinos.* As mentioned before, $B-L$ does not of course prevent the $d=5$, λ_1 and λ_2 - terms, regardless of the Higgs spectrum, because these terms conserve $B-L$.

To cure the situation mentioned above, we need to utilize symmetries beyond those of $SO(10)$. Consider first the presence of at least one extra $U(1)$ beyond $SO(10)$ of the type available in E_6, i.e. $E_6 \to SO(10)\times U(1)_\psi$, under which 27 of E_6 branches into $(16_1 + 10_{-2} + 1_4)$, where 16 contains $(Q, L \mid \overline{U_R}, \overline{D_R}, \overline{E_R}, \overline{\nu_R})$, with $Q_\psi = +1$; while 10 contains the two Higgs doublets $(H_1, H_2)^{(0,-2)}$ and a color-triplet and an anti-triplet $(H_3^{(-2/3,-2)} + H_{3^*}^{\prime(2/3,-2)})$, where the superscripts denote $(B-L, Q_\psi)$. Assume that the symmetry in the observable sector just below the Planck scale is of the form:

$$\mathcal{G}_{obs} = [\mathcal{G}_{fc} \subseteq SO(10)] \times \hat{U}(1)_\psi \times [U(1)'s]. \tag{12}$$

It is instructive to first assume that $\hat{U}(1)_\psi = U(1)_\psi$ of E_6 [68] and ignore all the other $U(1)$'s. Ignoring the doublet-triplet splitting problem for a moment, we allow the flavor-color symmetry $\mathcal{G}_{fc}$ to be as big as $SO(10)$. The properties of the operators in W given in Eq.(7), and the fields $\widetilde{\overline{N_R}}$, (H_1, H_2) and the singlet $\chi \subset 27$, under the charges Y, I_{3R}, $B-L$, Q_ψ and $Q_T \equiv Q_\psi - (B-L)$, are shown in Table 2. We see that the $d=4$ operators (η_i -terms) carry nonvanishing $B-L$, Q_ψ and Q_T, and are thus forbidden by each of these symmetries. Furthermore, note that when $\widetilde{\overline{N_R}} \subset 16$ and

$\widetilde{N'_L} \subset \overline{16}$ acquire VEV, the charges I_{3R}, $B-L$ as well as Q_ψ are broken, *but* Y *and* Q_T *are preserved.* Now Q_T would be violated by the VEVs of $(H_1, H_2) \sim 200$ GeV and of the singlets $\chi^{(27)}$ and $\overline{\chi}^{(\overline{27})}$. Assume that χ and $\overline{\chi}$ acquire VEVs ~ 1 TeV through a radiative mechanism, utilizing Yukawa interactions, analogous to (H_1, H_2). The $d = 4$ operators can be induced through nonrenormalizable terms of the type $16 \cdot 16 \cdot 16 \cdot [\langle \widetilde{\overline{N_R}} \subset 16 \rangle / M].[\langle 10 \rangle \langle 10 \rangle / M^2$ or $\langle \overline{\chi} \subset \overline{27} \rangle / M]$, where the effective couplings respect $SO(10)$ and $U(1)_\psi$. Thus we get $\eta_i \leq (10^{15.5}/10^{18})(1 \text{ TeV}/10^{18} \text{ GeV}) \sim 10^{-18}$, which is below the limit of $\eta_1 \eta_2 \leq 10^{-24}$. Thus, $B-L$ *and* Q_ψ, arising within E_6, suffice to control the $d = 4$ operators adequately, while permitting neutrinos to have desired masses.

Next consider the LLH_2H_2-term. While it violates I_{3R}, $B-L$ and Q_ψ, it is the only term that is allowed by Q_T. Such a term can arise through an effective interaction of the form $16 \cdot 16 \cdot (H_2 \subset 10)^2 \cdot \langle \widetilde{\overline{N_R}} \subset 16 \rangle^2 / M^3$, and thus with a strength $\sim 10^{-5} \cdot (10^{18} \text{GeV})^{-1}$, which is far below the limits obtained from ν-less double β-decay.

Although the two $d = 5$ operators $QQQL/M$ and $\overline{U}\,\overline{U}\,\overline{D}\,\overline{E}/M$ are forbidden by Q_ψ and Q_T, the problem of these two operators still arises as follows. Even for a broken E_6-theory, possessing $U(1)_\psi$-symmetry, the color-triplets H_3 and H'_{3^*} of 27 still exist in the spectrum. They are in fact needed to cancel the anomalies in $U(1)^3_\psi$ and $SU(3)^2 \times U(1)_\psi$ etc. They acquire masses of the form $M_3 H_3 H'_{3^*} + hc$ through the VEV of singlet $\langle \chi \rangle$ which breaks Q_ψ and Q_T by four units. With such a mass term, the exchange of these triplets would induce $d = 5$ proton-decay operators, just as it does for SUSY $SU(5)$ and $SO(10)$. We are then back to facing either the problem of doublet-triplet splitting (i.e. why $M_3 \geq 10^{17}$ GeV) or that of rapid proton-decay (for $M_3 \sim 1$ TeV). *In this sense, while the* E_6*-framework, with* $U(1)_\psi$*, can adequately control the* $d = 4$ *operators and give appropriate masses to the neutrinos (which* $SO(10)$ *cannot), it does not suffice to control the* $d = 5$ *operators, owing to the presence of color-triplets.* As we discuss below, this is where string-derived solutions help in preserving the benefits of a Q_ψ-like charge, while naturally eliminating the dangerous color-triplets.

6.3 Doublet-Triplet Splitting In String Theories: A Preference For Non-GUT Symmetries:

While the problem of doublet-triplet splitting does not have a compelling solution within SUSY GUTS and has not been resolved within string-derived GUTS [49], it can be solved quite simply within string-derived standard-like [69,70] or the $\mathcal{G}_{224}$-models [54], *because in these models, the electroweak doublets are naturally decoupled from the color-triplets after string-compactification.* As a result, invariably, the same set of boundary conditions (analogous to "Wilson lines") which break $SO(10)$ into a standard-like gauge symmetry such as $\mathcal{G}_{2311}$, either project out, by GSO projections, all color-triplets H_3 and H_3', from the "massless"- spectrum [70], or yield some color-triplets with extra $U(1)$ - charges which make them harmless [69], because they can not have Yukawa couplings with quarks and leptons. In these models, the doublet triplet splitting problem is thus solved from the start, because the *dangerous* color - triplets simply do not appear in the massless spectrum [71].

At the same time, owing to constraints of string theories, the coupling unification relations hold [42] for the string-derived standard-like or $\mathcal{G}_{224}$-models, just as they do for GUT-models. Furthermore, close to realistic models have been derived from string theories only in the context of such standard-like [69,70], flipped $SU(5) \times U(1)$ [38] and $\mathcal{G}_{224}$ models [54], but not yet for string-derived GUTS [49]. For these reasons, we will consider string-derived non-GUT models, as opposed to string-GUT-models, *as the prototype of a future realistic string model*, and use them as a *guide* to ensure *(a)* proton - stability and *(b)* light neutrino masses [72].

Now, if we wish to preserve the benefits of the charge Q_ψ (noted before), and still eliminate the color-triplets as mentioned above, there would appear to be a problem, because, without the color-triplets, the incomplete subset consisting of $\{16_1+(2,2,1)_{-2}+1_4\} \subset 27$ of E_6 would lead to anomalies in $U(1)_\psi^3$, $SU(3)^2 \times U(1)_\psi$ etc. This is where symmetries of string-origin come to the rescue.

6.4 Resolving the Puzzle of Proton-longevity through string-symmetries

The problem of anomalies (noted above) is cured within string theories in a variety of ways. For instance, new states beyond those in the E_6-spectrum invariably appear in the

string-massless sector which contribute toward the cancellation of anomalies, and only certain *combinations* of generators become *anomaly-free.* To proceed further, we need to focus on some specific solutions. For this purpose, we choose to explore the class of string-derived three generation models, obtained in Refs.[69] and [70], which is as close to being realistic as any other such model that exists in the literature (see e.g. Refs. [54] and [38]). In particular, they seem capable of generating qualitatively the right texture for fermion mass-matrices and CKM mixings. We stress, however, that the essential feature of our solution [14], relying primarily on the existence of extra symmetries analogous to $U(1)_\psi$, is likely to emerge in a much larger class of string-derived solutions.

After the application of all GSO projections, the gauge symmetry of the models developed in these references, at the string scale, is given by:

$$\mathcal{G}_{st} = [SU(2)_L \times SU(3)^C \times U(1)_{I_{3R}} \times U(1)_{B-L}] \times [G_M = \prod_{i=1}^{6} U(1)_i] \times G_H. \qquad (13)$$

Here, $U(1)_i$ denote six horizontal-symmetry charges which act non-trivially on the three families and distinguish between them. In the models of Refs. [69], [70], $G_H = SU(5)_H \times SU(3)_H \times U(1)_H^2$. There exists "hidden" matter which couples to G_H and also to $U(1)_i$.

A partial list of the massless states for the solution derived in Ref. [69], together with the associated $U(1)_i$-charges, is given in Table 3. The table reveals the following features:

(i) There are three families of quarks and leptons (1, 2 and 3), each with 16 components, including $\overline{\nu_R}$. Their quantum numbers under the symmetries belonging to $SO(10)$ are standard and are thus not shown. Note that the $U(1)_i$ charges differ from one family to the other. There are also three families of hidden sector multiplets V_i, $\overline{V}_i$, T_i and $\overline{T}_i$ which possess $U(1)_i$-charges.

(ii) The charge Q_1 has the same value $(\frac{1}{2})$ for all sixteen members of family 1, similarly Q_2 and Q_3 for families 2 and 3 respectively. In fact, barring a normalization difference of a factor of 2, *the sum* $Q_+ \equiv Q_1 + Q_2 + Q_3$ *acts on the three families and on the three Higgs doublets* $\overline{h_1}$, $\overline{h_2}$ *and* $\overline{h_3}$ *in the same way as the* Q_ψ *of* E_6 *introduced before.* The analogy, however, stops there, because the solution has additional Higgs doublets (see table) and also because there is only one pair of color triplets $(D_{45}, \overline{D}_{45})$ instead of three. Furthermore, the pair $(D_{45}, \overline{D}_{45})$ is *vector-like* with opposite Q_+-charges, while (H_3, H'_{3^*}), belonging to 27 of E_6, have the same Q_ψ-charge. In fact the pair $(D_{45}, \overline{D}_{45})$ can have an invariant mass conserving all Q_i-charges, but (H_3, H'_{3^*}) can not.

(iii) It is easy to see that owing to different $U(1)_i$-charges, the color-triplets D_{45} and $\overline{D}_{45}$ (in contrast to H_3 and H'_{3*}) can not have allowed Yukawa couplings to (qq) and (ql) - pairs. Thus, as mentioned before, they can not mediate proton decay.

(iv) Note that the solution yields altogether four pairs of electroweak Higgs doublets: (h_1, h_2, h_3, h_{45}) and $(\overline{h_1}, \overline{h_2}, \overline{h_3}, \overline{h_{45}})$. It has been shown [69] that only one pair – i.e. $\overline{h_1}$ or $\overline{h_2}$ and h_{45} – remains light, while the others acquire superheavy or intermediate scale masses. Owing to differing $U(1)_i$-charges, the three families have Yukawa couplings with three distinct Higgs doublets. Since only one pair ($\overline{h_1}$ and h_{45}) remains light and acquires VEV, it turns out that families 1,2 and 3 get identified with the τ, μ and e-families respectively [69]. The mass-heirarchy and CKM mixings arise through higher dimensional operators, by utilizing VEVs of appropriate fields and hidden-sector condensates.

Including contributions from the entire massless spectrum, one obtains: $TrU_1 = TrU_2 = TrU_3 = 24$ and $TrU_4 = TrU_5 = TrU_6 = -12$. Thus, all six $U(1)_i$'s are anomalous. They give rise to five anomaly-free combinations and one anomalous one:

$$\begin{aligned} U'_1 &= U_1 - U_2\,, \quad U'_2 = U_4 - U_5\,, \quad U'_3 = U_4 + U_5 - 2U_6\,, \\ \hat{U}_\psi &= U_1 + U_2 - 2U_3\,, \\ \hat{U}_\chi &= (U_1 + U_2 + U_3) + 2(U_4 + U_5 + U_6)\,, \\ U_A &= 2(U_1 + U_2 + U_3) - (U_4 + U_5 + U_6). \end{aligned} \tag{14}$$

One obtains $TrQ_A = 180$. The anomalous U_A is broken by the Dine-Seiberg-Witten (DSW) mechanism, in which the anomalous D-term generated by the VEV of the dilaton field is cancelled by the VEVs of some massless fields which break U_A, so that supersymmetry is preserved [73]. The solutions (i.e. the choice of fields with non-vanishing VEVs) to the corresponding F and D - flat conditions are, however, not unique. A few alternative possibilities have been considered in Ref. [69] (see also Refs. [54] and [38] for analogous considerations). Following our discussions in the previous subsection as regards non-availibility of 126 of $SO(10)$ or $(1, 3, \overline{10})$ of $\mathcal{G}_{224}$, I assume, for the sake of simplicity in estimating strengths of relevant operators, that $B - L$ is violated spontaneously at a scale $\sim 10^{15}$-10^{16} GeV by one unit (rather than two) through the VEVs of *elementary* sneutrino-like fields $\widetilde{\overline{N_R}} \subset 16_H$ and $\widetilde{N'_L} \subset \overline{16_H}$ (as in Ref. [54]). Replacing VEVs of these elementary fields by those of products of fields including condensates,

as in Ref. [69], would only lead to further suppression of the relevant unsafe higher dimensional operators and go towards strengthening our argument [14] as regards certain symmetries being sufficient in preventing rapid proton-decay [74].

A Longlived Proton: We now reexamine the problem of proton-decay and neutrino-masses by assuming that in addition to I_{3R} and $B-L$, or just Y, either $\hat{Q}_\psi \equiv Q_1+Q_2-2Q_3$, or $\hat{Q}_\chi \equiv Q_1+Q_2+Q_3+2(Q_4+Q_5+Q_6)$ (see Eq. (10)), or both emerge as good symmetries near the string scale, which are broken by the VEVs of (i) *s*neutrino-like fields $\sim 10^{15}$ - 10^{16} GeV, (ii) electroweak doublets and singlets (denoted by ϕ's) $\sim 1TeV$, and (iii) hidden-sector condensates. To ensure proton-stability, we need to assume that the hidden-sector condensate-scale is $\leq 10^{-2.5}M_{st}$. With the gauge coupling α_X, at the unification-scale M_X, having nearly the MSSM value of $.04-.06$, or even an intermediate value $\approx .16-.2$ (say), as suggested in Ref. [43], this seems to be a safe assumption for most string models (see discussions later). The roles of the symmetries Y, $B-L$, $\hat{Q}_\psi$, $\hat{Q}_\chi$ and $(\hat{Q}_\chi+\hat{Q}_\psi)$ in allowing or forbidding the relevant (B,L) - violating operators, including the higher dimensional ones, which allow violations of these symmetries through appropriate VEVs, are shown in Table 4. Based on the entries in this table, the following points are worth noting:

(i) Inadequacy of the Pairs $(Y,\ B-L)$; $(Y,\ \hat{Q}_\psi)$; $(Y,\ \hat{Q}_\chi)$ and $(B-L,\ \hat{Q}_\chi)$: Table 4 shows that no single charge nor the pairs $(Y,B-L)$, $(Y,\ \hat{Q}_\psi)$, $(Y,\ \hat{Q}_\chi)$ and $(B-L,\ \hat{Q}_\chi)$ give adequate protection against all the unsafe operators. Let us next consider other pairs of charges.

(ii) Adequate Protection Through the Pair $(B-L$ and $\hat{Q}_\psi)$ or the Pair $(\hat{Q}_\chi$ and $\hat{Q}_\psi)$: Using Table 4, we observe that the pair $(B-L$ and $\hat{Q}_\psi)$, as well as the pair $(\hat{Q}_\chi$ and $\hat{Q}_\psi)$, forbid all unsafe operators, including those which may arise from higher dimensional ones, with or without hidden-sector condensates. In fact, *members of the pairs mentioned above complement each other in the sense that when one member of a pair allows an unsafe operator, the other member of the same pair forbids it, and vice versa* – a remarkable team effort. Note that the strengths of the d=4 and d=5 operators are controlled by the VEVs $<\overline{h}_1/M>^2$, $<\Phi/M>^n$ and $<T_i\overline{T}_j/M^2>^2$, which give more than necessary suppression, even if the condensate-scale is as large as about 10^{15} GeV (see estimates below).

(iii) $\hat{Q}_\psi$ removes Potential Danger From Triplets in The Heavy Tower As Well: Color triplets in the heavy infinite tower of states with masses $M \sim M_{st} \sim 10^{18}$ GeV in

general pose a *potential danger* for all string theories, including those for which they are projected out from the massless sector [69]. The exchange of these heavy triplets, if allowed, would induce $d = 5$ proton-decay operators with strengths $\sim \kappa/M$, where κ is given by the product of two Yukawa couplings. Unless the Yukawa couplings are appropriately suppressed [75] so as to yield $\kappa \leq 10^{-7}$ [59], these operators would be unsafe. *Note, however, that string-derived solutions possessing symmetries like $\hat{Q}_\psi$ are free from this type of danger.* This is because, if $\hat{Q}_\psi$ emerges as a good symmetry near the string-scale, then the spectrum, the masses and the interactions of the color-triplets in the heavy tower would respect $\hat{Q}_\psi$. As a result, the exchange of such states can not induce $d = 5$ proton-decay operators, which violate $\hat{Q}_\psi$ (see Table 4).

In fact, for such solutions, the color-triplets in the heavy tower can appear only as *vector-like pairs*, with opposite $\hat{Q}_\psi$-charges (like those in 10 and $\overline{10}$ of $SO(10)$, belonging to 27 and $\overline{27}$ of E_6 respectively), so that they can acquire invariant masses of the type $M\{(H_3\overline{H_3} + H'_{3^*}\overline{H'_{3^*}}) + hc\}$, which conserve $\hat{Q}_\psi$. Such mass-terms cannot induce proton decay.

Thus we see that a symmetry like $\hat{Q}_\psi$ plays an essential role in safegaurding proton-stability from all angles [14]. Since $\hat{Q}_\psi$ distinguishes between the three families [76], it cannot, however, arise within single - family grand unification symmetries, including E_6. *But it does arise within string-derived three-family solutions (as in Ref. [69]), which at once know the existence of all three families.* In this sense, string theory plays a vital role in explaining naturally why the proton is so extraordinarily stable, in spite of supersymmetry, and why the neutrinos are so light.

Z'-mass and proton decay rate: If symmetries like $\hat{Q}_\psi$ and possibly $\hat{Q}_\chi$, in addition to I_{3R} and $B-L$, emerge as good symmetries near the string scale, and break spontaneously so that only electric charge is conserved, there must exist at least one extra Z'-boson (possibly more), in addition to the (almost) standard Z and a superheavy Z_H (that acquires a mass through *s*neutrino–VEV) [77]. The extra Z' boson(s) will be associated with symmetries like $\hat{Q}_T \equiv 2\hat{Q}_\psi - (B-L)$ and $\hat{Q}_\chi + \hat{Q}_\psi$, in addition to Y, that survive after *s*neutrino acquires a VEV. The Z' bosons can acquire masses through the VEVs of electroweak doublets and singlets (ϕ's), as well as through the hidden-sector condensates like $\langle \overline{T}_i T_j \rangle$, all of which break $\hat{Q}_T$ and $\hat{Q}_\chi + \hat{Q}_\psi$ (see Table 3). As mentioned before, we expect the singlet ϕ's to acquire VEVs, at least radiatively (like the electroweak doublets), by utilizing their Yukawa couplings with the doublets, which at the string-scale

is comparable to the top-Yukawa coupling. Since the ϕ's do not have electroweak gauge couplings, however, we would expect that their radiatively-generated VEV, collectively denoted by v_0, to be somewhat higher than those of the doublets ($v_{EW} \sim 200$ GeV) -*i.e.*, quite plausibly, $v_0 \sim 1$ TeV. Thus, in the absence of hidden-sector condensates, we would expect Z' to be light ~ 1 TeV.

If the condensates like $\langle \overline{T}_i T_j \rangle$ do form, however, they are likely to make Z' much heavier than 1 TeV. Denoting the strength of $\langle \overline{T}_i T_j \rangle$ by Λ_c^2, if $\Lambda_c \sim \Lambda_H$, where Λ_H is the confinement-scale of the hidden-sector, we would expect Λ_H and thus Z' to be either superheavy $\sim 10^{15}$-10^{16} GeV, or at least medium-heavy $\sim 10^{8}$-10^{13} GeV (see below).

The mass of the Z'-boson is correlated with the proton decay-rate. The heavier the Z', the faster is the proton-decay. Looking at Table 4, we see that the strength of the effective $d = 4$ operators ($\overline{U}\,\overline{D}\,\overline{D}$ etc.) is given by $\left(\langle \widetilde{\overline{N_R}}/M \rangle\right)\left(\langle T_i \overline{T}_j \rangle / M^2\right)^2 \sim 10^{-2.5}(\Lambda_c/M)^4$, and that of the $d = 5$ operator ($QQQL/M$) is given by $\left(\langle T_i \overline{T}_j \rangle / M^2\right)^2 \sim (\Lambda_c/M)^4$. The observed bound on the former ($\eta_{1,2} \leq 10^{-12}$) implies a rough upper limit of $(\Lambda_c/M)^4 \leq 10^{-9.5}$ and thus $\Lambda_c \leq 10^{15.5}$ GeV, while that on the latter (i.e. $\lambda_{1,2} \leq 10^{-7}$) implies that $\Lambda_c \leq 10^{16.2}$ GeV, where, for concreteness, we have set $M = 10^{18}$ GeV.

Thus, if $\Lambda_c \leq 1$ TeV, Z' would be light ~ 1 TeV, and accessible to LHC and perhaps NLC. But, for this case, or even if Λ_c is as heavy as 10^{15} GeV (say), proton-decay would be too slow ($\tau_p \geq 10^{42}$ yrs.) to be observed. On the other hand, if $\Lambda_c \sim 10^{15.4} - 10^{15.6}$ GeV, the Z'-bosons would be inaccessible; but proton decay would be observable with a lifetime $\sim 10^{32}$-10^{35} years [78]. To see if such a superheavy Λ_c is feasible, let us recall the discussion in Sec. 5, where it was noted that an intermediate unified coupling $\alpha_X \approx 0.2$ at $M_X \sim 10^{17}$ GeV (as opposed to the MSSM-value of $\alpha_X \approx 1/26$) is desirable to stabilize the dilaton and that such a value of α_X would be realized if there exists a vector-like pair of families having the quantum numbers of $16 + \overline{16}$ of $SO(10)$, in the $1 - 100$ TeV-region [43]. With $\alpha_X \approx 0.16$-0.18 (say), and a hidden sector gauge symmetry like $SU(4)_H$ or $SU(5)_H$ [69], a confinement scale $\Lambda_H \sim \Lambda_c \sim 10^{15.5} - 10^{16}$ GeV would in fact be expected. Thus, while rapid proton decay is prevented by string-derived symmetries of the type discussed here [14], *observable rate for proton decay ($\tau_p \sim 10^{32}$-10^{34} yrs.), which would be accessible to Superkamiokande and ICARUS, seems perfectly feasible and natural* [79].

In summary, $\hat{Q}_\psi$ is a good example of the type of symmetry that can safegaurd, in conjunction with $B - L$ or $\hat{Q}_\chi$, proton-stability from *all angles*, while permitting

neutrinos to have desired masses. It even helps eliminate the potential danger from contribution of the color-triplets in the heavy tower of states. In this sense, $\hat{Q}_\psi$ plays a very desirable role. I do not, however, expect it to be the only choice. Rather, I expect other string-solutions to exist, which would yield symmetries like $\hat{Q}_\psi$, serving the same purpose [80]. At the same time, I feel that *emergence of symmetries like $\hat{Q}_\psi$ is a very desirable constraint that should be built into the searches for realistic string-solutions.*

To conclude this section, the following remark is in order. For the sake of argument, one might have considered an $SO(10)$-type SUSY grand unification by including 126 of Higgs to break $B-L$ and ignoring string-theory constraints [66]. One would thereby be able to forbid the $d=4$ operators and give desired masses to the neutrinos [65]. But, as mentioned before, the problems of finding a compelling solution to the doublet-triplet splitting as well as to the gravity-linked $d=5$ operators would still remain. This is true not just for SUSY $SO(10)$, but also for SUSY E_6, as well as for the recently proposed SUSY $SU(5)\times SU(5)$ - models [81]. *By contrast, a string-derived non-GUT model, possessing a symmetry like $\hat{Q}_\psi$, in conjunction with $B-L$ or $\hat{Q}_\chi$, meets naturally all the constraints discussed above.* This shows that string theory is not only needed for a unity of all forces, but also for ensuring *natural consistency* of SUSY-unification with two low-energy observations – proton stability and light masses for the neutrinos.

7 Summary and Concluding Remarks

Turning now to a summary of the first part of this talk,

- I noted in sections 1 and 2 that non-conservations of baryon and lepton numbers are implied on the one hand by ideas of higher unification [1,2,3], and on the other hand, by the need for baryogenesis [8,9] and by neutrino-masses as well. The latter two in fact suggest some form of violation of $B-L$, which, very likely, includes a violation through heavy Majorana masses of the right-handed neutrinos.

- If $\Delta(B-L)=0$ decay modes of the nucleon (i.e. $p\to\bar{\nu}K^+, \mu^+K^\circ, \bar{\nu}\pi^+, e^+\pi^\circ$, etc.) turn out to be the only observed source of non-conservation of B and L, as opposed to $\Delta(B-L)\neq 0$-transitions exhibited in Table 1 (i.e. $p\to e^-\pi^+\pi^+, n\leftrightarrow\bar{n}$ and $nn\to ppe^-e^-$ etc.), there would be no signal for new physics at about 100 TeV. That would of course conform with conventional wisdom, which is based on simple mechanisms

for symmetry-breaking of SUSY GUTS and/or string-derived solutions, obtained to date. On the other hand, if the $\Delta(B-L) \neq 0-$ transitions such as $p \rightarrow e^-\pi^+\pi^+$ or $n-\bar{n}-$ oscillation do show at some level, that would clearly point to new physics at low intermediate scales $\sim 100TeV$. This will be counter to conventional thinking, but just for that reason that may be quite revealing. I comment on this issue further in the following.

• Confining to the $\Delta(B-L)=0$ decay modes of the proton, assuming that they are discovered at SuperKamiokande and/or ICARUS, we will learn much from knowing which decay-channels are prominent or dominant. First, prominence of $\bar{\nu}K^+$ and/or μ^+K^o-mode would be a *strong evidence* in favor of the dominance of $d=5$ over the $d=6$-operators, and thereby in favor of supersymmetry, though not necessarily for SUSY GUTS. Prominence of the μ^+K^o -mode would suggest large $tan\beta$ [37]. Second, prominence of $\bar{\nu}_\mu\pi^+$ and/or $\mu^+\pi^o$-mode, together especially with *non-observation* of the $e^+\pi^o$-mode would also provide the same signal. Third, prominence of the $e^+\pi^o$-mode would favor, in the context of supersymmetry, either the dominance of string-derived $d=4$ over $d=5$-operators (see Sec. 6 and Ref. 14), or, for example, the flipped $SU(5)\times U(1)'$ -model [38]. It would, of course, be compatible also with non-supersymmetric GUTS, whose unification-scales are raised, for example, through enriched Higgs-systems, so that the associated lifetimes exceed 10^{33} yrs.

It is worth commenting on the issue of $\Delta(B-L)=0$ versus $\Delta(B-L)\neq 0$ -transitions. Certain guidelines of simplicity, noted below, seem to suggest that the latter would be too slow to be observed. First, the straightforward meeting of the three gauge couplings, obtained in the context of either MSSM or ESSM, and the associated predictability of $sin^2\theta_W$ (see Sec. 5) would be lost, if one introduces low intermediate scale-physics (necessary for prominence of $\Delta(B-L)\neq 0$ -transitions) [25,26], and thereby somewhat arbitrary multi-stage running of the couplings. Second, neutrino masses that are relevant, especially for the MSW solution of the solar neutrino-puzzle and for $\bar{\nu}_\tau$ being hot dark matter, suggest a superheavy, rather than a low intermediate-scale, Majorana mass for the right-handed neutrinos (see Secs. 2 and 6). Furthermore, in contrast to low intermediate-scales, such superheavy scales (e.g. $<\widetilde{N_R}>\sim 10^{15.5}$ GeV, see Sec. 6) do arise naturally in the context of string-solutions (see e.g. Ref. 53); and, they do not alter the simple running of three gauge couplings, except near the point of unification, which may be good anyway to remove the mismatch between MSSM and string-unifications

(see Sec. 5). Thus, if one is permitted to possess a *theoretical prejudice*, based on grounds of simplicity, as narrated above, it would seem that low intermediate-scale physics of a nature that would lead to observable rates for $\Delta(B-L) \neq 0$-modes is not likely to be realized, at least in the context of current level of thinking.

Nevertheless, I believe that it is essential to keep an open mind as regards the planning of experiments, precisely to find out if one's prejudices are true after all. And, what if these prejudices turn out to be wrong? That has happened in the past. A case to the point is CP- violation. Imagine that CP-violation was not discovered in 1964 and that one did not know that it is needed to implement baryogenesis. As late as the early 70's, judged purely from the point of view of theoretical models, based on just (u,d,s,c)-quarks, there was no compelling *theoretical* motivation for CP-violation. In the context of renormalizable gauge theories, one would have had to introduce extra Higgs-scalars, new gauge interactions, complex Yukawa couplings and/or a third family of quarks and leptons to implement CP-violation. Apriori, it would have appeared to be an unnecessary complication to introduce such extra matter and/or extra parameters. Judged from this point of view, CP-violation might have appeared unnatural or unlikely. Yet, CP-violation was discovered; so was its need to implement baryogenesis; and also the third family. It is, however, revealing to note in this context that even now we do not know the precise origin of CP-violation. There is some analogy of this case with that of $(B-L)$-violation. We do know from baryogenesis and neutrino masses that, very likely, $B-L$ is violated (see Sec. 2). The issue that needs to be settled, notwithstanding the question of naturalness and simplicity of present theoretical models, is whether the rates for $(B-L)$-violating transitions would lie in an observable range. *There is no other way to settle this question except to search for such transitions with the highest possible precision.*

I, therefore, believe that experimental searches for both $(B-L)$-conserving–i.e. $p \to \bar{\nu}K^+, \bar{\nu}\pi^+, \mu^+K^o, e^+\pi^o$ etc. – as well as $(B-L)$-violating processes–i.e. $p \to e^-\pi^+\pi^+, n \leftrightarrow \bar{n}$-oscillation, neutrinoless double beta decay, etc.–are strongly motivated. For this reason, I rejoice in the starting of the SuperKamiokande and look forward to the starting of ICARUS. I also greatly welcome proposal to set up searches for $n-\bar{n}$ oscillation here at OakRidge, which aim to probe into oscillation-periods of $10^{10}-10^{11}$ sec.

The main purpose of this talk has been to address two issues:

(i) How to resolve the mismatch between MSSM and string-unification?, and especially,

(ii) How to prevent, *naturally*, rapid proton-decay in supersymmetry?

With regard to the first, I noted some alternative possibilities. Among these, the only one that has a chance of being directly tested at future high energy accelerators, including the LHC and the NLC, especially if the two vector-like families have masses below about 1.5 TeV, is the extended supersymmetric standard model (ESSM), which proposes a *semi-perturbative unification* with intermediate unified coupling ($\alpha_X \sim .2$) in four dimensions [43].

With regard to the second issue, I have stressed that

- the extreme smallness of the strengths of the $d = 4$ (i.e. $\eta_i \leq 10^{-12}$) and the color-triplet mediated and/or gravity-linked $d = 5$ operators (i.e. $\lambda_{1,2}(M_{st}/M) < 10^{-7}$) deserves a natural explanation. The problem in this regard is somewhat analogous to that of understanding the smallness (or the vanishing) of the cosmological constant. Rather than being merely accommodated by a *choice* of the Higgs multiplets and discrete symmetries, the small parameters associated with the $d = 4$ and the $d = 5$ operators should emerge as a *compelling feature* owing to *symmetries* of the underlying theory, which would provide the desired protection against these unsafe operators.

- The symmetries in conventional SUSY GUTS including $SO(10), E_6$ and $SU(5) \times SU(5)$ do not, however, suffice for the purpose–especially in the matter of suppressing naturally the $d = 5$ proton-decay operators. By contrast, I showed that a certain *string-derived symmetry*, which cannot arise within SUSY GUTS as mentioned above, but which does arise within a class of *three-generation string-solutions*, possessing non-GUT symmetries, suffices, in conjunction with $B - L$, to safeguard proton-stability from all potential dangers, including those which may arise from higher dimensional operators and the color-triplets in the heavy infinite tower of states [14]. At the same time, the symmetry in question permits neutrinos to acquire appropriate masses. We thus see that *just seeking for an understanding–as opposed to accommodating–proton-stability, in the context of supersymmetric unification, drives us to the conclusion that, at the fundamental level, the elementary particles must be string-like and not point-like.* It seems remarkable that just a low-energy observation that proton is so stable, together with the demand of naturalness in understanding this feature, can provide us with such a deep insight.

• It is intriguing that one needs a *family-dependent symmetry*, like $\hat{Q}_\psi$, to achieve the desired protection against rapid proton decay, which cannot be realized for one- or two-family string-solutions, but which does emerge for a class of solutions possessing three families.

• A related remark: the necessity of such a family-dependent symmetry, which cannot arise *within* conventional GUT symmetries, as well as the lack of a compelling mechanism for doublet-triplet splitting in SUSY GUT theories (string-derived or not) suggest that *the flavor-color gauge symmetry below the string-scale is very likely a non-GUT string-derived symmetry like* $\mathcal{G}_{2311}$ *or* $\mathcal{G}_{224}$ *, or even flipped* $SU(5) \times U(1)'$*, rather than a GUT-symmetry like* $SU(5)$*, or* $SO(10)$ *or* E_6. Recall that, owing to string-constraints [42], the benefits of coupling unification, quark-lepton unification and quantization of electric charge still hold for the former, just as they do for the latter.

• Last but not least, as discussed in Sec. 6, it is interesting that, while symmetries like $\hat{Q}_\psi$ provide the desired protection against rapid proton decay, observable rates for proton-decay (i.e. lifetimes of order $10^{32} - 10^{34}$ yrs) are nevertheless perfectly natural in the context of these solutions, provided, however, one assumes (at least for the class of solutions considered in Ref. [14]), a *semi-perturbative unification* with intermediate unified coupling ($\alpha_X \sim .18 - .2$) [43]. As discussed in Sec. 5, such intermediate coupling is suggested by ESSM, and it may well be needed to help stabilize the dilaton, while retaining the benefits of coupling-unification.

To conclude, the original motivations for a unity of the fundamental forces and that for questioning baryon and lepton-number non-conservations [1,2,3] still persist. Supersymmetry and superstrings, while retaining these motivations, provide a new perspective with regard to both issues. As discussed here, several models of SUSY GUTS and superstring-derived models do in fact suggest that proton decay should occur at a rate that is accessible to ongoing searches. Observation of proton decay would strengthen our belief in an underlying unity of all matter and of its forces. Determination of its dominant decay modes, would provide us with a *wealth of knowledge* regarding new physics at very short distances, spanning from 10^{-19} to 10^{-32} cm. The question now is an experimental one: Will proton decay be discovered at SuperKamiokande and/or ICARUS?

Acknowledgements

I wish to thank M. Dine, P. Langacker, R.N. Mohapatra, N. Polonsky, A. Raisin, F. Wilczek, E. Witten and especially K.S. Babu, K. Dienes, and A. Faraggi for most helpful discussions and communications on topics included in this talk. I wish to thank the organizers, especially Y. Kamyshkov and R.N. Mohapatra, for arranging a very fruitful meeting and for their hospitality. I also wish to thank Delores Kight for her care and efforts in typing this manuscript.

References

[1] J.C. Pati and Abdus Salam; Proc. 15th High Energy Conference, Batavia, reported by J.D. Bjorken, Vol. 2, p. 301 (1972); Phys. Rev. **8** (1973) 1240; Phys. Rev. Lett. **31** (1973) 661; Phys. Rev. **D10** (1974) 175.

[2] H. Georgi and S.L. Glashow, Phys. Rev. Lett. **52** (1974) 438.

[3] H. Georgi, H. Quinn, and S. Weinberg, Phys. Rev. Lett. **33** (1974) 451.

[4] V. Kuzmin, JETP Lett. 12, 228 (1970); R.N. Mohapatra and R. E. Marshak, Phys. Rev. Lett. 44, 1316 (1980); S.L. Glashow in Recent Developments in Gauge Theories, Cargése, 1979. For a recent model, see R.N. Mohapatra, hep-ph/9604414, Proc. this Conference.

[5] For the status and prospect of SuperKamiokande, see Y. Totsuka, Nucl. Phys. B (Proc. Suppl.) 48, 547 (1996). For a review of the status of IMB, Kamiokande and SuperKamiokande searches for proton decay, see J. Stone, talk at this conference. For the prospect of ICARUS and the scope for detecting various $\Delta(B-L)=0$ *as well as* $\Delta(B-L)\neq 0$ decay modes of the nucleon listed in Table 1, see in particular D. Cline, talk at this conference.

[6] For a review of the status of searches for ν -less Double beta decay, including planned experiments, see H. Klapdor-Kleingrothaus, Proc. this Conference.

[7] For limits from the ILL experiment on $n-\bar{n}$ oscillation, see M. Baldo-Ceolin et al., Padova preprint DFPD 94/EP/13. For proposed Oak Ridge experiment, see Y. Kamyshkov, these Proceedings.

[8] A.D. Sakharov, Pisma Zh. Eksp. Teor. Fiz. 5, 32 (1967).

[9] V. Kuzmin, JETP. Lett. 12, 335 (1970) (in Russian).

[10] For a review, see e. g. P. Langacker, invited talk, Erice School (1994), hep-ph/941339.

[11] Y.A. Gelfand and E.S. Likhtman, JETP Lett. **13** (1971) 323; J. Wess and B. Zumino, Nuc. Phys. **B70** (1974) 139; Phys. Lett. **49B** (1974) 52; D. Volkov and V.P. Akulov, JETP Lett. **16** (1972) 438.

[12] M. Green and J.H. Schwarz, Phys. Lett. **149B**, 117 (1984); D.J. Gross, J.A. Harvey, E. Martinec and R. Rohm, Phys. Rev. Lett. **54**, 502 (1985); P. Candelas, G.T. Horowitz, A. Strominger and E. Witten, Nucl. Phys. **B 258**, 46 (1985).

[13] S. Weinberg, Phys. Rev. **D 26**, 287 (1982); N. Sakai and T. Yanagida, Nucl. Phys. B197, 533 (1982).

[14] J.C. Pati, *"The Essential Role of String-Derived Symmetries in Ensuring Proton Stability and Light Neutrino Masses"* hep-ph/9607446, Physics Letters, to appear. Some preliminary aspects of this work were alluded to at the conference. Its main results, reported here, developed after the conference.

[15] V. Kuzmin, Va. Rubakov and M. Shaposhnikov, Phys. Lett. **155B**, 36 (1985). For a review, see A. Cohen, D. Kaplan and A. Nelson, Ann. Rev. Nucl. Part. Sc. **43**, 27 (1993).

[16] J.C. Pati and A. Salam, Phys. Rev. **D10**, 275 (1974); R. N. Mohapatra and J.C. Pati, Phys. Rev. **D11**, 566, 2558 (1975); G. Senjanovic and R.N. Mohapatra, Phys. Rev. **D12**, 1502 (1975).

[17] M. Gell-Mann, P. Ramond and R. Slansky, in *Supergravity*, ed. by D. Freedman and P. Van Nieuwenhuizen (North Holland 1979), p. 315; T. Yanagida, Proc. Workshop on "Unified Theories and Baryon Number of the Universe", eds. O. Sawata and A. Sugamoto, KEK, Japan (1979); R.N. Mohapatra and G. Senjanovic, Phys. Rev. Lett. **44**, 912 (1980).

[18] This mass-pattern goes with the MSW-explanation of the solar neutrino puzzle (see S.P. Mikheyev and A. Yu. Smirnov, Nuov. Cim. **9 C**, 17 (1986), and L.

Wolfenstein, Phys. Rev. **D 17**, 2369 (1978)), and the indirect ν_e-ν_μ - oscillation - explanation of the LSND-experiment (see K.S. Babu, J.C. Pati and F. Wilczek, Phys. Lett. **B 359**, 351 (1995)).

[19] If there was no L-R symmetry and no ν_R, ν_L's can still obtain Majorana masses through gravity-induced effects, using higher dimensional operators such as $\nu_L\nu_L\phi\phi/M$, where ϕ is the Higgs doublet, and M is a characteristic mass-scale. With $< \phi > \sim 250GeV$, and $M \sim 10^{18}GeV$, however, one obtains $m(\nu_L) \sim 10^{-7}eV$, which is too small to be relevant to the MSW solution for the solar neutrino puzzle.

[20] T.D. Lee and C.N. Yang, Phys. Rev. 98, 1501 (1955).

[21] For $SO(10)$: H. Georgi, in Particles and Fields (edited by C. Carlson), A.I.P. (1975); H. Fritzsch and P. Minkowski, Ann. Phys. (NY) **93**, 193 (1975). For E_6: F. Gursey, P. Ramond and P. Sikivie, Phys. Lett. **60 B**, 177 (1976).

[22] R.N. Mohapatra and G. Senjanovic (Ref. 17).

[23] See, e.g., J.C. Pati and A. Salam, Proc. First Workshop on Grand Unification, New Hampshire (April 1980), p. 115; J.C. Pati, A. Salam and U. Sarkar, Phys. Lett. **113B**, 330 (1983); T. Rizzo and G. Senjanovic, Phys. Rev. **D25**, 235 (1982); F. del Aguilla and L. Ibanez, Nucl. Phys. **B 177**, 60 (1981); D. Chang, R.N. Mohapatra, J.M. Gipson, R.E. Marshak and M. Parida, Phys. Rev. **D 31**, 1718 (1985).

[24] S. Weinberg, Phys. Rev. Lett. **43**, 1566 (1979); F. Wilczek and A. Zee, Phys. Rev. Lett. **43**, 1571 (1979).

[25] See R.N. Mohapatra, Proceedings this Conference and references therein.

[26] J.C. Pati, A. Salam and U. Sarkar (Ref. 23); J.C. Pati, Phys. Rev. D, Rap. Comm. **29**, 1549 (1984).

[27] J.C. Pati, Phys. Lett. **B 228**, 228 (1989); J.C. Pati, M. Cvetic and H.S. Sharatchandra, Phys. Rev. Lett. **58**, 851 (1987); K.S. Babu, J.C. Pati and H. Stremnitzer, Phys. Rev. Lett. **67**, 1688 (1991); K.S. Babu, J.C. Pati and H. Stremnitzer, *A hint from the inter-family mass-hierarchy: two vector-like families in the TeV range*, Phys. Rev. **D 51**, 2451 (1995).

[28] For a recent review of the preonic approach, see J.C. Pati, "Towards a Unified Origin of Forces, Families and Mass Scales," hep-ph/9505227, Proc. of the 1994 Int'l. Conf. on B-Physics, held at Nagoya, Japan (Oct. 26-29, 1994), pages 164-181, Eds. A. Sanda and S. Suzuki, Publ. World Scientific.

[29] For a theoretical extraction of $sin^2\theta_W$ from LEP data, and discussion of coupling-unification, see P. Langacker and N. Polonsky, Phys. Rev. **D 52**, 3081 (1995). The value quoted corresponds to $m_H = 100GeV$ and $m_t = 180GeV$.

[30] For a review, see e.g., P. Langacker, talk at Gatlinburg Conference, June 94, hep-ph 9411247 and talk at this conference.

[31] P. Langacker and M. Luo, Phys. Rev. **D 44** (1991) 817; U. Amaldi, W. de Boer and H. Furstenau, Phys. Lett. **B 260** (1991); J. Ellis, S. Kelley and D. V. Nanopoulos, Phys. Lett. **B 260** (1991) 131; F. Anselmo, L. Cifarelli, A. Peterman and A. Zichichi, Nuov. Cim. **A 104** (1991) 1817. Earlier analysis containing the essential physics of the two-loop effects in SUSY GUTS may be found in W. Marciano and G. Senjanovic, Phys. Rev. D 25, 3092 (1982) and M. Einhorn and D.R.T. Jones, Nucl. Phys. B 196, 475 (1982).

[32] M. Bastero-Gil and J. Perez-Mercader, Nucl. Phys. **B 450**, 21 (1995); M. Bastero-Gil, private communications (to appear); T. Binoth and J.J. van der Bij, Z. Phys. **C 58**, 581 (1993); L. Clavelli and P. Coulter, hep-ph9507261; J. Bagger, K. Matchev and D. Pierce, Phys. Lett. **348**, 443 (1995); P. Chankowski, Z. Pluciennik and S. Pokorski, Nucl. Phys. **B 439**, 23 (1995); R. Barbieri, P. Ciafaloni and A. Strumia, Nucl. Phys. **B 442**, 461 (1995). These papers include exact one-loop (rather than step-function) threshold effects.

[33] J. Hisano, H. Murayama and T. Yanagida, Phys. Rev. **D 49**, 4966 (1994); Nucl. Phys. **B 402**, 46 (1993); J. Hisano, T. Moroi, K. Tobe and T. Yanagida, Tohoku University preprint (TU-470), hep-ph/9411298.

[34] See P. Nath, Talk at the conference.

[35] S. Dimopoulos, S. Raby and F. Wilczek, Phys. Lett. **112 B**, 113 (1982).

[36] For earlier estimates on nucleon decay modes in SUSY GUT theories, and considerations of different regions of SUSY-parameter-space which lead to prominance of different decay modes, see S. Chada and M. Daniel, Phys. Lett. **137 B**, 374 (1984); M. Belayev and M. I. Vyotsky, Phys. Lett. **127 B**, 215 (1983); J. Milutnovic, P.B. Bal and G. Senjanovic, Phys. Lett. **140 B**, 324 (1984); P. Nath, A.H. Chamseddine and R. Arnowitt, Phys. Rev. **D 32**, 2348 (1985) and K. Enqvist, A. Masiero and D.V. Nanopoulos, Phys. Lett. **156 B**, 209 (1985). For recent more detailed analysis and estimates of rates for alternative nucleon decay modes, especially for SUSY SU(5), see Hisano et al. (Ref. 33), and for SUSY SO(10), see V. Lucas and S. Raby, hep-ph/9610293.

[37] For preliminary considerations of gluino-loops leading to possible prominence of $p \to \mu^+ K^o$-mode, see S. Chada, G.D. Coughlan, M. Daniel and G.G. Ross, Phys. Lett. **149 B**, 477 (1984). For recent considerations showing prominence of this mode in supergravity models for the case of large $tan\beta$, see T. Goto, T. Nihei and J. Arafune, Phys. Rev. **D 52**, 505 (1995); and in particular K.S. Babu and S.M. Barr, Phys. Lett. B 381, 137 (1996).

[38] I. Antoniadis, J. Ellis, J. Hagelin and D.V. Nanopoulos, Phys. Lett. **B231**, 65(1989). For a review, see J.L. Lopez and D.V. Nanopoulos, hep-ph/9511266)).

[39] Particle Data Group, L. Montanet et al., Phys. Rev. **D 50**, 1173 (1994).

[40] For an early review on this issue, see S. Weinberg, Summary talk, Proc. 26th Intl. Conf. on High Energy Physics, Dallas, Texas (1992).

[41] For a recent discussion, see K. Dienes, hep-th/9602045 (to appear in Phys. Rept.) and references therein.

[42] P. Ginsparg, Phys. Lett. **B 197**, 139 (1987); V.S. Kaplunovsky, Nucl. Phys. **B 307**, 145 (1988); Erratum: *ibid.* **B 382**, 436 (1992).

[43] J.C. Pati and K.S. Babu, *"The Problems of Unification-Mismatch and Low α_3: A Solution with Light Vector-Like Matter"*, hep-ph/9606215, Physics Lett., To appear.

[44] See e.g. M. Dine and N. Seiberg, Phys. Lett. **162 B**, 299 (1985), and in *Unified String Theories*, Ed. by M. Green and D. Gross (World Scientific, 1986).

[45] If one were to use point particle field theory for an SU(N) gauge theory as a rough guide, one might expect perturbation theory to break down if the ratio of the 2-loop to the 1-loop amplitude given by $\alpha_N N/(2\pi)$ exceeds about 0.2, i.e., if $\alpha_N \geq (.3,.15)$ for $N = 3, 6$ where α_N denotes the SU(N) gauge coupling ${g^2}_N/(4\pi)$. Assuming the MSSM spectrum and therefore $\alpha_X \simeq 0.04$, the question has however arisen, on grounds of necessity in this case, whether string-perturbation theory might break down even for such a weak coupling, see T. Banks and M. Dine, Phys. Rev. **D 50**, 7454 (1994). It seems fair to say that no convincing argument has arisen in favor of such a possibility.

[46] E. Witten, Nucl. Phys. **B 433**, 85 (1995); P. Horava and E. Witten, Nucl. Phys. **B 460**, 506 (1996); See J. Polchinski, hep-th/9511157, for a review and references therein.

[47] M. Dine and Y. Shirman, hep-th/9601175; M. Dine, hep-th/9508085.

[48] E. Witten, hep-th/9602070.

[49] See e.g. D. Lewellen, Nucl. Phys. **B 337**, 61 (1990); A. Font, L. Ibanez and F. Quevedo, Nucl. Phys. **B 345**, 389 (1990); S. Chaudhari, G. Hockney and J. Lykken, Nucl. Phys. **B 456**, 89 (1995) and hep-th/9510241; G. Aldazabal, A. Font, L. Ibanez and A. Uranga, Nucl. Phys. **B 452**, 3 (1995); ibid. **B 465**, 34 (1996); D. Finnell, Phys. Rev. **D 53**, 5781 (1996); A.A. Maslikov, I. Naumov and G.G. Volkov, Int. J. Mod. Phys. **A 11**, 1117 (1996); J. Erler, hep-th/9602032 and G. Cleaver, hep-th/9604183; and Z. Kakushadze and S.H. Tye, hep-th/9605221, and hep-th/9609027.

[50] K. Dienes and A. Faraggi, Nucl. Phys. **457**, 409 (1995); C. Bachas, C. Fabre and T. Yanagida, Phys. Lett. **B 370**, 49 (1996).

[51] J.A. Casas and C. Munoz, Phys. Lett. **B 214**, 543 (1988); L.E. Ibanez, Phys. Lett. **B 318**, 73 (1993); K. Dienes, A. Faraggi and J. March-Russell, hep-th/9510223; S. Chaudhuri, G. Hockney and J. Lykken, hep-th/9510241.

[52] H. Nilles and S. Steiberger, hep-th/9510009.

[53] In Ref. 42, a mass-scale of 1 TeV was used for the masses of the vector-like families. This was suggested by the SUSY-preon model (Ref. 27). With elementary quarks, this restriction is relaxed. This is because, following discussions in Refs. 27 and [43], it is easy to see that the masses of the known fermions restrict only the ratio of the VEVs of H_S and H_λ (see Ref. [43] for notations), where $< H_S >$ mixes chiral and vector-like families while $< H_\lambda >$ gives diagonal masses to the latter. I would in this note allow their masses to lie in the range of 1-100 TeV, which would still lead to intermediate unified coupling, as desired in Ref. [43]. Heavier masses of order 10-100 TeV are suggested by recent works on gauge-mediated SUSY-breaking, where vector-like quarks serve as messengers.

[54] I. Antoniadis, G.K. Leontaris and J. Rizos, Phys. Lett. **B 245**, 161 (1990).

[55] Z. Kakushadze and S.H. Tye (Ref. [49]).

[56] Such a see-saw pattern of mass-matrix arises naturally in the SUSY-preon model [27]. This is abstracted for elementary quarks [43] to preserve the explanation of inter-family mass-hierarchy. It remains to be seen whether such a pattern can be derived from a superstring theory for elementary quarks as well.

[57] An extension of the renormalization group analysis of Ref. [43] has recently been carried out by C. Kolda and J. March-Russell (hep-ph/9609480), by including 3-loop effects, which are found to preserve the essential features of the results of Ref. [43], for the case for which the extra matter is in $16 + \overline{16}$.

[58] See e.g. L. Maiani, G. Parisi and R. Petronzio, Nucl. Phys. **B 136**, 115 (1978).

[59] I. Hinchliff and T. Kaeding, Phys. Rev. **D 47**, 279 (1993).

[60] S. Dimopoulos and H. Georgi, Nucl. Phys. **B 193**, 150 (1981); N. Sakai, Z. Phys. **C 11**, 153 (1982).

[61] A. Masiero, D.V. Nanopoulos, K. Tamvakis and T. Yanagida, Phys. Lett. **B 115**, 380 (1982); B. Grinstein, Nucl. Phys. **B 206**, 387 (1982).

[62] S. Dimopoulos and F. Wilczek, in Proc. Erice Summer School (ed. by A. Zichichi), I.T.P. preprint NSF-ITP-82-07 (1981). For recent discussions on DW-mechanism, see K.S. Babu and S.M. Barr, Phys. Rev. **D 48**, 5354 (1993); ibid **D 51**, 2463 (1995).

[63] See, e.g., Z. Berezhiani, C. Csáki and L. Randall, Nucl. Phys. **B 444**, 61 (1995) and references therein.

[64] H. Kawai, D. Lewellen and S.H. Tye, Phys. Rev. Lett. **57**, 1832 (1986) and Nucl. Phys. **B 288**, 1 (1987); I. Antoniadis, C. Bachas and C. Kounnas, Nucl. Phys. **B 289**, 87 (1987).

[65] R.N. Mohapatra, Phys. Rev. **D 34**, 3457 (1986), A. Font, L. Ibanez and F. Quevedo, Phys. Lett. **B 288**, 79 (1989); S.P. Martin, Phys. Rev. **D 46**, 2769 (1992).

[66] K.R. Dienes and J. March-Russell, hep-th/9604112; K.R. Dienes, hep-ph/9606467.

[67] For an alternative solution of $B-L$ violation, and of neutrino masses using hidden-sector condensates, see A. Faraggi and E. Halyo, Phys. Lett. **B 307**, 311 (1993).

[68] Our discussion in this section is similar in spirit, though not in content, to that of Weinberg in Ref. [13].

[69] A. Faraggi, Phys. Lett. **B 278**, 131 (1992); Nucl Phys. **B 403**, 101 (1993); Nucl. Phys. **B 416**, 63 (1994). The full massless spectrum is given in the first paper.

[70] A. Faraggi, Phys. Lett. **B 274**, 47 (1992).

[71] Although doublet and triplet coexist in the flipped $SU(5)\times U(1)'$-model, the problem of doublet-triplet splitting is resolved in this model as well, owing to a *natural* missing-partner mechanism [38]. This too is a non-GUT-model like the $\mathcal{G}_{224}$-model [1,54], each of which possesses coupling unification at the level of strings, assuming that they originate from a string theory. One still needs to examine if the problems of $d = 4$ and gravity-linked $d = 5$ operators, which would seem to exist in the flipped $SU(5)$-model, can be resolved by utilizing extra symmetries of the type discussed in the text.

[72] If the problem of doublet-triplet splitting can be solved naturally for a string-derived GUT model, and if symmetries of a nature to be presented below can arise in these models, so as to prevent rapid proton decay, they would of course be just as acceptable as the string-derived non-GUT models.

[73] M. Dine, N. Seiberg and E. Witten, Nucl. Phys. **B 289**, 585 (1987).

[74] We remark that, while the vector-like $(16_H + \overline{16}_H)$ - pair or equivalently the $(B = (1,2,\overline{4}) + \overline{B}' = (1,2,4)\ )$ - pair, does not appear in the specific solutions of Ref. [69], existence of such pairs is fairly generic in string theories (see *e.g.* Refs. [54] and [55]). It is important to note, however, that if sneutrino-like fields belonging to 16_H and $\overline{16}_H$ acquire large VEVs (as in Ref. [54]), one must ensure that strengths of operators like $16_i \cdot 16_H \cdot 10_H$ and $16_i \cdot \overline{16}_H \cdot 1_H$ in the superpotential are strongly suppressed, so that ν_L-Higgsino mixing mass (which these operators would induce) remains below about 1 MeV. While such a suppression could happen through constraints of symmetries and the allowed pattern of VEVs, it turns out that this specific problem does not arise in models like those of Ref. [69]. This is because, as mentioned in the text, $< \widetilde{\overline{N}}_R >$ is effectively replaced in these models by VEVs of *product* of fields and a condensate, which naturally lead to sufficiently strong suppression of ν_L - $\tilde{H}$ mixing (especially if the condensate-scale is $\leq 10^{14}$ GeV) through relevant higher dimensional operators. I thank K.S. Babu for drawing my attention to this potential problem.

[75] As far as we can see, Yukawa couplings of the color-triplets in the heavy tower need not all be suppressed to the same extent as those of the electroweak doublets.

[76] Note $\hat{Q}_\psi$ assigns the same charge to all sixteen members of a given family. In this sense, $\hat{Q}_\psi$ (though not $\hat{Q}_\chi$) commutes with $SO(10)$.

[77] The possibility of extra Z' bosons, with or without a string-origin, has been considered by several authors. See e.g. M. Cvetic and P. Langacker, hep-ph/95111378 for a recent string-motivated analysis. The role of a string-derived symmetry (associated with an extra Z') in preventing rapid proton-decay, has not however been noted in these previous works.

[78] If $< \widetilde{\overline{N}}_R > \neq 0$, the d=4 operators (see table 4) lead to proton decay rate $\propto (\eta_1\eta_2)^2 \propto (\Lambda_c/M)^{16}$, which varies extremely rapidly with Λ_c. It is interesting that, despite this rapid variation, proton decay is observable for a plausible though narrow range of values of $\Lambda_c \approx 10^{15.5}$ GeV. If $< \widetilde{\overline{N}}_R >= 0$, as in Ref. [69] (see also remarks in Ref. [74]), only the d=5 operators with strengths $\sim (< T_i\overline{T}_j > /M^2)^2$ are relevant (see table 4). These will lead to proton decay rate $\propto (\Lambda_c/M)^8$, which would be observable if $\Lambda_c \sim 10^{16}$ GeV (see text). In contrast to the $d = 5$ operators, if the $d = 4$ operators ($\bar{U}\bar{D}\bar{D}$ and $QL\bar{D}$) induced as above dominate, they can yield (through $\tilde{d}_R$-exchange) strange as well as non-strange particle decay modes of the nucleon. Thus, through these operators, the $e^+\pi^o$-mode can be prominent or even dominant.

[79] In all these considerations, contribution of d=6 operators are neglected, because they are strongly suppressed if the relevant scale (M_X or M) exceeds 10^{16} GeV.

[80] For example, other pairs of string-derived symmetries such as $(\hat{F}, B-L)$, where $\hat{F} \equiv F_1 + F_2 - 2F_3$ and F_i acts as the fermion number on the ith family (i.e. $F_i \equiv (3B+L)_i = (1,1\,|\,-1,-1)$ for $(q,l\,|\,\overline{q},\overline{l})_i$), may also play a role analogous to the pair $(\hat{Q}_\psi, B-L)$. As an additional possibility, it would be interesting to explore whether the recently proposed variants of the solutions in Refs. [69] and [38], which yield a leptophobic Z' (see e.g. A. Faraggi, hep-ph/9604302 and J. L. Lopez and D. V. Nanopoulos, hep-ph/9605359), can be developed to provide a consistent Higgs-mechanism and also prevent rapid proton decay, utilizing extra symmetries, as discussed here.

[81] For alternative versions, see R. Barbieri, G. Dvali and A. Strumia, Phys. Lett. **333 B**, 79 (1994); R. N. Mohapatra, hep-ph/9601203 and S. M. Barr, hep-ph/9607359.

Family	States	Q_1	Q_2	Q_3	Q_4	Q_5	Q_6	$\hat{Q}_\psi$	$\hat{Q}_\chi$
1	q_1	1/2	0	0	-1/2	0	0	1/2	-1/2
	L_1	1/2	0	0	1/2	0	0	1/2	3/2
	$(\overline{U},\overline{E})_1$	1/2	0	0	1/2	0	0	1/2	3/2
	$(\overline{D},\overline{\nu_R})_1$	1/2	0	0	-1/2	0	0	1/2	-1/2
2	q_2	0	1/2	0	0	-1/2	0	1/2	-1/2
	L_2	0	1/2	0	0	1/2	0	1/2	3/2
	$(\overline{U},\overline{E})_2$	0	1/2	0	0	1/2	0	1/2	3/2
	$(\overline{D},\overline{\nu_R})_2$	0	1/2	0	0	-1/2	0	1/2	-1/2
3	q_3	0	0	1/2	0	0	-1/2	-1	-1/2
	L_3	0	0	1/2	0	0	1/2	-1	3/2
	$(\overline{U},\overline{E})_3$	0	0	1/2	0	0	1/2	-1	3/2
	$(\overline{D},\overline{\nu_R})_3$	0	0	1/2	0	0	-1/2	-1	-1/2
Color Triplets	$D_{45} = (3, -2/3, 1_L, 0)$	-1/2	-1/2	0	0	0	0	-1	-1
	$\overline{D_{45}} = (3^*, +2/3, 1_L, 0)$	1/2	1/2	0	0	0	0	+1	+1
Higgs doublets	$\overline{h_1} = (1, 0, 2_L, 1/2)$	-1	0	0	0	0	0	-1	-1
	$\overline{h_2} = (1, 0, 2_L, 1/2)$	0	-1	0	0	0	0	-1	-1
	$\overline{h_3} = (1, 0, 2_L, 1/2)$	0	0	-1	0	0	0	+2	-1
	$\overline{h_{45}} = (1, 0, 2_L, 1/2)$	1/2	1/2	0	0	0	0	1	1
Hidden Matter	$V_1, \overline{V}_1$	0	1/2	1/2	1/2	0	0	-1/2	2
	$T_1, \overline{T}_1$	0	1/2	1/2	-1/2	0	0	-1/2	0
	$V_2, \overline{V}_2$	1/2	0	1/2	0	1/2	0	-1/2	2
	$T_2, \overline{T}_2$	1/2	0	1/2	0	-1/2	0	-1/2	0
	$V_3, \overline{V}_3$	1/2	1/2	0	0	0	1/2	1	2
	$T_3, \overline{T}_3$	1/2	1/2	0	0	0	-1/2	1	0

Table 3: Partial List of Massless States from Ref. [69]. (i) The quark and lepton fields have the standard properties under $SU(3)^C \times U(1)_{B-L} \times SU(2)_L \times U(1)_{I_{3R}}$, which are not shown, but those of color triplets and Higgses are shown. (ii) Here $\hat{Q}_\psi \equiv Q_1 + Q_2 - 2Q_3$ and $\hat{Q}_\chi = (Q_1 + Q_2 + Q_3) + 2(Q_4 + Q_5 + Q_6)$ (see Eq. (5)). (iii) The doublets $\overline{h}_{1,2,3,45}$ are accompanied by four doublets $h_{1,2,3,45}$ with quantum numbers of conjugate representations, which are not shown. (iv) The $SO(10)$-singlets $\{\phi\}$ which possess $U(1)_i$-charges, and the fractionally charged states which become superheavy, or get confined [69], are not shown. In Ref. [69], since only $\overline{h_1}$ and h_{45} remain light, families 1, 2 and 3 get identified with the τ, μ and e - families respectively. Hidden matter $V_i, \overline{V}_i, T_i$ and $\overline{T}_i$ are $SO(10)$-singlets and transform as $(1,3),(1,\overline{3}),(5,1)$ and $(\overline{5},1)$, respectively, under $SU(5)_H \times SU(3)_H$.

Operators	Family Combinations	Y	$B-L$	$\hat{Q}_\psi$	$\hat{Q}_\chi$	$\hat{Q}_\chi+\hat{Q}_\psi$	If Allowed
$\overline{U}\,\overline{D}\,\overline{D}, QL\overline{D}, LL\overline{E}$	(a) All except (b)	$\surd$	$\times$	$\times$	$\times$	$\times$	unsafe
	(b) 3 fields from 3 different families	$\surd$	$\times$	$\surd$	$\times$	$\times$	unsafe
$(\overline{U}\,\overline{D}\,\overline{D}$ or $QL\overline{D})(\overline{N_R}/M)$	All	$\surd$	$\surd$	$\times$	$\surd$	$\times$	unsafe
$(\overline{U}\,\overline{D}\,\overline{D}$ or $QL\overline{D})(\overline{N_R}/M)\times$ $[(\overline{h_1}/M)^2$ or $(\text{“}\phi\text{”}/M)^n]$	All	$\surd$	$\surd$	$\surd$	$\times$	$\times$	safe
$(\overline{U}\,\overline{D}\,\overline{D}$ or $QL\overline{D})(\overline{N_R}/M)\times$ $(T_i\overline{T}_j/M^2)^2$	Some(†)	$\surd$	$\surd$	$\surd$	$\surd$	$\surd$	safe
$QQQL/M$	All	$\surd$	$\surd$	$\times$	$\surd$	$\times$	unsafe
$(QQQL/M)(N_L^i/M)_{i=1,2}$	e.g.$(1,2,1,3)$	$\surd$	$\times$	$\surd$	$\times$	$\times$	unsafe
$(QQQL/M)(N_L^i/M)(\overline{N}_R^j/M)$	All	$\surd$	$\surd$	$\times$	$\surd$	$\times$	safe(?)
$(QQQL/M)(T_i\overline{T}_j/M^2)^2$	Some(†)	$\surd$	$\surd$	$\surd$	$\surd$	$\surd$	safe
$\overline{U}\,\overline{U}\,\overline{D}\,\overline{E}/M$	All	$\surd$	$\surd$	$\times$	$\times$	(*)	unsafe
$LL\overline{h_i}\,\overline{h_i}/M$	All	$\surd$	$\times$	$\times$		(*)	safe

Table 4: The roles of Y, $B-L$, $\hat{Q}_\psi$, $\hat{Q}_\chi$ and $\hat{Q}_\chi+\hat{Q}_\psi$ in allowing or forbidding the relevant (B,L) violating operators. Check mark ($\surd$) means "allowed" and cross ($\times$) means "forbidden". The mark † signifies that the corresponding operator is allowed if either two of the four fields are in family (1 or 2) and two are in family 3, with $i=1$ and $j=3$; or all four fields are in family (1 or 2) with $i=1$ and $j=2$. The mark (*) signifies that $(\hat{Q}_\chi+\hat{Q}_\psi)$ forbids $\overline{U}\,\overline{U}\,\overline{D}\,\overline{E}/M$ for all family-combinations except when all four fields belong to family 3, and that it forbids $LL\overline{h_i}\,\overline{h_i}$ in some family-combinations, but not in others. In labelling the operators as safe/unsafe, we have assumed that $\langle\widetilde{\overline{N_R^i}}\rangle \sim 10^{15.5}$ GeV, $\langle\phi/M\rangle^n \leq 10^{-9}$ and $M \sim M_{st} \sim 10^{18}$ GeV, and that hidden sector condensate-scale $\Lambda_c \leq 10^{15.5}$ GeV (see text). Note that the pairs (Y, $B-L$), (Y, $\hat{Q}_\psi$), (Y, $\hat{Q}_\chi$) and ($B-L$, $\hat{Q}_\chi$) do not give adequate protection against the unsafe operators. But $\hat{Q}_\psi$, in conjunction with $B-L$ or $\hat{Q}_\chi$, gives adequate protection against all unsafe operators. This establishes the necessity of string-derived symmetries like $\hat{Q}_\psi$ (which can not emerge from familiar GUTs including E_6) in ensuring proton-stability.

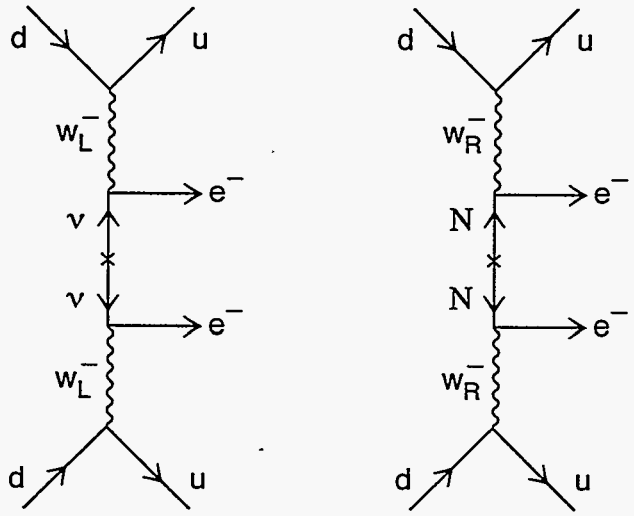

Fig.1 Neutrinoless Double Beta Decay: $nn \rightarrow ppe^-e^-$

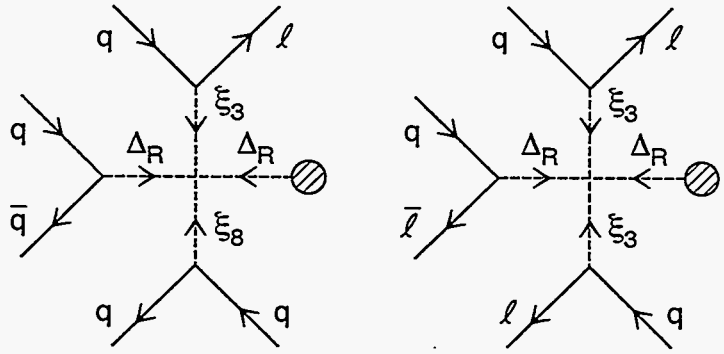

Fig. 2a,b Nucleon Decays into lepton + pions and into $\ell\ell\bar{\ell}$ + pions (ξ_3, ξ_8 and Δ_R are Higgs-scalars, see text).

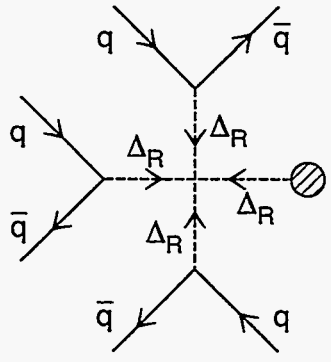

Fig. 3 $n-\bar{n}$ oscillation ($qqq \rightarrow \bar{q}\bar{q}\bar{q}$)

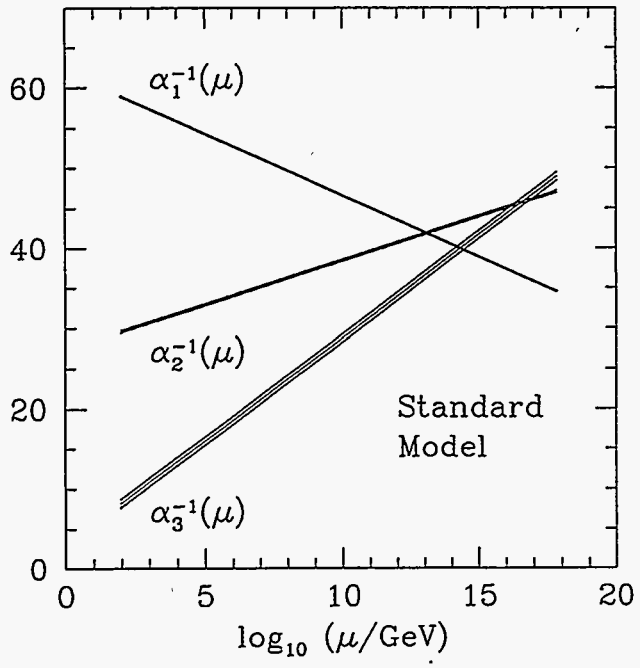

Fig. 4 (From Ref. 41)

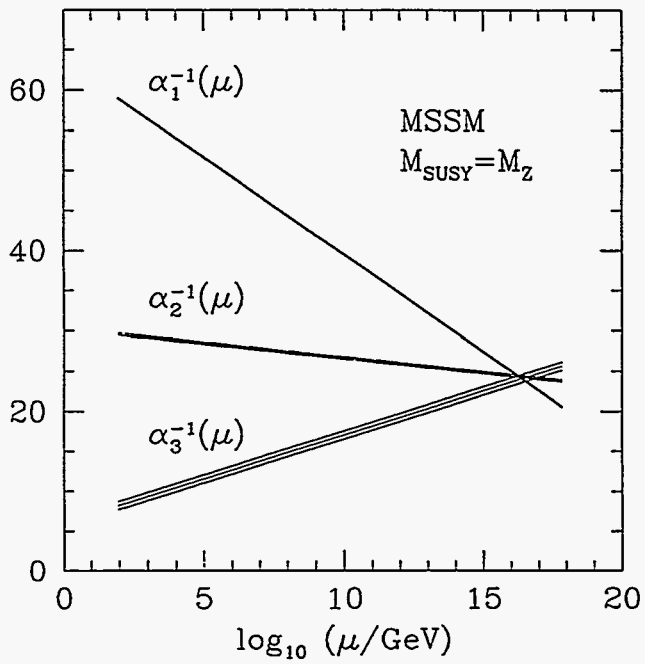

Fig. 5a (From Ref. 41)

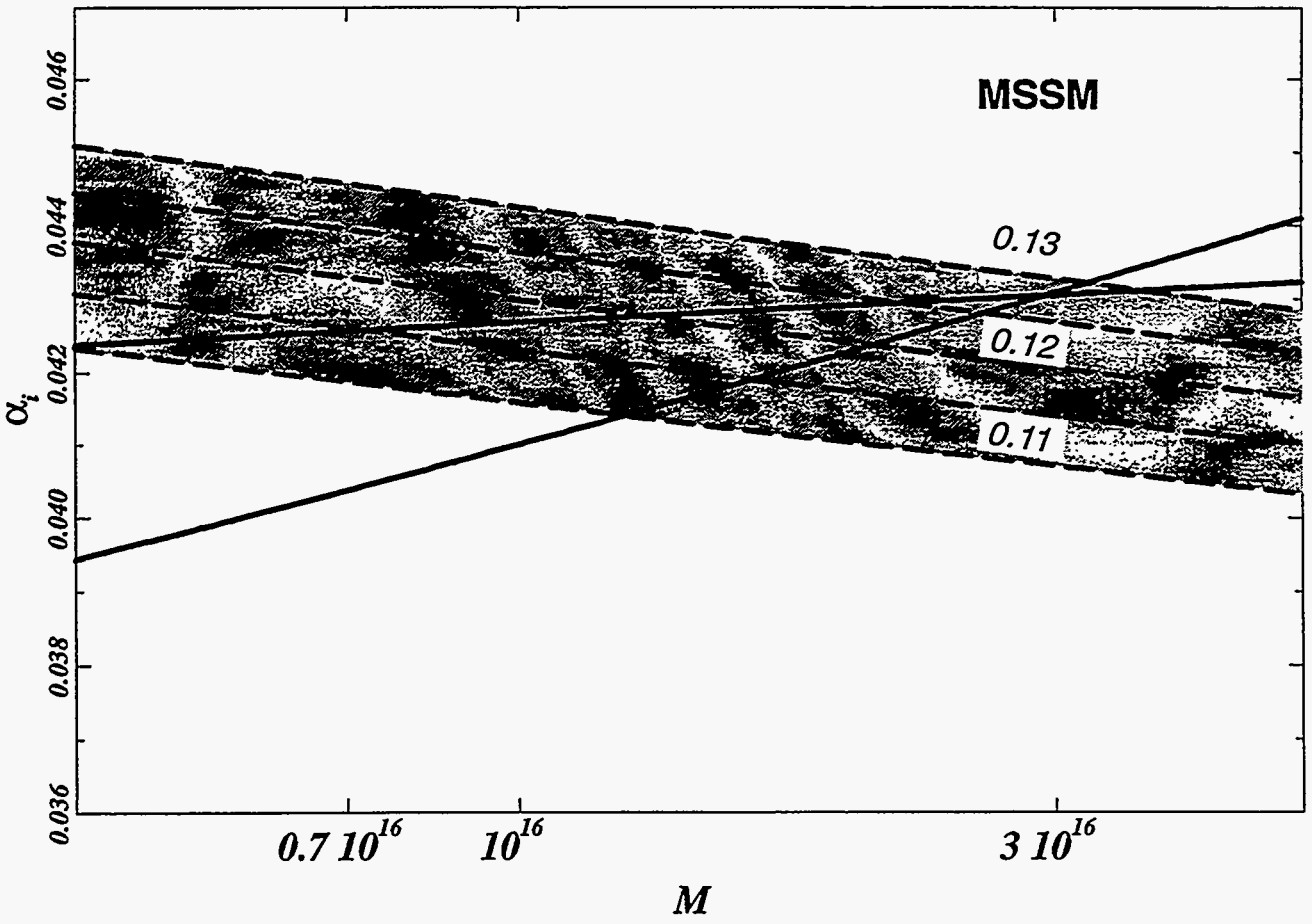

Fig. 5b Unification as a function of α_3 in MSSM (see Ref. 29)

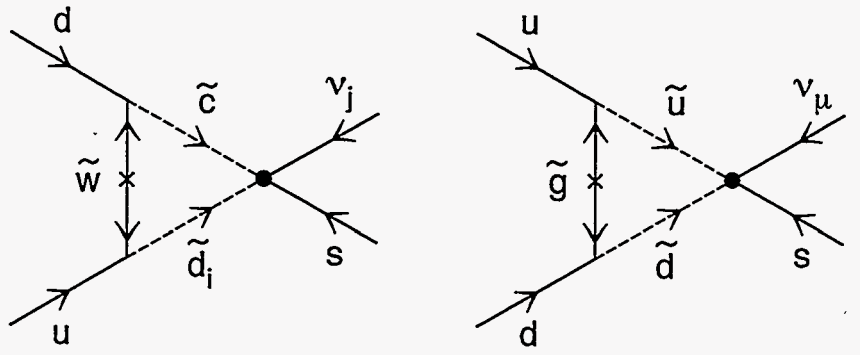

Fig. 6 Typical Diagrams for Proton Decay into $\bar{\nu}\kappa^+$ through d=5 operators

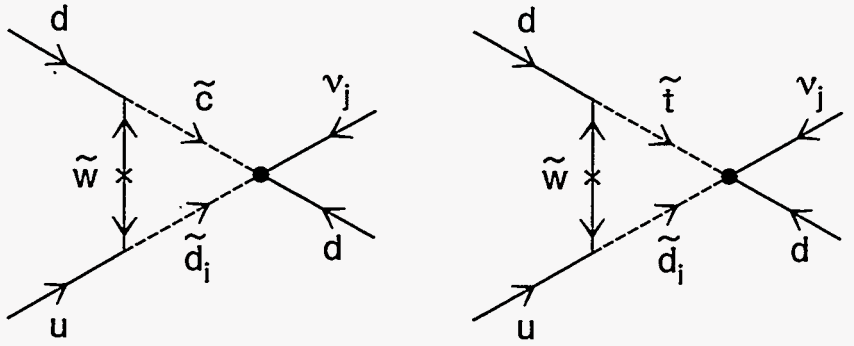

Fig. 7 Typical Diagrams for Proton Decay into $\bar{\nu}\pi^+$

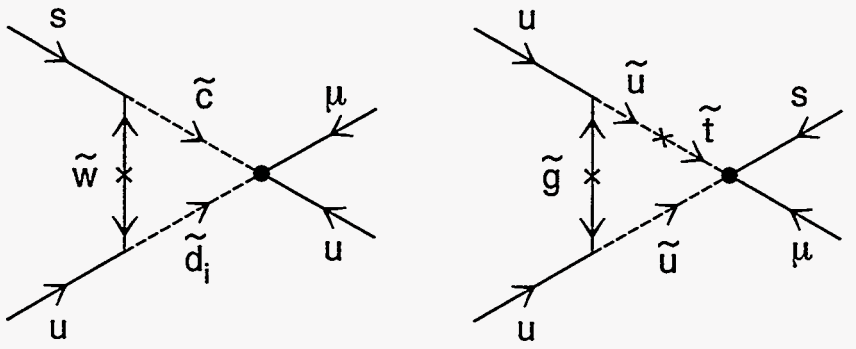

Fig. 8 Typical Diagrams for Proton Decay into $\mu^+\kappa^o$

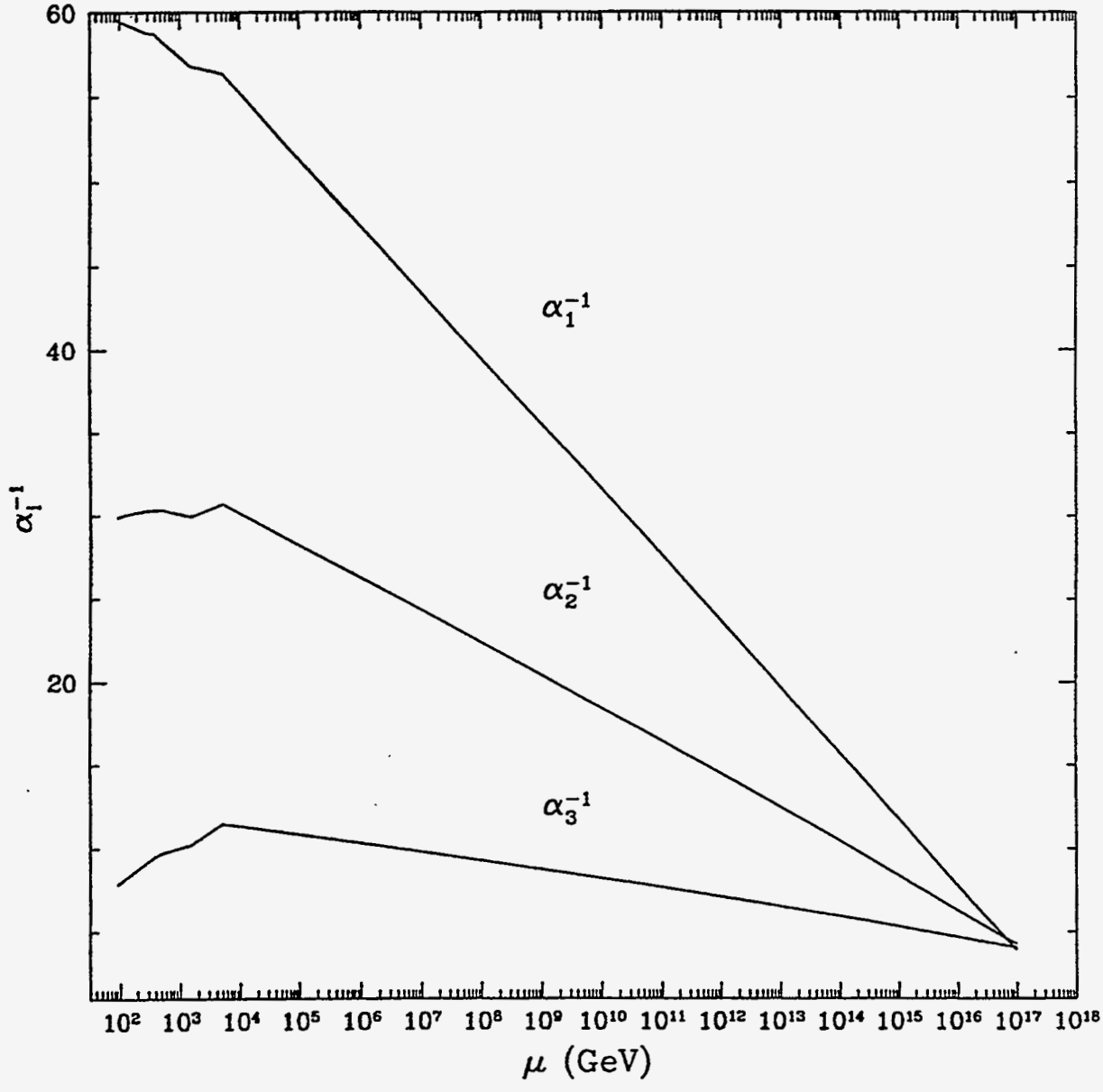

Fig. 9 Running of α_i^{-1} in ESSM (see sec. 5 and Ref. 43)

Baryon Instability in SUSY Models

Pran Nath
Department of Physics, Northeastern University
Boston, MA 02115
R. Arnowitt
Center for Theoretical Physics, Department of Physics
Texas AM University, College Station, TX 778

Abstract

A review is given of nucleon instability in SUSY models. The minimal SU(5) model is discussed in detail.

1. Introduction:

We begin by discussing proton instability in non-supersymmetric grand unification. The simplest unified model that accomodates the electro-weak and the strong interactions is the SU(5) model[1] and the instability of the proton arises here from the lepto-quark exchange with mass M_V. The dominant decay is the $e^+\pi^0$ mode and its lifetime can be written in the form[2]

$$\tau(p \to e^+\pi^0) \approx (\frac{M_V}{3.5 \times 10^{14} GeV})^4 10^{31\pm1} yr \tag{1}$$

The current experimental limit of this decay mode is[3]

$$\tau(p \to e^+\pi^0) > 9 \times 10^{32} yr, (90\% CL) \tag{2}$$

In non-SUSY SU(5) the $e^+\pi^0$ mode has a partial lifetime of $\tau(p \to e^+\pi^0) \leq 4 \times 10^{29\pm2}$ yr.Thus the non-SUSY SU(5) is ruled out because of the p-decay experimental limits. It is expected that the Super Kamiokande will increase the sensitivity of this mode to 1×10^{34}[4]. That would imply that theoretically the $e^+\pi^0$ mode would be observable if $M_V \leq 5 \times 10^{15}$ GeV. In supersymmetric grand unification current analyses based on unification of couplings constants already put a constraint on M_G of about 10^{16}[5]. Thus it seems not likely that the $e^+\pi^0$ mode would be observable in supersymmetry even in the next generation of proton decay experiments. Infact, reasonable estimates indicate that $\tau(p \to e^+\pi^0) > 1 \times 10^{37\pm2} yr$.

In supersymmetric unification the dominant instablity of the proton arises via baryon number violating dimension five operators[6, 7, 8, 9]. In SUSY SU(5) operators of this type arise from the exchange of Higgs triplet fields and they have chiral structures LLLL and RRRR in the superpotential after the superheavy Higgs triplet field is eliminated. The main decay mode of the

proton in these models is $\tau(p \to \bar{\nu}K)$.The current experimental limit for this decay mode is[3]

$$\tau(p \to \bar{\nu}K) > 1.0 \times 10^{32} yr \tag{3}$$

It is expected that Super Kamiokande will reach a sensitivity of 2×10^{33} yr[4] while ICARUS will reach a sensitivity of 5×10^{33} yr[10]. Thus it is an interesting question to explore to what extent the new generation of proton decay experiments will be able to test SUSY unified models.Actually we shall show that, unlike the prediction for the $e^+\pi^0$ mode, it is not possible to make any concrete predictions for the $\bar{\nu}K$ mode in SUSY models without inclusion of the low energy SUSY mass spectra which depends on the nature of supersymmetry breaking. Such an explicit supersymmetry breaking mechanism is provided in supergravity grand unification[11, 12], but not in MSSM.Thus it is only in supergravity grand unification[11] that one can make detailed meaningful predictions of proton decay lifetimes.

2. GUT Varieties

Even within supersymmetric framework there are many possibilities that may occur. The simplest of these is the minimal SU(5) model. However, one can have extended gauge groups such as $SU(3)^3$, SO(10),...etc. and also string inspired models such as SU(5)×U(1)[13].There has been several works in the literature where there is a suppression of dimension five proton decay operators.There are a variety of ways in which a suppression of p-decay can occur[13, 14, 15]. One possibility is that matter is embedded in some unusual fashion in the basic particle multiplets. Such a situation arises in the flipped $SU(5)\times U(1)$ model where one has an interchange $u \longleftrightarrow d$ and $e \longleftrightarrow \nu$ relative to the usual embeddings. The other possibilty is the presence of some discrete symmetry which might forbid the baryon number violating dimension five operators. In the following we discuss the condition that would forbid such operators in the general case. Let us assume that one has several Higgs triplets 1,2,..,N that couple with the matter fields. We make a field redefinition so that the linear combination that couples with matter is labelled $H_1, \bar{H}_1$ while the remaining Higgs triplet field have no couplings. We may write their interactions in the form

$$\bar{H}_{1x} J^x + \bar{K}_x H_1^x + \bar{H}_{ix} M_{ij}^{xy} H_{jy} \tag{4}$$

where J and K are given by

$$J^x = \lambda^2 \bar{M}_y M^{xy}, \; K_x = \lambda^1 \epsilon_{xyzuv} M^{yz} M^{uv} \tag{5}$$

Now the condition that the dimension five operators be suppressed is given by[16]

$$(M^{-1})_{11} = 0 \tag{6}$$

Of course satisfaction of the above condition would require either a finetuning or a discrete symmetry.It is generally found that the imposition of discrete symmetries can lead to unwanted light higgs doublets or light Higgs triplets[17] which would spoil the consistency of the unification of couplings with the LEP data. It is possible that string theory may generate the desired discrete symmetries which suppress proton decay without producing undesirable features alluded to above.However, more generally one can expect proton decay to occur in both supergravity and string models. The detailed nature of proton decay modes, their signatures and partial lifetimes would depend on the specifics of the model.

Another problem that surfaces in supersymmetric unified models is that of the doublet-triplet splitting. That is one needs a mechanism that makes the Higgs triplets which mediate proton decay heavy and the Higgs doublet which generate electro-weak breaking light.Normally one simply finetunes the parameters to generate this splitting. Other possibilities consist of the so called missing partner mechanism[18], where one uses 75 , 50 and $\bar{50}$ representations in SU(5) instead of the usual 24 plet to break SU(5). Here 50 contains a $(\bar{3}, 1)$ and the $\bar{50}$ contains a (3,1) part in SU(3)$\times SU(2)$ decomposition but no (1,2) pieces. Thus the Higgs triplets from the 50 and $\bar{50}$ will match up with the Higgs triplet states from the 5 and $\bar{5}$ when the 75 plet develops a superheavy VEV, leaving the Higgs doublets light. More recently a mechanism has been dicussed in the literature which makes use of higher global symmetries such as SU(6) in the GUT sector which lead to light Higgs as pseudo-Goldstone doublets[19] when the local SU(5) symmetry breaks.However, there is as yet no complete model which also gives acceptable pattern of masses to fermions for this mechanism.Several other mechanisms have also been discussed mostly in SO(10) frameworks[20, 21, 22] and make use of vacuum alignment, discrete symmetries etc to achieve the doublet-triplet splitting. In the following we shall assume that the doublet-triplet splitting is resolved and discuss the case of the minimal SU(5) model in detail .

3. Nucleon Instability in Supergravity SU(5)

We discuss now the details of proton decay in the minimal SU(5) model to get an idea of the sizes of the lifetimes of the various decay modes. The invariant potential of this model is given by

$$W_Y = -\frac{1}{8} f_{1ij} \epsilon_{uvwxy} H_1^u M_i^{vw} M_j^{xy} + f_{2ij} \bar{H}_{2u} \bar{M}_{iv} M_j^{uv} \tag{7}$$

Here the M_{xi}, M_i^{xy} stand for the three generations(i=1,2,3) of $\bar{5}, 10$ plet of

quarks and leptons and H_1, H_2 are the $\bar{5}, 5$ plet of Higgs which give masses to the down and up quarks. After spontaneous breaking of the GUT group SU(5)$\rightarrow SU(3)\times SU(2)\times U(1)$ and integration over the heavy fields one has the effective dimension five operators with baryon number violation given by $L_5 = L_5^L + L_5^R$ where[7, 8]

$$L_5^L = \frac{1}{M}\epsilon_{abc}(Pf_1^u V)_{ij}(f_2^d)_{kl}(\tilde{u}_{Lbi}\tilde{d}_{Lcj}(\bar{e}^c_{Lk}(Vu_L)_{al} - \nu^c_k d_{Lal}) + ...) + H.c.$$
$$L_5^R = -\frac{1}{M}\epsilon_{abc}(V^\dagger f^u)_{ij}(PVf^d)_{kl}(\bar{e}^c_{Ri}u_{Raj}\tilde{u}_{Rck}\tilde{d}_{Rbl} + ...) + H.c. \quad (8)$$

Here the Yukawa couplings f^u, f^d are related to the quark masses m^u and m^d as

$$m_i^u = f_i^u(sin2\theta_W/e)M_Z sin\beta$$
$$m_i^d = f_i^d(sin2\theta_W/e)M_Z sin\beta \quad (9)$$

where θ_W is the Weak angle and β is defined by $tan\beta = \frac{v_2}{v_1}$ where $v_2 =< H_2^5 >$ and $v_1 =< H_1^5 >$. Further, V is the Kobayashi-Maskawa (KM) matrix and P is a diagonal phase matrix with elements

$$P_i = (e^{i\gamma_i}),\ \sum_i \gamma_i = 0;\ i = 1, 2, 3 \quad (10)$$

The dimension five operators must be dressed by the exhange of gluinos, charginos and neutralinos to produce dimension six operators which produce proton decay Of all these exchanges the chargino exchange is the most dominant and is governed by the interaction

$$L_{ui}^{\tilde{W}} = \frac{ig_2}{\sqrt{2}}(cos\gamma_-\tilde{W}_1 + sin\gamma_-\tilde{W}_2)(V\gamma^0 d_L)_i - ig_2(2cos\beta M_W)^{-1}$$
$$(Ecos\gamma_+\tilde{W}_1 - sin\gamma_+\tilde{W}_2)(Vm^d\gamma^0 d_R)_i \quad (11)$$

where $\gamma_\pm$ are defined in the text preceding eq(30). The dressing loop diagrams which convert dimension five into dimension six operators also include squark and slepton exchanges. However, the sfermion states that are exchanged are not pure L or R chiral states. As will be discussed later, in Supergravity one has soft susy breaking terms which mix the L and the R terms so that one has a (mass)^2 matrix of the form

$$\begin{pmatrix} m^2_{\tilde{m}_{Rui}} & m_i^u(A_{ui}m_o - \mu ctn\beta) \\ m_i^u(A_{ui}m_o - \mu ctn\beta) & m^2_{\tilde{t}_{Lui}} \end{pmatrix} \quad (12)$$

where A, μ are parameters which will be discussed in sec5. The mass diagonal states are denoted by the scalar squark fields $\tilde{u}_{i(1,2)}$.These are related to the L and R chiral states as

$$\tilde{u}_{Ri} = cos\delta_{ui}\tilde{u}_{i1} + sin\delta_{ui}\tilde{u}_{i2},\ \tilde{u}_{Li} = -sin\delta_{ui}\tilde{u}_{i1} + cos\delta_{ui}\tilde{u}_{i2} \tag{13}$$

where δ_{ui} is defined by

$$sin2\delta_{ui} = -2m_{ui}(A_{ui}m_0 - \mu ctn\beta)/(\tilde{m}^2_{ui1} - \tilde{m}^2_{ui2}) \tag{14}$$

The chiral structure of the dimension six operators involves operators of the type LLLL, LLRR, RRLL and RRRR. Of these it is the operators of the first type,i.e., LLLL which are the most dominant. In general one finds many SUSY decay modes for the proton,i.e.,

$$\begin{gathered} \bar{\nu}_i K^+, \bar{\nu}_i \pi^+; i = e, \mu, \tau \\ e^+K^0, \mu^+K^0, e^+\pi^0, \mu^+\pi^0, e^+\eta, \mu^+\eta \end{gathered} \tag{15}$$

The dependences of the branching ratios on quark mass factors and on KM matrix elements is shown in Table1.Also exhibited are the enhancement factors, denoted by y_1^{tk} etc, from the third generation squark and slepton exchange contributions in the dressing loop diagrams.

Table 1: lepton + pseudoscalar decay modes of the proton [7, 8]

SUSY Mode	quark factors	CKM factors	3rd generation enhacement
$\bar{\nu}_e K$	$m_d m_c$	$V_{11}^\dagger V_{21} V_{22}$	$(1 + y_1^{tK})$
$\bar{\nu}_\mu K$	$m_s m_c$	$V_{21}^\dagger V_{21} V_{22}$	$(1 + y_2^{tK})$
$\bar{\nu}_K$	$m_b m_c$	$V_{31}^\dagger V_{21} V_{22}$	$(1 + y_3^{tK})$
$\bar{\nu}_e\pi, \bar{\nu}_e\eta$	$m_d m_c$	$V_{11}^\dagger V_{21}^2$	$(1 + y_1^{t\pi})$
$\bar{\nu}_\mu\pi, \bar{\nu}_\mu\eta$	$m_s m_c$	$V_{21}^\dagger V_{21}^2$	$(1 + y_2^{t\pi})$
$\bar{\nu}_\tau\pi, \bar{\nu}_\tau\eta$	$m_b m_c$	$V_{31}^\dagger V_{21}^2$	$(1 + y_3^{t\pi})$
eK	$m_d m_u$	$V_{11}^\dagger V_{12}$	$(1 + y_e^{tK})$
μK	$m_s m_u$		$(1 - V_{12}V_{21}^\dagger - y_\mu^{tK})$
$e\pi, e\eta$	$m_d m_u$		$(1 - V_{11}V_{11}^\dagger - y_e^{t\pi})$
$\mu\pi, \mu\eta$	$m_s m_u$	$V_{11}^\dagger V_{21}^\dagger$	$(1 + y_\mu^{t\pi})$

The dependence of y factors, which contain the third generation contributions, on quark masses and KM matrix elements is shown in Table2. The factors R_e, R_μ, etc that enter in the evaluation of y in table2 are the dressing loop integrals and their explicit form is given in ref.[8]

Table 2: Third generation factors.

y factor	evaluation of y
y_1^{tK}	$\frac{P_3}{P_2}\frac{m_t V_{31} V_{32}}{m_c V_{21} V_{22}} R_e$
y_2^{tK}	$\frac{P_3}{P_2}\frac{m_t V_{31} V_{32}}{m_c V_{21} V_{22}} R_\mu$
y_3^{tK}	$\frac{P_3}{P_2}\frac{m_t V_{31} V_{32}}{m_c V_{21} V_{22}} R_\tau$
$y_1^{t\pi}$	$\frac{P_3}{P_2}\frac{m_t V_{31}^2}{m_c V_{21}^2} R_e$
$y_2^{t\pi}$	$\frac{P_3}{P_2}\frac{m_t V_{31}^2}{m_c V_{21}^2} R_\mu$
$y_3^{t\pi}$	$\frac{P_3}{P_2}\frac{m_t V_{31}^2}{m_c V_{21}^2} R_\tau$
y_e^{tK}	$\frac{P_3}{P_1}\frac{m_t V_{32} V_{33} V_{31}^\dagger}{m_u V_{12}} R'_e$
y_μ^{tK}	$\frac{P_3}{P_1}\frac{m_t V_{21}^\dagger V_{32} V_{33} V_{31}^\dagger}{m_u} R'_\mu$
$y_e^{t\pi}$	$\frac{P_3}{P_1}\frac{m_t V_{31} V_{33} V_{31}^\dagger V_{11}^\dagger}{m_u} R''_e$
$y_\mu^{t\pi}$	$\frac{P_3}{P_1}\frac{m_t V_{33} V_{31}^\dagger}{m_u V_{11}} R''_\mu$

From tables 1 and 2 one finds that there is a hierarchy in the partial decay branching ratios of these modes which can be read off from the quark mass factors and the KM matrix elements. In making order of magnitude estimates for lifetimes it is useful to keep in mind that

$$muV_{11} : m_c V_{21} : m_t V_{31} \approx 1 : 50 : 500 \tag{16}$$

One can then roughly order the partial decay branching ratios for the various modes listed in table1 as follows

$$\begin{aligned} BR(\mu K) >> BR(\mu K), BR(\mu\pi) >> BR(\mu\pi) \\ BR(\bar{\nu}K) > BR(\bar{\nu}\pi) > BR(lK) > BR(l\pi) \\ BR(\bar{\nu}_\mu K) > BR(\bar{\nu}_\tau K) > BR(\bar{\nu}_e K),\ BR(\bar{\nu}_\mu\pi) > BR(\bar{\nu}_\tau\pi) > BR(\bar{\nu}_e\pi) \end{aligned} \tag{17}$$

One finds from the above that the most dominant decay modes of the proton are the $\bar{\nu}K$ modes.The dimension six operators which govern these are given by[7, 8]

$$\begin{aligned} L_6(N \to \bar{\nu}_i K) = [(\alpha_2)^2(2MM_W^2 sin2\beta)^{-1} P_2 m_c m_i^d V_{i1}^\dagger V_{21} V_{22}][F(\tilde{c}, \tilde{d}_i, \tilde{W}) + F(\tilde{c}, \\ \tilde{d}_i, \tilde{W})] + ([1 + y_i^{tK} + (y_{\tilde{g}} + y_{tildeZ})\delta_{i2} + \Delta_i^K]\alpha_i^L + [1 + y_i^{tK} - (y_{\tilde{g}} - \\ y_{\tilde{Z}})\delta_{i2} + \Delta_i^K]\beta_i^L + (y_1(R)\alpha_3^R + y_2^{(R)}\beta_3^R)\delta_{i3}) \end{aligned} \tag{18}$$

In the above $\alpha_i^{L,R}, \beta_I^{L,R}$ are defined by

$$\alpha_i^L = \epsilon_{abc}(d_{aL}\gamma^0 u_{bL})(s_{cL}\gamma^0 \nu_{iL}) \tag{19}$$

and $\alpha_i^R = \alpha_i^L(\mathrm{d}_L, u_L \to d_R, u_R)$, and $\beta_i^{L,R} = \alpha_i^{L,R}(d \longleftrightarrow s)$. Further y_i^{tk} gives the dominant contribution from the third generation and is defined by[7, 8]

$$y_i^{tK} = \frac{P_2}{P_3}\left(\frac{m_s V_{31} V_{32}}{m_c V_{21} V_{22}}\right)\left(\frac{F(\tilde{t}, \tilde{d}_i, \tilde{W}) + F(\tilde{t}, \tilde{e}_i, \tilde{W})}{F(\tilde{c}, \tilde{d}_i, \tilde{W}) + F(\tilde{c}, \tilde{e}_i, \tilde{W})}\right) \tag{20}$$

where the functions F are dressing loop integrals and would be defined explicitly below. The remaining contributions represented by Δ_i^K, $y_{\tilde{g}}$ (from gluino exchange) and $y_{\tilde{Z}}$(from neutralino exchange) are all relatively small.

The decay branching ratios of the p into the $\bar{\nu}_i K$ modes are given by the relation

$$\Gamma(p \to \bar{\nu}_i K^+) = \left(\frac{\beta_p}{M_{H3}}\right)^2 |A|^2 |B_i| C \tag{21}$$

where β_p is the three quark - vacuum matrix element of the proton and is defined by

$$\beta_p U_L^\gamma = \epsilon_{abc}\epsilon_{\alpha\beta} < 0 | d_{aL}^\alpha u_{bL}^\beta u_{cL}^\gamma | p > \tag{22}$$

The most recent evaluation of β_p is from lattice gauge calculations [23] and is

$$\beta_p = (5.6 \pm 0.5) \times 10^{-3} GeV^3 \tag{23}$$

The factors A and B_i of eq(21) are defined by

$$A = \frac{\alpha_2^2}{2M_W^2} m_s m_c V_{21}^\dagger V_{21} A_L A_S \tag{24}$$

$$B_i = \frac{1}{sin2\beta} \frac{m_i^d V_{i1}^\dagger}{m_s V_{21}^\dagger} [P_2 B_{2i} + \frac{m_t V_{31} V_{32}}{m_c V_{21} V_{22}} P_3 B_{3i}] \tag{25}$$

$$B_{ji} = F(\tilde{u}_i, \tilde{d}_j, \tilde{W}) + (\tilde{d}_j \to \tilde{e}_j) \tag{26}$$

where

$$F(\tilde{u}_i, \tilde{d}_j, \tilde{W}) = [E cos\gamma_- sin\gamma_+ \tilde{f}(\tilde{u}_i, \tilde{d}_j, \tilde{W}_1) + cos\gamma_+ sin\gamma_- \tilde{f}(\tilde{u}_i, \tilde{d}_j, \tilde{W}_1)]$$
$$-\frac{1}{2}\frac{\delta_{i3} m_i^u sin2\delta_{ui}}{\sqrt{2} M_W sin\beta} [E sin\gamma_- sin\gamma_+ \tilde{f}(\tilde{u}_{i1}, \tilde{d}_j, \tilde{W}_1) - cos\gamma_- cos\gamma_+ \tilde{f}(\tilde{u}_{i1}, \tilde{d}_j, \tilde{W}_2)$$
$$-(\tilde{u}_{i1} \to \tilde{u}_{i2})] \tag{27}$$

In the above $\tilde{f}$ is given by

$$\tilde{f}(\tilde{u}_i, \tilde{d}_j, \tilde{W}_k) = sin^2\delta_{ui} \tilde{f}(\tilde{u}_{i1}, \tilde{d}_j, \tilde{W}_k) + cos^2\delta_{ui} \tilde{f}(\tilde{u}_{i2}, \tilde{d}_j, \tilde{W}_k) \tag{28}$$

where

$$f(a,b,c) = \frac{m_c}{m_b^2 - m_c^2}[\frac{m_b^2}{m_a^2 - m_b^2} ln(\frac{m_a^2}{m_b^2}) - (m_a \rightarrow m_c)] \tag{29}$$

and $\gamma_\pm = \beta_+ \pm \beta_-$ where

$$sin2\beta_\pm = \frac{(\mu \pm \tilde{m}_2)}{[4\nu_\pm^2 + (\mu \pm \tilde{m}_2)^2]^{1/2}} \tag{30}$$

and

$$\sqrt{2}\nu_\pm = M_W(sin\beta \pm cos\beta) \tag{31}$$

$$sin2\delta_{u3} = -\frac{-2(A_t + \mu ctn\beta)m_t}{m_{\tilde{t}_1}^2 - m_{\tilde{t}_2}^2} \tag{32}$$

$$\begin{aligned} E &= 1\ , sin2\beta > \mu\tilde{m}_2/M_W^2 \\ &= -1, sin2\beta < \mu\tilde{m}_2/M_W^2 \end{aligned} \tag{33}$$

Finally C that enters eq(25) is a current algebra factor and is given by

$$C = \frac{m_N}{32\pi f_\pi^2}[(1 + \frac{m_N(D+F)}{m_B})(1 - \frac{m_K^2}{m_N^2})]^2 \tag{34}$$

where the chiral Lagrangian factors $f_\pi, D, F, ..$ etc that enter the above equation have the numerical values: $f_\pi = 139\ MeV$, $D = 0.76$, $F = 0.48, m_N = 938\ MeV$, $m_K = 495\ MeV, and\ m_B = 1154$.

4. Vector Meson Decay Modes of the Proton

The same baryon number violating dimension six quark operators that lead to the decay of the proton into lepton and pseudoscalar modes also lead to decay modes with lepton and vector mesons[24]. Although the vector mesons are considerably heavier that their corresponding pseudoscalar counterparts, decay modes invoving ρ, K^*, ω are still allowed. We list these below

$$\begin{aligned} &\bar{\nu}_i K^*, \bar{\nu}_i \rho, \bar{\nu}_i \omega; i = e, \mu, \tau \\ &eK^*, \mu K^*, e\rho, \mu\rho, e\omega, \mu\omega \end{aligned} \tag{35}$$

The quark, KM and third generation enhancement factors for the allowed vector meson decay modes is exhibited in table3. The branching ratios for the vector meson decay modes are typically smaller than the corresponding pseudo-scalar decay modes.

Table 3: lepton + vector meson decay modes of the proton

SUSY Mode	quark factors	CKM factors	3rd generation enhacement
$\bar{\nu}_e K^*$	$m_d m_c$	$V_{11}^\dagger V_{21} V_{22}$	$(1+y_1^{tK})$
$\bar{\nu}_\mu K^*$	$m_s m_c$	$V_{21}^\dagger V_{21} V_{22}$	$(1+y_2^{tK})$
$\bar{\nu}_\tau K^*$	$m_b m_c$	$V_{31}^\dagger V_{21} V_{22}$	$(1+y_3^{tK})$
$\bar{\nu}_e \rho, \bar{\nu}_e \omega$	$m_d m_c$	$V_{11}^\dagger V_{21}^2$	$(1+y_1^{t\pi})$
$\bar{\nu}_\mu \rho, \bar{\nu}_\mu \omega$	$m_s m_c$	$V_{21}^\dagger V_{21}^2$	$(1+y_2^{t\pi})$
$\bar{\nu}_\tau \rho, \bar{\nu}_\tau \omega$	$m_b m_c$	$V_{31}^\dagger V_{21}^2$	$(1+y_3^{t\pi})$
eK^*	$m_d m_u$	$V_{11}^\dagger V_{12}$	$(1+y_e^{tK})$
μK^*	$m_s m_u$		$(1-V_{12}V_{21}^\dagger - y_\mu^{tK})$
$e\rho, e\omega$	$m_d m_u$		$(1-V_{11}V_{11}^\dagger - y_e^{t\pi})$
$\mu\rho, \mu\omega$	$m_s m_u$	$V_{11}^\dagger V_{21}^\dagger$	$(1+y_\mu^{t\pi})$

5. Details of Analysis in Supergravity Unification

Next we discuss the details of the proton decay analysis in supergravity unification. As already indicated the low energy SUSY spectrum plays a crucial role in proton decay lifetime.In fact the spectrum that enters consists of 12 squark states, 9 slepton states, 4 neutralino states, 2 chargino states, and the gluino. There are thus 28 different mass parameters alone. In globally supersymmetric grand unification one has no way to meaningfully control these parameters and thus detailed predictions of p decay lifetimes in globally supersymmetric theories cannot be made. In supergravity unified models one has a well defined procedure of breaking supersymmetry via the hidden sector and the minimal supergravity unification contains only 4 SUSY parameters in terms of which all the SUSY masses can be predicted. Thus supergravity unification is very predictive. We give below a brief review of the basic elements of supergravity grand unification. These are: (1) supersymmetry breaks in the hidden sector by a superhiggs phenomenon and the breaking of supersymmetry is communicated gravitationally to the physical sector; (2) the superhiggs coupling are assumed not to depend on the generation index, and (3) one assumes the spectrum to be the MSSM spectrum below the GUT scale. After the breaking of supersymmetry and of the gauge group one can integrate over the superhiggs fields and the heavy fields and the following supersymmetry breaking potential in the low energy domain results [11, 12]:

$$V_{SB} = m_0^2 z_a z_a^\dagger + (A_0 W^{(3)} + B_0 W^{(2)} + h.c.) \tag{36}$$

where $W^{(2)}, W^{(3)}$ are the bilinear and trilear parts of the superpotential. There is also a gaugino mass term $L_{mass}^{\lambda} = -m_{1/2}\bar{\lambda}^\alpha \lambda^\alpha$. At this stage the theory has five SUSY parameters $m_0, m_{1/2}, A_0, B_0, and\ \mu_0$. Here μ_0 is the

Higgs mixing term which along with the other low energy quark-lepton- Higgs interactions is given by

$$W = \mu_0 H_1 H_2 + [\lambda_{ij}^{(u)} q_i H_2 u_j^c + \lambda_{ij}^{(d)} d_i H_1 d_j^c + \lambda_{ij}^{(e)} l_i H_1 d_j^c] \tag{37}$$

In the above H_1 is the light Higgs doublet which gives mass to down quark and leptons and H_2 give mass to the up quark. The number of SUSY parameters can be reduced after radiative breaking of the electro-weak symmetry. The radiative electro-weak symmetry breaking is governed by the potential

$$\begin{aligned} V_H = m_1^2(t)|H_1|^2 + m_2^2(t)|H_2|^2 - m_3^2(t)(H_1 H_2 + h.c.) \\ + \frac{1}{8}(g^2 + g_y^2)(|H_1|^2 - |H_2|^2)^2 + \Delta V_1 \end{aligned} \tag{38}$$

where ΔV_1 is the correction from one loop, and $m_1^2(t)$ etc are the running parameters and satisfy the boundary conditions $m_i^2(0) = m_0^2 + \mu_0^2; i = 1,2$, $m_3^2(0) = -B_0\mu_0$, $\alpha_2(0) = \alpha_G = (5/3)\alpha_Y(0)$. The breaking of the elctroweak symmetry is accomplished by the relations $\frac{1}{2}M_Z^2 = (\mu_1^2 - \mu_2^2 tan^2\beta)/(tan^2\beta - 1)$ and $sin2\beta = (2m_3^2)/(\mu_1^2 + \mu_2^2)$, where $\mu_i^2 = m_i^2 + \Sigma_i$ and Σ_i is one loop correction from ΔV_1.Using the above relations one can reduce the low energy SUSY parameters to the following:

$$m_0, m_{1/2}, A_0, tan\beta \tag{39}$$

Another result that emerges from radiative breaking of the electro-weak symmetry is that of scaling.One finds that over most of the parameter space of the theory $\mu^2 >> M_Z^2$ which gives[25, 26]

$$\begin{aligned} m_{\tilde{W}_1} \sim \frac{1}{3} m_{\tilde{g}}\ (\mu < 0); m_{\tilde{W}_1} \sim \frac{1}{4} m_{\tilde{g}}\ (\mu > 0) \\ 2m_{\tilde{Z}_1} \sim m_{\tilde{W}_1} \sim m_{\tilde{Z}_2}; m_{\tilde{Z}_3} \sim m_{\tilde{Z}_4} \sim m_{\tilde{W}_2} >> m_{\tilde{Z}_1} \\ m_H^0 \sim m_A \sim m_{H^\pm} >> m_h \end{aligned} \tag{40}$$

Corrections to the above are typically small $O(1/\mu)$ over most of the parameter space.

We discuss now the effects of the top quark which play an important role in limiting the parameter space of the model. Contraints from the top quark arise because there is a Landau pole in the top quark Yukawa coupling, i.e., $Y_0 = Y_t/(E(t)D_0)$ where $D_0 = 1 - 6Y_t F(t)/E(t)$, $Y_t = \lambda_t^2/4\pi$, $\lambda_t(Q)$ is the top-quark Yukawa coupling and is defined by $m_t =< H_2 > \lambda_t(m_t)$, and the functions E(t) and F(t) are as defined in ref[27].We see from the above that the top Yukawa has a Landau pole which appears at

$$m_t^f = (8\pi/\alpha_2(t))^{1/2}(Y_t^f(t))^{1/2} M_Z cos\theta_W sin\beta \tag{41}$$

where θ_W is the weak mixing angle.For some typical values of α_G and M_G one has $m_t^f \sim 200 sin\beta$. Now it is found that the same Landau singularity also surfaces in the other SUSY parameters because of the coupled nature of the renormalization group equations.Thus, for example, the trilinear soft SUSY parameter develops a Landau singularity: $A_0 = A_R/D_0 + A_0(nonpole)$, and $A_R = A_t - 0.6m_g$, where A_0 is the value of A_t at the GUT scale. A similar analysis shows that μ^2 and thus the stop masses become singular.Specifically one finds that $m_{\tilde{t}_1}^2 = -2x/D_0 + m_{\tilde{t}_1}^2(NP)$ and $m_{\tilde{t}_2}^2 = -x/D_0 + m_{\tilde{t}_2}^2(NP)$ where x=$Y_t A_R^2 F/E$. We note that the Landau pole contribution is negative definite and thus drives the stops towards their tachyonic limit. Especially the Landau pole contributions to $\tilde{t}_1$ are rather large and so its transition to the tachyonic limit is very rapid. Thus the condition that there be no tachyons puts a strong limit on the parameter space. One finds that the allowed values of A_t lie in the range $-0.5 < A_t < 5.5$.

6. Discussion of Results

Figure 1 gives the maximum lifetime of the $p \to \nu K^+$ mode for$\mu < 0$ as function of m_0 when all other parameters are varied over the allowed parameters space consistent with radiative breaking of the electro-weak symmetry and with the inclusion of the LEP1.4 constraints. The solid curve gives the maximum without the imposition of the cosmological relic density constraint while the dashed curve includes the relic density constraint.

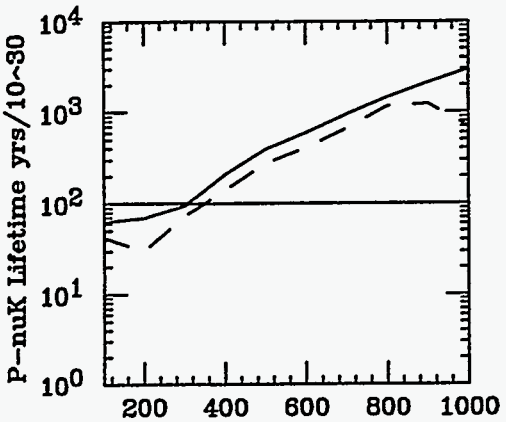

Fig 1: m0, mu<0

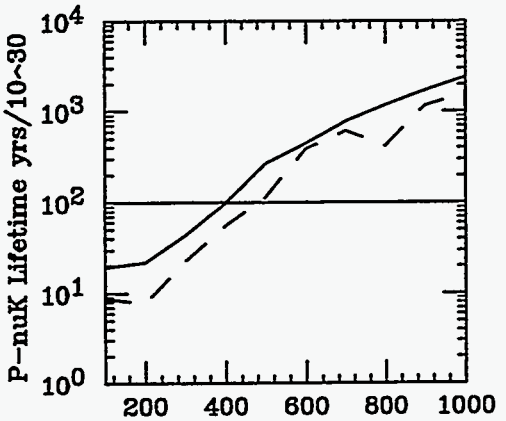

Fig 2: m0, mu>0

The solid horizontal line is the current experimental lower limit for this mode from IMB and Kamiokande. We see that the analysis shows that there exists a cosiderable part of the parameter space not yet explored by the current experiment, which will be accessible to SuperKamiokande and ICARUS.

Figure 2 gives the same analysis when $\mu > 0$.Comparison of figs 1 and 2 shows that the current experiment excludes a somewhat larger region of the parameter space in m_0 for $\mu > 0$ than for $\mu < 0$.Thus for $\mu > 0$ one eliminates the region $\mu < 400GeV$ while for $\mu < 0$ only the values $m_0 < 300GeV$ are eliminated. Figure 3 gives the plot of the maximum lifetime for the $p \to \bar{\nu}K$ mode as a function of gluino mass for the case $\mu < 0$ corresponding to Fig 1. We see that regions of the parameter space with lifetimes above the current limits lie below approximately 400 GeV when the dark matter constraint is imposed. Figure 4 is similar to Fig 3 except that $\mu > 0$.

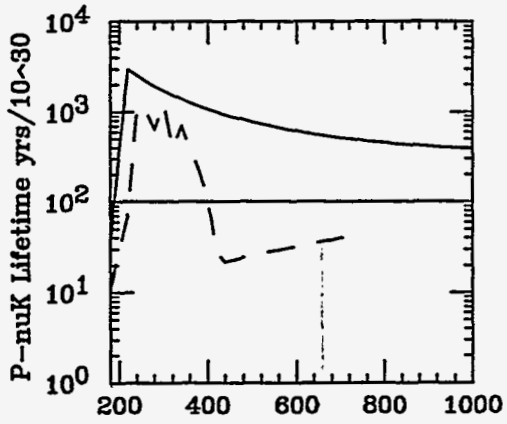

Fig 3: gluino mass, mu<0

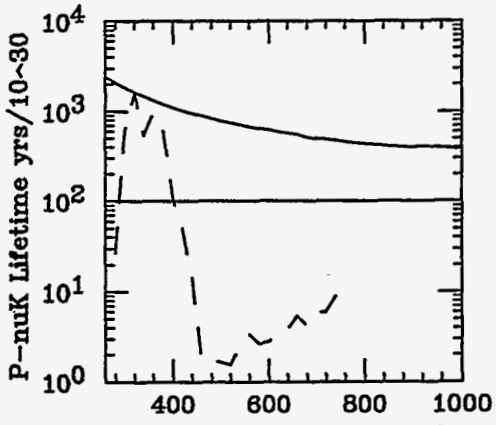

Fig 4: gluino mass , mu>0

7.Conclusion

In the above we have given a brief review of nucleon instability in supersymmetric unified theories. We have pointed out that no concrete predictions on proton decay lifetimes are possible unless the nature of the low energy SUSY mass spectrum which enters in the dressing loop diagrams is assumed. Thus no concrete predictions on proton lifetime can be made in globally supersymmetric grand unified theories. In contrast one can make predictions in supergravity unification since the SUSY breaking spectrum of the theory is characterised by four parameters.Further since there are 32 supersymmetric particles one has 28 predictions in the model, and thus supergravity grandunification is very predictive. An updated analysis of p-decay in the minimal SU(5) model was given including the constraints of LEP1.4.It is found that there exits a significant part of the parameter space which is not yet explored by the current proton lifetime limits on $p \to \bar{\nu}K$ from IMB and Kamiokande but which would become accessible to SuperKamiokande and ICARUS experiments. Finally we note that the minimal model can correctly accomodate the b/τ mass ratio[29]. However, it does not predict other quark lepton mass ra-

tios correctly and non-minimal extensions are needed for this purpose. These non-minimal extensions also affect the proton lifetime predictions.

Acknowledgements: This research was supported in part by NSF grant numbers PHY-19306906 and PHY-9411543.

References

1. H.Georgi and S.L.Glashow, Phys.Rev.Lett.**32**, 438(1974).

2. M.Goldhaber and W.J. Marciano, Comm.Nucl.Part.Phys.**16**, 23(1986); P.Langacker and N.Polonsky, Phys.Rev.**D47**,4028(1993).

3. Particle Data Group, Phys.Rev. **D50**,1173(1994).

4. Y.Totsuka, Proc. XXIV Conf. on High Energy Physics, Munich, 1988,Eds. R.Kotthaus and J.H. Kuhn (Springer Verlag, Berlin, Heidelberg,1989).

5. W.de Boer, Prog.Part. Nucl.Phys.**33**,201(1994).

6. S.Weinberg, Phys.Rev.**D26**,287(1982); N.Sakai and T.Yanagida, Nucl.Ph ys.**B197**, 533(1982); S.Dimopoulos, S.Raby and F.Wilcek, Phys.Lett. **112B**, 133(1982); J.Ellis, D.V.Nanopoulos and S.Rudaz, Nucl.Phys. **B202**,43(1982); B.A.Campbell, J.Ellis and D.V.Nanopoulos, Phys.Lett.**141B**,299(1984); S.Chadha, G.D.Coughlan, M.Daniel and G.G.Ross, Phys.Lett.**149B**,47(1984).

7. R.Arnowitt, A.H.Chamseddine and P.Nath, Phys.Lett. **156B**,215(1985).

8. P.Nath, R.Arnowitt and A.H.Chamseddine, Phys.Rev.**32D**,2348(1985).

9. J.Hisano, H.Murayama and T. Yanagida, Nucl.Phys. **B402**,46(1993).

10. ICARUS Detector Group, Int. Symposium on Neutrino Astrophsyics, Takayama. 1992.

11. A.H. Chamseddine, R. Arnowitt and P. Nath, Phys. Rev. Lett **29**. 970 (1982);P.Nath,Arnowitt and A.H.Chamseddine , "Applied N=1 Supergravity" (World Scientific, Singapore, 1984); H.P. Nilles, Phys. Rep. **110**, 1 (1984); R. Arnowitt and P. Nath, Proc of VII J.A. Swieca Summer School (World Scientific, Singapore 1994).

12. R.Barbieri, S.Ferrara and C.A.Savoy, Phys.Lett.**B119**, 343(1982); L.Hall, J.Lykken and S.Weinberg, Phys.Rev.**D27**, 2359(1983); P.Nath, R.Arnowitt and A.H.Chamseddine, Nucl. Phys.227,121(1983).

13. I.Antoniadis, J.Ellis, J.S.Hagelin and D.V.Nanopoulos, Phys.Lett.**B231**,65 (1987); ibid, **B205**, 459(1988).

14. K.S.Babu and S.M. Barr,Phys.Rev. **D48**, 5354(1998).

15. R.N.Mohapatra, UMD-PP-96-59(1996)/hep-ph/9601203.

16. R.Arnowitt and P.Nath, Phys.Rev. **D49**, 1479(1994).

17. C.D. Coughlan, G.G.Ross, R.Holman, P.Ramond, M.Ruiz- Altaba and J.W.F. Valle, Phsy.Lett.**158B**,401(1985).

18. B.Grinstein, Nucl.Phys.**B206**,387(1982);H.Georgi, Phys.Lett.**B115**,380 (1982).

19. K.Inoue, A.Kakuto and T.Tankano, Prog.Theor. Phys.**75**, 664(1986); A.Anselm and A.Johasen, Phys.Lett.**B200**,331(1988); A.Anselm, Sov. Phys.JETP**67**,663(1988); R.Barbieri, G.Dvali and A.Strumia, Nucl. Phys. **B391**,487(1993); Z.Bereziani and G.Dvali, Sov.Phys. Lebedev Inst. Report 5,55(1989);Z.Bereziani, C.Csaki and L. Randall, Nucl.Phys.**B44**,61 (1995).

20. S.Dimopoulos and F.Wilczek, Report No.NSF-ITP-82-07(1981) (unpublished).

21. K.S.Babu and S.M.Barr, Phys.Rev.**D50**,3529(1994).

22. D.Lee and R.N.Mohapatra, Phys.Rev.**D51** (1995).

23. M.B.Gavela et al, Nucl.Phys.**B312**,269(1989).

24. T.C.Yuan, Phys.Rev.**D33**,1894(1986).

25. R. Arnowitt and P. Nath, Phys. Rev. Lett. **69**, 725 (1992).

26. P. Nath and R. Arnowitt, Phys. Lett. **B289**, 368 (1992).

27. L.Ibanez, C.Lopez, and C.Munos, Nucl. Phys.**B256**, 218(1985).

28. P. Nath, J. Wu and R. Arnowitt, Phys.Rev.**D52**,4169(1995).

29. V.Barger, M.S.Berger, and P.Ohman, Phys.Lett. **B314**,351(1993).

Neutron-Anti-Neutron Oscillation as a Test of Grand Unification[1]

R.N. Mohapatra[2]
Department of Physics
University of Maryland
College Park, MD 20742

Abstract

We discuss the predictions for the neutron-anti-neutron ($N - \overline{N}$) process in various supersymmetric and non-supersymmetric grand unified theories. In particular it is pointed out that in a class of superstring inspired grand unified theories (of E_6 type) that satisfy the constraints of gauge coupling unification, breakdown of the $B - L$ symmetry occurs at an intermediate scale leading in turn to $\Delta B = 1$ type R-parity violating interactions naturally suppressed to the level of 10^{-5} to 10^{-7}. This in turn implies an $N - \overline{N}$ transition time of order 10^{10} to 10^{11} sec. which may be observable in the next generation of proposed experiments. These models also satisfy the conditions needed for generating the cosmological baryon asymmetry of the right order of magnitude.

---

[1]Invited talk presented at the "International workshop on the future prospects for baryon instability search proton decay and neutron oscillation" at Oak Ridge National Laboratory from March 28-30, 1996.

[2]Work supported by the National Science Foundation Grant #PHY-9119745 and a Distinguished Faculty Research Award by the University of Maryland for the year 1995-96.

I. Introduction:

The observed matter anti-matter asymmetry in nature is convincing enough as an evidence for the existence of baryon number violation in the fundamental interactions that describe physical processes. This is because of the three conditions for generating this asymmetry laid down originally by Sakharov in 1967: (i) existence of CP-violating and (ii) baryon number violating interctions plus (iii) the presence of out of thermal equilibrium conditions in the early universe. There are also strong theoretical hints in favor of $\Delta B \neq 0$ interactions: for instance, the standard model violates both baryon (B) and lepton (L) number via the triangle anomalies involving the electro-weak gauge bosons (although it conserves the linear combination $B-L$). The present consensus however is that these baryon violating effects are too weak to be observable in laboratory experiments. Similarly, most extensions of the standard model also imply such interactions in the sector beyond the standard model. Perhaps more compelling is the argument that the anomaly free gauge quantum number in most extensions of the standard model is indeed the $B-L$ symmetry alluded to above. If the present indications for non-zero neutrino mass from various terrestrial and extra terrestrial sources hold up with time, the only sensible theoretical way to understand it is to assume that the neutrino is a Majorana particle implying that the lepton number is broken by vacuum by two units ($\Delta L = 2$). Since B and L appear in combination with each other, if lepton number breaks by two units, there is no reason for baryon number not to break. In fact this reasoning was first noted by Marshak and this author[1] as a theoretical motivation for neutron- anti-neutron oscillation.

Once one accepts the existence of baryon number violating interactions, it becomes of crucial importance to learn about the possible selection rules obeyed by them. As is quite well-known[2], the different selection rules probe new physics at different mass scales and therefore contain invaluable information regarding the nature of short distance physics that is otherwise inaccessible. Two of the most interesting selection rules are: one in which $B-L$ is conserved such as the decay $p \to e^+\pi^0$ (or $p \to \bar{\nu}_\mu K^+$ as in supersymmetric theories) and a second one which obeys $\Delta(B-L) = 2$, such as $N-\bar{N}$ oscillation (which is the main theme of this workshop). These two processes probe two very different mass scales. To see this note that the process $p \to e^+\pi^0$ arises from the operator $uude^-$ (or $QQQL$ in the $SU(2)_L \times U(1)_Y$ invariant form) and it therefore scales like M^{-2} where M denotes the mass scale where the interaction originates. The present limits on proton lifetime then imply that $M \geq 10^{15}$ GeV or so. On the other hand, $N-\bar{N}$ oscillation arises from the operator of the form $u^c d^c d^c u^c d^c d^c$ which scales like M^{-5}. The limits on nonleptonic $\Delta B = 2$ nuclear decays or the $N-\bar{N}$ oscillation time from the ILL

experiment[3], implies that $M \geq 10^5$ GeV or so. Thus $N - \bar{N}$ oscillation has the additional properties that it also provides complementary probes of new physics near the TeV scale.

There is however as yet no laboratory evidence for any kind of $\Delta B \neq 0$ process. The first generation of experiments searching for evidence of baryon number violation have all reported their results as lower limits on the partial life times for the various decay modes of the proton (at the level of roughly 10^{32} to 10^{33} years). Those results have already had the important implication that the minimal non-supersymmetric $SU(5)$ model is ruled out as a grand unification theory. There are currently two experimental efforts to improve the discovery potential for proton decay to the level of 10^{34} years. These are the Super-Kamiokande[4] and ICARUS[5] experiments. To go beyond that would require a major innovation in experimental methods.

There is however encouraging news from the $N - \bar{N}$ oscillation front in this regard. As is well-known[6], the existence of neutron- anti-neutron oscillation inside nuclei leads to baryon instabilty which can also be probed in the proton decay searches (e.g. the disppearance of oxygen nuclei in water detectors). One can then use simple scaling arguments to relate the nuclear instability life time(τ_{nucl}) to the $N - \bar{N}$ oscillation time ($\tau_{N-\bar{N}}$) For more reliable nuclear physics calculations, see [7]:

$$\tau_{nucl} \simeq \left(\frac{\tau_{N-\bar{N}}}{6.6 \times 10^6 \ sec}\right)^2 \times 10^{30} \ yrs. \tag{1}$$

From this equation we see that a measurement of $\tau_{N-\bar{N}}$ to the level of 10^{10} sec. (as is contemplated by the Oak Ridge group[8]) would correspond to probing baryon instability to the level of almost 10^{37} yrs. This will take us far into the uncharted domain of baryon non-conservation not easily accessible in other experiments(albeit in a very special non-leptonic channel). This may be one of the strongest arguments for undertaking such an experiment. In this article, I will discuss elegant and plausible theoretical models that provide additional arguments in favor of conducting such an experiment since this can be a very useful way to discriminate between various grand unification theories.

This paper is organized as follows: in sec.II, the general theoretical arguments for $N - \bar{N}$ oscillation based on gauged $B - L$ symmetry are outlined; the predictions for $\tau_{N-\bar{N}}$ in non-supersymmetric theories and supersymmetric theories are given in sec.III and IV respectively; in sec.V, it is shown how baryon asymmetry can be generated in an $[SU(3)]^3$ string inspired SUSY GUT model which predicts observable $\tau_{N-\bar{N}}$; in sec.VI, some concluding remarks are presented.

II. Local $B-L$ symmetry and $N-\bar{N}$ oscillation:

As already mentioned, in the standard model, $B-L$ is an anomaly free global symmetry. However, it is not a gaugeable symmetry since it is not cubic anomaly free. This fact is connected with whether neutrino mass is zero or not. In the standard model neutrino mass vanishes because the right handed neutrino is not included in the spectrum; it is also the absence of ν_R that prevents $B-L$ symmetry from being a gaugeable symmetry. In order to generate neutrino mass, we must add ν_R to the spectrum of fermions in the standard model. As soon as this is done, $B-L$ becomes cubic anomaly free and becomes a gaugeable symmetry. This also incidentally restores quark-lepton symmetry to particle physics. The natural gauge symmetry of particle physics then becomes the left-right symmetric gauge group $SU(2)_L \times SU(2)_R \times U(1)_{B-L}$[9] which then not only explains the smallness of neutrino mass but it also makes weak interactions asymptotically parity conserving. It was noted in 1980[1, 10] that in formula for electric charge in the left-right symmetric model is given by:

$$Q = I_{3L} + I_{3R} + \frac{B-L}{2} \tag{2}$$

It follows from this equation[11] that since $\Delta Q = 0$, at distance scales where $\Delta I_{3L} = 0$, we have the relation

$$\Delta I_{3R} = -\frac{1}{2}(B-L) \tag{3}$$

Clearly, the violation of lepton number which leads to a Majorana mass for the neutrino is connected with the violation of right-handed iso-spin I_{3R}. The same equation also implies that for processes where no leptons are involved, it can lead to purely baryonic processes where baryon number is violated. In nonsupersymmetric theories, the simplest such process is neutron-anti-neutron oscillation since $u^c d^c d^c u^c d^c d^c$ is the lowest dimensional baryon number violating operator that conserves color, electric charge and angular momentum and does not involve any lepton fields. (The situation is different in supersymmetric theories as we will see in the next section.) This equation implies a deep connection between the Majorana mass for the neutrino and the existence of neutron-anti-neutron oscillation. Of course whether $N-\bar{N}$ transition appears with an observable strength depends on the details of the theory such as the mass spectrum, value of mass scales etc.

Before proceeding further, a few words about the notation: Let us call $G_{N-\bar{N}}$ as the strength of the six quark amplitude; $\delta m_{N-\bar{N}}$ as the transition mass for neutron-anti-neutron transition and $\tau_{N-\bar{N}} = h/2\pi\delta m_{N-\bar{N}}$ where h is Planck's constant. We hasten to clarify that while theories with local $B-L$ symmetry provide a natural setting for the neutron-anti-neutron oscillation to arise, it is possible to construct alternative models where one can have $N-\bar{N}$ oscillation. In such models however, the strength for this process is completely unrelated to other physics making them quite adhoc.

III. Predictions for $\tau_{N-\bar{N}}$ in non-supersymmetric unified theories:

There were many models for neutron-anti-neutron oscillation discussed in the early eighties[6]; most of these models are in the context of nonsupersymmetric higher unified theories. Here I present the simplest of them and summarize the general status of $\tau_{N-\bar{N}}$ transition in all these models in Table 1.

We will consider the gauge group $SU(2)_L \times SU(2)_R \times SU(4)_c$ which was suggested by Pati and Salam[9] in 1973. The recognition that $SU(4)_c$ contains the $B-L$ symmetry and has the potential to explain neutrino mass and applications to N-$\bar{N}$ oscillation came in the papers of Marshak and this author [1, 11]. In order to obtain neutron-anti-neutron oscillation process, the gauge symmetry breaking of the model has to be broken by the Higgs multiplets as in Ref.[11] i.e. a bidoublet $\phi(2,2,1)$, and a pair of triplets $\Delta_L(3,1,\bar{10}) + \Delta_R(1,3,\bar{10})$. This set of Higgs multiplets was different from the one originally used in Ref.[9] and brought out the physics of the model in a very clear manner. The quarks and leptons are assigned to representations as follows: $Q_L(2,1,4) + Q_R(1,2,4)$. Here leptons are considered as the fourth color. The allowed Yukawa couplings in the model are given by:

$$L_Y = y_q \bar{Q}_L \phi Q_R + f(Q_L Q_L \Delta_L + Q_R Q_R \Delta_R) + h.c. \tag{4}$$

Here we have omitted all generation indices and also denoted the couplings symbolically omitting charge conjugation matrices, Pauli matrices etc. The Higgs potential of the model can be easily written down; the term in it which is interesting for our purpose is $\lambda \epsilon^{ijkl}\epsilon^{i'j'k'l'}\Delta_{L,ii'}\Delta_{L,jj'}\Delta_{L,kk'}\Delta_{L,ll'} + L \to R + h.c.$.

In order to proceed towards our goal of estimating the strength of $N-\bar{N}$ oscillation in this model, we first note that the original gauge symmetry here is broken by the vev $\langle \Delta_{R,44} \rangle = v_{B-L} \neq 0$ to the standard model gauge group. The diagram of Fig.1 then leads to the six quark effective interaction below the scale v_{B-L} of the form $u_R d_R d_R u_R d_R d_R$ with strength $\lambda f^3 v_{B-L}/M^6_{\Delta_R}$. For the scale v_{B-L}

and M_{Δ_R} of order 100 TeV and for $h \approx \lambda \approx 10^{-1}$ this will lead to a strength for the six quark amplitude of about 10^{-29} GeV^{-5}. In order to convert it to $\delta m_{N-\bar{N}}$, we need the three quark "wave function" of the neutron at the origin. This has been estimated by various people[12] and usually yields a factor of about 10^{-4} or so. Using this , we expect $\tau_{N-\bar{N}} \simeq 6 \times 10^8$ sec. This is however only an order of magnitude estimate since the true value of the parameters that go into this estimate is unknown. But the main point that this example makes is that there exist very reasonable theories where neutron-anti-neutron oscillation is observable. Note that this model is a completely realistic extension of the standard model with many intersting features such as the smallness of neutrino mass naturally explained etc.

A natural question to ask at this point is whether there are grand unified theories where observable $N - \bar{N}$ oscillation can be expected. In simple nonsupersymmetric extensions of $SU(5)$ model, it is easy to show that[13] $N - \bar{N}$ transition amplitude is very highly suppressed. Let us therefore consider the $SO(10)$ model which contains the gauge group $SU(2)_L \times SU(2)_R \times SU(4)_c$. All the ingredients for a sizable $N - \bar{N}$ to exist are present in the model except that the scale v_{B-L} is constrained by gauge coupling unification. This question was studied in detail in Ref.[14] and a scenario of symmetry breaking was isolated where one could get a value for $v_{B-L} \simeq 100$ TeV. This would therefore lead to an observable $\tau_{N-\bar{N}}$ oscillation as before. The only problem is that in a low $SU(4)_c$ scale model, one has to introduce iso-singlet fermions to lift the degeneracy between quark and charged fermion masses implied by $SU(4)_c$ symmetry. While this procedure is quite harmless in partial unification models, it effects gauge coupling unification in a model such as $SO(10)$. This question has not been discussed yet in such models. For situation in other non-SUSY GUT theories, see Table 1.

IV. R-parity violation and $N - \bar{N}$ oscillation:

The particle physics of the nineties has perhaps a different "flavor" (set of prejudices ?) than the eighties. It is now widely believed that supersymmetry is an essential ingredient of physics beyond the standard model with supersymmetry breaking scale around a TeV in order to explain the origin of electroweak symmetry breaking. Furthermore if one believes that supersymmetry is the low energy manifestation of the superstring theories, then to the usual renormalizable Lagrangian of the supersymmetric theory, one must add non-renormalizable terms which are the low energy remnants of superstring physics. In the discussion of this section, we will use both these ingredients.

A simple way to explain supersymmetric theories is to note that corresonding

to every particle there is a super partner (spin half partner for a gauge boson or Higgs boson and spin zero partner for a fermion with identical internal quantum numbers in both cases) and there are a large number of relations between the coupling constants of the theory. In this article, we will denote the super partners of quarks and leptons by $\tilde{q}$ and $\tilde{L}$ respectively; super partners of W and Z bosons by $\tilde{W}$ and $\tilde{Z}$ etc. The extension of the standard model to include supersymmetry is under extensive investigation right now both from theoretical and experimental side.

One troubling aspect of the minimal supersymmetric extension of the standard model (MSSM) is that it allows for lepton and baryon number violating interactions with arbitrary strengths. This in a sense is a step backward from the standard model which automatically ensured that both baryon and lepton numbers are conserved to an extremely high degree as is observed. A simple way to see the origin of such terms is to note that $\tilde{L}$ which is the superpartner of the lepton doublet is exactly like a Higgs boson of the standard model except that it carries lepton number. But we know that the Higgs doublet of the standard model couples to quarks; similarly the $\tilde{L}$ field also couples to quarks as in the standard model: $Q\tilde{L}d^c$; but this clearly violates lepton number by an arbitrary amount. Similar terms can be written down which violate baryon number also with arbitrary strength. These are the so-called R-parity violating interactions. There exist very stringent upper limits on the various R-parity violating couplings[15] which range anywhere from 10^{-4} to 10^{-8} depending on the type of selection rules they break. Since the main reason for believing in supersymmetry is that it improves the naturalness of the standard model, it will be awkward to assume that the MSSM carries along with it the above fine-tuned couplings without any fundamental assumptions.

The general attitude to this problem is that when the MSSM is extrapolated to higher scales, new symmetries will emerge which either forbid the R-parity violating couplings or suppress it in a natural manner. A concrete proposal in this direction proposed some time ago[16] is that at higher energies the the gauge symmetry becomes bigger and includes $B-L$ as a subgroup. It is well-known that the $B-L$ symmetry is also important in understanding the smallness of the neutrino mass; therefore is not a completely new symmetry custom-designed only to solve the R-parity problem. It is easy to see that in the symmetric phase of a theory containing $B-L$ local symmetry, R-parity is conserved since $R=(-1)^{3(B-L)+2S}$. This however is not the end of the story since the $B-L$ must be a broken symmetry at low energies and if the $B-L$ symmetry is broken by the vev of a scalar field which carries odd $B-L$, then R-parity is again broken at low energies[16]. Examples of theories where R-parity is broken by such fields abound- the string inspired $SO(10)$ and E_6 being only two of them. On the other hand there are also many theories where $B-L$ is broken by fields with even $B-L$ values. In these models[17], R-parity

remains an exact symmetry, as is required if supersymmetry has to provide a cold dark matter particle. It remains to be seen whether these latter class of models can arise from some higher level compactification of superstring theories.

In this paper we focus on the first class of theories since it has been shown that they can arise from string theories in different compactification schemes. In this class of theories, R-parity breaking interactions arise once $B-L$ symmetry is broken. It is then easy to see that to suppress the R-parity breaking interactions to the desired level, $B-L$ breaking must occur at an intermediate scale[18] than at the GUT scale as is quite often done. The reason why all this is of interest to us is that while pure lepton number violating processes in these classes of models are likely to be highly suppressed, the $\Delta B = 2$ processes such as neutron-anti-neutron oscillation may arise at an observable rate. To see what kind of restrictions on R-parity breaking couplings are implied by the present lower limits on $N-\bar{N}$ transition time, let us start by writing down the general structure of R-parity violating interactions in the MSSM:

$$W_{RP} = \lambda_{ijk} L_i L_j e^c_k + \lambda'_{ijk} Q_i L_j d^c_k + \lambda''_{ijk} u^c_i d^c_j d^c_k \tag{5}$$

The coupling relevant in the discussion of neutron-anti-neutron oscillation is the λ''[19]. Due to the color structure of the coupling, it cannot lead to $N-\bar{N}$ oscillation in the tree level and one has to invoke electroweak loop effects. This has been studied in detail in the recent paper of Goity and Sher[20]. They conclude that the dominant contribution arises from the $u^c d^c b^c$ type coupling in conjunction with a box diagram that changes $dd \rightarrow bb$ and has the strength (see Fig.2):

$$G_{N-\bar{N}} = \frac{6\alpha^2_{wk} m_{\tilde{W}} m^2_b V_{ub} \tilde{V}_{ub} \lambda''^2_{123}}{M^8_{\tilde{b_L}}} GeV^{-5} \tag{6}$$

The V_{ub} and $\tilde{V}_{ub}$ above refer to the ub mixing angles in the quark and squark sector. The rest of the notation is self explanatory. The value of $\tilde{V}_{ub}$ is not known. In order to estimate the transition time for neutron-anti-neutron oscillation, we have to multiply by the wave function effect i.e. $|\psi(0)|^2$:

$$\delta m_{N-\overline{N}} = G_{N-\overline{N}} |\psi(0)|^2 \ GeV \tag{7}$$

Using the value for $|\psi(0)|^2 \simeq 3 \times 10^{-4} \ GeV^6$ from Ref.[12], we get

$$\delta m_{N-\overline{N}} \simeq 5 \times 10^{-22} \lambda''^2_{123} \left(\frac{100GeV}{M_{sq}}\right)^6 GeV \tag{8}$$

The ILL lower bound on $\tau_{N-\bar{N}} \geq .8 \times 10^8$ sec. can be translated into an upper bound on $\lambda''_{123} \leq 4 \times 10^{-6}$. There are uncertainties in this estimate coming from the value of squark mixings as well as the values of squark masses. Our goal will be to seek grand unified theories where values of λ'' in the general ball-park 10^{-6} to 10^{-7} are predicted so that one may confidently argue that those models provide a good motivation for carrying out the neutron oscillation experiment.

We will be guided in our choice of the models by the heterotic superstring theory compactified either fermionically or via the Calabi-Yau manifolds. It turns out that complete breakdown of the gauge symmetry in these cases automatically imply that R-parity, which is an exact symmetry above the GUT scale breaks down. Our goal will be to study the prediction of the strength R-parity violating interactions in these models consistent with the idea of gauge coupling unification. We will discuss two classes of theories: one based on the gauge group $SO(10)$ and another on $[SU(3)]^3$. In both cases we will restrict ourselves to only those Higgs representations allowed by the superstring compactification guidelines.

V. Spontaneous breaking of R-parity in string inspired $SO(10)$ model:

In the $SO(10)$ model, the matter fields belong to the spinor **16**-dimensional representations whereas the Higgs fields will belong to **45**, **54**, **16**+$\overline{\mathbf{16}}$ **10**-dim representations as is suggested by recent studies of level two models[21]. The symmetry breaking in these models is achieved as follows: The vev of the **45** and **54**-dim fields break the $SO(10)$ symmetry down to $SU(3)_c \times SU(2)_L \times SU(2)_R \times U(1)_{B-L}$ which is broken down to the standard model by the $\tilde{\nu^c}$ component of **16**+$\overline{\mathbf{16}}$ acquiring vevs. The question we now ask is what is the strength of $\Delta B = 1$ R-parity violating terms at low energies. Since the $\tilde{\nu^c}$ field has $B - L = 1$, it will induce the $\Delta B = 1$ terms at low energies. First point to note that they do not arise from renormalizable terms in the Lagrangian but rather only from the mass suppressed nonrenormalizable terms in the $SO(10)$ model. This imlies that they are automatically suppressed. The relevant terms are of the form $\mathbf{16}_H\mathbf{16}_m\mathbf{16}_m\mathbf{16}_m/M_{Pl}$. When $\tilde{\nu^c}$ vev is turned on, these type of terms lead to terms of type QLD^c, LLE^c as well as $U^cD^cD^c$. Their strength will be given by $\langle\tilde{\nu^c}\rangle/M_{Pl}$ and will therefore depend on the scale of $B - L$ breaking, which in turn is tied with the gauge coupling unification. Important point to note is that all the above terms have the same strength as a result of which a combination of the QLD^c and the $U^cD^cD^c$ terms at the tree level will lead to proton decay with strength $\simeq \frac{\alpha_W m_{\tilde{w}}}{4\pi M^2_{\tilde{q}}} \left(\frac{\langle\nu^c\rangle}{M_{Pl}}\right)^2$. The present limits then imply that $\langle\nu^c\rangle/M_{Pl} \leq 10^{-12}$.

This automatically implies that the effective λ'' type terms are also of this order leading to unobservable amplitudes for $N-\bar{N}$ transition.

VI. Observable $N-\bar{N}$ oscillation in $[SU(3)]^3$ model:

Let us now turn to the superstring inspired $[SU(3)]^3$ type models. The matter multiplets in this case belong to representations $\psi \equiv (\mathbf{3},\mathbf{1},\mathbf{3})$, $\psi^c \equiv (\mathbf{\bar{1}},\mathbf{\bar{3}},\mathbf{\bar{3}})$ and $F \equiv (\mathbf{\bar{3}},\mathbf{3},\mathbf{1})$ representations. The particle content of these representations can be given by: $\psi = (u,d,g)$, $\psi^c = (u^c,d^c,g^c)$,

$$F = \begin{pmatrix} H_u^0 & H_d^+ & e^+ \\ H_u^- & H_d^0 & \nu^c \\ e^- & \nu & n^0 \end{pmatrix} \tag{9}$$

ψ and ψ^c denote the quark multiplets and F denotes the leptonic multiplets. The Higgs fields will belong to F-type representations and will be denoted by H and $\bar{H}$ respectively. The gauge invariant couplings are then given as in the following superpotential:

$$f\psi\psi^c H + f'(\psi\psi\psi + \psi^c\psi^c\psi^c) + f''\psi\psi^c F + h_1 F^3 + h_2 H^3 + h_3 \bar{H}^3 + ... \tag{10}$$

where we have suppressed the generation indices. These terms are of course enormalizable. Again as in the case of the SO(10) model, the R-parity violating terms arise once the $\tilde{\nu_H^c}$ vev is inserted in the above operators. Again, as before, $\Delta B \neq 0$ terms will be induced by purely renormalizable terms thru tree diagrams of type shown in Fig.3. They lead to $u^c d^c d^c$ type terms[22] . It is these type of terms that are dominant and their strength can be estimated to be $ff'\langle\tilde{\nu^c}\rangle/\langle n^0\rangle$. The strength of $\Delta B \neq 0$ R-parity violating terms are dictated by gauge coupling unification.

Let us now see the constraints of proton decay on the couplings in this model. To see this, let us recall the superpotential in the above equation. Note that proton decay involves the couplings $f'f''$ whereas $\Delta B = 1$ non-leptonic terms involve ff'. Therefore unlike the SO(10) case, the two processes are decoupled from each other and we can suppress proton decay by imposing a symmetry that forbids the f'' term but not the f or f' terms.

Let us now proceed to discuss the constraint of gauge coupling unification on the $B-L$ breaking scale in these models. It turns out that if we assume that $[SU(3)]^3$ breaks down to $SU(3)_c \times SU(2)_L \times SU(2)_R \times U(1)_{B-L}$ at the GUT scale by the vev of the n^0 field, the spectrum of particles below it is same as for the $SO(10)$

case. We keep one additional color octet multiplet below M_U. The one and two loop unification in this case have been studied recently[23] and the result is that one finds $M_U \simeq 10^{18}$ GeV and $M_{B-L} \simeq 10^{13}$ GeV or so. The one loop unification graph is shown in Fig.4. We see from the discussion in the above sections that operators of type $u^c d^c d^c$ are induced with strength of order λf where $\lambda \simeq 10^{-5}$ as determined by the unification analysis and f is an unknown parameter (which could be assumed to be of order 10^{-1}). This leads to $\lambda'' \simeq 10^{-7}$ or so. It can lead to observable neutron-anti-neutron oscillation with $\tau_{N-\bar{N}}$ of order 10^{10} sec. We hasten to note that due to the unknown coupling f in the six-quark superfield operator, we cannot make an exact prediction; but given the uncertainties in the parameters, the neutron-anti-neutron oscillation time could be somewhere between 10^8 to 10^{10} sec. This is clearly accssible to the proposed Oak Ridge experiment which plans to search for neutron-anti-neutron oscillation upto a sensitivity of 10^{10} to 10^{11} sec.[8]. This should therefore throw light on the nature of this class of grand unified theories.

VII. Baryogenesis in the $[SU(3)]^3$ model:

In the section we present a brief outline of a scenario for baryogenesis in the $[SU(3)]^3$ model discussed above. The reason for this is that the nature of the selection rule for baryon number non-conservation and the possibility of baryogenesis in the early universe are intimately linked. Very crudely this connection can be stated as follows: the higher the dimensionality of the $\Delta B \neq 0$ operator, the lower is the temperature of its thermodynamic decoupling from the rest of the universe. Since before the decoupling temperatures is reached such processes can always erase any preexisting baryon asymmetry, there is a close connection between the mechanism for baryogenesis and the nature of baryon non-conservation. Clearly, since the N-$\bar{N}$ transition operator has dimension nine, it remains in equilibrium to very low temperatures and one must be careful.

We contemplate the following scenario for baryogenesis, where the lepton asymmetry of the universe is generated at temperatures of order 10^9 GeV or so below the temperature for inflation reheating. This lepton symmetry is converted to the baryon asymmetry due to sphaleron effects [24] as suggested in Ref.[25]. We now have to make sure that the $\Delta B = 1$ interaction is out of thermal equilibrium during the time when the sphalerons active in transforming the lepton number into baryon number i.e. from 10^9 GeV down to 100 GeV. In Fig.5, we have plotted the rates for the $\Delta B = 1$ process and the Hubble expansion rates for various values of the λ'' coupling. It appears that only for $\lambda'' \leq 10^{-7}$ or so, the conditions are favorable for baryogenesis. One could also treat this as a crude upper bound on the

magnitude of the $\Delta B = 1$ interaction from the baryogenesis consideration. This corresponds to a $\tau_{N-\bar{N}} \simeq 10^{10}$ sec. It is interesting that this is the range being expected from $[SU(3)]^3$ type theories and is also measurable in the $N - \bar{N}$ experiment being planned.

VIII. Conclusion:

In conclusion, it is clear that a dedicated search for neutron-anti-neutron oscillation to the level of 10^{10} sec sensitivity is going to prove extremely valuable in our understanding of physics beyond the standard model. A non-zero signal would rule out many grand unified theories such as the simple non-supersymmetric $SU(5)$ and E_6, supersymmetric $SO(10)$ models etc. and will be a strong indication in favor of a string inspired supersymmetric E_6 or $[SU(3)]^3$ type model. A negative signal to this level would imply restrictions on the baryogenesis scenarios and the accompanying particle physics models. A positive signal would also yield valuable information on the violation of equivalance principle between particle and anti-particle.

I would like to thank the Oak Ridge National laboratory for hospitality during the workshop.

References

[1] R. E. Marshak and R. N. Mohapatra, Phys. Lett.**91B**, 222 (1980).

[2] S. Weinberg, Phys. Rev. Lett. **43**, 1566 (1979); F. Wilczek and A. Zee, Phys. Rev. Lett. **43**, 1571 (1979).

[3] M. Baldo-ceolin et al, Padova preprint DFPD 94/EP/13.

[4] J. Stone, talk at this conference.

[5] D. Cline, talk at this conference.

[6] R. N. Mohapatra, Nucl. Instr. and Methods in Phys. Research, **A284**, 1 (1989).

[7] W. Alberico, these proceedings; J. M. Richard, these proceedings.

[8] see Y. Kamyshkov, these proceedings.

[9] J. C. Pati and A. Salam, Phys. Rev. **D10**, 275 (1974); R. N. Mohapatra and J. C. Pati, Phys. Rev. **D11**, 566, 2558 (1975); G. Senjanovic and R. N. Mohapatra, Phys. Rev. **D12**, 1502 (1975).

[10] A. Davidson, Phys. Rev. **D20**, 776 (1979).

[11] R. N. Mohapatra and R. E. Marshak, Phys. Rev. Lett. 44, 1316 (1980).

[12] J. Pasupathy, Phys. Lett. **114B**, 172 (1982); S. P. Misra and U. Sarkar, Phys. Rev. **D28**, 249 (1983); S. Rao and R. Shrock, Phys. Lett. **116B**, 238 (1982).

[13] R. N. Mohapatra, *Unification and Supersymmetry*, Springer-Verlag, (Heidelberg, 1992), second edition.

[14] D. Chang, R. N. Mohapatra, J. Gipson, R. E. Marshak and M. K. Parida, Phys. Rev. **D31**, 1718 (1985).

[15] C. S. Aulakh and R. N. Mohapatra, Phys. Lett. **119B**, 136 (1982); F. Zwirner, Phys. Lett. **132B**, 103 (1983); L. Hall and M. Suzuki, Nucl. Phys. **B231**, 419 (1984). For a review, see V. Barger, G. Giudice and T. Han, Phys. Rev. **D40**, 2987 (1989); for constraints from cosmological considerations, see B. Campbell, S. Davidson, J. Ellis and K. A. Olive, Phys. Lett. **B256**, 457 (1991).

[16] R. N. Mohapatra, Phys. Rev. **D34**, 3457 (1986); A. Font, L. Ibanez and F. Quevedo, Phys. Lett. **B228**, 79 (1989).

[17] S. P. Martin, Phys. Rev. **D46**, 2769 (1992); R. Kuchimanchi and R. N. Mohapatra, Phys. Rev. **D48**, 4352 (1993); R. N. Mohapatra, hep-ph/9601203; Dae-Gyu Lee and R. N. Mohapatra, Phys. Rev. **D51**, 1353 (1995).

[18] D. G. Lee and R. N. Mohapatra, Phys. Rev. **D52**, 4125 (1995); B. Brahmachari and R. N. Mohapatra, Phys. Lett. **B357**, 566 (1995).

[19] F. Zwirner, Ref.[15].

[20] J. Goity and M. Sher, Phys. Lett. **B346**, 69 (1995).

[21] S. C. Choudhuri, S. Chung and J. Lykken, Fermilab-Pub- 94/137-T; For a recent review, see K. Dienes, Phys. Rep. (to appear).

[22] R. N. Mohapatra and J. W. F. Valle, Phys. Rev. **D34**, 1436 (1986).

[23] M. Bastero-Gil, B. Brahmachari and R. N. Mohapatra, (to appear).

[24] V. Kuzmin, V. Rubakov and M. Shaposnikov, Phys. Lett. **191B**, 171 (1987); for a review, see A. Cohen, D. Kaplan and A. Nelson, Ann. Rev. Nucl. Part. Sc. **43**, 27 (1993).

[25] M. Fukugita and T. Yanagida, Phys. Lett. **174B**, 45 (1986).

Table 1

GUT model	Is $N-\bar{N}$ observable?	Implications
(NON SUSY)		
$SU(5)$	No	$\Delta(B-L)=0$
$SU(2)_L \times SU(2)_R \times SU(4)_c$	Yes	$M_c \simeq 10^5$ GeV
Minimal SO(10)	No	
E_6	No	
(SUSY GUT)		
$[SU(3)]^3$	Yes	Induced breaking of R-parity
$SO(10)$	No	

Table Caption: This table summarizes the observability of neutron-anti-neutron oscillation in various GUT models.

Figure Caption:

Fig 1: The Feynman diagram that leads to $N-\bar{N}$ oscillation in the $SU(2)_L \times SU(2)_R \times SU(4)_c$ model.

Fig 2: The diagram responsible for $N-\bar{N}$ oscillation in models with R-parity breaking.

Fig 3: The origin of the $u^c d^c d^c$ vertex in $[SU(3)]^3$ type model at low energies.

Fig 4: The running of gauge couplings in the one loop approximation in models with intermediate scales and unification at the string scale.

Fig 5: The comparision of the rates for baryon number violating processes in R-parity broken models with the Hubble expansion rate.

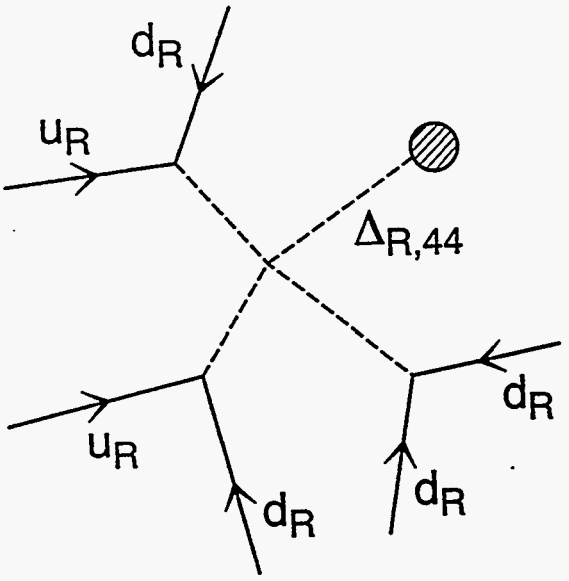

Fig. 1

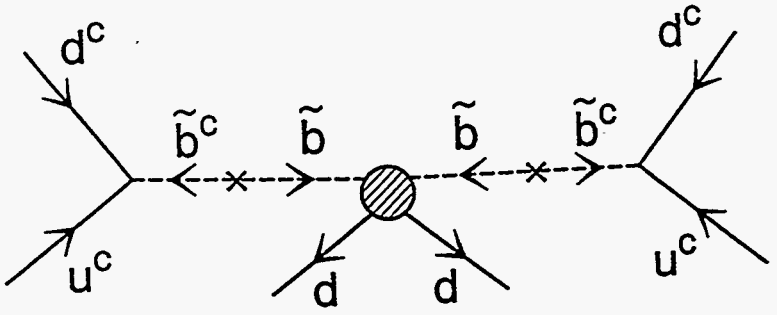

Fig. 2

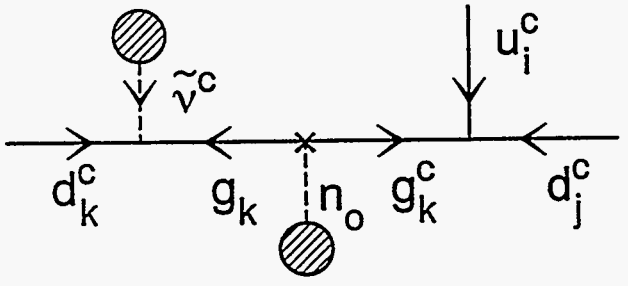

Fig. 3

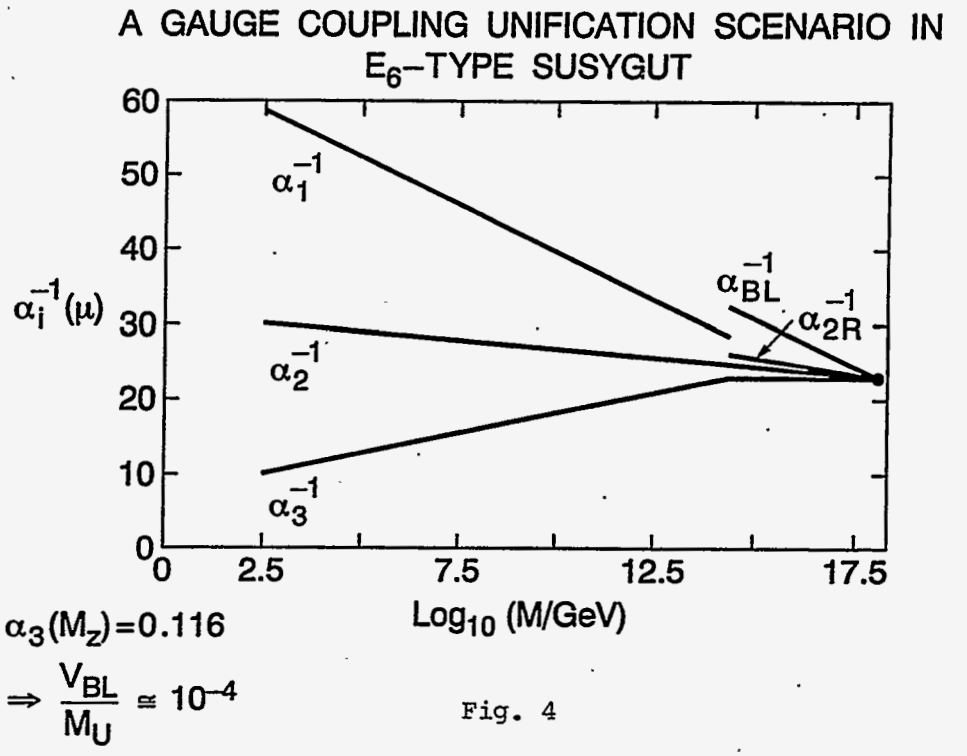
A GAUGE COUPLING UNIFICATION SCENARIO IN
E6–TYPE SUSYGUT
60
50
40
30
20
10
0
$\alpha_i^{-1}(\mu)$
α_1^{-1}
α_2^{-1}
α_3^{-1}
α_{BL}^{-1}
α_{2R}^{-1}
0
2.5
7.5
12.5
17.5
Log_{10} (M/GeV)
$\alpha_3(M_Z)=0.116$
$\Rightarrow \frac{V_{BL}}{M_U} \cong 10^{-4}$

Fig. 4

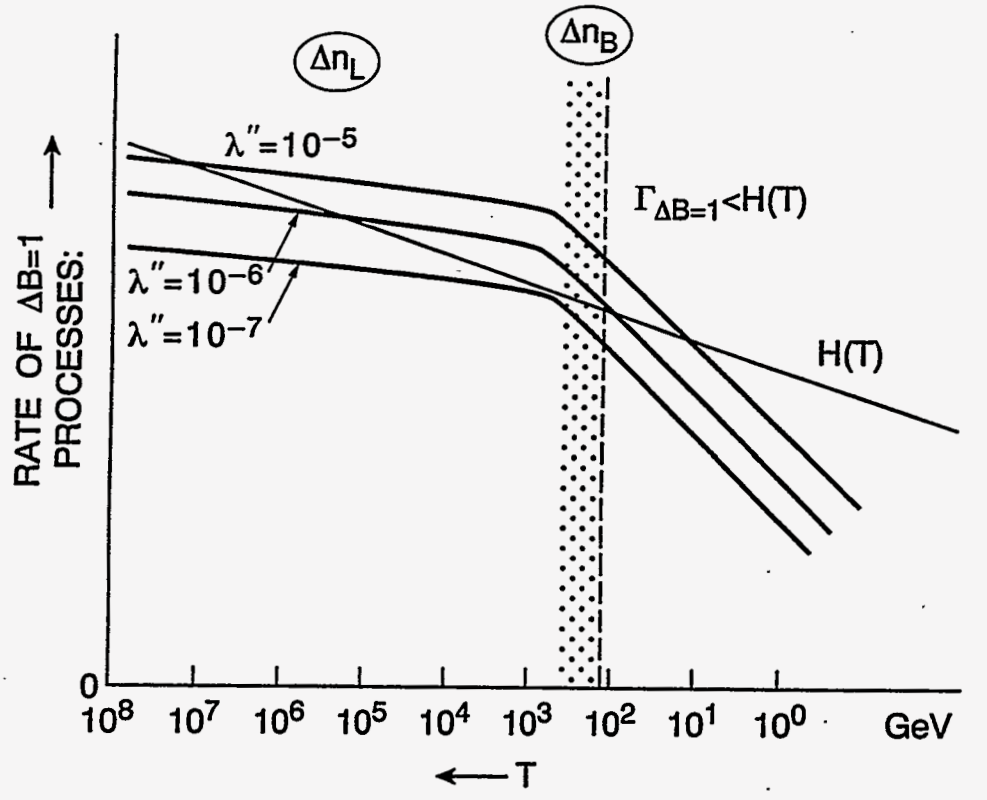
Δn_L
Δn_B
$\lambda''=10^{-5}$
$\Gamma_{\Delta B=1}<H(T)$
$\lambda''=10^{-6}$
$\lambda''=10^{-7}$
H(T)
RATE OF ΔB=1 PROCESSES:
0
10^8 10^7 10^6 10^5 10^4 10^3 10^2 10^1 10^0 GeV
T

Fig. 5

MIGHT FAST B-VIOLATING TRANSITIONS BE FOUND SOON?

Vadim A. Kuzmin

Institute for Nuclear Research of Russian Academy of Sciences,
60th October Anniversary Prosp. 7a, Moscow 117312, Russia
and
Max-Planck-Institut fuer Physik
Foeringer Ring 6, 80805 Muenchen, Germany

Abstract

We claim that there might exist a new interaction leading to very fast baryon-number violating processes quite observable in the laboratory conditions.

1. Baryon-Antibaryon Mixings and Oscillations.

It was conjectured few years ago [1] that there could take place very fast baryon-number violating transitions with quite observable rates which however escaped observation up to now due to some specifics of the interaction. Specifically, it was conjectured [1] that there could be a baryon-number violating coupling originating in particles of electroweak masses and coupling strengths, provided all three generations are simultaneously involved. An example of what I am talking about is given by the coupling

$$\epsilon_{ijk}\lambda\phi_i q_j q_k, \tag{1}$$

ϕ being color-triplet scalar fields, q being right-handed quark fields, λ being the coupling constant and $i,j,k = 1,2,3$ are family indices. Note that the corresponding scalar fields are quite generic in the context of any GUT. Being interested in various aspects of baryon- antibaryon mixings and oscillations, I exhibited special interest in the Ξ_b (bus) baryon as the lightest one composed of quarks of all three generations which might undergo a lot of mixing with its antiparticle (see Fig. 1).

By rapid transitions $(bus) \leftrightarrow (\bar{b}\bar{u}\bar{s})$ I mean that the transition time, $\tau_{bus\leftrightarrow\bar{b}\bar{u}\bar{s}}$, is not excluded to be of order of the weak decay lifetime,

$$\tau_{bus\leftrightarrow\bar{b}\bar{u}\bar{s}} \sim 10^{-13}s. \tag{2}$$

It does not seem that such couplings would result in problems with FCNC and/or hyperon $\leftrightarrow$ anti-hyperon transitions. It seems that the most stringent constraints on the magnitude of the coupling under consideration come from results of experimental searches of matter instability (proton decay, neutron-antineutron transitions in nuclei and in vacuum). However, what I am going to conjecture now, is the following. Remarkably enough, neutron-antineutron transitions originating from radiative electroweak corrections to the proposed interaction Fig. 1 being

tremendously suppressed in comparison with $(bus) \leftrightarrow (\bar{b}\bar{u}\bar{s})$ transitions by factor $\sim (G_F^2)^2 \sim 10^{-20}$ might be well in the right range for experimental searches, with

$$\tau_{n \leftrightarrow \bar{n}} \sim 10^7 - 10^8 s. \tag{3}$$

Thus, fast enough baryon-number violating transitions might be looked for both by investigation of wrong signature weak decays of (bus)-like baryons and by searches of $n\bar{n}$ transitions.

2. A Speculation on ALEPH Events.

One may speculate on a possible relation of the assumed existence of these new scalars ϕ mediating baryon-number violating transitions to presumably observed recently 4-jet events by ALEPH. Such features of ALEPH events as no missing energy, absence of b-quarks in jets, relatively large yield in comparison with expectations might be easily understood in the framework of our hypothesis. Indeed, our colored scalars ϕ are coupled to quarks only and not to leptons. Second, if a pair of produced particles (with masses 55 GeV), giving two jets after their decay, is assumed to be a pair of ϕ's with the family index $j = 3$, then one should not expect b-quarks in jets at all. Finally, if there is indeed some excess in number of events observed, it might be explained by large electric charge of some of ϕ's.

3. Conclusions.

New rich physics might be well quite nearby! Searches are worthwhile both at accelerators and in low energy experiments and may proceed in several directions. Among them are, obviously, the following ones.

1. Production of pairs $\phi\bar{\phi}$ at hadron and electron colliders (in experiments like ALEPH).

2. Production of (bus)-like baryon-antibaryon pairs, say, at e^+e^- colliders, and search for wrong signature decays of produced baryons and antibaryons. Wrong signature is due to baryon-antibaryon mixing.

3. Search for $n\bar{n}$ oscillations in free neutrons beam. It might be well that even present sensitivity is already almost sufficient and we are close to observation of this phenomenon. 4. Search for induced matter instability.

The proposed new interaction might have a deep impact on generation of the baryon asymmetry of the Universe.

Acknowledgements.

I am grateful to J.D. Bjorken, S. Pokorski, L. Stodolsky and V. Zakharov for many encouraging discussions and comments and to I. Tkachev for his stimulating interest in the work and enlightening discussions. I am grateful to Yu. Kamyshkov for his interest, enthusiasm and hospitality extended to me in Oak Ridge.

References

[1] V. Kuzmin (1991),private communication to J.D. Bjorken, see: J.D. Bjorken, What Lies Ahead, preprint SLAC-PUB-5673, Oct. 1991, 13 p.p. In : *Corpus Christi 1991, Proceedings, Superconducting Super Collider* 653-665, invited talk given at 1991 Symp. on the SSC: The Project, the Progress, the Physics, Corpus Christi, TX, Oct 13-17, 1991. Published in SSC Symposium 1991: 651-665 (QCD184:S7:1991).

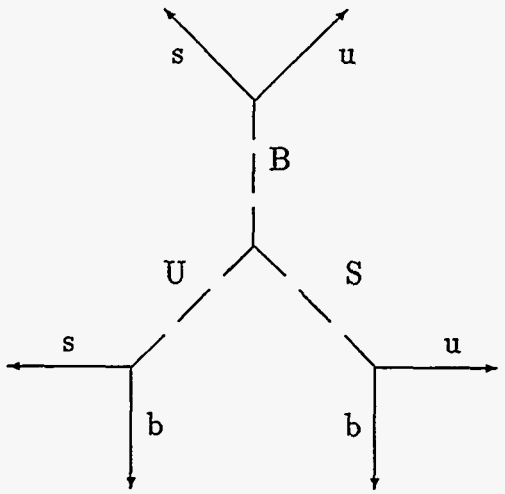

Fig. 1. $(bus) - (\bar{b}\bar{u}\bar{s})$ coupling. The dashed lines are color-triplet scalar fields ϕ; the solid lines are right-handed quark fields.

ELECTROWEAK BARYOGENESIS AND ANTIMATTER

A. G. Cohen
Physics Department, Boston University
590 Commonwealth Ave., Boston, MA 02215 USA

Abstract

I describe the current status of electroweak baryogenesis, and comment on the possible existence of domains of antimatter in the Universe.

1 Introduction

Although the dominant components of the Universe remain a mystery, one thing seems clear: in the vicinity of our galaxy there are photons, a small amount of matter (baryons, electrons and neutrinos), but practically no antimatter. This asymmetry between matter (baryons) and antimatter (antibaryons) has given rise to speculation that the fundamental forces of nature might be baryon number violating, generating this asymmetry during the early history of the Universe, and eventually leading to this workshop. Of course it is possible that for some unknown reason the initial conditions for the Universe at or prior to the time of the big bang distinguish between matter and antimatter, but we wish to avoid invoking such conditions if at all possible. We will therefore assume that the Universe contains a matter-antimatter symmetric distribution of material at very early times which must evolve into the asymmetric distribution we observe today. There are two possibilities for this evolution: either the antimatter is everywhere destroyed, or it is somehow moved to or left in locations distant from our own galaxy. The

former possibility is usually referred to as "baryogenesis", while the latter is usually referred to as impossible. We will first discuss the status of baryogenesis and its implications for baryon violation detection, and subsequently remark on the theoretcial possibility of distant domains of antimatter.

2 Observations and Evalutations

In quantifying the size of this baryon asymmetry it is convenient to quote the ratio of the baryon density to the photon density (or sometimes the photon entropy). The reason for using this ratio is simple: the expansion of the Universe leads to a dilution of the baryon density, and thus this quantity by itself evolves even in the absence of any interactions. However the photon density dilutes in a similar fashion, and thus the ratio is unaffected by this cosmic expansion. (Note that photon entropy production, as occurs during the era of electron-positon decoupling, can also cause this ratio to evolve; in a careful quantitative analysis these changes can be taken into account to relate this ratio at early times to the value measured today). Quantitatively, a combination of direct observations and theoretical computations lead to a value for the ratio of the baryon number density to the photon density of a few times 10^{-10}; the theoretical input comes from our understanding of the synthesis of light nuclei in the early Universe which directly constrains the baryon to photon entropy ratio, while the experimental input comes from measuring the luminous material in the visible portion of the cosmos. If the Universe had initially contained equal numbers of baryons and antibaryons, the rapid baryon-antibaryon annihilation rate in the early Universe would lead to a value for this ratio some ten orders of magnitude smaller than this observed value.

If however the number of baryons exceeds the number of antibaryons by some small amount than annihilation can not be totally efficient: we can at best annihilate all the antibaryons, leaving a small residual number of antibaryons. If this excess of baryons over antibaryons is one part in 10^8 than the residual number of baryons after annihilation would be in agreement with the observed baryon to photon ratio. In order for such an excess to be generated from initially symmetric conditions in the early Universe three requirements, first articulated by Sakharov,[1] are necessary:

1. C and CP Violation.

2. Baryon Violation.

3. Departure from Thermal Equilibrium.

Qualitative discussions of baryogenesis typically begin by identifying possible sources for these three ingredients. More quantitative treatments must of course include a mechanism by which these three ingredients can interact to produce an asymmetry.

In the late 1970s and early 1980s the dominant candidates for the origin of these three ingredients were Grand Unified Theories. These theories typically include interactions, either through new gauge bosons or through new Higgs-like scalars, which violate baryon number. In addition the existence of these new particles (notably the new Higgs-like scalars) allows for the possibility of new CP violation. Thus these theories can easily accomodate the first 2 requirements. The third condition can also arise in the context of these theories by having a "late decaying particle", whose decay rate is much smaller than its mass; but this is non-trivial to realize at a sufficiently large level. It often requires some amount of fine tuning of parameters in order to obtain a baryon asymmetry as large as that which is observed. Discussions of experimental signatures for baryon violation have largely focused on these theories.

In the mid 1980s an alternative to Grand Unified baryogenesis was suggested by Rubakov, Kuzmin and Shaposhnikov.[2] They pointed out that even the Standard Model of weak interactions has the potential to give rise to all three of Sakharov's requirements. Although they were not able to describe a mechanism by which these three ingredients in the SM could interact to produce the asymmetry which we observe, this sparked the notion that known physics could account for the baryon asymmetry.

3 The Standard Model

The first of Sakharov's ingredients, C and CP violation, is well known to be satisfied both in nature and in the Standard Model: experimentally we have reactions such as the semi-leptonic decay of the long-lived neutral K meson:

$$\Gamma(K_L^0 \to \pi^+ e^- \bar{\nu}) \neq \Gamma(K_L^0 \to \pi^- e^+ \nu) \tag{1}$$

while theoretically the $SU(2) \times U(1)$ theory of the weak interactions along with the phase θ_{CKM} in the CKM matrix is the origin of C and CP violating processes.

Although less widely recognized, and unverified experimentally, the standard model also contains baryon number violating interactions. As was first realized by t'Hooft,[3] just as barrier penetration in non-relativistic single-particle quantum mechanics can give rise to classically forbidden effects, similar non-perturbative quantum effects in the $SU(2) \times U(1)$ theory of the weak interactions allow transitions between states of differing baryon number. These effects are suppressed by a typical semi-classical tunneling factor, $\exp(-2\pi/\alpha) \sim 10^{-110}$ and are therefore too small to be obvserved laboratory in any laboratory experiment. In addition the symmetries of such processes restrict all such transitions to change baryon number by 3 units, which excludes porcesses like proton decay or neutron-antineutron oscillations. However at high temperatures there is no need to tunnel through any barrier, as thermal fluctuations will allow transitions over the *top* of any potential impediments. These are characterized by a Boltzmann rather than a semi-classical factor, $\exp(-E_s/T)$, where $E_s \sim M_Z/\alpha_{wk}$ is the barrier height. At sufficiently high temperature this factor ceases to be small, and baryon violating interactions can proceed at a reasonable rate.

The last ingredient, departure from thermal equilibrium, follows also from the standard model of weak gauge interactions. At laboratory temperatures these interactions are in a (weak) superconducting phase, accounting for the short range nature of weak forces via the Higgs mechanism. But at a high temperatures (expected to be about 100 GeV) these interactions should undergo phase transition to the unbroken (or "normal") phase in which the W and Z bosons are massless (along with the quarks and leptons which get their masses from electroweak symmetry breaking as well). In this phase the barrier preventing baryon violating transitions has disappeared altogether, leaving a rate per unit volume for baryon violating processes characterized by $\alpha_{wk}^4 T^4$. This phase transition can provide a source of non-equilibrium physics satisfying the last of Sakharov's conditions. Whether or not this is so depends on the details of the transition: if it is second order, particle masses and reaction rates vary smoothly during the phase transition, and no large non-equlibrium effects are present. If the transition is first order however, then the Higgs vev will be discontinuous at the transition, and may give rise to large non-equlibirum effects.

Having recognized that the standard model (and consequently any exten-

sion of the standard model) contains the necessary components for baryogenesis, the remaining question is how and if these ingredients can in fact interact in a way to produce the observed baryon asymmetry.

4 Electroweak Baryogenesis

Cohen, Kaplan and Nelson[4] have suggested a means by which the presence of CP violation may be communicated to baryon violating interactions in a non-equilibrium way which would give rise to a baryon asymmetry. This mechanism relies on the existence of an epoch in which regions of broken electroweak symmetry coexist with regions of unbroken electroweak symmetry, separated by phase boundaries (this would be the case for a classic first order phase transition that proceeds through nucleation of bubbles of the low-temperature phase as the Universe cools). From the discussion of baryon violation in the standard model we see that this also means that baryon violation will occur rapidly in the unbroken phase regions, while in the broken phase regions baryon violation is effectively shut off, provided the symmetry breaking (and hence the W and Z boson masses) is sufficiently large. The spatial separation of domains where baryon violation is rapid and domains where it is slow provides the connection between non-equilibrium physics and baryon violation necessary for baryogenesis.

The last ingredient, CP violation, typically arises through couplings of fermions (like the quarks and leptons). Fermions typically become massive only through the effects of electroweak symmetry breaking (this is the case for quarks, leptons and many fermions in extensions of the standard model), and consequently they can interact strongly with the phase boundaries that appear at the electroweak phase transiton; these interactions will in general be CP violating, and can have a large CP violating effect on the distributions of fermions in the neighborhood of these phase boundaries. Thus this provides a connection between CP violation and the non-equilibrium physics of the phase transition. Once the distributions become affected in the vicinity of these phase boundaries, the fermions can communicate the effects of CP violation to the baryon violating interactions which are occurring rapidly in the unbroken phase. Although complicated to compute in detail, the baryon asymmetry produced can be qualitatively summarized by the simple formula:

$$\frac{n_b}{n_\gamma} \sim \frac{\alpha^4}{100}\,\delta_{CP}$$

where δ_{CP} is an invariant measure of the size of CP violation.

5 The Standard Model (again)

Although the standard model (and by this we mean the model based on an $SU(2) \times U(1)$ gauge theory of three families of quarks and leptons with a single Higgs doublet) possesses the ingredients outlined in the previous section, it has two difficulties which prevent the generation of the observed baryon asymmetry entirely within the context of this model.

Firstly, in order for baryon violation to be effectively shut off in the regions of broken symmetry the phase transition must be rather strongly first order. Calculations[5,6] as well as lattice simulations[6–8] suggest that this happens only for Higgs masses lighter than current experimental bounds permit.

Secondly, the invariant size of CP violation in the standard model is quite small—note that CP violation is absent in this model if any two up type or down type quarks are degenerate in mass, or if any family mixing angles vanish. The result is that the parameter δ_{CP} is approximately 10^{-10}, which yields a baryon asymmetry nearly ten orders of magnitude smaller than the observed value.

Although a possible enhancement over this basic estimate has been suggested,[9] careful calculations indicate that the naïve estimate is essentially correct,[10–13] and the standard model is unlikely to be capable of producing the observed asymmetry.

Fortunately, almost any extension beyond this restrictive definition of the standard model has the potential for a more strongly first order phase transition, as well as substantial new CP violation. Examples of such extensions include essentially all popular models of electroweak symmetry breaking, such as multi-Higgs doublet models, Supersymmetric models, neutrino-mass models and Technicolor.

6 Antimatter

Our previous discussion has described a possible means for an initially baryon symmetric Universe to develope the asymmetry we believe exists in our local neighborhood. Although this asymmetry is typically assumed to be uniform throughout the entire Universe, the direct experimental evidence for this is

rather weak.

The observational constraints on domains of antimatter (regions in which baryogenesis produced not an excess of matter but instead an excess of *antimatter*) are carefully reviewed in the work of Steigman.[14] The conclusion is that within our local cluster (a distance of about 20 Mpc) very little antimatter is possible. However on distance scales larger than this, domains of antimatter are not excluded. For reference note that the Hubble size today is approximately two orders of magnitude larger than this minimum domain size.

Experimental searches for such domains are currently being discussed. If some of the cosmic rays we observe originated outside our local cluster of galaxies, then we would expect that some fraction of these cosmic rays should contain antimatter. The AMS experiment is designed to look for antinuclei in cosmic rays using a magnetic spectrometer placed in orbit above the earth.

Previous analyses of the viability of such domains have focused on high energy gamma rays produced in the regions of overlap between domains today. These results exclude such domains to a distance of approximately the size of clusters today, 20 Mpc. However if such regions do exist, they would have a significant impact on the evolution of the *early* Universe and might give rise to several other possible signatures. They would, for example, give rise to a diffuse gamma-ray background from the matter-antimatter annihilations that would have taken place near the domain boundaries in the early Universe; these high enery gammas would subsequently redshift and give rise to low energy gammas or X rays today. The high energy charged particles produced in matter-antimatter annihilations could also give rise to non-thermal distortions of the cosmic microwave background radiation

In recent work by various combinations of Cohen, De Rújula, Glashow and Gavela[15,16] , these constraints have been examined to determine whether a cosmology of this sort is still acceptable in view of recent measurements of the cosmic microwave background and the diffuse gamma ray background.

Although these computations are not yet complete, preliminary indications are that domains whose size today is smaller than the current Hubble size would give rise to an unacceptably large gamma ray background.

References

[1] A. D. Sakharov. *JETP Letters*, 5:24, 1967.

[2] V.A. Kuzmin, V.A. Rubakov, and M.E. Shaposhnikov. *Physics Letters B*, 155:36, 1985.

[3] G. t'Hooft. *Physical Review D*, 14:3432, 1976.

[4] A.G. Cohen, D.B. Kaplan, and A.E. Nelson. In J.D. Jackson, editor, *Annual Review of Nuclear and Particle Science*, volume 43, pages 27–70. 1993.

[5] M. Dine, R. Leigh, P. Huet, A. Linde, and D. Linde. *Physical Review D*, 46:550, 1992.

[6] M. Shaposhnikov. *Physics Letters B*, 316:112, 1993.

[7] K. Kajantie, K. Rummukainen, and M. Shaposhnikov. *Nuclear Physics B*, 407:356, 1994.

[8] K. Farakos, K. Kajantie, K. Rummukainen, and M. Shaposhnikov. *Physics Letters B*, 336:494, 1994.

[9] G. Farrar and M. Shaposhnikov. *Physical Review Letters*, 70:2833, 1993.

[10] M. Gavela, P. Hernandez, J. Orloff, and O. Pene. *Modern Physics Letters A*, 9:795, 1994.

[11] M. Gavela, P. Hernandez, J. Orloff, and O. Pene. *Nuclear Physics B*, 430:345, 1994.

[12] M. Gavela, P. Hernandez, J. Orloff, O. Pene, and C. Quimbay. *Nuclear Physics B*, 430:382, 1994.

[13] P. Huet and E. Sather. *Physical Review D*, 51:379, 1995.

[14] G. Steigman. In *Annual Review in Astronomy and Astrophysics*, volume 14, page 339. 1976.

[15] A.G. Cohen, A. De Rújula, and S.L. Glashow. in preparation.

[16] A.G. Cohen, A. De Rújula, and M.L. Gavela. in preparation.

Antimatter in Different Baryogenesis Scenarios

A.D. Dolgov
Teoretisk Astrofysik Center
Juliane Maries Vej 30, DK-2100, Copenhagen, Denmark
and
ITEP, Bol. Cheremushkinskaya 25, Moscow 113259, Russia.

Abstract

Possible mechanisms of abundant creation of antimatter in the universe are reviewed. The necessary conditions for that are: baryonic charge nonconservation, spontaneous breaking of charge symmetry or nonequilibrium initial state, and the formation of appropriate initial conditions during inflation. In this case the universe may be populated with domains, cells, or even stellar size objects consisting of antimatter.

1 Introduction

The problem that I am going to discuss is not directly related to the subject of this conference dedicated to experimental search of baryon nonconservation. Still there is one thing in common, all models of cosmological creation of antimatter request nonconservation of baryonic charge. There may be of course a production of antibaryons by e.g. decays or annihilation of new long-lived heavy particles (like quasistable neutralinos of supersymmetric models) which may proceed with baryonic charge conservation or even production of antinucleons by energetic cosmic rays but this is not what is usually understood as creation of antimatter.

We know from observations that the universe in our neighborhood is 100% charge asymmetric. There are only baryons and electrons and no their antiparticles in a comparable amount. Though the asymmetry is large now, in some sense it is very small. The number density of baryons, N_B, relative the number density of photons in the cosmic microwave background radiation, N_γ is:

$$N_B/N_\gamma \approx 3 \times 10^{-10\pm0.3}, \tag{1}$$

This means that the universe was almost charge symmetric at high temperatures, $T > (a\,few) \times 100$ MeV. At these temperatures the excess of baryonic charge was approximately one unit per 10^9 baryons. Still though the ratio (1) is very small, it is 9 orders of magnitude larger than it would be in the case of locally charge symmetric universe. We do not know if all the universe is charge asymmetric with the same universal magnitude of the charge asymmetry or the charge asymmetry is point dependent and can even change its sign. Nothing is known about the size of these locally asymmetric domains, l_B. Existing data indicate that $l_B > 10$ Mpc. Whether l_B is above or below the present day horizon, $l_h = 10$ Gpc, is an intriguing question and in what follows I will discuss the models which predict a relatively small value of l_B, so that antimatter may be accessible to observations.

It is very important for all these models as well as for the planned experiments on search of baryon nonconservation to know if baryonic charge is indeed nonconserved. At the present time cosmology gives the only "experimental" and a very strong argument in favor of nonconservation of baryons. In other words our existence strongly implies baryon nonconservation. This is not just that the baryon asymmetry of the

universe can be generated only if baryonic charge is nonconserved as was suggested 25 years ago by Sakharov [1]. (For possible but rather exotic exceptions see review paper [2].) There is something more, namely that sufficiently long inflation could not go with conserved baryonic charge [3, 2]. Since it seems that without inflation is impossible to make a suitable for life universe we have to assume that baryons are indeed nonconserved. The argument goes as follows. For successful solution of cosmological problems[4] inflationary stage should last sufficiently long (for a review see e.g. books [5, 3]). The duration of inflation τ should be larger than 60 Hubble times, $H_I\tau > 60$, where H_I is the Hubble constant during inflation such that the scale factor, which describes the universe expansion, behaves as $a(t) \sim \exp(H_I t)$. One may say that in order to create the observed number density of baryons, the initial baryonic charge density at the onset of inflation should be unnaturally large, at least $e^{180}(T_{Rh}/2.7K)^3$ times larger than at the present day. Here 2.7K is the temperature of the cosmic microwave background radiation today and T_{Rh} is the temperature at the end of inflation. Such a large number is of course not natural but it does not mean impossible. What makes inflation with conserved baryons impossible is the energy density considerations. The Hubble parameter is expressed through the cosmological energy density density ρ as $H = \sqrt{8\pi\rho/3m_{Pl}^2}$. To make an exponential expansion the parameter H must be approximately constant. It implies that in this regime the energy density does not change with the expansion but remains constant too. It is indeed realized in models where inflation is driven by a scalar (inflaton) field. Let us assume now that baryons are conserved. In accordance with eq.(1) the energy density associated with baryonic charge at the hot early stage of the universe evolution is about $10^{-10} - 10^{-9}$ of the total energy density. Let us go backward in time to even earlier period, when inflation took place. At this stage the energy density of all forms of matter is represented by the inflaton and remains constant in the course of contraction (remember we are going backward in time). However the energy density associated with baryonic charge cannot be constant because by assumption this charge is conserved. Correspondingly it changes with the scale factor as $\rho_B \sim a^{-4}$. It means that in less than 6 Hubble times the energy density of baryons becomes dominant and the total energy density could not remain constant. Thus with conserved baryons inflation can be only very short, $H_I\tau \leq 6$, which is by far below the necessary duration.

Thus we must conclude that baryonic charge in our universe is not conserved and the direct experimental search of the proton instability or neutron-antineutron oscillations is not only just experiments for putting an upper bound but the experiments for discovery really existing phenomenon. Unfortunately cosmology does not say anything about the magnitude of the effect. It very much depends upon the mechanism of baryonic charge nonconservation and one should keep in mind that the mechanism through which the observed baryon asymmetry of the universe has been created is not necessarily the same that leads to the proton decay or neutron-antineutron oscillations. Theory opens several possibilities to break B-conservation with different levels of creditability. The standard $SU(2) \times U(1)$-electroweak interactions are known to break baryonic current conservation by the chiral quantum anomaly[6]. This is a rather strong theoretical prediction but unfortunately manifestations of this phenomenon in low energy physics are extremely weak, they are suppressed by the tunnel penetration factor $\exp(4\pi \sin^2\theta_W/\alpha) \approx 10^{-170}$. At high temperatures the effect may be grossly amplified and may explain the observed baryon asymmetry of the universe[7] (for the reviews see the talk by A. Cohen at this Conference or review papers[2, 8]). Fortunately there are plenty of other mechanisms of B-nonconservation, which do not necessarily operate at ultrahigh energies, as for example the GUT's one does. Some of them are so efficient at low energies that the direct observation of the effect is almost at hand and, as M. Goldhaber said at the beginning of this meet-

ing, one should rush to the laboratory and to make the discovery (unfortunately he referred to the unsuccessful attempts to find proton decay in the first generation experiments). Let us hope that the second generation will make it.

2 General conditions for cosmological creation of antimatter.

Why at all may we expect that there are macroscopically large domains of antimatter in the universe? There is no rigorous theory which requests that. Moreover in all simple models of baryogenesis the baryon asymmetry is a universal constant over all the universe so that there is no place for antimatter. On the other hand simple modifications of baryogenesis scenarios will result in formation of domains with different signs of baryon asymmetry. To this end the following two conditions should be satisfied:

1. Different signs of C and CP-violation in different space points.

2. Inflationary (but moderate) blow-up of regions with different signs of charge symmetry breaking.

The first condition is realized in the model of spontaneous breaking of charge symmetry[9]. It is assumed that the Lagrangian is charge symmetric but the ground state is not. It can be realized by a complex scalar field which acquires a nonzero vacuum expectation value like the one in the usual Higgs mechanism. The effective potential of this field may e.g. have the form:

$$U(\phi) = -m^2|\phi|^2 + \lambda(\phi^4 + \phi^{*4}) + g^2T^2|\phi|^2 \qquad (2)$$

where the last term came from the temperature corrections, which force the system to the symmetric state at high temperatures[10]. At low temperatures the state $\langle\phi\rangle = 0$ becomes energetically unfavorable and a complex condensate is developed which through Yukawa coupling would give rise to breaking of C and CP by e.g. complex fermion masses. One can see that through this mechanism domains with opposite signs of C(CP)-odd phase are indeed formed. In these domains either matter or antimatter is generated by baryogenesis[11]. The universe in this model is charge symmetric on the average and asymmetric locally.

There are two serious problems which this model encounters. First is that the average size of the domains is too small. If they are formed in the second order phase transition, their size at the moment of formation is determined by the so called Ginzburg temperature and is approximately equal to $l_i = 1/(\lambda T_c)$ where T_c is the critical temperature at which the phase transition takes place and λ is the selfinteraction coupling constant. In this case different domains would expand together with the universe and now their size would reach $l_0 = l_i(T_c/T_0) = 1/(\lambda T_0)$ where $T_0 = 2.7$K is the present day temperature of the background radiation. If the phase transition is first order then the bubbles of the broken phase are formed in the symmetric background. In this case different bubbles initially are not in contact with each other, typically the distance between them is much larger than their size, and their walls may expand faster than the universe, even as fast as the speed of light. Thus to the moment when the phase transition is completed the typical size of the bubbles may be as large as the horizon, $l_f \approx t \approx m_{Pl}/T_f^2$. After that they are stretched out by the factor T_f/T_0 due to the universe expansion. To make the present day size around (or larger than) 10 Mpc we need $T_f \sim 100$ eV. It is difficult (if possible) to arrange

that without distorting successful results of the standard cosmology. Thus to make observationally acceptable size of the matter-antimatter domains, a superluminous cosmological expansion seems necessary. This solution was proposed in ref.[12] where exponential (inflationary) expansion was assumed. With this expansion law it is quite easy to overfulfill the plan and to inflate the domains above the present day horizon. Effectively it would mean a return to the old charge asymmetric universe without any visible antimatter. So some fine-tuning is necessary which would permit to make the domain size above 10 Mpc and below 10 Gpc.

The second cosmological problem which may arise in this model is a very high energy density and/or large inhomogeneity created by the domain walls[13]. This can be resolved if domain walls were destroyed at later stage by the symmetry restoration at low temperature or by some other mechanism [14, 15]. However there could be scenarios of baryogenesis in which domains of matter-antimatter may be created without domain walls. The basic idea of these scenarios is that baryogenesis proceeds when the (scalar) field which creates C(CP)-breaking or stores baryonic charge is not in the dynamically equilibrium state. These models are described in more detail in the following sections.

3 Antimatter in models with baryonic charge condensate.

In supersymmetric theories there exist scalar fields with nonzero baryonic charge, superpartners of quarks. Such fields (more exactly the electrically neutral colorless combination of squarks and sleptons) may form a classical condensate in the early universe, in particular at inflationary stage, if there are the so called flat directions in the potentials. Subsequent decay of this condensate would result in a considerable baryon asymmetry[16]. The picture can be visualized as follows. Evolution of a complex spatially homogeneous scalar field is described by the same equation as two-dimensional motion of a point-like body in the same potential $U(Re\phi, Im\phi) \rightarrow U(x, y)$. Baryonic charge density is equivalent in this language to the angular momentum of the mechanical motion of the body. The potential typically has the form of eq.(2). It is spherically symmetric at small ϕ and asymmetric and has flat directions at large ϕ. So for small values of the amplitude of ϕ baryonic charge is conserved while evolution of ϕ with a large amplitude goes with a strong baryonic charge nonconservation. If the mass of ϕ is smaller than the Hubble parameter during inflation, the field would climb up the potential slope due to infrared instability of scalar fields in De Sitter spacetime[17, 18, 19]. When inflation ends the field ϕ would evolve down to the equilibrium value. Depending upon the initial conditions it may rotate clock-wise or anticlockwise near the origin or in other words it would produce baryons or antibaryons in its decay. One sees at this example that even in the charge symmetric theory baryon asymmetry may evolve; charge asymmetry is created by asymmetric initial conditions which in turn are created by rising quantum fluctuations of the scalar baryonic field during inflationary stage. Of course at large scales the universe is charge symmetric. It is evident that there is no domain wall problem in this scenario. The characteristic size of domain with a definite sign of baryonic charge was estimated in ref.[2]. At the end of inflation it is equal to $L_{Bi} = H_I^{-1} \exp(\lambda^{-1/2})$. With λ around $10^{-3} - 10^{-4}$ such domains would be consistent with observations and still inside the present day horizon. Since it is natural to assume that the baryon asymmetry in this model gradually changes from a positive value through zero to a negative one, the annihilation at the boundaries of the domains would be much weaker than in the (usually assumed) picture of interactions of domains with sharp boundaries. Correspondingly the limits

on the magnitude of l_B would be considerably weaker. Note that not only the sign but also the magnitude of the baryon asymmetry in different domains in this scenario may be significantly different.

4 Alternating (and periodic?) matter-antimatter cosmic layers.

A relatively simple modifications of the baryogenesis scenario would permit to get a very interesting distribution of matter and antimatter in the universe ranging from strictly periodic flat alternating layers of matter and antimatter[20, 21, 22, 23] to cell structures with each cell formed by matter or antimatter with an average characteristic size which could easily be around 100 Mpc. The basic assumptions leading to this kind of structure are quite simple and even natural. Assume that there exists a complex scalar field ϕ with the mass which is smaller than the Hubble parameter at inflation, $m_\phi < H_I$. Assume also that the potential $U(\phi)$ contains nonharmonic terms (i.e. not only $m^2|\phi|^2$ but also e.g. $\lambda|\phi|^4$). Assume at last that a condensate $\langle\phi\rangle = \sigma(\vec{r})$ was formed during inflation. It is essential that the condensate σ is not a constant but a slowly varying function of $\vec{r}$. Such a condensate could be formed due to infrared instability of the scalar field mentioned in the previous section or in first order phase transition with very much inflated bubble walls. The characteristic scale at which ϕ essentially varies, l_ϕ, may be exponentially large due to inflation.

When inflation is over, the field ϕ relaxes down to its equilibrium value, oscillating near the minimum of the potential. If baryogenesis takes place very soon after the end of the inflation and the rate of the baryogenesis is large in comparison with the frequency of oscillations of ϕ, then the instant value of the amplitude of ϕ would be imprinted on the magnitude of the asymmetry because, as we mentioned above, a condensate of a complex scalar field gives rise to C(CP)-violation proportional to the field amplitude. Thus baryogenesis makes a snapshot of the magnitude of ϕ. Now since the potential $U(\phi)$ is not harmonic, the frequency of the oscillations of ϕ depends on the amplitude. By assumption the initial amplitude is not the same at different space points and so the frequency is also a function of $\vec{r}$. Because of that the initially smooth function $\phi(\vec{r})$ would turn into an oscillating one with a huge wave length of oscillations proportional to l_ϕ.

If ϕ oscillates around zero than its snapshot would show both positive and negative values. In the case that there are no other comparable sources of C(CP)-violation this model would produce approximately equal number of baryons and antibaryons situated on relatively thin layers or shells. If the equilibrium value of ϕ is nonzero or there is an explicit charge symmetry breaking, matter or antimatter would be produced more efficiently and the universe on the average would be more baryonic or antibaryonic.

5 Island universe model.

It is relatively simple to construct a cosmological model of the universe consisting of separate baryonic or antibaryonic islands floating in the sea of invisible matter or even of a baryonic island surrounded by the sea of antimatter[20, 21]. In the first case our chances to observe antimatter are minor because the distance between the islands is typically rather large and the probability of the collisions is low. In the second case antimatter may be possibly observed by the gamma ray background.

In short the scenario leading to the insular structure can be realized as follows. First, the charge symmetry should be spontaneously broken and the phase transition to the CP-odd phase should be first order with supercooling and formation of bubbles of the new phase inside the quasistable CP-symmetric phase. Second, there should be sufficiently long period of exponential expansion after the phase transition but not too long. Otherwise the sizes of the CP-odd bubbles would be either too small in contradiction with observations or too large so that we would never see the boundary. If the phase transition took place before the end of inflation but not far from it, the island size could be of the order of the present horizon size but still slightly smaller than the latter. When inflation ends and the Universe is (re)heated an excess of particles over antiparticles or vice versa is generated inside of the bubble by the normal process of baryogenesis. Outside of the bubbles where the charge symmetry is unbroken the baryonic charge density would be equal to zero. However it might be that there are two mechanisms of C(CP)-breaking, the spontaneous one operating inside the island and an explicit one operating everywhere. In that case the baryogenesis would proceed also outside the bubbles and may have either sign, in particular it is possible that the baryonic island would be in the antibaryonic sea. In that case one may expect a noticeable annihilation on the coast.

The size of the islands (or bubbles) depends upon the duration of inflation after the phase transition to C(CP)-odd phase took place. Normally the duration of inflation is very large in comparison with the minimal necessary one, $H_I\tau \approx 60$, and one would naturally expect that the size would be much larger than the present day horizon. To escape this conclusion one may introduce a coupling of the field ϕ, which creates charge symmetry breaking, to the inflaton field Φ, e.g. of the form:

$$L_{int} = \lambda' \mid \phi \mid^2 (\Phi - \Phi_1)^2 \qquad (3)$$

with $\lambda' > 0$ and Φ_1 is such that the inflaton field reaches and passes this value in the course of inflation. This interaction leads to effective time dependent mass of ϕ, $\Delta m^2(t) = \lambda'[\Phi(t) - \Phi_1]^2$, so that the state $\phi = 0$ is almost always classically stable with respect to small fluctuations and only when Φ is close to Φ_1 there is a period of instability. Quantum fluctuations of ϕ at that time increases and, if they exceed a critical value ϕ_c to the moment when the condition of stability becomes valid again, they do not return to the false vacuum state but would rise up to a nonzero complex value. Thus the bubbles of CP-odd vacuum can be formed. The average bubble size d and the distance l between them are very much model dependent. In particular the value of l can vary from 0 to infinity and correspondingly vary the odds for observing antimatter in such universe.

6 Very inhomogeneous baryogenesis.

The model considered in this section combines some of the ideas discussed above but in an extremal form. Namely the mechanism of baryogenesis was proposed[24] which creates a huge baryon asymmetry $N_B/N_\gamma = O(1)$ in relatively small regions with, say, stellar size over the normal homogeneous baryonic background with N_B/N_γ given by eq.(1). The probability of production of such high-B regions should be sufficiently small so that their number density is below the observational bounds. The sign of the baryon asymmetry in this regions is with equal probability positive or negative so we can expect both high density and small size baryonic and antibaryonic objects. There is no observational difference between the two if the density is so high that those objects collapsed at some early epoch into compact stellar remnants and black holes. This model presents a mechanism for early black hole formation from large amplitude isothermal fluctuations at small spatial scales. In this case, at least some

dark matter in the universe would be in the form of baryonic (and antibaryonic) black holes. Smaller uncollapsed bubbles of antibaryonic matter would be observable either as point-like sources of γ–radiation or, if they annihilated earlier, as some bright spots in the otherwise isotropic background radiation. If the number density of these objects were sufficiently high, early $p\bar{p}$–annihilation could result in the distortion of the spectrum of background radiation. Unfortunately there is too much freedom in the model to make any specific predictions. The amount of uncollapsed antimatter may vary from an unnoticeable amount to that in contradiction with existing data.

The basic idea of the model is to make the conditions in which the Affleck-Dine[16] mechanism of baryogenesis could be operative only in small spatial regions. In these regions the asymmetry may be huge since this mechanism suffers from overabundant baryoproduction in contrast to all other ones. This could be realized if the flat directions in the potential of the scalar baryonic field ϕ are separated from the origin (where the field is normally located) by a potential barrier. In this case the jump to the flat directions could be achieved only through the tunnel transition which is usually strongly suppressed. This ensures the desired suppression of the production of high B-bubbles. Once again the jump to the flat directions should be done during inflationary stage to make the bubbles macroscopically large at the present time. The necessary tuning may be achieved by a coupling between ϕ and the inflaton field.

Under reasonable assumptions about the production mechanism the mass distribution of the high density baryonic or antibaryonic bubbles is given by the expression[24]:

$$\frac{dn}{dM} = M_0^4 \exp[-\alpha - \beta \ln^2(M/M_0)] \tag{4}$$

The constants α, β, and M_0 are determined by the parameters of the potential of the ϕ-field and the Hubble constant during inflation. With the reasonable choice of the parameters it is possible to get M_0 in the interesting interval $(1 - 10^6)M_\odot$ where $M_\odot$ is the solar mass.

The cosmological evolution of such bubbles depends upon their size and the magnitude of the baryon asymmetry or, to be more precise, upon the ratio of their size, l_B and the Jeans wave length, λ_J. Bubbles of large size, $l_B > \lambda_J$, would form compact objects, either stars or black holes, at a very early stage of the evolution of the universe. Stars of antimatter could emit considerable energy due to annihilation of the accreted matter. With a sufficiently large amount of surrounding matter, they should radiate at their Eddington limit,

$$L_{Ed} = 3 \cdot 10^4 L_\odot \left(\frac{M}{M_\odot}\right) \tag{5}$$

where $L_\odot \approx 4 \cdot 10^{33}$erg/sec is the solar luminosity. The life-time of such objects is of the order of $5 \cdot 10^9$years. If the accretion rate is below the limiting one (e.g. due to the surrounding deficit of matter), the luminosities would be smaller and the life-times would be larger. Those objects can be observed as γ-ray sources isotropically distributed over the sky. A very interesting phenomena may take place in a collision of the antistar with a normal star. One would expect to observe together with a flux of gamma radiation rare events of antinuclei, in particular anti-helium-4.

7 Conclusion.

One cannot make any strong conclusion from this very speculative talk. What seems quite definite is that baryonic charge is not conserved. Hence proton is in principle unstable, neutron-antineutron oscillations should exist and this is matter of "only"

good luck to observe them in direct laboratory experiments. Unfortunately cosmology is absolutely helpless in predicting the magnitude of the effects.

The probability of observing big lumps of antimatter in the universe suffers from the similar uncertainty. The difference is however that in this case the existence of antimatter is by no means obligatory. While baryonic charge is definitely nonconserved, the universe may still contain only baryons. Another sad but very probable option is that the universe may be charge symmetric but antimatter is far beyond present day horizon. It means effectively that "our best of all possible worlds" does not contain antimatter. Unfortunately the models with inflationary expansion of the matter-antimatter bubbles would quite easily overexpand them too far. Still a rather simple coupling of the underlying scalar fields to the inflaton may stop inflating the bubbles at sufficiently early moment and make them comfortably (for possible observations) nearby. If this is true, very interesting configurations of matter-antimatter regions in the universe are possible, as it has been discussed above. Anyhow independently of theoretical speculations the idea of the charge symmetric universe looks so interesting and attractive that the searches for that just cannot be unsuccessful.

This paper was supported in part by the Danish National Science Research Council through grant 11-9640-1 and in part by Danmarks Grundforksningsfond through its support of the Theoretical Astrophysical Center.

References

[1] A. D. Sakharov, Pis'ma Zh. Eksp. Teor. Fiz. **5** 32 (1967).

[2] A.D. Dolgov, Phys. Repts. **222**, 311 (1992).

[3] A.D. Dolgov, M.V. Sazhin and Ya.B. Zeldovich, Basics of Modern Cosmology. Editions Frontiers. France, 1990.

[4] A. Guth, Phys. Rev. **D23** 347 (1981).

[5] A.D. Linde, Particle Physics and Inflationary Cosmology. Harwood Academic Publishers, 1990.

[6] G. t'Hooft, Phys. Rev. Lett. **37**, 8 (1976); Phys. Rev. **D14**, 343 (1976).

[7] V.A. Kuzmin, V.A. Rubakov, and M.E. Shaposhnikov, Phys. Lett. **B191**, 171 (1987).

[8] Cohen, A.G., D. B. Kaplan, and A. E. Nelson, Annu. Rev. Nucl. Part. Sci. 43 (1993).

[9] T.D. Lee, Phys. Rev. **D8**, 1226 (1973).

[10] D.A. Kirzhnits, Pis'ma ZhETF, **15**, 745 (1972)(for the review see e.g. A.D. Linde, Repts. Prog. Phys. **42**, 389 (1979)).

[11] R.W. Brown and F.W. Stecker, Phys. Rev. Lett. **43**, 315 (1979).

[12] K. Sato, Phys. Lett. **99B**, 66 (1981).

[13] Ya.B. Zel'dovich, I.Yu. Kobzarev, and L.B. Okun, ZhETF **67**, 3 (1974).

[14] R.N. Mohapatra and G. Senjanović, Phys. Rev. **D20**, 3390 (1979); Phys. Rev. Lett. **42**, 1651 (1979).

[15] V.A. Kuzmin, I.I. Tkachev, and M.E. Shaposhnikov, Phys. Lett. **105B**, 167 (1981).

[16] I. Affleck and M. Dine, Nucl. Phys. **B249**, 361 (1985).

[17] T.S. Bunch and P.C.W. Davies, Proc. Roy. Soc.(London), **A360**, 117 (1978).

[18] A.D. Linde, Phys. Lett. **116B**, 335 (1982).

[19] A. Vilenkin and L.H. Ford, Phys. Rev. **D26**, 1231 (1982).

[20] A.D. Dolgov, and N.S. Kardashev, Space Research Int. Preprint-1190 (1986).

[21] A.D. Dolgov, A.F. Illarionov, N.S. Kardashev, and I.D. Novikov, ZhETF. **94**, 1 (1987).

[22] M.V. Chizhov and A.D. Dolgov, Nucl. Phys. **B372**, 521 (1992).

[23] M. Chizhov and D. Kirilova, Preprint ICTP IC/95/172.

[24] A. Dolgov and J. Silk, Phys. Rev., **D47**, 4244 (1993).

AMS
A Magnetic Spectrometer for the International Space Station

Steven P. Ahlen for the AMS Collaboration
Physics Department, Boston University, Boston, MA 02215, USA

ABSTRACT

The AMS experiment will be flown on the Space Shuttle in 1998 during which it will face deep space for 100 hours. It will also be attached to the International Space Station in the year 2000 for three years of operation. AMS will: (i) search for antinuclei in the cosmic rays; (ii) measure the antiproton flux at the top of the earth's atmosphere; (iii) measure the positron flux at the top of the earth's atmosphere; (iv) measure high energy gamma rays from space; and (v) measure the isotopic composition of the light elements in the cosmic rays.

1. Introduction and Description of Instrument

The Alpha Magnetic Spectrometer (AMS) will go into a ten day orbit on the Space Shuttle in the Spring of 1998 during which it will be operated for 100 hours while viewing space. Also, it will be attached to the International Space Station in late 2000 for an exposure of three years. The primary goal of AMS is to search for antinuclei in the cosmic rays with a sensitivity 10,000 times greater than achieved previously. The energy range covered will be approximately 0.1 to 20 GeV/amu. Possible sources of antimatter include antigalaxies such as might exist in a baryon symmetric universe,[1,2] or compact objects made of antimatter.[3] AMS will also measure the abundances of positrons and antiprotons in the cosmic rays. These particles are known to be present, and may be made exclusively as products of collisions of cosmic ray nuclei and electrons with the interstellar medium. There have also been suggestions that they may have been produced as a result of interactions of non-baryonic dark matter particles in the halo of our galaxy.[4,5] Positrons will be identified from 1 to 100 GeV and antiprotons will be identified from 0.1 to 10 GeV. AMS will also function as a gamma ray telescope, covering the energy range from 0.1 to 300 GeV. With its size and energy range AMS will be able to continue the study of galactic and extragalactic gamma ray sources begun by the EGRET experiment,[6] which will no longer be operating when AMS is on the Space Station. Finally AMS will make improved measurements of the isotopic composition of the light elements in the cosmic rays, which will enhance our understanding of cosmic ray production and propagation in our galaxy.

For the Shuttle flight AMS will weigh 6900 pounds, and will include (see Fig. 1): 1) a two-ton cylindrical magnet made of Nd-Fe-B with an energy product of 50 MGOe; 2) six layers of silicon trackers with tracking resolution of better than 10 microns per layer; 3) four layers of scintillator to measure time-of-flight (TOF) and energy loss; 4) an anticoincidence scintillator lining the inside surface of the magnet. The geometrical factor of AMS will be 0.6 m^2 sr, and its integral of magnetic field times tracking distance will be 0.15 T m. The momentum resolution is about 6% at a few GeV/c/nucleon, and degrades at high energy due to tracking resolution, and at low energy due to multiple scattering. The maximum detectable rigidity is about 500 GV/c. The TOF resolution will be 100 ps/Z, where Ze is the charge of the particle. Charge magnitude is determined by using TOF data and energy loss data from the scintillators

and silicon detectors. The charge sign is determined from the sense of curvature in the magnetic field and from the sign of velocity from the sign of TOF. Mass is determined (up to a velocity of about 0.9 c) from the momentum and TOF measurements.

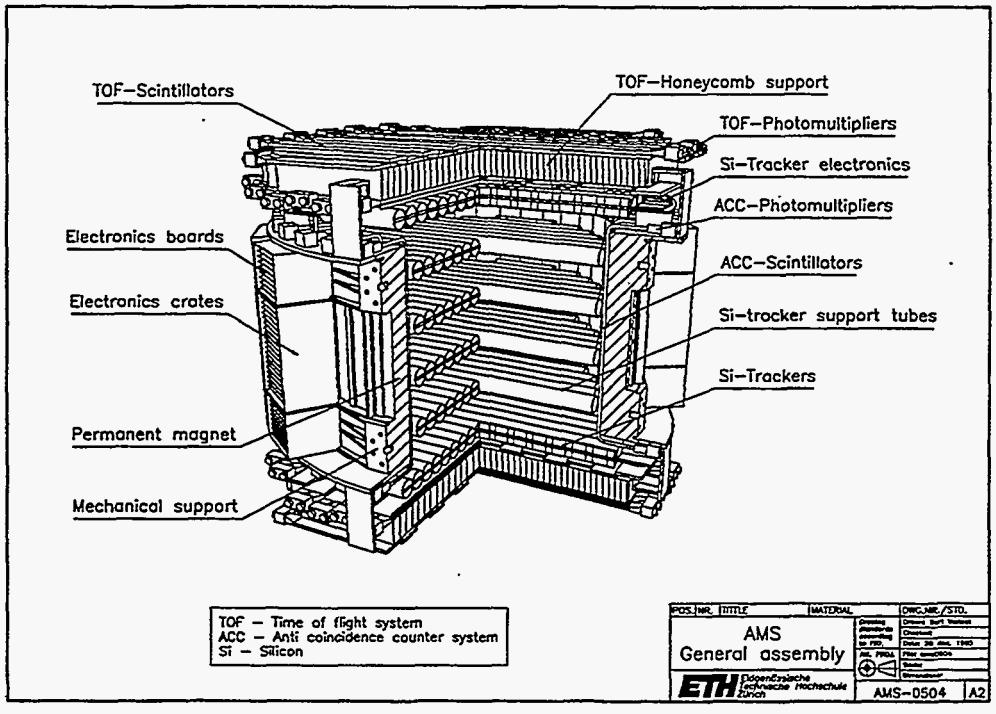

Fig. 1 AMS as it will be flown on the Space Shuttle in 1998.

For the three year mission on the Space Station, four items will be added to AMS (see Fig. 2): 1) a directional sensitive Cerenkov counter (DSC) made of lucite which will reduce antimatter background due to misidentified upward moving particles; 2) a straw tube transition radiation tracker (TRD) for positron identification; 3) a 1 mm thick tungsten converter plate to improve gamma ray detection efficiency; 4) a ring imaging cerenkov counter (RICH) to extend the range of precision velocity measurements available with the TOF, improving antimatter background rejection at high energy and extending the energy reach for antiproton measurements from 1 to 10 GeV.

2. Cosmic Ray Overview

To appreciate the potential for AMS to learn new things about the universe requires some understanding of the nature of cosmic rays. Fig. 3 shows the key observational information pertaining to composition and energy of the cosmic rays observed near earth. The current consensus is that most cosmic ray nuclei begin as stationary interstellar material accelerated to large energy by shock waves produced in the aftermath of supernova explosions, and that they leak out of galaxies after having passed through about 10 g/cm^2 of interstellar gas. The critical issue for AMS is the question of how much time it takes for cosmic rays to diffuse through various astrophysical objects.

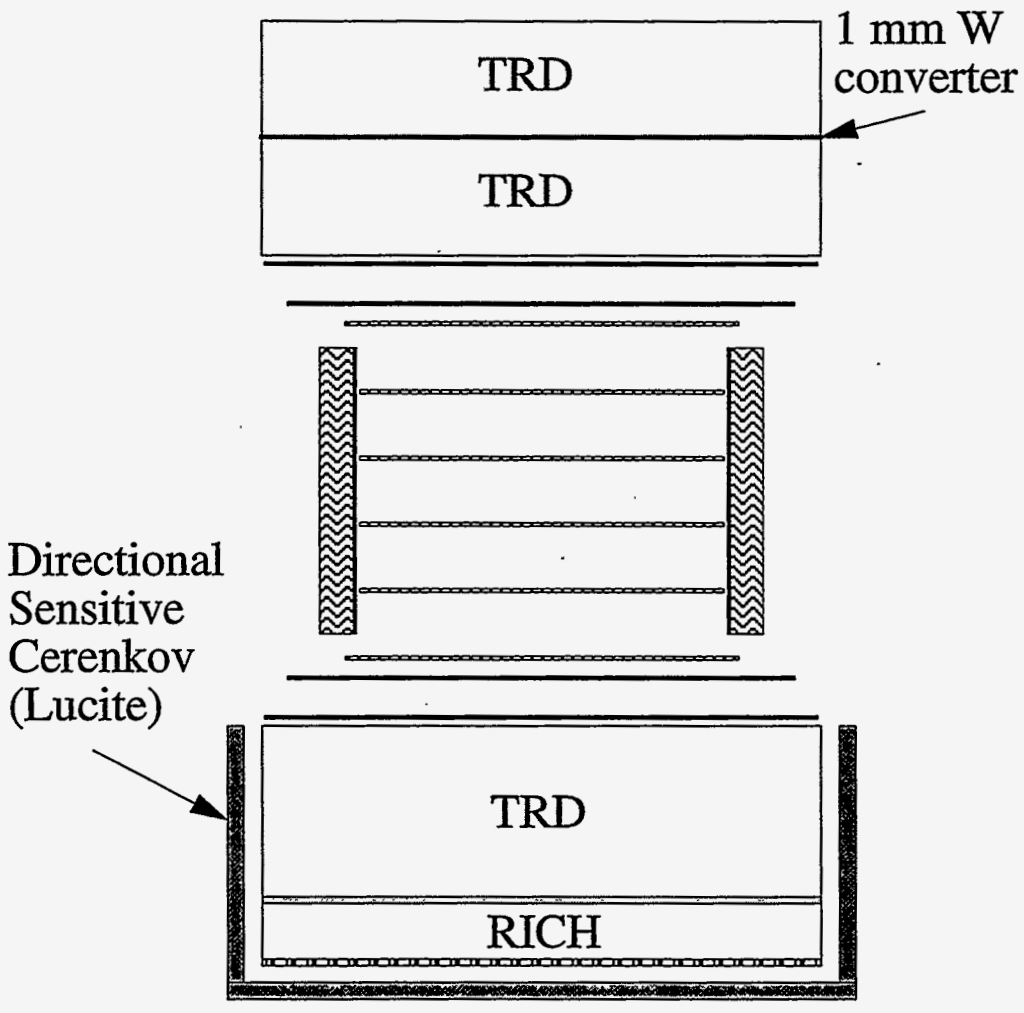

Fig. 2 AMS as it will be on the Space Station in 2000.

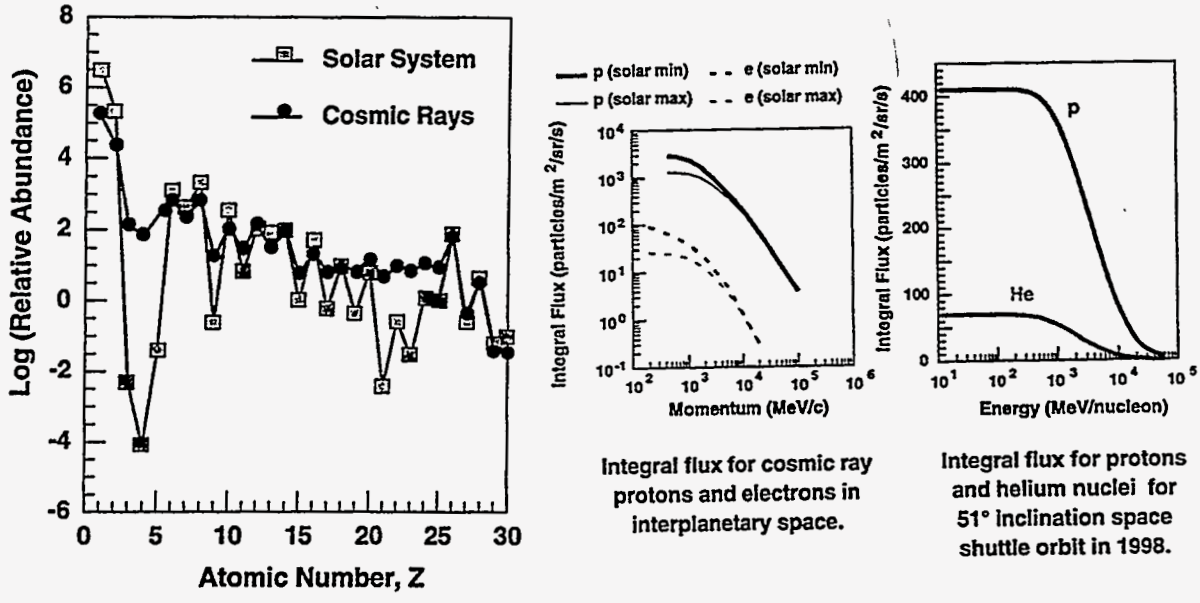

Fig. 3 Cosmic ray composition and energy spectra.

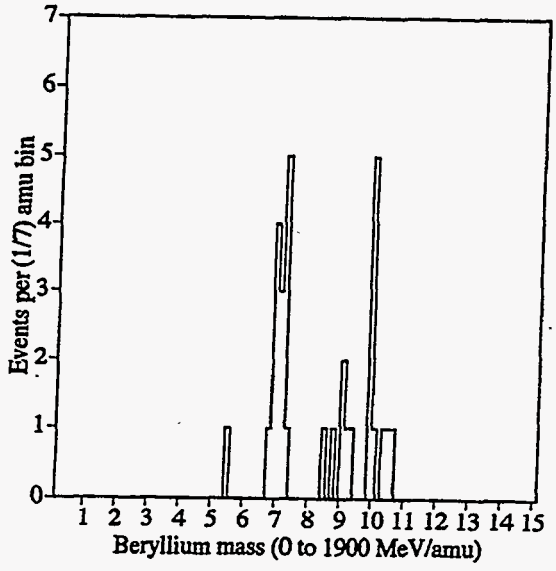

Fig. 4 Beryllium isotopic composition from the SMILI experiment.

The most significant evidence to date that relates to the above question is shown in Fig. 4. This is the mass histogram for cosmic ray beryllium with energies up to 1900 MeV/amu obtained from a recent balloon experiment (SMILI).[7] Since the isotope ^{10}Be is not present at the cosmic ray source, and is radioactive with a mean life of 2.3 My, it serves as a cosmic ray clock - absence of ^{10}Be implies cosmic rays take a very long time to leak out of the galaxy - presence of ^{10}Be in numbers comparable to the other isotopes of beryllium implies cosmic rays are young, probably escaping from our galaxy on a time scale equal to or less than a few million years. Indeed, using the data of Fig. 4 and performing detailed studies of cosmic ray propagation imply that at the 95% confidence level cosmic rays leak out of our galaxy with a mean confinement time of less than five million years.

Taking into account the size and distribution of stars and galaxies in the universe, it is straightforward to show that the ionization energy loss and nuclear interaction effects of very old cosmic rays (i.e. made after the first galaxies were formed about 15 billion years ago) is dominated by these effects in the gas of their parent galaxy (and in our galaxy if they happen to migrate to the earth). Of course cosmic rays do not move in straight lines in the universe because of the apparently pervasive presence of cosmic magnetic fields.[8,9] In our own galaxy the field strength is a few micro gauss, and is distributed throughout the disk of the galaxy. Cosmic rays spiral along field lines (with a gyroradius of about a micro pc for a 10 GeV proton) until they encounter changes in field direction due to the tangled nature of the field on scales of 10 to 100 pc. Assuming a random walk/diffusion type model (such as is commonly used in treating interactions of cosmic rays with the solar wind) with a mean free path of 30 pc, the beryllium measurement implies that cosmic rays leak out of the galaxy when they are less than 3 kpc from the plane of the disk. This is consistent with observations of the magnetic field structure of the galaxy (for which the magnetic halo extends to about 1 kpc from the plane of the disk). Note that it is the magnetic scale length which serves as the diffusion mean free path, not the gyroradius. If we had used the gyroradius we would have obtained an absurdly small disk thickness for cosmic ray confinement.

We can extend the diffusion argument to the scale of clusters of galaxies. In such structures, fields are also of the order of a micro gauss. As is the case with galactic fields, there is no clear understanding of the origin of the fields. Theories include:[10] 1) flux conservation following compression of material containing a primordial magnetic field; 2) remnant fields of extended radio sources; 3) magnetic fields ejected from galaxies (possibly produced by dynamo mechanisms); 4) conversion to magnetic energy of turbulent kinetic energy induced by the motion of galaxies through the intracluster medium. For our purposes, the mechanism is not as important as the observation that the scale length is of the order of tens of kpc, which implies that it takes tens of millions of years to leak out of the cluster field region (which has a size of about 1 Mpc).

To continue our discussion of cosmic ray diffusion beyond the cluster scale is purely speculative, since there are no hard data pertaining to the nature of magnetic fields between clusters of galaxies. The presence of a large intergalactic magnetic field between clusters of galaxies would not only have an impact on our search for antimatter, but would also have an impact on current theories of galaxy formation which typically ignore the possibility of such a field. Nevertheless, estimates for the strength of such fields have been made. Based on cosmological theory[11] they range from 10^{-65} to 10^{-10} gauss. Extrapolations from data have led some to believe in a pervasive tangled field of magnitude as large as a microgauss.[9] But again, the key parameter for AMS is the scale size, which tends to lie in the range from 1 to 10 Mpc for the theories as well as for the extrapolation of measurements. Assuming 3 Mpc, one calculates a time of 16 billion years to diffuse a distance of 100 Mpc, which is the distance between superclusters of galaxies. Thus, if the supercluster scale is the scale for a matter-antimatter domain structure of the universe, cosmic rays could diffuse from an antimatter supercluster to a matter supercluster in the age of the universe.

3. AMS Antimatter Sensitivity

Fig. 5 shows the sensitivity for a three year search with AMS for antihelium. Also shown is a curve calculated[12] assuming a symmetric universe (i.e. equal numbers

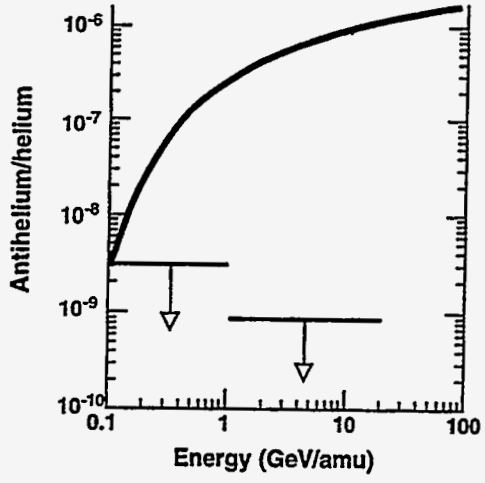

Fig. 5 Sensitivity (95% C.L.) of three year search for antimatter with AMS. Curve is conservative estimate for symmetric universe.

of galaxies and antigalaxies). The reduction in the antimatter fraction at low energy is due to the possible effects of an outflowing galactic wind from the plane of our galaxy. Note that current limits of antihelium are off the scale of the figure, being of the order of 10^{-5}. Antihelium nuclei (with mass 3) have been made in accelerator experiments.[13] Based on these measurements we estimate the ratio of secondary antihelium to helium in the cosmic rays to be of order 10^{-12}. Only about 0.01% of the secondary antihelium would have mass 4. By using TOF and the RICH to determine mass up to about 6 GeV/amu, the secondary antihelium nuclei can be rejected.

4. Antiprotons

Fig. 6 shows the state of measurements and theory of antiproton flux at the time of the AMS proposal in 1995. The dashed line is the expected solar modulated flux of antiprotons from standard propagation. The upper (lower) solid curve is the spectrum predicted if a 30 GeV (60 GeV) neutralino populates the galactic halo.[5] The points with error bars along the dotted line indicate the precision of measurements which could be made with AMS for 100 hours of data from the shuttle flight in 1998 (for which particle identification will be accomplished using TOF). The data point at 500 MeV is from the BESS experiment.[14] The point at 8 GeV is from an early measurement by Golden et al.[15] Fig 7 from ref. 16 shows more recent measurements from the IMAX experiment and calculations of secondary production of antiprotons.

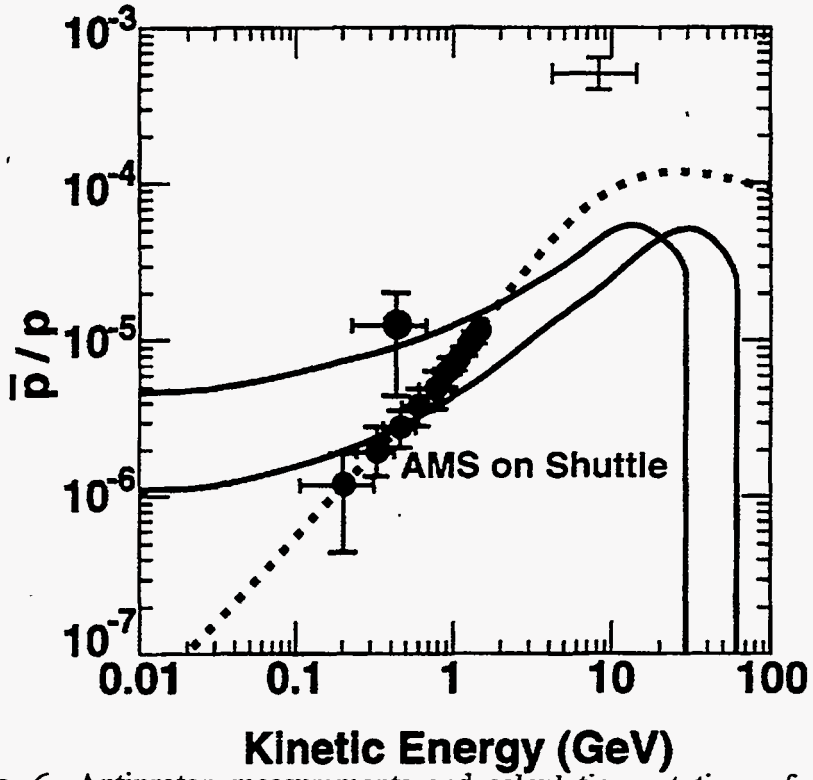

Fig. 6 Antiproton measurements and calculations at time of AMS proposal. Solid curves are predictions of dark matter models.

The RICH will extend the capability of AMS to reject electron and pion background for the antiproton measurement to higher energies. Fig. 8 shows the capabilities of a RICH based on aerogel with an index of refraction of n = 1.2. Such

indices are now available, and it has been shown[17] that aerogel with n = 1.03 can be made with sufficiently good optical quality to permit its use to form Cerenkov rings. We are pursuing an R&D program to investigate the environmental effects and the feasibility of using aerogel with n = 1.2 for ring imaging. The Cerenkov radiation will be measured with an array of small phototubes separated from the aerogel by an 8 cm gap, as indicated in Fig. 2.

In the three year exposure on the Space Station, AMS will observe about 1 million antiprotons. To date fewer than 100 antiprotons have been observed, preventing an accurate comparison of the energy spectrum with that predicted by standard propagation models.

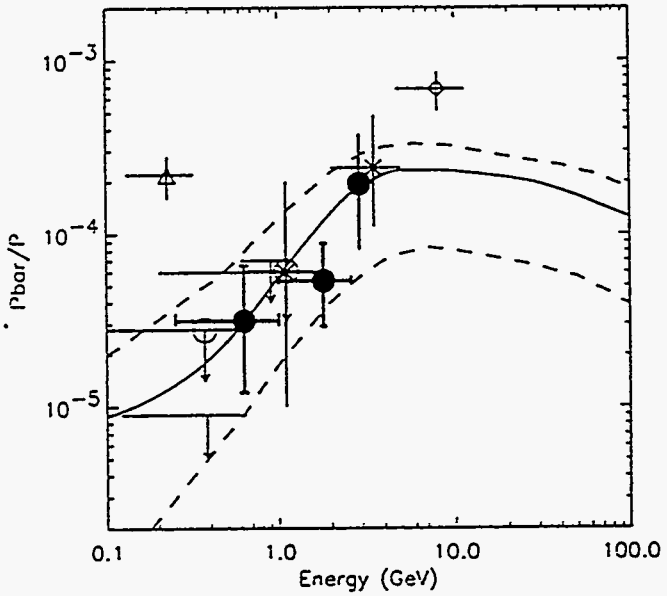

Fig. 7 Measurements (solid circles) of antiproton to proton ratio for IMAX experiment, and recent calculations of secondary production.

5. Positrons

Fig. 9 shows calculations of positron yield from a particular model[4] for a halo of non-baryonic dark matter. Fig. 10 shows recent measurements of positron fraction from the HEAT balloon experiment.[18] To enable the measurement of the positrons at the high energies needed to address the dark matter issue requires greater sensitivity than balloon experiments. AMS has such sensitivity. Furthermore, AMS will not be subject to the large background of atmospherically produced positrons which can be difficult for balloon experiments to deal with.

To measure positron flux, one must reject the large background of protons (there are about 1000 protons for every positron). The TRD tracker will accomplish this through the measurement of transition radiation clusters with 42 layers of kapton drift tubes interleaved with polypropylene fibers. Fig. 11 shows the proton rejection possible with various total TRD thickness. It is seen that with the large thickness anticipated for AMS the proton rejection should be more than sufficient from about 1 to more than 100 GeV.

To date, about 100 positrons above 10 GeV have been observed with balloon experiments. AMS will observe 3 million positrons in this range in three years.

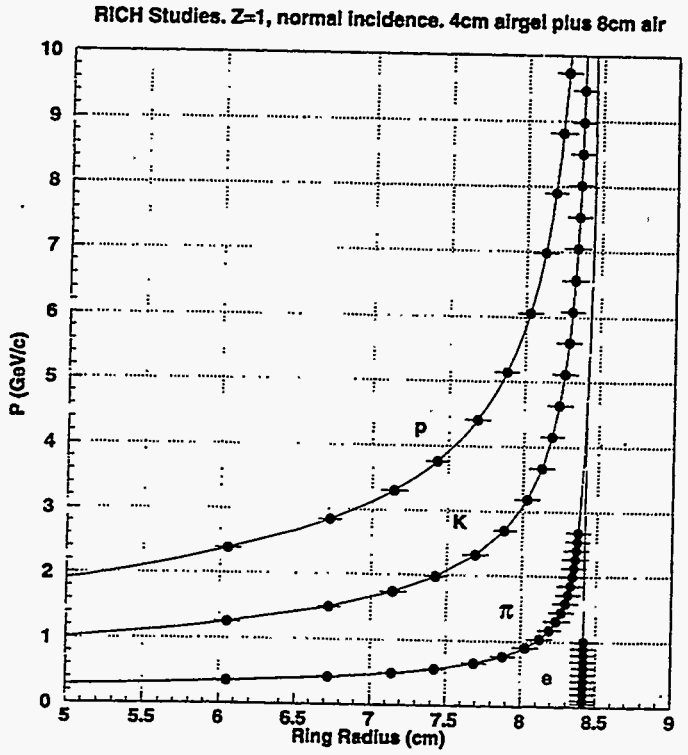

Fig. 8 Particle identification with an aerogel RICH.

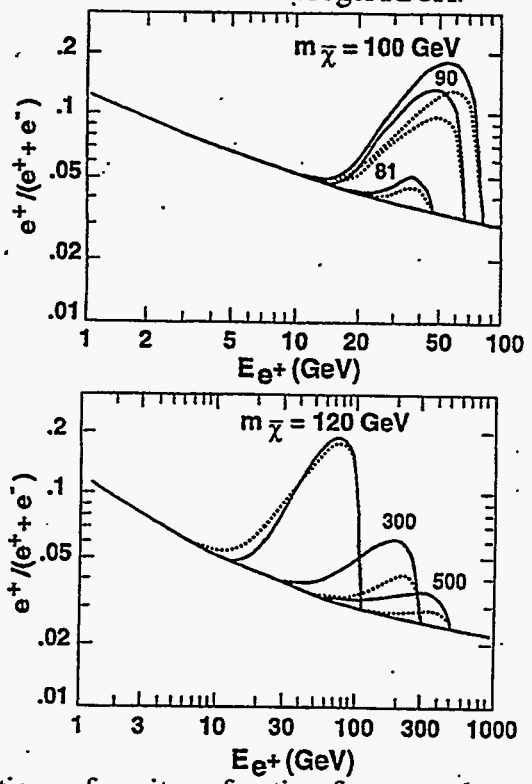

Fig. 9 Calculations of positron fraction from non-baryon dark matter model (ref. 4).

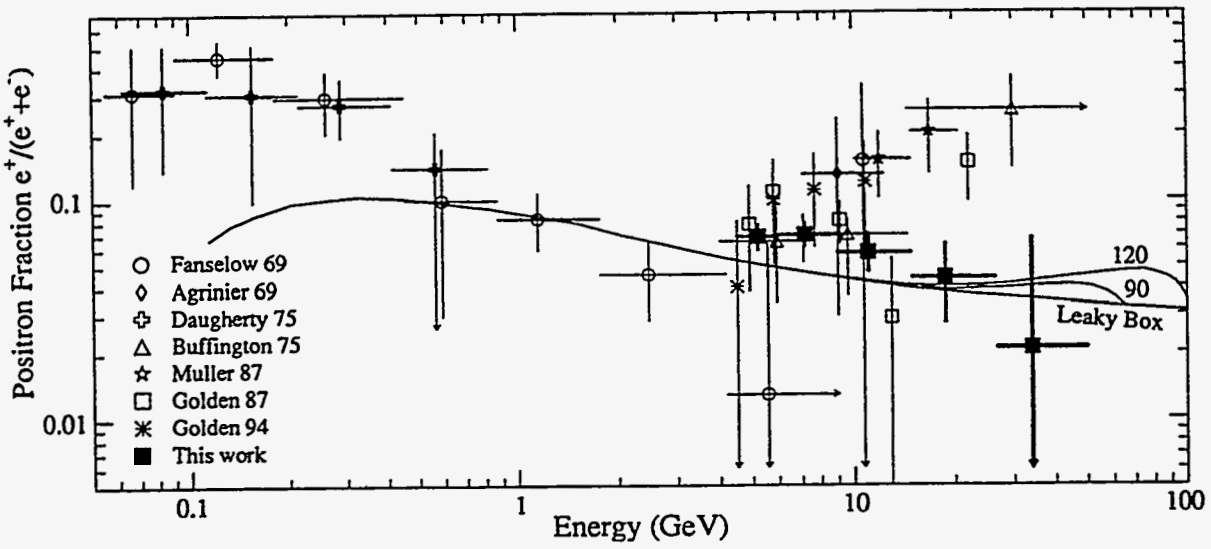

Fig. 10 Measurements of positron fractions from recent HEAT experiment (ref. 18).

6. Gamma Rays

The EGRET gamma ray experiment,[6] which is on the Compton Gamma Ray Observatory, has made a number of important discoveries, particularly those involving gamma ray emission from Active Galactic Nuclei (AGNs) and observations of high energy gamma rays from gamma ray bursters.

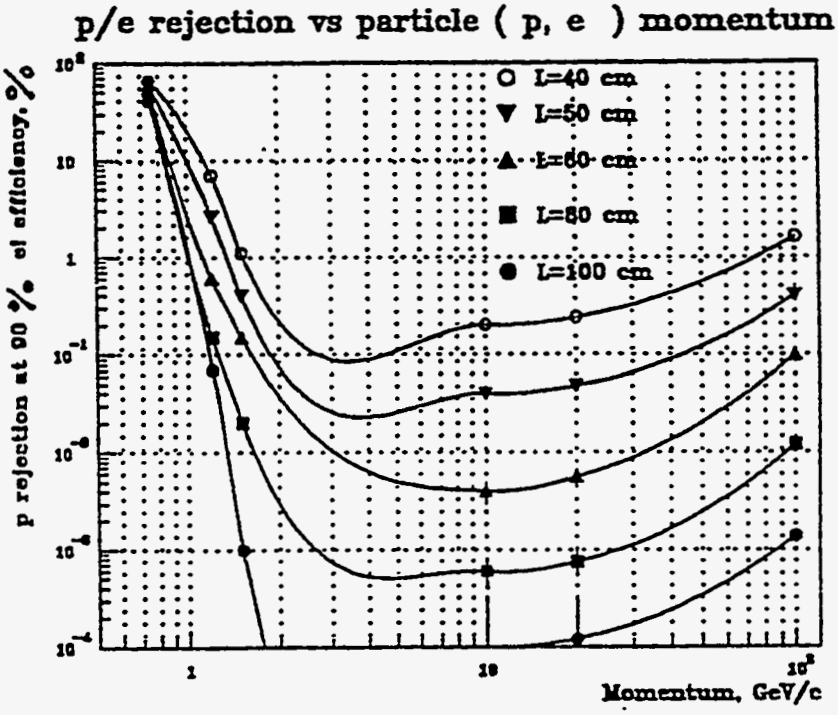

Fig. 11 Proton rejection capabilities with TRD.

Fig. 12 shows the gamma ray sources identified by EGRET. The gamma ray spectrum for one of the AGNs, Markarian 421, is shown in Fig. 13. On the same figure is shown the spectrum measured with the ground based gamma ray detector at the Whipple Observatory. The reduction at several hundred GeV may be due to the absorption of gamma rays by the diffuse intergalactic infrared background. If so, this could account for the fact that most AGNs are not detected by Whipple. In this regard it is important to note that Markarian 421 is one of only two AGNs seen both by Whipple and EGRET, and that this is the closest AGN in view of each telescope.

With the addition of the tungsten converter foil, AMS becomes a gamma ray telescope which can carry on the exciting program of observations begun by EGRET (which will turn off within a year or so due to depletion of spark chamber gas). Pairs produced in the tungsten can be measured in the magnetic spectrometer below. Comparison of the AMS and EGRET energy and pointing resolutions are shown in Fig. 14 and 15. AMS is better in both, and also has a higher energy reach than EGRET. Also, AMS has somewhat greater aperture than EGRET in the pair spectrometer mode. Finally, we are considering the use of the upper TRD module as a stand-alone gamma ray telescope. This has an order of magnitude greater geometry factor than EGRET, and is capable of measuring gamma ray directions from the tracking information of the straw tubes used in drift mode. The transition radiation also provides energy information, from about 1 to 20 GeV gamma ray energies, as is seen from Fig. 16.

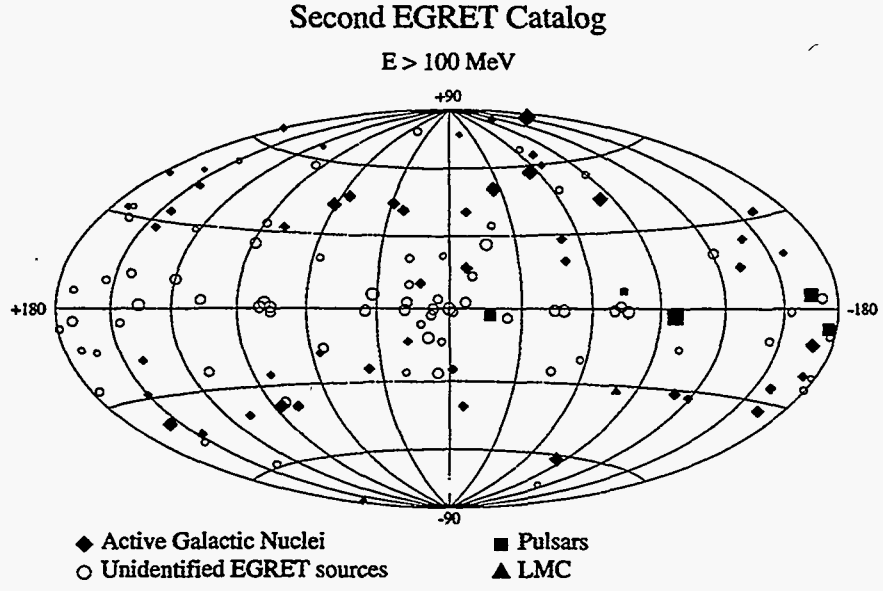

Fig. 12 Gamma ray sources detected by EGRET..

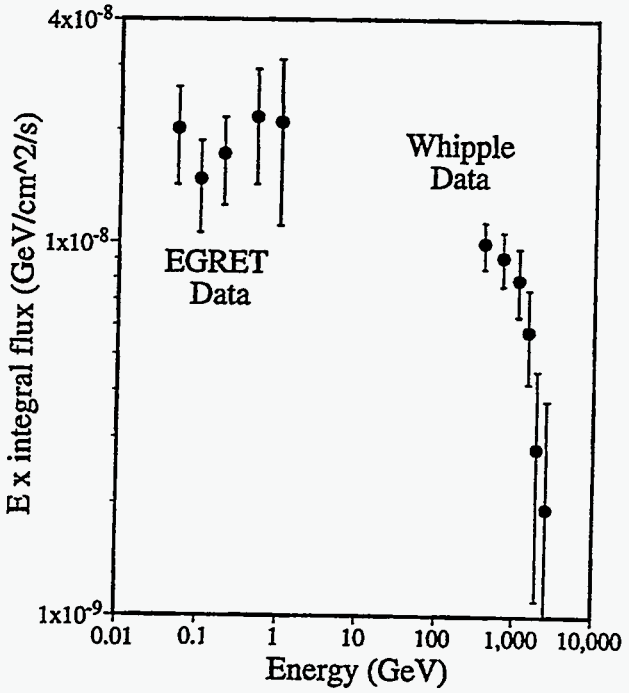

Fig. 13 Energy spectrum of Markarian 421 measured by EGRET and Whipple..

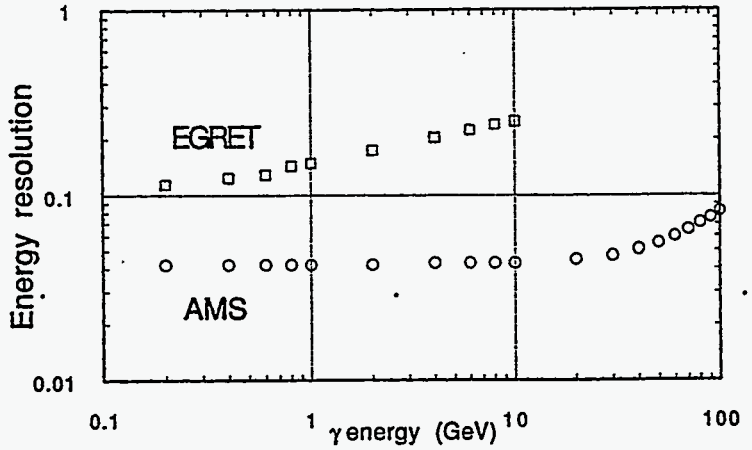

Fig. 14 Energy resolution for AMS and EGRET.

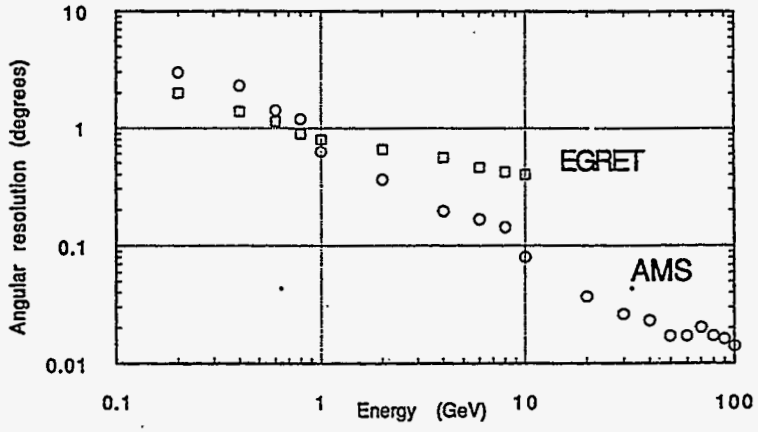

Fig. 15 Angle resolution for AMS and EGRET.

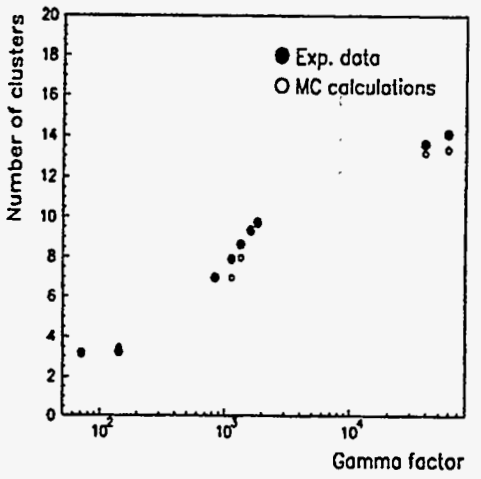

Fig. 16 Dependence of transition radiation on Lorentz factor..

References

1) R.W. Brown and F.W. Stecker, *Phys. Rev. Lett.* **43**, 315 (1979).

2) K. Sato, *Phys. Lett.* **99B**, 66 (1981).

3) A. Dolgov and J. Silk, *Phys. Rev. D* **47**, 4244 (1993).

4) M. Kamionkowski and M.S. Turner, *Phys. Rev. D* **436**, 1744 (1991).

5) Jungman and M. Kamionkowski, *Phys. Rev. D* **49**, 2316 (1994).

6) D.J. Thompson et al., "The Second EGRET Catalog of High-Energy Gamma-Ray Sources," NASA Goddard Space Flight Center (1996).

7) D. Loomba, presentation at APS meeting, Indianapolis, May 4, 1996.

8) C. Heiles, *Ann. Rev. Astron. Astrophys.* **14**, 1 (1976).

9) P.P. Kronberg, *Rep. Prog. Phys.* 325 (1994).

10) J.C. Carvalho, *Astron. Astrophys.* **281**, 641 (1994).

11) B. Ratra, *Ap.J.* **391**, L1 (1992).

12) S.P. Ahlen et al., *Ap.J.* **260**, 20 (1982)..

13) Y.M. Antipov, *Sov. J. Nucl. Phys.* **12**, 171 (1971).

14) K. Yoshimura et al., preprint, (1995).

15) R.L. Golden et al., *Phys. Rev. Lett.* **43**, 1196 (1979).

16) J.W. Mitchell et al., *Phys. Rev. Lett.* **76**, 3057 (1996).

17) D.E. Fields et al., *Nucl. Instr. Meth.in Phys. Res. A* **349**, 431 (1994).

18) S.W. Barwick et al., *Phys. Rev. Lett.* **75**, 390 (1995).

Double Beta Decay – Physics at Beyond Accelerator Energies

H.V. Klapdor–Kleingrothaus
Max–Planck–Institut für Kernphysik
P.O.Box 10 39 80, D–69029 Heidelberg, Germany

ABSTRACT

Double beta decay yields – besides proton decay – one of the most promising possibilities to probe beyond standard model physics at beyond accelerator energies. The possibilities include the neutrino mass, SUSY models, compositeness, leptoquarks, right–handed W bosons and others. We discuss the status and the future perspectives of $\beta\beta$ research, including applications some double beta technology can find in the search for dark matter and in high resolution balloon and satellite gamma–ray astronomy.

1. Introduction

Many central questions of particle physics are beyond the capabilities of modern accelerators. They can, however, to some extent be investigated via non–accelerator experiments (see, e.g.[1]). Table 1 and Fig.1 show some probable areas of research of future accelerators. LHC, for example, the main enterprise of High Energy Physics in the next decade, will cover physics up to scale of a few TeV and may search for the Higgs particle, some SUSY particles and others. In general, however, accelerator physicists at present are forced to search in the extreme 'low–energy' range of the parameter spaces of models of 'new physics' like SUSY or leptoquark signatures and others (see e.g.[3]). Many questions of modern physics have to be studied at higher energy scales: grand unification with or without supersymmetry, and with or without left–right symmetry, compositeness, leptoquarks, neutrino mass (e.g. see–saw–mechanism), Majorons,...

This explains the increasing trend to non–accelerator experiments in numerous underground laboratories and elsewhere. Double beta decay, and proton decay, to mention the most prominent examples, are among those, which yield the most promising possibilities to probe beyond the standard model (SM) physics at beyond accelerator energies and bridge the time gap to the occurence of future larger accelerators. Propagator physics has to replace direct observations. That this method is very effective, is obvious from important earlier research work and has been stressed, e.g. by.[4] Examples are the proporties of W and Z bosons derived from neutral weak currents and β–decay, and the top mass deduced from LEP electroweak radiative corrections. Also for accelerators, the search for new bosons or compositeness, for example, can be to some

	e^+e^- linear colliders	Proton colliders LHC,SSC
Higgs boson standard model	Mass $\leq$ 250 GeV all decay channels	Mass $\leq$ 180 GeV: rare decays Mass $\geq$ 180 GeV: $H \rightarrow ZZ \rightarrow 4l$
Higgs boson SUSY–extension	Complete coverage of the Higgs parameter space	Partial coverage of the Higgs parameter space
W, Z bosons standard model	Magnetic dipole and electric Gauge–theoretical structure of	quadrupole moments the electroweak forces
Extended gauge theories	New leptons (heavy neutrinos)	New gauge bosons and quarks
Top	Precise measurements of mass, dipole moments, decay current; Higgs and other rare decays	Higgs decays CP violation
Supersymmetry	Sleptons and electroweak Gauginos/Higgsinos	Squarks and gluinos

Table 1. Proposed areas of research for future accelerators (from [2]).

degree extended beyond kinematical production limits through the study of *indirect* effects from virtual particle exchange (see, e.g.[5]). For a recent review concerning the perspectives of proton decay we refer to.[4]

The potential of double beta decay includes investigation of the neutrino mass, of the parameter space of SUSY models, of right–handed W bosons, compositeness, leptoquarks, Majorons,...(see table 2). For these topics double beta decay is comfortably competitive to high–energy accelerators ([6,7] and various contributions in,[89–16]). To give just one example, inverse double beta decay $e^-e^- \rightarrow W^-W^-$ requires an energy of at least 4 TeV for observability, according to present constraints from double beta decay.[17] Similar energies are required to study leptoquarks.[5,7,18–21]

In the following chapter we shall sketch some of the connections between $\beta\beta$–decay and particle physics, including some comments on the status of nuclear matrix elements necessary to deduce particle physics information from experiment. Section 3 describes the experimental status of $\beta\beta$ research and its future perspectives. Sections 4,5 discuss applications of some $\beta\beta$–technology to dark matter search and high resolution balloon and satellite gamma–ray astronomy. Section 6 gives a conclusion.

2. Double beta decay and beyond standard model physics

We present an introductory outline of the potential of $\beta\beta$ decay for some representative examples like the problem of the mass of the neutrino, for SUSY models, heavy neutrinos, left–right symmetric models and the mass of the right–handed W boson, Majorons, compositeness, sterile neutrinos, including some brief comments on

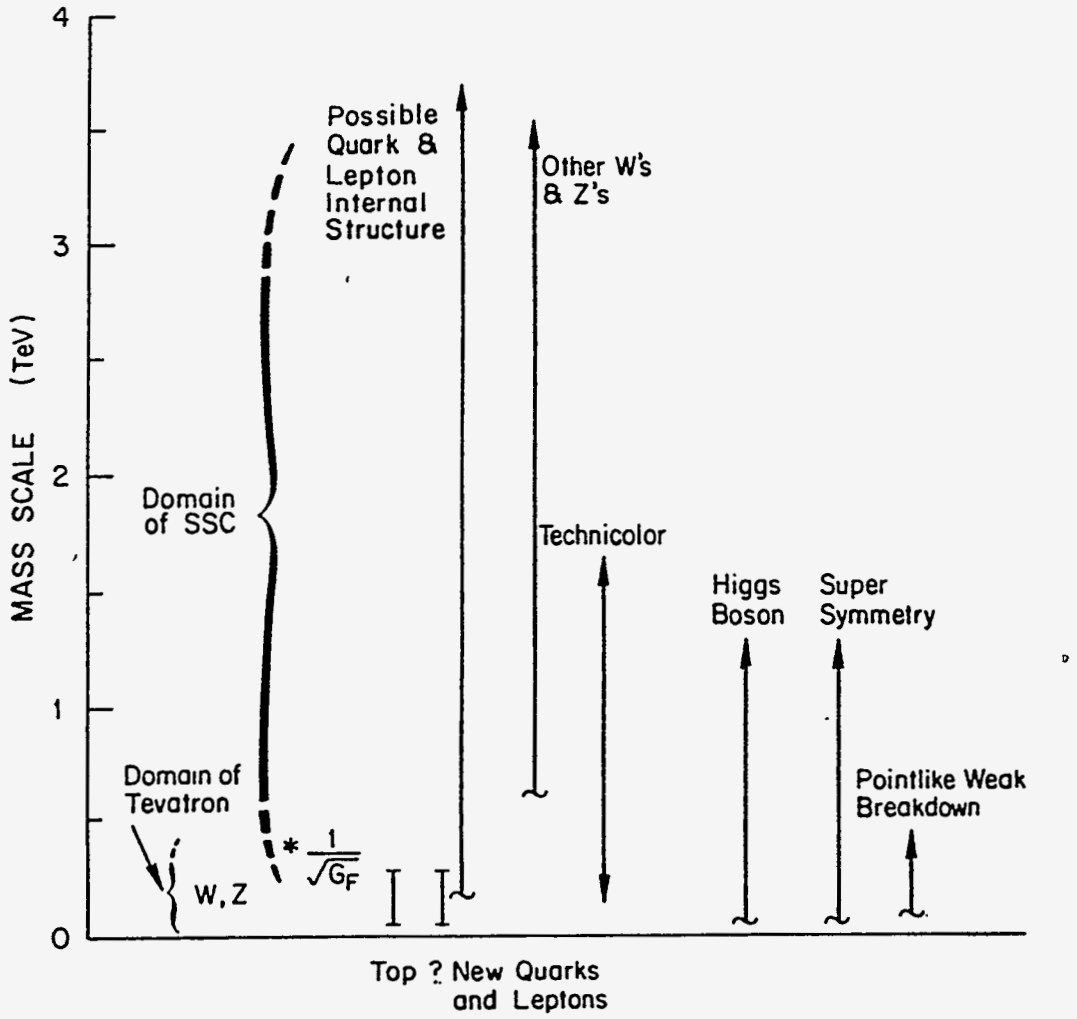

Fig.1 Mass scales and new phenomena made accessible to research by colliders (from[1,118])

Observable	Restrictions	
0ν:	via ν exchange:	Beyond the standard model and SU(5) model;
	Neutrino mass	early universe, matter–antimatter asymmetry
	Light Neutrino	Dark matter, L–R –symmetric models (e.g. SO(10))
	Heavy Neutrino	seesaw mechanism, compositeness
	Right handed weak currents	$V+A$ interaction, $W_R^{\pm}$ masses
	via photino, gluino, zino	SUSY models: Bounds for parameter space beyond
	(gaugino) exchange:	the range of accelerators (R–parity breaking
		interaction, squark and slepton masses)
$0\nu\chi$:	existence of the Majoron	Mechanism of (B-L) breaking
		-explicit
		-spontaneous breaking of the local/global
		B-L symmetry

Table 2. $\beta\beta$ decay and particle physics

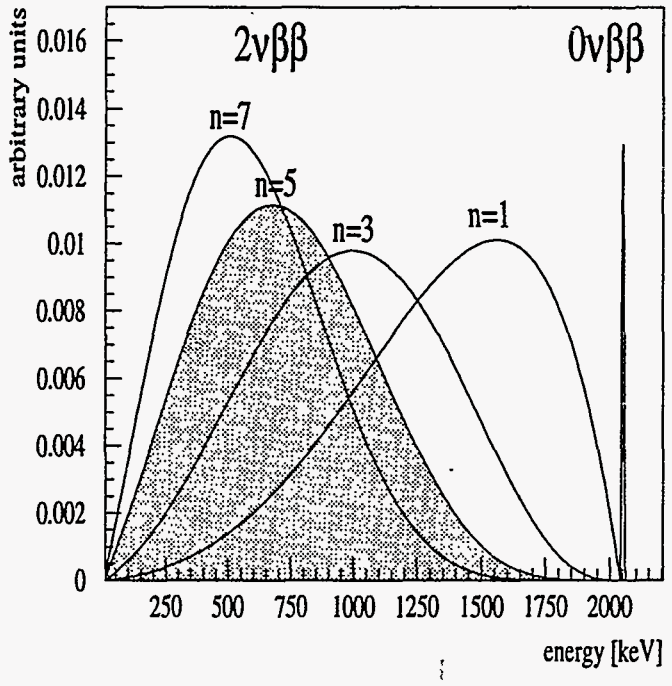

Fig.2 Spectral shapes of the different modes of double beta decay, n denotes the spectral index , n=5 for $2\nu\beta\beta$ decay (see text)

the status of the required nuclear matrix elements.

Double beta decay is a process violating lepton number conservation by $\Delta L = 2$. It can occur in several decay modes

$$ {}^{A}_{Z}X \rightarrow {}^{A}_{Z+2}X + 2e^{-} + 2\overline{\nu}_{e} \quad (1) $$

$$ {}^{A}_{Z}X \rightarrow {}^{A}_{Z+2}X + 2e^{-} \quad (2) $$

$$ {}^{A}_{Z}X \rightarrow {}^{A}_{Z+2}X + 2e^{-} + \phi \quad (3) $$

$$ {}^{A}_{Z}X \rightarrow {}^{A}_{Z+2}X + 2e^{-} + 2\phi \quad (4) $$

Fig.2 shows the corresponding spectra, for the neutrinoless mode (2) a sharp line at $E = Q_{\beta\beta}$, for the two-neutrino mode and the various Majoron–accompanied modes classified by their spectral index (see Päs,[8] Burgess[8]) continuous spectra. Important for particle physics are the decay modes (2)–(4).

The neutrinoless mode (2) needs not be necessarily connected with the exchange of a virtual neutrino. *Any* process violating lepton number can in principle lead to a process with the same signature as usual $0\nu\beta\beta$ decay (see below).

2.1. Mass of the electron neutrino

The neutrino is one of the best examples for the merging of the different disciplines of micro– and macrophysics. The neutrino plays, by its nature (Majorana or Dirac particle), and its mass, a key role for the structure of modern particle physics theories

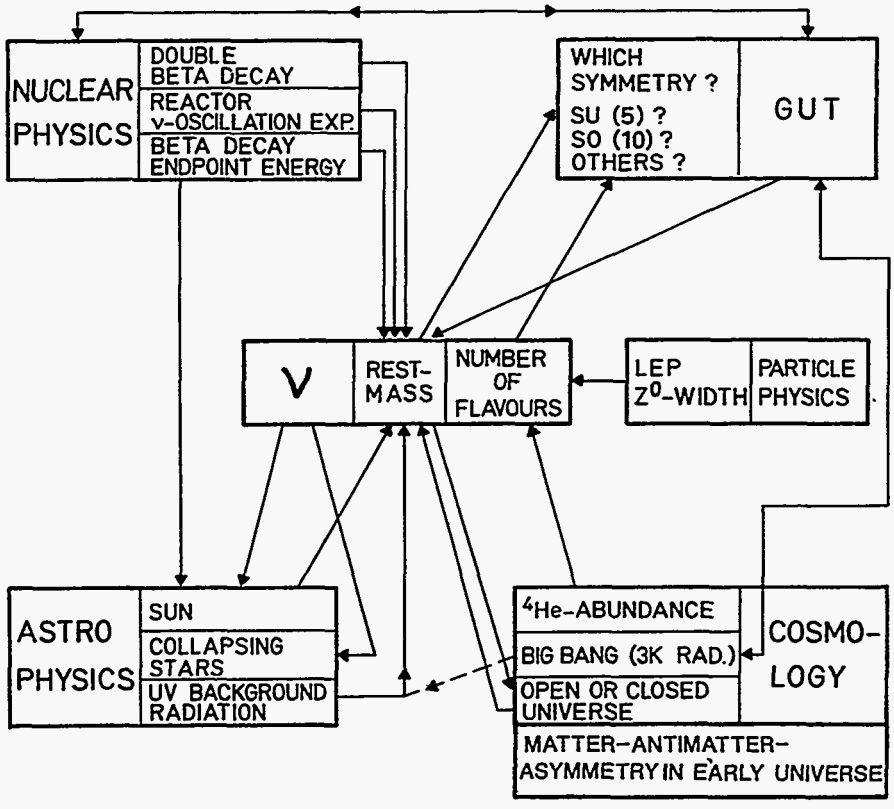

Fig.3 The neutrino and its role in micro– and macrophysics (from[87])

(GUTs, SUSYs, SUGRAs,...).[22–24] At the same time it is candidate for non–baryonic dark matter in the universe, and the neutrino mass is connected – by the sphaleron effect – to the matter–antimatter asymmetry of the early universe[25] (Fig. 3). Neutrino physics has recently entered an era of new actuality in connection with several possible indications of physics beyond the standard model (SM) of particle physics which are at present discussed: The lack of solar (^7Be) neutrinos, the atmospheric ν_μ deficit and mixed dark matter models could all be explained by non–vanishing neutrino masses. Recent GUT models, for example an extended SO(10) scenario with S_4 horizontal symmetry could explain these observations and would predict degenerate neutrino masses within 1–2 eV.[26] Also other GUT models used for interpreting the solar neutrino deficit favour degenerate neutrino scenarios with masses in the 0.1–1 eV range[27–30] over the old, well–known see–saw mechanism which is based on some rather arbitrary arguments (see Fig. 4). Also the recently claimed indication of ν oscillations from the LSND experiment at Los Alamos,[31] has been interpreted with degenerate neutrino masses around 2.5 eV.[32,33] This brings double beta decay experiments into some key position, since with some second generation $\beta\beta$ experiments like the HEIDELBERG–MOSCOW experiment using large amonts of enriched $\beta\beta$–emitter material the predictions of or assumptions in such scenarios can now be tested.

At present $\beta\beta$ decay is the most sensitive of the various existing methods to determine the mass of the electron neutrino (see Fig. 5). It further provides a unique possibility of deciding between a Dirac and a Majorana nature of the neutrino (Fig. 6).

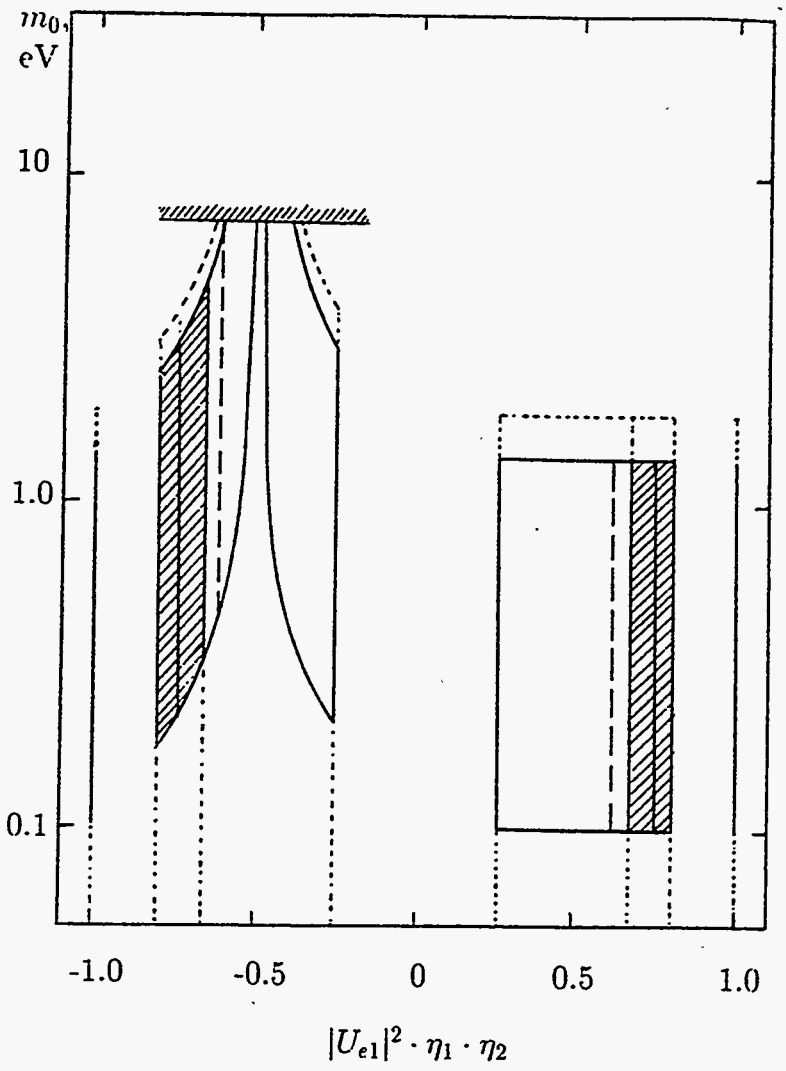

Fig.4 Values of the mass m_0 of the degenerate neutrinos and the mixing parameters $|U_{e1}|^2$ for which the MSW and vacuum oscillation solutions of the solar neutrino problem can be reconciled with an observable Majorana mass $|m_{ee}| = (0.1 - 1.4)eV$. Solid lines correspond to two–neutrino contributions in m_{ee} and to two–neutrino oscillations/conversions. The regions of the large mixing MSW solution are hatched; the small mixing solution is shown as a vertical line at $|U_{e1}|^2 \cdot \eta_1\eta_2 \simeq \pm 1$. For an appreciable contribution of the third neutrino state in m_{ee} the regions are larger: the dashed lines correspond to the case of three degenerate neutrinos, the dotted lines correspond to the case of large m_3, so that $m_3|U_{e3}|^2 = 0.5eV$. The upper bound on the electron antineutrino mass from the tritium experiments is also shown (from[27]).

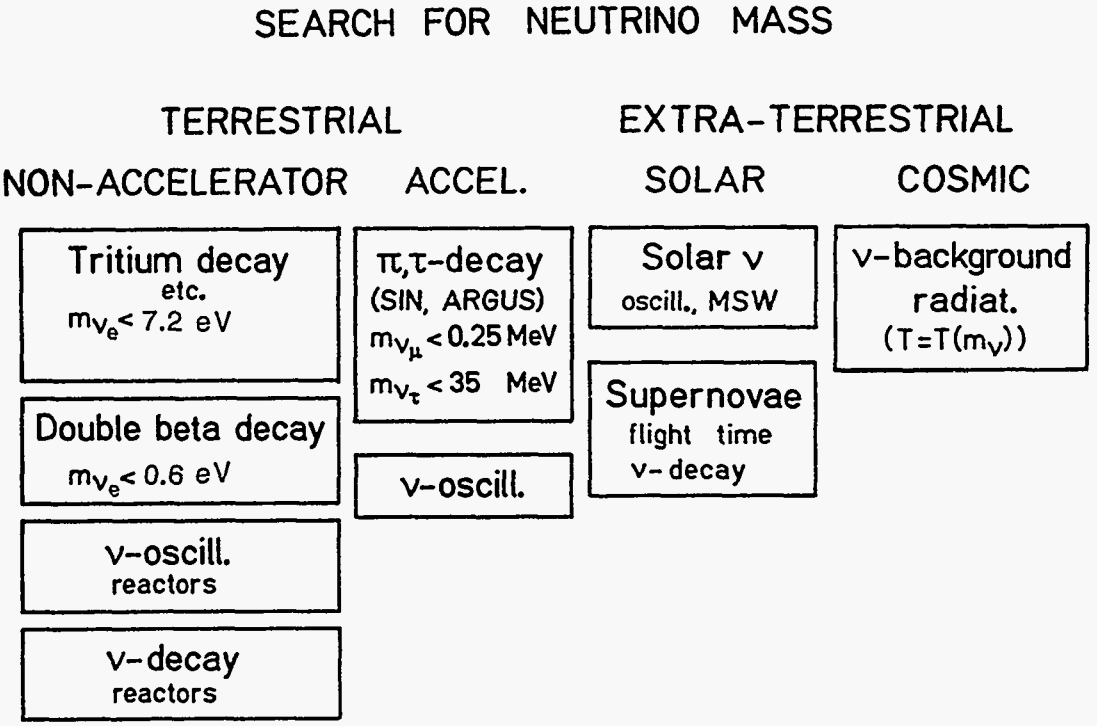

Fig.5 Classification of experiments investigating the neutrino mass (from[87]).

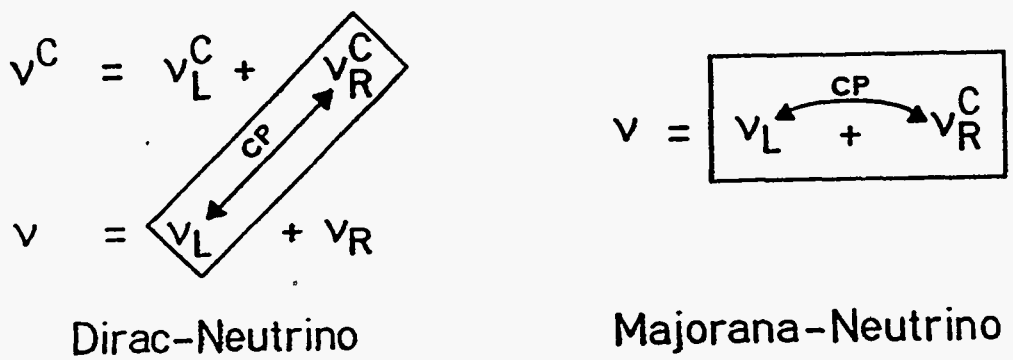

Fig.6 Possible assignments of the experimentally known (in boxes) neutrino states (of one family) in the theoretical description for Dirac and Majorana fields

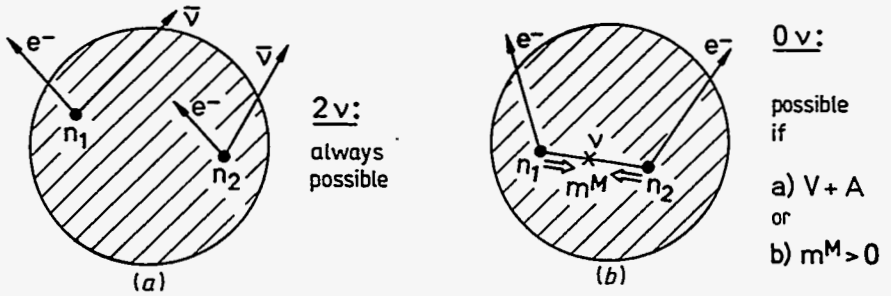

Fig.7a Schematic representation of 2ν and 0ν double beta decay

Neutrinoless double beta decay can be triggered by exchange of a light or heavy left-handed Majorana neutrino as shown in Fig. 7. (For exchange of a heavy *right*–handed neutrino see section 2.3) The propagators in the first and second case show a different m_ν dependence: Fermion propagator $\sim \frac{m}{q^2-m^2} \Rightarrow$

$$a) \quad m \ll \dot{q} \rightarrow\sim m \quad \textit{'light' neutrino} \tag{5}$$

$$b) \quad m \gg q \rightarrow\sim \frac{1}{m} \quad \textit{'heavy' neutrino} \tag{6}$$

The half–life for $0\nu\beta\beta$ decay induced by exchange of a light neutrino is given by

$$T^{0\nu}_{1/2}(0^+_i \rightarrow 0^+_f) = C_{mm}\frac{\langle m^2_\nu\rangle}{m^2_e} + C_{\eta\eta}\langle\eta\rangle^2 + C_{\lambda\lambda}\langle\lambda\rangle^2 + C_{m\eta}\frac{m_\nu}{m_e} + C_{m\lambda}\langle\lambda\rangle\frac{\langle m_\nu\rangle}{m_e} + C_{\eta\lambda}\langle\eta\rangle\langle\lambda\rangle \tag{7}$$

or, when neglecting the effect of right–handed weak currents, by

$$T^{0\nu}_{1/2}(0^+_i \rightarrow 0^+_f) = C_{mm}\frac{\langle m_\nu\rangle^2}{m^2_e} = (M^{0\nu}_{GT} - M^{0\nu}_F)^2 G_1 \frac{\langle m_\nu\rangle^2}{m^2_e} \tag{8}$$

where G_1 denotes the phase space integral, $\langle m_\nu\rangle$ denotes an effective neutrino mass

$$\langle m_\nu\rangle = \sum_i m_i U^2_{ei}, \tag{9}$$

respecting the possibility of the electron neutrino to be a mixed state (mass matrix not diagonal in the flavor space)

$$|\nu_e\rangle = \sum_i U_{ei}|\nu_i\rangle \tag{10}$$

The effective mass $\langle m_\nu\rangle$ could be smaller than m_i for all i for appropriate CP phases of the mixing coefficiants U_{ei}. In general not too pathological GUT models yield $m_{\nu_e} = \langle m_{\nu_e}\rangle$ (see[22]).

η,λ describe an admixture of right–handed weak currents, and $M^{0\nu} \equiv M^{0\nu}_{GT} - M^{0\nu}_F$ denote nuclear matrix elements.

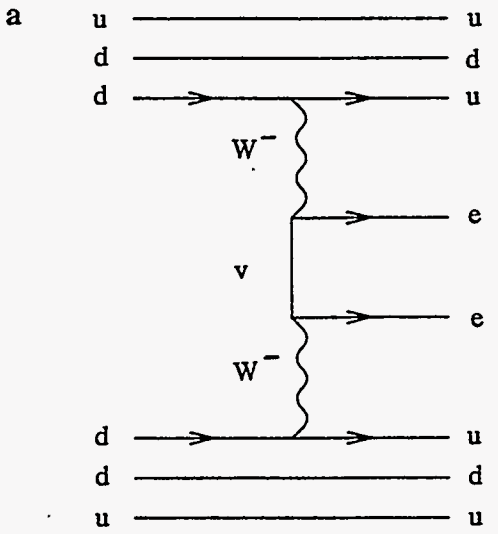

Fig.7b Feynman Graph for neutrinoless double beta decay triggered by exchange of a left–handed light or heavy neutrino

Nuclear matrix elements:

A detailed discussion of $\beta\beta$ matrix elements for neutrino induced transitions including the substantial (well–understood) differences in the precision with which 2ν and $0\nu\beta\beta$ rates can be calculated, can be found in.[23,34-36] After the major step of recognizing the importance of g.s. correlations for the calculation of $\beta\beta$ matrix elements,[37,38] in recent years the main groups used the QRPA model for calculation of $M^{0\nu}$. The different groups obtained very similar results for $M^{0\nu}$ when using a realistic nucleon–nucleon interaction,[35,36,39] consistent with shell model approaches,[40,41] where the latter are possible. Some deviation is found only when a non–realistic nucleon–nucleon interaction is used (e.g. δ force, see[42] and also[43]). Also use of a by far too small configuration space like in recent shell model Monte Carlo (SMMC) calculations[44] can hardly lead to reliable results. On the other hand refinements of the QRPA approach by going to higher order QRPA (see[45,46])lead only to minor changes for the $0\nu\beta\beta$ ground state transitions. An effect of inclusion of the proton–neutron pairing force is discussed by.[47] The corresponding results for $0\nu\beta\beta$ decay presented by[48] should be checked. The results of high-lying GT strength (in the GTGR and in the Δ resonance) have been studied early already.[38]

Since the usual QRPA approach does ignore deformation, some larger uncertainty in these approaches may occur in deformed nuclei. This shows up for example in different results obtained for ^{150}Nd by QRPA and by a pseudo SU(3) model as used by.[49] Calculation of matrix elements of all double beta emitters have been published by.[50,36] Fig. 8 shows typical uncertainties of calculated $0\nu\beta\beta$ rates originating from our limited knowledge of the particle–particle force, which is the main source of the uncertainty in those nuclei where this QRPA approach is applicable.

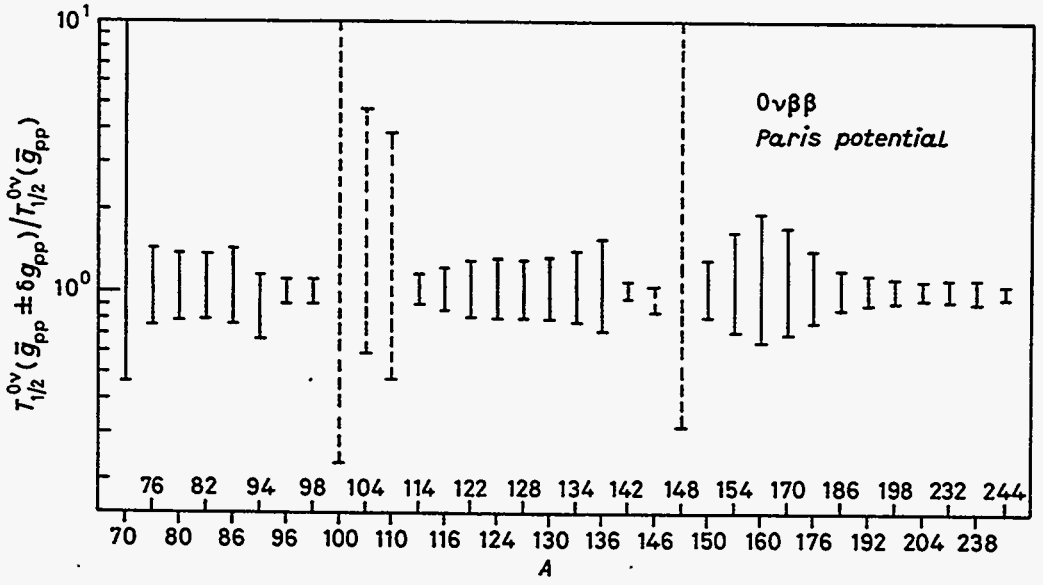

Fig.8 Illustration of the variation of the 0ν decay rates within the probable range of the particle–particle interaction g_{PP}. The dashed "error bars" indicate isotopes for which the matrix elements are evaluated close to the collapse of the RPA or at $g_{PP} < \overline{g_{PP}}$ (from[36]).

2.2. Supersymmetry

Supersymmetry (SUSY) is considered as prime candidate for a theory beyond the standard model, which could overcome some of the most puzzling questions of today's particle physics (see, e.g.[51,52]). Accelerator experiments have hunted for signs of supersymmetric particles so far without success. Lower limits on masses of SUSY particles are at present in the range of 20–100 GeV,[53] mainly from experiments at LEP and TEVATRON.

SUSY particles differ from usual particles not only in their masses but also in R–parity, assigned to be $R_P = 1$ for usual particles and $R_P = -1$ for SUSY particles. Conservation of R–parity has been imposed ad hoc to the minimal supersymmetric extension of the standard model (MSSM) to ensure baryon number and lepton number conservation. Attention has, however, been focused also on SUSY theories with R–parity violation. In such theories $0\nu\beta\beta$ decay can proceed by exchange of supersymmetric particles like gluinos, photinos,... (Fig. 9). This process has exactly the same experimental signature, as $0\nu\beta\beta$ decay via neutrino exchange. Thus $0\nu\beta\beta$ decay can be used to restrict R–parity violating SUSY models.[6,12,24,54,55] Fig. 9 shows the Feynman graphs for SUSY contributions to $0\nu\beta\beta$ decay, partly first presented by.[6,54] From these

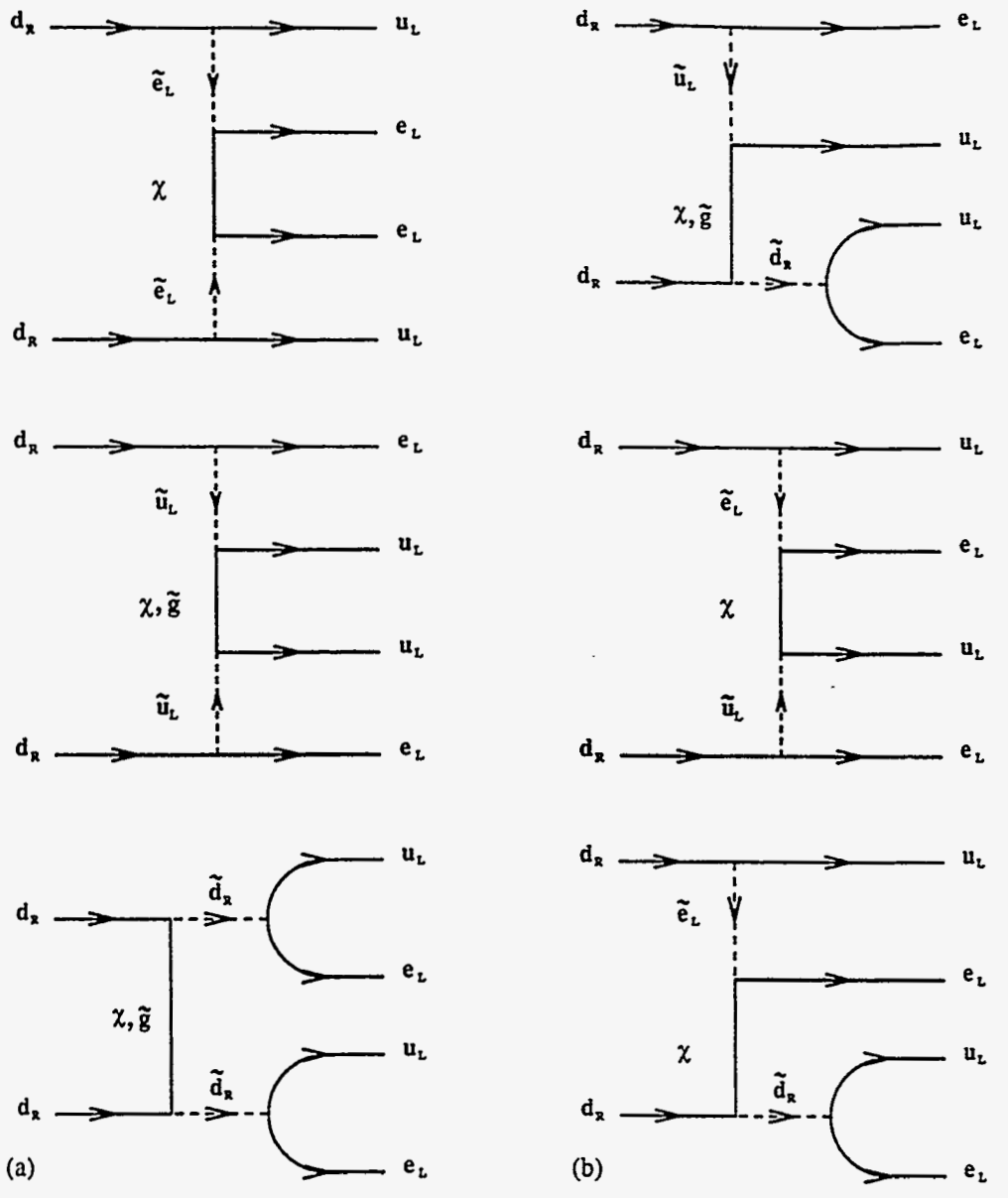

Fig.9 Feynman graphs for the supersymmetric contributions to $0\nu\beta\beta$ decay (from[6]).

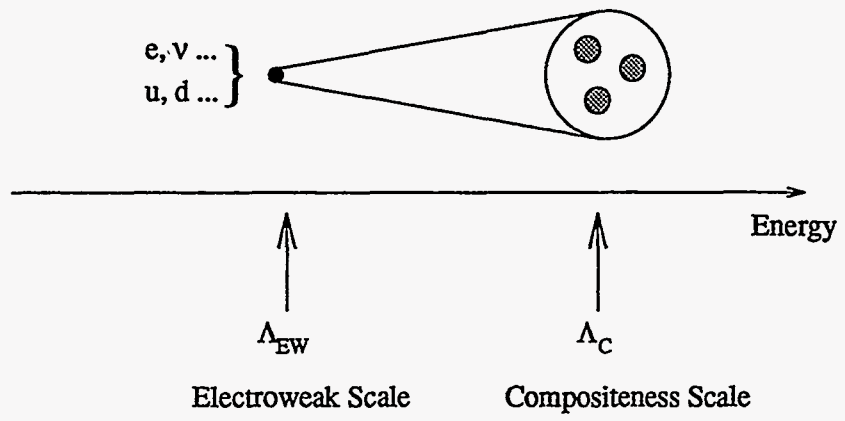

Fig.10 The idea of compositeness: at a (still unknown) energy scale Λ_C (the compositeness scale) quarks and leptons might show an internal structure (from[10]).

graphs one derives[6] under some assumptions

$$[T^{0\nu}_{1/2}(0^+ \rightarrow 0^+)]^{-1} \sim G_{01}(\frac{\lambda'^2_{111}}{m^4_{\tilde{q},\tilde{e}} m_{\tilde{g}\chi}} M)^2 \qquad (11)$$

where G_{01} is a phase space factor, $m_{\tilde{q}\tilde{e}\tilde{g}\chi}$ are the masses of supersymmetric particles involved: squarks, selectrons, gluinos, and neutralinos. λ'_{111} is the strength of an R–parity breaking interaction, and M is a nuclear matrix element. For the matrix elements and their calculation see.[12]

2.3. Heavy neutrinos and right–handed W Boson

Heavy *right–handed* neutrinos appear quite naturally in left–right symmetric GUT models. They offer in some natural way via the see–saw mechanism explanation for the small neutrino masses compared to other fermions and can explain also naturally parity violation. However the symmetry breaking scale for the right–handed sector is not fixed by the theory and thus the mass of the right–handed W_R boson and the mixing angle between the mass eigenstates W_1, W_2 are free parameters. $0\nu\beta\beta$ decay taking into account contributions from both, left– and right–handed neutrinos have been studied theoretically by.[13,56] The former gives a more general expression for the decay rate than introduced earlier by.[57] From a $0\nu\beta\beta$ experiment one can deduce a limit on m_{W_R} as function of the mass m_N of the right–handed heavy neutrino (see[13] and section 3).

2.4. Compositeness

Although so far there are no experimental signals of a substructure of quarks and leptons, there are speculations that at some higher energy ranges beyond 1 TeV or so there might exist an energy scale Λ_C at which a substructure of quarks and leptons (preons) might become visible[10,52,58](Fig. 10).

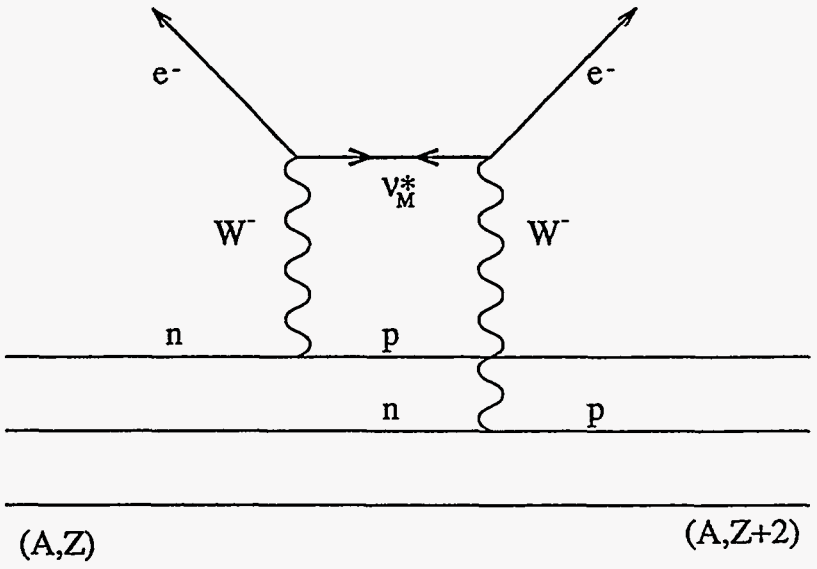

Fig.11 Neutrinoless double beta decay ($\Delta L = +2$) mediated by a composite heavy Majorana neutrino (from[10]).

The main consequences of compositeness of quarks and leptons are (1) modifications to the gauge boson propagators and the interaction vertices with fermions, and additional effective four–fermion interactions through constituent exchange (2) highly massive excited states which couple to the ordinary fermions through gauge interactions. This is discussed in detail in.[10] Lower bounds on the compositeness scale have been deduced from accelerator experiments at LEP,[59] Fermilab,[60] HERA[5] and from a theoretical analysis of the effect of contact interactions in the leptonic τ decay.[61] They are all in the range of $\Lambda_C \geq 1.6$ TeV.

The *masses* of the excited leptons (l^*) and quarks (q^*) should not be lower than the compositeness scale Λ_C. Already in 1982 it was shown[62] that precise measurements of the anomalous magnetic moment of the electron give bounds on the masses of the excited states and thus the compositeness scale.

Limits on the masses of excited leptons from accelerators are $m_{e^*} > 127$ GeV,[63] $m_{e^*,\nu^*} > 91$ GeV,[64] $m_{\nu^*} > 180$ GeV[65,66] $m_{q^*} > 540$ GeV.[67]

A possible low energy manifestation of compositeness could be neutrinoless double beta decay, mediated by a composite heavy Majorana neutrino (Fig. 11), which then should be a Majorana particle.

Recent theoretical work shows (see Panella[8] and Takasugi[8]) that the bounds which can be derived from double beta decay are at least of the same order of magnitude or better than those coming from the direct search of excited states in high energy accelerators (see also section 3).

2.5. Majorons

The existence of new bosons, so–called Majorons, can play a significant role in new physics beyond the standard model, in the history of the early universe, in the evolution of stellar objects, in supernovae astrophysics and the solar neutrino problem.[68,69] In many theories of physics beyond the standard model neutrinoless double beta decay can occur with the emission of Majorons

$$2n \rightarrow 2p + 2e^- + \phi \tag{12}$$

$$2n \rightarrow 2p + 2e^- + 2\phi. \tag{13}$$

In the classical Majoron model invented by Gelmini and Roncadelli in '81,[70] the Majoron is the Nambu–Goldstone boson associated with the spontaneous breaking of the $B-L$–symmetry and so generates Majorana masses of neutrinos. This was expected[68] to give a sizeable contribution to double beta decay. It was, however, ruled out, as also the doublet Majoron[73] by LEP[74] since it should contribute the equivalent of two neutrino species to the width of the Z^0. On the other hand, Majoron models in which the Majoron is an electroweak isospin singlet[71,72] are still viable. The drawback of the singlet Majoron is that it requires a severe finetuning in order to preserve existing bounds on neutrino masses and at the same time get an observable rate for Majoron accompanied $0\nu\beta\beta$ decay.

To avoid such an unnatural fine–tuning in recent years several new Majoron models were proposed,[75–77] where the term Majoron denotes in a more general sense light or massless bosons with couplings to neutrinos.

The main novel features of these "New Majorons" are that they can carry leptonic charge, that they need not be Goldstone bosons and that emission of two Majorons can occur. The latter can be scalar–mediated or fermion–mediated (Fig. 12). Table 3 shows some features of the different Majoron models according to.[76,77] L denotes the leptonic charge, n the spectral index defining the phase space of the emitting particles, M the nuclear matrix elements. For details we refer to Päs et al.[8],[16] Burgess[8].[78]

The half–lifes are according to[79,80] in some approximation given by

$$[T_{1/2}]^{-1} = | < g_\alpha > |^2 \cdot |M_\alpha|^2 \cdot G_{BB_\alpha} \tag{14}$$

for $\beta\beta\phi$-decays, or

$$[T_{1/2}]^{-1} = | < g_\alpha > |^4 \cdot |M_\alpha|^2 \cdot G_{BB_\alpha} \tag{15}$$

for $\beta\beta\phi\phi$–decays. The index α indicates that effective neutrino–Majoron coupling constants g, matrix elements M and phase spaces G differ for different models.

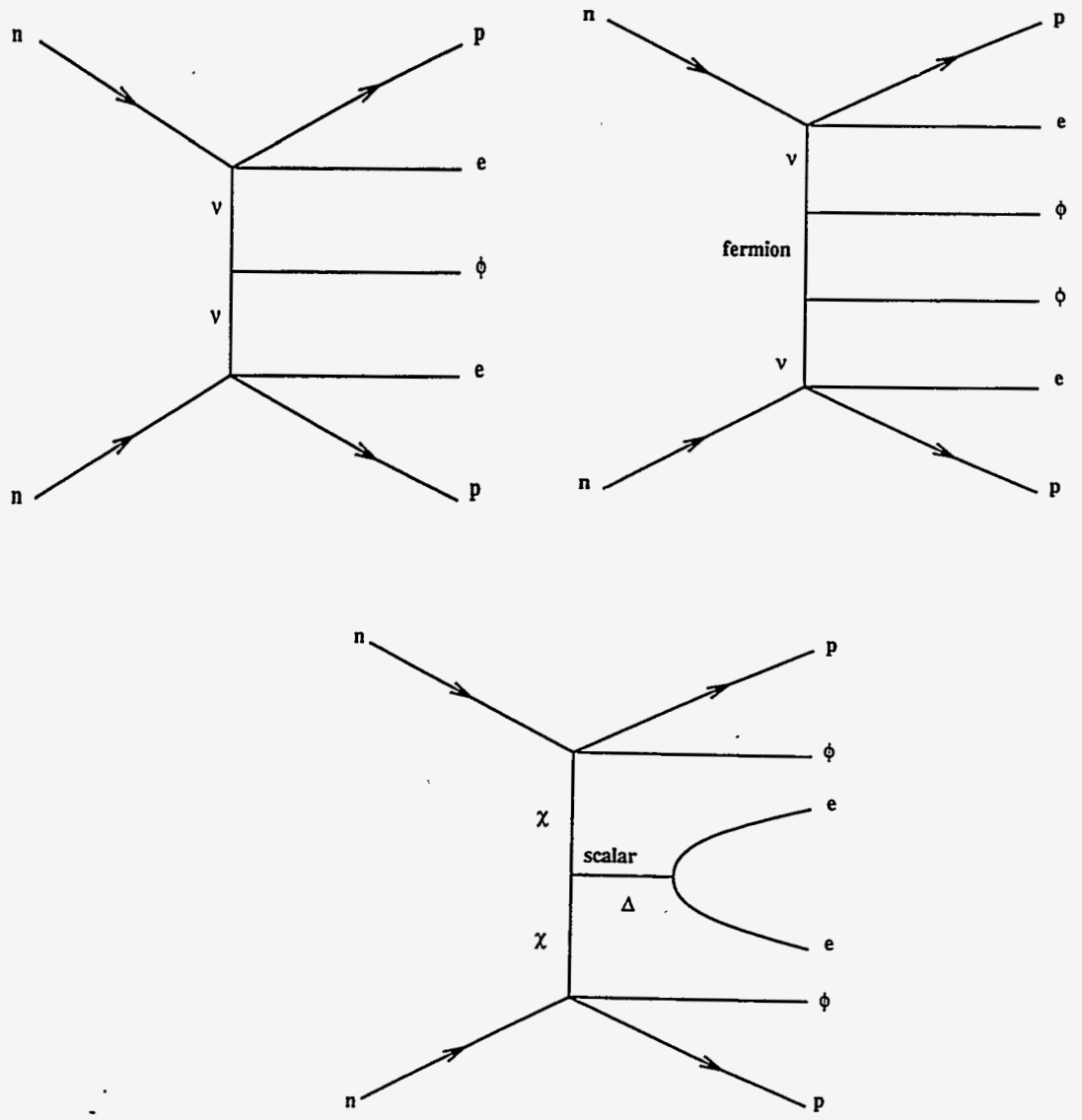

Fig.12 Feynman graphs for $\beta\beta\phi$ decays (a), fermion–mediated $\beta\beta\phi\phi$ decays (b), and scalar–mediated $\beta\beta\phi\phi$ decays (c)

case	modus	Goldstone boson	L	n	Matrix element
IB	$\beta\beta\phi$	no	0	1	$M_F - M_{GT}$
IC	$\beta\beta\phi$	yes	0	1	$M_F - M_{GT}$
ID	$\beta\beta\phi\phi$	no	0	3	$M_{F\omega^2} - M_{GT\omega^2}$
IE	$\beta\beta\phi\phi$	yes	0	3	$M_{F\omega^2} - M_{GT\omega^2}$
IIB	$\beta\beta\phi$	no	-2	1	$M_F - M_{GT}$
IIC	$\beta\beta\phi$	yes	-2	3	M_{CR}
IID	$\beta\beta\phi\phi$	no	-1	3	$M_{F\omega^2} - M_{GT\omega^2}$
IIE	$\beta\beta\phi\phi$	yes	-1	7	$M_{F\omega^2} - M_{GT\omega^2}$
IIF	$\beta\beta\phi$	Gauge boson	-2	3	M_{CR}

Table 3. Different Majoron models according to Bamert/Burgess/Mohapatra[75]. The case IIF corresponds to the model of Carone[76].

model	$T_{1/2}(< g >= 10^{-4})$	$T_{1/2}(< g >= 1)$	$T_{1/2exp}$
IB,IC,IIB	$4 \cdot 10^{22}$	$4 \cdot 10^{14}$	$1.67 \cdot 10^{22}$
ID,IE,IID	10^{38-42}	10^{22-26}	$1.67 \cdot 10^{22}$
IIC,IIF	$2 \cdot 10^{28}$	$2 \cdot 10^{20}$	$1.67 \cdot 10^{22}$
IIE	10^{38-42}	10^{22-26}	$3.37 \cdot 10^{22}$

Table 4. Comparison of half–lives calculated for different $< g >$–values for the new Majoron models with experimental best fit values (from [15])

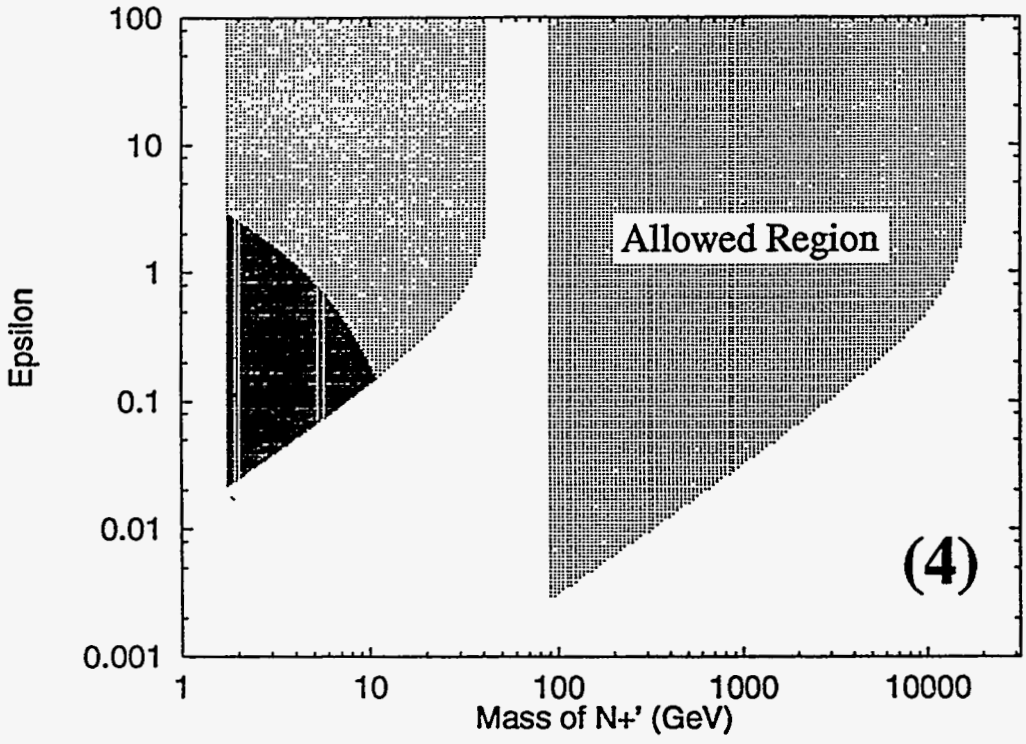

Fig.13 Regions of the parameter space ($\epsilon - M_{N'_+}$ plane) yielding an observable signal (shaded areas) (from[83]). Darker area: 'natural' region, lighter shaded: Finetuning needed, to keep m_{ν_e} below 1 eV. $M_{N'_+}$: mass eigenstate, ϵ: strength of lepton number violation in mass matrix

Nuclear matrix elements:

According to Table 3 there are five different nuclear matrix elements. Of these M_F and M_{GT} are the same which occur in $0\nu\beta\beta$ decay. The other ones and the corresponding phase spaces have been calculated for the first time by.[16,81] The calculation of the matrix elements show (see Päs et al.[8]) that the new models predict, as consequence of the small matrix elements very large half–lives and that unlikely large coupling constants would be needed to produce observable decay rates (see Table 4).

2.6. Sterile neutrinos

Introduction of sterile neutrinos has been claimed to solve simultaneously the conflict between dark matter neutrinos, LSND and supernova nucleosynthesis.[82] Neutrinoless double beta decay can investigate several effects of heavy sterile neutrinos.[83]

If we assume having a light neutrino with a mass $\ll 1$ eV, mixing with a much heavier (m ≥ 1 GeV) sterile neutrino can yield under certain conditions a detectable signal in current $\beta\beta$ experiments.

In models with two (or more) sterile neutrinos, the sterile neutrinos can mix

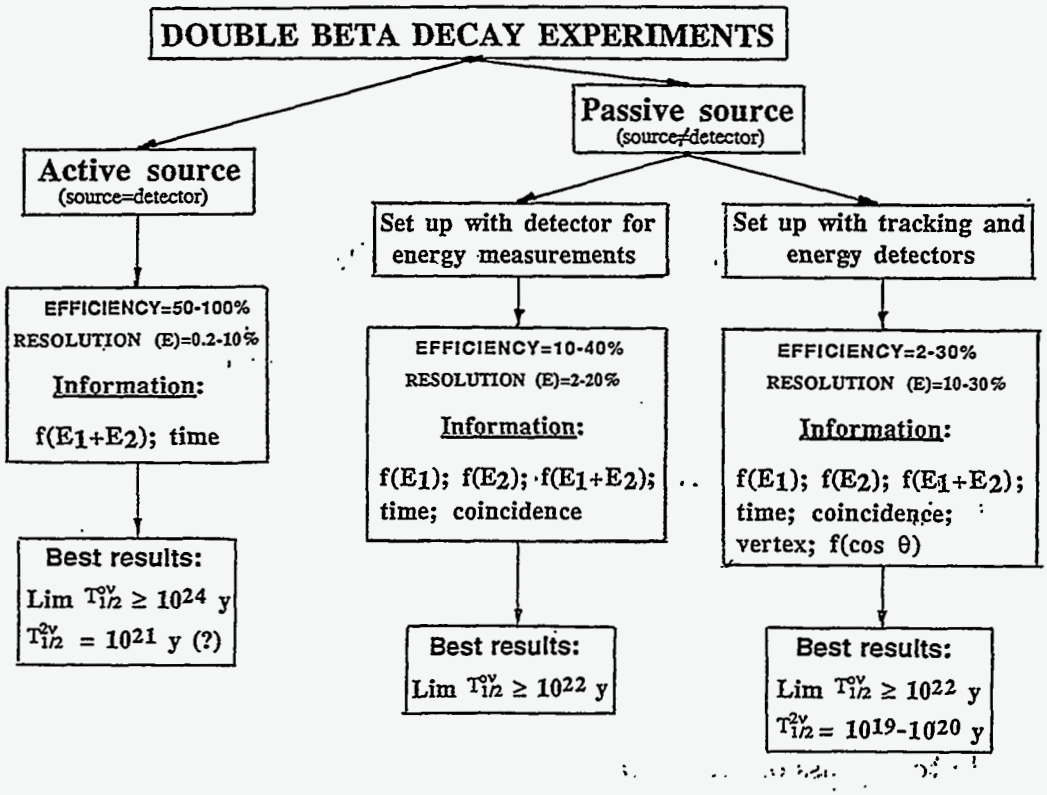

Fig.14 Classification of $\beta\beta$ decay experiments (from[87])

appreciably even in the limit $m_{\nu_e} \to 0$ and so can be potentially visible in many processes.[84] Neutrinoless double beta decay proceeds in these models through the virtual exchange of the heavier (i.e. GeV scale or higher) neutrinos. Fig. 13 shows the mass ranges leading to a $0\nu\beta\beta$ signal close to observability (shaded areas).

3. Double Beta Decay Experiments: Status and Perspectives

We can differentiate between two classes of direct (non–geochemical) $\beta\beta$ decay experiments (Fig. 14):

a) active source experiments (source = detectors)

b) passive source experiments

In the first class of experiments the $\beta\beta$ process usually is identified only on the basis of the distribution of the total energy of the electrons. The second class of experiments yields in principle more complete information on the $\beta\beta$ events by measuring time coincidence, tracks and vertices of the electrons and their energy distribution. But also time projection chambers (TPCs) using $\beta\beta$ active counting gas are belonging to the first class – such as the Gotthard ^{136}Xe experiment.

It is obvious from Fig. 23, which shows an overview over measured $0\nu\beta\beta$ half–life limits and deduced mass limits, that the largest sensitivity for $0\nu\beta\beta$ decay is obtained at present by active source experiments, in particular ^{76}Ge[85–87] and ^{136}Xe.[88] The main reason is that large source strengths can be used (simultaneously with high energy

resolution), in particular when enriched $\beta\beta$ emitter materials are used.

Other criteria for the "quality" of a $\beta\beta$ emitter are:

- a small product $T^{0\nu}_{1/2} \cdot \langle m_\nu \rangle^2$, i.e. a large matrix element $M^{0\nu}$ or phase space
- a $Q_{\beta\beta}$ value beyond the limit of natural radioactivity (2.614 MeV)

The future of $\beta\beta$ experiments will be dominated by use of enriched detectors, ^{76}Ge playing a particular favourable role here, and enriched source material such as ^{136}Xe, ^{100}Mo, ^{116}Cd. Some of these experiments may probe the neutrino mass in the next years down to 0.1 eV, see Fig. 23b. A detailed discussion of the various experimental possibilities can be found in.[1] A useful listing of existing data from the various $\beta\beta$ emitters is given in.[89]

3.1. The HEIDELBERG–MOSCOW experiment

3.1.1. Status

The HEIDELBERG–MOSCOW experiment[85–87,90,91] (Fig. 15) is now exploring the sub–eV range for the mass of the electron neutrino. With five enriched (86% of ^{76}Ge) detectors of a total mass of 11.5 kg taking data in the Gran Sasso underground laboratory the experiment has reached its final setup. The experiment gives at present for most parameters the sharpest limits from double beta decay. They are discussed in detail in[8] by B.Maier, M. Hirsch, H. Päs, O.Panella, E. Takasugi. Since these results are representative in that they set the scale of this type of experiments, they will be briefly listed up here. Fig. 16 shows the spectrum taken in a measuring time of 17.70 or 13.6 kg y, respectively.

Half–life of neutrinoless double beta decay

The deduced half–life limit for $0\nu\beta\beta$ decay is

$$T^{0\nu}_{1/2} > 7.4 \cdot 10^{24} y \ (90\% C.L.) \tag{16}$$

$$> 12.7 \cdot 10^{24} y \ (68\% C.L.) \tag{17}$$

Neutrino mass

Light neutrinos: The deduced upper limit of an (effective) electron neutrino Majorana mass is, with the matrix element from[36]

$$\langle m_\nu \rangle < 0.56 eV \ (90\% C.L.) \tag{18}$$

$$< 0.43 eV \ (68\% C.L.) \tag{19}$$

This is the sharpest limit for a Majorana mass of the electron neutrino so far.

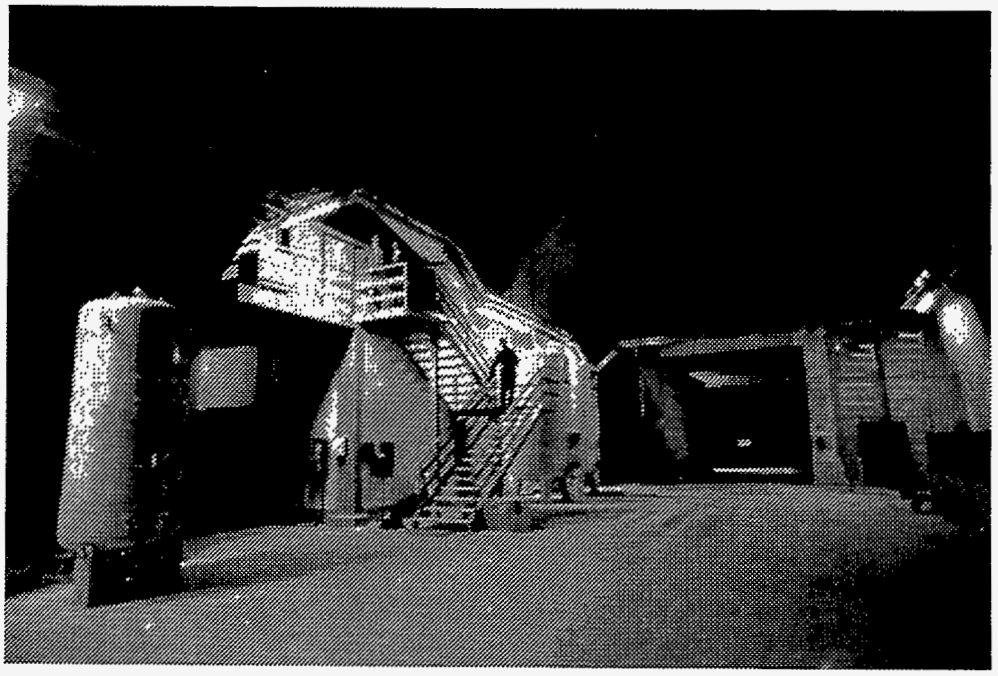

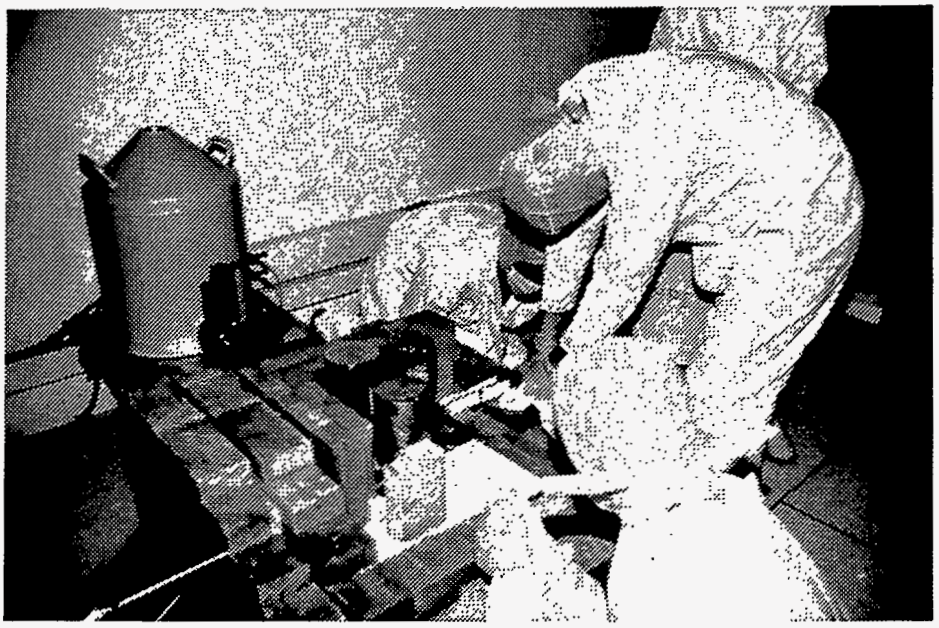

Fig.15 The $\beta\beta$ laboratory of the HEIDELBERG-MOSCOW experiment in the Gran Sasso near Rome (a), Mounting of the first enriched detectors under low–level conditions (b).

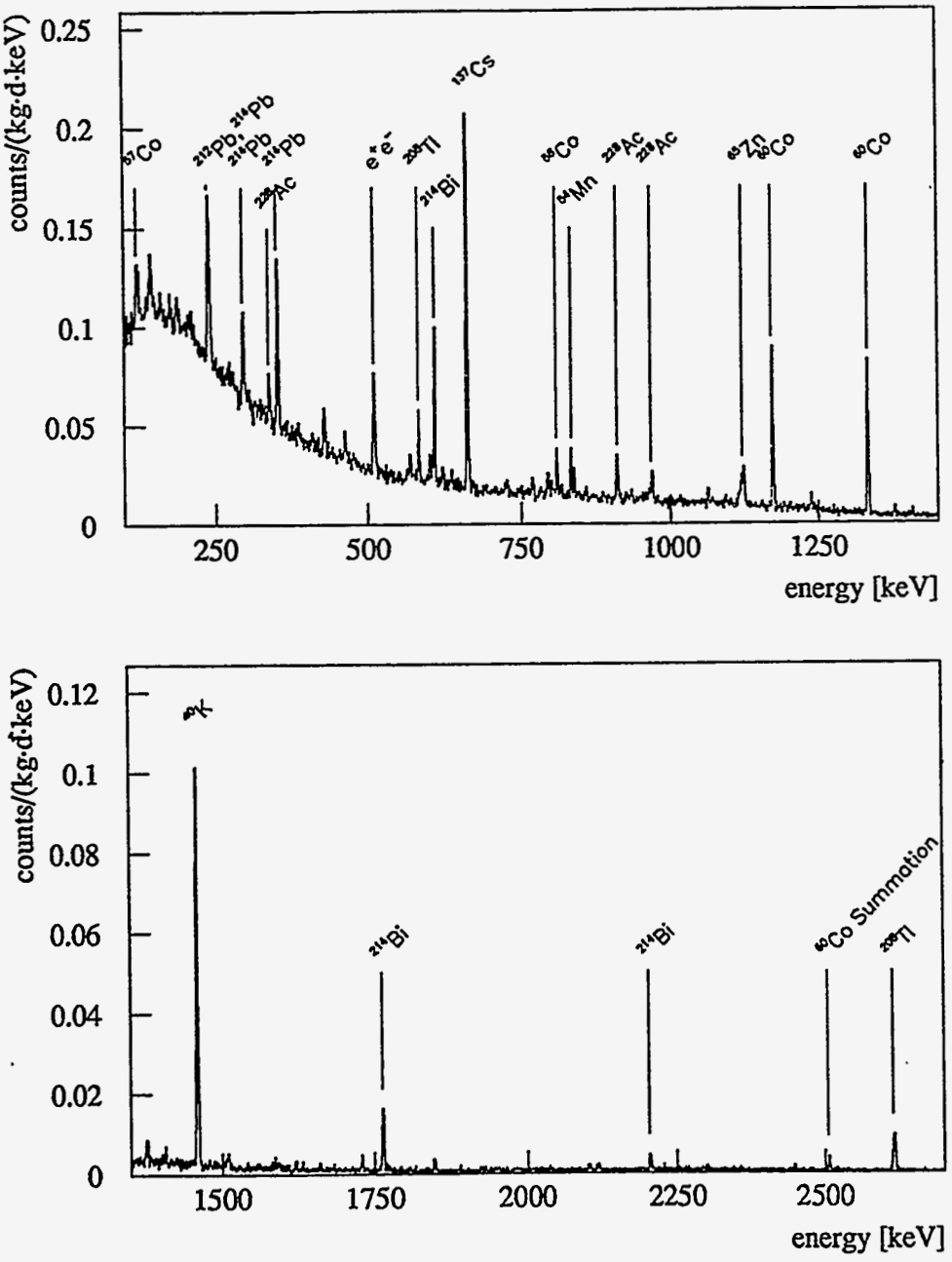

Fig.16a Integral spectrum of the enriched ^{76}Ge detectors of the HEIDELBERG-MOSCOW experiment after 17.70 kg y of measurement.

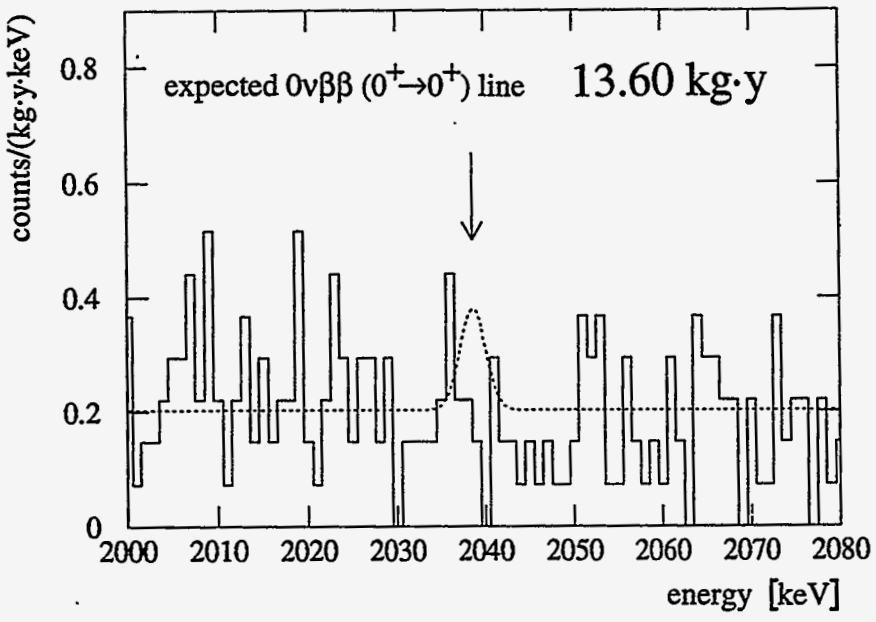

Fig.16b Region of interest in the combined spectrum of Fig.16a after subtraction of the first 200 days of measurement of each detector, leaving 13.60 kg y of measuring time. The dotted curve corresponds to the signal excluded with 90%$C.L.$ It corresponds to $T^{0\nu}_{1/2} > 7.4 \cdot 10^{24}$ y.

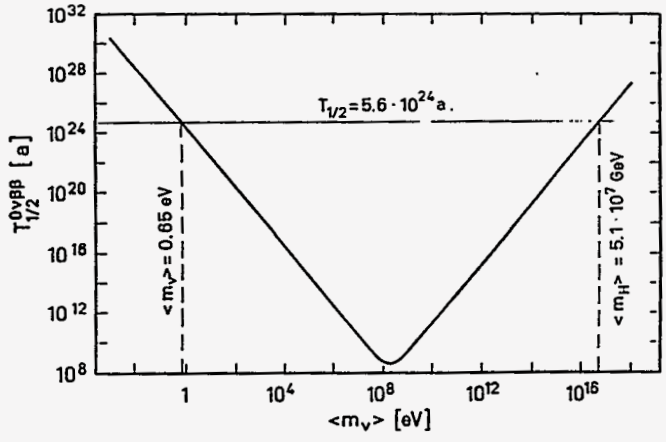

Fig.17 Considering the dependence of the nuclear matrix element on the neutrino mass yields also a lower limit of a heavy left–handed neutrino, of $\langle m_H \rangle > 5.1 \cdot 10^7$ GeV (from[85])

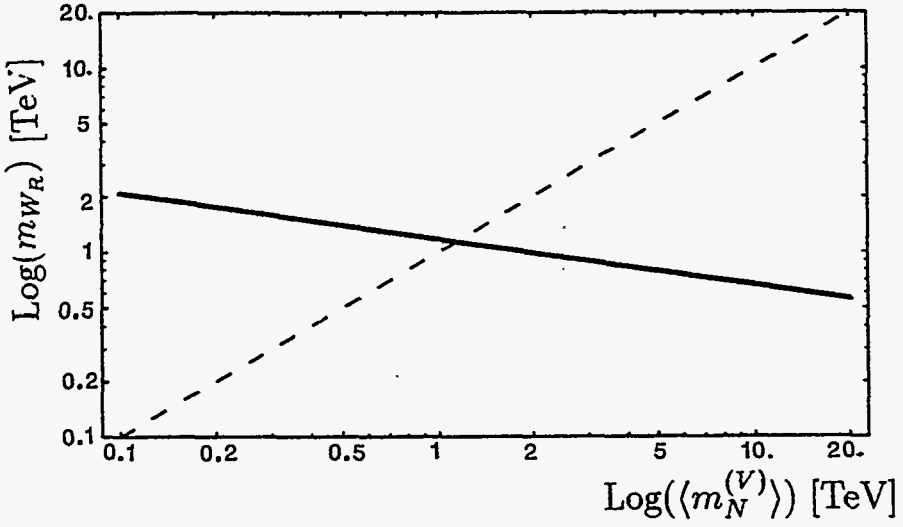

Fig.18 Area excluded from the HEIDELBERG–MOSCOW experiment (below the curves) in the plane of the right–handed W boson mass versus the mass of a heavy right–handed neutrino. The full line is the constraint from $0\nu\beta\beta$ decay, the dotted line is the requirement of vacuum stability (from[13])

Superheavy neutrinos: For a superheavy *left*–handed neutrino we deduce ([85] and Fig. 17) exploiting the mass dependence of the matrix element (for the latter see[35]) a lower limit

$$\langle m_H \rangle \geq 5.1 \cdot 10^7 GeV \tag{20}$$

For a heavy *right*–handed neutrino the relation obtained to the mass of the right–handed W boson is shown in Fig. 18 (see[13]).

Right–handed W boson

For the right–handed W boson we deduce[13] a lower limit of

$$m_{W_R} \geq 1.1 TeV \tag{21}$$

SUSY parameters

New constraints on the parameters of the minimal supersymmetric standard model with explicit R–parity violation are deduced[6,12] from the $0\nu\beta\beta$ half–life limit, which are more stringent than those from other low–energy processes and from the largest high energy accelerators (Fig. 19).

Compositeness

Evaluation of the $0\nu\beta\beta$ half–life limit for exchange of excited Majorana neutrinos ν^* yields under some assumptions[11] as lower mass bound of an excited neutrino

$$m_{\nu^*} > 5.9 \cdot 10^4 TeV \tag{22}$$

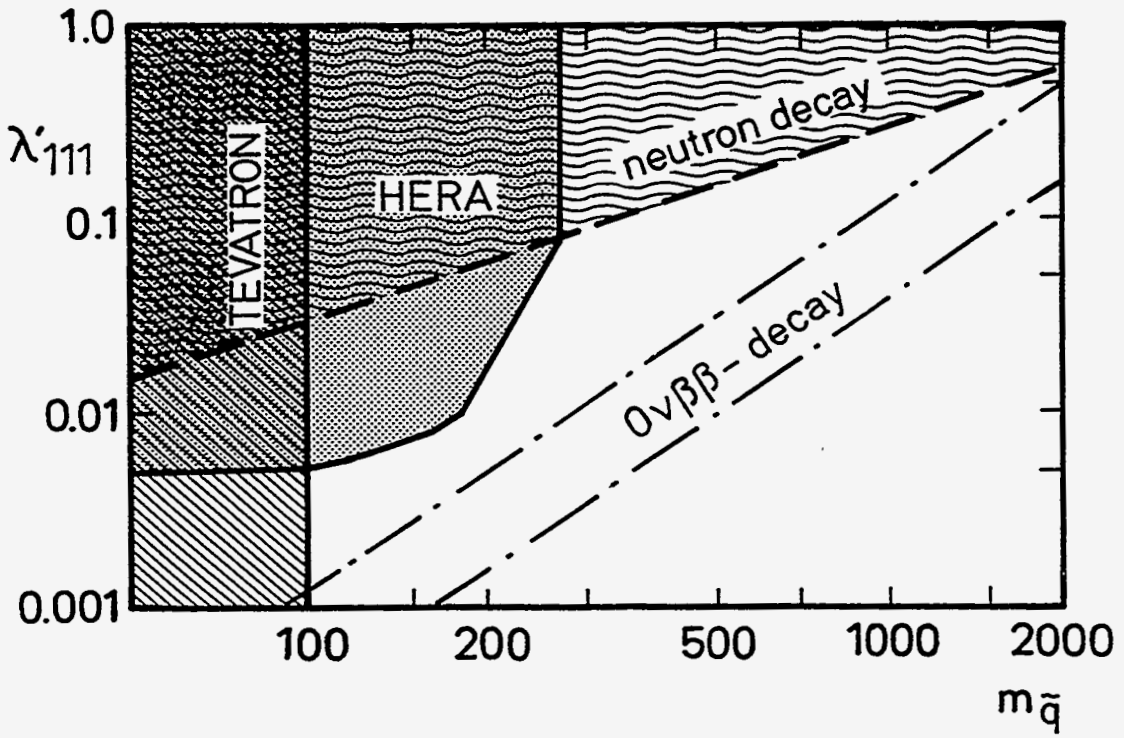

Fig.19 Comparison of limits on the R–parity violating MSSM parameters from different experiments in the λ'_{111}–$m_{\tilde{q}}$ plane. The dashed line is the limit from charged current universality according to.[119] The vertical line is the limit from the data of Tevatron.[120] The thick full line is the region which might be explored by HERA.[121] The two dash–dotted lines to the right are the limits obtained from the half–life limit for $0\nu\beta\beta$ decay of ^{76}Ge, for gluino masses of (from left to right) $m_{\tilde{g}}$ =1TeV and 100 GeV, respectively. The regions to the upper left of the lines are forbidden (from[6]).

This is the most stringent bound so far.

The bounds deduced on the compositeness scale in different models are roughly of the order of magnitude as those coming from high energy experiments (see Panella,[8] Takasugi[8]).

Half–life of $2\nu\beta\beta$ decay

The experiment produced for the first time a high statistics $2\nu\beta\beta$ spectrum ($\sim$ 20000 counts). The deduced half–life is[86]

$$T^{2\nu}_{1/2} = (1.77^{+0.01}_{-0.01}(stat.)^{+0.13}_{-0.11}(syst.)) \cdot 10^{21} y \tag{23}$$

Majoron–accompanied decay

From fits like those shown in Fig. 20, fitting simultaneously the 2ν spectrum and one selected Majoron mode, experimental limits for the half–lives of the decay modes of the newly introduced Majoron models (C. Burgess[8]) are given for the first time (H. Päs et al.[8]).

The small matrix elements and phase spaces for these modes (see Päs et al.[8]) already determined that these modes by far cannot be seen in experiments of the present sensivity if we assume typical values for the neutrino–Majoron coupling constants around $\langle g \rangle = 10^{-4}$ (see table 4).

3.1.2. Perspectives

The HEIDELBERG–MOSCOW experiment will probe the neutrino mass within 5 years down to the order of 0.1 eV (Fig. 21). This limit will be reached taking into account the current background of 0.1 counts/kg y keV in the $0\nu\beta\beta$ region and a further reduction by a factor of $\sim$ 5 by digital puls shape analysis (DPSA). The new DPSA method which we developed[92] allows for the first time in a very efficient, and reliable way to discriminate between multiple site (MSE) and single site events (SSE) (see also B. Maier et al.[8]). Examples of the second class are the interaction of a beta particle, of the first class multiple Compton scattering events. Fig. 22 shows the result of the first application of this method with one of the enriched detectors in the Gran Sasso for a measuring time of 156 kg d. In Fig. 22a the analyzed MSE and in Fig. 22b the corresponding SSE spectrum of the double beta decay energy region is plotted. The original spectrum (equals the sum of the MSE and SSE spectra) contains 15 counts, while the SSE spectrum contains two, reflecting a drastic background reduction. The energy of the central count in the SSE spectrum is (2038.5 $\pm$ 3.6) keV corresponding exactly to the $Q_{\beta\beta}$ value. According to its shape the pulse is a clear single site event and thus a clear double beta candidate. The strong reduction of the background by the new DPSA method, with the potential of reducing the background in the $0\nu\beta\beta$ region to $\leq$ 0.02 counts/kg y keV, will be essential for the further experiment.

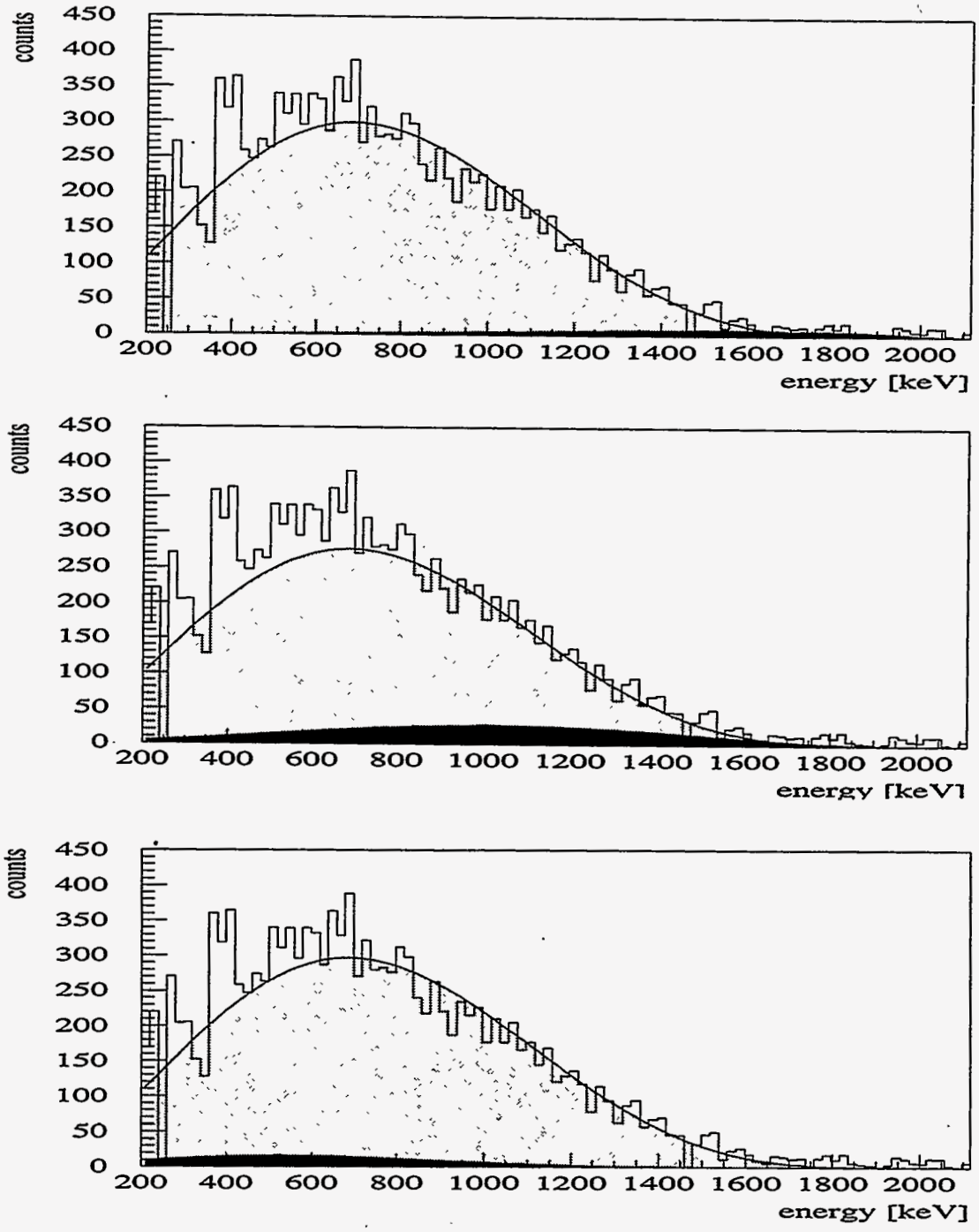

Fig.20 Simultaneous fit of the HEIDELBERG–MOSCOW experiment to $2\nu\beta\beta$ decay and
a) 'Ordinary' Majoron (n=1), yielding a half–life bound of $T_{1/2} > 7.91 \cdot 10^{21} y(90\% C.L.)$
b) 'Charged Majoron' or 'Double Majoron' (n=3), yielding a half–life bound of $T_{1/2} > 5.85 \cdot 10^{21} y(90\% C.L.)$
c) 'Double Majoron' (n=7), yielding a half–life bound of $T_{1/2} > 6.46 \cdot 10^{2}1 y(90\% C.L.)$
(from[16])

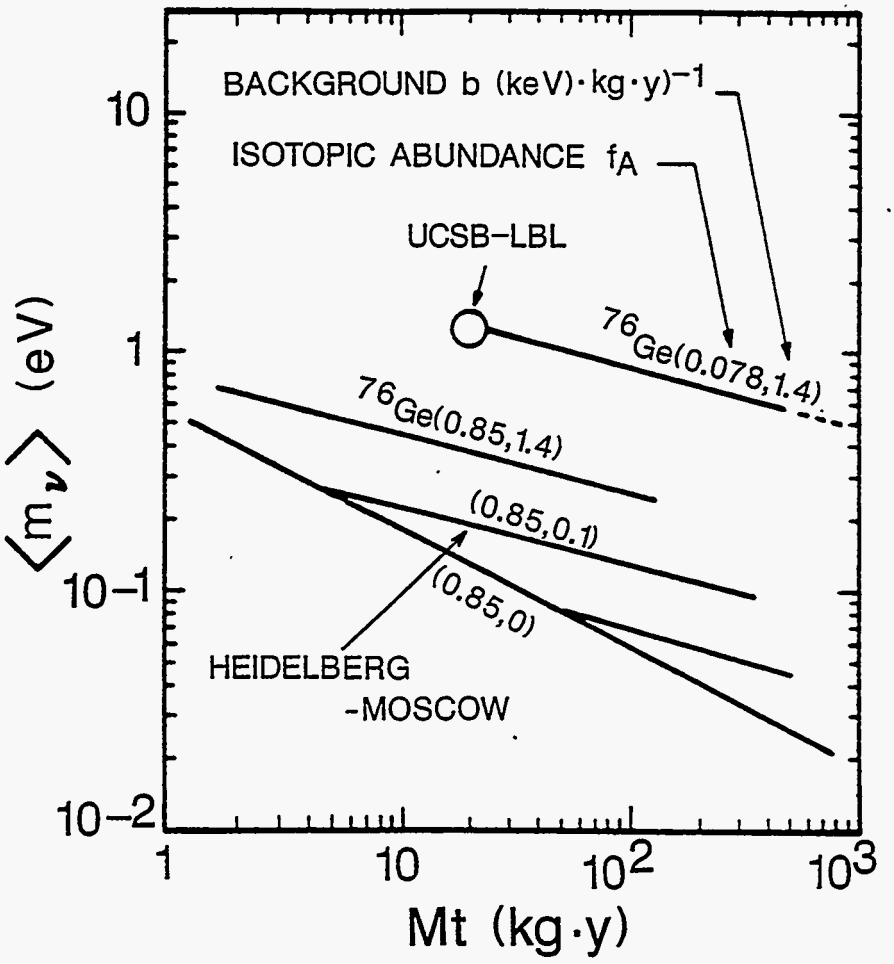

Fig.21 The ranges of neutrino mass which can be probed with Ge detectors of different enrichment in ^{76}Ge, as function of the product detector mass times measuring time (kg y)

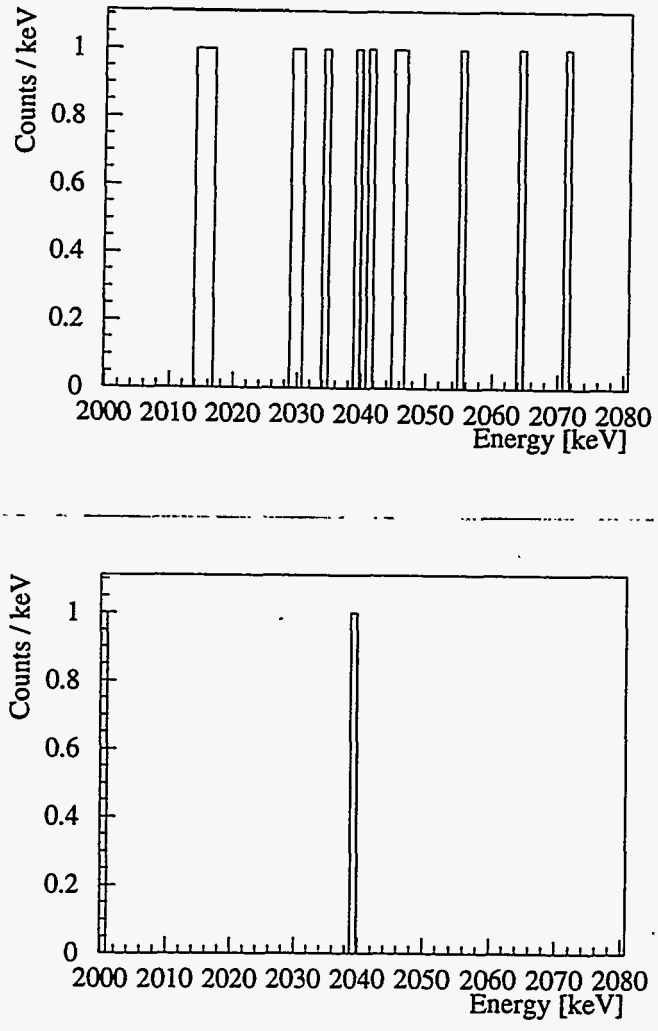

Fig.22 First test application of digital pulse shape analysis with an enriched ^{76}Ge detector in the Gran Sasso laboratory in a measuring time of 166 kg d. a) MSE spectrum b) SSE spectrum, demonstrating a drastic reduction of the background (from[92])

3.2. General Perspectives

Figs. 23a,b show the future perspectives of $\beta\beta$ decay experiments for the next decade. They show the present results and aims of the most promising double beta decay experiments in comparison with the HEIDELBERG-MOSCOW experiment. The best presently existing limits besides the HEIDELBERG-MOSCOW experiment (filled bars in Fig. 23), with half–life limits above 10^{21}a, have been obtained with the isotopes: ^{48}Ca,[93] ^{82}Se,[94] ^{100}Mo,[95] ^{116}Cd,[96] ^{130}Te,[97] ^{136}Xe[98] and ^{150}Nd.[99] These and other double beta decay setups presently under construction or partly in operation such as NEMO,[100] the Gotthard ^{136}Xe TPC experiment,[101] the ^{130}Te cryogenic experiment,[97] a new ELEGANT ^{48}Ca experiment using 64 g of ^{48}Ca,[102] a hypothetical experiment with an improved UCI TPC[99] assumed to use 1.6 kg of ^{136}Xe, etc., will not reach or exceed the ^{76}Ge limits. The limit given for the NEMO experiment (see Piquemal et al.[1048]) in Fig. 23 may even be very optimistic if claims about the effect of proton-neutron pairing on the $0\nu\beta\beta$ nuclear matrix elements by[48] will turn out to be true. As pointed out recently by Raghavan,[103] even use of an amount of about 200 kg of enriched ^{136}Xe or 2 tons of natural Xe added to the scintillator of the KAMIOKANDE detector or similar amounts added to BOREXINO (both primarily devoted to solar neutrino investigation) would hardly lead to a sensitivity larger than the present ^{76}Ge experiment. An interesting future candidate might be a ^{150}Nd bolometer exploiting the relatively large phase space of this nucleus (see[99]). The way outlined by[105] proposing a TPC filled with 1 ton of liquid enriched ^{136}Xe and identification of the daughter by laser fluorescence may not be feasible in a straight-forward way.

It is obvious that the HEIDELBERG-MOSCOW experiment will give the sharpest limit for the electron neutrino mass till the end of the decade and longer. For further improvements beyond the region of < 0.1 eV one has to think of *very large* experiments with *much bigger* source strength.

4. Dark matter search with enriched Ge detectors

The best laboratory limits on dark matter (WIMPs) are obtained at present by search with Germanium detectors. The HEIDELBERG–MOSCOW experiment allowed for the first time a search for dark matter with isotopically enriched material. Data taken with a 2.9 kg detector in 166 kg d were used to set limits on spin–independently interacting WIMPS.[107] A background level of 0.102 ± 0.005 events /kg d keV was achieved (average value between 11 and 30 keV), which is better than in other dedicated dark matter experiments with Ge detectors. The existing cross section limits for WIMP masses above $\sim$ 150 GeV were improved (Fig. 24) compared to other recent work, and Dirac neutrinos could be excluded as the dominant component of the dark halo in the mass range 26 GeV to 4.7 TeV. Since the cross section for sneutrino–nucleus interactions is four times larger than for Dirac neutrino–nucleus interactions the measured limit of Fig. 24 rules out also heavy sneutrinos as dark matter in scenarios of a minimal supersymmetric standard model.[108] The potential of ^{76}Ge dark matter detectors for search for neutralinos in relation to the non–zero spin ^{73}Ge has been carefully

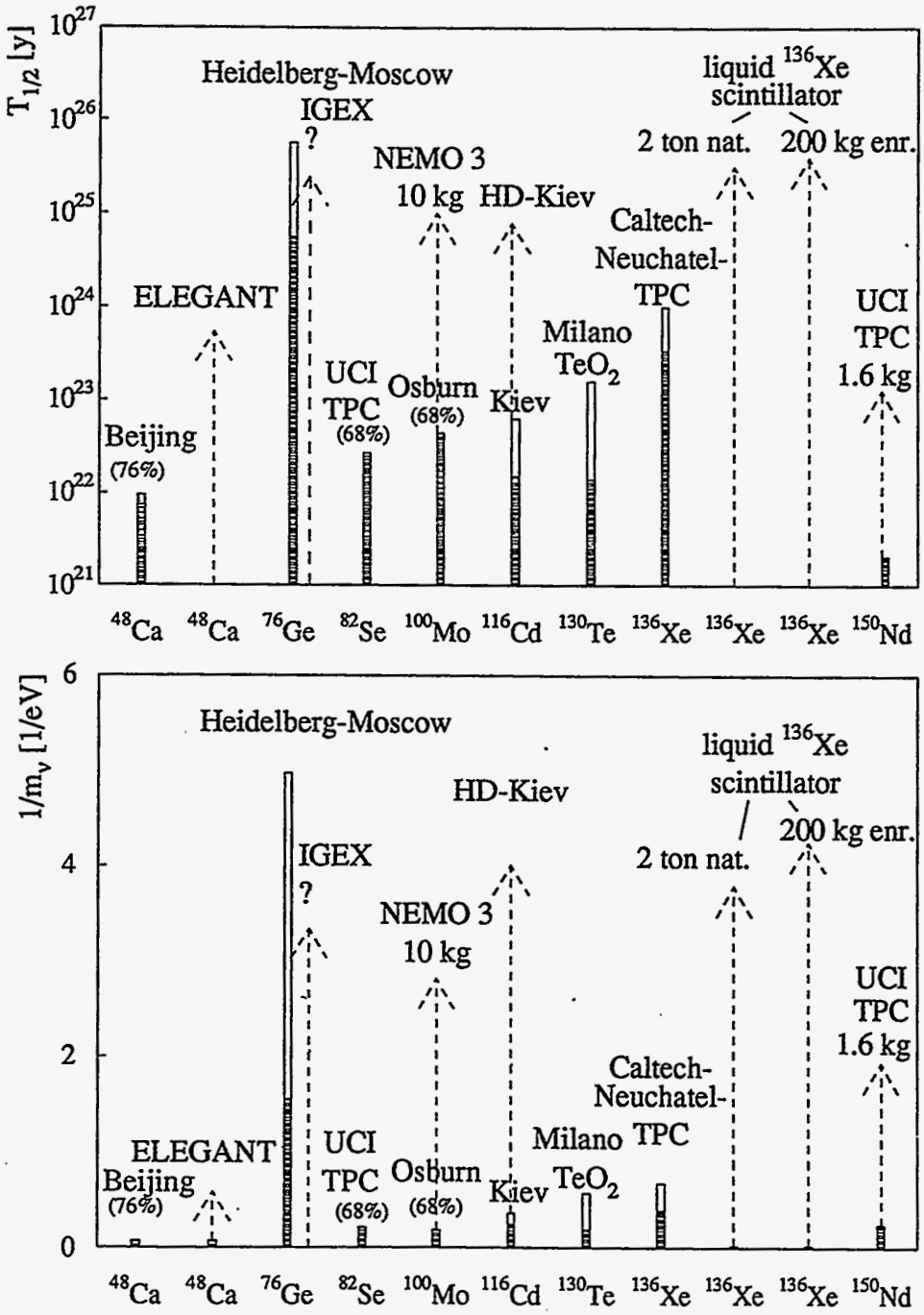

Fig.23 Present situation, 1995, and expectation for the near future until the year 2000, of the most promising $\beta\beta$–experiments concerning accessible half–life (a) and neutrino mass limits (b). The filled bars correspond to the present status, open bars correspond to "safe" expectations and dashed lines correspond to long–term planned or hypothetical experiments.

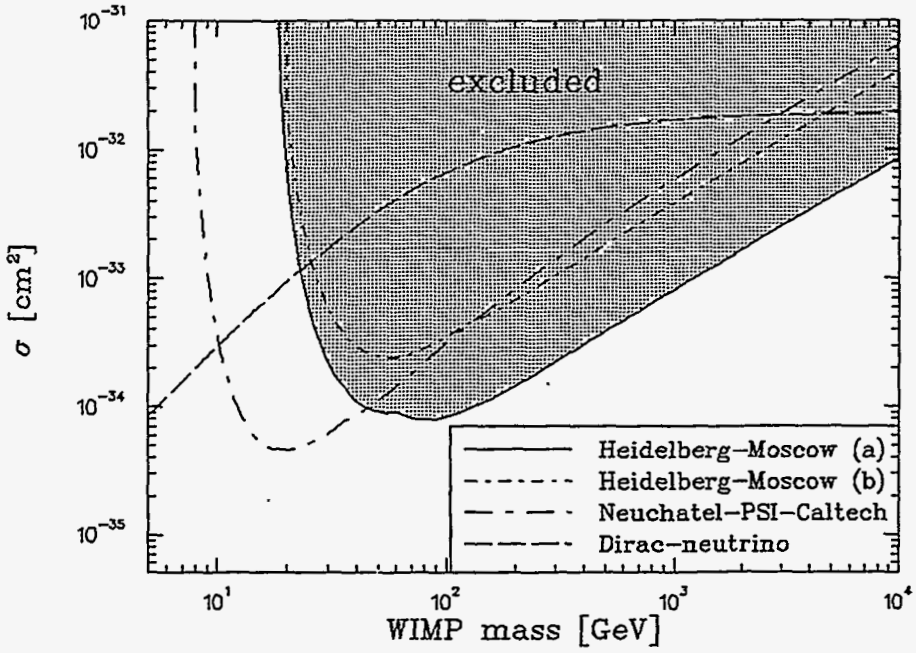

Fig.24 Exclusion limits for elastic scattering cross sections of WIMPS on ^{76}Ge from the HEIDELBERG–MOSCOW experiment (a) not corrected (b) corrected for loss of coherence, compared with the best results compared with a natural detector.[109] WIMPs of a given mass with cross sections σ beyond the lines are excluded. The expected cross section for Dirac neutrinos with standard weak coupling is shown as a dashed line (from[87,107])

investigated recently[110] (see also S. Kovalenko et al.[8]).

For dark matter search the progress obtained with enriched ^{76}Ge is shown in Figs. 25,26. Enriched ^{76}Ge and ^{73}Ge detectors allow to improve the LEP limits on Dirac or Majorana WIMPs considerably (see, e.g.[1]). A major step in sensivity improvement is expected on long terms from cryogenic detectors (see Fig. 25 and[111]). Similarly interesting and realizable on shorter time scale could be the new HEIDELBERG project planning to use ionisation Ge detectors in a special new configuration (see Fig. 26 and[124]).

5. γ–line astrophysics

The fact demonstrated for the first time by the Heidelberg–Moscow experiment, that the technology of production of enriched HP detectors can be handled, is also of interest for high–resolution γ–line astrophysics by balloons and satellites.[112,106,114–117]Use of enriched ^{70}Ge detectors in the ESA project INTEGRAL (International Gamma Ray Astrophysics Laboratory) was expected to reduce the β background dominating in or-

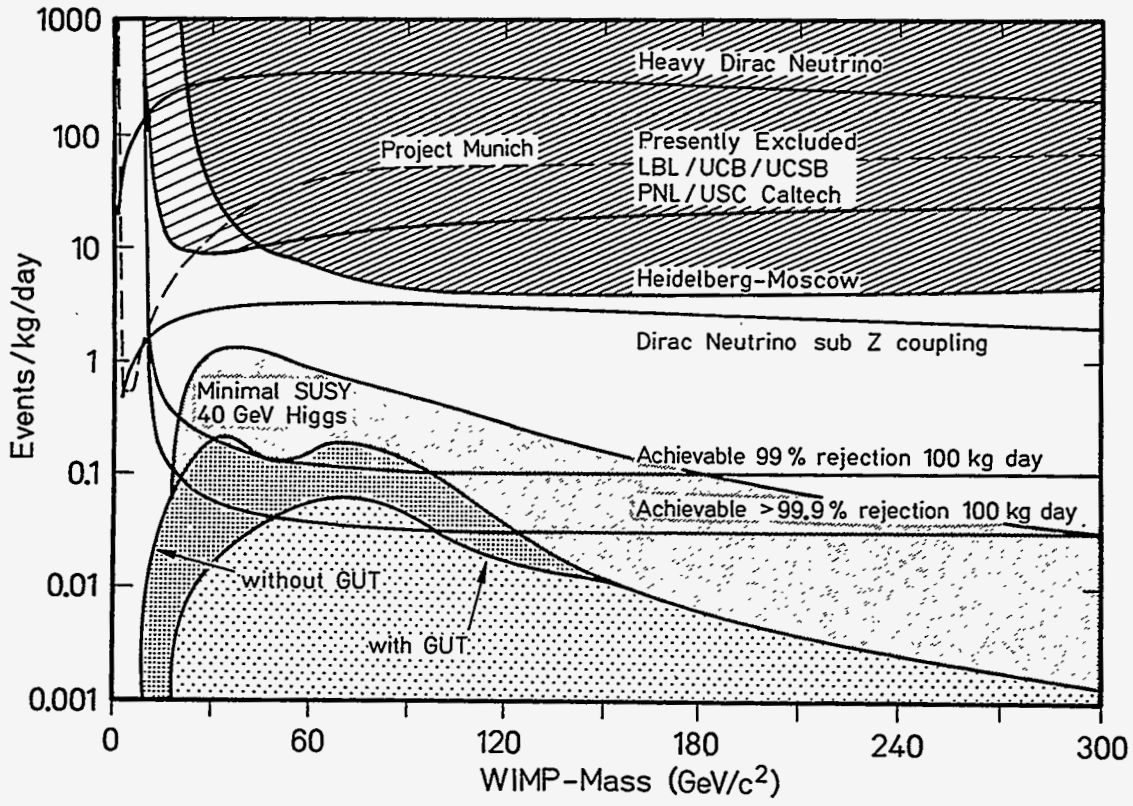

Fig.25 Current detection bounds for WIMPs with Ge ionisation detectors (shaded regions) and anticipated increase in the sensitivity with Ge cryodetectors (the Berkeley project: curves 99 and 99.9 %). The figure shows also expected values for spin–independently and spin–dependently interacting WIMPs in various GUT models (after[1,87,110,111,122]). Also shown is the sensitivity range of the Munich cryodetector project CRESST[123]

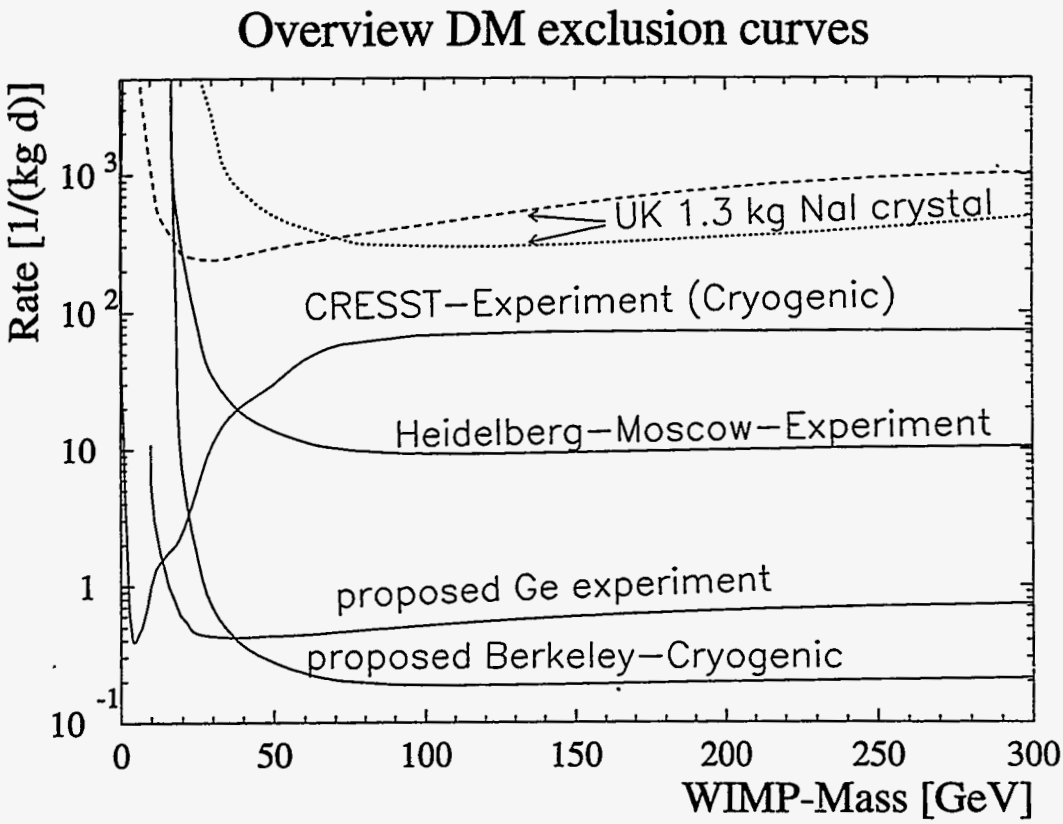

Fig.26 Current detection bounds for WIMPs from the HEIDELBERG–MOSCOW experiment,[107] and the UK experiment,[113] the present claimed goal of the Berkeley cryo detector project and the expectation for the new HEIDELBERG project using ionisation Ge detectors in a special configuration (from[124])

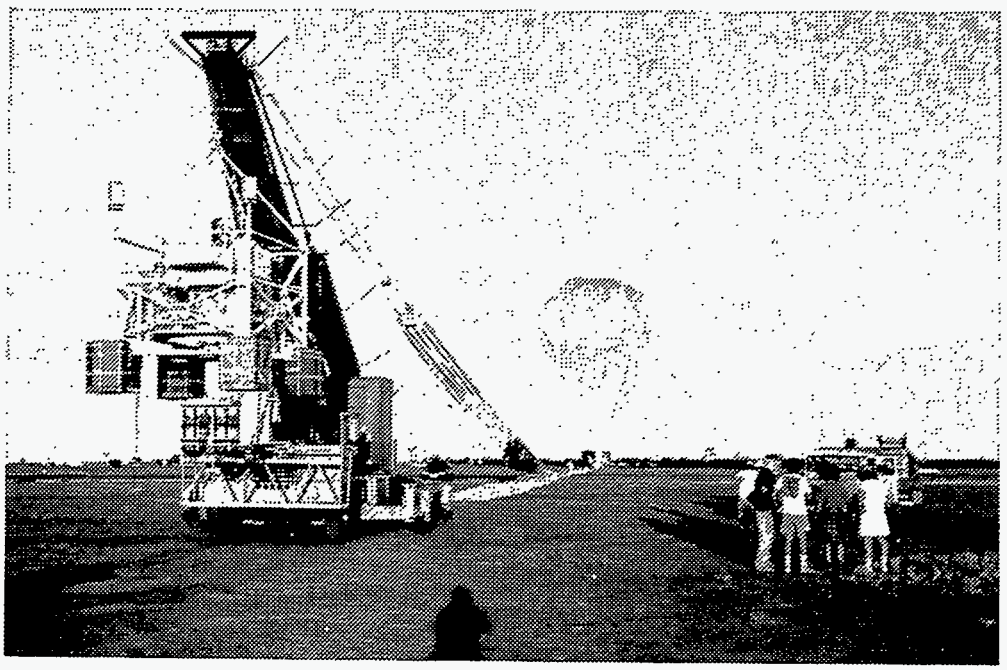

Fig.27 Balloon campaign GRIS in Alice Springs (Australia), May 1992 with one enriched ^{70}Ge detector (from,[87] see[106,115])

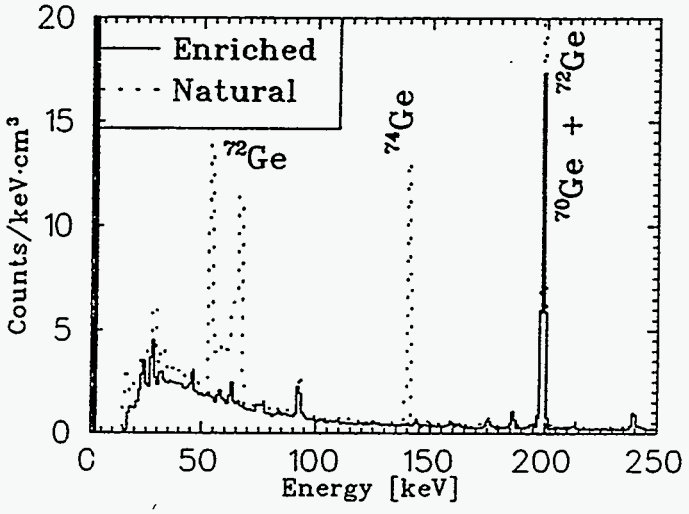

Fig.28 Background spectra for natural and enriched (95 % in ^{70}Ge) Ge detectors in the low energy regime, in the balloon campaign GRIS (see[106.115–117])

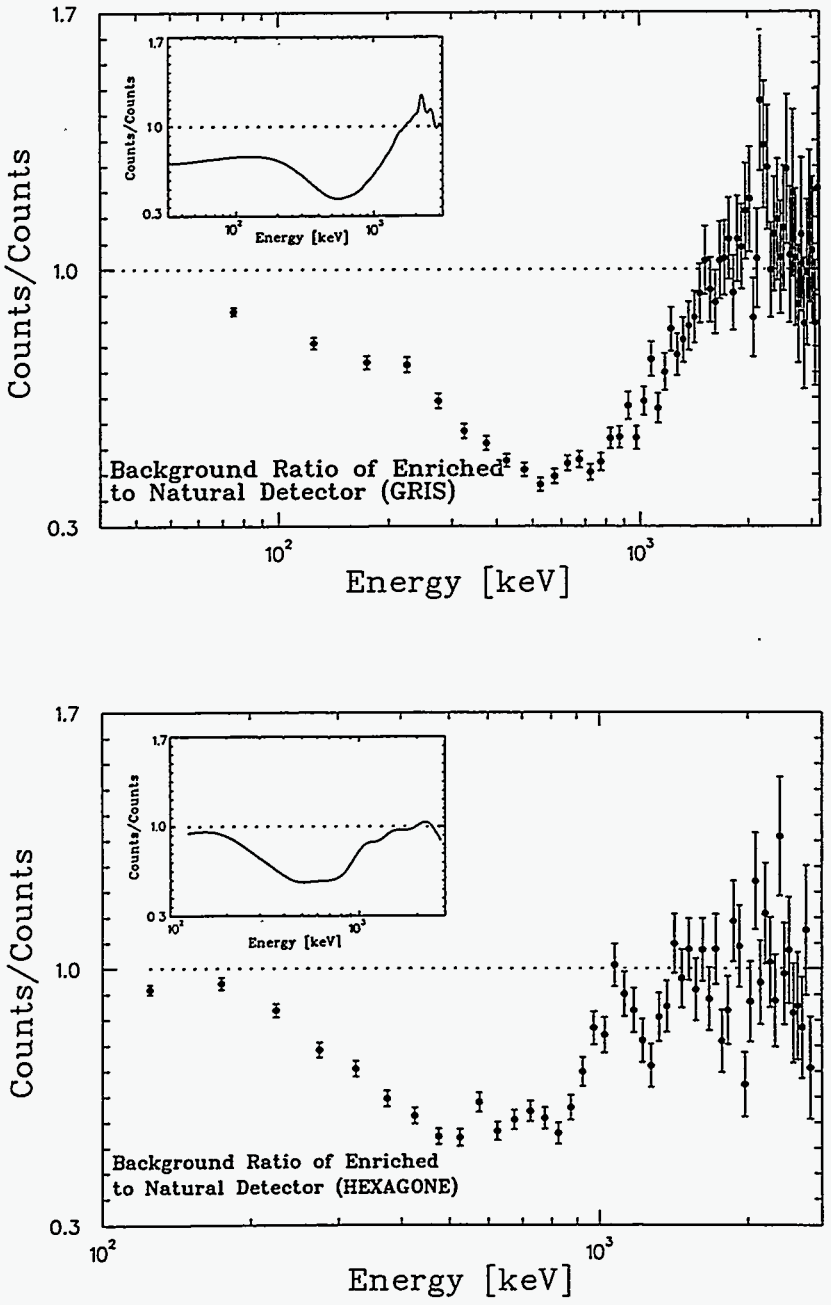

Fig.29 Background ratio of enriched (95 % in ^{70}Ge) to natural Ge detector in the GRIS and HEXAGONE balloon campaigns in Australia, 1992 (see[106,115,117]).

bit, by an order of magnitude.[114] This has recently been checked in balloon flights using detectors of enriched ^{70}Ge built in a collaboration between NASA, MPI Heidelberg and Kurchatov Institute,[87,106,115] (Figs. 27–29).

The complete elimination of lines at 53.4, 66.7 and 139.7 keV in the enriched detector (see Fig. 28) is important for cyclotron lines studies in the spectra of GRB's and X-ray pulsars. The effect on the background at energies 2–3 MeV from β^+ decay ignored in earlier[114] simulations is understood and included in a complete background simulation program for the first time.[116,117]

The INTEGRAL satellite mission aims at the study of a variety of astrophysical questions by high resolution γ spectroscopy, including a variety of γ–ray line producing processes like e^+e^- annihilation connected with black holes in the center of the Galaxy, radioactive elements produced in supernova explosions, neutron capture and cyclotron processes in strong magnetic fields and many others, like imaging and positioning of celestial γ ray sources.

The progress made in the use of enriched Germanium detectors and in understanding the background in orbit[116,117] helps considerably starting a new era of experiments in γ astronomy.

6. Conclusion

Double beta decay has a broad potential for providing important information on modern particle physics beyond present and future high energy accelerator energies which will be competitive for the next decade and more. This includes SUSY models, compositeness, left–right symmetric models, leptoquarks, and the neutrino mass. For the latter double beta decay now is particularly pushed into a key position by the recent possible indications of beyond standard model physics from the side of solar and atmospheric neutrinos, dark matter COBE results and others. New classes of GUTs basing on degenerate neutrino mass scenarios which could explain these observations, can be checked by double beta decay in near future. The HEIDELBERG–MOSCOW experiment has reached a leading position among these new $\beta\beta$ experiments and as the first of them now yields results in the sub–eV range.

It may be of interest to put the potential of $\beta\beta$ decay concerning the neutrino mass in relation with other methods. At present none of the other methods to obtain information on the neutrino mass reaches the sensitivity of $0\nu\beta\beta$ decay. The limit from the supernova SN87A is around 20 eV.[125] Solar,[126] atmospheric,[127] reactor and accelerator neutrino oscillation experiments, including running and future approaches like the CERN experiments NOMAD and CHORUS[128] or the reactor experiments CHOOZ and San Onofre[129,130] do not yield model-independent information on the neutrino mass and in particular on the ν_e mass, but determine a difference of neutrino mass eigenvalues of different (usually unknown) flavours squared. For example, different GUT model assumptions lead for the solar neutrino experiments - even when assuming for a moment that they might see an MSW effect which is not clear at present - to masses for ν_e in a range uncertain by eight orders of magnitude (10^{-7} to several

eV) (see, e. g.[22,26]). Model-independent information complimentary to that from $\beta\beta$ decay comes however, from tritium β decay experiments. Their present lowest limit is 7.2 eV,[131] about an order of magnitude less sharp than that of $0\nu\beta\beta$ decay, but it is independent of the nature (Dirac or Majorana particle) of the neutrino. Thus both types of experiment are needed to determine the most general neutrino mass matrix.

We summarize also that a by–product of $\beta\beta$ decay is the first search for dark matter with enriched ^{76}Ge detector material. The results yield the *sharpest* limits for WIMP masses beyond $\sim$ 150 GeV, excluding Dirac neutrinos as the dominant component of the dark halo of our Galaxy in the mass range 26 GeV to 4.7 TeV. The results also rule out heavy sneutrinos as dark matter in scenarios of a minimal supersymmetric standard model.

Finally it may be stressed that the technology of producing and using enriched HP germanium detectors, which have been produced for the first time for the HEIDELBERG–MOSCOW experiment, has found meanwhile applications also in high resolution γ astrophysics with balloons and satellites.

References

1. H. V. Klapdor–Kleingrothaus, A. Staudt, Non–Accelerator Particle Physics, IOP Publ., Bristol, Philadelphia, 1995; and Teilchenphysik ohne Beschleuniger, Teubner Verlag, Stuttgart, 1995
2. P.M. Zerwas, Phys. Bl. 49 (1993) 187
3. W. Buchmüller and G. Ingelman, Proc. Workshop Physics at HERA, Hamburg, Oct. 29–30 (1991)
4. C. Rubbia, Proc. TAUP 95, Toledo, Sept. 17–21 (1995)
5. H1 Collab., Phys. Lett. **B 353** (1995) 578, Z. Phys. **C 64** (1994) 545
6. M. Hirsch, H.V. Klapdor–Kleingrothaus, S.G. Kovalenko, Phys. Rev. Lett. 75 (1995) 17
7. M. Hirsch, H.V. Klapdor–Kleingrothaus, S. Kovalenko, in preparation
8. H.V. Klapdor–Kleingrothaus and S. Stoica (Eds.), Proc. *Int. Workshop on Double Beta Decay and Related Topics*, Trento, 24.4.–5.5.95, World Scientific Singapore
9. R.N. Mohapatra, in[8]
10. O.Panella, in[8]
11. E.Takasugi, in[8]
12. M. Hirsch, H.V. Klapdor–Kleingrothaus, S.G. Kovalenko, in[8]
13. M. Hirsch, H.V. Klapdor–Kleingrothaus, in[8]
14. S. Petcov, in[8]
15. J.W.F. Valle, in[8]
16. H. Päs *et al.*, in[8]
17. G. Belanger, F. Boudjema, D.London, H. Nadeau, Preprint hep-ph/9508317, August 1995
18. E. Baver, M. Leurer, Phys. Rev. **D 51** (1995) 260
19. M. Leurer, Phys. Rev. **D 49** (1994) 333
20. D. Choudhury, hep-ph/9408250 (1994)

21. J. Blümlein, E. Boos, A. Pukhov, preprint DESY 94-072 (April 1994)
22. P.Langacker, in 'Neutrinos' (Springer: Heidelberg, New York), 1988, ed. H.V. Klapdor, p. 71
23. K. Grotz, H.V. Klapdor, 'The Weak Interaction in Nuclear, Particle and Astrophysics' (Adam Hilger: Bristol, Philadelphia) 1990
24. R.N. Mohapatra, P.B. Bal, 'Massive Neutrinos in Physics and Astrophysics' (World Scientific, Singapore) 1991
25. V. Kuzmin, V. Rubakov, M. Shaposhnikov, Phys. Lett. **B 185** (1985) 36; M. Fukugita, T. Yanagida, Phys. Rev. **D 42** (1990) 1285; G. Gelmini, T. Yanagida, Phys. Lett. **B 294** (1992) 53; B. Campbell *et al.*, Phys. Lett. **B 256** (91) 457
26. D.G. Lee, R.N. Mohapatra, Phys. Lett. **B 329** (1994) 463
27. S.T. Petcov, A.Yu. Smirnov, Phys. Lett. **B 322** (1994) 109
28. A. Ioanissyan, J.W.F. Valle, Phys. Lett **B 322** (1994) 93
29. H. Fritzsch and Zhi-zhong Xing, preprint hep-ph/9509389
30. R.N. Mohapatra, S. Nussinov, Phys. Lett. **B 346** (1995) 75
31. C. Athanassopoulos *et al.* (LSND–Collaboration), Phys. Rev. Lett. **75** (1995) 2650 and D. Smith, in[8]
32. J.R. Primack, J. Holtzman, A. Klypin, D.O. Caldwell, Phys. Rev. Lett. 74 (1995) 2160
33. G. Raffelt, J. Silk, preprint hep-ph/9502306
34. K. Muto, H.V. Klapdor, in 'Neutrinos (Springer: Heidelberg, New York) 1988, ed. H.V. Klapdor, p. 183
35. K. Muto, E. Bender, H.V. Klapdor, Z. Phys. **A 334** (1989) 177,187;
36. A. Staudt, K.Muto, H.V. Klapdor–Kleingrothaus, Europhys. Lett. **13** (1990) 31
37. H.V. Klapdor, K. Grotz, Phys.Lett. **B142** (1984) 323
38. K. Grotz, H.V. Klapdor, Nucl. Phys **A 460** (1986) 395
39. T.Tomoda, A. Faessler, Phys. Lett. **B199** (1987) 475
40. K. Muto, E.Bender, H.V. Klapdor–Kleingrothaus, Z. Phys **A** 339 (1991) 435
41. W.C. Haxton, G.J. Stephenson, Progr. Part. Nucl. Phys. 12 (1984) 409
42. P.Vogel, M.R. Zirnbauer, Phys. Rev. Lett. **57** (1986)3148
43. P.Vogel, in[8]
44. P.B. Radha *et. al*, preprint nucl-th/9510052 (Oct. 1995)
45. S. Stoica, in[8]
46. J. Suhonen, in[8]
47. A. Faessler, in[8]
48. F. Simkovic, Proc. TAUP 95, Toledo, 17–21 Sept. 1995
49. J. Hirsch *et al.*, preprint 1995
50. K. Grotz, H. V. Klapdor, Phys. Lett. **B 157** (1985) 242
51. H. E. Haber, in Proc. on Recent Advances in the Superworld, Houston, April 14-16 (1993)
52. R.N. Mohapatra, Unification and Supersymmetry (Springer: Heidelberg, New York) 1986 and 1992
53. Particle Data Group, Phys. Rev. **D 50** (1994)

54. M. Hirsch, H.V. Klapdor–Kleingrothaus, S. Kovalenko, Phys. Lett. **B 352** (1995) 1
55. R.N. Mohapatra, Phys. Rev. **D 34** (1986) 3457
56. M. Doi, T. Kotani, Progr. Theor. Phys. 89 (1993) 139
57. R.N. Mohapatra, Phys. Rev. **D 34** (1986) 909
58. I.A. D'Souza. C.S. Kalman, Preons, Models of Leptons , Quarks and Gauge bosons as Composite Objects (World Scientific, Singapore) 1992
59. ALEPH Collab., Z.Phys. **C 59** (1993) 215
60. CDF Collab., Phys. Rev. Lett. **67** (1991) 2148
61. J.L. Diaz Cruz, O.A. Sampayo, Phys. Lett. **B 306** (1993) 395; Phys. Rev. **D 49** (1994) R2149
62. F.M. Renard, Phys. Lett. **B 116** (1982) 264
63. O. Adriani *et al.*, Phys. Lett. **B 288** (1992) 404
64. ALEPH Collab., Phys. Rep. 216 (1992) 343
65. M. Derrik, *et al.* (ZEUS Collab.), Z. Phys. **C 65** (1995) 627
66. F. Raupach (H1 Collab.), Proc. Int. Europhys. Conf. on High En. Phys., Marseille, 1993, Edition Frontieres, Gif–Sur–Yvette, France 1994. Eds J. Carr, M. Perrothet
67. F. Abe *et al.* (CDF Collab.), Phys. Rev. Lett. 72 (1994) 3004
68. H.M. Georgi, S.L.Glashow and S. Nussinov, Nuc. Phys. **B 193** (1981) 297
69. J.Friemann, H.Haber, K.Freese, Phys. Lett. **B 200** (1988) 115; J. Bahcall, S. Petcov, S. Toshev and J.W.F. Valle, Phys.Lett. **B 181** (1986) 369; Z. Berezhiani and M. Vysotsky, Phys. Lett. **B 199** (1988) 281.
70. G.B. Gelmini and M. Roncadelli, Phys. Lett. **B 99** (1981) 411
71. Y. Chikashige, R.N. Mohapatra and R.D. Peccei, Phys. Lett. **B 98** (1981) 265; Phys. Rev. Lett. **45** (1980) 265
72. Z.G. Berezhiani, A. Yu. Smirnov, J.W.F. Valle, Phys.Lett. **B 291** (1992) 99
73. C.S. Aulakh and R.N. Mohapatra, Phys. Lett. **B 119** (1982) 136
74. J. Steinberger, Phys. Rep. **203** (1991) 345
75. C.P. Burgess, J.M. Cline, Phys. Lett. **B 298** (1993) 141; Phys. Rev. **D 49** (1994) 5925
76. P. Bamert, C.P. Burgess, R.N. Mohapatra, Nucl. Phys. **B 449** (1995) 25
77. C.D. Carone, Phys. Lett. **B 308** (1993) 85
78. C.P.Burgess, in[8]
79. R.N. Mohapatra and E. Takasugi, Phys. Lett. **B 211** (1988) 192
80. M. Doi, T. Kotani, E.Takasugi, Progr. Theor. Phys. Suppl. **83** (1985) 1
81. M. Hirsch, H. V. Klapdor–Kleingrothaus, S. G. Kovalenko, H. Päs, preprint hep-ph/9511227
82. J.T. Peltoniemi, preprint hep-ph/9506228
83. P. Bamert, C.P. Burgess, R.N. Mohapatra, preprint UMD-PP-95-11 (august 1994)
84. A. Pilaftsis, Phys. Rev. **D 49** (1993) 2398
85. HEIDELBERG–MOSCOW collab., Phys. Lett. **B 356** (1995) 450
86. B. Maier *et al.*, in[8]
87. H.V. Klapdor–Kleingrothaus, Progr. Part. Nucl. Phys. **32** (1994)261
88. G. Gervasio, in[8]

89. V.I. Tretyak, Yu. Zdesenko, At. Data Nucl. Data Tables **61** (1995) 43
90. H.V. Klapdor–Kleingrothaus, MPI–H 1987, proposal
91. HEIDELBERG–MOSCOW collab., Phys. Rev. Lett. **70**, (1993) 2853
92. F. Petry, H.V. Klapdor–Kleingrothaus, B. Maier, subm . to Nucl. Instr. Meth., 1995
93. Ke You et al., Phys. Lett. **B 265** (1995) 53
94. S. R. Elliott et al., Phys. Rev. **C 46** (1992) 1535
95. M. Alston-Garnjost et al., Phys. Rev Lett. **71** (1993) 831
96. F. A. Danevich et al., Phys. Lett. **B 344** (1995) 72
97. A. Alessandrello et al., Phys. Lett **B 335** (1994) 519
98. J.-C. Vuilleumier et al., Phys. Rev. **D 48** (1993) 1009
99. M. K. Moe, Prog. Part. Nucl. Phys. **32** (1994) 247; Nucl. Phys. (Proc. Suppl.) **B 38** (1995) 36
100. NEMO Collaboration, Nucl. Phys. (Proc. Suppl.) **B 35** (1994) 369
101. V. Jörgens et al., Nucl. Phys. (Proc. Suppl.) **B 35** (1994) 378
102. K. Kume (ELEGANT collaboration), in[8]
103. R. S. Raghavan, Phys. Rev. Lett. **72** (1994) 1411
104. F. Piquemal *et al.*, in[8]
105. M. K. Moe, Phys. Rev. **C 44** (1991) R931
106. S. D. Barthelmy et al., Astrophys. J. **427** (1994) 519
107. HEIDELBERG–MOSCOW collab., Phys. Lett. **B 336** (1994) 141
108. T. Falk, A. Olive, M. Srednicki, Phys. Lett. **B339** (1994) 248
109. D. Reusser *et al.* Phys. Lett. **B 255** (1991) 143; E. Garcia *et al.* Phys. Rev. **D 51** (1995) 1458
110. V. A. Bednyakov, H.V. Klapdor–Kleingrothaus, S.G. Kovalenko, Phys. Lett. **B 329** (1994) 5, Phys. Rev. **D 50** (1995) 7128
111. B. Sadoulet, Nucl. Phys. **B** (Proc. Suppl.) 35 (1994) 117
112. H.V. Klapdor–Kleingrothaus, AIP Conf. Proc. 232 (1991) 464 and J. Phys. **G 17** (1991) 537
113. J.J. Quenby *et al.*, Phys. Lett. **B 351** (1995) 70
114. N. Gehrels, Nucl. Inst. Meth. **A 292** (1990) 505
115. S.D. Barthelmy *et al.*, AIP Conf. Proc. 280 (1993) 1166
116. J. Bockholt, H.V. Klapdor–Kleingrothaus, in preparation
117. J. Bockholt, H.V. Klapdor–Kleingrothaus, Nucl. Phys. **B** (Proc. Suppl.) 35 (1994) 403
118. Physics through the 1990's: Nuclear Physics, (Washington: National Academy Press) 1986
119. V. Barger, G.F. Guidice, T. Han. Phys.Rev. **D 40** (1989) 2987
120. D.P. Roy, Phys.Lett. **B 283** (1992) 270
121. J. Butterworth, H. Dreiner, Nucl. Phys. **B397** (1993) 3 and H. Dreiner, P. Morawitz, Nucl. Phys. **B428** (1994) 31
122. D.O.Caldwell, Progr. Part. Nucl. Phys. 32 (1994) 109
123. P.Ferger, Progr. Phys. Lett. **B** 323 (1994) 95

124. Y. Ramachers, *et al.* (HEIDELBERG-MOSCOW Collab.), Proc. Second Workshop of 'The Dark Side of the Universe', Rome, Nov. 13–14, 1995
125. E. W. Kolb, A. J. Stebbins, M. S. Turner, Phys. Rev. **D 35** (1987) 3598
126. P. Anselmann et al., Phys. Lett. **B 327** (1994) 377
127. Y. Suzuki, Nucl. Phys. (Proc. Suppl.) **B 35** (1994) 407
128. K. Winter, Proc. Neutrinos '94, Nucl. Phys. **B** (Proc. Suppl.) 38 (1995) 211
129. P. Vogel, Proc. Neutrinos '94, Nucl. Phys. **B** (Proc. Suppl.) 38 (1995) 204
130. M. Chen *et al.*, Proc. TAUP '93, Nucl. Phys. **B** (Proc. Suppl.) 35 (1994) 447
131. Ch. Weinheimer et al, Phys. Lett. **B 300** (1993) 210

THE IGEX DOUBLE BETA DECAY EXPERIMENT WITH PULSE SHAPE DISCRIMINATION

F. T. Avignone, III

Department of Physics and Astronomy, University of South Carolina, Columbia, SC 29208
(Representing the IGEX Collaboration)*

ABSTRACT

The International Germanium Experiment (IGEX) has six detectors, containing > 90 fiducial moles of ^{76}Ge operating underground. Data thus far yield $T_{1/2}^{2\nu} = (1.1 \pm 0.1) \times 10^{21}$ y and $T_{1/2}^{0\nu} > 4.2 \times 10^{24}$ y(90%CL)if interpreted as a null experiment, or $T_{1/2}^{0\nu} > 3.3 \times 10^{24}$ y(95%CL) in a more conservative case.

1. Introduction

The guns of neutrino physics continue to smoke, and in this conference we saw clear indications of increasing smoke from the reports on four solar neutrino experiments and several atmospheric neutrino experiments. Nevertheless, there is still no real evidence for new physics. Reports in this volume clearly show how the sensitivity of proton decay, n-$\bar{n}$ oscillation, solar neutrino and atmospheric neutrino experiments will be improved in the near future. These are indeed exciting developments. In this context, what is the interest in double-beta ($\beta\beta$) decay?

2. Double-beta Decay

Double-beta ($\beta\beta$) decay is thus far the only practical way to determine if neutrinos are Majorana particles. The theorem of Kayser, Petkov, and Rosen states that interpreted in the context of any gauge theory, the observation of neutrinoless (0ν) $\beta\beta$-decay would constitute unambiguous proof that at least one neutrino eigenstate has non-

*IGEX is a collaboration involving the institute of Nuclear Research (INR) Moscow, the Institute for Theoretical and Experimental Physics (ITEP) Moscow, Pacific Northwest National Laboratory (PNNL), the University of South Carolina, and the University of Zaragoza.

zero mass[1]. This is an extension of the black-box theorem of Schechter and Valle [2]. Recent evidence from atmospheric μ/e ratios that might imply neutrino flavor oscillations, provides new strong justification for pursuing a direct observation of $0\nu\ \beta\beta$-decay. Accordingly, it is important to search for evidence of Majorana masses down one tenth of an electron volt or below.

It is also important to measure the shape of the continuum from $2\nu\ \beta\beta$-decay with precision to search for the emission of majorons in $0\nu\ \beta\beta$-decay. It should be emphasized that the death of doublet and triplet-majoron models by the width of the Z^o-decay, is by no means the end of viable majoron theories [3]. The best currently available technology for precision measurements of the continuum to probe majoron physics, utilizes large intrinsic germanium detectors, isotopically enriched to 86% in ^{76}Ge.

The decay rate for lepton-number violating ($\Delta\ell = 2$) $\beta\beta$-decay with the emission of electrons only ($0\nu\ \beta\beta$-decay) can be written as follows* :

$$\lambda_{\beta\beta}^{0\nu} = G^{0\nu}(E_0, Z)\,\langle m_\nu \rangle^2 \left| M_f^{0\nu} - (g_A/g_V)\, M_{GT}^{0\nu} \right|^2 . \qquad (1)$$

In equation (2), $G^{0\nu}$ is the two-body phase-space factor, including coupling constants, $M_f^{0\nu}$ and $M_{GT}^{0\nu}$ are the Fermi and Gamow-Teller nuclear matrix elements respectively; g_A and g_V are the axial-vector and vector, relative weak coupling constants. The quantity $\langle m_\nu \rangle$ is a weighted mixture of eigenstate neutrino masses given by:

$$\langle m_\nu \rangle \equiv \left| \sum_{k=1}^{2n} \lambda_k^{CP} \left(U_{ek}^L\right)^2 m_{\nu_k} \right| , \qquad (2)$$

where λ_k^{CP} is the k^{th} CP eigenvalue (± 1 for CP conservation), U_{ek}^L are the elements of the matrix that diagonalizes the neutrino-mass-matrix, m_{ν_k} is the mass of the k^{th} neutrino eigenstate, and n is the number of eigenstates. The neutrinos exchanged must be Majorana neutrinos to be absorbed on a vertex identical to that of emission, and have some right handed helicity, perhaps due to finite mass.

3. Recent Results from IGEX

Aside from the technical developments and the successful fabrication of three large (~2kg) and three smaller (~0.7kg) detectors, some interesting physics results have already emerged from IGEX-II thus far. A block of data equivalent to 12.92 mole years has been analyzed to extract the half life of $2\nu\ \beta\beta$-decay of ^{76}Ge. The spectrum below the maximum of the $2\nu\ \beta\beta$–decay distribution at ~750 keV is dominated by a continuum we have interpreted as bremsstrahlung from the decay of ^{210}Pb, however, the half-life can be determined from the portion of the spectrum above this energy. The signal-to-noise ratio from 750 keV to the end of the $2\nu\ \beta\beta$-decay spectrum is 2.95.

The background from $^{57,58}Co$, ^{54}Mn, and ^{65}Zn formed internal to the crystal by cosmic ray neutrons, as well as that from external sources, is clearly identifiable in the

* This expression only includes the exchange of massive Majorana neutrinos.

spectrum. The measured peak intensities were used with a well documented Monte Carlo model to make the corrections. The results of previous measurements and spallation code calculations were used to make the corrections for ^{60}Co and ^{68}Ge formed cosmogenically in the crystal [4].

The correction to the low energy portion of the spectrum due to the bremsstrahlung from ^{210}Pb in the inner lead shield was made in a manner described in detail in our earlier work[5]. The shape of the spectrum was measured in a shield of lead with a very high level of ^{210}Pb. Monte Carlo models were used to obtain the response of the 2.1 kg detector from that of the 0.75 keV detector used in the measurement. The intensity of the bremsstrahlung was a free parameter while the spectral shape was fixed.

Data were analyzed for the two smaller detectors. Together they represented 6.37 mole-years, resulting in a half-life of $(0.9 - 1.1) \times 10^{21}$y. Data from the two larger detectors (12.92 kg yr) were analyzed yielding a half-life of $\sim 1.1 \times 10^{21}$y with an uncertainty of ~10%. The data from all 4 detectors analyzed separately yielded similar half-lives.

The central value continues to be roughly 30% to 40% shorter than that of the MPIH-Kurchatov-INFN experiment. This disagreement could have an interesting impact on the interpretation of 0ν ββ data. If there is as much as 30% disagreement in the measured 2ν ββ-decay half-life, there could be errors in one or both of the methods of correcting for internal and external background, or there are systematic errors in the measurements of the detector fiducial volumes. In the latter case, probably the error is in the experiment associated with the longer half-life, because if the dead layers are underestimated, the upper bound on the number of atoms is fixed by the total detector masses which are all known within a fraction of 1%. Therefore no experiment will result in a half-life too short due to an error in skin depth if the total mass is known accurately.

In the IGEX experiment there was only one count in the 10 keV window centered at 2038 keV in 23.7 mole · y of data. To a 95% confidence level, there are fewer than 3 counts, hence the bound on the 0ν ββ-decay half life is:

$$(\ln 2)(23.7 \text{ mole} \cdot \text{y})\left(6.022 \times 10^{23}\right)/3 = 9.89 \times 10^{24}\,\text{y}/3 \text{ or } T^{0\nu}_{1/2} > 3.3 \times 10^{24}\,\text{y(95\%CL)}$$

$$\text{corresponding to } \langle m_\nu \rangle < 0.85 \text{ eV},$$

using the same matrix elements applied in the analysis of the MPIH-Kurchatov-INFN experiment, which has already achieved a better exclusion. Since the one event lies at the very edge of the 10 keV window, the experiment could also be analyzed as a null experiment, in which case $T^{2\nu}_{1/2} > 4.2 \times 10^{24}\,\text{y(90\%CL)}$. These results will be updated at Neutrino-96 in Helsinki.

4. Towards A Zero-Background Experiment

The background levels of isotopically enriched ^{76}Ge on ββ-decay experiments appear to be reaching an asymptotic value of ~0.1 to 0.15 counts/keV/kg/yr. Further improvement requires identifying individual pulses from a background strongly dominated

by internal ^{68}Ge and ^{60}Co produced throughout the crystal by spallation reactions generated by cosmogenic neutrons[4,6]. The ^{60}Co content is long lived and not directly observable when internal, but it can be evaluated by directly observing the internal electron capture decays of ^{56,57,58}Co during the first few months the detector is underground. The ^{68}Ge and ^{60}Co dominate the background in the energy region of 2 MeV. Fortunately, the overwhelming majority of the events from these decays produce characteristic multi-site pulse-shapes that can be identified and eliminated. Accordingly our detectors are no longer only calorimeters, but can distinguish between single-site events, characteristic of $\beta\beta$–decay, and multiple-site events from background.

5. Principles of Pulse Shape Discrimination (PSD).

PSD is an old subject[7]; only recently have intrinsic -Ge detectors become large enough and digital electronics fast enough to render it effective for our purposes[8,9]. The basic idea is depicted in Fig. A where the detector circuit charging curves are approximated by straight lines. A change in displacement current occurs when the electrons (holes) reach the outer (inner) conductor. The change to slope-zero occurs at the final collection. The artificially smoothed curve depicts what one would expect with instrumental distortion.

In 1989 an extensive experimental study by Feffer et al.[9] yielded characteristic shapes of single-site events produced at various radii. Figure B shows three current pulses representing averages of many experimental samples observed in their Compton-Scattering coincidence experiment. The pronounced peak closest to the left edge of the graph represents an event occurring near the outer conductor. The electrons acquire a high velocity and are collected early. The holes decrease in velocity as they move inward and are collected later. The curve on the right is the opposite scenario, but it is always the electrons that move most rapidly near their point of collection because the magnitude of the field is very strong at the outer regions.

The electric field in a depleted intrinsic Ge detector is obtained theoretically by solving Poison's equation subject to the boundary conditions $\varphi(r_2)-\varphi(r_1)=V$, the detector bias. The $\sim 10^{10}$ p-type impurities per cm^3 create a space charge density ρ. The magnitude of the field is given by:

$$E(r)=|\rho/\varepsilon|\, r-\frac{V-1/4|\,\rho/\varepsilon|\,\left(r_2^2-r_1^2\right)}{r\ln(r_2/r_1)}. \qquad (3)$$

It is typically an order of magnitude stronger at the positive outer conductor at r_2. The drift velocity is given by an empirical expression[10].

$$\vartheta_d=\frac{\mu_0 E(r)}{\left[1+\alpha E(r)\right]^{1/\beta}}, \qquad (4)$$

where α and β are measured parameters and μ_0 is the mobility.[10]

The effective value of ρ/ε for a given detector can be determined experimentally using the following depletion voltage equation:

$$V_D = (\rho/2\varepsilon)\left\{r_1^2 \ln(r_2/r_1) - 1/2\left(r_2^2 - r_1^2\right)\right\} \qquad (5)$$

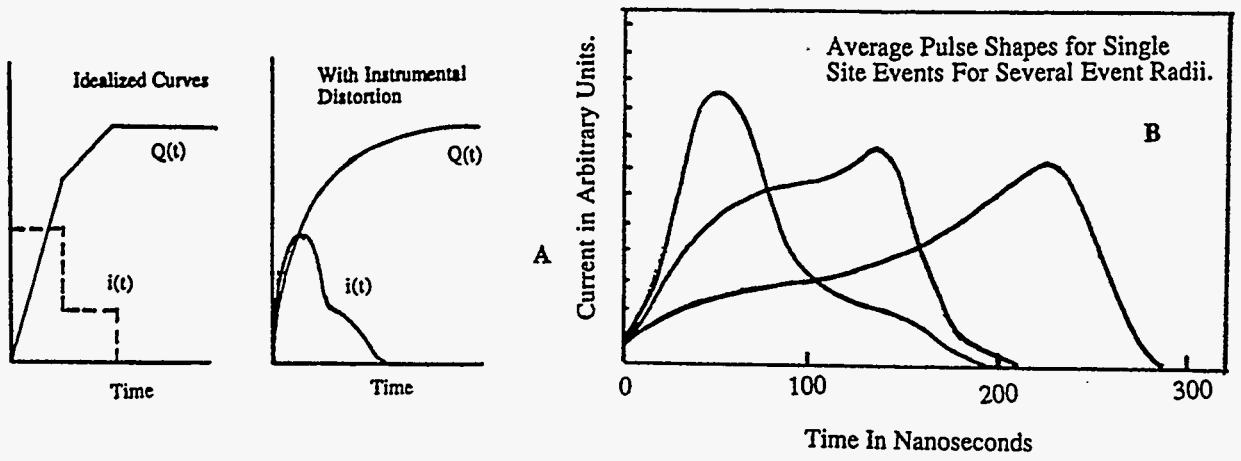

Fig. A. Sketch of an idealized linear charging curve with slope changes at the collections of charges and holes; a smoothed version expected from instrumental effects.
Fig. B. the experimental current traces of pulses taken from reference (9).

6. Experimental Pulse Shapes from IGEX

In Figures 1-6 on the next page show the output traces of an early stage of preamplification recorded with a LeCroy 9360 fast digital oscilloscope using a high impedance FET probe. The upper traces represent the amplified current, however with some feedback compensation. The lower traces are the numerically calculated derivatives. The current pulses are stored with a sampling rate of 10 gigahertz, approximately 4000 points per pulse.

Figures 1, 2, and 3 are excellent examples of pulses from single site events. Each tick mark on the horizontal axes represents 100 ns, while vertical axis ticks represent 50 mV each. In all three cases, the collection of holes occurred early at the inner conductor in roughly 100 ns. The electrons were collected beginning at roughly 400 ns and ending at approximately 450 ns.

Figures 4, 5, and 6 are clear examples of pulses from multi-site events. Figures 4 and 6 are clearly dominated by two or more major collection pairs. Figure 5 has two or more early collections occurring in the first 250 ns, with a later collection, or collections, occurring at approximately 500 ns.

While we are able to reduce the background by a factor of roughly 10, we have recently discovered a further improvement in electronic circuitry that will definitely improve the level of confidence of our PSD selection, and possibly also improve the suppression of background.

ACKNOWLEDGEMENTS

The complete list of authors contributing to this work follows: F. T. Avignone, III, C. E. Aalseth, R. L. Brodzinski, J. I. Collar, E. Garcia, D. Gonzáles, F. Hasenbalg, W. K. Hensley, I. B. Kirpichnikov, A. A. Klimenko, H. S. Miley. A. Morales, J. Morales, A. Ortiz de Solórzano, S. B. Osetrov, V. S. Pogosov, J. Puimedón, J. H. Reeves, C. Sáenz, A. Salinas, M. L. Sarsa, A. A. Smolnikov, A. S. Starostin, A. G. Tamanyan, A. A. Vasenko, S. I. Vasiliev, and J. A. Villar.

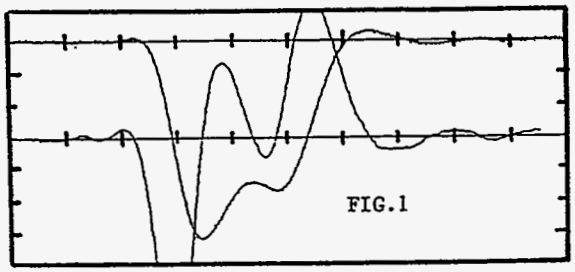

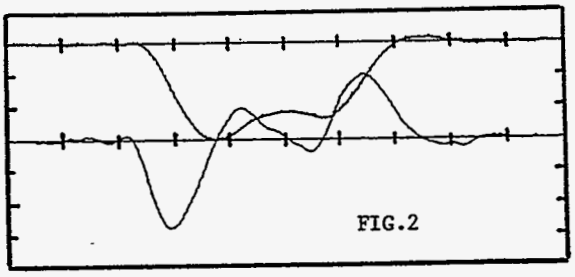

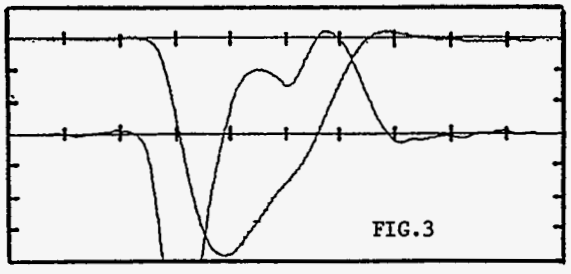

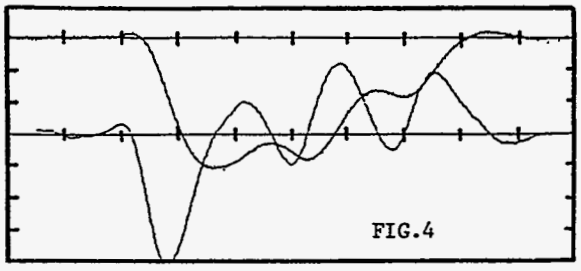

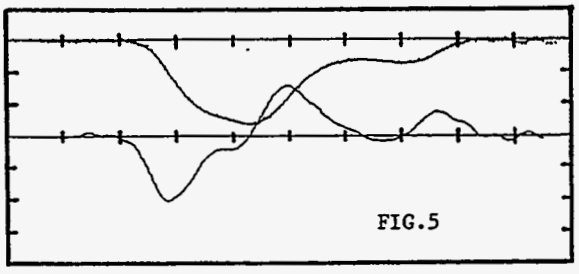

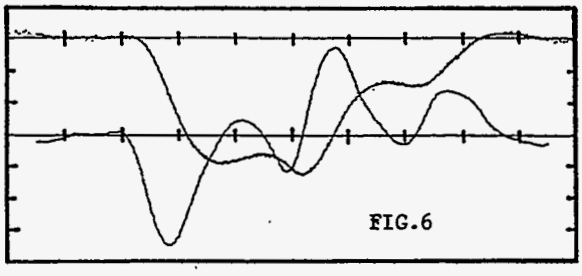

Figures 1 - 6 are taken directly from the fast digital oscilloscope (top trace) and their derivatives (bottom trace). Figures 1 - 3 are interpreted as single-site events. Figure 4 - 6 are interpreted as multiple-site events. More details are given in the text.

REFERENCES

1. B. Kayser, Proc. XXIII Int. Conf. on High Energy Physics ed. S. C. Loken, World Scientific, Singapore (1987) p.945.

2. J. Schechter and J. W. F. Valle, Phys. Rev. D25, 2951 (1982).

3. Z. G. Berezhiani, A. Yu Smirnov and J. W. F. Valle, Phys. Lett. B291, 99 (1992).

4. F. T. Avignone, III et al., Nucl. Phys. B (Proc. Suppl.) 28A, 280 (1992).

5. F. T. Avignone, III et al., Phys. Lett. B256, 559 (1991).

6. R. L. Brodzinski et al., J. Radioanalytical and Nucl. Chem. 93, 61 (1995).

7. Glen F. Knoll, "Radiation Defection Measurement," 2nd Ed. John Wiley & Sons.

8. F. Petry et al., Nucl. Instr. and Meth. A332, 107 (1993).

9. P. T. Feffer et al. SPIE Vol. 1159 EUV, X-Ray and Gamma Ray Instrum. for Astr. and Atomic Physics 1159, 287 (1989).

10. T. W. Raudorf and R. H. Pehl, Nucl. Instr. and Meth., A255, 538 (1987).

Study of Atmospheric Neutrino Interactions and Search for Nucleon Decay in Soudan 2

W.A. Mann, W. Leeson and D. Wall
Physics Department, Tufts University
Medford, MA 02155

For the Soudan 2 Collaboration
Argonne National Laboratory, University of Minnesota, Oxford University,
Rutherford Appleton Laboratory, Tufts University, Western Washington University

ABSTRACT

Preliminary results from 1.52 fiducial kiloton years are presented. In 27% of single track and shower events, we observe a final state proton to accompany the lepton. The distribution of lepton–proton opening angle is consistent with threshold neutrino quasi–elastic kinematics in iron nuclei. Using 102 contained single track and single shower events, we measure the atmospheric ν_μ/ν_e ratio–of–ratios to be $0.75 \pm 0.16(stat) \pm 0.14(sys)$. The conjecture that an anomalous flavor ratio originates with proton decay $p \rightarrow e^+\nu\nu$ is examined using single shower events. We search for nucleon decay modes $N \rightarrow l^\pm + hadrons$ among 55 contained multiprong events and find no candidates. We find no candidates for $p \rightarrow \nu K^+$ ($K^+ \rightarrow \mu^+\nu$) among Soudan "track plus recoil proton" topologies.

I. Detector and Data

Soudan 2 is a fine-grained iron tracking calorimeter which is currently taking data with its full mass of 963 tons in a cavern 2090 mwe underground at Soudan, Minnesota. The site is 730 kilometers "as the neutrino flies" from Fermilab, where a neutrino beam will be aimed at Soudan to enable study of ν oscillations with long baseline. The present experiment began logging contained events in April 1989 when the detector was one–quarter of its final mass. A total fiducial exposure of 2.75 kiloton years (kty) has been recorded as of April 1996. The data reported here represent the initial 1.52 kty exposure ('89 to end '93).

The calorimeter's particle detection elements are 1.5–cm diam., 1–m–long, slightly conductive drift tubes. The drift tubes are embedded in sheets of insulating mylar which carry copper strips. Graded high voltage applied to the strips creates an axial electric field within each tube, directed from either tube end to the middle of each tube. Electrons, initiated by a charged particle traversal, drift down the tube and are collected at the tube ends by crossed pairs of anode wires and cathode pads. The third coordinate for the tube traversal is deduced from the drift time. The mylar sheets with tubes and additional polystyrene insulation are interleaved with 1.6 mm corrugated steel sheets to form a stack with honeycomb lattice cross section. The steel sheets with tubes and insulation are stacked 240 layers high, then compressed and enclosed in a gas-tight steel enclosure. The resulting structure constitutes a standard, stand alone calorimeter tracking module of dimensions 1x1x2.5 m weighing 4.3 tons. The assembled calorimeter consists of 224 of these modules; it has mean density 1.6 g/cm^3, 9.7 cm radiation length, and 80 cm nuclear interaction length. Soudan's modular design allows test beam calibration to be carried out, and enables portions of the calorimeter to be installed or repaired while the rest of the detector is taking data [1].

The calorimeter is surrounded on all sides by a cavern-liner active shield array. The shield consists of 1570 8–cell extruded aluminum manifolds which comprise a hermetic double–layer of proportional tubes with digital readout [2].

In the Soudan 2 experiment, raw data passes the hardware trigger requirement at a rate of 0.5 Hz. Information for each trigger event consists of anode channel versus time (X–Z), and cathode channel versus time (Y–Z) pulse profiles, where the pulse height in each time bin is digitized by a 6–bit flash ADC. Time information and pulse shape profiles are used to match anode and cathode pulses, yielding a three dimensional reconstruction for each gas crossing in the event. Trigger events are subsequently processed by two levels of contained–event software filters whose data quality and rough containment cuts reduce the number of events one thousandfold. All events are then subjected to two levels of physicist scans. The initial scan rejects 'obvious' non-contained or background events; a more severe set of containment requirements is imposed by the final scan. Events for which zero coincident hits are recorded by the shield array are candidate neutrino interactions or candidate nucleon decays. These events are classified according to topology as "single track" or "single shower" (mostly quasi–elastic neutrino interactions) or as "multiprong" (mostly inelastic charged or neutral current reactions).

Selected views of three different contained events, illustrating the three topology categories, are shown in Figure 1. Figs. 1a,b show anode–time and cathode time views of a single track muon accompanied by a heavily–ionizing recoil proton. Here, ionization energy dE/dx loss is clearly visible as each track ranges to stopping. Figs. 1c and 1d show typical single shower and multiprong events respectively. The obvious topological differences between the shower in Fig. 1c and the muon track in Figs. 1a,b illustrate how readily the distinction between ν_μ and ν_e flavor can be made in this high resolution detector.

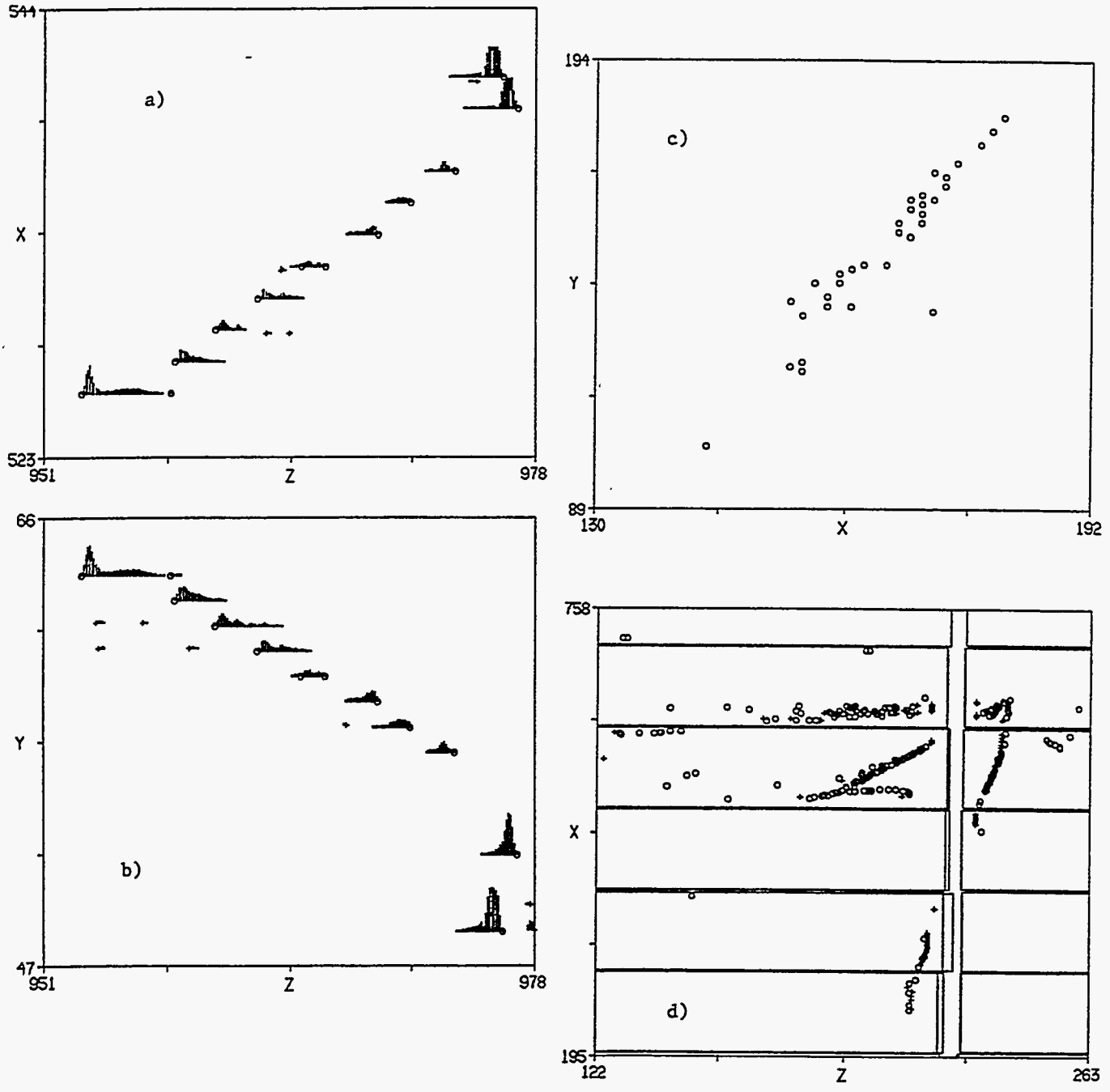

Figure 1: Contained events recorded in Soudan 2. Figs. 1a,b show two views of a "single track" muon accompanied by a heavily-ionizing proton. Typical "single shower" and "multiprong" events are shown in Figs. 1c,d respectively.

II. Track and Shower Events

Contained single track and single shower events are expected to be predominantly charged current quasi-elastic reactions:

$$\nu_\mu + n \rightarrow \mu^- + p, \quad (1)$$
$$\bar{\nu}_\mu + p \rightarrow \mu^+ + n, \quad (2)$$
$$\nu_e + n \rightarrow e^- + p, \quad (3)$$
$$\bar{\nu}_e + p \rightarrow e^+ + n. \quad (4)$$

Due to the presence of reactions (1) and (3), a fraction of each sample can be expected to contain visible recoil protons which would not be detected in a water Cherenkov experiment.

Figures 2a,b show the lepton momentum distributions (preliminary) for contained single track and shower samples from the 1.52 kty exposure. Events in each bin which have a visible recoil proton in the final state are denoted with shaded histogramming. For track events (reactions (1) and (2)), momenta are determined from track ranges in the calorimeter medium. The momentum resolution $\Delta p/p$ for muons is about 8%. For shower events (reactions (3) and (4)), electron momenta are estimated based upon totals of ionized tube crossings, and the resolution is typically 26 – 35 %. This difference between our lepton momentum resolutions is reflected in the relative shapes of the Fig. 2 distributions. Concerning contents of the lowest bins in Fig. 2, some caution is warranted; neutrino events with fewer tube crossings are more readily imitated by background processes.

Separation of single track from single shower events sets the stage for determination of the flavor composition ν_μ/ν_e of the atmospheric neutrino flux. Before presenting the Soudan measurement however, we point out that single track and shower events have other interesting attributes which are observable in a fine–grained calorimeter. As summarized below in Table I, we observe a visible recoil proton from the event vertex to accompany 32% of the muon tracks and 21% of the electron showers. Interpreted in terms of reactions (1) through (4), events with a recoil proton are necessarily initiated by ν_μ or ν_e neutrinos and not by $\bar{\nu}_\mu$ or $\bar{\nu}_e$ anti–neutrinos. That is, proton "tags" enable neutrino events to be distinguished from anti–neutrino events. Information of similar kind is provided by endpoint decays on stopped tracks, of which we observe 9 among 53 single track events. In Soudan's iron medium, μ^- tracks usually undergo nuclear absorption before they can decay, whereas stopped μ^+ particles always decay ($\mu^+ \rightarrow e^+\nu\bar{\nu}$). As a result, observation of track endpoint decays provides discrimination between quasi–elastic ν_μ versus $\bar{\nu}_\mu$ reactions. The detector efficiencies for these observations can be reliably ascertained, and so measurement of the atmospheric antineutrino to neutrino ratio $\bar{\nu}_\mu/\nu_\mu$ should be feasible in Soudan 2 once a fiducial exposure exceeding three kiloton-years is achieved.

The track and shower subsamples which have visible recoil protons, can be used to investigate the distribution of lepton–proton opening angle and its correlation with lepton momentum. These observables provide checks on our understanding of threshold kinematics of quasi–elastic reactions, in particular of the crucial role

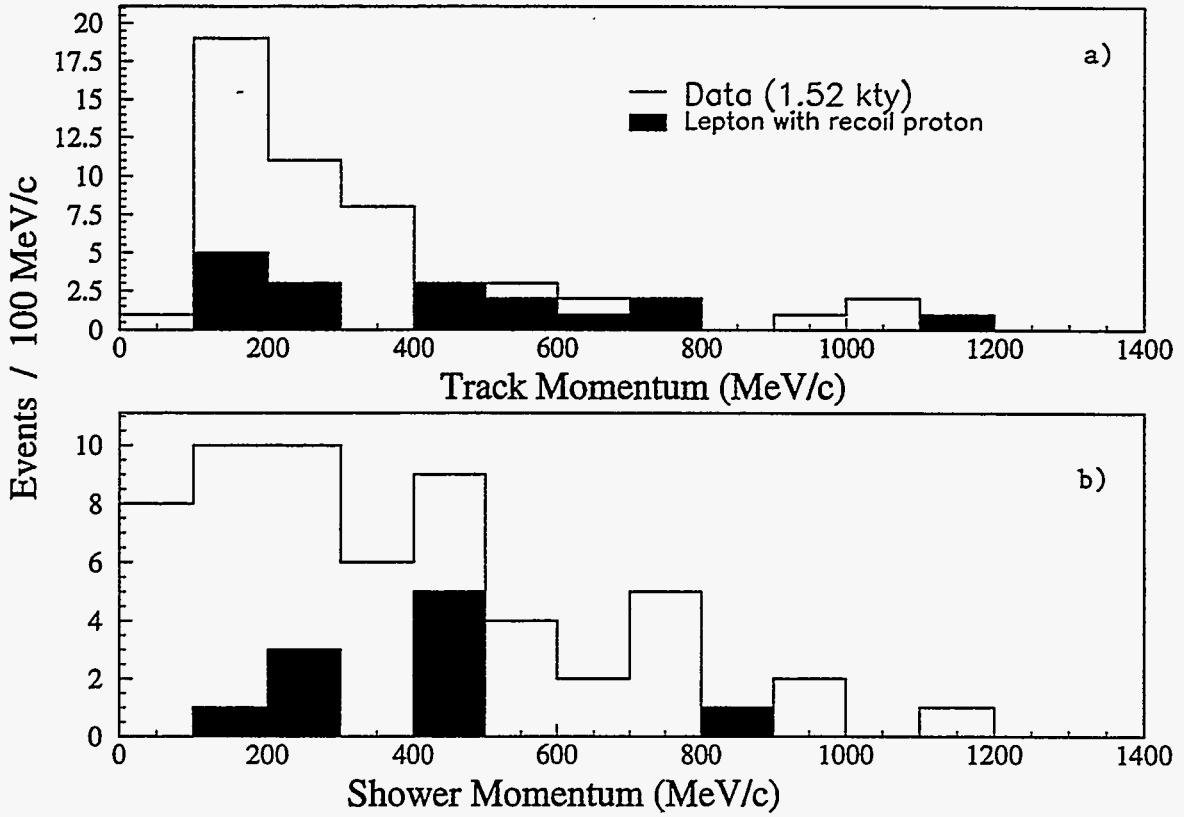

Figure 2: Lepton momentum distributions: a) for single track events; b) for single shower events. Events in which a visible recoil proton accompanies the lepton are shown shaded.

Topology	No. Events	
track	29	
track + proton at vertex	15	(total single track
track + endpoint decay	7	events = 53)
track + proton + decay	2	
shower	41	(total single shower
shower + proton at vertex	11	events = 52)

Table I: Attributes of Soudan 2 single track and single shower events.

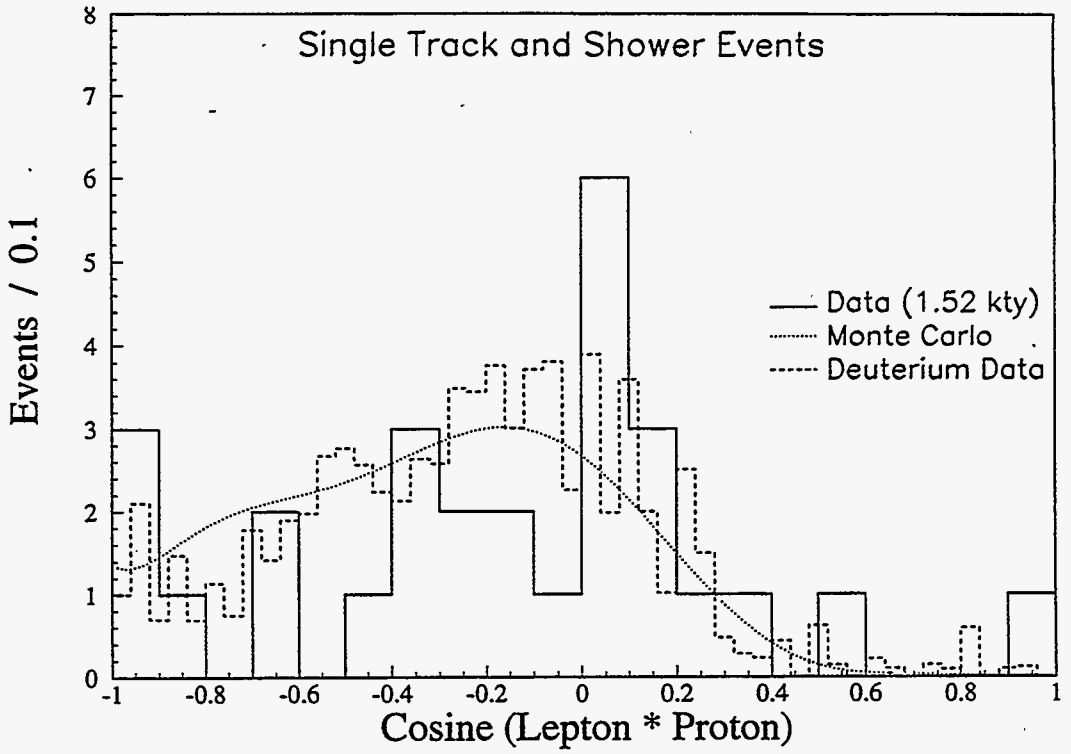

Figure 3: Distributions of cosine of lepton–proton opening angles. The solid histogram shows Soudan events; distributions from deuterium bubble chamber reactions (1) and from simulation of quasi–elastic interactions in iron, are given by the dashed histogram and doted curve respectively.

played by Fermi motion of target neutrons within iron nuclei. From calculations and from our data, opening angle distributions are found to be $\nu_\mu - \nu_e$ flavor blind, consequently track–plus–proton and shower–plus–proton samples can be combined. Cosines of lepton–proton opening angles from Soudan events are presented in Fig. 3 (solid histogram). The angles are remarkably large. The elastic character of quasi–elastic events gives rise to the broad pile–up around 90°; however for events with slow leptons, there is sizable rate for angles in the backward hemisphere. Figure 3 summarizes comparisons made with two other event samples. Opening angles for quasi–elastic reactions (1) recorded in the deuterium–filled ANL 12–foot diameter bubble chamber [3] are shown by the dashed histogram. For the latter data, interaction protons are required to satisfy $P_p \geq 500$ MeV/c, and the events have been weighted so that the sample's E_ν content matches that which would be obtained from an atmospheric ν_μ flux. The dotted curve shows results from a Monte Carlo calculation for ν_μ quasi–elastics generated using the Bartol atmospheric flux [4] and interacting on iron nuclei. The target neutron momenta are assigned according to a Fermi gas model for the Fe nucleus [5]. All three distributions are broader than that obtained using simulated interactions on stationary neutrons. In particular, opening angle cosines greater than 0.2 are not accessible in the absence of Fermi motion.

III. Atmospheric Neutrino Anomaly

Kamiokande and IMB–3 have reported [6, 7] the ratio of single ring muon–type events to electron–type events to be anomalously low. Experimental results are usually expressed in terms of the neutrino flavor ratio–of–ratios R_ν:

$$R_\nu \equiv \frac{(\nu_\mu/\nu_e)_{Data}}{(\nu_\mu/\nu_e)_{MC}} \simeq \frac{(track/shower)_{measured}}{(track/shower)_{predicted}} \quad . \tag{5}$$

In the absence of unknown effects, R_ν will equal unity. In the water Cherenkov experiments however, R_ν is measured to be four standard deviations below 1.0 with a value more nearly 0.60. Observations by the Frejus planar iron tracking calorimeter have not confirmed the anomaly [8].

An R_ν measurement based upon Soudan's 1.52 kty exposure is currently being finalized; we report here a new, albeit preliminary value. Improvements incorporated into the new analysis include the following:

i) The neutrino event Monte Carlo (MC) has been improved to include more accurate low energy scattering for nucleons, more realistic representation of detector geometry, intranuclear scattering of produced hadrons, and variation of the neutrino flux with the solar cycle. The simulation is now fully tuned to test beam measurements; detector noise effects are included.

ii) MC events,which are now completely indistinguishable from data by eye, are introduced into the data stream prior to scanning and their identity is unknown to scanners. In this way we ensure that any scanning bias is common to both data and MC.

iii) Event selection and corrections have benefited from analysis of backgrounds originating with cosmic ray muon–induced fluxes of neutrons and photons in the cavern.

iv) A detailed accounting of systematic effects has been carried out [9]. Possibilities for residual bias have been checked by having two independent groups scan and analyze the data using somewhat different procedures and acceptances.

For the flavor ratio analysis, 50 single track events and 52 single shower events passed our criteria, to be compared with 351.6 track events and 272.7 shower events from the MC simulation. The fractional event counts of the MC samples reflect corrections made for neutral contaminants entering the ν samples as the result of shield array inefficiency (+6% correction, little flavor bias), and for ν event losses resulting from random hits in the shield (−5% correction, no flavor bias). Based upon these samples, our preliminary measurement is

$$R_\nu = 0.75 \pm 0.16(stat) \pm 0.14(sys). \tag{6}$$

The systematic error assignment is conservative; it may decrease when our review of differences between the two independent analyses is completed. Although the Soudan 2 result does not by itself show a significant atmospheric neutrino anomaly,

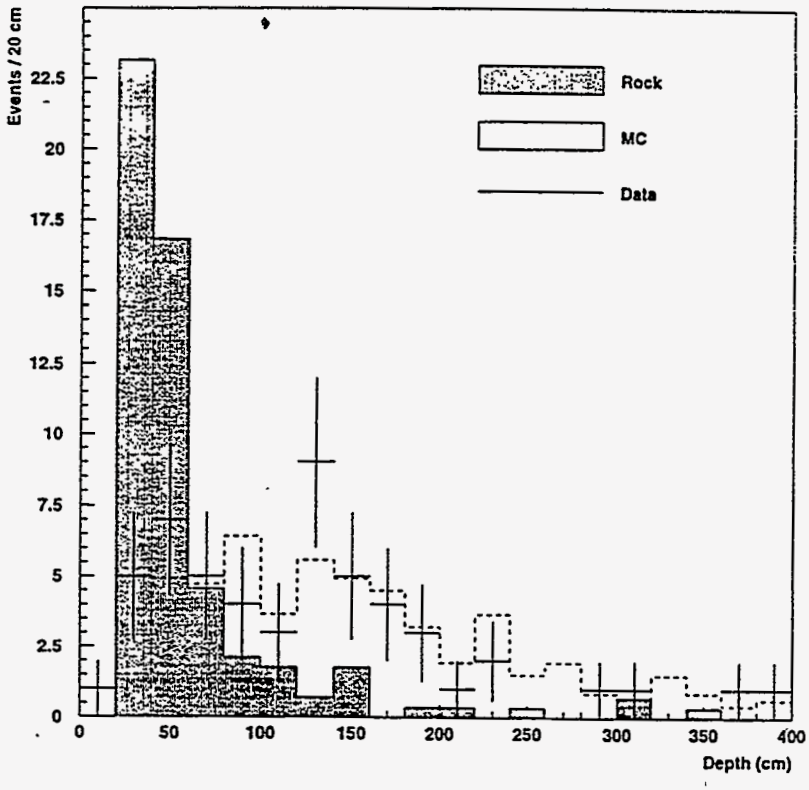

Figure 4: Distributions of shortest distance to detector exterior for shower events from data (crosses), neutrino MC (dashed), and rock (shaded) samples.

our value of R_ν is below 1.0 and is in agreement with the high statistics water Cherenkov measurements.

For experiments at intermediate depths such as IMB, Soudan, and Kamiokande, it is important to establish that contained event samples are not contaminated by events produced by photons or neutrons emerging from cavern rock ("rock events"). These neutral particles originate with inelastic interactions of cosmic ray muons at the depth of the detector. Fortunately, rock events exhibit characteristic attenuations in Soudan's calorimeter medium, whereas neutrino events distribute uniformly throughout the detector volume. In Figure 4 we show distributions of shortest distance between vertex position and detector exterior, for our single shower events (crosses), for our neutrino MC shower events (dashed histogram), and for shield–tagged shower events (shaded histogram). Our contained single shower sample follows the neutrino MC distribution and shows no sign of clustering near detector edges as observed with the rock events.

IV. R_ν Anomaly and Proton Decay

If indeed the atmospheric flavor ν_μ/ν_e composition is anomalous, then a fundamental uncertainty in atmospheric neutrino background estimates for nucleon decay searches is implied. "Unless this situation is resolved, background subtracted searches for nucleon decay will be severely hampered in future nucleon decay detectors" [10]. To interpret the low R_ν ratio, one needs to know whether the μ–like events of the numerator are too few, whether e–like events of the denominator are

too numerous, or whether a combination of both circumstances is actually the case. A popular view (Refs. [6]) is that there exists an apparent dearth of muon–neutrino events, accompanied perhaps by a mild excess of electron–neutrino events [7], which is interpreted as evidence that neutrino oscillations deplete the muon–neutrino flux over distances of 10 to 10,000 kilometers. The oscillation interpretation is usually formulated using absolute neutrino fluxes calculated by the Bartol group [4] or by Honda *et al.* [11]; these happen to be the highest in the literature. A different view, formulated by us, assumes that the expected number of ν_μ events has been detected, and that there is an excess of electron–like events that can be ascribed to predominant nucleon decay via the mode $p \rightarrow e^+\nu\nu$. In our original presentation of the proton decay scenario [12], we utilized absolute atmospheric neutrino fluxes calculated by Bugaev and Naumov [13], which are distinctly lower in absolute rate than the Bartol or Honda *et al.* fluxes. However the essential argument can be restated in a way which does not rely on an absolute neutrino flux calculation [14].

In essence, we assume the distribution of muon momentum from the 7.7 kty exposure of Kamiokande to be free of any "new physics". Also, we assume neutrino cross–sections to be the same for corresponding ν_μ and ν_e charged current channels. Then we use the number of μ–like events in each momentum bin, together with the experimental detection efficiencies and the expected e–like to μ–like event ratio 1:2, to predict the number of e–like events to be observed. Proceeding in this way, we find there to be an excess of e–like events over and above the expectation inferred from the μ–like event distribution and the conventional neutrino flux flavor ratio. Upon subtracting bin–by–bin from the e–like event data, the rate expectation inferred from the distribution of μ–like events, we obtain the distribution of excess e–like events in Figure 5. The excess is localized to the shower momentum interval 100 – 500 MeV/c. The shape is well–described by the positron momentum spectrum from the proton decay mode

$$p \rightarrow e^+ + \nu + \nu. \qquad (7)$$

In Figure 6 we reproduce Kamiokande measurements for R_ν versus lepton momentum from 4.92 kty and 7.7 kty analyses. With the statistical gain in the more recent data, the anomaly appears mildly enhanced in the 300 to 700 MeV/c interval while being mildly diminished both below and above this regime. These trends coincide with the shape of $p \rightarrow e^+\nu\nu$ phase space.

Scrutiny of the anomaly as $p \rightarrow e^+\nu\nu$ hypothesis will be made feasible by the steady accumulation of contained single shower events in the Soudan experiment. The e–like event excess indicated in Fig. 5 should emerge, for example in the lepton momentum distribution from shower events as in Fig. 2b, at a rate of 6 to 11 events per kiloton year. It is of interest to examine the 200 – 600 MeV/c region of Fig. 2b for evidence of an excess. If only the relativistic $e^\pm$ particles were being imaged as in a Cherenkov experiment, one might consider the populous 400–500 MeV bin to show promise for a signal. Alas, in more than half of the events in this bin, a final state proton is observed to accompany the shower (events shown shaded). Such events, having visible baryon number in the final state, are highly unlikely to be proton decay. With the shower–plus–proton events removed from consideration, no obvious excess is discernible in Soudan's 1.52 kty single shower sample. Detailed

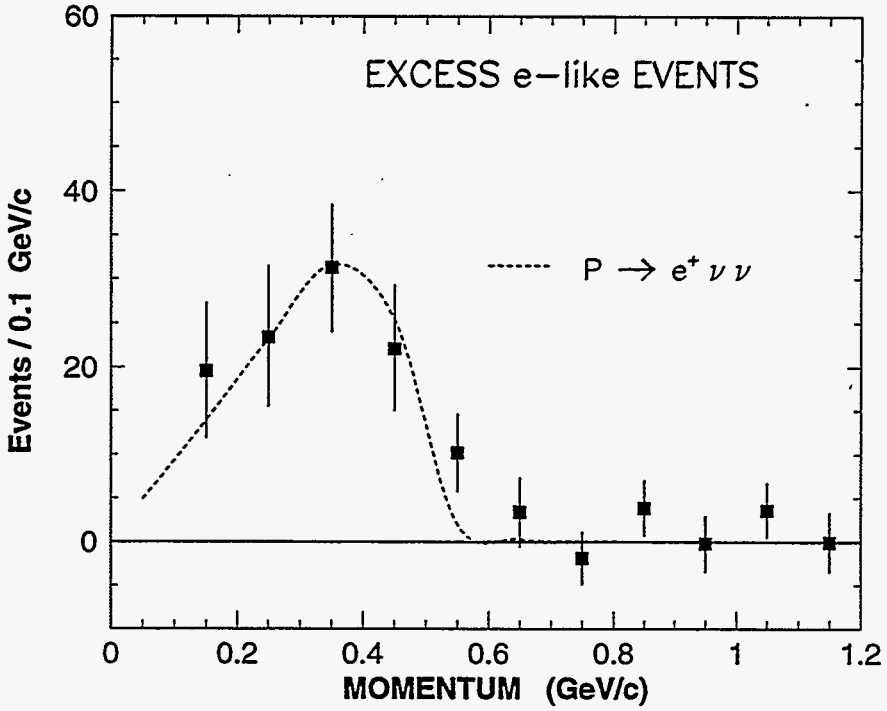

Figure 5: Excess e–like events inferred from the 7.7 kty exposure of Kamiokande (solid squares). Superimposed is the phase space momentum distribution for positrons originating from $p \to e^+\nu\nu$ in water medium (dashed line).

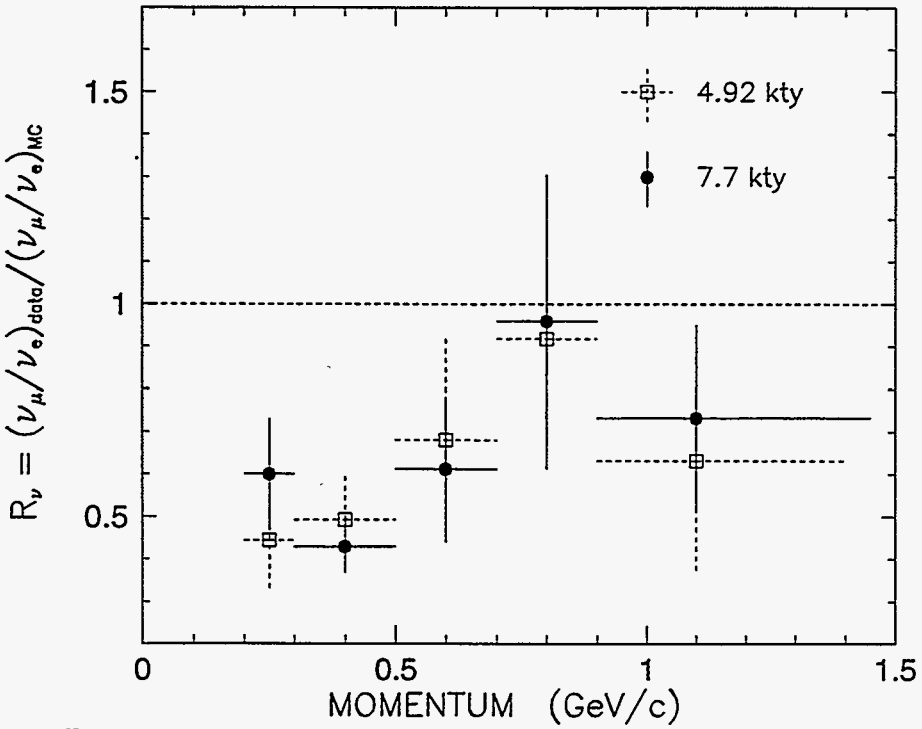

Figure 6: R_ν in Kamiokande data given in bins of lepton momentum from 0.2 to 1.5 GeV/c. Proton decay into $e^+\nu\nu$ would populate the region below 600 MeV/c.

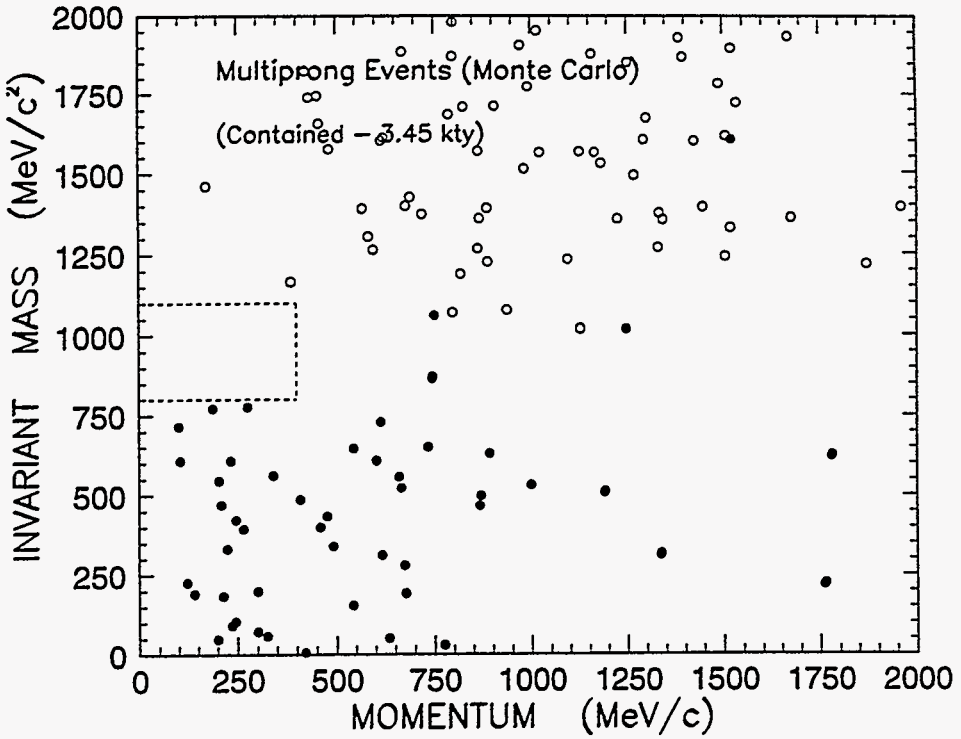

Figure 7: Invariant mass versus the visible final state momentum for the multiprong Monte Carlo sample. Events with a visible recoil protons are shown with open circles.

analysis however requires a larger sample; we look forward to new data from Soudan and from SuperKamiokande.

V. Baryon Instability Search

A. Nucleon decay into charged lepton modes

We observe 55 contained multiprong events in our 1.52 kty exposure. Using particle identification and reconstruction techniques similar to methods for heavy liquid bubble chamber experiments, a four–momentum vector is determined for each track or shower outgoing from the event vertex. From the four–vectors, variables useful to baryon instability searches can be constructed. For multiprongs, it is informative to plot the invariant mass of each event against the magnitude of the net vector momentum. Diplots of these variables are shown in Figure 7 for an atmospheric neutrino MC sample of 3.45 kty [15], and in Figure 8 for our contained multiprongs. In either Figure, the rectangular area bordered by the dashed line depicts the kinematical region compatible with nucleon decays into charged lepton modes:

$$N \rightarrow l^{\pm} + hadrons, \qquad l = e \text{ or } \mu. \tag{8}$$

The delineated region is the 'neighborhood' of nucleon mass having Fermi momentum around 250 MeV/c, with allowance for detector resolution and for the Fermi motion spread within iron nuclei. Nucleon decay modes which yield multiprongs

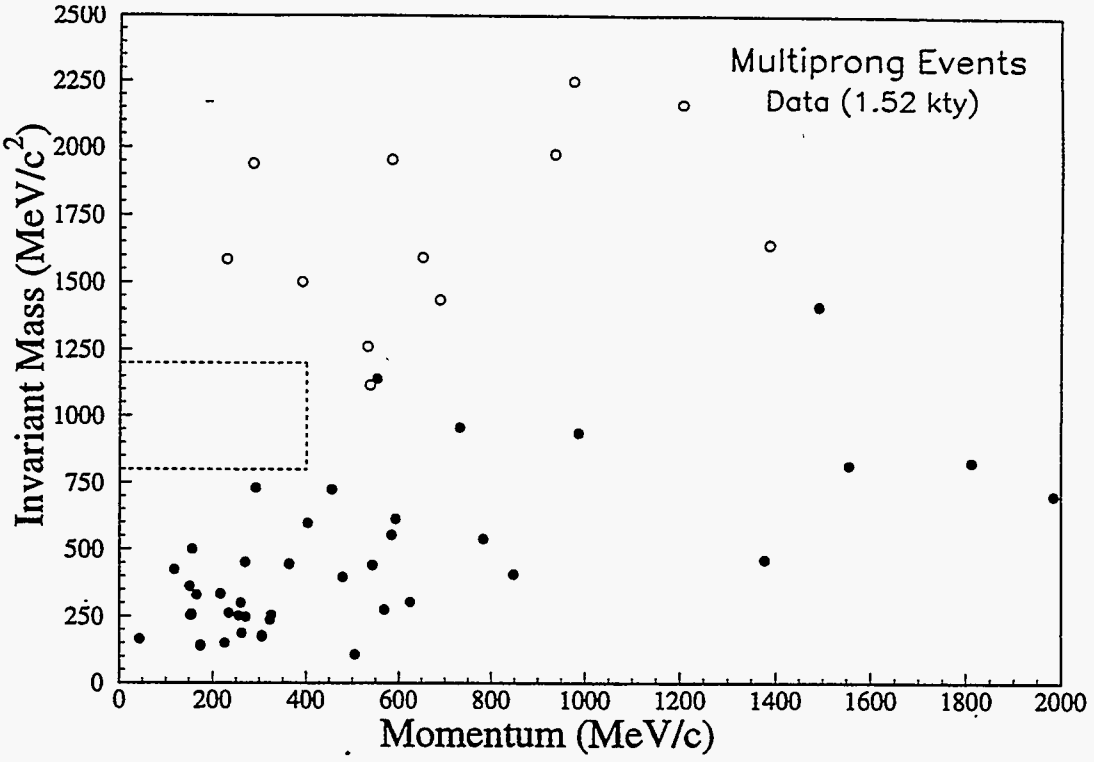

Figure 8: Invariant mass versus the visible final state momentum for the multiprong data sample. Events with visible final state protons are shown with open circles.

together with a final state neutrino, e.g. $n \to \nu K^0$, would populate a region below and slightly to the right of the rectangular area. Directly above the rectangular area, from 1.0 to about 2.0 GeV in invariant mass, is the region of occurrence for $n - \bar{n}$ oscillation events. Sizable fractions of both MC and data multiprong samples include events which have visible recoil protons (open circle events); these can be excluded from consideration as nucleon decay or $n - \bar{n}$ oscillation candidates. We note that the data roughly distributes as does the neutrino MC sample. Fig. 7 indicates that the neutrino background for nucleon decay modes (8) is low, being of order ≤ 0.3 neutrino background events per kiloton year. From Figure 8 we conclude that no nucleon decays via reactions (8) and no $n - \bar{n}$ oscillation candidates, are observed in the initial 1.52 kty exposure of Soudan 2.

B. Proton decay into $\bar{\nu}K^+$

The proton decay mode favored by supersymmetric grand unified theories is

$$p \to \bar{\nu} + K^+. \tag{9}$$

The Soudan calorimeter can image this process with compelling detail, provided that it occurs with an accessible lifetime. We focus here on decays wherein the K^+ subsequently decays – after ranging to a stop – into $\mu^+\nu$ (BR = 63.5%). This decay sequence gives rise to a candidate track plus recoil topology in the Soudan detector, of appearance akin to the quasi-elastic $\mu^- p$ event shown in Figs 1a,b. Careful scrutiny will however discern features which distinguish (9) from quasi-elastics (1), and from other neutrino reactions [16]:

i) Since the K^+ decays at rest, the muon track will have – to the accuracy afforded by detector resolution – the momentum 236 MeV/c.

ii) In contrast to a produced charged hadron whose ionization is least in the vicinity of the event vertex, the K^+ track should exhibit a stopping ionization increase as it approaches the apparent vertex.

iii) Sixty percent of daughter μ^+'s will have endpoint decays which make two or more tube hits displaced from the track endpoints.

From Fig. 2a it can be seen that three track plus recoil events have muon momenta between 200 and 300 MeV/c. In two of these events, however, the μ^+ momenta are too high to be compatible with signature *i)*. In the remaining event, the candidate K^+ track has ionization increasing in the direction away from the vertex and hence is incompatible with signature *ii)*. In conclusion, we report that no candidate decays $p \to \nu K^+$ $(K^+ \to \mu^+\nu)$ are observed in Soudan's initial 1.52 kiloton–year exposure.

VI. Status and Outlook

The Soudan 2 detector is performing as designed and continues to record quality data. The experiment's high resolution imaging of contained events will provide new perspectives on atmospheric neutrino interactions and on baryon instability. For optimal investigation of these phenomena, we intend to accumulate a fiducial exposure of five kiloton–years. The prerequisite live–time will be achieved before the millenium, at which point preparation for long baseline neutrino oscillation experimentation will be the dominant activity at the site.

References

[1] J.L. Thron, Nucl. Instr. Meth. **A283**, 642 (1989).

[2] W.P. Oliver *et al.*, Nucl. Instr. Meth. **A276**, 371 (1989).

[3] See R. Merenyi *et al.*, Phys. Rev. **D 45**, 743 (1992), and references therein.

[4] T. K. Gaisser, T. Stanev, G. Barr, Phys. Rev. **D 38**, 85 (1988); G. Barr, T. K. Gaisser, T. Stanev, Phys. Rev. **D 39**, 3532 (1989).

[5] A. Bodek and J. L. Ritchie, Phys. Rev. **D 23**, 1070 (1981).

[6] K.S. Hirata *et al.*, Phys. Lett. **B 205**, 416 (1988); K.S. Hirata *et al.*, Phys. Lett. **B 280**, 146 (1992).

[7] D. Casper *et al.*, Phys. Rev. Lett. **66**, 2561 (1991); R. Becker–Szendy *et al.*, Phys. Rev. **D 46**, 3720 (1992).

[8] Ch. Berger *et al.*, Phys. Lett. and **B 227**, 489 (1989); Phys. Lett. **B 245**, 305 (1990); K. Daum *et al.*, Z. Phys. C **66**, 417 (1995).

[9] H.M. Gallagher, Ph.D. Thesis, University of Minnesota, 1996, unpublished.

[10] T. Haines, K. Kaneyuki, C. Mc Grew, R. Mohapatra, E. Peterson, D. Cline, *in*: Proceedings of the 1994 Snowmass Summer Study, Ed. E.W. Kolb and R.D. Peccei, World Scientific (1995).

[11] M. Honda, K. Kasahara, K. Hidaka and S. Midorikawa, Phys. Lett. **B 248**, 193 (1990); Phys. Rev. **D 52**, 4985 (1995).

[12] W.A. Mann, T. Kafka and W. Leeson, Phys. Lett. **B 291**, 200 (1992).

[13] E. V. Bugaev and V. A. Naumov, Phys. Lett. **B 232**, 391 (1989).

[14] W.A. Mann, T. Kafka and W. Leeson, *in*: Proceedings of the DPF92 Meeting, Fermilab, 10–14 November 1992; p. 1330; Soudan 2 Report PDK–590, July 1994.

[15] William R. Leeson, Ph.D. Thesis, Tufts University, 1995, unpublished.

[16] Steven Werkema, Ph.D. Thesis, University of Minnesota, 1989, unpublished.

ICARUS EXPERIMENT *

P. Benetti[a], A. Bettini[b], P. Boccaccio[c], E. Calligarich[a], F.Carli[d], C.Carpanese[b], F. Casagrande[e], D.Cavalli[f], F. Cavanna[g], P. Cennini[h], S. Centro[b], A. Cesana[a], C.Cinquini[d],S. Cittolin[h], D. Cline[i], L.K. Ding[l], R. Dolfini[a], D. Dzialo Giudice[e], A.Ferrari[f], F.Gianotti[f], A. Gigli Berzolari[a], W. Hong[i], X. Li[e], Y. Li[l], F. Lu[l], J.M. Ma[l], G. Mannocchi[e], M.Martelli[d], F. Mauri[a], G.Maurin[h], L. Mazzone[a], C. Montanari[a], G. Muratori[i], E. Olejarczyk[g], S. Otwinowski[i], J. Park[i], D.Pascoli[b], A. Pepato[b], L. Periale[m], G. Piano Mortari[g], A. Piazzoli[a], P. Picchi[e], F. Pietropaolo[b], A. Placci[h], J.F. Qiu[l], A. Rappoldi[a], G.L. Raselli[a], S.Resconi[f], J.P. Revol[h], M. Rossella[a], C. Rubbia[h], P.Sala[f], D. Scannicchio[a], F. Sergiampietri[n], H.Y. Sheng[l], S. Suzuki[m], M. Terrani[a], W.H. Tian[h], P.Torre[a], K.L Tung[l], S. Ventura[b], M. Verdecchia[g], C. Vignoli[a], H.G. Wang[i], J.Y. Zeng[l], B. Zhang[l], M. Zhou[i]

[a]Dipartimento di Fisica e INFN, Università di Pavia, via Bassi 6, Pavia, Italy
[b]Dipartimento di Fisica e INFN, Università di Padova, via Marzolo 8, Padova, Italy
[c]Lab. Naz. di Legnaro dell'INFN, via Romea 4, Legnaro (PD) , Italy
[d]Dipartimento di Meccanica Strutturale e INFN, Università di Pavia, via Abbiategrasso 209, Pavia, Italy
[e]Lab. Naz. di Frascati dell'INFN, via E. Fermi 40, Frascati (Roma), Italy
[f]Dipartimento di Fisica e INFN, Università di Milano, via Celoria, Milano, Italy
[g]Dipartimento di Fisica e INFN, Università dell'Aquila, via Vetoio, L'Aquila, Italy
[h]CERN, CH-1211 Geneva 23, Switzerland
[i]Department of Physics, UCLA, Los Angeles, CA 90024, USA
[l]Institute of High Energy Physics, Beijing, People's Republic of China
[m]ICGF del CNR di Torino, corso Fiume 4, Torino, Italy
[n]INFN Pisa, via Livornese 1291, 56010 S. Piero a Grado, Pisa, Italy

ABSTRACT

We briefly describe the current status of the ICARUS programme, including the 3 ton prototype R&D studies. The next step of the project will be the construction of a 600 ton module to be operated in the LNGS underground laboratory. A detailed description of the proton decay detection capability and of the lifetime limits achievable, both with the 5,000 ton final detector and with the 600 ton module are reported.

1.Introduction

As is well known, bubble chambers have played a fundamental role in Particle Physics. They provide unbiased events, in 3 dimensions, with the possibility of adding a magnetic field. Because of the high density of the liquid medium, bubble chambers can combine target and detector

* presented by F.Mauri

functions. Unambiguous discovery can be claimed at single (few) event level.

However, bubble chambers are not continuously sensitive, hard and costly to build and dangerous if operated underground.

An ideal detector for search of rare events in an underground laboratory, such as proton decay and neutrino interactions, would be a high resolution detector with an electronic read-out, a so called *electronic bubble chamber*.

With this aim, in 1985 the ICARUS programme was presented[1]. The final goal of the experiment is the construction of a multi-kton detector to study a variety of fundamental physics issues in the underground Gran Sasso laboratory[2]. After many years of intense R&D work, culminated in more than 4 years of continuous operating the 3 ton prototype at CERN[3], we are now ready to build and operate a 600 ton module in the Gran Sasso underground laboratory[4].

2.The 3 ton prototype

In 1989 the ICARUS collaboration decided to build a reasonable scale prototype[3] detector aiming to solve the main technological problems:

a) The liquid argon must be kept ultra pure even in the presence of a large number of feedthroughs for the signals and the high voltage, and with wire chambers, cables, etc. in the clean volume. The contamination of electronegative molecules must be kept to around 0.1 ppb to allow drifts on long distances (metres) without capture of the ionization electrons;

b) All the materials employed in the construction of the detector must be extremely clean and non-degassing and the feedthroughs between pure argon and the outside world must be completely tight to avoid contamination due to leaks;

c) The wire chambers must be able to perform non-destructive readout with several wire planes with a few mm pitch; they must be built out of non-contaminating materials and must stand the thermal stress of going from room to liquid argon temperatures; the precision and the reliability of the mechanics must be high and a good knowledge of the electric field in the detector must be granted;

d) In order to obtain a good signal-to-noise ratio, low-noise preamplifiers must be developed. It must be remembered that we work with no amplification in the liquid; the signal is very small, of the order of 10 000 electrons for a minimum-ionizing track in a 2 mm wire pitch;

e) Given the large amount of digitizations of the three-dimensional image, software architectures and algorithms must be developed for data reduction.

The cryostat, shown schematically in Figure 2.1, consists of two coaxial vertical stainless steel (AISI 304L) vessels. The shape of both the external

(1 in Figure) and the internal (2) vessels is a cylinder with hemispherical bottoms. The outer vessel has a diameter of 1.5 m, a height of 3.3 m and a wall thickness of 3 mm. The inner vessel has a diameter of 1.05 m, a height of 3.08 m and a wall thickness of 3 mm. The total internal volume is 2.61 m^3.

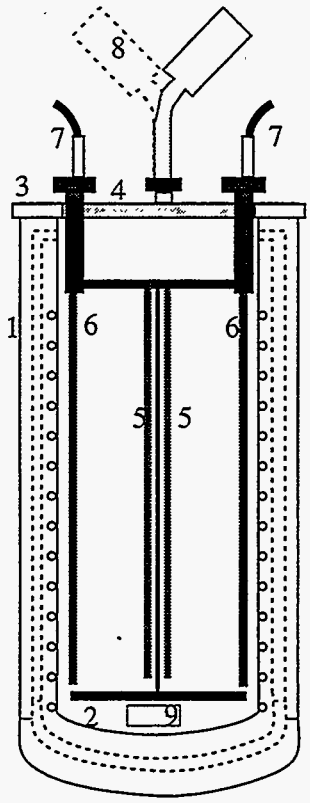

Fig. 2.1 : Schematic view of the mechanics of the detector. 1 is the outer vessel, 2 the inner vessel, 3 the annular flange, 4 the circular flange, 5 the wire chambers, 6 the cathodes, 7 the high-voltage feedthroughs, 8 the boxes containing the preamplifiers (two out of eight shown), 9 the purity monitor.

There are two wire chambers on each side of the central septum. Each chamber consists of three planes of wires. The first plane is a screening/focusing grid followed by the induction plane and finally by the collection plane. The induction plane is made by doublets of sense-wires (each doublet is read out by one amplifier) separated by 0.6 mm; the centres of two adjacent doublets are separated by 2 mm and there is a screen wire between them. The collection plane is made of sense-wires at a 2 mm pitch separated by screen wires.

The wires (stainless steel, 100 μm in diameter) are kept in position and under tension on the frame of the chamber by a structure made out of MACOR bars. They are held by small conical tubes crimped around them, while the tubes are held in turn by the holes drilled in the MACOR

bar. Their diameter is 150 μm. In the case of the doublets of the induction plane we insert both wires in the same tube (300 μm in diameter).

3. The 600 ton module

It appears to us that the best way to reach the sensitive mass needed to fulfil our scientific goals is to go through an intermediate step between the 3 ton detector in operation at CERN and the major engineering design of the multikiloton detector[3]. A few hundred ton detector will insure that our extrapolation between 3 tons and a few thousand tons is done in the most efficient way.

This step-wise strategy will allow us to develop progressively, at the Gran Sasso Laboratory, (1) the infrastructure needed to build and operate our large detector, (2) the *in situ* experience needed in terms of safety but on a still modest liquid argon volume, and (3) to obtain a definitive and practical evaluation of our engineering choice for the final phase.

It quickly appeared to us, that a few hundred ton detector would at the same time allow an important first step in our scientific programme. While a sensitive mass in excess of a few thousand tons of liquid argon is clearly needed to achieve the 10^{34} years range in proton decay lifetime in a number of proton decay channels, many exotic channels have only been poorly investigated so far or not at all, and would be easily covered in this first phase. Atmospheric and solar neutrinos are areas which could be completely clarified in establishing whether the effects observed by Kamiokande and Homestakes are instrumental or genuine. Therefore we have chosen a detector size which is the largest which can be transported from an outside laboratory to the Gran Sasso Laboratory: two half detectors with a cross-section of 3.9 by 4.2 metres and a length of 19 metres, corresponding to a total internal volume of 465 m^3 and a sensitive mass of 540 tons of liquid argon. Moreover, we decided to use a 3 mm wire pitch instead of the 5 mm foreseen for the 5000 ton module, in order to allow for higher precision measurements. This is particularly beneficial for solar neutrinos, especially when this is combined also with the presence of a neutron absorber around the entire volume, in order to reduce the radioactivity background to a negligible level.

This intermediate step opens in addition the possibility to explore a new route towards larger detector volumes: the construction of a number of identical 600 ton detectors installed next to one another.

4. Proton decay detection

4.1 The multi kton detector

Thanks to its large sensitive mass (4.7 kton)[4] and to its spatial and energy resolution capabilities, ICARUS is an ideal device for nucleon decay detection, in particular for those channels that are not accessible to

Cherenkov detectors due to the complicated event topology, or because the emitted particles are below the Cherenkov threshold ($K^{\pm}$). Unlike the other large detectors for proton decay, ICARUS, with its excellent tracking and particle identification capabilities providing a much more powerful background rejection, can perform exclusive decay mode measurements. In particular, it is possible to distinguish between atmospheric neutrino events and true nucleon decays. Our Monte Carlo simulation has already verified this point for a number of decay channels.

We have performed a detailed event simulation based on the standard GEANT Monte Carlo code and the realistic events obtained contain very long tracks with redundant information, allowing particle identification and measurement of their energies with great precision.

Table 4.1 : Efficiency (ε), as defined in the text, for various nucleon decay modes

Decay mode	ε	Decay mode	ε
$p \rightarrow e^+ \pi^0$	0.42	$n \rightarrow e^+ \pi^-$	0.4
$p \rightarrow \nu \pi^+$	0.42	$n \rightarrow \mu^+ \pi^-$	0.37
$p \rightarrow \mu^+ \pi^0$	0.38	$n \rightarrow \nu \pi^0$	0.42
$p \rightarrow \nu K^+$	0.85	$n \rightarrow e^- K^+$	0.85
$p \rightarrow e^+ \pi^+ \pi^-$	0.13	$n \rightarrow e^+ \rho^-$	0.08
$p \rightarrow e^+ \rho^0$	0.08	$n \rightarrow e^+ \pi^- \pi^0$	0.13

Particle identification benefits greatly from the ability to measure the ionization loss (*dE/dx*). In particular, using *dE/dx* versus range only, an excellent separation is obtained between pions and kaons. As a consequence, many exclusive channels will be searched for simultaneously, both for proton and neutron decays for which discoveries can occur at the one-event level. This is certainly the main strength of the ICARUS technique.

In the absence of background, the limit on the nucleon lifetime reachable in T years of observation is given by the simple formulae:

$\tau_p > 1.2 \times M \times T \times \eta$ (10^{32} year) (90 % C.L.) for the proton (1a)

$\tau_n > 1.4 \times M \times T \times \eta$ (10^{32} year) (90 % C.L.) for the neutron (1b)

where M is the detector mass in kton and η is the overall detection efficiency.

In order to reduce neutrino-induced backgrounds we make use of the ability of ICARUS to fully reconstruct the events. Proton decay events are characterized by a definite value of the total energy and by the fact that the total momentum of the decay products must be zero. These features, which are true for a free nucleon, are also approximately verified for a nucleon bound in a nucleus, provided the decay products do not rescatter before escaping the nucleus. As a consequence, we also include in our

definition of detection efficiency $\eta = \varepsilon_D \cdot \varepsilon$ the probability ε that the decay products do not interact with the nucleus in which they were produced, and the reconstruction efficiency ε_D.

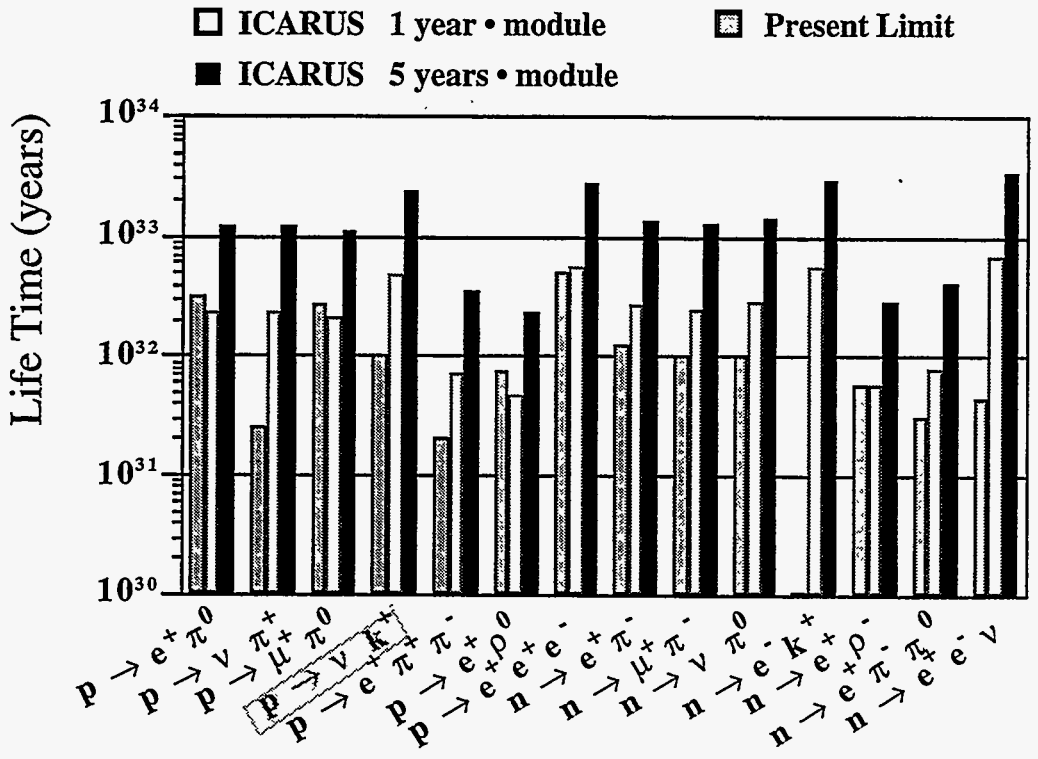

Fig. 4.1 : Comparison of present nucleon decay limits with the sensitivity of ICARUS for one and five years

These nuclear effects, the distortions of the energy and momentum distributions due to the nucleon Fermi motion, and the reinteraction of decay particles with the nucleus have been studied by Monte Carlo simulation methods.

Table 4.1 lists, for some of the main decay modes under consideration, the computed probabilities (ε) for the nucleon decay products to escape the argon nucleus without interacting.

For example, for the decay mode $p \rightarrow \nu + K^+$ we obtain $\varepsilon = 0.85$ and a corresponding lifetime limit $\tau_p > 4.7 \times 10^{32}$ (90% C.L.) years for one year of data-taking. In ten years of operation, ICARUS will be able to reach a proton lifetime of 5×10^{33} years for this most interesting decay mode. This would increase the present limit by about two orders of magnitude. For this decay mode in particular (as for many others) we don't expect to have any significant background.

Except for channels such as $p \rightarrow e^+ \nu \nu$ for which the topology is identical to that of atmospheric ν_e charged-current events, the background corresponding to a data-taking period of one year is negligible. In order to obtain a preliminary estimate of the sensitivity of ICARUS, we have assumed that for all the other decay modes the background is indeed also negligible.

In summary, many nucleon decay modes can be searched for simultaneously and, after only one year of data taking, ICARUS will reach or exceed most present limits (Figure 4.1). The equivalent of five years of data will take us to the unexplored region between 10^{33} and 10^{34} years for some of the most relevant channels.

With the huge mass of liquid argon it is possible to conceive a measurement of the neutron-antineutron oscillations, taking into account the big reduction factor due to the nuclear potentials[6]. The efficiency to detect a neutron-antineutron oscillation (5 pions in average) in ICARUS is very high. The achievable limit for free n-n oscillation in one year running is of the order of 4.0×10^8 s, better than the present one[7].

4.2 The 600 ton module

Even with a relatively low mass, our test module can provide important contributions to the proton decay search, in particular for those decay modes (referred in the following as *exotic decay modes*) with high multiplicities (3 or 4 particles in the final state) or, more generally, with signatures particularly difficult to identify with previously used detector techniques.

One example of such decay modes is $p \rightarrow e^+ \nu \nu$ which has been emphasised in our proposal[2] because it can be interpreted as the source of the excess electron-like events in the Kamiokande and IMB experiments. This type of event belongs to a class of decay modes with $\Delta B = -\Delta L$ which is one of the distinguishing features of $SU(4)^{colour}$ Grand Unification Theories. This model has been first proposed by J. Pati and A. Salam[5] in 1973.

With a sensitive mass of about 540 tons the ICARUS prototype can probe in one year, lifetimes up to 1.5×10^{32} years. Moreover, this module will have three readout planes and a better space resolution (3 mm^3 instead of 5 mm^3) with respect to the one foreseen for the big ICARUS, and therefore it will be even better suited for the analysis of complicated topologies. In this sense the physics programme of the 600 ton module will be, at least in part, complementary to the one of the full detector.

Table 4.2 reports the rates and the background expected for a 540 ton prototype in some of the channels characteristic of the Pati-Salam model, assuming that the nucleon lifetime is at the current experimental limit.

The ICARUS technique is particularly well suited to identify these decay modes, or any decay mode involving several charged particles in

the final state. The detector techniques used so far, especially water Cherenkov detectors, do not allow to study these decay modes in an exclusive way, as can be seen from the relatively modest present limits. For most of them the background in ICARUS is expected to be negligible, hence one single event is sufficient for a discovery.

Table 4.2: For a number of exotic decay modes, the detection efficiency (including the fiducial volume cut), the present limits, the rates in the 600 ton module corresponding to the present limit are given.

Decay Mode	Efficiency	Present Limit (10^{31} years)	Events (year^{-1})
$p \rightarrow e^- \kappa^+ \pi^+$	0.36 (.9)	2.0	2.6
$p \rightarrow \mu^- \kappa^+ \pi^+$	0.36 (.9)	0.5	10.5
$p \rightarrow \bar{\nu} \pi^+$	0.36 (.85)	2.5	2.0
$p \rightarrow e^+ \nu \nu$	0.72 (.85)	1.1	9.6
$p \rightarrow \mu^+ \nu \nu$	0.68 (.8)	2.1	4.7
$n \rightarrow \mu^- e^+ \nu$	0.54 (.6)	4.7	2.1
$n \rightarrow e^- \kappa^+$	0.68 (.8)	3.2	3.8
$n \rightarrow \mu^- \kappa^+$	0.64 (.75)	5.7	2.0
$n \rightarrow e^- e^+ e^- \pi^+$	0.36 (.9)	0.1	12
$n \rightarrow e^- e^+ e^- \kappa^+$	0.81 (.9)	0.1	27
$n \rightarrow \mu^- e^+ e^- \pi^+$	0.36 (.9)	0.1	12
$n \rightarrow \mu^- e^+ e^- \kappa^+$	0.81 (.9)	0.1	27

Table 4.2 also reports the detection efficiencies for the various channels. These efficiencies include the requirement that the events are contained in the detector. For nucleon decay events, with the present geometry for the 600 ton module, it turns out that the containment request does not reduce very much the fiducial volume. Considering that a certain segmentation with relatively large dead zones (for supporting frames, internal electronic boards, etc.) will be probably present also in a single 5000 ton detector, the above consideration favours a strategy of using several 600 ton modules to reach the 5000 ton sensitive mass.

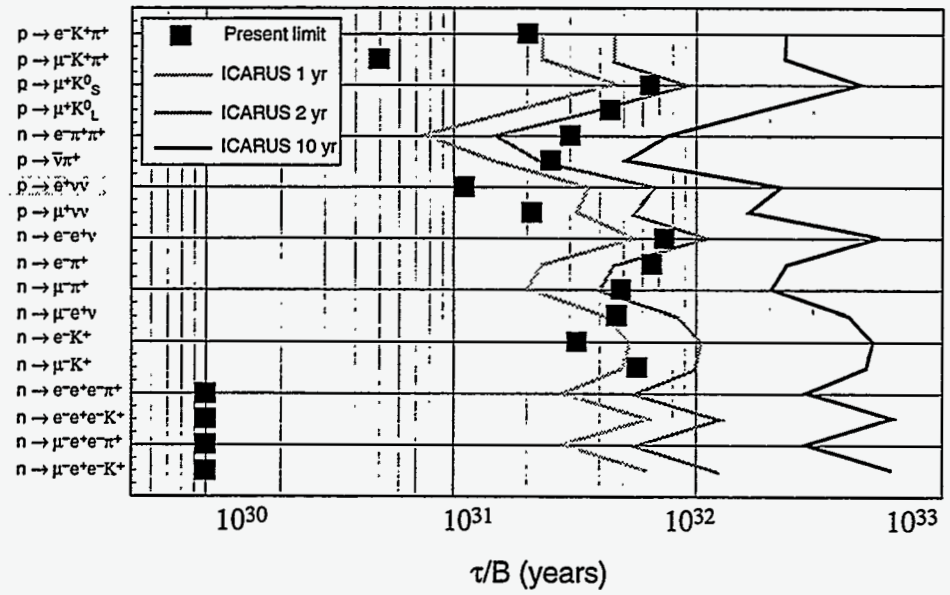

Fig. 4.2 : Present limits for a number of "exotic" proton and neutron decays together with the 90% ICARUS sensitivity, with the 600 ton module and for data taking periods of 1, 2 and 10 years.

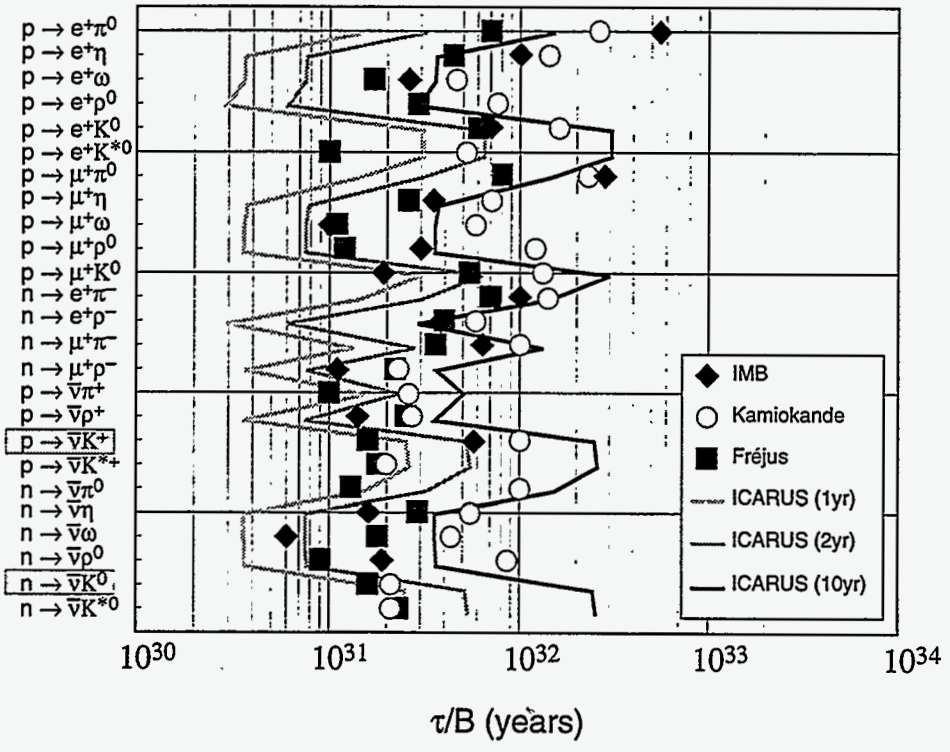

Fig. 4.3 : Present limits for a number of "standard" proton and neutron decays together with the 90% ICARUS sensitivity, with the 600 ton module and for data taking periods of 1, 2 and 10 years.

With our 600 ton module, in a few years, we will be able to explore a lifetime region exceeding 10^{32} years for most of the channels reported in the above tables, with a considerable improvement (a factor 5 to 100) of the present limits for the exotic channels (see Figure 4.2). It is clear that with one single module we cannot reach the lifetime limit of 10^{34} years (Figure 4.3) which is needed to fully test the minimal SUSY Gran Unification Theory and which is the final goal for the 5000 ton detector. We will nevertheless satisfy completely what is our requirement for this first phase of our programme and namely to extend the present knowledge of the nucleon stability over the widest possible range of decay modes at the same level of the presently best studied channels.

5. Conclusion

After many years of intense R&D studies, with more than 4 years of continuous operating the 3 ton prototype at CERN, the ICARUS experiment is now ready to start the construction of a 600 ton module to installed in the underground Gran Sasso Laboratory. As is reported in § 3, this step is intended to pursue two main goals:

- to establish all the important technical developments, such us the cryostat design, the read-out chamber technique, the electronics immersed in LAr, needed to scale up the detector size from 3 ton to several kton;
- to realize a complete physics programme, including atmospheric and solar neutrinos study, proton decay detection, at least in the exotic channels.

This step has already been approved and funded by Istituto Nazionale di Fisica Nucleare, for the Italian groups, and by DOE for the UCLA group.

The construction of the cryostat will start soon in Italy and the foreseen completion of the whole detector and the start of data taking at the LNGS is expected for the year 1999.

References

[1] ICARUS collaboration, INFN/AE-85/7 Frascati (1985).
[2] P.Cennini et al., LNGS - 94/99 I (1993) and II (1994).
[3] P.Benetti et al., Nucl. Instr. and Meth. **A 332**, 395 (1993),
P.Cennini et al., Nucl. Instr. and Meth. **A 345**, 230 (1994).
[4] P.Cennini et al., LNGS - 95/10 (1995).
[5] J.C.Pati, A.Salam, Phys. Rev. Lett. **31**, 661 (1973).
[6] W.M.Alberico et al., Phys.Lett. **114B**, 266 (1982),
C.B.Dover, A.Gal, J.M.Richard, Phys. Rev. **C31**, 1423 (1985)
[7] M.Takita et al., Phys. Rev. **D34**, 902 (1986),
C.H.Berger et al., Phys. Lett. **240B**, 237 (1990).

STUDY OF RARE SIGNALS WITH THE ICARUS DETECTOR

David B. Cline
Department of Physics and Astronomy, University of California Los Angeles
405 Hilgard Avenue, Los Angeles, California 90095-1547 USA

ABSTRACT

The ICARUS detector concept of imaging rare events is very well matched to the search for supersymmetric proton decay. We describe very briefly the R&D programs carried out by the ICARUS team over the past 10 years, emphasizing the enormous dynamic range. We discuss the signal and background for the decay, $p - K^+\bar{\nu}_\mu$. We also discuss the search for exotic neutrino processes and the use of the ICARUS method for a liquid-xenon detector to reach very low energy-recoil processes for the detector of SUSY WIMPs.

1. The Search for Proton Decay

The current generation of detectors has nearly exhausted the lifetime range up to ~ 10^{32} years. The scaling rules for the proton decay search are:

$$\tau_p \propto N_p \text{ (protons in detector)} \quad , \quad S/N >> 1 \quad , \tag{1}$$

$$\tau_p \propto \sqrt{N_p} \quad , \quad S/N \leq 1 \quad , \tag{2}$$

where S is the signal for proton decay and N is the background. In the latter case, a background subtraction is required, which reduces the statistical power of the detector.

In order to explore the τ_p ~ 10^{32}-10^{34}-yr region, we choose between two options:

1. Construction of very large detectors (M ~ 10^5 tons) that will have $S/N \leq 1$, or
2. Construction of detectors with M ~ 10^4 tons with $S/N >> 1$, with extreme pattern recognition for unique event selection.

In both cases, the background must be known, but in the $S/N >> 1$, we must know N precisely in order to subtract the background. We illustrate this part for the decay, $p - K^+\bar{\nu}_\mu$, given in Table 1.

Table 1. Current situation in search for $p - K^+\bar{\nu}_\mu$

Mode	Candidates	Gb[a]	Group
K_{μ_2}	11	8.6	KAM I/II 4.92Kt.y.
K_{μ_2}	6	4.7	IMB (90) 3.76Kt.y.
$K_{\mu_2} K_{\pi_2}$	1	1.8	Frejus 9.98Kt.y.
K_{π_2}	3	15.1	IMB

[a]Region of K_{μ_2} in $(\mu/e)/(\mu/e)_{cal} < 1$

[b]$\tau/B \geq 6 \times 10^{31}$ y 90% C.L.

The ICARUS detector method of detecting particles by ionization and scintillation light in noble gas–liquid has been developed over the past 10 years, starting with small prototype detectors up to the 3-ton liquid-Ar detector that has been operating at CERN for the past five years.[1-3] In addition, we have been operating a 2-kg liquid-Xe detector for the past two years.[4,5]

The features of ICARUS that make it a very sensitive detector for rare processes are given in Table 2.[1-3] One of the most important is the vast dynamic range that, as we shall show, goes down to almost 10 keV.[4,5]

The two types of proton decay that ICARUS is being designed for are shown in Fig. 1, where (A) is for a Pati–Salam model and (B) is for the currently favored, SUSY–GUT model.[1,3] We believe the predictions of the latter, which are illustrated in Table 3 and Fig. 2, should be taken seriously.

Of course there are other tests of SUSY–GUT, as illustrated in Table 4. One very interesting result of the SUSY–GUT concept is the extrapolation to the GUT scale, as shown in Fig. 3.[1] We note that the X mass that would be derived from this extrapolation would give a lifetime for $p \rightarrow \pi^0 e^+$ in excess of 10^{35} years. Thus in our opinion, the only viable options to detect proton decay in the near future are the processes shown in Fig. 1 (A and B). The ICARUS detector is well matched to these decay modes.[3] In Fig. 4, we show the limits for various proton decay modes that can be searched for with the 600-ton ICARUS.[3]

2. ICARUS Sensitivity to SUSY–GUT Predictions

The preferred decay mode of $p - K^+\bar{\nu}_\mu$ is uniquely searched for by ICARUS. Figure 5 shows the spectrum of energy deposition for the K^+ decay and illustrates that the detector efficiency can be ~ 85%.[1] Figures 6 (A) and (B) show two simulated events, indicating how unique the signal will be.[1]

Table 2. Unique features of ICARUS.

• Detect particles by ionization (water Č detetors observe only fast particles ($\beta \approx 1$) Sensitive to all charged particles in event
• Detect range and ionization to make a particle ID (water Č attempt ID by Č ring, etc.)
• Clear study of the vertex of events to help resolve ν interaction vs p decay
• Large dynamic range (~ 10s keVs → 100 GeV)

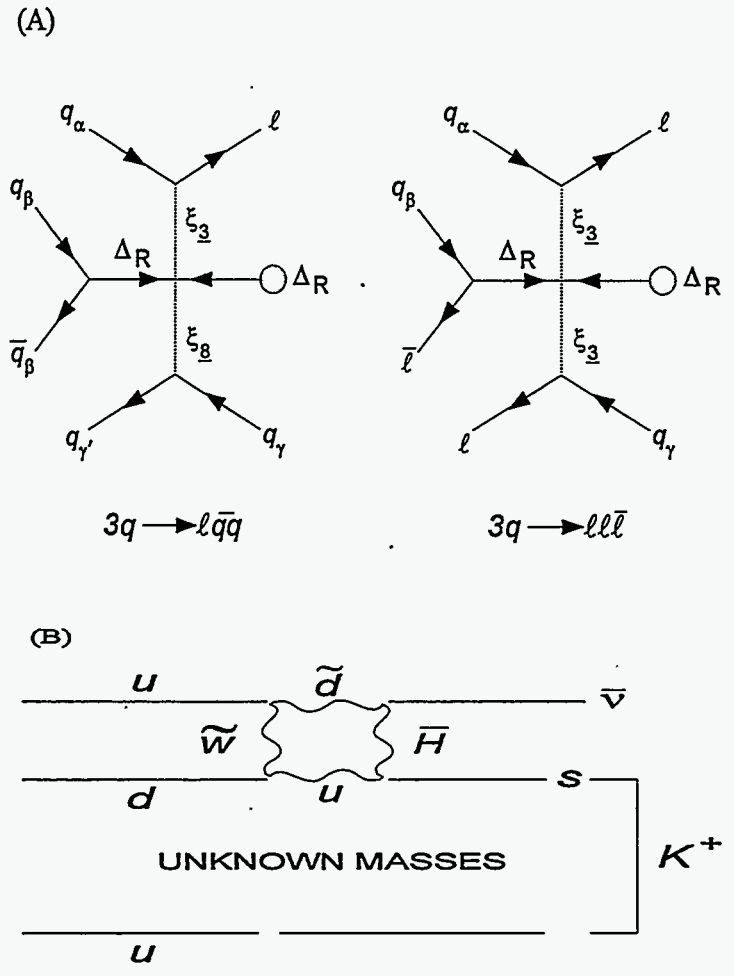

Fig. 1. (A) Feynman diagrams for proton decay into $\ell q\bar{q}$ and $\ell\ell\bar{\ell}$ in the Pati–Salam model, and (B) SUSY–GUT $p - K^+\bar{\nu}_\mu$ decay research.

Table 3. Why should we pay attention to SUSY- GUT predictions? (- Experimentalists)

(Is SUSY science or religion?)

- If a theory has some measured predictions, it should be testable. (SUSY/SUSY-GUTs have "testable" predictions)
- If a new technique is available (e.g., electron drift over large distances in liquid Ar), it should be used.
- Current data are remarkably near expectations for SUSY-GUT
  - $\Omega h^2 \sim 1$
  - $\sin^2\theta_W$ very near $\sin^2\theta_W$ (observed)
  - α extrapolation to GUT scale

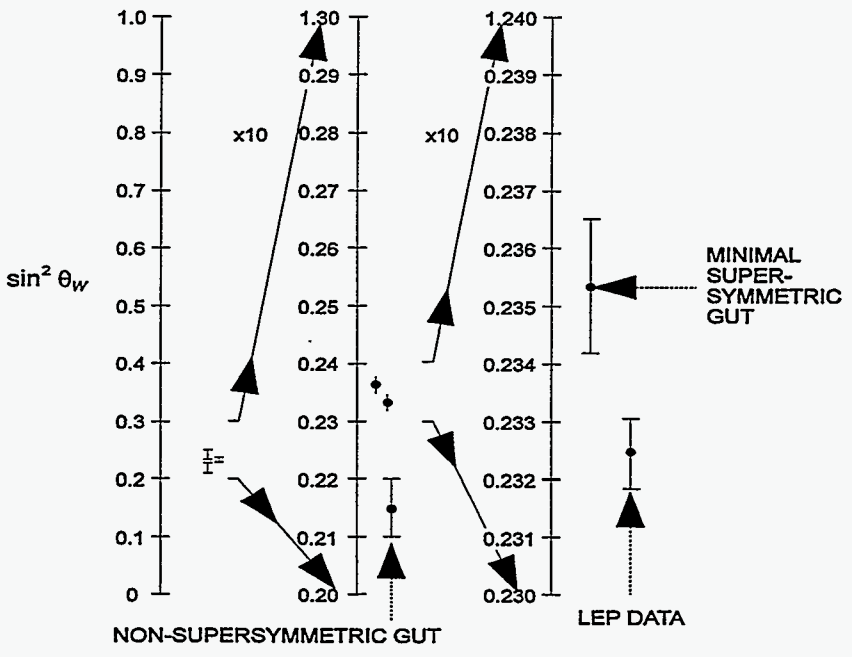

Fig. 2. Gee-whizz plot showing how well GUT predictions of $\sin^2\theta_W$ agree with the experiment data (from Ref. 6).

Table 4. Testable predictions of supersymmetric theories.

1. Discover SUSY particles at LHC (FNAL): $\tilde{q}$, $\tilde{\ell}$, $\tilde{W}$, ...
2. Observe proton decay: $p - K^{+}\bar{\nu}_{\mu}$
3. Detect SUSY dark matter: $\tilde{z}$ (neutralino)

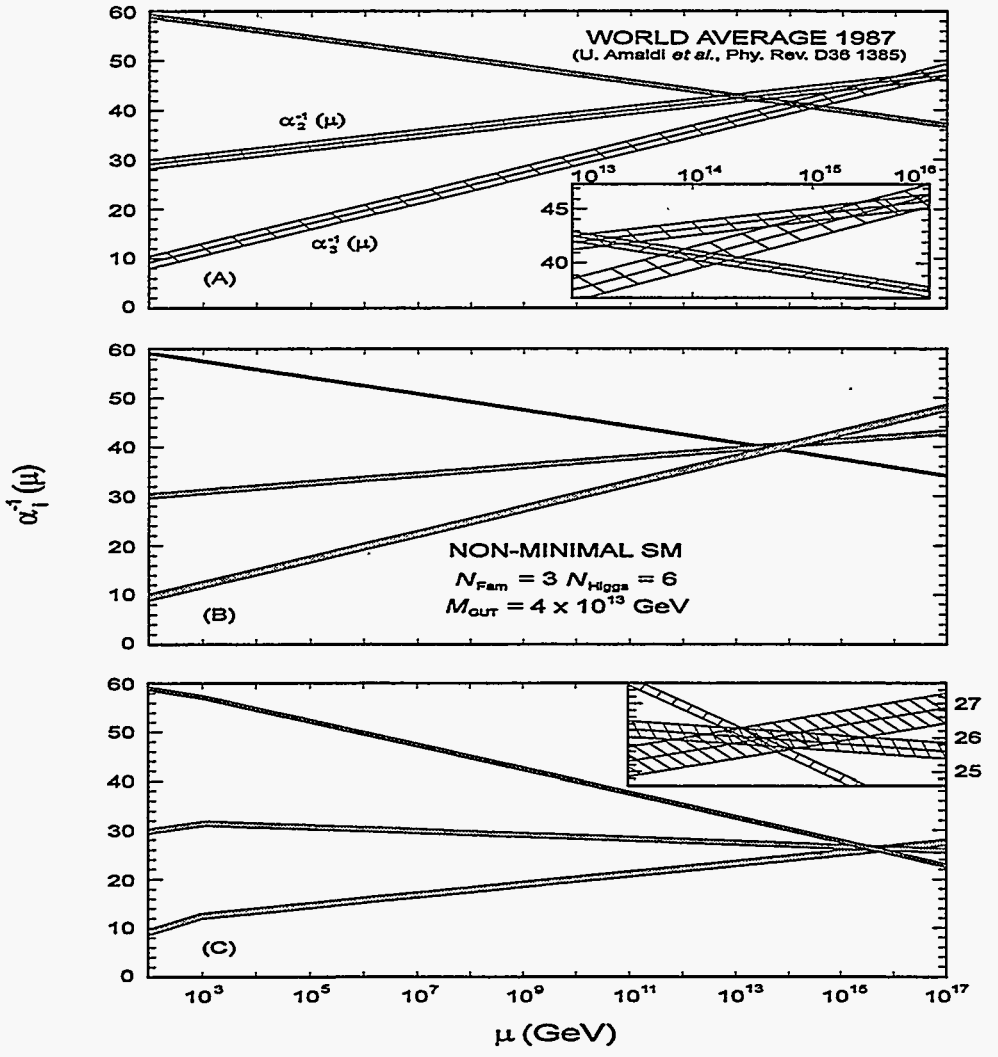

Fig. 3. Extrapolation to the GUT scale.

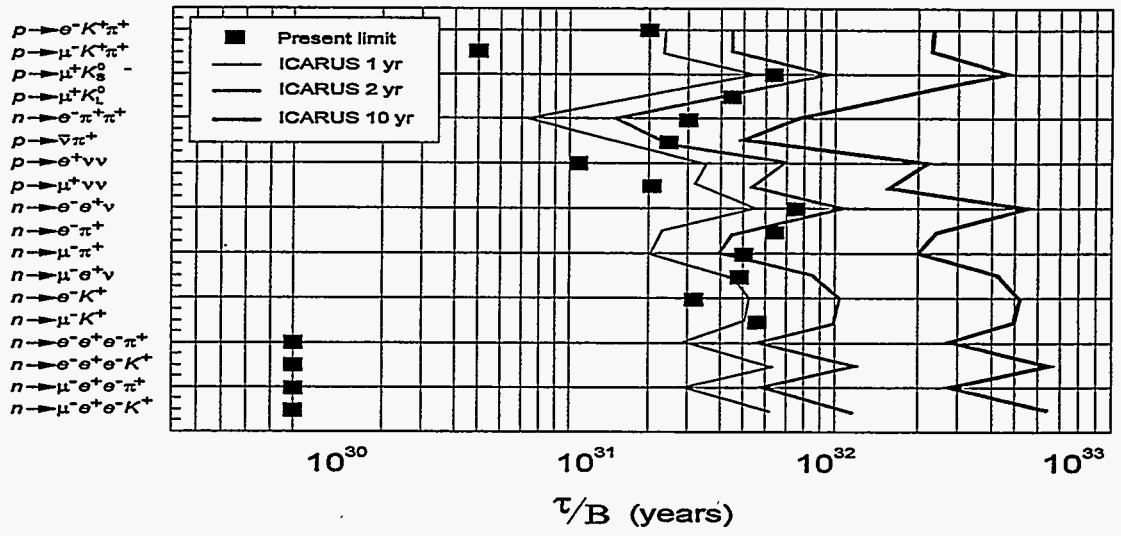

Fig. 4. Present limits for a number of "exotic" proton and neutron decays, together with the 90% ICARUS sensitivity, with the 600-ton module.

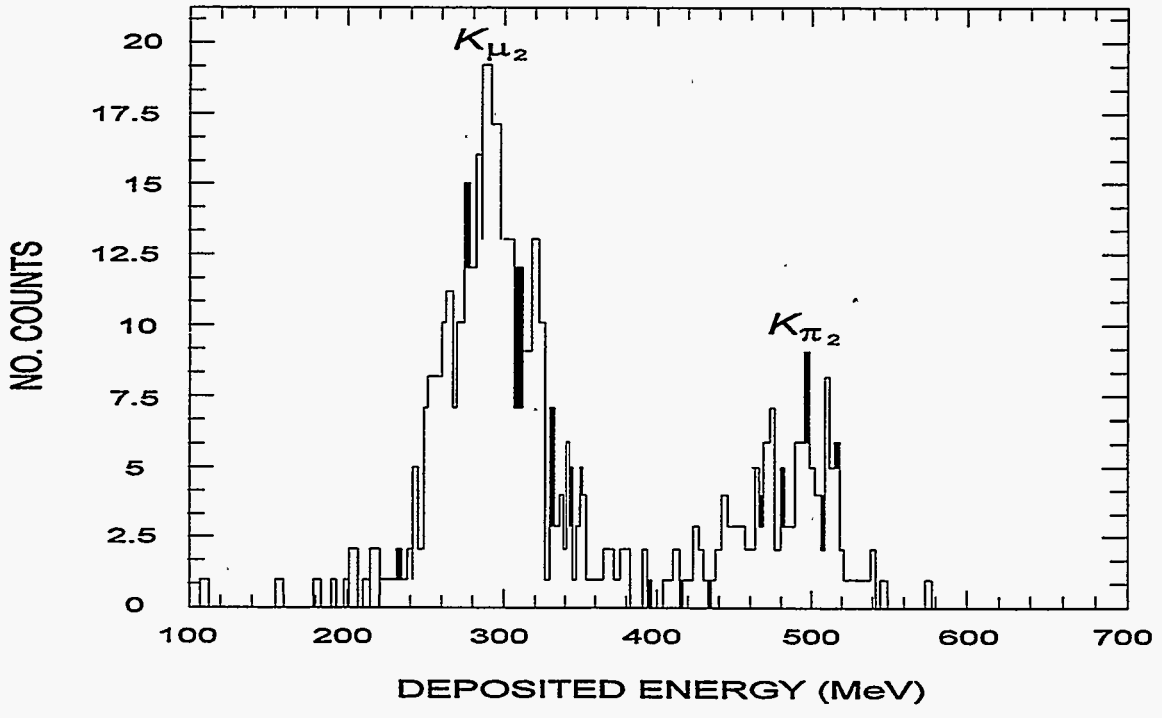

Fig. 5. Spectrum of energy deposition for the k^+ decay. [The two peaks correspond to the decay modes: $k^+ \rightarrow \mu^+\nu$ (64%) and $k^+ \rightarrow \pi^+\pi^0$ (21%).]

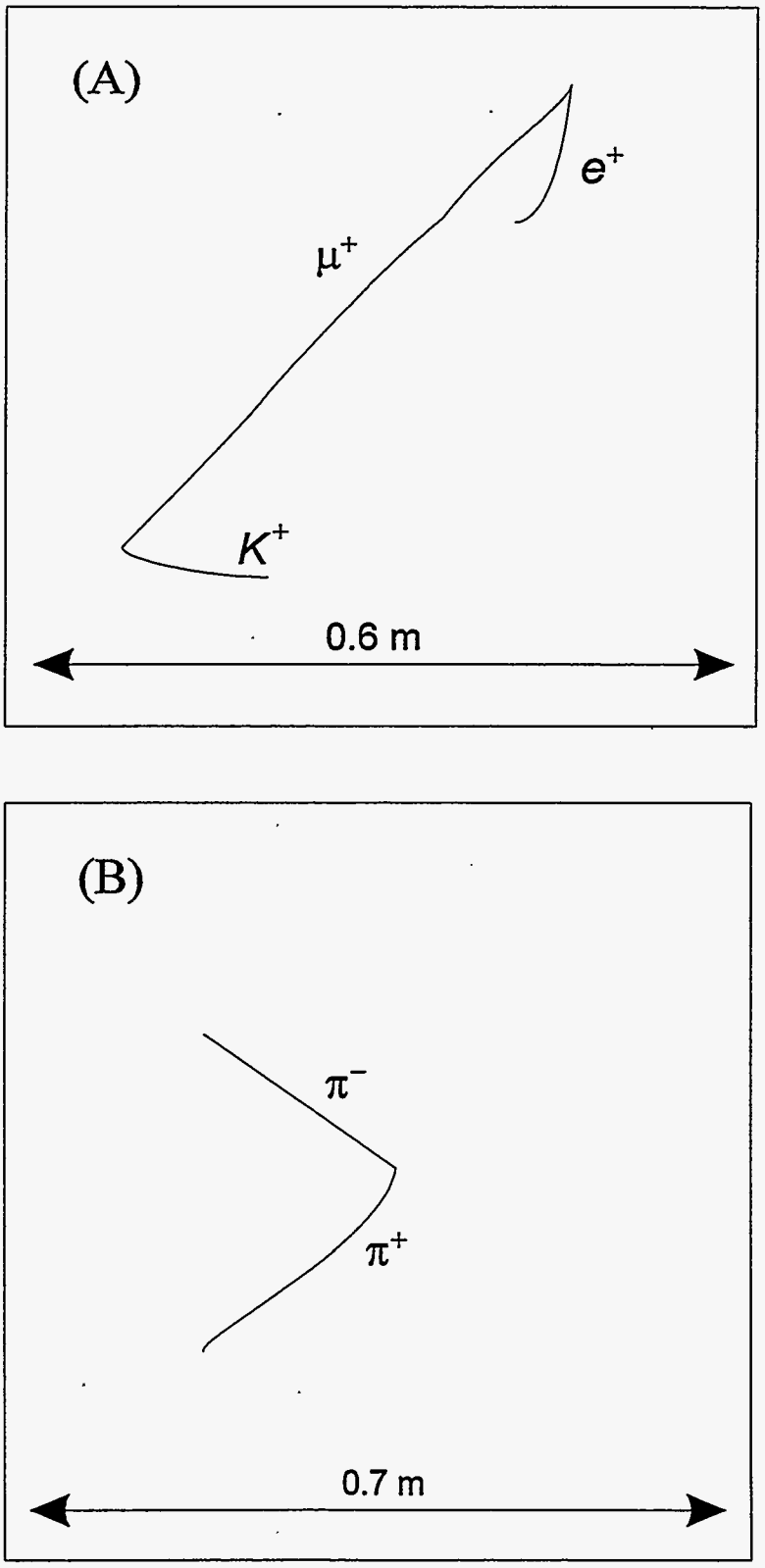

Fig. 6. Simulated $p - K^+\bar{\nu}_\mu$ with k_{μ_2} decay and (B) $n \rightarrow K^0\,\bar{\nu}_\mu$ in ICARUS.

We have carried out a careful background study to show that $\tau \geq 10^{33}$ years can be achieved with the 5000-ton ICARUS. The reason the background is so small is that the neutrino reaction

$$\nu_\mu + N \rightarrow \nu_i + K^+ + X(s = 0) \quad , \tag{3}$$

is forbidden, since it is a flavor-changing weak-neutral-current process. In fact, it may be possible to reach 10^{34} years for this decay with enough operating time! In Table 5, we show the limits (or discovery) that can be reached with the 5000-ton ICARUS.[1]

3. Other Rare Processes with ICARUS

There is a very interesting window of discovery for new sources of 20–30 MeV neutrinos, as shown in Fig. 7. We will not discuss solar neutrinos here, but simply remark that ICARUS can make a unique contribution to this subject as well.[7]

4. Low-Energy Studies with a Liquid-Xenon Detector

In the early 1990s, as the ICARUS technique was being perfected, we considered the possibility of detecting very small recoil energies with the detector.[4,5] We considered the pulse shape and relative scintillation-light output to be important factors needed to discriminate against various radioactive backgrounds. I gave a follow-up talk at a meeting at Waseda University in 1992.[4]

In 1992, a subset of the ICARUS group started the study of liquid Xe for the purpose of WIMP detection.[5] The first report of this work was given in 1992 at Waseda University and was published in the proceedings of the conference.[5] Figure 8(A) shows the initial experimental setup. Table 6 presents a schematic view of the reasons that liquid Xe is potentially an excellent WIMP detector.[4] The scope traces in Fig. 8(B) provide the essential discrimination method.[5] The ratio of primary to secondary scintillation light is very sensitive to the initial ionization of the source; the γ, β, and α particles are clearly separated.[5] In addition, the pulse shapes provide discriminations against background. More recently, this group has constructed a larger detector [Fig. 9(A)] and carried out very detailed tests of the discrimination methods [Fig. 9(B,C)].[8]

A successful test of the detection of a recoil Xe nucleus using neutron scattering has been carried out recently, and it shows clear evidence that SUSY–WIMPs will give a strong, unique signal on a discriminating liquid-Xe detector. The 2-kg detector shown in Fig. 9(A) will be taken to the Mt. Blanc Laboratory in the Spring of 1996 to test backgrounds further and to perform a first search for SUSY–WIMPs using this technique.[8]

Acknowledgements

I wish to thank members of the ICARUS team for their great work on the R&D and detector design presented here. I also wish to thank the ICARUS–WIMP team, including H. Wang and P. Picche.

Table 5. Sensitivity of 5-k ton ICARUS for various proton and neutron decay modes and for a data-taking period of five years.

Decay mode	Sensitivity[a]	No. of events[b]
$p \to e^+\pi^0$	1.2×10^{33}	2.7
$p \to \bar{\nu}\pi^+$	1.2×10^{33}	2.7
$p \to \mu^+\pi^0$	1.5×10^{33}	2.4
$p \to \bar{\nu}K^+$	2.4×10^{33}	5.4
$p \to e^+\pi^+\pi^-$	3.5×10^{32}	0.8
$p \to e^+\rho^0$	2.4×10^{32}	0.5
$p \to e^+e^+e^-$	2.7×10^{33}	6.4
$n \to e^+\pi^-$	1.4×10^{33}	3.1
$n \to \mu^+\pi^-$	1.2×10^{33}	2.9
$n \to \nu\pi^0$	1.4×10^{33}	3.3
$n \to e^-K^+$	2.9×10^{33}	6.6
$n \to e^+\rho^-$	3.0×10^{32}	0.6
$n \to e^+\pi^-\pi^0$	4.1×10^{32}	1.0
$n \to e^+e^-\nu$	3.3×10^{33}	7.8

[a]90% C.L. limit expressed in years and for one module.
[b]corresponds to a nucleon lifetime of 10^{33} years.

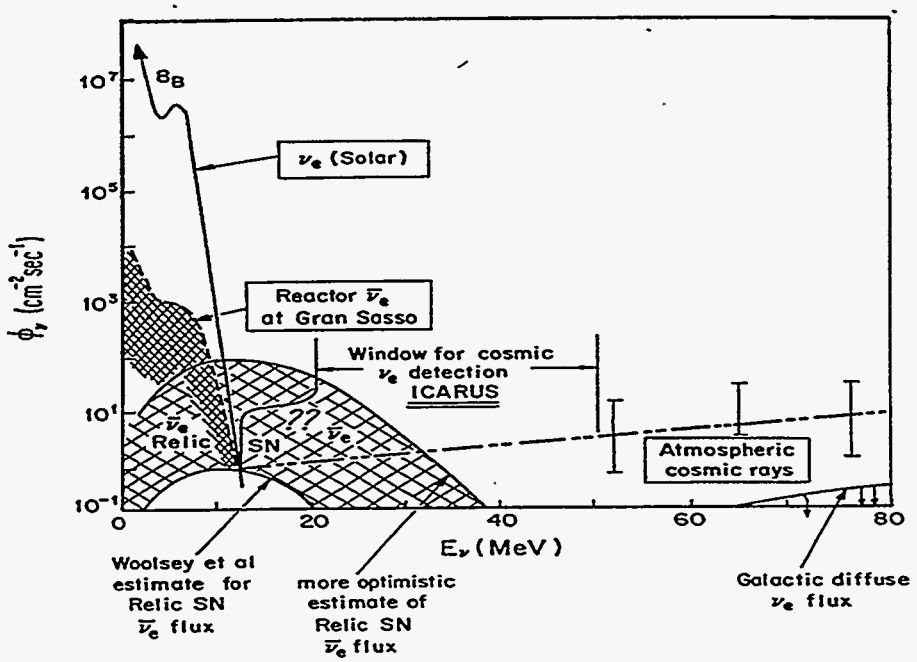

Fig. 7. Window of neutrino sources in which new, possibly cosmological, sources could be detected with ICARUS.

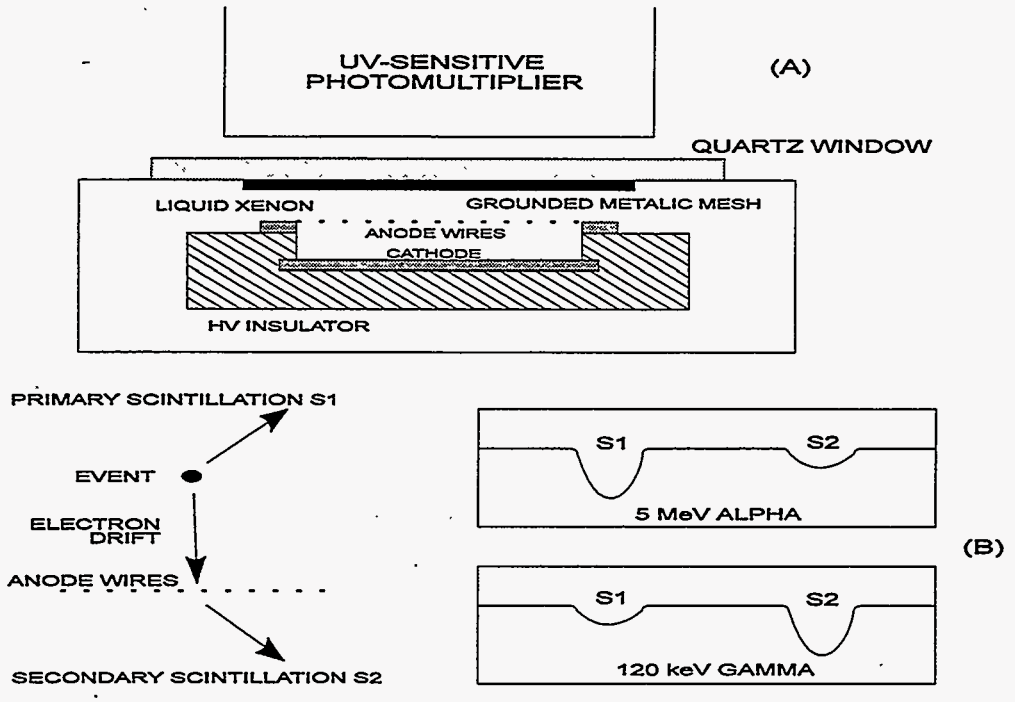

Fig. 8. (A) Geometry of liquid-xenon test chamber, and (B) Observed primary and secondary scintillation signals showing S1/S2 >> 1 for α events and << 1 for γ events.

Table 6. Signature and background in liquid xenon.

Recoil Nuclei
• Heavily ionizing particle
• High recombination, hence
• Mainly scintillation light is produced
Radioactivity
• Minimum ionizing particle
• Low recombination, hence
• Both charge and light are produced
<u>In liquid Xe</u>
• Both charge and light are visible
• This provides an efficient way for signal-to-background rejection
<u>Moreover, in Xe</u>
• No long-lived natural isotopes are present
• Xe^{127} has longest decay time (≈36 d)

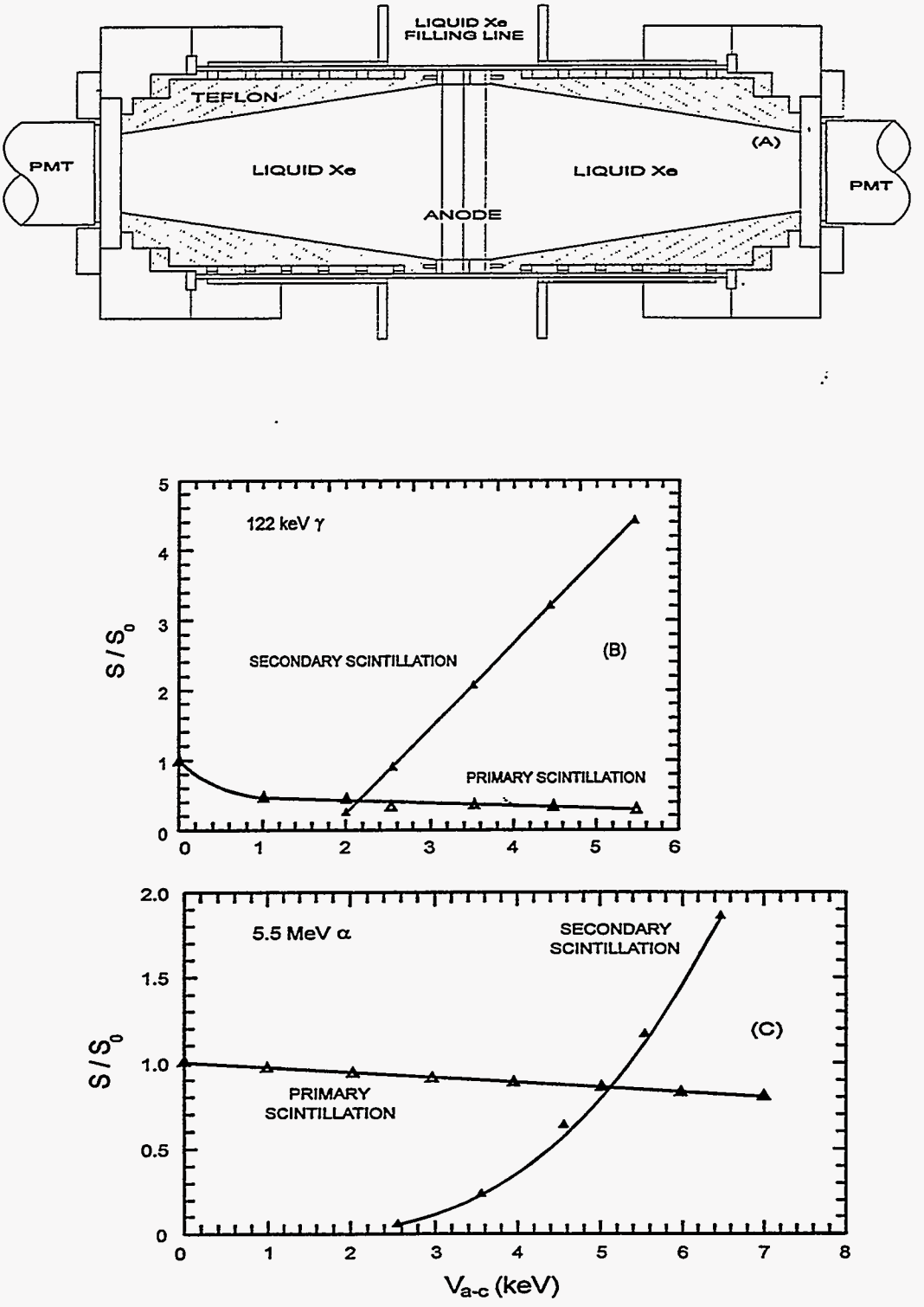

Fig. 9. (A) A 2-kg detector that has been constructed for tests at Mt. Blanc and a possible WIMP search; (B) Variations of the secondary scintillation intensity as a function of $V_{a\text{-}c}$ for photons; and (C) The same as B but for α particles.

References

[1]The ICARUS Collaboration, "ICARUS II, a Second-Generation Proton Decay Experiment and Neutrino Observatory at the Gran Sasso Laboratory," LNGS-94/99, Vols. I & II, Proposal, 1993; also P. Cennini *et al.*, Nucl. Instrum. Methods **A345** (1994) 230-243.
[2]CERN-Harvard-Milano-Padova-Roma-Tokyo-Wisconsin Collaboration, "Searching for New Underground Phenomena with High Resolution Visual Techniques and Magnetic Analysis," proposal for the Gran Sasso Laboratory, INFN/AE-85/7, Frascate (1985).
[3]The ICARUS Collaboration, "A First 600-Ton ICARUS Detector Installed at the Gran Sasso Laboratory," LNGS-94/99, Vols. I & II, Proposal Addendum (May 1995).
[4]D. Cline, Nucl. Instrum. Methods **A327**, 178-186 (1993).
[5]P. Benetti *et al.*, Nucl. Instrum. Methods **A327**, 203-206 (1993).
[6]J. Ellis, CERN Report #TH/95-316, hep-ph 9512335 (1995).
[7]J. N. Bahcall, M. Baldo Ceolin, D. B. Cline, and C. Rubbia, Phys. Lett. **B178**, 324 (1986).
[8]D. B. Cline, "On a Discriminating Liquid-Xenon Detector for SUSY Dark-Matter Observation," UCLA report APH-0084, to be published in the Proceedings of the UCLA Int. Conf. on Imaging Detectors in High Energy & Astroparticle Physics, Feb. 1995 (World Scientific, Singapore, in press).

Gas Detector for proton decay search

V.Lubimov
Institute for Theoretical and Experimental Physics,Moscow,Russia

Abstract

Megaton detector - the Big gas Drift Chamber(BDC)[1] for the study of proton decay is discussed.

1 Introduction

The discovery of the proton decay would be of fundamental importance for understanding of the Theory of Grand Unification. In the framework of SU(5) models[2] it was possible to make a prediction of the proton lifetime($\sim 10^{29\pm2}$ years). This prediction was ruled out already by the first results from IMB collaboration in 1983[3]. Presently the experimental upper limit for the proton decay time is set on the level $\tau_p > 1 - 8 * 10^{32}$ years[4]. However in some sophisticated models such as SUSY or SO(10) the proton lifetime is predicted to be at the level of$\sim 10^{35\pm1}$ years[5]. There are about a dozen of proton decay current experiments and projects now[6–10]. For instance the SUPERKAMIOKANDE experiment(50 000 *ton* water Cerenkov detector)[11] will have a chance to provide the measurable limit for the proton lifetime up to about 10^{34} years, depending on the proton decays mode and the reasonable background from the neutrino induced events.

However, to reach the SUSY scale to test their prediction one should be able to construct the detector with big fiducial mass, bigger compared with the present experiments. In this talk we present the idea which was developed more than 10 years[1] ago how it is possible technically to increase the mass of the detector by several order of magnitude.

2 Size optimization of homogeneous detector for proton decay

In order to answer the above questions we will try to optimize the detector size. Let $V = L^3$ to be a volume of the detector filled with any sensitive (active) substance. (For a moment the practical way how the sensitivity of the substance can be achieved is out of our consideration).

The detector mass:

$$M = L^3 * \rho \tag{1}$$

with ρ being the density in ton/m^3 $(= g/cm^3)$.

Maximum range of the charge particle produced in the proton decay is:

$$R \approx \frac{M_p/2}{dE/dx} * \frac{1}{\rho}; \quad \frac{dE}{dx} \approx 2.5 \frac{MeV}{g/cm^2} = 0.25 \frac{GeV}{ton/m^2}; \quad R = \frac{2}{\rho}\,[m] \tag{2}$$

Decay products should not leave the detector, therefore we shall consider proton decays only within the volume V_f :

$$V_f = L_f^3 = (L - 2R)^3; \quad L_f = L - 2R \tag{3}$$

The rest of the volume V, i.e. the walls of thickness R which surround the volume V_f serves as active shielding.

It isn't reasonable to have $V_f << V$ since the main cost of the detector in this case is the cost of shielding. Another extreme is $V_f \approx V$. This leads to very large size of the detector and disproportionate expenses.

Reasonable choice would correspond to

$$V_f \approx \frac{1}{2}V \quad \text{and} \quad (L - 2R)^3 = \frac{1}{2}L^3 \tag{4}$$

Solving this equation one can express the size of detector in terms of the maximum range of particles Eq.2 :

$$L \approx 10R = \frac{20}{\rho}\,[m] \quad \text{and} \; L_f \approx 8R = \frac{16}{\rho} \tag{5}$$

One sees here that the size of detector is determined by maximum range and hence by substance density.

The detector mass therefore is:

$$M = \frac{8000}{\rho^2}\,[ton], \; M_f \simeq \frac{4000}{\rho^2}\,[ton] \tag{6}$$

If the water ($\rho = 1$) is used in the detector then $L = 20\ m$, $L_f = 16\ m$, $M = 8000\ ton$, $M_f = 4000\ ton$. These values are practically the same as in the IMB-detector:

$$L = 21\ m, \; L_f = 16\ m, \; M = 10000\ ton, \; M_f = 4000\ ton.$$

It shows that IMB-detector parameters were well optimized.

Thus the detector mass of 10^4 *ton* is the optimum and close to its limiting value if the water ($\rho = 1$) was chosen as a sensitive substance of the detector. Nevertheless the mass of homogeneous detector can be considerably increased if one would accept at the first sight paradoxical decision to take the sensitive substance of of lower density. According to Eq.6 for the substance density $\rho = 0.1\ ton/m^3$ the mass of the detector of the optimized size increases to $M \approx 10^6$ ton and the mass in the fiducial volume to $M_f \simeq 5 * 10^5\ ton$.

The detector size then is $L = 200\ m$, $L_f = 160\ m$. But gases at high pressure can have density of about $0.1\ ton/m^3$, whereas the most effective and informative gaseous detector is the drift chamber.

3 The Big gas Drift Chamber (BDC) as the detector for proton decay

Fig.1 shows the scheme of 3-dimensional (No. of wires, A-amplitude, t-drift time) drift chamber.

Sensitive anode wires in the drift chamber are arranged with the spacing d. Measured coordinates of the particle tracks are X_i (coordinate of i-th wire) and Y_i(coordinate measured by drift time T_i at i-th wire)*.

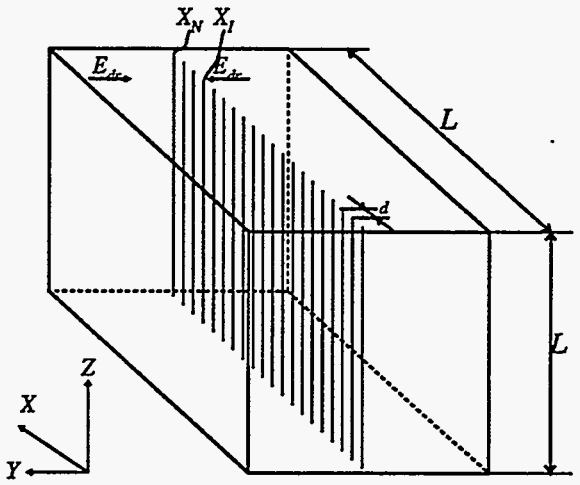

Figure 1. The scheme of Big gas Drift Chamber (BDC).

One remarkable property of the 3-dimensional drift chamber have to be noted. The detector sensitive volume (and consequently the mass) depends on L as L^3 while the number of sensitive wires (and hence the number of electronic channels) $N = L/d$ is proportional to L. The latter is correct if the wire spacing d doesn't depend on L, for instance when minimum technologically reasonable spacing d is chosen. For the proton decay events there are no reasons to keep spacing d at minimum. The accuracy of track reconstruction depends on the number of points measured on the tracks. We can fix this number for the proton decay track with maximum range:

$$n = R/d \tag{7}$$

Thus, track length reconstruction will be ensure with the same fixed accuracy for the tracks of any length R.

The total number of wires in the detector:

$$N = L/d = L * n/R \tag{8}$$

*Third space coordinate can be measured, for instance, by the charge division method.

Optimization of detector size (Eq.4) provides the relation between L and R (Eq.5): $L = 10R$. Therefore

$$N = 10n \tag{9}$$

i.e. the total number of wires in a detector doesn't depend on the detector size L (as well as on the density or the pressure of the gas).

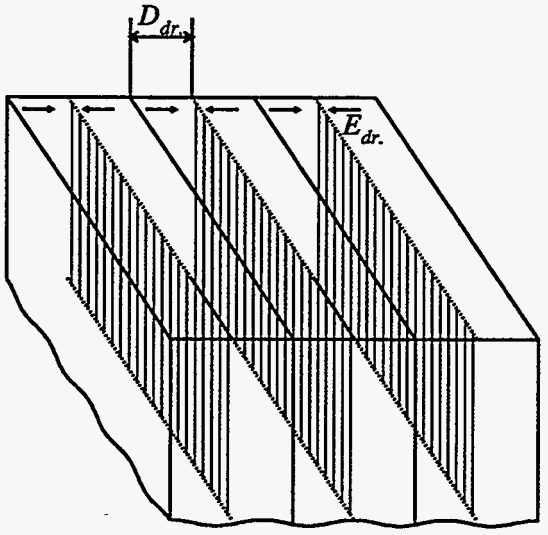

Figure 2. The scheme of division of BDC into separate drift layers.

It is reasonable to divide the detector volume into several parts in order to avoid too large drift gaps (Fig.2). The layers of the thickness $\sim 2R$ ($D_{drift} \sim R$) would divide the detector into $L/2D_{drift} = 5$ nearly independent parts. The number of wires will be increased to:

$$N_t = N * \frac{L}{2D_{drift}} = 10n * \frac{10R}{2R} = 50n \tag{10}$$

Again the number of wires N_t is independent on the size of detector. We can choose the maximum number of measured points on the track $n = 50$. Thus the total number of anode wires of the length L will amount $N_t = 2500$[†].

Some characteristics of a Big gas Drift Chamber are shown in Table1 for the detector dimensions $L = 50$, 100 and 200 m. When the size of detector increases the length of the tracks increases proportionally too. The accuracies of geometrical and kinematical parameters remains unchanged. But the detector mass increases (like $\sim L^2$) and amounts for for $L = 200\ m$ $\sim 10^6\ ton$.

[†]Since the events looked for are rare, the rate of external radiation is rather low (quite different from accelerator experiments) and there are no particular need to know exactly the place inside the detector where nucleon decay occurs one can connect several anode wires in parallel. Thus the number of electronic channels for information readout can be reduced to $N_{parallel} = N\frac{2R}{L} = 100$!. This certainly doesn't degrade the accuracy of track measurements and reconstruction of the event geometry

$L\ [m]$	50	100	200
$\rho\ [ton/m^3]$ ‡	0.4	0.2	0.1
$P\ [atm]$	400	200	100
$d\ [m]$	0.1	0.2	0.4
$R = D_{drift}\ [m]$	5	10	20
$M\ [ton]$	$5 * 10^4$	$2 * 10^5$	$8 * 10^5$
$M_f\ [ton]$	$2.5 * 10^4$	10^5	$4 * 10^5$
$t_{drift}\ [msec]$	0.5	1	2
$\langle \Delta X \rangle = \langle \theta \rangle_{Mult.scatt.} * d\ [mm]$	1	2	4
No. of nuclons in M_f	$1.5 * 10^{34}$	$6 * 10^{34}$	$2.4 * 10^{35}$
No. of decay/year $(\tau_p = 10^{33})$	15	60	240
No. of decay/year $(\tau_p = 10^{35})$	0.15	0.60	2.4

Table 1. Some characteristics of BDC for different detector dimensions

For the detected tracks one can expect the following accuracies:

1. Angular accuracy $\Delta\theta \sim 10^{-2} = 0.6^o$ is defined by multiple scattering in the gas on the length of wire spacing.

2. Energy of charge particle is measured by its range and the sum of energy losses: $\Delta E/E \sim 2..3\%$.

3. Ionizing stopping power of particles can be determined by multiple ($n = 50$) dE/dx – measurements on the track with $\Delta I/I \sim 4\%$.

4. The direction of particle motion along the track is defined from dE/dx measurements as well ($1/8R$ is enough to distinguish either directions).

5. Measurements of multiple Coulomb scattering allow to find the particle momentum with accuracy $\Delta P/P \sim 15..20\%$§.

6. Measurements of the range, total energy loss (energy), dE/dx (velocity) and multiple scattering allow to make particle identification. Besides, since $R * \rho/X_0 \sim 4.5$ and $R * \rho/\lambda_{hadr} \sim 2$ (X_0, λ_{hadr} - radiation length and nuclear absorption length) the interaction details of particle with the gas will allow separation of μ, π, e and other particles.

Thus, practically all the nucleon decay modes can be unambiguously interpreted.

There are some technical details of proposed BDC. The drift chamber is filled with the "cold" gas (low electronic temperature) where the diffusion spread is relatively

‡gas density at NTP was assumed $\rho_0 = 10^{-3}\ [\frac{ton}{m^3}]$

§These estimates of kinematical parameter were made for the track of maximum length. For shorter tracks of length l the accuracies of the parameter are worse by factor $\sqrt{R/l}$

small like in methane or others natural gases. Electric field in the drift gap is $\sim 0.1\, V/(cm\, mm\, Hg)$, drift velocity $\sim 1\ cm/\mu sec$, total drift time is about 1 millisecond. The maximum drift time limits the rate of cosmic muons to the level of $\sim 100\ sec^{-1}$. This requires the detector to be installed deeply underground (depth $\geq 1500\ m$ of water equivalent).

One of the most serious technological problems is how to build the vessel for such detector? The size of the vessel must be of the order of hundred meters and it must stand the pressure of few hundred atmospheres.

To make this vessel one can use the underground explosion of nuclear charge of proper power. This method is known to be used for creation reservoirs for the gas condensate storage. Cavities produced by this method are absolutely hermetic under the gas storage pressure of few hundred atmospheres. To be a convenient access into the cavity the explosion should be made in the vicinity of the existing shaft[¶].

The radio-activity induced in the walls of the cavity is certainly somewhat dangerous. Nevertheless this is not fatal for the detector for the following reasons. First the energy of the induced radio-activity (few MeV) is hundred times less than the energy of the proton decay. Therefore the radio-activity can not imitate the proton decay events but produces only some excessive rate in the chamber. Secondly, there are shielding of the detector with the thickness at least equal R (~ 4.5 and ~ 2 radiation and nuclear absorption lengths respectively), which will suppress the electron-gamma radiation of the walls by factor $10^3 - 10^4$. And finally, exploitation experience of gas reservoirs created by nuclear explosion shows that after some exposure ($\sim$ one year) gas comes to consumers without the traces of radio-activity.

We had discussed how the enormous mass of 10^6 *ton* can be made sensitive and how the vessel for such a detector can be created. One additional problem, the problem of background on the proper level of detector mass, have to be discussed here in order to demonstrate the feasibility of the idea.

The main source of the background in such a detector will be cosmic neutrino interactions. Any underground set up cannot avoid this sort of background. The suppression of neutrino induced events can be made using geometrical and kinematical characteristics of events. The efficiency of suppression will depend on the detector "quality", i.e. on the space and angular accuracies of tracks reconstruction, on energy resolution $\Delta E/E$, on the possibility of particle identification etc. We can compare, for example, the characteristics of experiment of Irvin-Michigan-Ohaio-Harvard-Padua-Visconsin(IMOHPV)[12] (water, Cherenkov light collection) group with the proposed detector BDC(Table2).

The correlations angle-energy of π and μ is different for the proton decay and neutrino induced events. For BDC detector the allowed region for proton decay events in the plot $E(\mu + \pi)$ vs $\theta_{\mu\pi}$ is smaller compared with IMOHPV experiment by the factor $\sim$ 600. In general, for any pair combination (two dimensional plot) of variables BDC detector gains on average a factor $\sim 10^3$ as compared with proposal of IMOHPV. For three dimensional combination this factor is $10^4 - 10^5$. Thus, the

[¶]Such an experience was practically realized

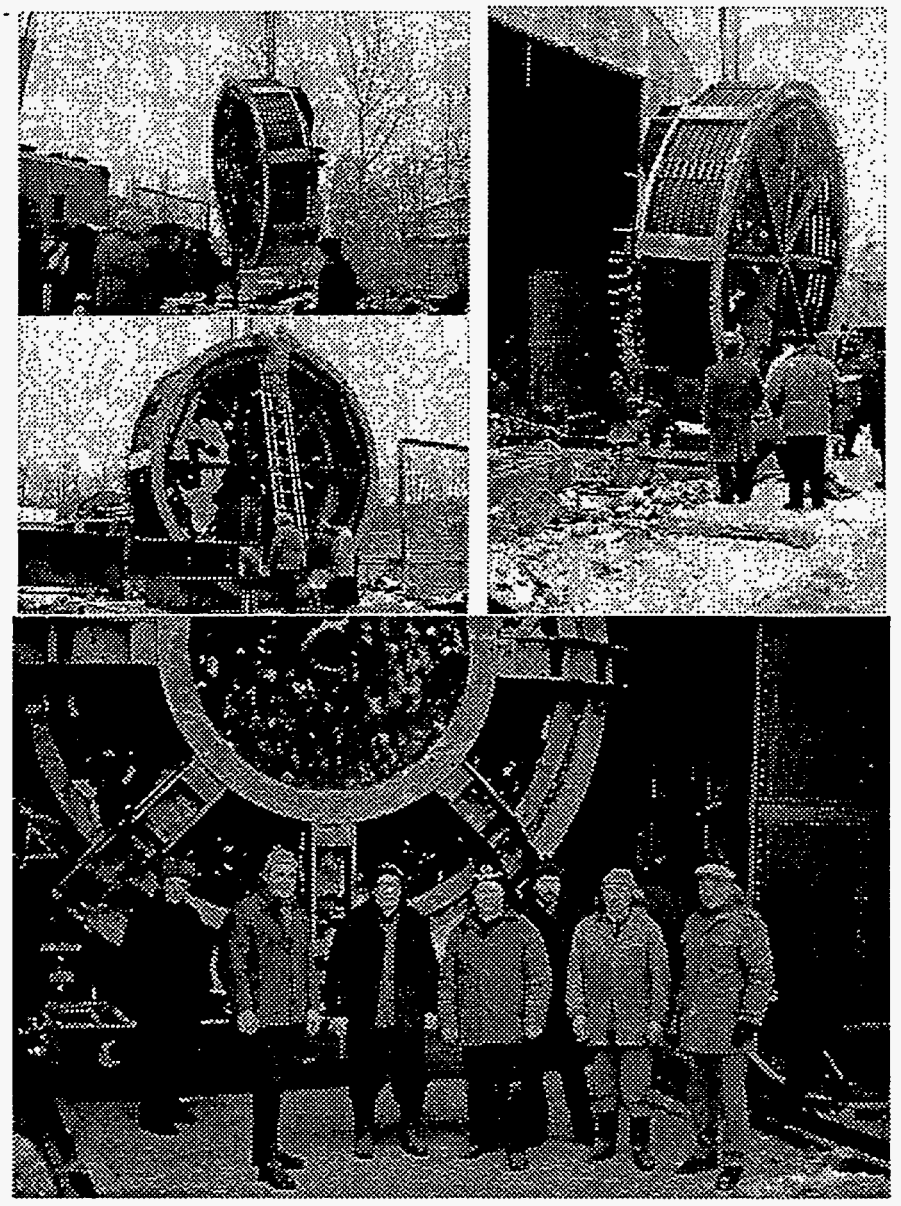

Figure 3. Winter '95-'96. Transportation of the magnet for double β-decay detector.

	IMOHPV	BDC	Factor
$M_f[ton]$	$5*10^3$	$4*10^5$	100
ΔX_{vertex}	20 cm	$few\ mm$	100
$\Delta\theta$ $(angular accuracy)$	20^o	0.6^o	30
$\Delta E/E$	50%	2..3%	20
$Background\ events/year$	3	10^{-2}	10^3-10^5
τ_{proton} $limit$	10^{32}	10^{35}	10^3

Table 2. Comparison of the characteristics of BDC detector with IMOHPV[12]

background suppression level in BDC ("quality" of the detector) allows to realize the detector mass of 10^5-10^6 ton and explore the proton life time up to the level $\sim 10^{35}$ years.

4 Conclusion

At the conclusion we would like to point that the idea to use the detector with small density and large size can be applied not only for the experiment of the proton decay.[13] The simplest examples are:

- ν_e, e scattering of the sun neutrino.
- Double β-decay.
- The search the exotic particles such as monopoles etc.

As the first step of the program of using BDC detectors, in ITEP there were proposed experiment[14] for the double decay searches. The construction of the detector with the following parameters:

$$V = 13\ m^3;\quad M = 10\ kg\ of\ Xe^{136}\ (95\%\ enriched)$$

$$Magnet\ \ Diameter \sim 6\ m$$

is completed. At Figs.3,4 ITEP detector for search of neutrinoless double β-decay is shown. The results obtained with the test prototype of the detector for the search of the two-neutrino double β decay are published.[15]

Through the paper we discussed the possibility to improve the experimental detector for the detecting of proton decay and show how one can increase the fiducial mass of the detector by few order of magnitude with BDC. However the same consideration can be applied to the not homogeneous detector. It is paradoxical point of view that to increase the mass of the detector one built up the detector from the material with large density rather than to increase the volume. Let us consider the

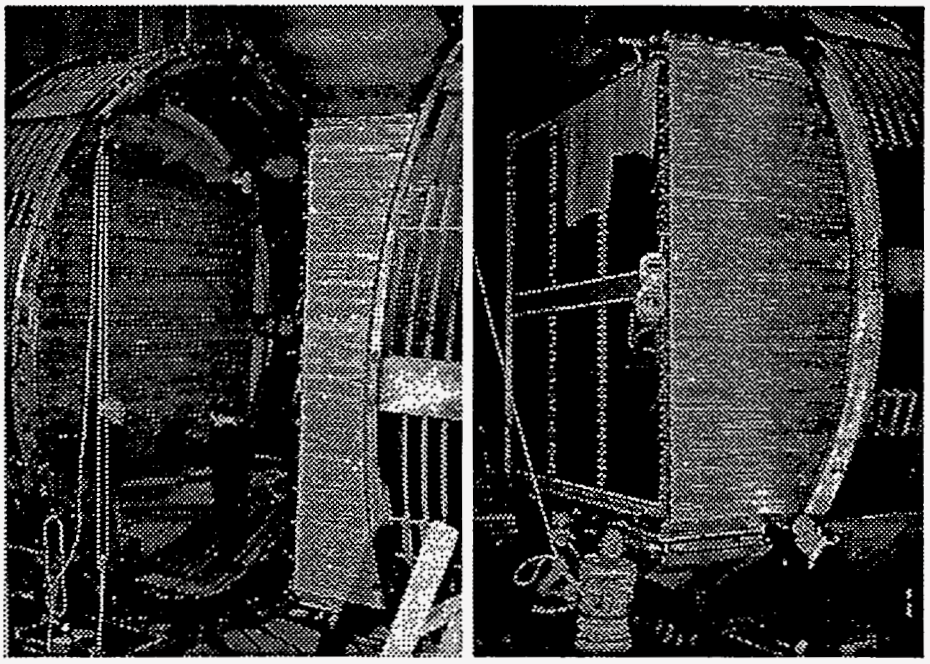

Figure 4. Spring '96. ITEP double β-decay experiment "on-floor".

detector uses tracking calorimetry with iron plates interleaved by tracking planes. Let us make the **scaling transformation**: we will increase in 10 times the sizes of sensitive elements but keeping the same the thickness of iron plates. The volume of such detector will increase as the L^3 but the average density drops as the $1/L$, so at the end we have the factor of $\sim$ 100 for the fiducial mass of the detector with the same number of sensitive elements and the same accuracy of events reconstruction.

I am grateful to Dmitriy Ozerov for the help in preparation of the manuscript.

5 REFERENCES

[1] V.Lubimov,*On the possibility of the proton decay searches up to the level of* 10^{35} *years*, ITEP-158 (1982).

[2] H.Georgi and S.L.Glashow, Phys. Rev. Lett. **32**, 438 (1974)
M.Golbhaber and W.J.Marciano, Comm. Nucl. Part. Phys. **16**, 23 (1986)

[3] IMB Collab., G. Blewitt et all.,*Linits on the nucleon lifetime in water from IMB*, In *Santa Fe 1984, Proceedings, The Santa Fe Meeting*, 377-379

[4] L. Montanet et al.,*REVIEW OF PARTICLE PROPERTIES. PARTICLE DATA GROUP.*, Phys. Rev. **D50**, 1173-1823 (1994)

[5] Jorge L. Lopez,*SUPERSYMMETRY: from the Fermi scale to the Planck scale* DOE-ER-40717-23, Jan 1996. 58pp., Submitted to Rept.Prog.Phys
and references therein

[6] Kamiokande Collab., K.S. Hirata et al.,*Experimental limits on nucleon lifetime for lepton + meson decay modes.*, Phys. Lett. **B220**,308 (1989)
[7] Frejus Collab.,C. Berger et al.,*Lifetime limits on (B-L) violating nucleon decay...*, Phys. Lett. **B269**, 227-233 (1991)
[8] IMB Collab., W. Gajewski et al.,*Search for proton decay into* $e^+ \pi^0$ *in IMB-3 detector*, Phys. Rev.,**D42** (1990)
[9] Soudan Collab., J. Bartelt et al.,*Monopole flux and proton decay limits from the SOUDAN-I detector.*, Phys. Rev. **D40**, 1701 (1989), Phys. Rev. **D36** 1990 (1987)
[10] B.Barish,*Baryon Instability Workshop: Summary Talk*, Caltech, March 30, 1996
[11] Y. Totsuka,*KAMIOKANDE and SUPERKAMIOKANDE*, ICRR-359-96-10, Mar 1996.
[12] J. Blandino et al.,*A multi-kiloton detector to conduct a sensitive search for nucleon decay.Proposal of HHPW collaboration*, Proc. of the International Conf. on Neutrino Physics and Astrophysics (1981).
[13] V.Lubimov,*"Archaeological" means of investigation of elementary particles*, ITEP-18 (1983)
[14] S.Boris et al.,*On a possibility of measurement of the double neutrinoless* β *decay in* Xe^{136}*. (in Russian)*, ITEP-47 (1982)
[15] V.A.Artemiev et al.,*Measurement of the* ^{150}Nd *Half-Life* $T_{1/2}(2\beta 2\nu)$ *with a Time Projection Chamber in a Magnetic Field*, Phys. Atom. Nucl. **1**, 6 (1996)

$n\bar{n}$ SUPPRESSION IN INTRANUCLEAR TRANSITIONS [1]

W.M. Alberico
Dipartimento di Fisica Teorica dell'Università di Torino
and INFN, Sezione di Torino
via P.Giuria 1, 10125 Torino, Italy

Abstract

We review the problematics connected with the occurrence of $n\bar{n}$ oscillations inside nuclei, leading to a specific $\Delta B = 2$ nuclear instability mode, for which a few experimental lower bounds have been till now established and are under way. Assuming the same mechanism as for the free neutron conversion, the influence of the nuclear medium turns out to be crucial in determining the global nuclear lifetime: indeed the newly formed antineutron state feels a considerably different mean field, with an imaginary absorptive part which accounts for the annihilation. As a result, the $n\bar{n}$ conversion is substantially suppressed, in the nuclear medium, with respect to the free process. Different theoretical approaches are reviewed, and the corresponding estimates for the suppression factor are confronted: the results are rather stable and make it a sensible tool for comparing with the free $n\bar{n}$ oscillation search.

1 Introduction

The interest for $n\bar{n}$ oscillations has been recently renewed both from the theoretical point of view, with the development of Grand Unified Schemes allowing for this process within reasonable mass scale parameters, and from experimental proposals which could realistically set up new limits on free $n\bar{n}$ oscillations (ORNL) or intranuclear processes (Superkamiokande, Icarus).

It is thus a good point to review the existing theoretical estimates of the influence, on the process, of nuclear medium effects; the latter indeed provide an important bridge between measurements of nuclear instability rates and the free oscillation time for an $\bar{n}$ conversion occurring in a beam of free neutrons.

The fundamental process is described by the $\Delta B = 2$ Hamiltonian

$$H_{n\bar{n}} = \epsilon_{n\bar{n}} \int d^3x \, \bar{\Psi}(x) \sigma_1 \Psi(x) \tag{1.1}$$

[1] Invited talk presented at the International workshop on Future Prospects of Baryon Instability Search in p–decay and $n\bar{n}$ oscillation experiments, at Oak Ridge National Laboratory, March 28-30, 1996.

$\epsilon_{n\bar{n}}$ being the transition mass (sometimes referred to as δm), σ_1 the usual Pauli matrix acting on the two–dimensional $(n, \bar{n})$ space spanned by the vectors Ψ:

$$\Psi(x) = \begin{pmatrix} \psi_n(x) \\ \psi_{\bar{n}}(x) \end{pmatrix} \tag{1.2}$$

the antineutron field being the customary charge conjugated of the neutron one: $\psi_{\bar{n}}(x) = \psi_n^C(x)$. The $n\bar{n}$ oscillation time for a process occurring in free space is then the inverse transition mass ($\hbar = c = 1$):

$$\tau_{n\bar{n}} = \frac{1}{\epsilon_{n\bar{n}}} \tag{1.3}$$

Two different approaches are mainly conceived in order to experimentally determine $\tau_{n\bar{n}}$:

- the *direct* measurement of an $\bar{n}$ component in a freely propagating beam of neutrons (or spallation sources)
- indirect limits stemming from $n\bar{n}$ oscillations occurring in nuclei and detectable by general purposes experiments, set up for nuclear instability search.

In the first instance the probability of finding at time t an antineutron component in an initially pure neutron state turns out to be

$$P(\bar{n}, t) = \frac{\epsilon_{n\bar{n}}^2}{\epsilon_{n\bar{n}}^2 + \Delta E^2} \sin^2 \left\{ t\sqrt{\epsilon_{n\bar{n}}^2 + \Delta E^2} \right\} \tag{1.4}$$

$2\Delta E$ being the energy gap between the n and $\bar{n}$ states, eventually due to external perturbative fields (as, for example, the Earth magnetic field). When ΔE is made negligibly small with respect to $\epsilon_{n\bar{n}}$, then the above probability more simply reduces to $P(\bar{n}, t) \approx \epsilon_{n\bar{n}}^2 t^2$.

The present experimental limit on $\tau_{n\bar{n}}$ has been set by the measurements at ILL (Grenoble)[1, 2] to be

$$\tau_{n\bar{n}} > 0.86 \times 10^8 sec \qquad (90\% CL) \tag{1.5}$$

A significant improvement by two or possibly three orders of magnitude is expected to be possible with the proposed experiment at ORNL[3, 4].

Besides specific and direct measurements of the free $n\bar{n}$ oscillation time, we will focus here on other existing and future experiments aimed at the discovery of

baryon and/or lepton number violating processes which might occur in nuclei. The $n\bar{n}$ conversion, followed by the $\bar{n}$ annihilation with the surrounding nucleons into a nucleus with mass number decreased by 2 and a certain number of pions, provides a source for nuclear instability induced by the $\Delta B = 2$ Hamiltonian (1.1).

Multipurpose experiments like Kamiokande, Frejus, Icarus (some of them already operating since a few years) could reveal unusual nuclear decays like the ones induced either by proton decay or by $n\bar{n}$ oscillations. Apart from the intrinsic technical difficulties in disentangling the occurrence of such processes from the overwhelming background, the extraction of the $n\bar{n}$ oscillation time is, in this case, somewhat complicated by its occurrence inside the nuclear medium, which strongly interacts with both the initial neutron and the antineutron resulting from the oscillation process.

This argument has been suggested and debated since the 80's [5, 6, 7, 8, 9] and can be understood in simple terms by considering the following $n\bar{n}$ mass matrix:

$$M = \begin{pmatrix} U_n & \epsilon_{n\bar{n}} \\ \epsilon_{n\bar{n}} & U_{\bar{n}} + iW_{\bar{n}} \end{pmatrix} \tag{1.6}$$

which contains the interaction potentials of the neutron and the antineutron with the residual nucleus, the $\bar{n}$ potential being a complex quantity with an imaginary (absorptive) part which is related with the $\bar{n}$ annihilation.

Diagonalization of (1.6) leads to two mass eigenstates $N_{\pm}$ with eigenvalues

$$\begin{aligned} m_+ &= < U_n > + \frac{\epsilon^2_{n\bar{n}} (< U_n - U_{\bar{n}} >)}{< U_n - U_{\bar{n}} >^2 + < W_{\bar{n}} >^2} \\ &\quad - i\epsilon^2_{n\bar{n}} \frac{W_{\bar{n}}}{< U_n - U_{\bar{n}} >^2 + < W_{\bar{n}} >^2} \end{aligned} \tag{1.7}$$

$$m_- = < U_{\bar{n}} > - i < W_{\bar{n}} > \tag{1.8}$$

where appropriate nuclear mean values of the interaction potentials have been introduced. The $|N_+ >$ state, belonging to the eigenvalue (1.7), contains the conversion of a neutron into an antineutron and the subsequent nuclear decay, with lifetime

$$\tau_+^{-1} \equiv T_A^{-1} = \epsilon^2_{n\bar{n}} \frac{W_{\bar{n}}}{< U_n - U_{\bar{n}} >^2 + < W_{\bar{n}} >^2} \equiv \epsilon^2_{n\bar{n}} T_R^{-1} \tag{1.9}$$

which allows us to define the "nuclear factor" T_R. Eq.(1.9) can be equivalently rewritten as

$$T_A = \tau^2_{n\bar{n}} T_R \tag{1.10}$$

which puts in evidence the different time scales involved by the $n\bar{n}$ oscillation time ($\tau_{n\bar{n}}$) and nuclear decay lifetimes (T_A). Indeed, as it will be shown in the next Section, thē nuclear quenching factor T_R turns out to be rather large, involving several orders of magnitude (it is typically of the order of 10^{23} sec^{-1}). According to (1.10), experimental limits on nuclear stability (say $T_A > T_0^{exp}$), together with the theoretical determination of T_R, allow to establish lower limits on $\tau_{n\bar{n}}$ as well.

2 Theoretical approaches

The existing estimates of T_R can be roughly divided into two categories, the first one being based on a potential model approach, the second one directly stemming from the S–matrix formulation along with two–body NN and $N\bar{N}$ interactions. One should, however, keep in mind that the two formulations are essentially equivalent, notwithstanding that they are focussed on different aspects of the many–body treatment of the problem.

2.1 The optical model approach

After the first rough estimates of the nuclear factor T_R, Dover *et al.*[10, 11] afforded an exact calculation based on the available N–nucleus and $\bar{N}$–nucleus optical potentials. The starting point is the (single–particle) nuclear Hamiltonian

$$H = \frac{p^2}{2M} + U_n P_+ + (U_{\bar{n}} + iW_{\bar{n}})P_- + H_{n\bar{n}} \equiv H_0 + H_{n\bar{n}} \tag{2.1}$$

acting onto the two–dimensional $n\bar{n}$ space. In eq.(2.1) $P_\pm = \frac{1}{2}(1 \pm \sigma_3)$ are the projection operators onto n ($\bar{n}$) states and $H_{n\bar{n}}$ is the $n\bar{n}$ transition Hamiltonian given in eq.(1.1). The eigenvalue equation for H,

$$(H_0 + H_{n\bar{n}}) \begin{pmatrix} \psi_n \\ \psi_{\bar{n}} \end{pmatrix} = E \begin{pmatrix} \psi_n \\ \psi_{\bar{n}} \end{pmatrix} \tag{2.2}$$

provides two coupled differential equations for the neutron and antineutron states:

$$\left(\frac{p^2}{2M} + U_n(x) - E_\alpha\right) \psi_{n,\alpha}(x) \simeq 0 \tag{2.3}$$

$$\left(\frac{p^2}{2M} + U_{\bar{n}}(x) + iW_{\bar{n}}(x) - E_\alpha\right) \psi_{\bar{n},\alpha}(x) = -\epsilon_{n\bar{n}} \psi_{n,\alpha}(x) \tag{2.4}$$

where the small coupling term ($-\epsilon_{n\bar{n}}\psi_{\bar{n}}$) to the $\bar{n}$–state is usually neglected in solving the wave equation for the neutron, while the inhomogeneous term is essential in equation (2.4), in order to justify the creation of an $\bar{n}$ inside the nuclear medium.

The n–nucleus optical potential $U_n(x)$ included in the Hamiltonian is choosen to reproduce the neutron binding energies, E_α, in the considered nucleus, while the complex $\bar{n}$–nucleus optical potential, $U_{\bar{n}}(x) + iW_{\bar{n}}(x)$ is adapted to fit energy shifts and widths of the $\bar{p}$–atom levels as well as low–energy $\bar{p}$–nucleus scattering data measured at LEAR. Its imaginary part accounts for the annihilation width of the antiparticle inside the nuclear medium. For an $\bar{n}$ in the state $\psi_{\bar{n},\alpha}$ the latter turns out to be:

$$\Gamma_\alpha = -2 \int d^3x \; |\psi_{\bar{n},\alpha}(x)|^2 \, W_{\bar{n}}(x). \tag{2.5}$$

The total nuclear annihilation width, obtained by averaging (2.5) over all possible occupied states,

$$< \Gamma_A >= \frac{< \Gamma_\alpha >}{N} = \frac{1}{N} \sum_\alpha n_\alpha \Gamma_\alpha, \tag{2.6}$$

N being the number of neutrons in the nucleus and n_α the occupation number of the state α, gives the inverse nuclear lifetime ($T_A^{-1} =< \Gamma_A >$).

¿From eq.(2.4) it appears that $\psi_{\bar{n},\alpha} \propto \epsilon_{n\bar{n}}$, so that $\Gamma_\alpha \propto \epsilon_{n\bar{n}}^2 = \tau_{n\bar{n}}^{-2}$. It is thus appropriate to explicitly factorize this factor in $< \Gamma_A >$ or, according to (1.10), to set:

$$T_R^{-1} = \frac{\tau_{n\bar{n}}^2}{N} \sum_\alpha n_\alpha \Gamma_\alpha. \tag{2.7}$$

This quantity is the above mentioned nuclear quenching factor and depends *only* on nuclear physics aspects, but not on the strength of the $n\bar{n}$ conversion.

Typical $\bar{n}$–nucleus optical potentials utilized in ref.[10, 11] are of Woods-Saxon form:

$$U_{\bar{n}}(x) = -\frac{V_0}{1 + e^{(r-R_V)/a_V}} \tag{2.8}$$

$$W_{\bar{n}}(x) = -\frac{W_0}{1 + e^{(r-R_W)/a_W}} \tag{2.9}$$

($r = |\vec{x}|$). The best fits to the available $\bar{p} - N$ data are obtained by employing potentials with a shallow real part and a deep (strong) imaginary part; it is worth

mentioning, however, that equivalently good fits can be obtained with set of parameters (in particular V_0, W_0) sometimes differing by one order of magnitude.

Dover *et al.*[11] estimated T_R [eq.(2.7)] for the ^{16}O nucleus, for which the Kamiokande experiment[12] provided in '86 the following lower limit of the nuclear lifetime:

$$T_A > T_0^{exp} = 4.3 \times 10^{31} y. \tag{2.10}$$

Eq.(1.10) translates then (2.10) into a lower limit for the $n\bar{n}$ oscillation time:

$$\tau_{n\bar{n}} \geq \sqrt{\frac{T_0^{exp}}{T_R}}. \tag{2.11}$$

By employing various models for the $\bar{n}$–nucleus potential, the authors of ref.[11] found the following range of T_R values (which expresses the "uncertainty" on the theoretical estimate):

$$0.46 \leq T_R \leq 1.93 \quad (\times 10^{-23} sec^{-1}). \tag{2.12}$$

Then, by employing (2.10), one gets:[2]

$$0.84 \leq \tau_{n\bar{n}} \leq 1.72 \quad (\times 10^8 sec). \tag{2.13}$$

We remark that the uncertainty in the T_R value, stemming from the different nuclear models employed in the calculation, is appreciably attenuated in $\tau_{n\bar{n}}$, due to the power 1/2 which relates the two quantities.

A simpler approach, still based on the potential model, starts from eq.(1.9) and evaluates T_R in terms of averages over the nuclear density[14]; for example, the average of the real part of the $\bar{n}$–nucleus potential is given by:

$$< U_{\bar{n}} >= \frac{\int_0^\infty dr r^2 \rho(r) U_{\bar{n}}(r)}{\int_0^\infty dr r^2 \rho(r)} \tag{2.14}$$

When the same $\bar{n}$–nucleus potential is employed, this approximation yields T_R values which are approximately twice the "exact" result[11]; thus the resulting limits on $\tau_{n\bar{n}}$ turn out to be somewhat overestimated.

---

[2]The numbers in [11] differ somewhat from (2.13) since in '85 the authors were using a previous (lower) limit for the nuclear lifetime, provided by the IMB collaboration[13].

2.2 S–matrix approach

This method can be developed not only starting from an optical model (single particle) hamiltonian, but also from the full many-body nuclear Hamiltonian

$$H = H_{SM} + V_{NN} + V_{N\bar{N}} + H_{n\bar{n}} \tag{2.15}$$

where H_{SM} is a suitably choosen shell model Hamiltonian, $V_{NN(\bar{N})}$ are short-cut notations for the two–body interaction terms, referring to the nucleon–nucleon (nucleon–antinucleon) potentials, respectively (e.g. $V_{NN} = \sum_{i>j} V_{NN}(i,j)$) and $H_{n\bar{n}}$ is the transition Hamiltonian (1.1).

The time evolution of a nuclear system described by (2.15) embodies a finite probability for the process:

$$(A,Z) \implies (A-1,Z,\bar{n}) \implies (A-2,Z) + n\pi \tag{2.16}$$

where a certain number n of pions (most probably 4 or 5) are produced in the final state, by annihilation of the $\bar{n}$ in the nucleus. The S–matrix for the $n-\bar{n}$ conversion and the subsequent evolution of the system up to a certain time t reads:

$$S(t,0) = U(t,0)T\left\{e^{-i\int_0^t dt' H_{n\bar{n}}(t')}\right\} \tag{2.17}$$

where the evolution operator is

$$U(t,0) = e^{-i\int_0^t dt'[V_{NN}+V_{N\bar{N}}]} \tag{2.18}$$

and

$$H_{n\bar{n}}(t) = U^{-1}(t,0)H_{n\bar{n}}U(t,0). \tag{2.19}$$

The decay probability of the initial nucleat state $|\Psi_A>$ is then determined by:

$$|<\Psi_A|S(t,0)|\Psi_A>|^2 = 1 - \Gamma_A t + \ldots \tag{2.20}$$

where the nuclear width, neglecting terms of order $O(\epsilon^4_{n\bar{n}})$, reads:

$$\Gamma_A \equiv \epsilon^2_{n\bar{n}} T_R^{-1} = \epsilon^2_{n\bar{n}} \sum_i |a_i|^2 \frac{\Gamma_i}{(\Delta M_i)^2 + \Gamma_i^2/4} \tag{2.21}$$

In the above the coefficients $|a_i|^2$ represent the probability that the wavefunction resulting from the $n\bar{n}$ conversion contains the quasi–nuclear state $|(A-1,Z,\bar{n})_i>$,

with energy $E_{i(\bar{n})}$ and annihilation width Γ_i into the nuclear state $|A-2, Z>$. Using two–body NN and (complex) $N\bar{N}$ interaction potentials:

$$\Delta M_i \equiv E_{i(n)} - E_{i(\bar{n})} = < i|V_{NN}|i > - < i|Re\, V_{N\bar{N}}|i > \quad (2.22)$$

$$\Gamma_i = -2 < i|Im\, V_{N\bar{N}}|i > . \quad (2.23)$$

Closure approximation

Since $\sum_i |a_i|^2 = 1$, if Γ_i and ΔM_i have only a weak dependence upon the state $|i>$, then eq.(2.21) reduces to

$$\Gamma_A \simeq \epsilon^2_{n\bar{n}} \frac{< \Gamma >}{< \Delta M >^2 + < \Gamma >^2 /4}, \quad (2.24)$$

where quantities averaged over the available quasi–nuclear states have been introduced.

We have followed this approach[15, 16, 17] within the framework of two different nuclear models:

(a) A nuclear matter description, which starts from the Hartree–Fock basis implemented by the local density approximation;

(b) A standard nuclear shell model, together with the above mentioned closure approximation.

In case (a) the states $|i>$ are expressed through single particle wave functions labelled by the wave number $\vec{k}$ and the coefficients $a_i \equiv a(\vec{k})$ are constants. With appropriate normalization and *without* resorting to the closure approximation, equation (2.21) can then be rewritten as:

$$T_R^{-1} = \frac{4}{A} \frac{\Omega}{(2\pi)^3} \int d^3k \theta(k_F - k) \frac{\Gamma_a(k)}{[\Delta M(k)]^2 + \Gamma_a^2(k)/4} \quad (2.25)$$

where (s, t are spin, isospin quantum numbers)

$$\Delta M(k) = V_n(k, s, t) - V_{\bar{n}}(k, s, t) \quad (2.26)$$

$V_{n(\bar{n})}(k, s, t)$ being the Hartree–Fock (Hartree only for the antineutron) fields felt by the neutron (antineutron) as a result of the two–body interaction potentials contained in H [eq.(2.15)], while $\Gamma_a(k)$ is the annihilation width of an antineutron in the state $(\vec{k}, s, t)$, stemming from $ImV_{N\bar{N}}$ (for detailed definitions see ref.[16]).

The local density approximation is then applied by averaging (2.25) over the nuclear volume with a locally defined Fermi momentum

$$k_F(r) = \left\{ \frac{3\pi^2}{2} \rho(r) \right\}^{1/3}, \tag{2.27}$$

$\rho(r)$ being the phenomenological nuclear density distribution (e.g. the usual Fermi parameterization).

In this approach there are two crucial ingredients: the nuclear model description and the two-body NN and $N\bar{N}$ interactions. Estimates of T_R made in the past[15, 16] utilized a schematic OBEP (One Boson Exchange Potential) for V_{NN} and $Re\, V_{N\bar{N}}$, together with the short range complex $N\bar{N}$ potential of Richard and Sainio[18]. The T_R values (in units of 10^{23} sec^{-1}) obtained for ^{16}O and ^{56}Fe are, within the allowed range of the model parameters:

$$^{16}\mathrm{O}: \qquad 1.80 \leq T_R \leq 2.12 \tag{2.28}$$

$$^{56}\mathrm{Fe}: \qquad 2.49 \leq T_R \leq 4.76, \tag{2.29}$$

the first one being comparable with the estimate of Dover *et al.*[11], previously reported within the potential model approach.

This method has mainly two advantages: it avoids the closure approximation and, at the same time, it allows a sensible estimate of T_R for any mass number A, by simply changing the nuclear density parameters. Obviously more specific shell effects on the dynamics of the neutron and antineutron involved in the process cannot be accounted for. One could notice that T_R turns out to be a rather smooth function of A, growing from about 1 to 2.5 in the mass range up to 60, and then asymptotically reaching a value of about 3 for the largest mass numbers (all values are in units of 10^{23} sec^{-1}).

As mentioned at point (b), we have also evaluated[17] the r.h.s. of (2.21) within a standard shell model description, implemented by the closure approximation; the average quantities entering into (2.24) are thus defined as:

$$< V_n > \; = \; \frac{1}{2A} \sum_{\{\alpha\}} < \alpha_1 \alpha_2 | V_{NN} | \alpha_1 \alpha_2 >_{\mathcal{A}} \tag{2.30}$$

$$< V_{\bar{n}} > \; = \; \frac{1}{2A} \sum_{\{\alpha\}} < \alpha_1 \alpha_2 | Re\, V_{N\bar{N}} | \alpha_1 \alpha_2 >_{\mathcal{D}} \tag{2.31}$$

$$< \Gamma_a > \; = \; -\frac{1}{A} \sum_{\{\alpha\}} < \alpha_1 \alpha_2 | Im\, V_{N\bar{N}} | \alpha_1 \alpha_2 >_{\mathcal{D}} \tag{2.32}$$

where the α_i's label all quantum numbers (n, l, j, τ) which identify a single particle state in the Harmonic Oscillator shell model and the summations are extended to the set $\{\alpha\}$ of states which are occupied in the (initial) ground state of the considered nucleus.

Concerning the nucleon–nucleon (antinucleon) interaction, in ref.[17] the most recent parameterization of the NN and $N\bar{N}$ Paris potentials has been employed (with the customary spin, spin–orbit, tensor and quadratic spin–orbit contributions): the latter was fitted to the whole available set of $p\bar{p}$ data, including polarization observables.

Calculations have been performed again in ^{16}O and ^{56}Fe (in order to update previous estimates and compare with the above mentioned nuclear matter approach) and also in ^{40}Ar nucleus, in view of the future measurements of nuclear instability expected from ICARUS[19]. The results are the following (the range for the estimated T_R values stemming from different sets of parameters of the $N\bar{N}$ Paris potential, which fit the $p\bar{p}$ data with comparable accuracy):

$$^{16}\mathrm{O} \qquad T_R = (1.7 \div 2.6) \times 10^{23}\mathrm{sec}^{-1} \tag{2.33}$$

$$\text{which, for} \quad T_A > 4.3 \times 10^{31}\mathrm{yr} \quad (90\%CL, ref.[12])$$

$$\text{ensues:} \quad \tau_{n\bar{n}} > (0.7 \div 0.9) \times 10^{8}\mathrm{sec}; \tag{2.34}$$

$$^{56}\mathrm{Fe} \qquad T_R = (2.2 \div 3.4) \times 10^{23}\mathrm{sec}^{-1} \tag{2.35}$$

$$\text{which, for} \quad T_A > 6.5 \times 10^{31}\mathrm{yr} \quad (90\%CL, ref.[20])$$

$$\text{ensues:} \quad \tau_{n\bar{n}} > (0.8 \div 1.0) \times 10^{8}\mathrm{sec}; \tag{2.36}$$

and finally

$$^{40}\mathrm{Ar} \qquad T_R = (2.1 \div 3.2) \times 10^{23}\mathrm{sec}^{-1} \tag{2.37}$$

which will provide limits on $\tau_{n\bar{n}}$ once the first ICARUS data will be available for this channel.

In concluding this Section one important remark concerns the relative stability of the estimated nuclear suppression factor: different models and approximations for both the nuclear model description and the neutron/antineutron interactions with the nuclear medium provide T_R values which *do not differ* by more than $10 \div 15\%$. Even by allowing for somewhat larger deviations, one can see that the expected lower limit for the $n\bar{n}$ oscillation time is now of the order of 10^8 sec, which makes it quite interesting the possibility of exploring free neutron oscillation times up to one or two orders of magnitude larger than previously done.

3 Criticism and conclusions

In the recent past there have been some unjustified rumors about the nuclear suppression factor being of order unity, thus leading to limits for the $n\bar{n}$ oscillation time of the same order as the nuclear instability limits[21], which would make hopless any direct search for free neutron–antineutron oscillations.

This author claims that the S–matrix approach is inconsistent with the potential model approach, thus pointing to an incorrect use of the latter for the evaluation of $n\bar{n}$ oscillations in the nucleus; this "inconsistency" has been clearly disproved by Krivoruchenko[22], with a careful analysis of the nuclear decay probability as determined by the time dependent S–matrix evolution of the nuclear states.

However an even more unfortunate mistake occurs in ref.[21] within the attempt of establishing a comparison with the potential model results: the author obtains the following probability of $n\bar{n}$ conversion with subsequent $\bar{n}$–nucleus decay:

$$W(t) = \epsilon_{n\bar{n}}^2 t^2 \left(\frac{1}{2} + \frac{1}{\Gamma t} + \frac{1}{\Gamma^2 t^2} \left[e^{-\Gamma t} - 1 \right] \right) \tag{3.1}$$

where the nuclear annihilation width is (more or less correctly) assumed to be $\Gamma \simeq 100$ MeV. Then the two extreme situations are considered:

- $\Gamma t << 1$, identified with some low density limit (and thus free space oscillations), in which case (3.1) reduces to $W(t) \simeq \epsilon_{n\bar{n}}^2 t^2$;
- $\Gamma t >> 1$, which should refer to the decay in the nuclear medium and gives, from (3.1), $W(t) \simeq \frac{1}{2} \epsilon_{n\bar{n}}^2 t^2$.

According to this calculation the nuclear suppression factor would turn out to be of order 1/2 and $\tau_{n\bar{n}}$ of the same order as the nuclear decay lifetime (10^{31} yr)!

But, as clearly pointed out in ref.[23], formula (3.1) is **wrong**: within the same assumptions of [21] the correct expression should read:

$$W(t) = \frac{4\epsilon_{n\bar{n}}}{\Gamma} t \left[1 - \frac{2}{\Gamma t} \left(1 - e^{-\Gamma t/2} \right) \right], \tag{3.2}$$

from which the limit $\Gamma t >> 1$ (oscillations in the medium) turns out to be:

$$W(t) \simeq \frac{4\epsilon_{n\bar{n}}^2}{\Gamma} t \tag{3.3}$$

and the corresponding nuclear lifetime:

$$T_A = \frac{\Gamma}{4}\tau_{n\bar{n}}^2 \equiv \frac{\Gamma}{4\epsilon_{n\bar{n}}}\tau_{n\bar{n}} >> \tau_{n\bar{n}}, \tag{3.4}$$

in qualitative (and semiquantitative) agreement with all previous evaluations in the existing literature.

A more serious criticism can be developed about the extraction of the "free" $n\bar{n}$ oscillation time from measurements of nuclear lifetime: the oscillation process indeed could be intrinsically modified in the presence of the nuclear medium. This was qualitatively pointed out long ago by Kabir[24] and semi–quantitatively considered by Dover *et al.*[11].

i) Based on the analogy between $n\bar{n}$ and β decay processes (both being induced by essentially zero range operators at very low momentum transfers) one can argue that the possible medium modifications are of long range character, like the ones, e.g., induced by two–body pionic correlations. The estimated correction to the transition mass should not exceed $15 \div 30\%$[11], which would not be a dramatic effect.

ii) Another source of uncertainty for the evaluation of $n\bar{n}$ oscillations in the medium can be ascribed to the occurrence of alternative direct $\Delta B = 2$ processes, which are suppressed in free space because of energy conservation[25]; typically one can envisage generic neutron–antibaryon oscillations like:

$$n \longrightarrow \bar{N}\pi \tag{3.5}$$

$$n \longrightarrow \bar{\Lambda} \tag{3.6}$$

which could lead to the same decay products but, in order to occur, require energy balance from the interactions with the nuclear medium. No quantitative estimates of the decay widths associated to these processes exist, but they should incoherently add to the one considered till now (both within the optical model and the S–matrix approach); as a result the limits on $\tau_{n\bar{n}}$ derived from nuclear decay observations would be less restrictive than presently believed, but still the estimated limit can be regarded as a conservative one.

In conclusion one can consider the existing estimate of the nuclear suppression factor as fairly reliable, although further improvements can still be pursued; but it is clear by now that these will not modify the order of magnitude of the effect. On the other hand the above mentioned ambiguities in the definition of $n\bar{n}$ transitions inside the nuclear medium can be clarified and serious theoretical estimates of these nuclear modifications should be provided. But we strongly need further experiments to go on, both on the issue of *free* $n\bar{n}$ oscillations and of nuclear instability search: hopefully theory can provide a reliable bridge in both directions.

References

[1] M. Baldo–Ceolin *et al.*, Phys. Lett. **B263** (1990) 95;

[2] M. Baldo–Ceolin *et al.*, Z. Physik **C 63** (1994) 409;

[3] Yu. A. Kamyshkov *et al.*, in Proceedings of TAUP95 (Toledo), September 1995

[4] Yu. A. Kamyshkov *et al.*, in PSI-Proc.95-02, P-10

[5] V.A. Kuzmin, JEPT Lett. **12** (1970) 228;

[6] R.N. Mohapatra et al., Phys. Rev. Lett. **44** (1980) 1316; Phys. Lett. **B94** (1980) 183;

[7] K.G. Chetyrkin et al., Phys. Lett. **99B** (1981) 358;

[8] Riazuddin, VPI-HEP–81/4 (1981);

[9] P.G. Sandars, J. Phys. G **6** (1980) L161;

[10] C.B. Dover, A. Gal and J.M. Richard, Phys. Rev. **D27** (1983) 1090;

[11] C.B. Dover, A. Gal and J.M. Richard, Phys. Rev. **C31** (1985) 1423;

[12] H. Takita *et al.* (Kamiokande), Phys. Rev. **D34** (1986) 902;

[13] T.W. Jones *et al.*, Phys. Rev. Lett. **52** (1984) 720;

[14] C.Y. Wong, A.K. Kerman, G.R. Satchler and A.D. MacKellar, Phys. Rev. **C29** (1984) 574;

[15] W.M. Alberico, A. Bottino and A. Molinari, Phys. Lett. **114B** (1982) 266;

[16] W.M. Alberico, J. Bernabeu, A. Bottino and A. Molinari, Nucl. Phys. **A429** (1984) 445;

[17] W.M. Alberico, A. De Pace and M. Pignone, Nucl. Phys. **A523** (1991) 488;

[18] J.M. Richard and M.E. Sainio, Phys. Lett. **110B** (1982) 349;

[19] see the contribution of F.Mauri (ICARUS collaboration) in these Proceedings;

[20] Ch. Berger *et al.* (Fréjus coll.), Phys. Lett. **B240** (1989) 237;

[21] V.I. Nazaruk, Phys. Lett. **337B** (1994) 328;

[22] M.I. Krivoruchenko, Preprint ITEP–95–37/March 1995;

[23] C.B. Dover, A. Gal and J.M. Richard, Phys. Lett. **B344** (1995) 433;

[24] P.K. Kabir, Phys. Rev. Lett. **51** (1983) 231;

[25] J. Basecq and L. Wolfenstein, Nucl. Phys. **B224** (1983) 21.

POSSIBLE $n-\bar{n}$ TRANSITIONS AND THE INFLUENCE OF OTHER INTERACTIONS

P. K. KABIR
INSTITUTE OF NUCLEAR AND PARTICLE PHYSICS
J. W. BEAMS LABORATORY
UNIVERSITY OF VIRGINIA, CHARLOTTESVILLE, VA 22904, USA

ABSTRACT

Baryon nonconserving $\Delta B=2$ interactions can induce both $n-\bar{n}$ transitions as well as disintegration of complex nuclei. Assertions that lower limits on lifetimes of complex nuclei imply corresponding lower limits for the characteristic period of $n-\bar{n}$ oscillation, are shown to be based on assumptions which are not well-founded. The claim that the two time-scales should be similar is certainly wrong.

1. Introduction

The possibility of $n-\bar{n}$ transformations arises naturally in a class of theories[1] which aim to unify weak and strong interactions. I was asked to discuss the relation between this effect for isolated neutrons and the closely connected question of stability of complex nuclei, especially in the light of a recently published claim[2] that the characteristic time $\tau_{n\bar{n}}$ for free $n-\bar{n}$ oscillation should be almost the same as the lifetime T_c for disintegration of complex nuclei through the associated nucleon-antineutron annihilation following $n-\bar{n}$ transformation. If the latter were true, existing limits[3,4] on T_c, - of the order of 10^{31} years or longer, - could immediately be translated into corresponding limits for $\tau_{n\bar{n}}$, which would make the prospects for laboratory searches for $n-\bar{n}$ transformation extremely unpromising.

In Section 2, I review earlier theoretical arguments[5] for a possible relationship between $n-\bar{n}$ transformations and consequent nuclear instability, and argue that it is unwise to presume too close a connection between the two. Section 3 analyzes recent theoretical objections to the representation of interactions of the neutron, other than the one which may induce $n-\bar{n}$ transitions, by effective potentials. Claims made in Ref. 2 are found to be unjustified and should be disregarded. Application of similar reasoning to the case of interaction with external magnetic fields leads to the conclusion that suppressive effects of magnetic interactions on $n-\bar{n}$ transitions do not require continuous shielding; appropriately chosen intermittent compensating fields[6] can serve just as well.

2. $n-\bar{n}$ Transformations in Nuclei

To describe the possibility of $n-\bar{n}$ transitions, it is convenient to represent the state of a "neutron" by a 2-component hyperspinor (similar to the isospinor used to represent the two possible charge states of a nucleon):

$$\Psi = \begin{bmatrix} \Psi_n \\ \Psi_{\bar{n}} \end{bmatrix} \tag{1}$$

whose two components are the amplitudes to find the particle as a neutron or an antineutron, respectively. Using units $\hbar=c=1$, the time evolution of Ψ is governed by

$$i\, d\,\Psi/dt = M\,\Psi \tag{2}$$

with

$$M = \begin{bmatrix} m_n + V_n & \epsilon \\ \epsilon & m_n + V_{\bar{n}} \end{bmatrix} \tag{3}$$

where m_n is the mass of a free neutron (or antineutron, assuming nTCP-invariance) and ϵ describes the strength of $n-\bar{n}$ transitions, assumed equal by time-reversal invariance; ϵ can be taken as real. V_n is the potential experienced by a neutron, while $V_{\bar{n}} = U_n - iW_n$ is the corresponding complex potential felt by an antineutron. These potentials depend, in principle, on position. Their spatial variation can be easily taken into account [as described, for example, by Alberico and Richard]. For our qualitative discussion, it suffices to treat them as constants. Diagonalization of M yields two complex eigenvalues with corresponding eigenstates which can be identified respectively with the states of a neutron and an antineutron in the nucleus. The shorter-lived state disappears at a rate given by the imaginary part of the optical potential for antineutrons, in the limit when ϵ, the measure of transitions to the neutron state, is neglected. The width (decay rate) of the longer-lived "neutron" state is given, for $|\epsilon| << |V_n - V_{\bar{n}}|$, by

$$\Gamma = 2\, W_n \,|\, \epsilon/V_n - V_{\bar{n}} \,|^2 \tag{4}$$

$$= \epsilon \,.\, 2\,\epsilon\, W_n/|\, V_n - V_{\bar{n}} \,|^2 \tag{4a}$$

$$= 2\,\epsilon^2\, W_n/\,[(\, U_n - V_n\,)^2 + W_n^2] \tag{4b}$$

The first expression, Eq. 4, has a simple interpretation as the disappearance rate of antineutrons in the nucleus, multiplied by the (probability) admixture of antineutrons in the "neutron" state induced by the mixing interaction ϵ. Since both V_n and $V_{\bar{n}}$ must vanish when the nuclear density goes to zero, the admixing potential ϵ is most effective in the outer regions of the nucleus, through dimunition of the denominator factor in Eq. 4. This aspect will be elaborated in Richard's talk. The separation of the factors in the form, Eq. 4a, serves to show the suppression of the disappearance rate of neutrons in the nucleus, relative to the free oscillation rate ϵ, by the enormous factor $|\, \epsilon/\Delta V_n \,|$. If the curly-bracketed "nuclear physics" factors in the third form are taken as known[7], Eq. 4b furnishes a direct connection between the rate of disappearance of neutrons within nuclei - a spectacular and easily detectable phenomenon - and the $n-\bar{n}$ oscillation time $\tau_{n\bar{n}} = 1/\epsilon$. This is the basis for the frequently quoted assertion that the measured lower

limits for T_c, for the lifetimes of complex nuclei, furnish corresponding lower limits for the period of $n-\bar{n}$ oscillations.

What is overlooked in this line of reasoning is that the ϵ which appears in Eqs. 4 is not necessarily the same ϵ which determines the period for free neutron-antineutron oscillation. It has been argued[8] that there are good reasons to expect that they should *not* be the same. In the quark description of elementary particles, which underlies the theories of $n-\bar{n}$ transformation, the requisite interactions are mediated by fields whose quanta are so massive that, for nuclear physics applications, the 6-quark $n-\bar{n}$ transition operator may be safely treated as a contact interaction $(d_c d)^2\ \bar{u}_c u$, where the particle symbols represent quark fields evaluated at the *same* space-time point. As such, the $n-\bar{n}$ transition amplitude depends on the overlap between quark fields, viz. the short-distance correlations between quarks. *Anything* which affects this correlation will correspondingly affect the rate of these processes. In his opening talk, Professor Goldhaber drew attention to the possibility of previously unknown interactions between quarks, suggested by recent results[9] reported by the CDF collaboration at Fermilab, according to which the frequency of "jets" produced in high energy collisions at the Tevatron, with $p_T > 200\ GeV/c$, is found to systematically exceed the expectation from QCD calculations. Julian Noble and I concluded that, if the discrepancy is real, it could be explained by a possibly universal repulsion between quarks, mediated by a neutral vector field with mass of order $200\ GeV/c^2$ or more, whose effects would not be readily recognized in lower energy reactions. The occurrence of such a short-range repulsion between quarks would introduce Gamow-type suppression factors for processes involving even shorter-range quark-quark interactions, such as those postulated for $n-\bar{n}$ transformation. While this would certainly modify the strength of $n-\bar{n}$ transitions in terms of the primary interactions, it is not obvious how it would affect the relation between $n-\bar{n}$ oscillations and nuclear lifetimes. Nevertheless, it should serve as a cautionary note before drawing far-reaching conclusions.

Another effect, which can modify the rate of $n-\bar{n}$ transformations within nuclei relative to that in free neutrons, arises from the fact that nucleons are themselves complex dynamical structures, and the distribution of quarks inside a free nucleon could differ significantly from the distribution in a nucleon (to the extent that we may view the latter as a separate object) when it is bound within a nucleus. A qualitative explanation which accounts for much of the so-called EMC effect[10] is that a nucleon bound inside a nucleus becomes enlarged[11], with a radius 10-30% greater than that of a free nucleon. This can be used to make a rough estimate[12] of the corresponding inhibition of $n-\bar{n}$ transitions within nuclei. If $n-\bar{n}$ transitions proceed through an essentially point-like interaction, the transformation will occur only when all three quarks of a neutron are found at the same point. While the first quark could be anywhere in the nucleon, the chance that each of the other quarks should be at the same place as the first, is inversely proportional to the neutron volume for each. Treating the motions of the quarks as independent, the overall probability amplitude will be inversely proportional to the *square* of the neutron volume. For a radial expansion by 10 to 30% this would yield, according to Eq. 4, a reduction by a factor of 3.1 to 23 for the nuclear disintegration rate.

A more fundamental objection to the identification of the parameter ϵ in nuclei

with the value ϵ_0 for a free neutron, arises from the recognition that there are many other mechanisms for catalysis of $n-\bar{n}$ transformation in the presence of other nucleons, which cannot possibly occur for a free neutron, which are of the same order in the baryon-nonconserving interactions. While this had been noted quite generally in Ref. 8, an interesting explicit example[13] has recently been presented by Krivorichenko. In relativistic quantum theory, a fermion and its antiparticle necessarily have opposite parity, consequently a purely *scalar* $\Delta B = 2$ interaction could not possibly induce the transformation of a free neutron into an antineutron, but in the presence of other particles, as in a nucleus, the parity-reversal required to change a neutron into an antineutron could be compensated by a change of relative orbital motions. Limits on ϵ from nuclear stability provide information which is complementary to that which can be obtained from searches for free $n-\bar{n}$ transitions.

3. Microscopic vs. Potential Description of "Other" Interactions

The preceding analysis followed earlier authors by representing interactions of neutrons and antineutrons, other than the $n-\bar{n}$ transition interaction of primary interest, by effective potentials. This procedure has been questioned by Nazaruk[2], who claims that a correct microscopic approach leads to vastly different conclusions. Detailed rebuttals of Nazaruk's claims have already been presented[14], apparently without convincing Nazaruk, so I shall try instead to justify the validity of the conclusions reached by the potential description, using more direct physical arguments based on the microscopic description.

In the hyperspin analogy introduced in Eq. 1, the neutron is identified with hyperspin "up" while the "down" hyperspin state corresponds to the antineutron. The quasi- Hamiltonian, Eq. 3, governing hyperspin motion can be written as

$$M = [m_n + (V_n + V_{\bar{n}})/2].I + (V_n - V_{\bar{n}})/2.\sigma_z + \epsilon.\sigma_x . \qquad (3')$$

In the absence of potentials $V_n, V_{\bar{n}}$, the hyper-"B_x" field causes precession of the hyperspin about the x-axis in hyperspin-space with anglar frequency ϵ; this is just the free $n-\bar{n}$ oscillation. In the presence of a strong hyper-"B_z" field, $|V_n - V_{\bar{n}}| >> \epsilon$, the precession now takes place about an axis z' making an angle $\theta \approx \epsilon/|V_n - V_{\bar{n}}|$ with the z-axis, in the x-z plane, with an angular frequency essentially given by $|V_n - V_{\bar{n}}|/2$. Consequently, an initial hyperspin-"up" (neutron) state will never be able to develop much of an antineutron (hyperspin "down") admixture because the maximum angle that this hyperspin can make with the z-axis, by precessing about z', will be limited to 2θ. Damping, arising from the imaginary term in Eq. 3, will assure that the final state will be oriented along z', making an angle θ with z. This is the geometrical interpretation of the suppression factor appearing in Eq. 4.

In a microscopic description of the interactions suffered by a neutron (or an antineutron) in the nucleus, the particle is not subject to a slowly-varying potential. Rather, the potentials V_n and $V_{\bar{n}}$ are simply phenomenological representations of the *average* effect of many separate interactions with the constituent particles of the nucleus, which could be regarded as a series of random encounters. Since the interactions are

different for neutrons and for antineutrons, in the hyperspin picture, these sporadic interactions would be represented by replacing the potential terms in Eq. 3' by fluctuating terms proportional either to I or to σ_z. Terms proportional to I do not affect the hyperspin while those proportional to σ_z rotate the hyperspin-state by corresponding angles around the z-axis. The magnitudes of these z-rotations, which vary essentially randomly, will be typically very much larger than the small angles produced by the slow monotonic precession about the x-axis induced by ϵ. Consequently, depending on the azimuth in which the hyperspin finds itself, the ϵ-precession will sometimes move the hyperspin away from the z-axis and sometimes towards it, cancelling out any secular drift away from the z-axis, on average. Therefore, a microscopic description, of *strong* interactions which distinguish n from $\bar{n}$, yields the same conclusion as the potential description employed earlier. Using either description, one unavoidably concludes that $n-\bar{n}$ transitions are severely suppressed by strong interactions in the nucleus which distinguish n from $n-\bar{n}$.

Application of an external magnetic field provides a situation where a constant hyper-"B_z" potential actually describes the different interactions experienced by a neutron and an antineutron. Since a neutron and an antineutron have opposite magnetic moments, hyperspin "up" and "down" states will have magnetic energies [for the *same* orientation of the true spin (angular momentum)] which differ by $2V_M = 2\mu B$. Since searches for free $n-\bar{n}$ transformations are able to observe neutrons for at most a small fraction of an oscillation period $2\pi/\epsilon$, the initial precession of the hyperspin about the x-axis, induced by ϵ, is only weakly affected by the precession about the z-axis forced by V_M. Consequently, the requirement of magnetic shielding, to eliminate the suppressive effect of V_M, is much less stringent than would be required to observe a sizeable fraction of an oscillation period. Our preceding discussion of the hyperspin analogy shows that the elimination of the magnetic suppression can be accomplished either by complete shielding or by intermittent application of appropriately chosen counter-fields[6]. The latter may offer some experimental advantages.

4. Conclusions and Acknowledgments

The relationship of possible $n-\bar{n}$ transitions to the stability of complex nuclei has been critically examined. It is found that the two types of experiments furnish complementary information about possible $\Delta B = 2$ interactions. In particular, lower limits for lifetimes of complex nuclei do not necessarily yield corresponding lower limits for $n-\bar{n}$ oscillation periods. The claim, that a "correct" microscopic description of nuclear interactions does not suppress the rate of $n-\bar{n}$ transitions in complex nuclei, is shown to be incorrect. Total magnetic shielding, to remove the suppressive effect of the Earth's magnetic field, can be replaced by intermittent magnetic "compensation".

I thank the organizers for arranging a very stimulating meeting, and inviting me to present my views. My research is partially supported by the U.S. Department of Energy.

References

1. R. Mohapatra, P. Nath, and J. C. Pati, in these Proceedings.
2. V. I. Nazaruk, Phys. Lett. **B337**, (328) (1994), and preprints INR-995 and INR-998 (1995).
3. H. Takita et al. (Kamiokande), Phys. Rev. **D34**, (902) (1986).
4. Ch. Berger et al. (Frejus), Phys. Lett. **B240**, (237) (1989).
5. For a review and a list of earlier references, see C. Dover, A. Gal, and J-M. Richard, Nucl. Instr. & Methods, **A284**, (13) (1989).
6. P. Kabir, S. Nussinov, and Y. Aharonov, Phys. Rev. D ... (1983?)
7. While determinable in principle from other experiments, in practice there is considerable uncertainty about their actual values. According to Ref. 5, the "nuclear factor" is relatively insensitive to these uncertainties.
8. P. K. Kabir, Phys. Rev. Lett. **51**, (231) (1983).
9. K. Abe et al. (CDF), described in Science, Feb. 7, (1996).
10. J. J. Aubert et al. (EMC), Phys. Lett. **B123**, (275) (1983).
11. F. E. Close, R. G. Roberts, and G. G. Ross, Phys. Lett. **B129**, (346) (1983).
12. P. K. Kabir, Nucl. Instr. & Methods, **A284**, (13) (1989).
13. M. Krivorichenko, private communication from Yu. Kamyshkov, (1996).
14. C. Dover, A. Gal, and J-M. Richard, Phys. Lett. **B344**, (433) (1995); M. Krivorichenko, ITEP preprint, (1995), hep-ph/9503300 (1995).

NEUTRON–ANTINEUTRON OSCILLATIONS AT THE SURFACE OF NUCLEI

Carl B. Dover[1]
Physics Department
Brookhaven National Laboratory
Upton, N.Y., U.S.A.

Avraham Gal
Racah Institute of Physics
The Hebrew University, Jerusalem, Israel

Jean-Marc Richard
Institut des Sciences Nucléaires–CNRS–IN2P3
Université Joseph Fourier, Grenoble, France

Abstract

We discuss some aspects of possible neutron–antineutron oscillations in nuclei. The phenomenon occurs mostly at the surface of nuclei, and hence *i)* is not very sensitive to medium corrections and *ii)* makes use of the antinucleon-nucleus interaction in a region probed by experiments at CERN.

The relevance of neutron–antineutron oscillations for testing physics beyond the standard model was stressed in several contributions at this Workshop, in particular by Mohapatra [1]. The question now is how to detect neutron–antineutron oscillations, or how to set an upper limit on their rate. We refer to Alberico's talk for a comprehensive survey [2]. In the present contribution, we wish to stress some properties of the potential-model approach, which in our opinion make it rather reliable.

Consider for instance an S-wave neutron in deuterium. It is governed by a radial Schrödinger equation

$$u''(r) + m\,[E - V_n(r)]\,u(r) = 0, \tag{1}$$

where notations are obvious. With a $n \leftrightarrow \bar{n}$ transition potential ϵ, the wave function gets an antineutron component $\bar{u}(r)$ which to leading order is given by the inhomogeneous equation

$$\bar{u}''(r) + m\,[E - V_{\bar{n}}(r)]\,\bar{u}(r) = m\epsilon u(r), \tag{2}$$

where E and u are now frozen. This leads to an estimate of the decay width of deuterium in terms of the annihilation part of the antineutron potential

$$-\frac{\Gamma}{2} = -\frac{1}{2T} = \int_0^\infty \bar{u}^2(r)\mathrm{Im}V_{\bar{n}}(r)\mathrm{d}r. \tag{3}$$

[1]Deceased

It is rather straightforward to generalise these equations to larger nuclei, once each neutron is described by its appropriate shell-model wave-function.

Such a set of equations gives results which are stable with respect to variations of the basic ingredients, as stressed, e.g., by Ericson and Rosa-Clot [3] in a different context. Moreover, this formalism provides the relative contribution of each neutron shell, and within a shell, the weight of the various parts in the integration over the distance r.

This analysis was carried out in Ref. [4], and its results were confirmed in further investigations [5]: neutron–antineutron oscillations, if any, occur mostly in outer shells, and near the surface of the nucleus. In particular:

- nuclei with weakly-bound neutrons offer more favourable rates. As discussed during the oral presentation, heavy water would be slightly better than ordinary water, because of the loosely-attached neutron in deuterium.
- the antineutron wave function is peaked outside the nuclear density.

These properties survive changes in the assumed shape of the neutron potential, and can be explicitly seen in toy models such as square-well or separable potentials, for which calculations can be performed analytically.

This peripheral character of nuclear instability can be explained as follows. In nuclear medium, a neutron which considers the possibility of oscillating is immediately refrained to do so when it feels the large gap between the average potentials V_n and $V_{\bar{n}}$. Far away, this gap vanishes, for both potentials go to zero. On the other hand, one would not care too much about an antineutron at large distance from the centre, as it has no nucleon to interact with. The best compromise takes place at the surface, where the neutron is free enough to oscillate, and the medium is still dense enough to annihilate freshly-produced antineutrons.

The peripheral character of neutron oscillations in nuclei has two important consequences:

- Contrary to the neutron potential V_n (and its by-product $u(r)$, the neutron wave function) which is well constrained by decades of phenomenological studies, the antineutron potential $V_{\bar{n}}(r)$ is not well known inside the nucleus. However, experiments at the LEAR facility of CERN with antiprotonic atoms, or with antiproton beams scattered on nuclear targets, provide stringent constraints on this interaction near the nuclear surface [6]. This is precisely the domain we need for neutron oscillations.
- Deeply inside a nucleus, the transition operator ϵ could be renormalised, or receive new contribution. This is discussed, e.g., by Kabir [7]. The quasi-free neutrons which contribute to most of the decay of the nucleus experience an ϵ potential which is identical or very close to τ^{-1}, where τ is the oscillation period of free neutrons.

The comparison between free-neutron and bound-neutron experiment has been the subject of intense debates, and one of the authors (J.M.R.) would like to acknowledge discussions on the subject at I.L.L., Grenoble, with the late R. Marshak and W. Mampe. As long as negative results are obtained, bound nuclei provide a rather reliable lower bound on the oscillation period τ. The scaling properties of Eqs(2-3) implies for

τ a relation

$$T = T_R \tau^2 \tag{4}$$

to the lifetime T of a given nucleus. When the nuclear factor T_R is computed with the typical medium-size nuclei used in proton-decay experiments, one gets that $T \geq 10^{32}$ y implies $\tau \geq 10^8$ s [8], comparable to the latest result with free neutrons at Grenoble [9]. The perspective of checking directly $\tau \geq 10^{11}$ s in the foreseen experiment at Oak Ridge corresponds to limits on T which are not conceivably reachable in underground experiments.

Acknowledgements

J.M.R. would like to thank the organisers for their kind invitation, making possible many stimulating and fruitful discussions with other participants. The hospitality provided by the theory group at Oak Ridge, and in particular T.D. Barnes, is also gratefully acknowledged.

References

[1] R.N. Mohapatra, Contribution to this Workshop (preprint hep-ph/9604414).

[2] W. Alberico, Contribution to this Workshop.

[3] T.E.O. Ericson and M. Rosa-Clot, Nucl. Phys. A405, 497 (1983)

[4] C.B. Dover, A. Gal and J.-M. Richard, Phys. Rev. D27, 1090 (1983).

[5] C.B. Dover, A. Gal and J.-M. Richard, Phys. Rev. C31, 1423 (1985); Nucl. Instr. Meth. , A284, 13 (1989); Phys. Lett. B 344, 433 (1995).

[6] See, e.g., C.B. Dover, in Proc. 1st Workshop on Intense Hadron Facilitites and Antiproton Physics, ed. T. Bressani, F. Iazzi, and G. Pauli (Italian Phys. Soc., Bologna, 1990).

[7] P.K. Kabir, Contribution to this Workshop.

[8] C.J. Batty, M. Fidecaro and H.B. Prosper, Nucl. Phys. A446, 473 (1987).

[9] M. Baldo-Ceolin *et al.*, Z. Phys. C63, 409 (1994).

$n - \bar{n}$ TRANSITIONS IN NUCLEI AND MIXING OF NUCLEAR STATES WITH A AND $A - 2$

L. A. Kondratyuk*
Institute of Theoretical and Experimental Physics
117259, Moscow, B. Cheremushkinskaya 25, Russia

Abstract

The new lower limit on the period of $n-\bar{n}$ oscillations $\tau_{n\bar{n}} > (8 \div 11) \times 10^8\, sec$ which follows from stability of Fe is found. This limit is almost by 10 times larger than previous estimations.

In this paper I present new lower limit on the period of $n - \bar{n}$ oscillations which follows from stability of nuclei. This limit is considerably larger than previous estimations [1-8]. In §1 I consider the mixing of sectors with $A = 2$ and $A = 0$ in deuterium to emphasize once more the difference of $n - \bar{n}$ oscillations in medium and in free space. In §2 the deuteron decay due to the $n - \bar{n}$ transition is analyzed. The $n - \bar{n}$ oscillations in nuclei are considered in §3 with a special attention to the binding effect. The new limit on $\tau_{n\bar{n}}$ from stability of Fe is presented.

1 Mixing of sectors with $A = 2$ and $A = 0$ in deuterium

When the $n-\bar{n}$ transition occurs inside a deuteron, the latter can decay into hadrons (mesons): $d \to h$. The Hamiltonian which describes the two-channel problem $p \to d, d \to h$ and $h \to h$ can be written as follows

$$\hat{H} = \begin{pmatrix} E_1 & V_{12} \\ V_{21} & E_2 \end{pmatrix} \tag{1}$$

If we take the initial state containing only the $A = 2$ component, then the admixture of the $A = 0$ component at the time t will be equal to

$$< h(t)|d >= V_{12} \frac{e^{iE_{21}t} - 1}{E_{21}} \tag{2}$$

*E-mail address: KONDRATYUK@VXITEP.ITEP.RU

where $E_{21} = E_2 - E_1$. The probability to find the h component at the time t is

$$w_{21}(t) = 2|V_{12}|^2 \frac{1 - cos(E_{21}t)}{E_{21}^2} \tag{3}$$

It is important that the transition $d \to h$ occurs to continuum with the density of states $\rho(E_2)$. This is the main reason why the transition probability for large time intervals

$$\gamma_{21} = \int dE_2 \rho(E_2) w_{21}(t) = 2\pi |V_{12}|^2 \rho(E_2 = E_1)t \tag{4}$$

is proportional to t (see e.g. [9]).

This is very different from the $n-\bar{n}$ oscillations in a free space where the transition occurs from discrete to discrete state. If in the latter case we start at $t = 0$ from the neutron state the probability to find $\bar{n}$ at the time $t \ll E_{21}^{-1}$ is proportional to t^2

$$w_{21}(t) \approx \varepsilon_{n\bar{n}}^2 t^2 \tag{5}$$

where $\varepsilon_{n\bar{n}} = V_{12}(n \to \bar{n})$.

If we know the lower limit for the life time of deuteron T, we would find the upper limit on $|V_{12}|^2$ using eq. (4)

$$2\pi |V_{12}|^2 \rho(E_2 = E_1) < \frac{1}{T} \tag{6}$$

The amplitude of the transition $d \to h$ is proportional to $\varepsilon_{n\bar{n}}$

$$V_{12} = D\varepsilon_{n\bar{n}} \tag{7}$$

where D is the constant which is calculated in §2.

Therefore we can find lower limit on the $n - \bar{n}$ oscillation period

$$\tau_{n\bar{n}} = \varepsilon_{n\bar{n}}^{-1} > (T_0 T)^{1/2} = (\frac{T_0}{T})^{1/2} T \tag{8}$$

where $T_0 = 2\pi D\rho(E_2 = E_1)$ is the characteristic time which depends on the $\bar{n}p$ annihilation probability and is of the order of $10^{-22} \div 10^{-23}$ sec.

As $T \geq 10^{31} \div 10^{32} y \approx 10^{38} \div 10^{39}$ sec the parameter $(T_0/T)^{1/2}$ is very small $\leq 10^{31}$ and this small factor describes the suppression of $n - \bar{n}$ oscillations in nuclei [1-8].

Note that in r ecent paper [10] it was clamed that the probability of $n-\bar{n}$ transition in nuclei is also proportional to t^2. In this case the small factor $(T_0/T)^{1/2}$ in eq. (8) would be absent. However this statement contradicts to eq. (4) which follows from general principles of quantum mecanics. It might happen only in the case when a very narrow meson state with the mass very close the mass of deuteron would exist.

2 $n-\bar{n}$ transition in deuteron

In the first approximation in $\varepsilon_{n\bar{n}}$ the amplitude of the deuteron decay into the final state f containing mesons can be written in the following form

$$M(d \to f) = \varepsilon_{\bar{n}n} \int \frac{d^3\vec{n}}{(2\pi)^3} \varphi_d(\vec{n}) \frac{1}{B_d + \vec{n}^2/m} \cdot \frac{1}{\sqrt{m}} A(\bar{n}p \to f) \tag{9}$$

where m is the nucleon mass, $\varphi_d(\vec{n})$ is the deuteron wave function in the momentum space, B_d is the binding energy of deuteron and $A(\bar{n}p \to f)$ is the amplitude of the $\bar{n}p$-annihilation into the meson state f.

Introducing the induced $\bar{n}p$ wave function

$$\psi_{\bar{n}}(r) = \int \frac{d^3\vec{n}}{(2\bar{n})^3} e^{i\vec{n}\vec{r}} \varphi_d(\vec{n}) \frac{1}{B_d + \vec{n}^2/m} \frac{1}{\sqrt{m}} \tag{10}$$

and taking into account that the radius of $\bar{n}p$ annihilation is much smaller than the deuteron radius $r_{ann} \ll r_d$ we can write

$$M(d \to f) = \varepsilon_{n\bar{n}} \psi_{\bar{n}}(\vec{r} = 0) A(\bar{n}p \to f) \tag{11}$$

The amplitude $M(d \to f)$ should be singular at $B_d \to 0$ when the radius of deuteron becomes very large. To demonstrate this let us take the Hülthen model of the deuteron wave function

$$\psi_d(r) = N \frac{e^{-\alpha r} - e^{-\beta r}}{r} \tag{12}$$

where $\alpha^2 = mB_d$ and $\beta \approx 5.2\alpha$. In this case

$$\psi_{\bar{n}}(r = 0) \approx 0.2\sqrt{\frac{m}{\alpha}} \tag{13}$$

which is divergent when $\alpha = \sqrt{mB_D} \to 0$. Note that this divergence is related with the contribution of the first term in eq. (12), i.e. with the contribution of large r. The second term is introduced to have correct behaviour of the wave function at $r \to 0$. Numerically we have for $B_d \approx 2.23 MeV$

$$\psi_{\bar{n}}(r = 0) \approx 0.9 \tag{14}$$

The total width of the deuteron

$$\Gamma_d = \sum_f |M(d \to f)|^2 \frac{1}{2m_d} d\phi_f \tag{15}$$

can be expressed through the $\bar{n}p$ annihilation cross section

$$\sigma^{ann}_{\bar{n}p} = \sum_f |A(\bar{n}p \to f)|^2 \frac{1}{4p_{c.m.}\sqrt{s}} d\phi_f \tag{16}$$

or through the imaginary part of the $\bar{n}p$ scattering length $a_{\bar{n}p}$

$$\Gamma_d = \varepsilon^2_{n\bar{n}}|\psi_{\bar{n}}(\vec{r}=0)|^2 2p_{c.m.}\sigma^{ann}_{\bar{n}p} = -\varepsilon^2_{n\bar{n}}|\psi_{\bar{n}}(\vec{r}=0)|^2 8\pi Im a_{\bar{n}p} \qquad (17)$$

Eq.(17) is very different from the formula for the annihilation width Γ_a which was used as ansatz by Dover, Gal and Richard [5]

$$\Gamma_a = -2\int d^3r|\psi(r)|^2 W_{\bar{n}p}(r) \qquad (A1)$$

Here $\psi(r)$ is the solution of the inhomogeneous Schrödinger equations with the $\bar{n}p$ complex optical potential

$$V_{\bar{n}p} = U_{\bar{n}p}(r) + iW_{\bar{n}p}(r) \qquad (A2)$$

and the source $\varepsilon_{\bar{n}n}\psi_d(r)$ with $\psi_d(r)$ being the deuteron wave function.

This ansatz was also used by other authors (see e.g. [6-8]) and is equivalent to the assumption that $\bar{n}p$ interaction can be described by the one-channel optical approach. The approach which is used here is based on the nonrelativistic diagram technique and takes into account that $\bar{n}p$ interaction is multichannel. In principle within our approach it is possible to express the probabilities for different exclusive channels of deuteron decay through partial widths of $\bar{n}p$ annihilation. The unitarity condition permits to express the total decay width of deuteron through the observable quantity: the imaginary part of $\bar{n}p$ scattering length.

The possibility to avoid the use of optical potential is important because the experimental $\bar{N}N$ scattering length can be described using completely different values for its strength and radius. As we show in §3 two different approaches give similar numerical values for Γ_a in the deuteron case. However for complex nuclei there are drastic differences: in the approach (A1) the $n\bar{n}$ oscillations occur mainly on the surface of nucleus while in our approach all the volume of nucleus gives contribution.

3 $n-\bar{n}$ transition in nuclei

It is convenient to introduce the amplitude A_1 which describes the three–step process:
i)$n-\bar{n}$ transition in nucleous with the atomic number A;
ii)scattering of antineuteron on the $A-1$ nuclear cluster;
iii) inverse transition $\bar{n}-n$ with formation of the initial nucleus.
This amplitude can be written in the following form

$$A_1 = \varepsilon_{n\bar{n}}\int \frac{d^3\vec{n}_1}{(2\pi)^3}\varphi(\vec{n}_1)\frac{1}{B+\vec{n}_1^2/2\mu}\frac{1}{\sqrt{2\mu}}\cdot$$

$$T_{\bar{n}N}(0)S(\vec{n}_1-\vec{n}_2)\varepsilon_{n\bar{n}}\frac{d^3\vec{n}_2}{(2\pi)^3}\varphi(\vec{n}_2)\frac{1}{B+\vec{n}_2^2/2\mu}\frac{1}{\sqrt{2\mu}} \qquad (18)$$

where B is the average binding energy of neutron, μ is the reduced mass of the $n-(A-1)$ system, $T_{\bar{n}N}(0)$ is the forward $\bar{n}N$ scattering amplitude and $S(\vec{n}_1-\vec{n}_2)$ is the form factor of the $A-1$) nuclear cluster.

The imaginary part of this amplitude is related to the decay width of A nucleous as follows -

$$-ImA_1 = m\frac{\Gamma}{N} \tag{19}$$

where N is the number of neutrons.

Generally speaking the amplitude $T_{\bar{n}N}(0)$ should be taken off-shell. However taking into account that the binding is small ($B \sim 8MeV$) we can ignore off–shell effects and express $T_{\bar{n}N}(0)$ through the $\bar{n}N$ absorption probability and the $\bar{n}N$ scattering length

$$-ImT_{\bar{n}N}(0) = 2p_{c.m.}\sqrt{s}\sigma_{\bar{n}N} = -8\pi\sqrt{s}Ima_{\bar{n}N} \tag{20}$$

Introducing $T_{\bar{n}N}(0)$ we avoid the use of optical potential (see e.g. refs. [5-8]) and express the decay width of nucleous in terms of observable quantity $Ima_{\bar{n}N}$.

As in the deuteron case we introduce the induced $\bar{n}$ wave function

$$\phi_{\bar{n}}(r) = \int \frac{d^3\vec{n}}{(2\pi)^3} e^{i\vec{n}\vec{r}} \varphi(\vec{n}) \frac{1}{B + \vec{n}^2/2\mu} \frac{1}{\sqrt{2\mu}} \tag{21}$$

and rewrite the amplitude A_1 in the following form

$$A_1 = \varepsilon^2_{n\bar{n}} \int d^3\vec{r}\rho(\vec{r})|\psi_{\bar{n}}(\vec{r})|^2 T_{\bar{n}N}(0) \tag{22}$$

where

$$\rho(r) = \int e^{-i\vec{n}\vec{r}} S(\vec{n}) \frac{d^3\vec{n}}{(2\pi)^3} \tag{23}$$

For the estimation we take the neutron wave function in the form

$$\varphi(\vec{n}) = N[\frac{1}{\vec{n}^2 + \alpha^2} - \frac{1}{\vec{n}^2 + \beta^2}] \tag{24}$$

where $\alpha^2 = 2\mu B$,

$$N = (\frac{8\pi\alpha\beta(\alpha+\beta)}{(\beta-\alpha)^2})^{1/2},$$

β is the cut-off parameter and we take it to be equal to 0.5 GeV. As we shall see below the result is not very sensitive to the choice of β.

The amplitude A_1 should be singular at $B \to 0$. Indeed for the wave function (24) we get

$$A_1 = \varepsilon^2_{n\bar{n}} T_{\bar{n}N}(0) D_A \sqrt{\frac{\mu}{B}} \tag{25}$$

and if $B \to 0$, $A_1 \to 1/\sqrt{B}$.

Calculating A_1 for ^{56}Fe with $\rho = \rho_0$ for $R \leq R$ and $\rho = 0$ for $> R$ with $R = 4.1fm, B = 8.8MeV$ we find $D_{Fe} = 0.3$. Note that the first term in the wave function (26) gives dominant contribution (~ 90)%.

Summarising §2 and 3 we can write the decay widths per neutron

$$\frac{\Gamma(Fe)}{N} = \varepsilon^2_{n\bar{n}} C^2_{Fe} 8\pi Ima_{\bar{n}N} \tag{26}$$

for iron and

$$\Gamma^{(d)} = \varepsilon_{n\bar{n}}^2 C_d^2 8\pi Im a_{\bar{n}p} \tag{27}$$

for deuteron with $C_{Fe} = 3$ and $C_d \approx 0.8$.

The imaginary part of $a_{\bar{p}p}$ is known from the width of $\bar{p}p$ atom. It is in the interval (see e.g. [11])

$$Im a_{\bar{p}p} = (0.7 \div 1.2) fm \tag{28}$$

The data of OBELIX collaboration [12] show that at $p_{lab} \geq 60 MeV/c$ the annihilation and total cross sections of $\bar{p}p$ and $\bar{n}p$ are almost the same within 20%. Therefore we take

$$a_{\bar{n}N} = \frac{Z}{A} a_{\bar{n}p} + \frac{N}{A} a_{\bar{n}n} \approx a_{\bar{p}p} \tag{29}$$

In this case we get

$$\frac{\Gamma_{Fe}}{N} = \varepsilon_{\bar{n}n}^2 (3.5 \div 6) \times 10^{-22} sec \tag{30}$$

$$\Gamma_d = \varepsilon_{\bar{n}n}^2 (0.5 \div 0.8) \times 10^{-22} sec \tag{31}$$

where $\varepsilon_{n\bar{n}}$ is in sec^{-1}.

It is useful to compare annihilation widths for deuteron, O^{16} and Fe calculated in ref.[5]:

$$\Gamma_d = \varepsilon_{n\bar{n}}^2 (0.36 \div 0.37) \times 10^{-22} sec$$

$$\frac{\Gamma(O^{16})}{N} = \varepsilon_{n\bar{n}}^2 (0.3 \div 2.2) \times 10^{-23} sec$$

$$\frac{\Gamma(Fe)}{N} = \varepsilon_{n\bar{n}}^2 (0.6 \div 0.9) \times 10^{-23} sec$$

In view of experimental uncertainties for $a_{\bar{n}N}$ our values for Γ_d are not very different. However we predict that the probability for neutron to annihilate in O^{16} or Fe is much higher than in deuteron while the ansatz (A1) leads to the prediction that it is much smaller.

According to the data of Frejus collaboration [13]

$$T_{Fe} > 6.5 \times 10^{31} yr \approx 2 \times 10^{39} sec$$

Using this limit we find the lower limit for the period of $n - \bar{n}$ oscillations

$$\tau_{n\bar{n}}^2 = \varepsilon_{n\bar{n}}^{-2} > [(8 \div 11) \times 10^8 sec]^2 \tag{32}$$

If for the deuteron $T_d \approx T_{Fe}$ then

$$\tau_{n\bar{n}}^{(d)} > (3 \div 4) \times 10^8 sec \tag{33}$$

The limit (32) for $\tau_{n\bar{n}}^2$ is by two order of magnitude higher than the limit

$$(\tau_{n\bar{n}}^{(Fe)})^2 > [(0.8 \div 1.0) \times 10^8 sec]^2 \tag{34}$$

found by Alberico, De Pace and Pignone [7].

Using the result of KAMIOKANDE for O^{16} [14]

$$T(O^{16}) > 2.4 \times 10^{31} yr$$

Dover, Gal and Richard [5] found the lower limit for $\tau^2_{n\bar{n}}$

$$(\tau_{n\bar{n}}(0^{16}))^2 > [(1 \pm 0.3) \times 10^8 sec]^2 \tag{35}$$

which is very close to the result of Alberico et.al (34) for Fe and is also by two orders of magnitude lower than the result (32).

The most recent lower limit on the $n - \bar{n}$ transition time in a free space reached by the ILL–Grenoble experiment [15] is

$$\tau_{n\bar{n}} > 8.6 \times 10^7 sec \tag{36}$$

This limit is approximately by 10 times smaller than the lower limit (32) on $\tau_{\bar{n}n}$ deduced from Frejus experiment [13].

As it was pointed out in refs.[16-17] the proposed experiment on the search for free $n - \bar{n}$ oscillations at Oak Ridge can reach $\tau_{n\bar{n}}$ by 10 times larger than the limit given by (32).

I am grateful to L. B. Okun for useful remarks and Yu. Kamyshkov for useful discussions.

References

[1] V. A. Kuzmin, JETP Lett. 13, 335 (1970); K. G. Chetyrkin et al., Phys. Lett. 99 B, 358 (1981)

[2] R. N. Mohapatra and R. E. Marshak, Phys. Lett. 94B, 183 (1980)

[3] P. G. Sandars, J. Phys. G9, L161 (1980)

[4] Riazzuddin, Phys. Rev. D25, 885 (1982)

[5] C. B. Dover, A. Gal and J .M. Richard, Phys. Rev. D27, 1090 (1983) Phys. Rev. C31, 1423 (1985)

[6] W. M. Alberico, A. Bottino and A. Molinari, Phys. Lett. 114 B. 266 (1982)

[7] W. M. Alberico, A. De Pace and M. Pignone, Nucl. Phys. A523, 448 (1991)

[8] C. Y. Wong et al., Phys. Rev. C29, 574 (1984)

[9] L. D. Landau and E. M. Lifshitz, "Quantum mechanics" Nauka, Moscow 1974.

[10] V. I. Nazaruk, Phys. Lett. B337, 328 (1994)

[11] J. Carbonell and K. V. Protasov, J. Phys. G18, 1863 (1992)

[12] S. Tessaro, Ph.D. Thesis, University of Trieste, 1995

[13] Ch. Berger et al., (Fréjus collaboration) Phys. Lett. B240, 237 (1989)

[14] M. Takita et al. (KAMIOKANDE). Phys. Rev. D34, 902 (1986)

[15] M. Baldo-Ceolin et al., Z. Phys. C63, 409 (1994)

[16] Yu. Kamyshkov et al., Proc. of the 3d International Conference on Nucleon-Antinucleon Physics (NAN-95), Yadernaya Fizika N9-10 (1996)

[17] Yu. Kamyshkov, Talk at the Workshop on Baryon Instability Searches, Oak Ridge, March 1996.

A RECENT NEUTRON-ANTINEUTRON SEARCH EXPERIMENT AT ILL

D. Gibin
Dipartimento di Fisica "G. Galilei", University of Padova and
I.N.F.N. Sezione di Padova - Padova, Italy

Abstract

The experimental search for neutron-antineutron oscillations which has been recently completed at the ILL high flux reactor at Grenoble is described. In this research the most sensitive limit on the oscillation time has been established. The characteristic features of the experiment are described in some detail and their improvement for a better limit discussed.

1 Introduction

The stability of matter plays a very central one in our understanding of the fundamental interactions and is particularly intriguing because we really don't know any deep reason for it, while there are various hints suggesting that the baryon number B has only an approximate validity. The possibility of baryon number non conservation via an interaction characterized by $\Delta B = 2$, $\Delta L = 0$ can give rise to $n \rightleftharpoons \overline{n}$ mixing and consequently may induce $n \rightleftharpoons \overline{n}$ oscillations, which are described by an oscillation time $\tau_{n\overline{n}}$ and could take place via a first order process.

The underground proton decay type experiments were able to set the lower limit $\tau_{n\overline{n}} > 10^8 s$ [6] by using measurements of nuclear lifetime. In this case, however, the evaluation of $\tau_{n\overline{n}}$ depends on nuclear model assumptions [7]. It was also pointed out that, since the strength of the $n \rightleftharpoons \overline{n}$ transitions needs not be the same for free neutrons and neutrons bound in nuclear matter [8], the only model independent measurement of $\tau_{n\overline{n}}$ can come from experiments on free neutrons.

If the $n \rightleftharpoons \overline{n}$ oscillations are possible, an initially pure neutron state develops an antineutron component oscillating in time:

$$P(\overline{n},t) = \frac{\delta m^2}{\delta m^2 + \Delta E^2} \sin^2\left(\sqrt{\delta m^2 + \Delta E^2} \cdot t\right) \qquad (1)$$

where $\delta m = (\tau_{n\overline{n}})^{-1} \leq 6 \cdot 10^{-29}$ MeV [2] is the $n \rightleftharpoons \overline{n}$ transition energy and ΔE is half of the energy gap between the n and $\overline{n}$ states due to the external field perturbations, either nuclear or electromagnetic.

The transition amplitude attains its maximum for $\Delta E = 0$, i.e. when neutrons propagate freely, in absence of external forces. In this ideal case for $t \ll \tau_{n\bar{n}}$, the transition probability (1) becomes

$$P(\bar{n}, t) \simeq \left(\frac{t}{\tau_{n\bar{n}}}\right)^2 . \tag{2}$$

i.e. the antineutron component increases proportionally to t^2.

However neutrons in nature are not free and even in the case of artificially produced unbound neutrons which are propagating in vacuum (where $\Delta E_N = 0$) the tiny interaction with the earth magnetic field ($B \simeq .5$ Gauss) gives a strong suppression to the oscillation amplitude: $\Delta E_B \simeq 3.10^{-18} MeV$ implying an amplitude $\leq 10^{-22}$.

An important feature of the experiments using neutron beams consists in the fact that eq. (2) correctly describes the time evolution of the $\bar{n}$ component, provided that external field perturbations are reduced to such a level that

$$\Delta E \cdot t \ll 1. \tag{3}$$

The condition (3) is defined as the *quasi free condition* [9].

For a quasi free neutron beam the $\bar{n}$ component can be described in terms of the experimental parameters as follows:

$$\frac{\overline{N}}{\epsilon} = I\,T\,\left(\frac{1}{\tau_{n\bar{n}}}\right)^2 \left(\frac{L}{v}\right)^2 \tag{4}$$

where $\overline{N}$ is the number of detected antineutrons, ϵ is the antineutron detection efficiency, I is the neutron intensity, T the running time, L the propagation region length and v the neutron velocity. Eq. (4) shows explicitly that an experiment using free neutrons needs a very intense beam of slow neutrons, a long propagation region evacuated and well shielded against the B field , a well designed target, to annihilate the possible antineutrons of the beam, and a detector with large solid angle coverage and with good energy and space resolutions to unambiguously identify the sought for annihilation events.

Two previous experiments performed with neutron beams obtained, at the 90% C.L., the lower limits $\tau_{n\bar{n}} \geq 10^6$ s [4] and $\tau_{n\bar{n}} \geq 0.5 \cdot 10^6$ s [5]. The $N\overline{N}$ 2 experiment, described in the following, was designed to measure in a neutron beam the $n \rightleftharpoons \bar{n}$ oscillations for $\tau_{n\bar{n}}$ up to $\sim 10^8$s.

The beam had an integrated intensity of $3 \cdot 10^{18}$ neutrons/s with an average velocity $v \approx 600\ m\ s^{-1}$ and propagated for a time $t \simeq 0.11$ s in a region where residual pressure and magnetic field were maintained at the values required by the quasi free condition. The final antineutron detection efficiency was $\epsilon \simeq 0.5$. No antineutrons were detected during the experiment, which gave a limit of

$$\tau_{n\bar{n}} \geq 0.86 \cdot 10^8 \quad s \tag{5}$$

at 90 % C.L.

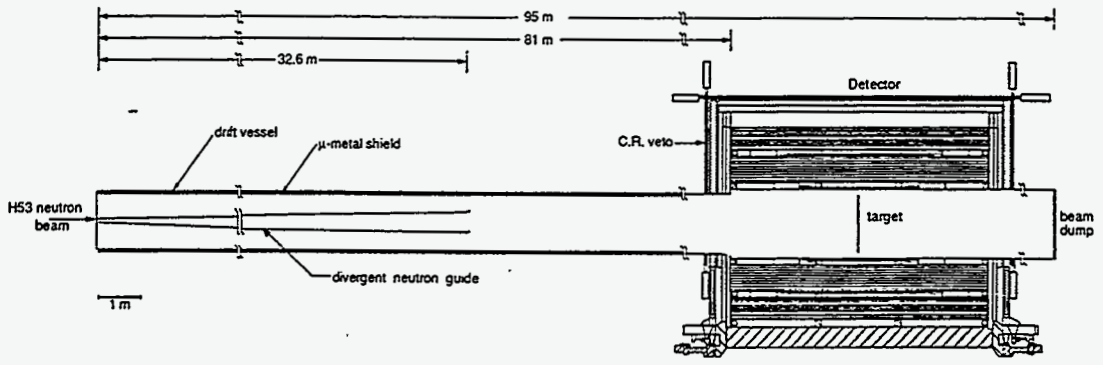

Figure 1: The $N\overline{N}$ experimental set-up

2 Experimental set-up

The experiment was realized at the 58 MW High Flux Reactor(HFR) at the Institute Laue-Langevin (ILL) in Grenoble, which could provide intense sources of slow neutrons. Figure 1 shows a sketch of the experimental set-up [2] [3].

The most severe constraints were the associated beam noise and the cosmic ray background.

2.1 Neutron source

The neutrons from the HFR were moderated to liquid D_2 temperature (25 K) at the Horizontal Cold Source and then injected in a system of neutron guides which transported them to the experimental area [10]. The neutron guides make possible to propagate intense neutron beams over long distances, while keeping practically constant the neutron beam intensity, cross-section and divergence with respect to the beam axis. The H53 line which was carrying the beam to the $N\overline{N}$ experiment was a sequence of totally reflecting neutron guides, ^{58}Ni coated, $63\,m$ long, $6\times12\,\mathrm{cm}^2$ cross-section. This system was slightly bent in order to eliminate γ's and fast neutrons coming directly from the reactor. The H53 neutron intensity was measured to be $I_0 \simeq 1.7\cdot10^{11}$ n s^{-1} [11]. The neutron energy spectrum and angular divergence are shown in figure 2 as a function of the wavelength λ. The neutron average wavelength was $\lambda \simeq 6.5\mathring{A}$ corresponding to an energy of $2\cdot10^{-3}$ eV and a velocity of 600 m s^{-1}. The average angular divergence with respect to the beam axis was 5.7 mrad, varying from 0 up to 40 mrad.

At the entrance of the $N\overline{N}$ beam line the neutron intensity was measured to be $I_0 \simeq 1.3\cdot10^{11}$ s^{-1}, while the beam properties, energy and divergence distributions, were measured to be practically unchanged after the exit of H53.

2.2 Neutron propagation region

The propagation region had to be carefully designed to allow an effective flight time $t \simeq 0.11$ s under the *quasi free condition* in a feasible way. First of all the drift vessel

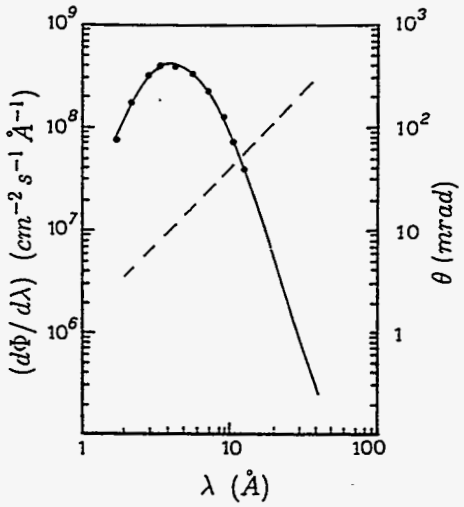

Figure 2: The neutron beam spectrum (full line) and the maximum neutron angular divergence (dashed line) as a function of the neutron wavelength λ.

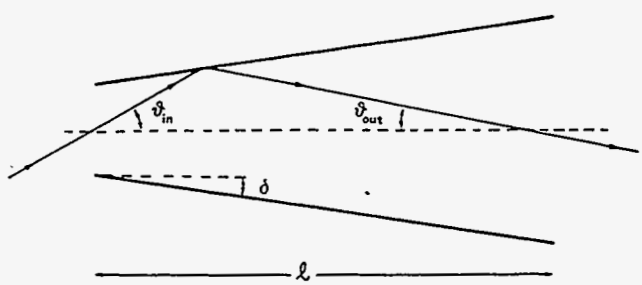

Figure 3: Effect of a reflection of a neutron on the divergent guide walls.

had to fully contain the neutron beam, otherwise the radiation coming from neutron captures on the walls would have produced an intolerable noise in the detector.

Given the H53 neutron divergence, the beam cross-section would have grown to a diameter of several meters at the detector. Therefore a system was devised which allowed to keep the neutron beam cross-section at the target within 1 m^2. It consisted of a straight beam guide with slightly divergent walls. Due to the wall divergence, δ, the neutron divergence was reduced, after each reflection, of 2δ [11] [12], see fig.3.

A Monte Carlo was developed to study the beam propagation and to design the divergent guide. The divergent guide was designed in order to optimize the effective propagation time, given the constraints on the total available length and on the beam dimensions at the target. Had it been possible to have a longer propagation region it would have been possible to squeeze the beam dimensions even more by using a longer less divergent guide. This had not been possible because of the presence of a nearby highway. The realized divergent guide reduced the neutron divergence by a factor of 2.7 on average (Fig. ??)[11] [12]. It consisted of 33 reflecting elements, coated with

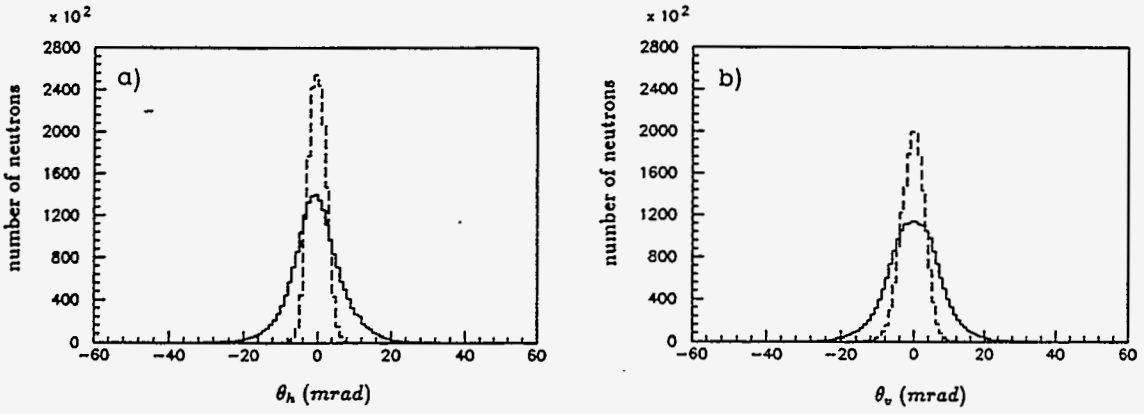

Figure 4: The distribution of the horizontal (a) and vertical (b) neutron angular divergence at the entrance (full line) and at the exit (dashed line) of the neutron divergent guide.

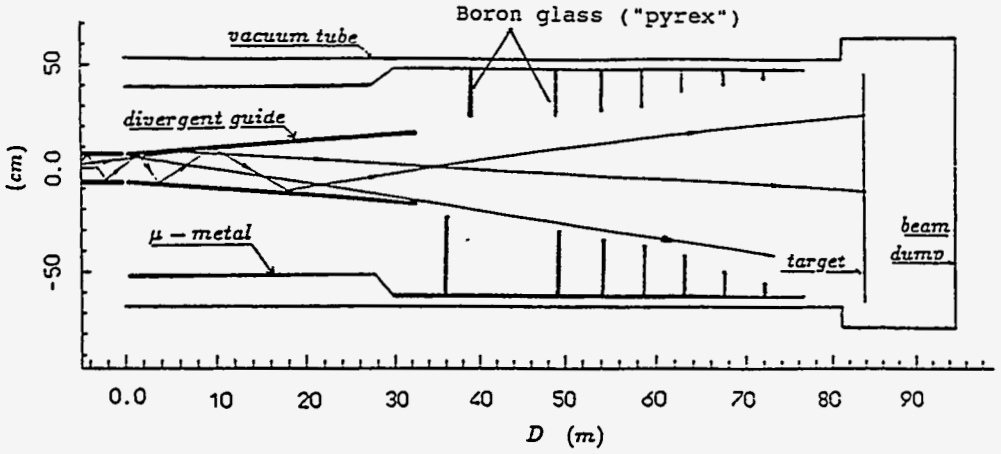

Figure 5: The quasi free propagation region.

with natural nickel. Each element, $1\,m$ long, with the walls at an angle $\delta = 3\,mrad$ with respect to the beam axis [11].

The oscillation region was a stainless steel drift vessel 81 m long, 1.2 m diameter, 0.5 cm thick. The divergent guide was installed inside the drift vessel at the neutron entrance. A passive μ metal shield was installed coaxially inside the drift vessel (see Fig. 5), in order to shield the oscillation region from the earth's magnetic field as well as from any other stray field. The following annihilation region of the drift vessel was an Al tube $5.6\,m$ long, $1.4\,m$ diameter and 0.8 cm thick. The antineutron annihilation target was suspended in the central part of the annihilation region. It consisted of a carbon foil $130\,\mu m$ thick and 110 cm diameter. The distance from the outer edge of the target to the wall - 15 cm - was chosen based on a M.C. study on the separation between events on the wall and those on the target. The main characteristics of

the target were: an annihilation probability for $\overline{n}$ larger than 99% [13]; a low Z to preserve the peculiar features of the annihilation events; a high transparency to the neutron beam and a mass of $\sim 180\,g$. The inner of the annihilation region was lined with ^6LiF, $2\,mm$ thick, to absorbed the neutrons scattered by the target [14].

The last part of the drift vessel, a stainless steel tube 7.8 m 0.5 cm thick, $1.4\,m$ diameter was closed by a stainless steel disk, covered with a 0.4 cm thick layer of ^6LiF and acting as an efficient neutron beam dump.

In their flight through the propagation region the neutron were bent downward by gravity. To compensate for this vertical displacement, the drift vessel was lowered with respect to the beam axis by 6.7 cm in the first part and 9 cm in the rest.

Measurements showed that only a very small fraction of the incoming neutron beam (2.5%) was lost along the divergent neutron guide. A further small fraction (2.7%) was lost along the drift vessel, after the divergent guide, due to the vertical fall of the free neutrons. To prevent these last stray neutrons from impinging on the walls eight rings of boron enriched glass were installed inside the drift vessel at different distances along the oscillation region. In this way this component of the beam produced a practically negligible noise level at the detector.

The neutron beam intensity was measured by gold foil activation in several positions along the beam line and was found in very good agreement with the M.C. calculations [15], [11].

The neutron intensity at the target was measured to be $I \simeq 1.25 \cdot 10^{11}$ s^{-1}. The full neutron beam was contained in the target, but a 10^{-3} fraction which flew directly to the beam dump.

2.3 The quasi free condition

The M.C. of the beam was used to evaluate the effective free neutron propagation time, taking into account of all the characteristics of both the beam and of the propagation region. In the computation it was assumed that, for each neutron, the useful length of free propagation was the distance travelled inside the shielded region starting from its last reflection on the divergent guide. The value of the effective time for neutron oscillation then was computed to be: $\langle t^2 \rangle^{1/2} = (0.109 \pm 0.002)\,s$. The $\overline{n}$ probability distribution foreseen by the MC on the target is shown in Fig. 6 [11].

To insure that the quasi free condition (3) be satisfied by the whole neutron beam, it was evaluated that the residual gas pressure in the propagation region had to be constrained [16] to the value $p_{res} < 10^{-2} Pa$. During the experiment two turbomolecular pumps maintained $p_{res} \simeq 2 \cdot 10^{-4} Pa$ in the whole drift vessel.

Moreover, to fulfill the condition (3), the oscillation region had to be shielded against any magnetic field: the required suppression of the Earth's magnetic field was of the order of 10^{-3}. The screening of the field was obtained by means of a passive mu-metal shield (76 m long, 1.1 m diameter and 1 mm thick), very effective in reducing the transverse field component, and of an active shield (a 80 m long solenoid wound around the vacuum pipe) to screen the longitudinal component of

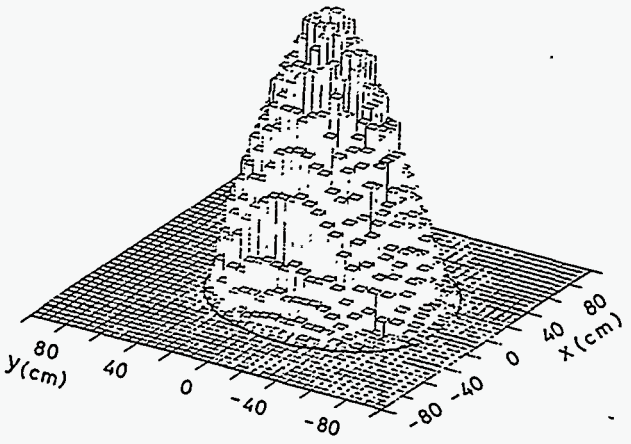

Figure 6: The expected $\overline{n}$ distribution on the target.

the field [17]. The residual magnetic field was measured to be $B < 10$ nT over the full length but sudden short variations around the mu-metal junctions. The field was continuously monitored during the experiment and twice a day it was measured over the full length. The efficiency for the quasi free condition defined as [17], [18]

$$\eta = \frac{P(\overline{n}, t, B)}{P(\overline{n}, t, B = 0)} \tag{6}$$

had an average value during the experiment $\langle \eta \rangle = (0.984 \pm 0.003)$.
The residual magnetic field was also directly checked by using the neutrons as magnetic probes, with the "neutron spin magnetometry" method described in [19] and found in excellent agreement with the other measurements.

2.4 The detector

The $\overline{n}$ -annihilation detector (Fig. 7) was organized in four quadrants around the target and covering a solid angle $\Delta\Omega/4\pi = 0.94$. It was a tracking device composed of limited streamer tubes (LSTs) ($0.9 \times 0.9 \times 500 cm^3$) [20] and scintillation counters (SCs).

The detector was composed of three sections: a vertex detector, a SC hodoscope and a calorimeter. The vertex detector closer to the target was the inner part. It was made of 10 LST planes supported by Aℓ honeycomb plates 2 cm thick. Its average density, $\rho = 0.3\, g\, cm^{-3}$, together with the high track sampling made it possible to measure the directions of the charged particles produced in the $\overline{n}$ -annihilation events.

The SC hodoscope on one side provided the fast signals for the first trigger level via a specially designed mean timer [21], and on the other allowed to measure the time of flight (TOF) of the particles. A layer of SC $2\, cm$ thick, $21\, cm$ large, equipped with light guides and photomultipliers (PMT) at both ends, were placed in front and on the back of the vertex detector. The inner SC's were $210\, cm$ long, the outer ones $300\, cm$ long, and covered a solid angle $\Delta\Omega/4\pi = 0.8$ around the annihilation

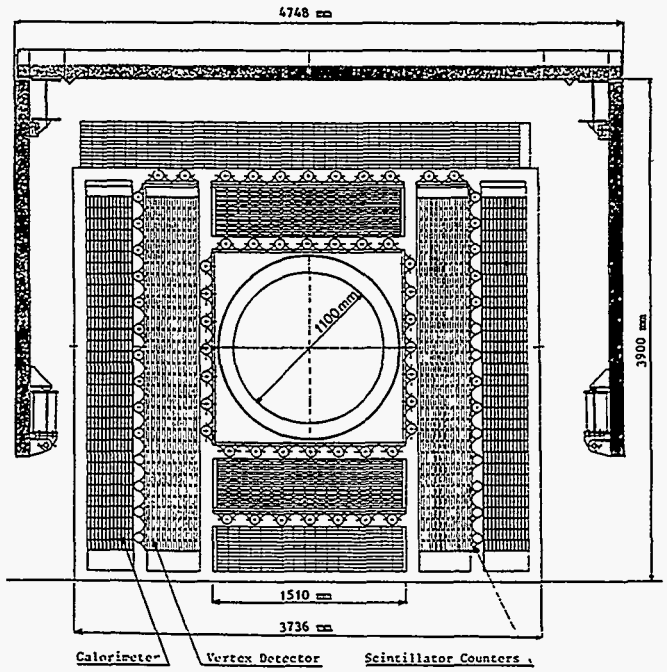

Figure 7: The $\overline{n}$ -annihilation detector (cross-sectional view)

target. The TOF was used primarily to discriminate genuine $\overline{n}$ -annihilation events, in which all the particles travel from the inner to the outer planes, against events due to neutral cosmic rays, in which a particle can fly towards the target from the outer to the inner SC. MC simulations of $\overline{n}$ -annihilation events (see below) showed that with TOF resolution $\sigma_{TOF} = 700\,ps$ the requirement of the right TOF sign would have rejected only 0.2 % of the annihilations. During the experiment the TOF resolution was regularly monitored with cosmic ray (C.R.) muons and found $\sigma_{TOF} \sim 600\,ps$. The time stability and accuracy was checked once per day by flashing the scintillators with short ($\Delta t = 200\,ps$) laser light pulses. Both the day by day check and the comparison between laser and C.R. timing allowed the timing stability at the $150\,ps$ level during the whole experiment [22] to be maintained.

The third part of the detector was a calorimeter. It was placed behind the external scintillator layer and consisted of 12 LST planes alternated with planes made of *Al-Pb-Al* sandwiched plates, 0.3-0.2-0.3 cm thick respectively.

The streamer signals on LST were collected by x and y pickup strips and read out by 32 channels digital cards. More than 60000 electronic channels were implemented. The read-out control and data compression were carried out by a specially designed CAMAC module (STROC) [23]. The LST system was continuously monitored and the percentage of disconnected streamer tubes never exceeded the 2% level.

An active veto shielding against charged Cosmic Rays completely overlayed the detector. The C.R. veto was made of 235 plastic SC's covering a total area of $95\,m^2$. To improve the geometrical veto efficiency as well as to reject C.R. induced high energy showers produced in the detector, a part of the SC's, covering an additional area of

5×4 m^2, was placed below the 80 cm concrete platform supporting the detector. Each veto counter was equipped with two light guides and two PMTs, whose signals, in order to reduce the dead time of the experiment, were processed by mean timers of the type mentioned above. The veto system was continuously monitored and the dead time measured by a dedicated processor [24].

Moreover, to shield the apparatus against neutral C.R., a passive veto was placed between the calorimeter and the veto counters, which was also designed to prevent possible autovetoing of $\overline{n}$ annihilation event. It consisted of planes of lead, $10\,cm$ thick, canned into boxes of stainless steel chosen to avoid magnetic field distortions.

3 Trigger and data acquisition

The first trigger level was provided by a coincidence of an inner and an outer SC on the same detector quadrant, in anticoincidence with the C.R. veto counters. It was expected to have an efficiency $\epsilon_{trig} = 0.8$ for $\overline{n}$ -annihilation events in the target. However the noise due to neutron captures in the annihilation target was too high [14]: bout $1MHz$ of counts in the SC inner shell and $\sim 2000Hz$ for this first trigger. Consequently it had to be enforced by the following requirements, compromising between efficiency and acceptable trigger frequency [25]:

a) At least one charged track crossing the same vertex detector quadrant in which the SC coincidence occurred. A charged track was defined by a coincidence of signals from at least 4 out of 10 LST planes. This requirement reduced the trigger rate to $\simeq 800$Hz.

b) At least one SC firing in another quadrant, and in addition at least a second track in the detector, either in the vertex detector or in the calorimeter, reducing the trigger rate to $\simeq 6$Hz.

c) A total number of hits $N_h \geq 120$ recorded in the full LST detector. This requirement was introduced in order to eliminate spurious triggers due to random superposition of beam associated noise in the detector. For this purpose a hardware adder was properly designed and constructed [26].

The trigger rate was 4 Hz. A sizable fraction, $\simeq 32\%$, was found to be due to spurious trigger, originated by the high level of the radiation associated with the beam, and were discarded. Of the remaining 2.7 Hz, 2.4 were due to C.R. muons traversing the apparatus which did not trigger the veto. The C.R. veto inefficiency was measured to be lower than $\sim 5 \cdot 10^{-3}$. Finally ~ 0.3 Hz were due to cosmic neutral particle interactions in the detector.

In order to determine ϵ_{trig}, a sample of 10^4 $\overline{n}$ -annihilation events were generated in the target through a M.C.. It was found $\epsilon_{trig} = 77\%$.

The trigger status was continuously monitored and the counting rates were recorded during every experimental run.

The data acquisition system [27] was based on a DEC MicroVax II computer inserted in a Local Area Vax Cluster environment together with 4 workstations to execute on-line monitor, event display and off-line analysis.

The dead time fraction for the trigger and data acquisition system was 1.2% due and 5% for the veto system.

4 Data Analysis

The experiment was taking data from August 1989 to April 1991 when the data taking was ended by the ILL reactor breakdown. The effective running time was $T = 2.4 \cdot 10^7 s$, the number of useful events was $6.8 \cdot 10^7$.

In order to study the C.R. event frequency and configuration, data were taken during $\sim 10^6$ s with the neutron beam off, obtaining a trigger rate for neutral interaction events of 0.3 Hz, in excellent agreement with the trigger rate obtained during the $n \rightleftharpoons \overline{n}$ runs. In addition, the comparison of the C.R. events produced during beam on and beam off periods provided a detailed analysis of the beam associated noise. To disentangle the sought for $\overline{n}$ signal the events were required to have

i) vertex inside the annihilation target,

ii) visible energy between 1 and 2 GeV,

iii) energy and momentum isotropically distributed,

These selection criteria were implemented in the analysis in two subsequent phases: software filter and final analysis.

4.1 Simulation of the annihilation event

A special M.C. program was developed for the analysis (MCA)[28]. In this program $\overline{n}$-annihilation events were generated in the target, according to the characteristics of the $\overline{n}$ annihilation in Carbon. The tracks of the produced particles were simulated inside the detector, taking into account the particle and the measured detector properties.

The streamer tube response to charged tracks was modelled using the measured hit multiplicity distributions on LST planes, measured with atmospheric muons crossing the apparatus at different incidence angles. In addition the vertex detector as well as the calorimeter detector response to electromagnetic showers, determined by measuring a sample of π^0 produced in the detector , was used in the MCA event simulations [29] The SC energy threshold and time resolution, experimentally measured, were also included in the MCA.

A sample of 10000 events simulated by the MCA were translated to a format identical to the experimental one. Moreover randomly distributed hits on LST's and on SC's, due to the beam associated noise as measured in the experimental events, were properly associated to each MCA event. The MCA events were finally processed through all the filters and analysis programs used for the experimental events.

4.2 Software filter

The $6.8 \cdot 10^7$ triggers went through a software filter [30], where the selection criteria were applied in the sequence described below. This sequence was chosen to minimize the global computer time needed for event selection.

a) *The event visible energy.* This criterion was chosen with the twofold purpose of discarding most of the C.R. events: neutral interactions as well as muons passing through the apparatus. In both cases the average energy deposition in the detector was smaller than 1 GeV.

A careful experimental analysis was performed in order to estimate the event visible energy by means of the measurement of N_h: the event number of hits on the LST after subtraction of the isolated hits, randomly generated by neutron beam noise. The experimental correlation between N_h and energy was then compared and found to be in very good agreement with the correlation N_h-energy of the pions produced in MCA generated events. Subsequently a relation between E_{vis} and N_h for the events was determined by averaging over the MCA generated events. As a result the relation $E_{vis} = (185 + 2.2N_h)MeV$ was determined within a 20 % accuracy. On this basis, it was decided to select events with $N_h > 300$ namely $E_{vis} > (850 \pm 170)MeV$.

Furthermore, the barycenter of hits was determined for each event and events were accepted if in the cross sectional view, orthogonal to the beam axis, they were inside a circle of radius $r = 80$ cm, centered in the center of target. For the $\overline{n}$ - annihilation events the hit barycenter practically coincided with the event vertices. In addition, events consistent with a single straight track traversing down the detector, were identified as crossing muons and discarded. It turned out that 90 % of the $6.8 \cdot 10^7$ collected events did not satisfy these requirements. On the contrary, 85 % of the MCA generated events had $N_h > 300$ and the hit barycenter in the region chosen, and only 0.7% of them satisfied the single straight track hypothesis.

b) *Time of flight.* SC signals not associated with charged tracks were disregarded as due to the beam related noise. The average value of the inner SC's, $\langle T_{SC} \rangle_{in}$, as well as the average value of the outer SC's, $\langle T_{SC} \rangle_{out}$, were computed. Events were rejected when at least one SC time was 2.5 ns away from the average.

The MCA generated events which satisfied the previous selection criterion were analyzed in the same way and the value of
D = $(\langle T_{SC} \rangle_{out} - \langle T_{SC} \rangle_{in})$ was calculated for each event. It was then determined that value D was well inside the region $0 < D < 5$ ns for all but a 4%. With this requirement 16.4% of the events were retained, with an efficiency for $\overline{n}$ -annihilation event detection of 96%.

c) *Event Vertices.* A pattern recognition routine was used to identify the particle tracks of each event and to determine the coordinates of their vertex. Events were retained if they had at least three tracks and vertex inside the region defined by the coordinates $R = (x^2 + y^2)^{1/2} < 60$ cm, and $|z| < 32$ cm (x=y=z=0 were the coordinates of the target center).

In order to test the quality of this procedure as well as the efficiency for $\overline{n}$ - annihilation detection, the vertices of several thousand experimental and MCA gen-

erated events were measured by a physicist with an interactive program and then compared with those provided by the pattern recognition routine. The agreement was good with the exception of a small fraction of events, about 10%, which had one or more particles interacting in the detector or which were incorrectly associated with a crossing particle.

In addition, since the event tracks were expected to be isotropically distributed, events were accepted if their tracks projected in the cross sectional plane orthogonal to the beam axis were contained inside an angle larger than 170°. The event vertex requirements were satisfied by 1.2% of the experimental events, and by 90% of the MCA events.

At the end of the software filter analysis, $1.2 \cdot 10^4$ events were left, corresponding to $1.8 \cdot 10^{-4}$ of the original sample. The efficiency of this procedure was $\epsilon_{filter} = 0.72$. Table 1 displays the effects of the various criteria on the experimental and on the MCA events.

Table 1: Percentages of experimental and simulated events selected by the filter criteria sequentially applied.

Filter requirements	% of accepted events	% of accepted MonteCarlo
Energy	10.0	85.0
TOF	16.4	96.0
Vertex	1.2	89.0
TOTAL	0.018	72.0

4.3 Final analysis

The events surviving the filter chain were visually inspected in two independent scannings. 100 MCA generated events were mixed with the $1.2 \cdot 10^4$ events in order to estimate the scanning efficiency for $\overline{n}$ annihilation, which resulted to be $\epsilon_{scan} = 98\%$.

Most of surviving events were C.R. muons crossing the apparatus, with an associated electromagnetic activity, or events in which the vertex was incorrectly reconstructed. The scanners were instructed to recognize and reject these events.

After the visual inspection 403 events were left. These events were accurately examined by physicists: particle tracks were reconstructed and the times recorded by PMTs were considered: 68 events, clearly induced by incoming charged C.R., were disregarded.

The vertices of the 335 remaining events were then reconstructed with an interactive program.

To evaluate the quality of the measurement, a sample of 250 experimental events was measured, chosen in the vicinity of the target, with the vertices on the beam tube, in the region where the tube was isolated from the SC planes. It turned out

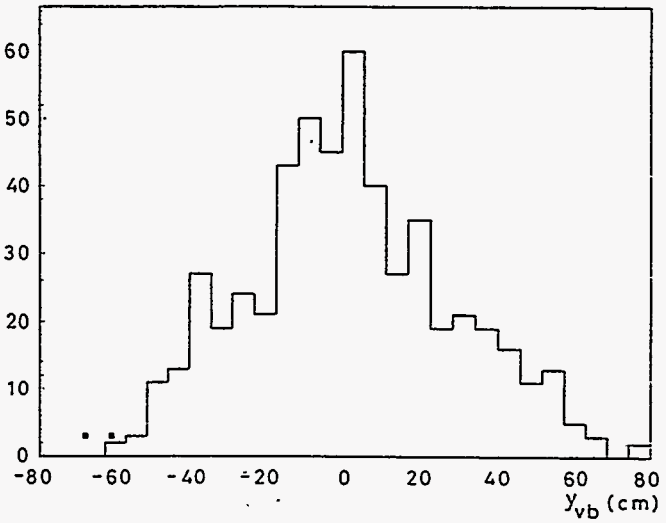

Figure 8: Distribution of the difference between the vertical coordinates of vertices and the barycenter of the hits for the MCA events (histogram) and the two experimental events(black squares)

that the resolution on R, measured in the detector plane orthogonal to the beam axis was ± 3.8 cm. The same type of measurement was performed on a sample of 200 MCA events, which had been accepted by the previous selection criteria. They provided a resolution on R of 4.5 cm, in very good agreement with the resolution of the experimental events; furthermore the z coordinate of the 200 MCA events was measured with a resolution of 4.2 cm.

According to these results it was then required that $\overline{n}$ -annihilation candidate event vertices satisfy the conditions $R \leq 55cm$ and $\mid z \mid \leq 15cm$.

Only 5, out the 335 remaining events, satisfied these conditions.

The visible energies of the 5 remaining events were measured directly. The track lengths were measured, π^0 were reconstructed and then the event energies were properly evaluated. Three events, which turned out to have a visible energy $E_{vis} < 800$ MeV, were disregarded. The remaining 2 events were rejected on the basis of the isotropy requirements. The barycenter of their hits lay far below their vertices, a characteristic of the C.R. interactions. The MCA $\overline{n}$ -annihilation event sample, satisfying the previous requirements, showed that the distribution of the difference y_{vb} between the vertical position of vertex and hit barycenter was peaking at 0 and greater than -60 cm, see Fig. 4.3 . The y_{vb} values of the two remaining events from the final sample were measured and found $y_{vb} < -60$ cm. The events were then discarded as due to C.R. interactions.

250 MCA generated events, surviving the previously defined filter, were processed together with the 335 experimental events in order to determine the efficiency of this procedure for the detection of $\overline{n}$ -annihilation events, which resulted to be 97%.

Thus the overall efficiency ϵ for $\overline{n}$ annihilation detection was:

$$\epsilon = \epsilon_{trig} \cdot \epsilon_{filter} \cdot \epsilon_{analysis} = 0.52 \pm 0.02$$

5 The present limit on $\tau_{n\overline{n}}$

Table 2 summarizes the experimental data.
No candidate $\overline{n}$ -annihilation was found in $2.4 \cdot 10^7$ s running time, and the lower limit for $\tau_{n\overline{n}}$

$$\tau_{n\overline{n}} \geq \left(\frac{I\,T\,(1-d)\,\langle\eta\rangle\,\epsilon\,\langle t^2\rangle}{\overline{N}} \right)^{1/2} = 0.86 \cdot 10^8 s \qquad (7)$$

was set at 90 % C.L..

Table 2: Experimental data

I, neutron intensity	$(1.25 \pm 0.06) \cdot 10^{11}\, s^{-1}$
$\langle t^2 \rangle^{1/2}$, neutron "quasi free" propagation time	$0.109 \pm 0.002\, s$
T, effective running time	$2.40 \cdot 10^7\, s$
d, experimental dead time	6.2%
$\langle\eta\rangle$, "quasi free" condition efficiency	0.984 ± 0.003
ϵ_{trig}, trigger efficiency	0.77
ϵ_{filter}, filter efficiency	0.72
$\epsilon_{analysis}$, analysis efficiency	0.95
ϵ, $\overline{n}$ detection efficiency	0.52 ± 0.02
$\overline{N}$, number of candidate events	0 (2.3 at 90 % C.L.)

6 What next?

We have discussed the situation on the $n \rightleftharpoons \overline{n}$ search as it is at the moment. Now we want to what are the parameters to work with in order to reach a better sensitivity. As it was said in the introduction the $n \rightleftharpoons \overline{n}$ oscillation sensitivity depends on: the neutron intensity I, the length of the propagation region L, the neutron velocity v, the $\overline{n}$ detection efficiency ϵ and the running time T. The last two parameters depend mostly on on the quality of the detector: a point which we recommend for the detector is the reconstruction of the tracks and of their direction of flight, i.e. a good granularity and a sensitive TOF in order to keep under control the background. The sensitivity depends on the square root of I: certainly increasing I is very important, however a lot of care has to be put on the reduction of the natural background coming with the neutrons themselves. The sensitivity depends linearly on L and is inversely proportional to v. L has to be taken as long as possible, in general is fixed by external conditions. In order to have the maximum sensitivity, once fixed the total length, it is not possible to disentangle in a simple way the length and the divergence of the

divergent guide as well as the value of the neutron velocity, but the three parameters have to be optimized at once. In this evaluation it is worthwhile to remind that the background is proportional to the material in the detector (beam cross section) and the noise is proportional to the neutron halo (I and L); at the same time gravity plays a not negligible role for long propagation times.

References

[1] For a review, see: R.N. Mohapatra, NUCL. INSTR. AND METH. *A*284, (1989) 1.

[2] M. Baldo-Ceolin et al., PHYS. LETT. 236*B*, (1990) 95.

[3] M. Baldo-Ceolin et al., Z. PHYS. *C*63, (1994) 409.

[4] G. Fidecaro et al., PHYS. LETT. 156*B*, (1985) 122.

[5] G. Bressi et al., Z. PHYS. 43*C*, (1989) 175.
G. Bressi et al. IL NUOVO CIMENTO 103*A*, (1990) 731.

[6] K. Nakamura, *"Proceed. of the 25th International Conference on High Energy Physics"* , Singapore (1990), pg. 281, and bibliography therein

[7] C.B. Dover, A. Gal and J.M. Richard, PHYS. REV. *C*31, (1985) 1423.
W.M. Alberico, A. De Pace and M. Pignone NUCL. PHYS. *A*523, (1991) 488. and bibliography therein

[8] P.K. Kabir, PHYS. REV. LETT. 51, (1983) 231.
J. Baseq and L. Wolfenstein, NUCL. PHYS. *B*224, (1983) 21.
P.K. Kabir and J.Noble, Univ. of Virginia - Preprint (1989).

[9] M. Baldo-Ceolin, Proceed. of the "Conference on Astrophysics and Elementary Particles: Common Problems", Accademia Nazionale dei Lincei", Roma (1980) 251.
R.E. Marshak and R.N. Mohapatra: Phys.Lett. 94B (1980) 183.

[10] P. Ageron: NUCL. INSTR. AND METH. *A*284, (1989) 197.

[11] T. Bitter et al, NUCL. INSTR. AND METH. *A*321, (1992) 284.

[12] A. Guglielmi: Progress in Nuclear Energy, Vol. 24, (1990), 429.
T. Bitter, Ph.D. thesis, Heidelberg, 1989.

[13] See e.g. "Physics at LEAR in the ACOL Era", ed. U. Gastaldi et al., Ed. Frontieres, Gif-sur-Yvette, France (1985).

[14] F. Eisert et al. , NUCL. INSTR. AND METH. *A*313, (1992) 477.

[15] A. Guglielmi, Nucl. Instr. and Meth. A325, (1993) 241.

[16] G. Costa and P. Kabir, PHYS. REV. *D28*, (1983) 667.

[17] T. Bitter et al., NUCL. INSTR. AND METH. *A309*, (1991) 521.
W.Lippert, Ph.D. thesis, Heidelberg, 1990

[18] U. Kinkel, Z. Phys C54, (1992) 573.

[19] T. Bitter and D. Dubbers, NUCL. INSTR. AND METH. *A239*, (1985) 461.
U. Schmidt et al., NUCL. INSTR. AND METH. *A320*, (1992) 569.
P. El-Muzeini, Ph.D. thesis, Heidelberg, 1991.

[20] E. Iarocci, NUCL. INSTR. AND METH. *A217*, (1983) 30.

[21] A. Cavestro et al., NUCL. INSTR. AND METH. *A305*, (1991) 488.

[22] M. Baldo-Ceolin et al. Nuovo Cimento A105, 1679 (1992).

[23] A. Cavestro et al., NUCL. INSTR. AND METH. *A313*, (1992) 571.

[24] G.L. Raselli, Ph.D. thesis, Pavia, 1991.

[25] M. Baldo-Ceolin et. al, IEEE TRANS. ON NUCL. SCI. 38 – 2, (1991) 471.

[26] A. Cavestro et al., *"A fast trigger processor for limited streamer tubes"* , NUCL. INSTR. AND METH. *A364*, (1995) 328.

[27] M. Mezzetto, Ph.D. thesis, Padova, 1986.

[28] D. Gibin, Ph.D. thesis, Padova, 1989.

[29] E. Brunello, Degree Thesis, Padova 1990.
M.Genoni, Ph.D. thesis, Pavia, 1991.

[30] D. Gibin et M.Mezzetto *"A software filter for the $n\overline{n}$ experiment"* , DPFH /92/$N\overline{N}$ /1, Padova, 1992.

PRESENT AND FUTURE NEUTRON SOURCES

Colin D. West
Neutron Sciences Program
Oak Ridge National Laboratory
Oak Ridge, Tennessee 37831, USA

ABSTRACT

The main types of neutron source that might have the right characteristics (including a large source area and a high neutron flux) for n-nbar experiments are described, and the characteristics of some existing and planned examples are given. Overall, reactors (either steady-state or pulsed) look more attractive than accelerator-driven sources. New ideas for very cold and ultracold neutron sources may have significant implications for future experiments.

Overview of High Intensity Neutron Sources

Table 1 shows the main options for high flux neutron sources, with an example of an existing or proposed facility of each type. The highest total production rate, by far, from any existing type of source is associated with fission reactors. For many experiments, the time-averaged neutron flux (neutrons per square centimeter per second) is a more important parameter than overall production, and here again reactors lead among the existing sources. However, some experiments can take advantage of the high instantaneous neutron flux found at the pulsed spallation neutron sources. In such cases, one should also seriously consider the merits of pulsed reactors, which have, at present, much higher peak neutron fluxes than any spallation source. The advantage of the spallation sources is that they can produce a shorter pulse of neutrons (e.g., a typical spallation source may have a thermal neutron pulse width of the order of tens of microseconds, whereas even the most specialized of pulsed reactors (the IBR-II) gives a 300-μs pulse, and millisecond durations are more usual). Furthermore, delayed neutrons from the fission process give rise to a higher background between pulses from a reactor than from a spallation source. It is not clear, however, that there is any advantage to the shorter pulse for any of the n-nbar experiments that have been discussed.

The next sections discuss and compare the neutron source types that are, or may soon be, available.

High Flux Steady-State Reactors

Table 2 lists the seven reactors with a steady thermal neutron flux of more than 5×10^{14} $cm^{-2} \cdot s^{-1}$ available outside the core (reactors with a very high flux only inside the core would not seem to be suitable for the n-nbar experiments that have been proposed so far).

These reactors all operate at a fairly high power level, meaning there are many fissions taking place and therefore many neutrons being produced. They also have compact cores, so that these neutrons leave the core through a rather small area, leading to a high flux.

Another matter of importance is the area of the beam that might, in principle, be available, and Table 2 also gives the area of the existing, planned, or possible beams.

Table 1. High flux neutron sources

Typical parameters (approx.)			Examples					
Source type (material)	Net neutron production per particle or event	Heat deposition, MeV/neutron	Facility	Power,[a] MW	Average net neutron production rate (10^{16} s^{-1})	Max. flux 10^{14} $cm^{-2} \cdot s^{-1}$ Average	Peak	Notes
Photoneutron (W)	.03/electron	~3,000	ORELA	.06	~.01			Peak production rate is 5×10^{18} s^{-1}
Nuclear stripping (D-L)	.05/deuteron	~1,000	IFMIF[b]	10	~10	20	20	Conceptual design only. Unmoderated flux. Very small volume (~100 mL) of high flux
Fission (^{235}U)	1.4/fission	~125	ILL	57	~300	14	14	Thermal flux in reflector
Spallation (Ta, 1 GeV)	20/proton	~25	ISIS	0.2	~1	.015	15	Equivalent 4π thermal flux at moderator surface
Fusion (D-T)	1/reaction	~3	ITER[b,c]	1,500[b]	~50,000	~10		~10 Unmoderated flux at first-wall and blanket

[a]In the case of the fission reactor, thermal power is quoted. The utility electrical power input to a research reactor facility (for coolant pumps, HVAC, etc.) is typically a few percent of the thermal power. For beam devices, the beam power is quoted: utility electrical input is typically a few times the beam power.

[b]Conceptual design only.

[c]During 1000-s pulse.

Table 2. Research reactors with accessible high flux for external experiments

	Peak thermal flux in reflector region, 10^{14} cm^{-2} · s^{-1}		Peak thermal flux at beam tube or thimble nose, 10^{14} cm^{-2} · s^{-1}		Area of beam tube or thimble, cm^2	Notes
	Unperturbed	Perturbed	Unperturbed	Perturbed		
HFIR (100 MW)	17	15	15	12	80	Present beam tubes
"	"	"	"	"	150	Upgraded[a] HB-2,-3, or -4
"	"	"	16	<14[b]	130-730	Upgraded[c] HB-2 beam tube
ILL	14	—	11	—	80	Beam tube
"	"	—	10	—	450	Vertical cold source thimble
SM-2/-3	18		>5	—	~60	
BR-2	5		0.5		730	
HFBR (60 MW)	11		~8	~4	60	Present beam tube
"			~6	—	1000	Upgraded cold source thimble
PIK[d]	*13*		*12*	—	*100-500*	*Tubes up to 25 cm diam. can be fitted*
	"		*3.5*	—	*~300*	
FRM-II[e]	*8*					*Vertical cold source*

[a]Diameter increased from 4 in. to 5 1/2 in., 100 MW.

[b]Perturbed flux at 4 in. beam tube is 14 x 10^{14} cm^{-2} · s^{-1}, but the larger beam tube would perturb the flux by an additional, unknown amount.

[c]Diameter increased to 12 in., 100 MW.

[d]Under construction.

[e]Design phase.

Pulsed Reactors

If n-nbar experiments can be devised that take advantage of the peak flux, rather than the time-averaged flux, of a neutron source, then pulsed sources would be interesting. For example, if a pulsed source of ultracold neutrons were constructed, it would be possible in principle to fill a storage vessel to almost the same time-average flux as the peak flux in the pulse (although this has not been fully demonstrated in practice). The value of such a device would depend, in part, on the extent to which the neutron oscillation clock is reset at each reflection. Perhaps other kinds of experiments can also be devised to make use of the time structure of pulsed sources.

TRIGAs are generally small (few megawatt) reactors, with tremendous safety margins, and with inherent safety during reactivity and power transients because of an enormous negative temperature coefficient of reactivity. This is put to good use in pulsed TRIGAs that are able, for some milliseconds, to reach gigawatt power levels three orders of magnitude higher than their long-term heat removal capability. During the pulse, of course, the instantaneous neutron flux can be very high—more than 100 times greater than the steady-state reactors discussed in the previous section.

TRIGAs are usually pulsed at less than 1 Hz, but W. L. Whittemore[1] has proposed a scheme that would give 25 Hz to 50 Hz pulses with a peak thermal neutron flux at the beam tube nose of up to 8×10^{15} $cm^{-2} \cdot s^{-1}$, with a pulse width of a few milliseconds. This is an exciting, low cost concept.

In addition to TRIGAs, two special purpose reactors, TREAT (now shut down) in the United States and CABRI in France, were built for nuclear safety research into the effects of large reactivity transients. At Dubna, Russia, a very specialized liquid sodium-cooled, fast reactor, with a rotating reflector was designed and built specifically to provide short pulses of thermal and cold neutrons for beam experiments.

General characteristics of these pulsed reactors are shown in Table 3.

Pulsed Spallation Sources

In these sources a beam of protons, usually at approximately 1 GeV, in pulses typically ~1-μs wide, is fired into a high-Z target. The primary particles collide with nuclei, which are left in an excited state from which neutrons, protons, and pions "evaporate" with high energy: this is the spallation process. These secondary particles, in turn, go on to strike other nuclei, inducing further spallations.

The total yield of neutrons can be increased by using a fissionable target material such as ^{238}U or a fissile material such as ^{235}U in a subcritical assembly. However, such targets involve much greater heat deposition per neutron produced (see Table 1), so that power densities are high and heat removal is a problem. Also, the release of delayed neutrons from the fission process raises the background in between pulses. The cladding and extra coolant needed effectively dilutes the fissionable or fissile material. Finally, fissile targets in particular raise greater regulatory and safety concerns.

ISIS used a ^{238}U target at one time, yielding about twice as many neutrons per proton as a heavy metal nonfissionable material. However, irradiation damage led to target failures, and they switched to tantalum. IPNS retrofitted a fissile, subcritical enriched uranium booster target in place of their ^{238}U design and found a 2-1/2-fold increase in flux in a typical beam (i.e., after moderation), with a tolerable background.

In order to maintain the narrow pulse width that is the selling point of spallation sources, the neutron moderators must be physically small (~cms), because in a larger moderator the slow moving, thermalized neutrons would be spread out in time. This is

Table 3. Pulsed reactors with a peak thermal neutron flux greater than 5×10^{16} cm$^{-2} \cdot$ s^{-1}

Facility name	Ave. power, MW	Peak power, GW	Φ_{th} Ave., 10^{14} cm$^{-2} \cdot$ s^{-1}	Φ_{th} Peak, 10^{16} cm$^{-2} \cdot$ s^{-1}	Type	Location
GA-TRIGA F	1.5	6	0.4	19	TRIGA-F	USA
CABRI	20	20	1.9	15	Pool	France
Pitesti	0.5	22	0.06	10	TRIGA-II[a]	Romania
NSRR	0.3	23	.013	10	TRIGA	Japan
TREAT[b]	.08	18	.004	10	Graphite	USA
KAERI	2	2	0.7	6	TRIGA-III	S.Korea
IBR-II	2	15	0.5	1[b]	Special!	Russia
University	0.1-1.5	1-7	0.1-3	1-10	TRIGA reactors	USA

[a]Dual core.
[b]This is the flux at the surface of an external, short pulse (320 μs) light water moderator.

even more true for the cryogenic moderators of a cold neutron source. Often, neutron absorbers are included in or around the reflectors and moderators to shorten the pulse further. As a result, typically only 10—20% of the neutrons entering the moderator are accessible, even in principle, to the beam tubes or guides. Systems with poisoning, for pulse shortening, are said to be "decoupled" and give much shorter pulses, but lower flux, than others.

Table 4 gives some characteristics of existing pulsed spallation sources. The peak and time-averaged fluxes are much lower than the ones listed in Table 3 (but the pulses are shorter and more frequent). Several planned or proposed new machines are listed in Table 5. The European Spallation Source (ESS) and the long-pulse concept would be comparable in average and peak flux to the existing reactors of Table 3. The pulse repetition frequency (PRF) would be much higher than any existing reactor, and similar to Whittemore's concept; however, it is not clear that this parameter is relevant to the n-nbar experiments.

Overall Comparison of Pulsed and Steady-State Sources

Figure 1 is a very simplified comparison of the existing and proposed reactors and spallation sources on the basis of two parameters only—peak and average flux. Existing reactors, pulsed and steady-state, offer higher fluxes by both measures than existing spallation sources. Proposed new spallation sources would approach the peak and average flux of the existing pulsed reactors, but not the average flux of the steady-state reactors.

Table 4. Existing pulsed spallation sources

Facility name	Beam power, kW	Target	PRF, Hz	Φ_{th}[a] Ave, 10^{14} cm^{-2}·s^{-1}	Φ_{th}[a] Pk, 10^{16} cm^{-2}·s^{-1}	Location
KENS	3	^{238}U	20	.0007	.018	Japan
IPNS	7	^{238}U	30	.0014	.024	USA
"	"	^{235}U	"	.0035	.060	"
LANSCE[b,c]	75	W	20	.0085	.21	USA
"	"	"	"	.011	.28	"
ISIS[c]	200	Ta	50	.015	.15	UK
"	"	^{238}U	"	.030	.30	"

[a]Calculated 4π equivalent of thermal neutron current from a moderator surface.
[b]The two values for LANSCE correspond to 100 mm x 100 mm and 120 mm x 120 mm moderator fields of view.
[c]Measured values for LANSCE and ISIS may be low by as much as 20%.

Table 5. Pulsed spallation sources (planned or proposed)

Facility name	Beam power, kW	Target/ moderator	PRF, Hz	Φ_{th} Ave, 10^{14} cm^{-2}·s^{-1}	Φ_{th} Pk, 10^{16} cm^{-2}·s^{-1}	Location
ESS	4,000	1st/[a]	40	0.5	6.0	Europe
ESS	1,000	2nd/[b]	10	1.5	12.0	Europe
IPNS-II	750	/[a]	30	0.13	2.3	USA
LANSCE-II	1,000	/[a]	60	0.16	1.3	USA
ORSNS	1,000	Hg/[a]	60	0.13	0.7[c]	USA
Long pulse[d] Bauer and LANL	1,000		60	~1-2	~10-30	

[a]Decoupled, poisoned moderator.
[b]Coupled moderators.
[c]This calculation took explicit account of pulse shape; the other figures may be based on a simpler "full width at half max." scaling, which would result in larger numbers.
[d]The long pulse concept calls for ~1 ms proton pulses. The other designs propose ~1 μs pulse.

Figure 1

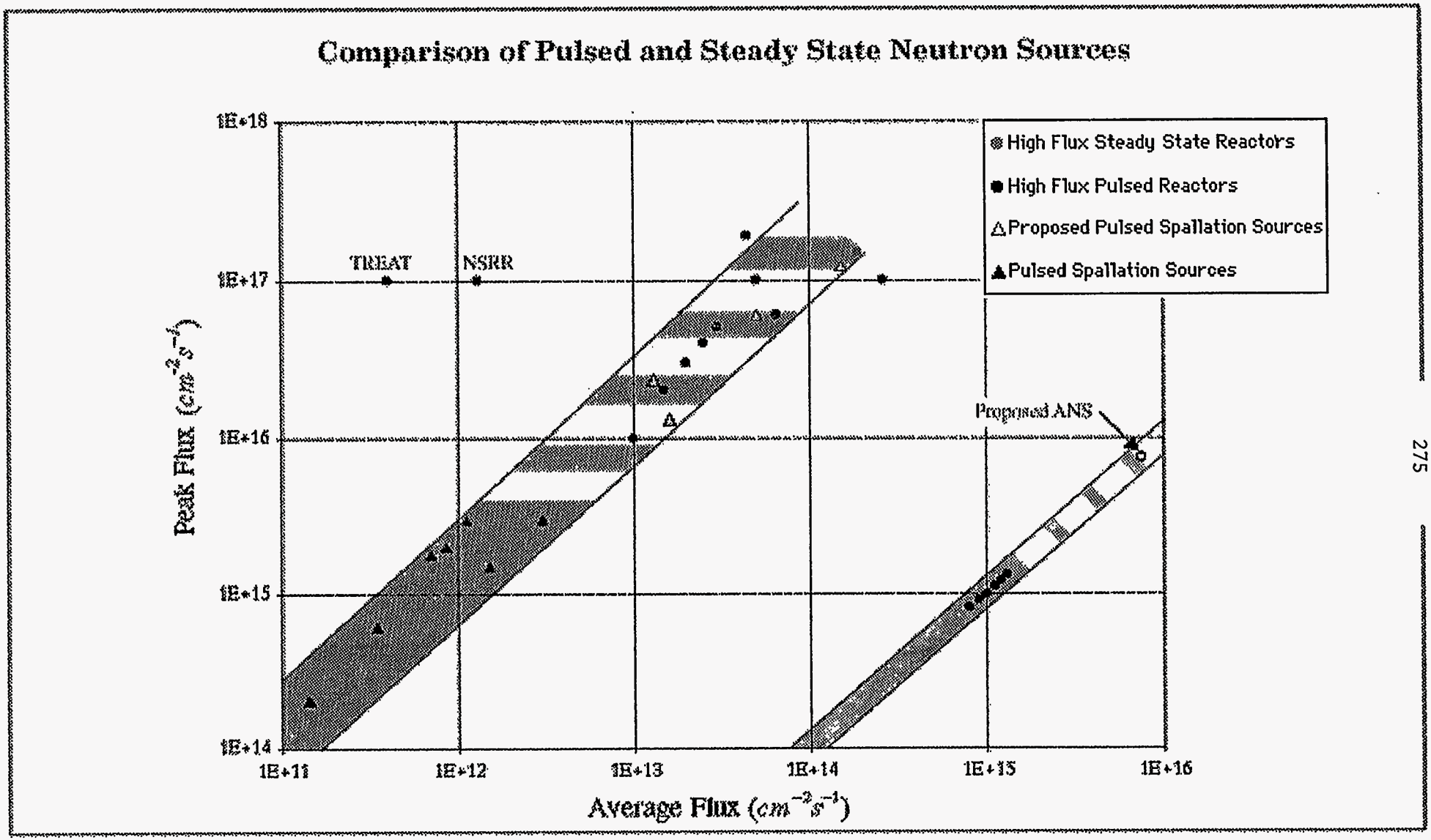
Comparison of Pulsed and Steady State Neutron Sources
High Flux Steady State Reactors
High Flux Pulsed Reactors
Proposed Pulsed Spallation Sources
Pulsed Spallation Sources
TRIGA
NSRR
Proposed ANS
1E+18
1E+17
1E+16
1E+15
1E+14
1E+11
1E+12
1E+13
1E+14
1E+15
1E+16
Peak Flux ($cm^{-2}s^{-1}$)
Average Flux ($cm^{-2}s^{-1}$)

Cold and Ultracold Neutron Sources

Crōw, Esibov, and Steyerl[2] developed a concept for an ultracold neutron (UCN) turbine based on a long-pulse spallation source. The optimum pulse length, in a certain sense, was ~2 ms. For a 1 MW, 2.5-ms pulse, 60 Hz spallation source, with a time-averaged flux in the cold source of 10^{14} cm$^{-2} \cdot$ s^{-1}, they calculated a UCN flux of 10^5 cm$^{-2} \cdot$ s^{-1}.

Unfortunately, there is at present no 1-MW pulsed spallation source in existence. However, as we have seen, several TRIGAs with equivalent or higher flux, and millisecond pulse lengths, are in operation and potentially accessible and could be considered for such experiments. The longer pulse length would be no drawback for such slow neutrons.

Trevor Lucas[3] has proposed flowing frozen methane pellets through a cryogenic chamber as a cold neutron moderator. The pellets, resident in the radiation field for only a short time, could overcome the radiolysis and stored energy ("burping") problems associated with solid methane, making it a safe and reliable moderator even at high-power neutron sources. Experiments on pellet fabrication, based on techniques developed to produce deuterium pellets for the fusion program, are planned at Oak Ridge.

An exciting possibility is that the small pellets, with a high-heat transfer area, might be cooled to ~10 K, or even less if desirable, by helium. This might lead to an intense source of very cold neutrons if such a moderator were placed at a high flux pulsed or steady-state neutron source. With methane, the necessary cold or very cold moderator thickness is quite small (~centimeters), and D. L. Selby[4] has proposed that it may be practical to consider a very large area (~0.1 m^2 or more) slab design that would intercept and moderate a very large number of neutrons even at a medium flux reactor. In that case, one could seriously consider seeking space at a TRIGA reactor, where such a large area cold source, and a very long-term experiment, might be accommodated at low cost and without dispossessing many other users. There are about 60 TRIGAs operating in the world; tables 6 and 7, respectively, list university TRIGAs in the United States and some nonuniversity facilities in the United States and elsewhere.

Summary

The most powerful existing facilities are reactors and spallation sources. The top six or so steady-state research reactors in the world offer an accessible thermal neutron flux ~10^{15} cm$^{-2} \cdot$ s^{-1}, and with the termination of the Advanced Neutron Source Project in the United States, there are no plans anywhere in the world for more intense steady-state sources of neutrons for research.

Peak thermal fluxes ~10^{17} cm$^{-2} \cdot$ s^{-1} are readily available at existing pulsed reactors. The pulses are typically 1—10 ms long (only 0.3 ms at IBR-II), with average fluxes ~10^{14} cm$^{-2} \cdot$ s^{-1} in some cases.

Existing pulsed spallation sources have two orders of magnitude lower average flux and one-to-two orders of magnitude lower peak flux than many of the pulsed reactors. The shorter pulse length at the spallation sources (tens of microseconds vs milliseconds) is a big advantage for thermal and epithermal neutron scattering work but not necessarily for the proposed n-nbar experiments.

Proposed short-pulse spallation sources, not yet under construction, would have average and peak fluxes within an order of magnitude of those available at pulsed

Table 6. University TRIGA reactors in the United States

Place	TRIGA type	Steady state power, MW	$\emptyset_{th}$, 10^{14} cm^{-2} · s^{-1}	Also pulsed?
Penn. State	Conv.	1.0	.33	Yes
Univ. of Wisconsin	Conv.	1.0	.32	No
Oregon State	MK II	1.0	.30	No
Univ. of Texas	MK II	1.1	.27	No
Univ. of Illinois	MK II	1.5	.22	Yes
Texas A&M	Conv.	1.0	.20	Yes
Reed College	MK I	0.25	.10	No
Kansas State	MK II	0.25	.10	Yes
Washington State	Conv.	1.0	.07	Yes
Univ. of CA - Irvine	MK I	0.25	.05	Yes
Univ. of Utah	MK I	0.1	.045	No
Cornell Univ.	MK II	0.5	.04	No
Univ. of Maryland	Mod.	0.25	.03	No
Univ. of Arizona	MK I	0.1	.02	Yes
Univ. of Illinois	—	.01	?	No

Table 7. Some other TRIGAs (there are about 60 worldwide, about half in the United States and half elsewhere)

Place	Type	Steady-state power, MW	$\emptyset_{th}$ 10^{14} cm^{-2} · s^{-1}
Pitesti, Romania	Dual core	14.0	2.6
KAERI, Korea	Mark III	2.0	0.65
Phillipine Nuclear Research Inst.	Conv.	3.0	0.6
Nuclear Energy Unit, Malaysia	Mark II	1.0	0.5
Center for Nuclear Techniques, Indonesia	Mark II	1.0	0.4
Inst. Nacional de Inv. Nucl., Mexico	Mark III	1.0	0.33
McClellan AFB,[a] USA	Mark II	1.0[b]	0.2

[a]Last year, this base was one of several placed on a "base closing" list by the U.S. Congress.

[b]Being upgraded to 2.0 MW.

reactors, and a future long-pulse spallation source has been proposed that would be competitive with today's pulsed reactors in peak and average flux.

New ideas continue to be developed for very cold and ultracold sources. The combination of a UCN source and an existing pulsed TRIGA reactor might provide some inexpensive, accessible opportunities for novel work (proof-of-principle or actual experiments) right now. If an n-nbar experiment could take advantage of such a facility, there are a number of places around the world that have low operating costs and that might be accessible; however, previous proposals (with weaker sources ?) for such n-nbar experiments have not looked promising.

References

1. William L. Whittemore, A Continuously Pulsed TRIGA Reactor: An Intense Source for Neutron Scattering Experiments, *Proceedings of the Fourth Meeting of the International Group on Research Reactors*, ORNL/CONF-9505218, pp 140, Lockheed Martin Energy Research, Corp., Oak Ridge National Laboratory (1995).

2. M. L. Crow, L. Esibov, and A. Steyerl, A Multilayer Neutron Turbine Source for a Long-Pulse Spallation Source, *Nuclear Instruments and Methods A* (in press).

3. A. T. Lucas, A Solid Methane/Hydrogen Moderator for Short-Pulsed Spallation Sources, *Proc. of the ICANS-IX Meeting*, Los Alamos, NM (1988).

4. D. L. Selby, Oak Ridge National Laboratory, private communication to C. D. West, Oak Ridge National Laboratory (March 1996).

5. G. S. Bauer, Some General Reflexions on "Long Pulse" Neutron Sources, *Journal of Neutron Research* (in press).

Data Sources

Table 1 G. S. Bauer, Medium-Power Spallation Neutron Sources for Research Applications, *Proc. Intl. Conf.* "Neutrons and Their Applications," published by SPIE, **Vol. 2339**, Crete, Greece (June 12-18, 1994).

Table 2 Private communications from W. L. Whittemore, General Atomics, Nuclear Research Reactors in the World, Dec. 1994 ed., International Atomic Energy Agency, Vienna, Austria, *Proc. of the Fourth Meeting of the International Group on Research Reactors,* ORNL/CONF-9505218, Lockheed Martin Energy Research, Corp., Oak Ridge National Laboratory (1995).

Table 3 Private communications, Nuclear Research Reactors in the World, Dec. 1994 ed., International Atomic Energy Agency, Vienna, Austria, *Proc. Third Asian Symposium on Research Reactor*, Hitachi, Ibaraki, Japan (1991).

Table 4 G. S. Bauer, Medium-Power Spallation Neutron Sources for Research Applications, *Proc. Intl. Conf.* "Neutrons and Their Applications," published by SPIE, **Vol. 2339**, Crete, Greece (June 12-18, 1994).

Table 5 G. S. Bauer, Some General Reflexions on "Long Pulse" Neutron Sources, *Journal of Neutron Research* (in press).

Table 6 Private communications from W. L. Whittemore, General Atomics, Nuclear Research Reactors in the World, Dec. 1994 ed., International Atomic Energy Agency, Vienna, Austria, *Proc. of the Fourth Meeting of the International Group on Research Reactors,* ORNL/CONF-9505218, Lockheed Martin Energy Research, Corp., Oak Ridge National Laboratory (1995).

Table 7 Private communications from W. L. Whittemore, General Atomics, Nuclear Research Reactors in the World, Dec. 1994 ed., International Atomic Energy Agency, Vienna, Austria, *Proc. of the Fourth Meeting of the International Group on Research Reactors,* ORNL/CONF-9505218, Lockheed Martin Energy Research, Corp., Oak Ridge National Laboratory (1995).

PROSPECTS FOR NEUTRON–ANTINEUTRON TRANSITION SEARCH

Yuri Kamyshkov
Oak Ridge National Laboratory, Oak Ridge, TN 37831 and
Physics Department, University of Tennessee, Knoxville, TN 37996

ABSTRACT

Presently-available sources of free neutrons can allow an improvement in the discovery potential of a neutron-antineutron transition search by four orders of magnitude as compared to that of the most recent reactor-based search experiment performed at ILL in Grenoble [1]. This would be equivalent to a characteristic neutron-antineutron transition time limit of $>10^{10}$ seconds. With future dedicated neutron-source facilities, with further progress in cold-neutron-moderator techniques, and with a vertical experiment layout, the discovery potential could ultimately be pushed by another factor of ~100 corresponding to a characteristic transition time limit of $\sim 10^{11}$ seconds. Prospects for, and relative merits of, a neutron-antineutron oscillation search in intranuclear transitions are also discussed.

1. Introduction

Experimental search for baryon instability [2] discussed at this workshop is motivated by two major physics concepts: (a) "baryon asymmetry of the universe" [3] based on the observation that matter is more abundant in the universe than antimatter although both are believed to have been formed in equal amounts at the time of origin, and (b) the idea of unification of particles and their interactions [4, 5]. Both of these concepts involve the nonconservation of baryon number, B, either in the form of proton decay ($\Delta B=1$ transition) or as a neutron-antineutron oscillation ($\Delta B=2$ transition). In different versions of unification models either $\Delta B=1$, or $\Delta B=2$ transitions, or both, are expected to take place. Since the original simplest SU(5) model [5], which predicted unification at an energy scale of $\sim 10^{15}$ GeV and a proton life time of $\sim 10^{29\pm2}$ years, was ruled out by experiments [6], other unification schemes have been advanced in which certain new physics related to baryon instability may prevail at the scale of $\sim 10^5$–10^6 GeV which is intermediate between electroweak and unification scales (for most recent review of these schemes see Refs. 7, 8, and 9). The neutron-antineutron transition is one of the processes which might belong to such new intermediate-energy-scale physics. There are no conservation laws of nature which would forbid the transition of $n \to \bar{n}$ except the conservation of baryon number [10].

The possibility of neutron-antineutron oscillations was first considered in [11] and used as a mechanism for explanation of baryon asymmetry of the universe. In the context of unification models, $n \to \bar{n}$ oscillations were first discussed in [12]. The most recent theoretical review of neutron-antineutron oscillations in the framework of unification and supersymmetric models is given in [9].

Since the $n \to \bar{n}$ transition at the quark level is described by a 6-fermion operator, the corresponding amplitude (for dimensional reasons) should be proportional to m^{-5}, where m is the characteristic energy scale which cannot be very large in order to produce any observable rates of $n \to \bar{n}$ [9]. Thus, the experimental observation of $n \to \bar{n}$ oscillations would indicate a $\Delta B=2$ baryon instability and point to the new physics energy scale of $\sim 10^5$–10^6 GeV.

An interesting possibility which might lead to an alternative mechanism of $n \to \bar{n}$ transitions has been discussed by V. Kuzmin [13]. He assumed that the interaction of quarks inside baryons consisting of quarks of different generations (for example *bus*) can be mediated by the color-triplet scalar field coupled to the right components of the quarks. For neutral *bus*-type baryons such a scalar field might result in baryon-antibaryon oscillations with a characteristic time of $\sim 10^{-12}$ s. Neutron-antineutron oscillations, according to V. Kuzmin, will then arise from this interaction, being additionally suppressed by ~20 orders of magnitude by CKM-matrix quark-mixing probabilities, with a characteristic transition time of $\sim 10^8$ s.

There are two complementary experimental methods which can be used for an $n \to \bar{n}$ search: (a) utilizing free neutrons from reactors or neutron spallation sources and (b) with neutrons bound inside nuclei. The results of the most recent experiment [1] performed by method (a) are presented in [14] in these proceedings. The future prospects of $n \to \bar{n}$ search in intranuclear transitions — method (b) — were addressed in [15,16] at this workshop. In this paper we discuss the present status of both methods and their relative merits for the prospects of future experimental searches. In the conclusion arguments are presented for why experimental searches by both methods are necessary.

2. Experiments with Free Neutrons

The discovery potential of an $n \to \bar{n}$ transition search experiment can be characterized by the probability of production of antineutrons in the beam of neutrons. This probability (in vacuum, in the absence of external fields) depends on the observation time t as [12]

$$P_{n\bar{n}} = (t / \tau_{n\bar{n}})^2, \tag{1}$$

where $\tau_{n\bar{n}}$ is the characteristic $n \to \bar{n}$ transition time. It is assumed in this expression that neutrons and antineutrons have equal masses (as required by CPT conservation) and that the gravitational interaction with the earth is the same for neutrons and antineutrons. Thus, we can define the *discovery potential* of an $n \to \bar{n}$ search experiment as the product of the number of neutrons per second, N_n, used in the experiment and the square of the averaged neutron time-of-flight $\bar{t}$ through the experimental volume,

$$D.P. = N_n \cdot \bar{t}^2 \ \text{[neutrons·seconds]} \tag{2}$$

The most recent experimental search for $n \to \bar{n}$ with free neutrons [1] was performed at the 58-MW research reactor at the Institute Laue-Langevin (ILL) in

Grenoble. The experiment had a discovery potential ~$1.5 \cdot 10^9$ n·s, and, for approximately one year of operation, set a limit of $\tau_{n\bar{n}} \geq 8.6 \cdot 10^7$ s. This experiment is described in detail in a talk [14] at this workshop. Some of the major features of this experiment are also listed in Table 1 below. This state-of-the-art experiment has improved the $n \rightarrow \bar{n}$ transition discovery potential relative to that of the best previous reactor experiment [17] by a factor of ~7,000. In the rest of this paper we will define the discovery potential of the ILL-experiment as 1 and we will express the discovery potentials of other different possible experimental options relative to it.

It is clear from equation (2) that for a larger discovery potential, a higher flux of neutrons from the reactor is desirable. Since the discovery potential is proportional to t^2, it is also desirable to increase the "neutron observation time" t. The latter requires the use of low-velocity neutrons, i.e., neutrons thermalized in a cold moderator to the lowest possible temperature.

The general scheme of an $n \rightarrow \bar{n}$ search experiment is as follows: neutrons emitted from the cold moderator are propagated in the vacuum in a volume (shielded against earth's magnetic field down to the level of few nT) where the $n \rightarrow \bar{n}$ transitions can occur. Produced antineutrons propagating along the initial neutron path would be detected as a few-meson star with a total energy release of ~1.8 GeV resulting from the annihilation with a thin carbon target. In the simplest configuration, the $n \rightarrow \bar{n}$ search experiment would consist of a neutron source (cold neutron moderator) with area A_s, a flight path of the length L, and an antineutron annihilation detector with area A_d. The areas A_s and A_d should be chosen as large as possible to intercept the maximum number of neutrons from the reactor, but they are limited by practical constraints. For a fixed detector area the intercepted solid angle of neutron emittance (number of neutrons used by the detector) will be proportional to L^{-2}, and for a given spectrum of neutron velocities the square of the neutron time of flight is

$$\bar{t}^2 = L^2 / \bar{V}^2 . \qquad (3)$$

Thus, in such an experimental configuration, the discovery potential (2) does not depend on the distance L between the source and the target. An example of this kind of experimental approach is given in a 1982 proposal by a Harvard-ORNL-UT group [18]. Major parameters of the experiment proposed in [18] and the expected discovery potential are listed in Table 1 below.

A new approach proposed by an ORNL-UT-Harvard-UW group [19] for reactor or spallation source experiments is based on the property of neutrons to be focused by means of reflection from surfaces of certain materials. In this approach [20-22] the *elliptically-shaped reflector* intercepts neutrons emitted from the source within a large solid angle and focuses them onto the annihilation target. Since the intercepted solid angle is now determined by the acceptance of the focusing reflector and does not depend on the distance, the overall discovery potential (2) will be proportional to L^2 which provides an additional means by which the experiment can be improved. A possible layout for such a reactor experiment is illustrated schematically in Figure 1.

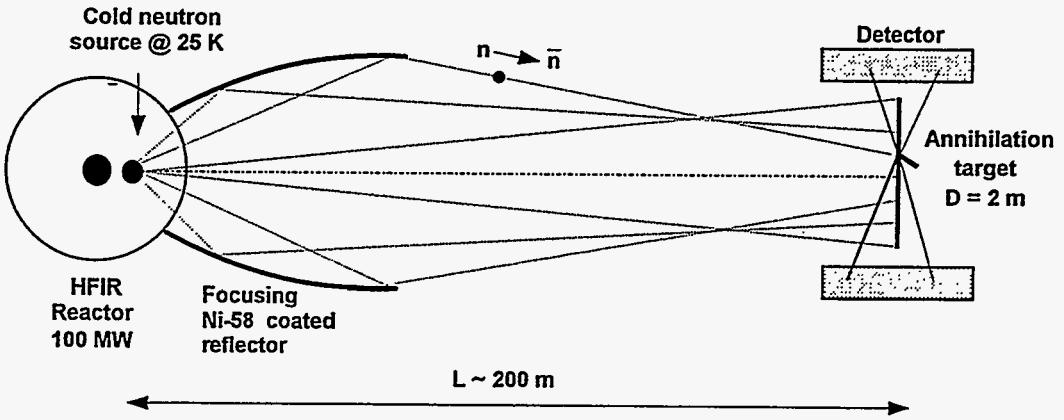

Figure 1. Conceptual layout of an experiment with a large elliptical focusing reflector for an $n \rightarrow \bar{n}$ transition search at a reactor (not to scale).

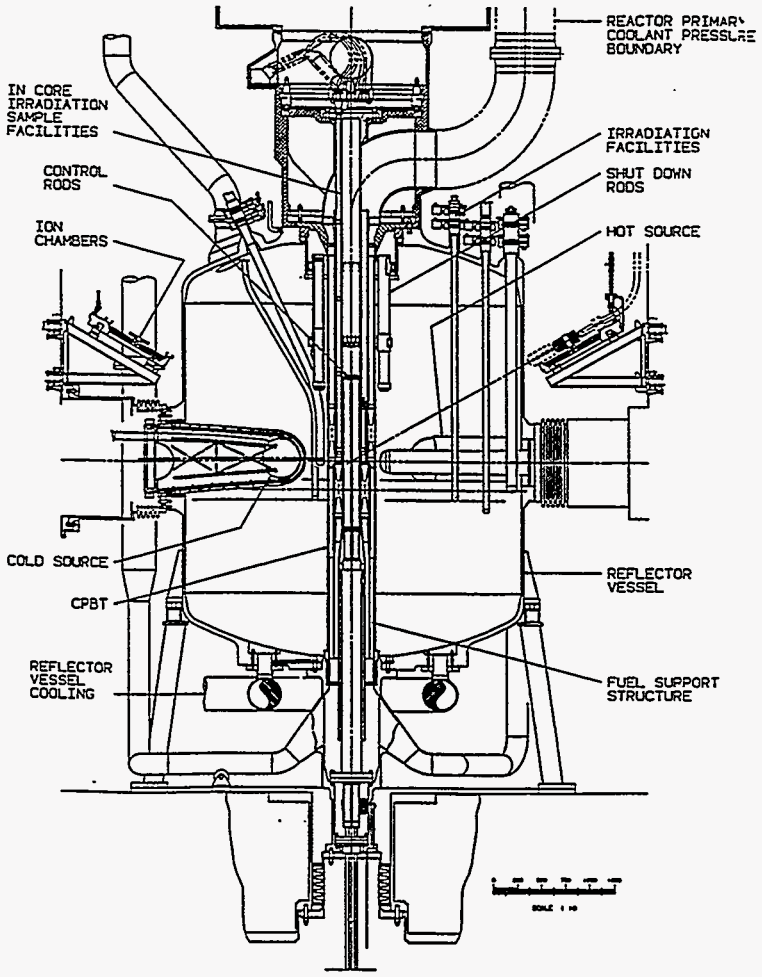

Figure 2. ANS reactor with compact core, heavy water reflector, and 40 cm diameter liquid deuterium moderator. The ANS project at ORNL was discontinued in 1995.

Originally this approach was developed for an $n \to \bar{n}$ search experiment proposed for the 330-MW Advanced Neutron Source (ANS) research reactor which had been planned for construction at ORNL. The high neutron flux, the availability of a large-area liquid-deuterium cold neutron moderator, and the possibility of modifying the reactor shield in an optimum way would have allowed, for one year of operation, an increase in the discovery potential of a factor ~13,000 relative to that of the ILL experiment. Figure 2 shows the large liquid-deuterium cold neutron moderator layout of the ANS reactor which would have been the best contemplated source of neutrons for an $n \to \bar{n}$ search experiment. Unfortunately, the ANS project was discontinued in the development phase [23]. Some features and the discovery potential of the ANS-based experiment are given for comparison in Table 1 below.

Table 1. Comparison of neutron-antineutron search experiments.

Neutron source	ILL' 94	ORR' 82	ANS	HFIR (upgraded with D_2O reflector)
Status	Completed experiment	Rejected proposal	Discontinued project	Possible option
Power (MW)	58	30	330	100
Reactor's max. thermal neutron flux ($n/cm^2/s$)	$1.5 \cdot 10^{15}$	$1.5 \cdot 10^{14}$	$7 \cdot 10^{15}$	$2 \cdot 10^{15}$
Moderator	Liq. D_2 @ 25	D_2O @ 300 K	Liq. D_2 @ 25 K	Liq. D_2 @ 25 K
Source area	6×12 cm^2	Ø 42 cm	Ø 40 cm	Ø 40 cm
$\varnothing_{det}$ (m)	1.1 m	1.0 m	2.0 m	2.0 m
L_{free} (m)	76	20	~300	~150
n/s @ target	$1.25 \cdot 10^{11}$	$2 \cdot 10^{13}$	$4.4 \cdot 10^{13}$	$5.1 \cdot 10^{13}$
$\sqrt{\langle t^2 \rangle}$ (s)	0.109	0.01	0.672	0.384
Detector efficiency	0.48	~ 0.5	~ 0.5	~ 0.5
Operation time (s)	$2.4 \cdot 10^7$	$3 \cdot 10^7$	$3 \cdot 10^7$	$9 \cdot 10^7$
Discovery potential $N \cdot \langle t^2 \rangle$ (n·s)	$1.5 \cdot 10^9$	$2 \cdot 10^9$	$2 \cdot 10^{13}$	$0.75 \cdot 10^{13}$
$\tau_{n\bar{n}}$ limit, s (90% CL)	$8.6 \cdot 10^7$	$1.1 \cdot 10^8$	$1.1 \cdot 10^{10}$	$1.0 \cdot 10^{10}$

The high-flux neutron sources available at the present time and in the foreseeable future are reviewed by C. West [24] in these proceedings. The Oak Ridge 100-MW High Flux Isotope Reactor (HFIR) has the highest steady thermal-neutron flux among the research reactors. This reactor has a compact highly enriched fuel core, a beryllium reflector, a pressure vessel with a diameter of 8', and four horizontal beam openings: three

with 8" diameter and one with 12" diameter (Figure 3). At the present time it is not equipped with cold neutron moderators. In one of the upgrade options of the HFIR reactor a heavy-water reflector and a large liquid-deuterium moderator of the ANS-type [25] would be installed. The openings in the reactor vessel in this case could be enlarged to accommodate the thimbles of the large cold moderators. This option is shown schematically in Figure 4. If implemented, such an upgrade would not only provide an excellent opportunity for the $n \rightarrow \bar{n}$ search but at the same time would also make available (similar to the ANS cold-source design) several cold-neutron beams for neutron scattering experiments. The discovery potential of an $n \rightarrow \bar{n}$ search experiment performed at the upgraded HFIR facilities could be a factor of ~5,000 higher than that of the ILL experiment. The gain in the discovery potential results from the following factors: higher reactor power, larger area of the cold-neutron emitting source, larger area of the annihilation detector, and, most importantly, from the use of a large-acceptance elliptical focusing reflector. This would be the most preferred option of implementation of a new reactor experiment. For 2-3 years of operation a discovery-potential gain (relative to the ILL experiment) of more than 10,000 can be envisaged which, if $n \rightarrow \bar{n}$ transitions are not found, would result in a new transition limit of 10^{10} seconds. The essential features of the upgraded HFIR option are shown in Table 1 for comparison with other experiments.

In the case that the heavy-water reflector upgrade of the HFIR reactor will not be implemented, the next-best possibility would be to use the radial HFIR beam which has a 12"-diameter opening. A medium-size cold moderator would be required in this beam in order to enhance the discovery potential up to ~1,000 times relative to that of the ILL experiment. This and other options with their discovery potentials for various combinations of beams and cold moderators are shown in Table 2.

The calculations of the discovery potential for different options of the $n \rightarrow \bar{n}$ search experiment have been performed with a Monte-Carlo neutron-transport code which takes into account the brightness of the neutron source with appropriate normalization, the cold moderator and beam layout, beam collimation, reflection of the neutrons off the material of the focusing reflector, and the effects of gravity. The dimensions and parameters of the reflector have been optimized to maximize the discovery potential for the various options of experimental layout and of cold moderators.

Effects of gravity (more important at low neutron velocities) produce significant defocusing if the length of the horizontal experiment is too large. This effect limits the advantages of using a very cold neutron source. The defocusing gravity effect can be eliminated in a layout with a vertical neutron flight path. This layout would be most efficient if the neutrons were thermalized in the cold moderator to the lowest possible temperatures. At the present time the lowest experimentally achieved temperatures of thermalized neutron Maxwellian distributions are in the range of 20-40K. The possibility of thermalization of neutrons to temperatures as low as 1-10K has not been sufficiently studied either theoretically or experimentally. This situation is addressed in References 22 and 26. For some options in Table 2, a temperature for the neutron spectrum of 1K was assumed, which, in practice, might not be achievable.

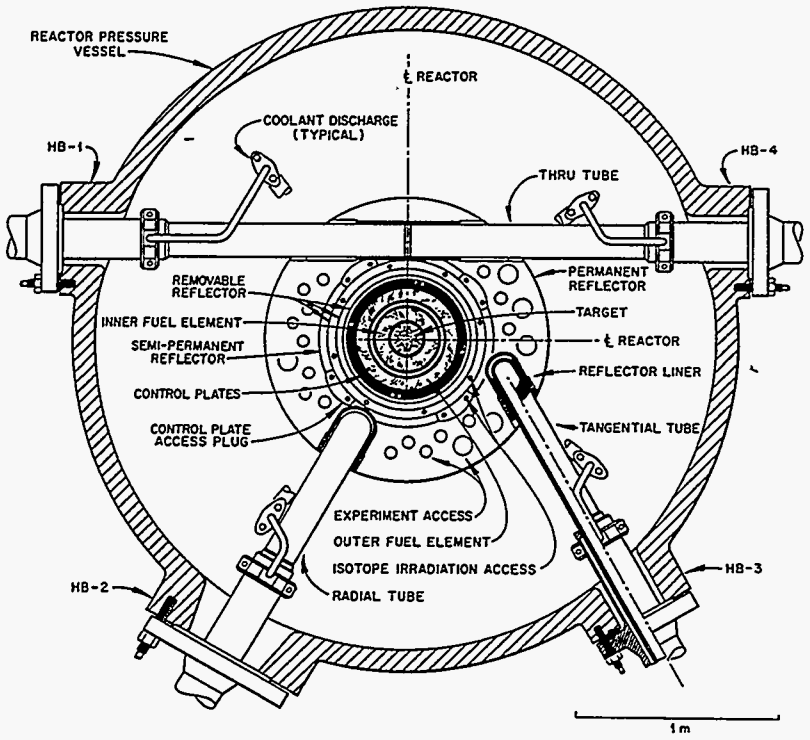

Figure 3. Current layout of neutron beams at the HFIR reactor in the present configuration.

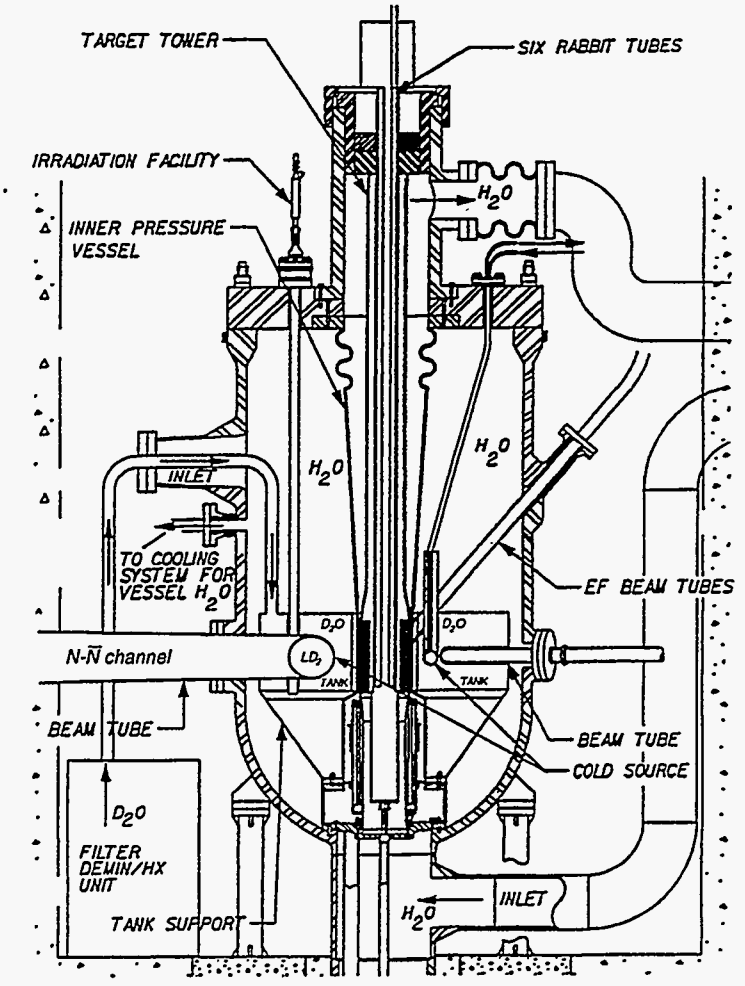

Figure 4. Upgrade option of HFIR reactor using a heavy-water reflector and a large cold moderator.

Table 2. Experimental options for neutron-antineutron transition search.

Neutron source	Neutron moderator	Discovery potential gain for one year of operation
ILL (1991) *completed experiment*	Large liquid D_2	× 1
ANS *discontinued project*	Large liquid D_2	× 13,000
HFIR *with enlarged radial beam opening, upgraded to D_2O reflector*	Large liquid D_2 or solid CH_4	× 5,000
HFIR *12" radial beam with modified Be reflector*	Liquid H_2	× 1,000
HFIR *8" tangential beam with modified Be reflector*	Small liquid H_2	× 100–400
HFIR *12" radial beam no modifications*	No cold moderator	× 50
New ANS-type reactor *vertical layout of experiment*	Super-cold moderator *thermalizing neutrons @ 1K*	up to × 1,000,000
Long pulse 1-MW neutron spallation source	Large-area liquid H_2 *coupled, not poisoned moderator*	× 500
Long pulse 1-MW neutron spallation source, *vertical layout*	Super-cold moderator *thermalizing neutrons @ 1K*	× 16,000

For the next generation of experiments, several improvement factors are essential in order to stretch the discovery potential level beyond the feasibility limits of HFIR. These factors are: (a) high flux neutron sources similar to ANS reactor, (b) newly developed super-cold neutron moderators, and (c) vertical experimental layouts combined with a focusing reflector. The combination of all of these factors in a next generation experiment should, hopefully, allow a total gain-factor of up to 10^6 relative to the present ILL level, or, it should allow the establishment of a $n \rightarrow \bar{n}$ transition-time limit of $>10^{11}$ s.

Neutron spallation sources, although delivering very high neutron peak fluxes, cannot compete [24] with reactors when it comes to the average neutron flux, which is most important requirement for a progress of $n \rightarrow \bar{n}$ search. To enhance the advantages of pulse operation for neutron spectroscopy, moderators at spallation neutron sources are very often operated in the "decoupled" and "poisoned" modes which reduces substantially the average neutron flux. An experiment with a vertical layout is more likely to be built at the spallation source than at the reactor where the location of various reactor services and where safety regulations result in more restrictive environment. The combination of a vertical layout and a super-cold neutron moderator at the spallation neutron source could provide a discovery potential which is competitive with that of a midrange reactor experiment (see Table 2).

3. Intranuclear Transitions

Since the potentials of neutrons and antineutrons inside the nucleus are different, the intranuclear $n \to \bar{n}$ transition is strongly suppressed. The lifetime of a nucleus for an $n \to \bar{n}$ intranuclear transition T_A is related to free neutron oscillation time $\tau_{n\bar{n}}$ as

$$T_A = T_R \cdot \tau_{n\bar{n}}^2 , \tag{4}$$

where T_R is the nuclear suppression factor.

The following simple speculation [27] allows obtaining a very approximate estimate of the nuclear suppression factor. The neutrons bound inside the nuclei can be considered "free" for a time Δt given by:

$$\Delta t \sim 1 / E_{binding} \sim 1 / 10MeV \sim 10^{-22} s , \tag{5}$$

and will "experience" this condition $N = 1/\Delta t$ times per second. The intranuclear $n \to \bar{n}$ transition probability per unit time, $1/T_A$, is then, according to (1):

$$\frac{1}{T_A} = \left(\frac{\Delta t}{\tau_{n\bar{n}}}\right)^2 \cdot \left(\frac{1}{\Delta t}\right). \tag{6}$$

The comparison of (6) with (4) shows that $T_R \sim 1/\Delta t \sim 10^{22}\ s^{-1}$.

The nuclear suppression factor has been evaluated with different methods by several authors during the past two decades. Most recent theoretical discussions and new reevaluations, as well as references to the previous work, can be found in [28-31]. According to [28], for oxygen, argon, and iron, the suppression factor has a value of $T_R \sim 2 \cdot 10^{23}\ s^{-1}$.

Experimentally, intranuclear $n \to \bar{n}$ transitions have been searched for in nucleon stability experiments IMB, Kamiokande, and Fréjus [32]. For example, the limit for the intranuclear $n \to \bar{n}$ transition lifetime for iron nuclei set by the Fréjus experiment is $T_A \geq 6.5 \cdot 10^{31}$ years which, according to (4) and the suppression factor T_R from [28], corresponds to a free $n \to \bar{n}$ transition time limit of $\tau_{n\bar{n}} \geq (8\text{-}10) \cdot 10^7\ s$.

During the next decade, the large next-generation nucleon stability experiments, SuperKamiokande and Icarus, will improve the $n \to \bar{n}$ transition limit. After a few years of operation the SuperKamiokande detector, commissioned in April this year, will be able to set an $n \to \bar{n}$ transition limit of $T_A \geq 10^{33}$ years [15] which will correspond, according to (4) and the suppression factor T_R from [28], to a free $n \to \bar{n}$ transition limit of $\tau_{n\bar{n}} \geq 4 \cdot 10^8\ sec$.

A new possibility for an intranuclear $n \to \bar{n}$ transition search has been recently considered by an ORNL-UTK group [16]. The idea is based on the measurement of the concentration of long-lived isotopes (with a lifetime in the range of million years) which may be the remnants of $n \to \bar{n}$ intranuclear transitions accumulated among the parent nuclides contained in deeply-deposited nonradioactive ores. As an example, the search for technetium isotopes ^{97}Tc, ^{98}Tc, and ^{99}Tc in deep-mined tin ore is discussed in [16]. In case of favorable backgrounds this approach can provide a limit for intranuclear $n \to \bar{n}$ transitions up to $T_A \approx 10^{34}$ years.

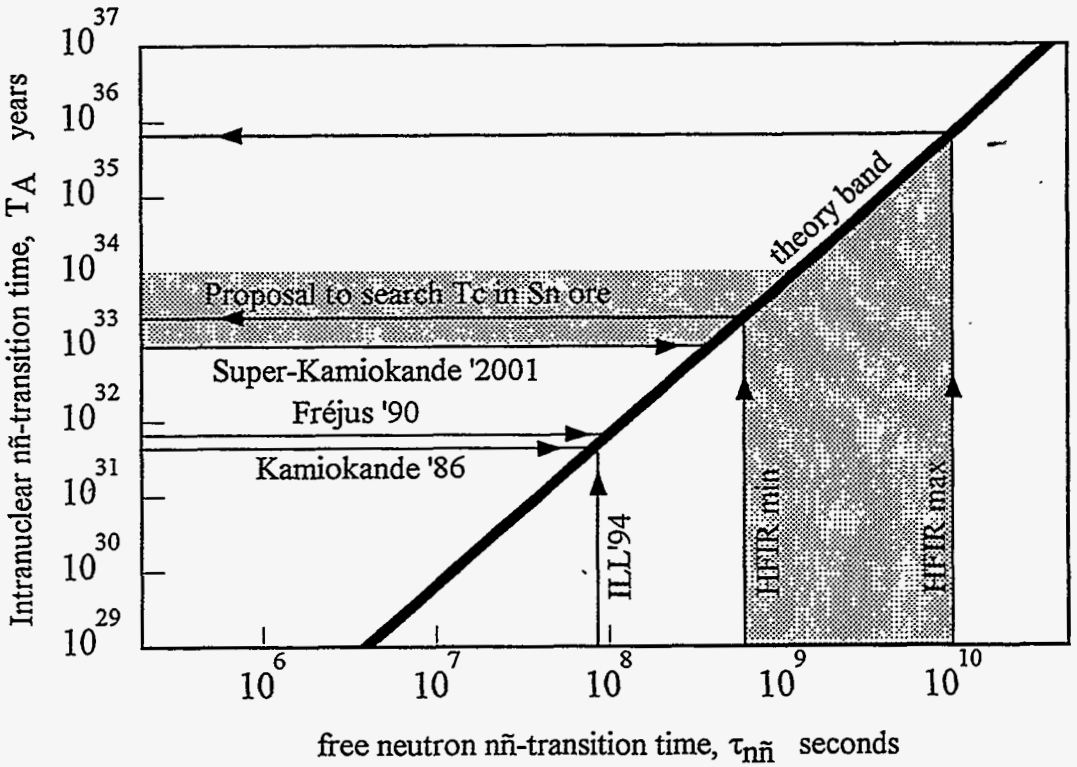

Figure 5. Comparison of $n \to \bar{n}$ searches in intranuclear transitions (T_A) to those in free neutron experiments ($\tau_{n\bar{n}}$). The slope and the width of the nuclear model band relating these two processes corresponds to $T_A = T_R \cdot \tau_{n\bar{n}}^2$, where T_R is the nuclear suppression factor taken from [28].

4. Conclusions

Different methods for $n \to \bar{n}$ transition searches are compared in Figure 5. At the present time the experimental free-neutron transition limit and limits from intranuclear transition experiments are in agreement with each other as related by theoretical calculations [28] via the nuclear suppression factor T_R. If the experimental limits for an intranuclear $n \to \bar{n}$ transition will be improved to the level of 10^{33}–10^{34} years, this will

correspond to an equivalent limit for the free-neutron transition time of $\sim 10^9$ s. Future reactor or spallation-source experiments with free neutrons have a much higher potential for $n \to \bar{n}$ discovery and can realistically set the limit for $n \to \bar{n}$ transitions as high as 10^{10} s (and ultimately at 10^{11} sec if all experimental possibilities will be stretched to their limits).

The current phenomenology of $n \to \bar{n}$ transitions is based on the assumption that neutrons and antineutrons have equal masses (as required by CPT conservation) and that the gravitational interaction with the earth is the same for neutrons and antineutrons. These assumptions, although perfectly acceptable by modern theories, require, in themselves, experimental confirmation. Strictly speaking, we do not know experimentally even whether antineutrons are attracted or repulsed by the gravitational field of the earth, and the neutron-antineutron mass difference is known with an accuracy of only ~ 100 KeV [6].

It was pointed out in [33] that a positive observation of $n \to \bar{n}$ transitions would allow a test of the CPT theorem (which predicts that the mass of a particle is equal to the mass of the antiparticle) with unprecedented accuracy. A similar conclusion can be drawn regarding the difference of gravitational interactions of neutrons and antineutrons.

The presence of, either a mass difference, Δm, or of a gravitational interaction difference of neutrons and antineutrons would result in the suppression of transitions of free neutrons to antineutrons. The intranuclear $n \to \bar{n}$ transitions, as was pointed out in [33], are not suppressed. This is correct provided that the mass difference, or the difference in the gravitational potentials of neutrons and antineutrons are considerably less than the difference of neutron and antineutron nuclear potentials (~ MeV range). The experimental observation of intranuclear $n \to \bar{n}$ transitions together with the suppression of the corresponding rate of transitions in experiments with free neutrons would indicate the presence of Δm or a difference of gravitational interaction. If both types of experiments would measure matching $n \to \bar{n}$ transition rates, it will allow the setting of unprecedentedly low limits on Δm or on the difference of gravitational interaction of particles and antiparticles. The Δm-sensitivity in such a case would be of the order of $1/t$, where t is the time of neutron observation in the free-neutron experiment. In one of the HFIR-based free-neutron experiment options, $t \sim 0.4$ s and the corresponding $\Delta m/m$ sensitivity can be as low as $\sim 10^{-24}$. Both kinds of $n \to \bar{n}$ search experiments (intranuclear and with free neutrons) are necessary in order to address the question of the neutron and antineutron mass difference.

I would like to thank Yu. V. Efremenko, V. A. Kuzmin, R. N. Mohapatra, F. Plasil, and C. D. West for useful and stimulating discussions. This research is sponsored by the Laboratory Directed Research and Development Program of the Oak Ridge National Laboratory, managed for the U.S. Department of Energy by Lockheed Martin Energy Research Corp., under Contract No. DE-AC05-96OR22464.

5. References

1. M. Baldo-Ceolin et al., Z. Phys. C **63** (1994) 409-416.
2. M. Goldhaber, these proceedings.
3. A. D. Sakharov, JETP Lett. **5** (1967) 24.
4. J. C. Pati and A. Salam, Phys. Rev. D **8** (1973) 1240.
5. H. Georgi and S. L. Glashow, Phys. Rev. Lett. **32** (1974) 438;
   H. Georgi, H. R. Quinn, S. Weinberg, Phys. Rev. Lett. **33** (1974) 451.
6. Review of Particle Properties, Phys. Rev. D **54** (1996) 562.
7. P. Nath, these proceedings.
8. J. C. Pati, these proceedings.
9. R. N. Mohapatra, these proceedings.
10. M. Gell-Mann and A. Pais, Phys. Rev. **97** (1955) 1387.
11. V. A. Kuzmin, JETP Lett. **12** (1970) 228;
    V. A. Kuzmin, Izvestiya AN SSSR, ser. phys. **35** (1971) 2088.
12. S. L. Glashow, Harvard report, HUTP-79/A059;
    R. N. Mohapatra and R. E. Marshak: Phys. Lett. **91**B (1980) 222,
    Phys. Rev. Lett. **44** (1980) 1316, Phys. Lett. **94**B (1980) 183;
    M. V. Kazarnovsky et al., Pis'ma Zh. Eksp. Teor. Fiz. **32** (1980) 88.
13. V. A. Kuzmin, these proceedings.
14. D. Gibin, these proceedings.
15. J. Stone, talk at this workshop.
16. Yu. Efremenko et al., these proceedings.
17. G. Fidecaro et al., Phys. Lett. **156**B (1985) 122.
18. M. S. Goodman et al., A Sensitive Search for Neutron-Antineutron Transitions, Proposal of Harvard University–ORNL–University of Tennessee, 1982, ORNL/PHYS-82/1. This proposal was rejected by DOE.
19. Members of ORNL-UT-Harvard-UW N-Nbar Collaboration: W. Bugg, H. Cohn, G.Condo, Yu. Efremenko, Yu. Kamyshkov, S. Lamoreaux, R. Lillie, A. T. Lucas, F.Plasil, S. Raman, M. Rennich, D. Selby, K. Shmakov, C. West, R. Wilson, G. Young.
20. Yu. Kamyshkov et al., in the proceedings of the NAN-95 Conference, ITEP, Moscow 1995; Yadernaya Fizika, No. 9-10, 1996.
21. Yu. Kamyshkov et al., in the proceedings of the TAUP-95 Conference, Toledo, Spain 1995, Nuclear Physics B (Proc. Suppl.) **48** (1996) 460.

22. Yu. Kamyshkov et al., in the proceedings of the ICANS-XIII Meeting, PSI, Villigen, Switzerland 1995, p. 843.
23. Advanced Neutron Source (ANS) 330-MW reactor with compact core, heavy water reflector, and large-area liquid deuterium cold moderators was an ORNL project discontinued in 1995 in the development phase; see ANS close-out document on CD-ROM, ORNL/M-4674.
24. C. D. West, these proceedings.
25. High Flux Isotope Reactor Futures Group Report, ORNL/TM-13002, 1995.
26. S. K. Lamoreaux, these proceedings.
27. V. A. Kuzmin, private communication.
28. W. Alberico, these proceedings.
29. P. K. Kabir, these proceedings.
30. J.-M. Richard et al., these proceedings
31. L. A. Kondratyuk, these proceedings.
32. T. W. Jones et al., IMB Collaboration, Phys. Rev. Lett. **52** (1984) 720; M. Takita et al., Kamiokande experiment, Phys. Rev. D **34** (1986) 902; Ch. Berger et al., Fréjus Collaboration, Phys. Lett. B **240** (1990) 237-242.
33. Yu. Abov, F. Djeparov, L. Okun, JETP Lett. **39** (1084) 493.

Antineutron annihilation event generator for $n \longrightarrow \bar{n}$ search experiment.

Ye.S.Golubeva[1], A.S.Iljinov[1] and L.A.Kondratyuk[2]

[1] Institute for Nuclear Research, Russian Academy of Sciences,
117312 Moscow, Russia
[2] Institute of Theoretical and Experimental Physics,
117259 Moscow, Russia

Abstract

Event generator for $n \rightarrow \bar{n}$ search experiment has been developed on the basis of the optical-cascade model of annihilation of slow antinucleons on nuclei. Available data on annihilation on nuclei of antiprotons at rest and antineutrons in flight have been analyzed in the framework of this model. Good agreement between the theory and experimental data on $\bar{p}A$ annihilation at rest has been observed that confirms a rather high accuracy of the event generator.

One of the possible ways to search for $n \leftrightarrow \bar{n}$ oscilation is the use of high intensity cold ($\sim 40K^0$) neutron beam [1]. But there is a problem of efficient detection of rare antineutrons in the background of high neutron flux ($\sim 10^{13} n/s$). The detection of antineutrons is based on the possibility to annihilate on nuclear target into multipion system. Carbon is prefered as a target material because its low neutron capture cross section ($\sim 12mb$) and high annihilation cross section ($\sim 5kb$). It is necessary to know the detail characteristics of cold $\bar{n}$ annihilation on ^{12}C nuclei for detector design. There are no corresponding experimental data and the goal of present work is to develop the generator for slow $\bar{n}$ annihilation events on ^{12}C nucleus. The model proposed here is based on intranuclear cascade model. We shall use, as a basis, the optical-cascade model of annihilation of slow $\bar{n}$ [2] and stopped $\bar{p}$ [3] on nuclei.

Annihilation of slow antinucleon on nucleus is a multistage process:
1st stage - antinucleon absorption by nucleus,
2nd stage - annihilation of antinucleon on the intranuclear nucleon,
3rd stage - the intranuclear cascade initiated by the annihilation pions,
4th stage - the de-excitation of residual nucleus.

The main idea of the optical-cascade model was to formulate the initial conditions for the intranuclear cascade in the framework of the optical model.

So, the 1st stage of the process was described by the optical model. Optical calculation showed that absorption of a slow antinucleon takes place at the far periphery of a nucleus. Usually the radial dependence of the absorption probability is approximated by the Gaussian [2,3]:

$$P_{abs}(r) \sim exp[-(r - R_{med})^2/2\sigma_a^2] \qquad (1)$$

where $R_{med} = R_{1/2} + 1.1fm$ ($R_{1/2} = 2.36fm$ is the half-density radius of a nucleus) and $\sigma_a = 1fm$.

The 2nd stage, namely the elementary $\bar{N}N$-annihilation, can be described by the modified statistical model [4]. This model describes well not only the multiplicities and energy spectra of pions produced in $\bar{p}p$-annihilation, but also different correlations between pions of different charge. The number of pions emitted from $\bar{N}N$-annihilation event lies between 2 and 8; the pion multiplicity distribution has a narrow peak at $n_\pi = 5$. The everage energy of produced pions $E_\pi \approx 230MeV$ is close to the energy of (3,3)-resonance.

The 3rd stage of the process is described by the intranuclear cascade (INC) model. The INC model has been successfully used in analyzing the inelastic interactions of intermediate-energy nucleons and pions with nuclei. The very detailed description of physical foundations and applications of INC model for analysis of different nuclear reactions is presented in the book [5].

Finally, the 4th stage of the process was described in the framework of the evaporation (medium-weight residual nuclei) or explosive breake-up (light residual nuclei) model of decay of highly excited nuclei [6].

Each event of $\bar{N}$-nucleus annihilation is simulated by Monte-Carlo technique. The total exclusive description of annihilation process is realized by this method.

Using the optical-cascade model, we described successfully the experimental data on stopped $\bar{p}$-annihilation on light nuclei (^{12}C, ^{14}N) obtained at LEAR [7-9]. Data [10,11] on annihilation of antiprotons on light nuclei

in flight obtained at the senior-generation of accelerators and the only measurement of 750 MeV $\bar{n}$-annihilation on ^{12}C [12] have been also described on the basis of our INC model [13] (the 1st stage of the process is absent in this case).

Because of surface character of $\bar{N}$A-annihilation at rest, most of annihilation pions escape from the nucleus. In the case of light ^{12}C nuclei the effects of rescattering and nuclear absorption of pions are not large and, as a result, the average numbers of emitted pions and average pion energy ($E_\pi = m_\pi + T_\pi$) are close to the values corresponding to the $\bar{N}N$-annihilation in vacuum (tab.1).

Table 1. Average multiplicities and energy of pions after $\bar{p}$C annihilation at rest.

	M_{π^+}	M_{π^-}	M_{π^0}	E_π, MeV
Exp.[7]	1.25 ± 0.06	1.59 ± 0.08	1.73 ± 0.10	380 ± 2
calc.	1.17	1.61	1.91	367

Fig.1 presents the distribution on the number of emitted charged pions n_{π^+-} and figs.2 and 3 show the distribution on the total pion charge $Q = n_{\pi^+} - n_{\pi^-}$. These characteristics demonstrate that most of annihilation pions are emitted from nucleus because the absorption of antinucleon takes plase in the diffuse nuclear layer. As it is seen from fig.3 the most probable Q values for for $\bar{p}$C annihilation are $Q = 0$ ($\bar{p}p$-annihilation) and $Q = -1$ ($\bar{p}n$-annihilation), but for $\bar{n}$C-annihilation most probable Q values are: $Q = 0$ ($\bar{n}n$-annihilation) and $Q = +1$ ($\bar{n}p$-annihilation). The FSI effects contribute to the broadening of initial distribution in the regions of negative and positive Q-values.

The annihilation pions can interact with intranuclear nucleons knocking-out nucleons from the target nucleus. It is seen from fig.4 that the "tail" of the distribution $W(n_p)$ streches out into the region $n_p = 5$. This is an evidence of almost complete desintegration of light ^{12}C nucleus in the case where the annihilation occurs deeply inside the nuclear interior, but the probability of these events is small. Fig.5 presents the momentum spectrum of charged pions emitted in $\bar{p}C$ annihilation at rest. The pion spectra extend up to $1GeV/c$ and have maximum at $200MeV/c$. The average momentum of pions $\approx 330MeV/c$ ($230MeV$) which is close to (3,3)-resonance.

The energy spectrum of protons that are knocked-out from the target

nucleus by pions or emitted in the de-excitation of the residual nuclei, is softer than the pion spectrum (see fig.6) and is described by the expression

$$N(E) = N_1 exp(-E/T_1) + N_2 exp(-E/T_2) \tag{2}$$

with the slope parameter $T_1 = 7MeV$ and $T_2 = 66MeV$ [9].

The developed optical-cascade model describes well the available experimental data on annihilation of antiprotons at rest on light nuclei ^{12}C, ^{14}N. This model can predict rather correctly the characteristics of nuclear absorption of slow antineutrons.

In the present work we shall describe the 1st stage of $\bar{n}C$-annihilation in the framerwork of optical model more correctly than in paper [2]. In distinction from antiprotons, slow antineutrons are absorbed by nucleus from the S-wave of continuum. The antineutron wave function can be found from the solution of the wave equation:

$$(\vec{\nabla}^2 + k^2)\Psi(\vec{r}) = V_{opt}(\vec{r})\Psi(\vec{r}), \tag{3}$$

where k is the antineutron momentum. The complex optical potential is given by

$$V_{opt}(\vec{r}) = -4\pi[f_{\bar{n}p}(0)\rho_p(\vec{r}) + f_{\bar{n}n}(0)\rho_n(\vec{r})] \tag{4}$$

where $f_{\bar{n}p}(0)$ and $f_{\bar{n}n}(0)$ are the $\bar{n}p$ and $\bar{n}n$ forward scattering amplitudes in the lab. system, $\rho_p(\vec{r})$ and $\rho_n(\vec{r})$ are the proton and neutron densities. Here we took $\rho_p(\vec{r}) = \rho_n(\vec{r}) = \rho(\vec{r})$. The wave equation was solved numerically by dividing the potential on N radial zones with constant densities. In each j-th zone the radial wave function was taken in the form:

$$\tilde{\Phi}_j(r) = r\Psi_j(r) = A_j e^{i\kappa_j r} - B_j e^{-i\kappa_j r} \tag{5}$$

where $\kappa_j^2 = k^2 - V_{opt}(r_j)$. The complex constants A_j and B_j were found from the continuity conditions for $\tilde{\Phi}(r)$ and $\tilde{\Phi}'(r)$. We took initial conditions $B = A = 1$ at $r = 0$, then the solution at $r \gg R$ has the form

$$\tilde{\Phi}(r) = A_\infty \frac{\sin(kr + \delta)}{k} \tag{6}$$

where $\delta = -ka_{\bar{n}A}$ with $a_{\bar{n}A}$ being the complex $\bar{n}A$ scattering length. For small k

$$\tilde{\Phi}(r) = A_\infty(r - a_{\bar{n}A}). \tag{7}$$

When A_∞ and δ were found we renormalised our solution dividing it by A_∞:

$$\Phi(r) = \frac{1}{A_\infty}\tilde{\Phi}(r) \tag{8}$$

The imaginary part of the $\bar{n}A$ scattering amplitude can also be found from the expression

$$ImF_{\bar{n}A}(0) = -Ima_{\bar{n}A} = \int ImV_{opt}(r) \mid \Phi(r) \mid^2 4\pi dr \tag{9}$$

Therefore the consistency of the solution can be checked comparing the values of $Ima_{\bar{n}A}$ found from Eq.7 and Eq.9.

The radial distribution (see fig.7) of the $\bar{n}$ absorption probability can be written as

$$P_{abs}(r) \sim \rho(r) \mid \Phi(r) \mid^2 \tag{10}$$

The calculations for ^{12}C were done using the density $\rho(r)$ in the form:

$$\rho(r) = \rho(0)\left(1 - C\frac{r^2}{R_{1/2}^2}\right) \Big/ \left(1 + exp\frac{r - R_{1/2}}{t}\right), \tag{11}$$

were $R_{1/2} = 2.36fm$, $t = 0.52fm$, $c = 0.15$.

The real and imaginary parts of $\bar{p}p$ scattering length are known from the shift and width of $\bar{p}p$ atomic levels. Different experiments give the values (see ref.[14]) of $Rea_{\bar{p}p}$ and $Ima_{\bar{p}p}$ in the following ranges: $Rea_{\bar{p}p} = (0.7 \div 1.2)fm$ and $Ima_{\bar{p}p} = -(0.6 \div 1.3)fm$. The imaginary part of $\bar{n}p$ scattering length can be estimated from the data of OBELIX collaboration [15]: $Ima_{\bar{n}p} \approx (0.3 \div 0.5)fm$. The value $Rea_{\bar{n}p}$ can not be found because of rather large experimental uncertainties. We calculated $\sigma_{ann}(^{12}C)$ taking different values of

$$f_{\bar{n}N}(0) = -2\left(\frac{Z}{A}a_{\bar{n}p} + \frac{N}{A}a_{\bar{n}n}\right)$$

where $a_{\bar{n}n} = a_{\bar{p}p}$ (see table 2). In our calculations we used $f_{\bar{n}N}(0) = (-1 + 1.7i)fm$. In this case $\sigma_{ann}(^{12}C) = 5.11kb$.

Table 2. σ_{ann} and R_{med} for ^{12}C at different values of $f_{\bar{n}N}(0)$.

$f_{\bar{n}N}(0), fm$	$-1+1.7i$	$-1+i$	i	$2i$	$1+i$
σ_{ann}, kb	5.1	4.1	8.5	7.6	11.6
R_{med}, fm	3.26	3.19	2.83	3.11	2.69

In the framerwork of proposed model the following characteristics of slow $\bar{n}$ absorption by ^{12}C nuclei were calculated:

- multiplicity distributions of π^+, π^-, π^0;
- multiplicity distributions of protons and neutrons;
- energy spectra of protons and pions;
- energy carried by pions;
- energy carried by charged particles.

These characteristics are very similar to ones for $\bar{p}$C absorption, except of the charged pion multiplicity distributions which are different due to different charges of initial states (see table 3).

Table 3. Average multiplicities of particles after $\bar{n}$C and $\bar{p}$C annihilation at rest.

	M_{ch}	M_{π}	M_{π^+}	M_{π^-}	M_{π^0}	M_{pr}
$\bar{n}$C	4.00	4.73	1.63	1.19	1.92	1.19
$\bar{p}$C	3.99	4.69	1.17	1.61	1.92	1.22

Summary

The optical-cascade model of slow $\bar{n}$-annihilation on ^{12}C nuclei was developed. The first stage of the process – absorption of slow antineutron – is described in the framework of optical model. The optical-cascade model, which describes well the experimental data on stopped antiproton annihilation, describes the second stage of the process – interaction of annihilation pions with target nucleus. In the framework of this model the characteristics of slow antineutron annihilation on ^{12}C nucleus are predicted. This model can be used as $\bar{n}C$ event generator for detector design and optimization in the $n \leftrightarrow \bar{n}$ search experiments at the beams of cold neutrons.

The authors are grateful to Yu.A.Kamyshkov and Yu. Efremenko for useful discussions.

References

[1] Yu. Kamyshkov et al., Proc. of the 3d International Conference on Nucleon-Antinucleon Physics (NAN'95) Phys.of Atomic Nuclei No.8-9 (1996)

[2] A.S.Iljinov, V.L.Matushko and S.E Chigrinov, Sov.J. Nucl. Phys. 36(1982) 878

[3] A.S.Iljinov, V.I.Nazaruk and S.E.Chigrinov, Nucl.Phys. A382(1982) 378

[4] S.I.Orfanidis and V.Rittenberg, Nucl.Phys. B59(1973) 570

[5] A.S.Iljinov, M.V.Kazarnovsky and E.Ya.Paryev, Intermediate-Energy Nuclear Physics, CRC Press, 1994

[6] A.S.Botvina, A.S.Iljinov and I.N.Mishustin, Nucl.Phys. A507(1990) 649

[7] E.D.Minor et al., Z.Phys.A-Atomic Nuclei 336(1990) 461

[8] P.Hofmann et al., Nucl.Phys. A512(1990) 669

[9] J.Riedlberger et al., Phys.Rev.C40(1989) 2717

[10] W.M.Bugg et al., Phys.Rev.Lett. 31(1973) 475

[11] L.S.Agnew et al., Phys.Rev. 118(1960) 1371

[12] H.J.Besch et al., Z.Phys.A 292(1979) 197

[13] Ye.S.Golubeva et al., Nucl. Phys. A483 (1988) 539

[14] J.Carbonell and K.V.Protasov, J.Phys.G18(1992)1863

[15] S.Tessaro, P.H.D.Thesis, University of Trieste, 1995

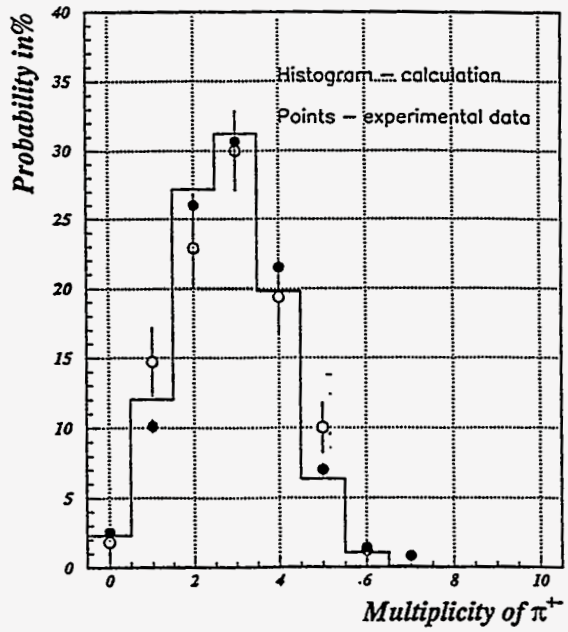

Figure 1: Production probability (in %) of a given number of charged pions π^{+-} in the stopped antiproton absorption on ^{12}C nucleus.

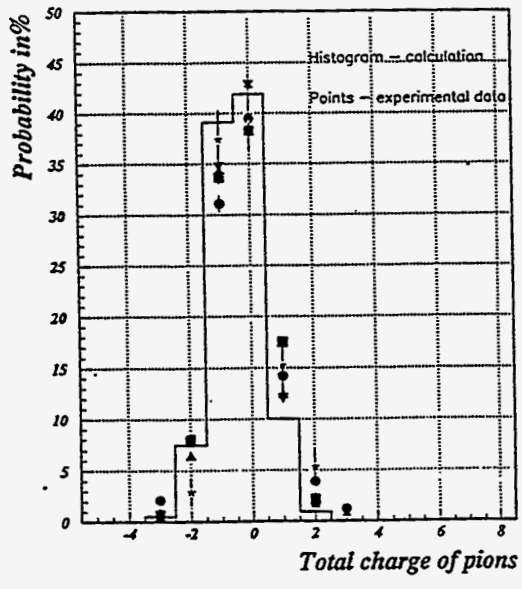

Figure 2: Probability (in %) of the interactions with a given charge Q carried away by pions in the stopped antiproton absorption on ^{12}C nucleus.

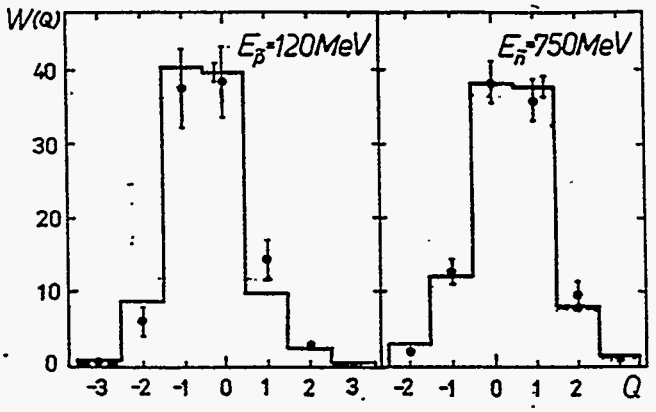

Figure 3: Probability (in %) of the interactions with a given charge Q carried away by pions in the antiproton annihilation at $120MeV$(left) and antineutron annihilation at $650MeV$(right) on ^{12}C nucleus.

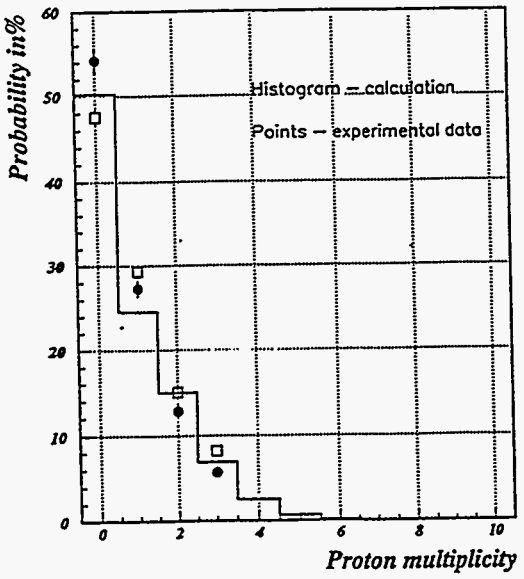

Figure 4: Production probability (in %) of a given number of protons in the stopped antiproton absorption on ^{12}C nucleus.

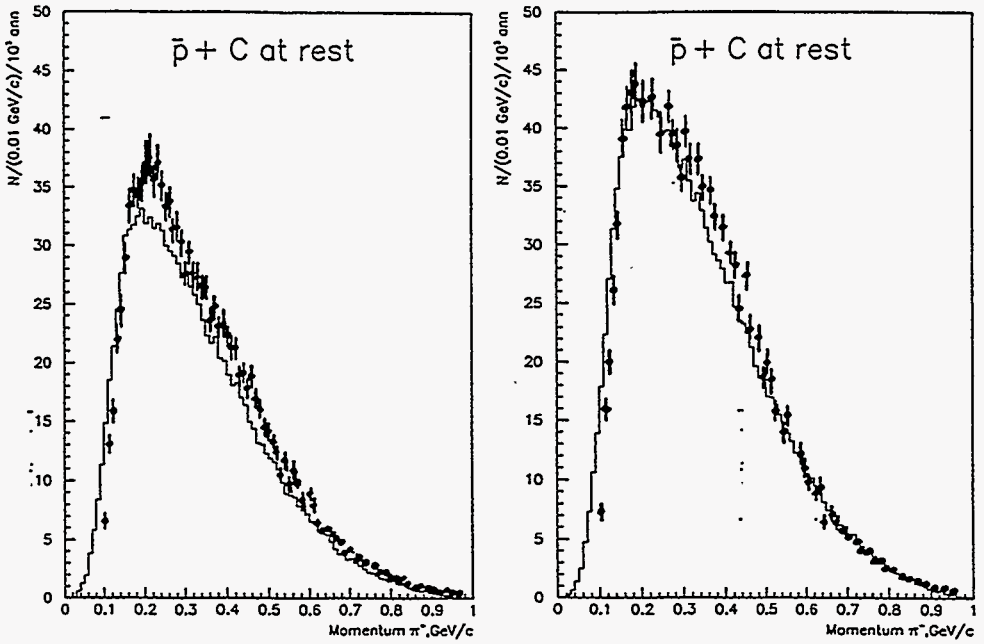

Figure 5: Momentum distribution of the π^+ and π^- mesons in the stopped antiproton absorption on ^{12}C nucleus.

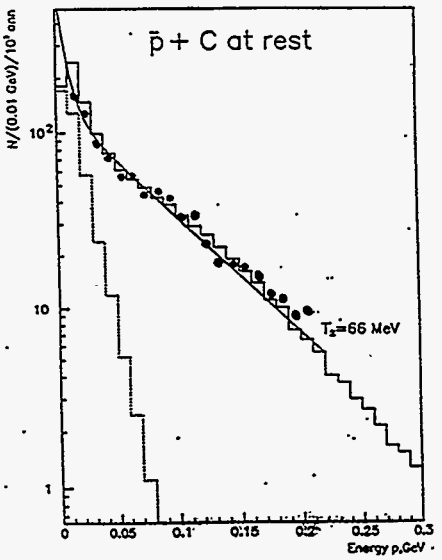

Figure 6: Energy spectra of protons in the stopped antiproton absorption on ^{12}C nucleus. Solid histogramm is INC+evaporation calculation. Dotted histogram is the contribution of evaporated protons. Line is the parametrization from [9]. Points are the experimental data [8].

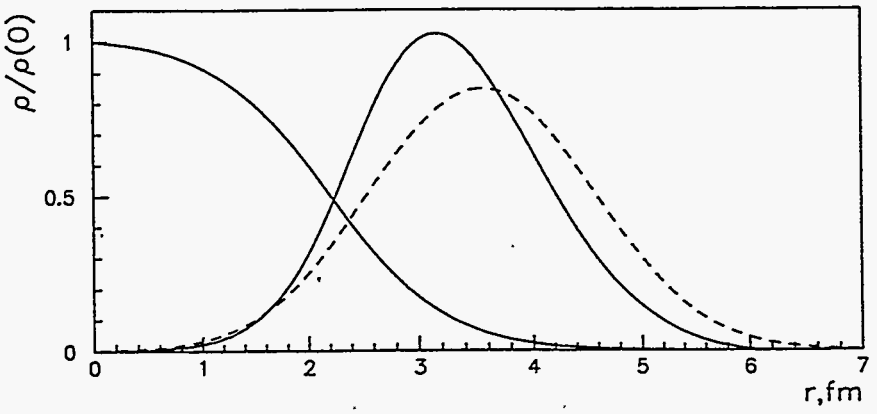

Figure 7: The radial distribution of the $\bar{n}$ absorption probability (solid curve) and $\bar{p}$ absorption probability (dotted curve), ρ is the nuclear density.

PROSPECTS FOR BARYON INSTABILITY SEARCH WITH LONG-LIVED ISOTOPES

Yu. Efremenko[ab], W. Bugg[b], H. Cohn[b], Yu. Kamyshkov[ab], G. Parker[a], F. Plasil[a]

[a] Oak Ridge National Laboratory, Oak Ridge, TN 37831
[b] University of Tennessee, Knoxville, TN 37996

ABSTRACT

In this paper we consider the possibility of observation of baryon instability processes occurring inside nuclei by searching for the remnants of such processes that could have been accumulated in nature as rare long-lived isotopes. As an example, we discuss here the possible detection of traces of ^{97}Tc, ^{98}Tc, and ^{99}Tc in deep-mined non-radioactive tin ores.

Introduction

The possible experimental observation of baryon instability remains among the most fundamental problems of modern physics [1]. The observed "baryon asymmetry" of the Universe [2] and some Unification Theories including Supersymmetric Models [3,4,5] require either nucleon-decay (with baryon number change by $\Delta B=1$) or neutron-antineutron transitions (with baryon number change by $\Delta B=2$) with rates stretching the limits of present experimental capabilities. Future prospects for proton decay and neutron-antineutron transition searches by traditional detection techniques have been reviewed in a number of contributions to this Workshop [1,6,7,8,9]. These techniques are based, in general, on the direct detection in real time of the final products of baryon transformation leading to the disappearance of one or two nucleons inside the nuclei corresponding to $\Delta B=1$ and $\Delta B=2$, respectively.

In 1975 a geochemical approach to the search for baryon instability was proposed by Rosen [10]. This method is based on the observation of residual nuclei (noble gases) which are the remnants of intranuclear nucleon decay accumulated in ores during a period of time that is comparable to the age of earth crust. Later Evans and Steinberg [11], using existing data [12] on the concentrations of stable isotopes of xenon in a $\sim 2.5 \cdot 10^9$ year-old telluride ore and comparing these with the abundance of xenon isotopes in the atmosphere, obtained a lower limit for the nucleon life time of $1.6 \cdot 10^{25}$ years. The result is based on the assumption that the excess of ^{129}Xe concentration in the ore (as compared to different Xe-isotopes in the ore and in the atmosphere) can be attributed to proton decay. Although this limit is a few orders of magnitude lower than the limits obtained from exclusive nucleon decay modes in real-time decay experiments [1,6] it is often interpreted in the literature as being independent of the nucleon decay mode [13]. We believe that this is a misinterpretation of the results of Ref. 11. These results are applicable only to certain particular plausible nucleon decay modes which do not have hadrons in the final state such

as $p \rightarrow e^+ 6\nu$, $p \rightarrow e^+ \gamma$, $n \rightarrow 3\nu$, $n \rightarrow \gamma\nu$, etc. The results may also be related to other nucleon decay modes after a mode-dependent correction factor is applied. The correction factor can be obtained via nuclear theory calculations of the type described in Ref. 14 which take into account transmutation of nuclides resulting from interactions of nucleon decay products with daughter nuclei. Evans and Steinberg also pointed out in [11] that: "The possibility of further large improvement of the nucleon lifetime limit using geochemical techniques would seem unlikely because of uncertainties in the estimation of background effects over geological timespans."

New approach with long-lived isotopes

The new approach we discuss here relies on the observation of traces of rare long-lived nuclides in ancient ores which are remnants of intranuclear baryon-number-violating processes. The life time of such nuclides should be large enough to allow accumulation of the baryon-number-violating signal and small enough (as compared to the age of the ore) to exclude the primordial abundance of these nuclides. Nuclides with a life time in the region of $\sim 10^6$ years are good candidates for such a search. This life time region is also appropriate for the reliable reconstruction of the geological history (stability) of the initial ore. The ore should, preferably, include no traces of fissionable or radioactive elements and should be obtained from a large burial depth in order to avoid cosmic-particle-induced background yield of the nuclides of interest. This ore should be mined in as large amounts as possible and should allow simple processing for the extraction of the nuclides of interest. We assume that chemical extraction can be used for the initial separation of the base element and for concentration of the residues. Considerable progress made in laser selective photoionization spectroscopy during the last decade [15] should allow, in a final step, the detection of single atoms of chosen isotopes with a typical efficiency ~ 1% in milligram samples. For technetium isotopes a detection limit of $5 \cdot 10^6$ atoms and an efficiency of 0.4% have already been demonstrated [16]. The detection of single atoms of francium with a typical efficiency of ~ 1% was achieved in [17]. These examples suggest that a detection limit for technetium at the level of a few hundred atoms would be possible.

We have identified a parent-daughter combination of nuclides which represents a transmutation which is favorable from the point of view of these requirements. This is a transmutation of tin into three isotopes of technetium: ^{97}Tc with (half-life time) $\tau_{97} = 2.6 \cdot 10^6$ years; ^{98}Tc with $\tau_{98} = 4.2 \cdot 10^6$ years; and ^{99}Tc with $\tau_{99} = 2.1 \cdot 10^5$ years. The probability of a parent-daughter transmutation with $\Delta A \sim 20$ and $\Delta Z = 7$ is determined by final-state interactions [14], i.e. it is decay-mode dependent. Since none of the technetium isotopes exist in the nature (technetium was discovered in the remnants of cyclotron bombarded molybdenum [18]) its chemical extraction will not be obscured by the presence of stable isotopes.

Assuming that the initial extraction of the technetium can be performed on a large scale as a by-process in the mining industry [18], and assuming that background processes, which will be discussed later, are favorable, one can expect detectable amounts of technetium to signal the baryon instability at the level of $\sim 10^{33}$–10^{34} years. Although different decay modes will have different transmutation efficiencies, the limit obtained by

this method will not permit identification of the particular decay mode involved or even to distinguish between $\Delta B=1$ and $\Delta B=2$ processes. Intranuclear neutron-antineutron transformations ($\Delta B=2$) in Sn with multi-pion final states will have nuclide transmutation efficiencies spread over a wide range of ΔA and ΔZ (Figure 1). Our choice of parent-daughter nuclides provides a higher sensitivity to $\Delta B=2$ processes than to those modes of nucleon decay with $\Delta B=1$ where ΔA and ΔZ values are expected to be lower.

A large ΔA gap between selected parent and daughter nuclides should be favorable from the point of view of suppression of background processes induced by low-energy cosmic rays, solar neutrinos, and neutrons and alpha particles from natural radioactivity since all of these processes result in smaller transmutations of the initial nuclide. However, interactions of high-energy muons, as discussed below, can, in some instances, produce rather large ΔA-transmutations.

Selection of tin (Sn) as a parent nuclide has some advantages. Tin is an abundant element with several stable isotopes with $Z=50$ and with an average mass of $A=118.7$. In nature the major source of tin is the mineral cassiterite (SnO_2). It consists of dense (~7 g/cm^3) hard granules. The world annual production of SnO_2 is $1.6 \cdot 10^5$ tons. The major deep mining areas for cassiterite are in Bolivia, Peru, Australia and England. Some of the cassiterites are found at a depth of more than a mile. As was pointed out in [18] it is likely that the industrial extraction scheme of tin from cassiterite can be modified in a simple and inexpensive way to allow the extraction of technetium with high efficiency from large quantities of tin ore as a by-process.

To estimate the yield of technetium isotopes we have calculated the spectrum of final-state nuclides resulting from neutron-antineutron transformations in tin nuclei followed by intranuclear cascades (the latter is described in Ref. 19). The results of these calculations are shown in Figure 1. The sizes of the boxes in this figure are proportional to the probability of the specific (A, Z) isotope production. Filled boxes correspond to the stable isotopes, and hatched boxes to long-lived isotopes of technetium. The arrows show the direction of natural radioactive transformations between nuclides. It is important to notice that isotopes with mass number of 97 and Z higher than 43 are unstable and have a relatively short life time. As a result of a chain of successive decays these isotopes are transmutated to ^{97}Tc and, therefore, essentially enhance its cumulative branching (ξ) to a total of 3.07 %. For the other two Tc isotopes the situation is not as favorable because the existance of stable isotopes of ruthenium ($Z=44$) terminates the corresponding decay chains earlier. Thus, the branching for ^{98}Tc is 0.56% and for ^{99}Tc it is 0.38%.

To estimate the sensitivity of our approach let us consider, for example, the extraction of the ^{97}Tc isotope from an initial sample of ore containing 1 ton of tin (N_n number of neutrons). We will ignore, for the time being, the processes which might lead to the background production of technetium in the ore. These processes will be considered in the next section. We will assume that the detection of single atoms by laser selective photoionization spectroscopy methods can be performed with an efficiency of 1% in the absence of a spurious background. This assumption corresponds rather closely to the presently-achieved level of detection efficiency [16, 17] but does require further refinement of the laser selective photoionization technique. Thus, assuming that the detection limit in laser selective photoionization spectroscopy (n_{min}) can be as low as 100

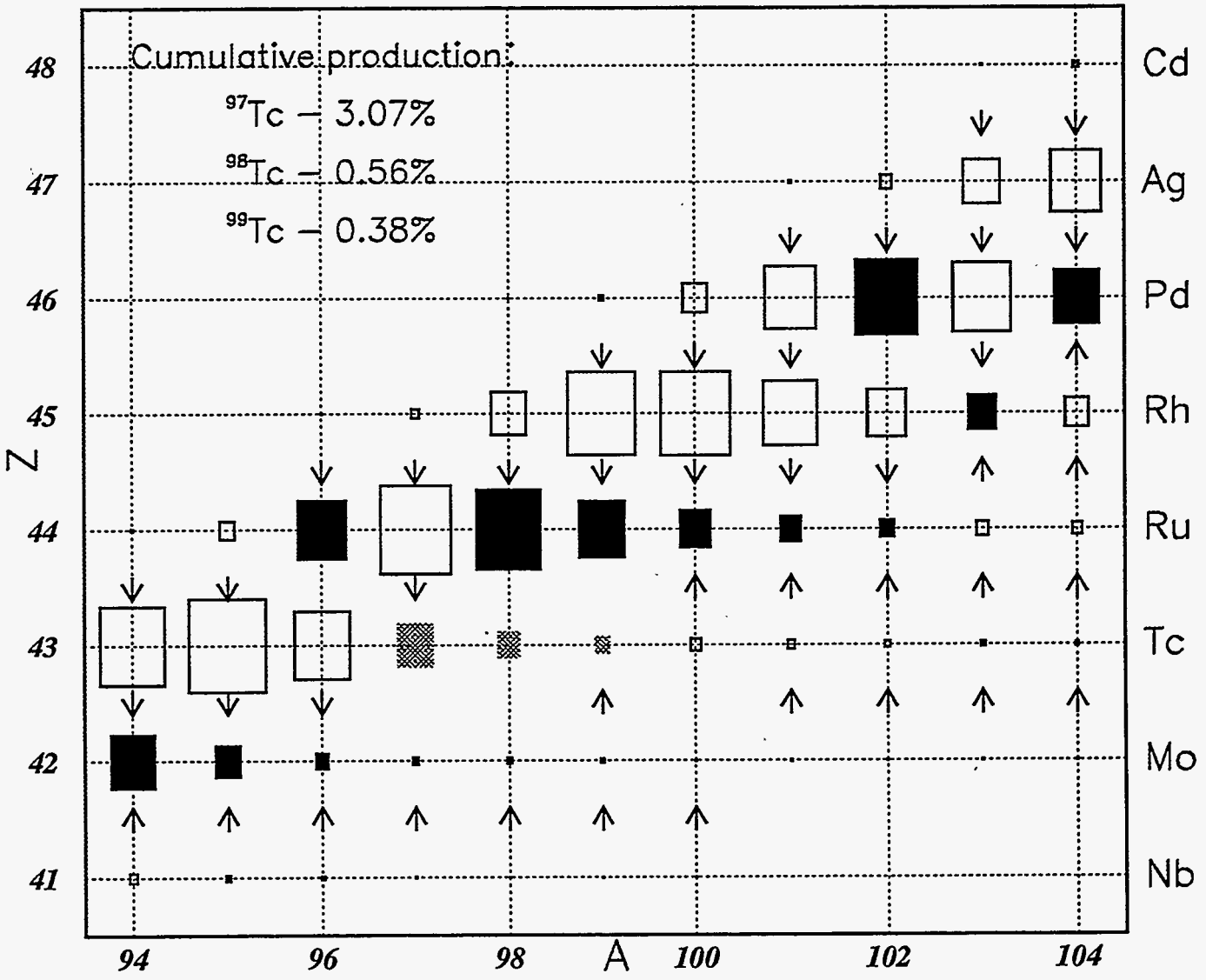

Fig 1. Yields of isotopes as a function of A and Z resulting from intranuclear neutron-antineutron transitions in tin, as calculated from the model of Ref. [19]. Open boxes indicate unstable isotopes, black boxes indicate stable isotopes, and hatched boxes indicate long lived technetium isotopes. The arrows show the direction of natural ß-decay. The sizes of boxes are proportional to the calculated isotope yields.

atoms, we can estimate the characteristic time for the case of neutron-antineutron transitions (^{97}Tc branching $\xi_{97} = 0.0307$) from:

$$\tau_{n-\bar{n}} = \frac{N_n \cdot \bar{\xi}_{97} \cdot \tau_{97}}{n_{min}} = \frac{6.022 \cdot 10^{23} \cdot 68.69/118.69 \cdot 10^6 \cdot 0.0307 \cdot 2.6 \cdot 10^6}{100} \cong 2.8 \cdot 10^{32} (\text{years / ton})$$

Thus, the processing of an initial amount of ore corresponding to 10^3–10^5 tons of tin could, potentially, result (in case of favorable background) in a neutron-antineutron intranuclear transition limit of 10^{33}–10^{34} years. For comparison, the limit of 10^{33} years for neutron-antineutron intranuclear transitions can be obtained from a five-year operation of the Super-Kamiokande detector which has a total active mass of 50,000 tons [6].

In practice, the experiment to search for technetium in tin ore would consist of two major stages: (a) efficient processing of a large amount of ore from deeply buried deposits including chemical separation of tin and concentration of technetium to a milligram-level sample, and (b) determination the concentration of technetium isotopes in the sample by laser selective photoionization spectroscopy methods.

Background

Neutron-antineutron transitions or nucleon decay are not the only mechanisms that might contribute to the production of isotopes of technetium in the tin ore. The following sources of background have to be considered: (a) natural radioactivity; (b) interaction of cosmic rays (mainly muons) with tin nuclei; (c) interaction of cosmic or solar neutrinos with possible admixtures of molybdenum present in the tin ore; and (d) technetium contamination during ore processing and sample analysis. We consider each in turn below.

(a) Natural radioactivity. If some amount of uranium is present in the ore, a background concentration of technetium will be produced due to spontaneous and/or induced fission processes. Nuclides with atomic masses of 90-100 are positioned at the maximum of the mass-yield curves for ^{235}U and ^{238}U fission, and have the yields of about 6%. It is known that primary fission fragments have the most probable Z-values that are lower than the Z-values for the stable isotopes of the same mass. As a result, the primary fission fragment yield of technetium is rather low. However, for nuclei with A=99, all isotopes with charge less then 43 are unstable with quite a short life time. They result in the chain of fast successive decays which lead to an accumulation of ^{99}Tc at the level of ~ 6% of fission products. For ^{98}Tc and ^{97}Tc isotopes the situation is quite different. Stable isotopes of ^{98}Mo, and ^{97}Mo terminate the decay chains and are the end products of unstable isotopes with lower Z which have been produced as primary fission fragments. As a result, the yield of ^{98}Tc and ^{97}Tc in uranium fission is the result of primary fission only. Unfortunately, there is only limited quantitative experimental information in the literature on the production of ^{98}Tc by fission and no data at all for ^{97}Tc.

In order to estimate the yield of ^{98}Tc and ^{97}Tc isotopes we used the usual Z-parametrization of the fission-fragment distribution [20] in the form $P(Z)=(c\pi)^{-1/2}\cdot\exp[-(Z-Z_p)^2/c]$ where parameter c is related to the width of the distribution ($c \sim 0.80 \pm 0.14$) and Z_p is the most probable value of Z of fragments with a given mass number. In figure 2a the

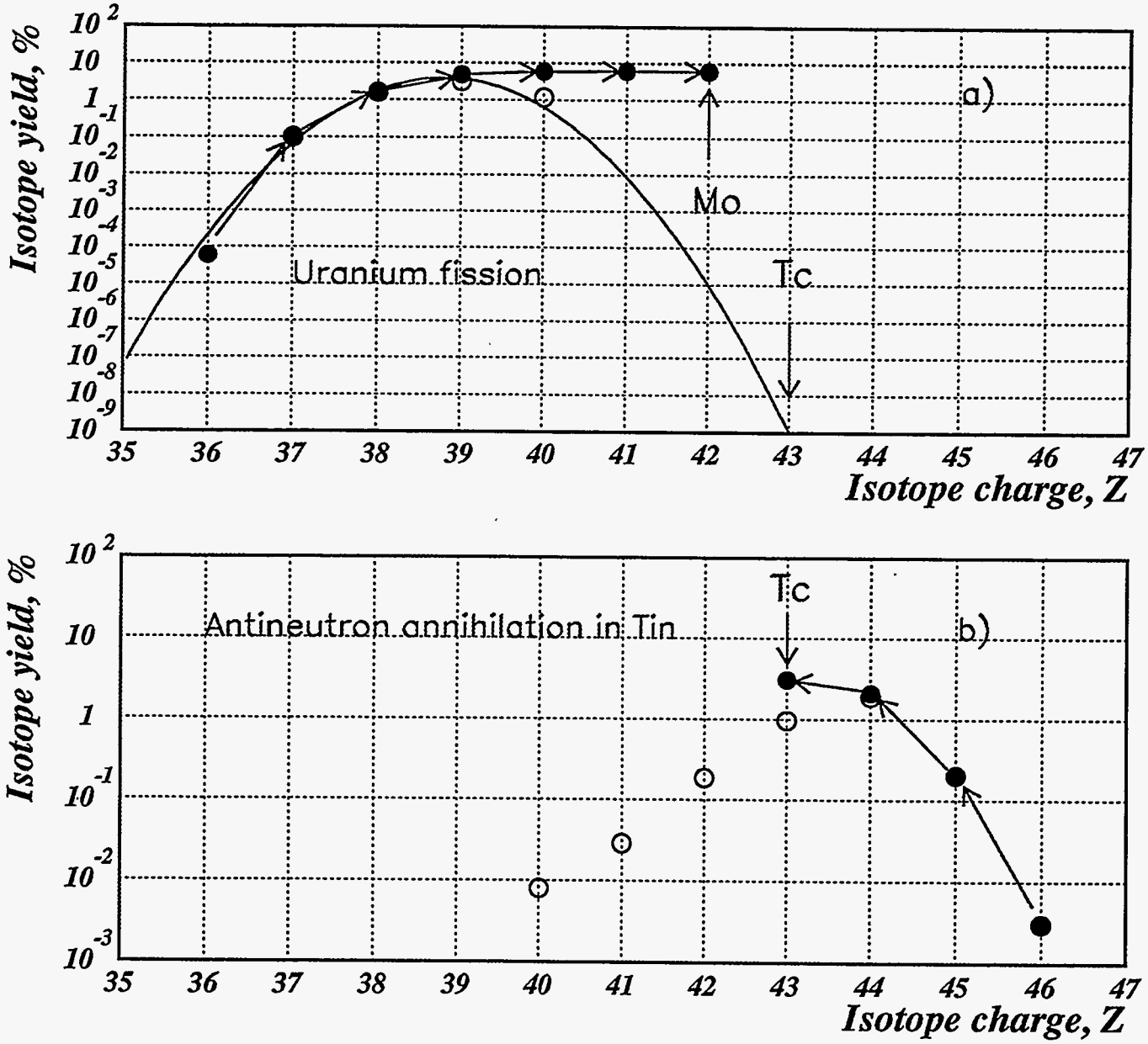

Fig 2. Cumulative yields of isotopes with mass number 97 produced by a) uranium fission [20], and b) antineutron annihilation in tin [19]. Open circles are for primary-produced isotopes; solid circles are for cumulative yields.

cumulative yield of isotopes (primary + decay) with mass number 97 produced by uranium fission is shown by the filled circles. The open circles in the figure represent the experimental data for primary-produced isotopes. The curve depicts the parametrization function with parameters c=0.8 and Z_p=38.8. Using this and similar parametrization for mass 98, we obtained the yield per fission event of $1 \cdot 10^{-11}$ for ^{97}Tc and of $7 \cdot 10^{-10}$ for ^{98}Tc isotopes. Shown in figure 2b is the yield of nuclides with mass 97 resulting from assumed neutron-antineutron intranuclear transformations in a natural mix of tin isotopes as calculated [19] from the model mentioned earlier [14]. Open circles are for primary-produced isotopes; solid circles and arrows indicate cumulatative yields.

Typical uranium concentrations in the earth crust are of the order of one ppm [21] and the uranium concentration in deeply buried tin ores has not been measured. The spontaneous fission life time of ^{238}U is $8 \cdot 10^{15}$ years. For ore with 1 ppm uranium concentration (by number) this should result in technetium concentrations of ~ 17 atoms of ^{97}Tc, 1,880 atoms of ^{98}Tc, and $8 \cdot 10^9$ atoms of ^{99}Tc isotopes per ton of tin. If the concentration of uranium in the initial material is known (the rate of induced uranium fission can be estimated from the known concentration of uranium and from the measured neutron flux in the deposit) the corresponding uranium background contributions can be calculated and subtracted from the measured amounts of technetium isotopes. Simultaneous measurement of all three technetium isotopes should provide additional constraints on the subtraction of the contributions of uranium fission, both spontaneous and induced. This would, in turn, require that the yields of ^{98}Tc and ^{97}Tc isotopes per uranium fission be determined experimentally with an appropriate accuracy. In Table 1 below we show estimated yields of Tc isotopes due to spontaneous uranium fission for two uranium concentrations of 1 ppm and 10 ppb representing pessimistic and optimistic levels.

(b) Cosmic rays. The main component of cosmic rays that penetrate to large underground depths consist of muons. The flux of muons is quickly attenuated with depth. After the first 500 meters of water equivalent it is ~ 1 muon$\cdot$m$^{-2}\cdot$s^{-1}. At a depth of ~ 4 km of water equivalent (~1 mile of rock), it is reduced to ~ $5.5 \cdot 10^{-5}$ muon$\cdot$m$^{-2}\cdot$s^{-1} [22]. At this depth the number of muon-nucleus inelastic interactions with a transferred energy E_{tr} > 100 MeV is about 0.11 per year in 1 ton of rock, as can be calculated from Ref. 23. The spectrum of these muons and their energy transfer in inelastic collisions with nuclei can be calculated from the known sea-level muon spectrum [24] and from the muon energy losses [23].

We pointed out earlier that the large ΔA of selected parent-daughter combination should be helpful for the suppression of background technetium production initiated by muon interactions with tin. This, however, is true only for low-energy muons. If the energy transferred to the tin nuclei by scattered muons is sufficiently large (~ > 200 MeV) it might result in inelastic interactions with a wide spectrum of ΔA losses. Since no direct experimental data on isotope production by high-energy muons are available, we estimated this effect by using the Rudstam formula [25] with parameters from [26]. In this way we calculated the concentration of technetium isotopes produced by muons per ton of initial tin at a depth of one mile of standard rock (ρ=2.65 g$\cdot$cm^{-3}) as $2.08 \cdot 10^3$ for ^{97}Tc, $0.63 \cdot 10^3$ for ^{98}Tc, and 22 for ^{99}Tc. We hope that the accuracy and reliability of these estimates can be further improved if some model (for example, [27]) that fits all the existing

experimental data on the yield of isotopes in high-energy collisions for all particles can be employed and if measurements of isotope yields resulting from interactions with virtual photons can be performed (for example, in the electron beam at SLAC). In Table 1 below we give the estimated yields of technetium isotopes due to cosmic muon interactions with tin for two burial depths of 1 mile and 2 miles, corresponding to pessimistic and optimistic background levels.

(c) Solar neutrino background. If molybdenum is presented in the ore the following reactions $^{97}Mo(\nu,e)^{97}Tc$ and $^{98}Mo(\nu,e)^{98}Tc$ might also produce technetium isotopes. In Ref. 28 the authors estimated the total production rate for ^{97}Tc due to this reaction to be $5.9 \cdot 10^{-36}$ atoms per ^{97}Mo-atom per second. Thus, assuming 1 ppm level (by number) of ^{97}Mo in the initial tin ore (abundance of ^{97}Mo is 9.55%) we obtain a concentration of ^{97}Tc at the level of ~ 2.5 per ton of initial tin. For the ^{98}Tc, due to the higher threshold of the $^{98}Mo(\nu,e)^{98}Tc$ reaction, the corresponding concentration is much smaller (see Table 1). The same authors estimated the contribution of another source of background associated with the presence of molybdenum, the process $^{97}Mo(p,n)^{97}Tc$. Their conclusion was that the yield of technetium for this process will be below the level of solar-neutrino production. If the concentration of molybdenum does not exceed the few-tens of ppm level, this source of background can be neglected.

(d) Technetium contamination during processing and analysis. It is very often quoted in the literature that technetium "was never found in nature". This is not quite correct. For example, tiny amounts of ^{99}Tc were found in uranium ores in the Belgium Congo [29]. Moreover, starting in 1945, technetium began to be produced in large quantities "artificially" in nuclear weapon tests and in nuclear reactors. To date, the total amount of technetium produced in nuclear weapon tests in the atmosphere is estimated to be 250 kg [30]. This includes a total of ~ 3 mg of ^{98}Tc, or ~ $3.5 \cdot 10^4$ atoms per square meter of the earth's surface. The distribution of technetium obviously is not uniform. The highest concentration should be found in the top layers of soil near the nuclear explosion sites. Measurements [31] of ^{99}Tc concentration in the soil in Japan have shown the presence of ~ $6 \cdot 10^{11}$ atoms per 1 kg of soil at the surface. This concentration falls quickly with increasing depth. At a depth of ~ 25 cm below the surface it is already lower by a factor ~100. The concentration of ^{98}Tc should be lower by factor of ~10^8 and concentration of ^{97}Tc by another factor of ~ 70. Thus, we expect the artificial technetium contamination of tin ores from the deeply buried deposits to be negligible. We also anticipate that all necessary precautions can be taken in order to avoid contamination during the ore processing, transportation, and during analysis of the samples.

Discussions and conclusions

We now can include background effects in the estimates of the possible achievable limits in the search for baryon instability via the detection of long-lived isotopes of technetium in nature. The baryon instability signal can be treated as a statistically significant excess over the background in concentrations of technetium isotopes in deep deposits of tin ores. We use the assumptions discussed above and summarized here as follows: (a) large volumes (up to 10^5 tons) of tin ore can be processed industrially with technetium extraction as an inexpensive by-process; (b) tin ore deposits from depths

between 1 and 2 miles (4-8 km of water equivalent) can be used; (c) the concentration of uranium in the tin ore is in the range of 10 ppb to 1 ppm and can be determined; (d) the chemical extraction efficiency of technetium will be ~ 25%; and (e) the minimum detection level of laser selective photoionization spectroscopy of technetium isotopes is 100 atoms, corresponding to an efficiency of ~ 1% with no ion detection background. Under these assumptions we have calculated the background contributions from different sources for the three isotopes of technetium considered above. These calculations are summarized in Table 1 below and are also presented in Figure 3 in term of the estimated discovery potential of the proposed method for ^{97}Tc and ^{98}Tc isotopes, assuming the optimistic and pessimistic background scenarios from table 1.

Table 1. Expected concentrations of technetium isotopes (atoms per ton) in deep-deposition of tin ores.

Isotope:	^{97}Tc	^{98}Tc	^{99}Tc
Expected Tc yield due to baryon instability:			
$\tau_{isotope}$, years	$2.6 \cdot 10^6$	$4.2 \cdot 10^6$	$2.1 \cdot 10^5$
$n \rightarrow \bar{n}$ branching, ξ	0.0307	0.0056	0.0038
Yield atoms/ton for $\tau_{n\bar{n}}=10^{32}$ yr	278	82	2.8
Pessimistic background yield:			
Yield atoms/ton due to cosmic μ (at depth of ~1 mile of rock)	2077	626	22
Yield atoms/ton due to 1 ppm of ^{238}U	17	1,880	$8 \cdot 10^9$
Optimistic background yield:			
Yield atoms/ton due to cosmic μ (at depth of ~2 mile of rock)	2.6	0.8	0.03
Yield atoms/ton due to 10 ppb of ^{238}U	0.17	19	$8 \cdot 10^7$
Yield atoms/ton due to solar ν	2.5	<1	–

The discovery potential in Figure 3 is expressed in metric tons of initial tin needed to be processed in order to establish the excess technetium concentration signal over the background level as 2.3 sigma (90% CL) of statistical fluctuation of the background. Additional requirement imposed on the estimated discovery potential limit is that the

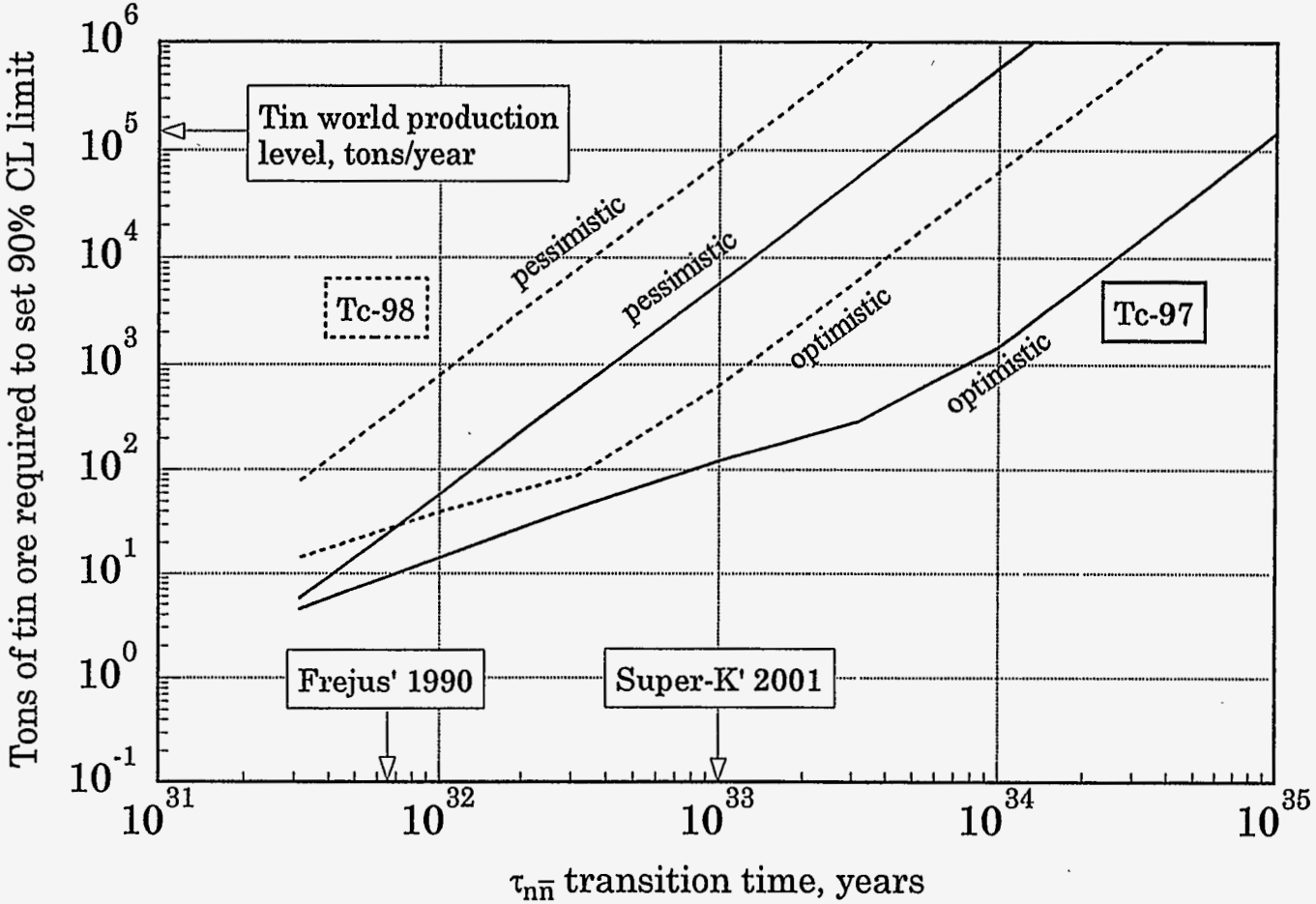

Fig 3. Amount of initial tin ore to be processed in order to establish, at 90% confidence level, the excess concentration of technetium isotopes due to intranuclear neutron-antineutron transitions in tin relative to background concentration of technetium. "Optimistic" and "pessimistic" assumptions used for background calculations are explained in the text.

minimum detected number of atoms be higher than 10. It is also assumed that the background can be estimated reliably and that systematic errors can be minimized as a result of direct measurements, related to the technetium production processes, made at different depths and extrapolated to the working depth.

Simultaneous detection of all three isotopes, together with direct measurements of uranium concentrations in the ore, muon flux measurements, and determination of the yield of technetium isotope production in uranium fission should provide additional constraints on the determination of contributions of different backgrounds. The efficiency of chemical extraction of technetium should be measured in the industrial environment with samples of known concentration entered at the beginning of the separation process. A minimum detection level of 100 atoms of technetium by the laser selective photoionization spectrometry methods needs to be demonstrated. Also, it will be very important to locate tin mines with a burial depth of deposits of more than a 4,000 m of water equivalent.

We would like to thank D. S. Burnett (Caltech), P. Degtyarenko (ITEP), Ye. S. Golubeva (INR), M. Goldhaber (BNL), A. S. Iljinov (INR), J. Parks (UTK), A. Puretzky (ORNL), and C. Y. Wong (ORNL) for usefull and stimulating discussion. This research was sponsored by the Laboratory Directed Research and Development Program of the Oak Ridge National Laboratory, managed for the U.S. Department of Energy by Lockheed Martin Energy Research Corp., under Contract No. DE-AC05-96OR22464.

References:

1. M. Goldhaber, these proceedings.

2. A. D. Sakharov, JETP Lett. **5** (1967) 24.

3. J. C. Pati, these proceedings.

4. R. N. Mohapatra, these proceedings.

5. P. Nath, these proceedings.

6. J. Stone, these proceedings.

7. A. Mann, these proceedings.

8. D. Gibin, these proceedings.

9. Yu. A. Kamyshkov, these proceedings.

10. S. P. Rosen, Phys.Rev.Lett. **34** (1975) 774.

11. J. C. Evans, Jr., R. I. Steinberg, Science **197** (1977) 989; also R. I. Steinberg, J. C. Evans, Jr., E. L. Fireman, in Proceedings of the International Conference on Neutrino Physics, Elbrus, USSR, June 1977.

12. E. W. Hennecke, O. K. Manuel, D. D. Sabu, Phys.Rev. **C 11** (1975) 1378.

13 Review of Particle Properties, Phys.Rev. **D 50** (1994) 1675.

14 A. S. Il'inov, M. V. Mebel', and S. E. Chigrinov, Yad.Fiz. **37** (1983) 18-26.

15 V. S. Letokhov, V. I. Mishin, A. A. Puretzky, Prog. Quant. Electr. **5** (1977) 139-303.

16 H.-U. Hasse et al., in proceedings of the Seventh International Symposium on the Resonance Ionization Spectroscopy 1994, pp 499-502 (1995).

17 S. V. Andreev, V. S. Letokhov, V. I. Mishin, Phys. Rev. Lett. **59** (1987) 1274.

18. G. W. Parker, these proceedings.

19. Ye. S. Golubeva et al., these proceedings.

20. R. Vandenbousch, J. R. Huizenga, "Nuclear Fission", Academic Press, NY 1973.

21. B. Mason, "Principles of Geochemistry", Wiley, NY 1966.

22. Ch. Berger et al. (Frejus Collaboration), Phys. Rev. **D40** (1989) 2163.

23. W. Lohman, R. Kopp, R.Voss, "Energy Loss of Muons in the Energy Range 1-10,000 GeV", CERN 85-03 (1985).

24. L. V. Volkova, G. T. Zatsepin, L. A. Kuz'michev, Yad. Fiz **29** (1979) 1252-1265.

25. G. Z. Rudstam, Naturf. **21a** (1966) 1027.

26. G. G. Jonsson, K. Lindgren, Physica Scripta Vol.**15** (1977) 308-310.

27. J. Jastrzebski et al., Phys.Rev. **C 47** (1993) 216.

28. G. A. Cowan, W. C. Haxton, Science, Vol. **216** (1982) 51-54 .

29. B. T. Kenna, P. K. Kuroda, J. Inorg. Nucl. Chem. **23** (1961) 142.

30. K. Yoshihara, Topics in Current Chemistry **176** (1996) 17.

31. S. Morita, K. Tobita, M. Kurabayashi, Radiochim Acta **63** (1993) 63.

SEARCH FOR TECHNETIUM IN NATURAL TIN METALLURGICAL RESIDUES*

G. W. Parker
Chemical Technology Division, Oak Ridge National Laboratory
P.O. Box 2008, Oak Ridge, Tennessee 37831-6221

ABSTRACT

Possible instability of baryons inside the nuclei might result in accumulation of rare isotopes in natural ores.† In this respect, isotopes of technetium have certain advantages that can be useful in the search for technetium in nonradioactive ores by chemical methods. In this paper, we review the history of technetium research and discuss a new approach to the search for natural technetium associated with tin ores which appears to offer a rare possibility of discovering a smelting operation by-product such as flue dust, in which the volatile technetium heptoxide (Tc_2O_7), like rhenium heptoxide (Re_2O_7), would be expected to concentrate. Our concept of a search for technetium in these materials would be based on the assumption that traces of rhenium could occur in the ore and could be traced most easily by neutron activation of small samples. Such a procedure would confirm that an enrichment from the ore to the flue dust actually occurs with the rhenium and therefore should occur with technetium. Furthermore, this occurrence should identify the best location to search for technetium.

1. INTRODUCTION

Possible instability of baryons inside the nuclei might result in accumulation of rare isotopes in natural ores. Since the technetium does not have stable isotopes, its detection in nonradioactive ores might be an indication for baryon instability processes.† We consider a new approach to the chemical extraction and concentration of the traces of natural technetium from the tin ores. This new approach is based on a comparison of the boiling points of these two oxides, showing them to be remarkably close, 311°C for Tc_2O_7 and 362°C for Re_2O_7. In a given air-cooled stack, therefore, technetium would deposit a little higher in the stack. However, there would be significant overlap.

Existing experience of extraction of technetium is related exclusively to the artificially produced element 43 from uranium fission or from cyclotron bombarded molybdenum. So far, natural technetium has not been detected in nonradioactive ores. Section 2 will give a review of more than 70 years of history of technetium search and existing extraction techniques.

Since our new approach is based on a chemical similarity of technetium and relatively more abundant element rhenium, we will discuss the existing methods of rhenium extraction in Sect. 3.

---

*Research sponsored by Oak Ridge National Laboratory, managed by Lockheed Martin Energy Research Corp. for the U.S. Department of Energy under contract number DE-AC05-96OR22464.

†See the paper by Yu. Efremenko in these proceedings.

These two chemical extraction processes (technetium and rhenium), coupled with the sensitive neutron activation analysis, are expected to form the basis for our search for naturally occurring technetium.

2. ISOLATION OF ELEMENT 43 FROM URANIUM FISSION (HISTORICAL REVIEW)

In 1925, Noddack, Tacke, and Berg[1] reported the discovery of two new elements of the manganese group and presumed them to be of atomic numbers 43 and 75. Later work has substantiated their claim on element 75 (now known as rhenium), but their work on element 43 has not yet been confirmed.

In 1937 and again in 1939, articles appeared by Perrier and Segré,[2-3] defining some of the physical and chemical properties of a long-lived radioactive component extracted from cyclotron bombarded molybdenum, which they declared to be element 43. A later paper in 1939 by Seaborg and Segré[4] discussed the decay scheme of a 6.6-h 43 isotope, which was also extracted from cyclotron bombarded molybdenum, and concluded that it should exhibit a ground state half-life in excess of 40 years.

As early as 1943, the classified literature of the Manhattan Project contained references and possible analytical schemes for element 43, and Glendenin[5] suggested in November 1943 that the half-life exceeded 3000 years. Until late 1945, experimental evidence failed to show that even trace amounts of a long-lived activity existed in fission product mixtures. Schuman[6] announced in February 1946 a new fission product activity that carried well on Re_2S_7 and followed the 6.6-h 43 daughter activity of 67-h ^{99}Mo with an estimated half-life of $\sim 3 \times 10^5$ years.

However, in all of these cases, the amounts isolated were of such small magnitude that only radiochemical techniques were available for identification purposes. Motta et al.[7-8] investigated neutron induced activities in ruthenium and molybdenum during most of 1946 and reported two isotopes of element 43, one of ~90-d half-life and another 2 to 4×10^6 years.

2.1 FIRST SMALL SCALE RADIOCHEMICAL ISOLATION OF ^{99}Tc

Early in 1946, active investigation was begun by the author[9] in an attempt to isolate visible amounts of the long-lived isotope of element 43 from fission. The general scheme for isolation conceived consisted of dissolving long-bombarded uranium slugs, precipitating the acid insoluble sulfides on suitable carrier, filtering, dissolving the precipitate, and distilling the 43 from the dissolved precipitate with H_2SO_4. A number of tracer experiments were run using the 6.6-h 43 isotope that resulted in the following conclusions.

1. The uranium slugs were dissolved in HCl rather than HNO_3, as has been usual. This eliminated a changeover step from the nitrates.
2. Because the chloride solution as it is formed in the dissolver contains so much solid material, probably UCl_4, an oxidation step was necessary to change the UCl_4 to UO_2Cl_2. It was found that H_2O_2 addition followed by Br_2 and aeration gave a solution which could be handled successfully.

In August 1946, the preliminary tracer experiments were complete, and the process was transferred to a shielded cell, adapted to remote control, and hot runs started. Yields were collected and combined from the first 5 slugs, processed, and precipitated as the carrier-free sulfide. Samples were prepared for spectrographic analysis, and spectrograms were photographed by D. Timma[10] in September 1946. Samples were prepared to produce the X-ray emission spectra[11] that was successfully photographed with appropriate standards in December 1946 (Fig. 1). The sample shown by the X-ray spectra is chiefly element 43. The lines of element 43 measured were $K_{\alpha 1}$, $K_{\alpha 2}$, $K_{\beta 1}$, and $K_{\beta 2}$. The agreement of the observed wave length assignment and calculated values are apparent in Table 1. The chemical and physical history of the material, together with the controlled conditions in obtaining the X-ray spectra, is conclusive evidence that this material is element 43.

Table 1. Observed and calculated values for X-ray lines of element 43.

Element	Line	Calculated XU	Observed XU
43	$K_{\alpha 2}$	677.77	677.8
43	$K_{\alpha 1}$	673.37	673.5
43	$K_{\beta 1}$	600.14	601.4
43	$K_{\beta 2}$	589.18	589.9

2.2 HOT CELL INSTALLATION FOR LARGE SCALE EXTRACTION OF TECHNETIUM

In the process of selecting a carrier for technetium suitable for a precipitation process to be used in the recovery of ^{99}Tc from radiochemical wastes, a method employing perrhenate as a carrier and tetraphenyl arsonium chloride (TPA chloride) as the precipitant was first proposed because of the unique similarity between the pertechnetate ion and the perrhenate ion. For several reasons, including the cost of rhenium and the difficulty of later separating it from the technetium, a substitute carrier that could be used liberally and separated easily was sought. The pilot-plant size installation is shown in Fig. 2.

Besides perrhenate, it has been found that any of a certain type of anion, especially those comprising the perhalogen acids perchlorate and periodate, will form an efficient carrier for pertechnetate. Of these, periodate is the most effective, although for decontamination perchlorate is more satisfactory. Besides these, fluoborate (BF_4^-) is at least as good as if not better than perrhenate, while permanganate is fair but forms an explosive mixture. The fact that anions of the type XY_4^- form the only good carriers seems to support the formula TcO_4^-. A few anions of the form $XY_4^=$, such as $CrO_4^=$ or $S_2O_8^=$, carry in a much weaker fashion with large excesses of the reagent. The flow plan,[12] including the crude precipitation and the purification process used to recover a total of 18 g of technetium, is shown in Fig. 3.

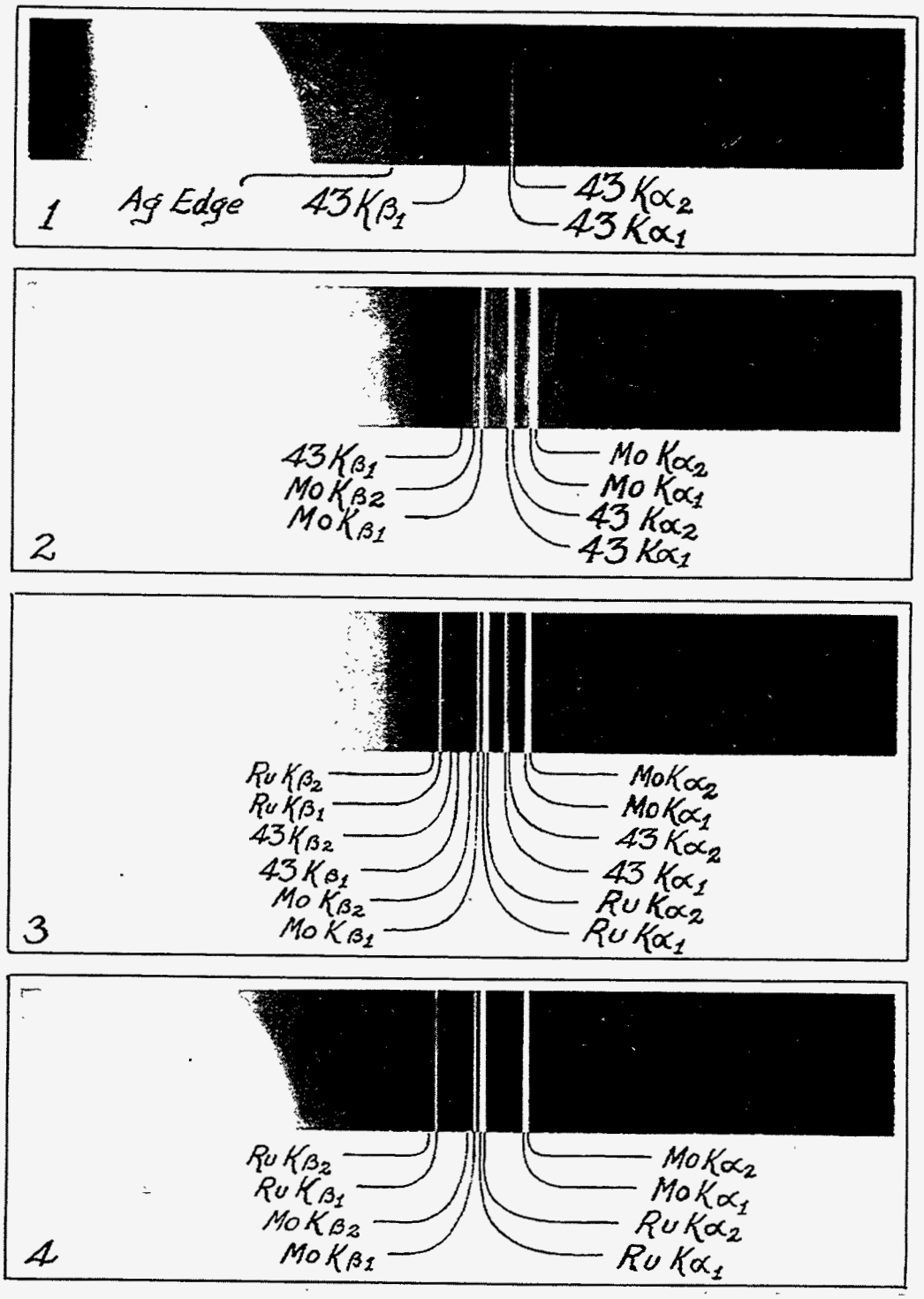

Fig. 1. First X-ray spectrograms of element 43 with adjacent molybdenum 42 and ruthenium element 44 (December 1946).

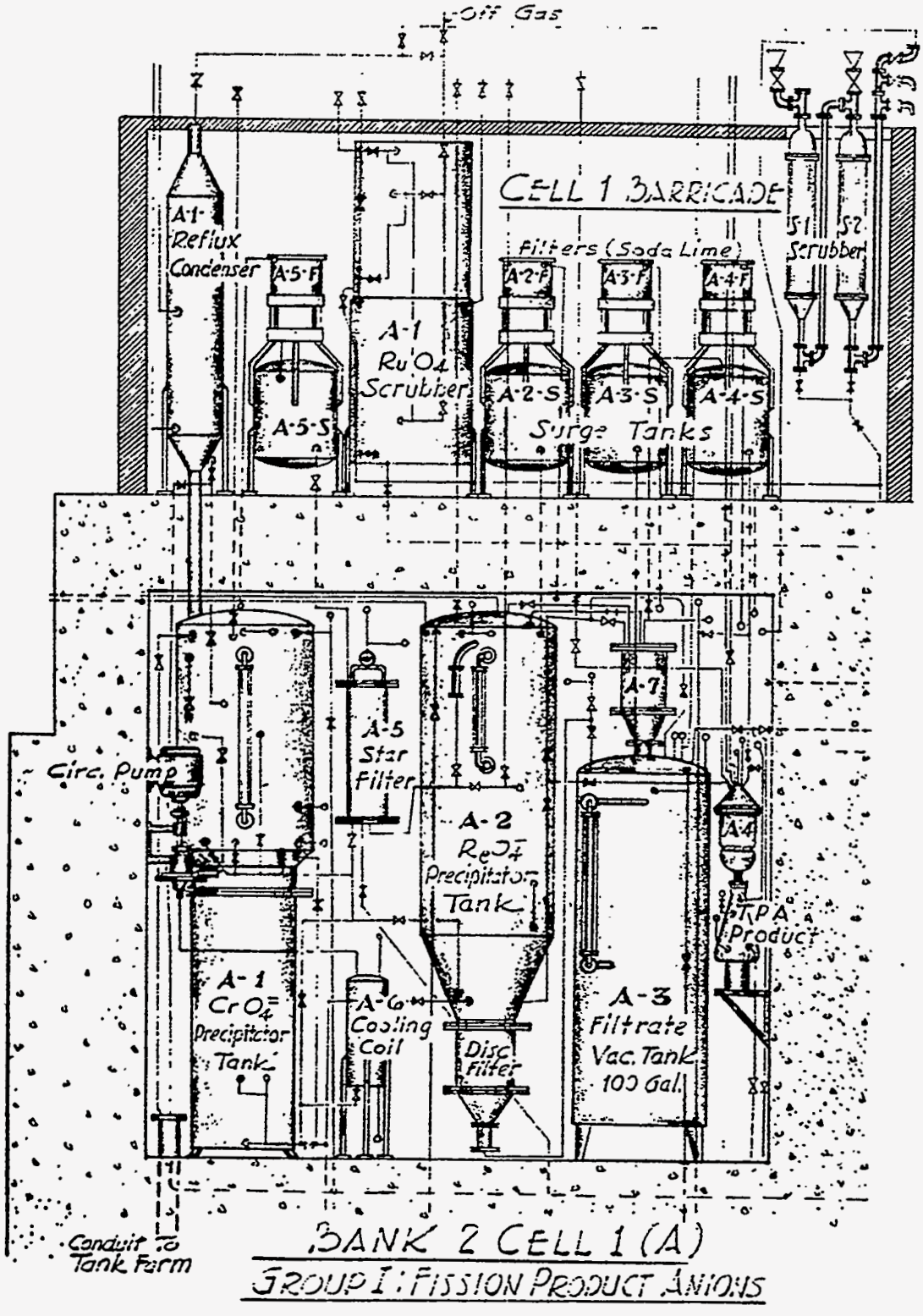

Fig. 2. Hot-cell process for technetium recovery.

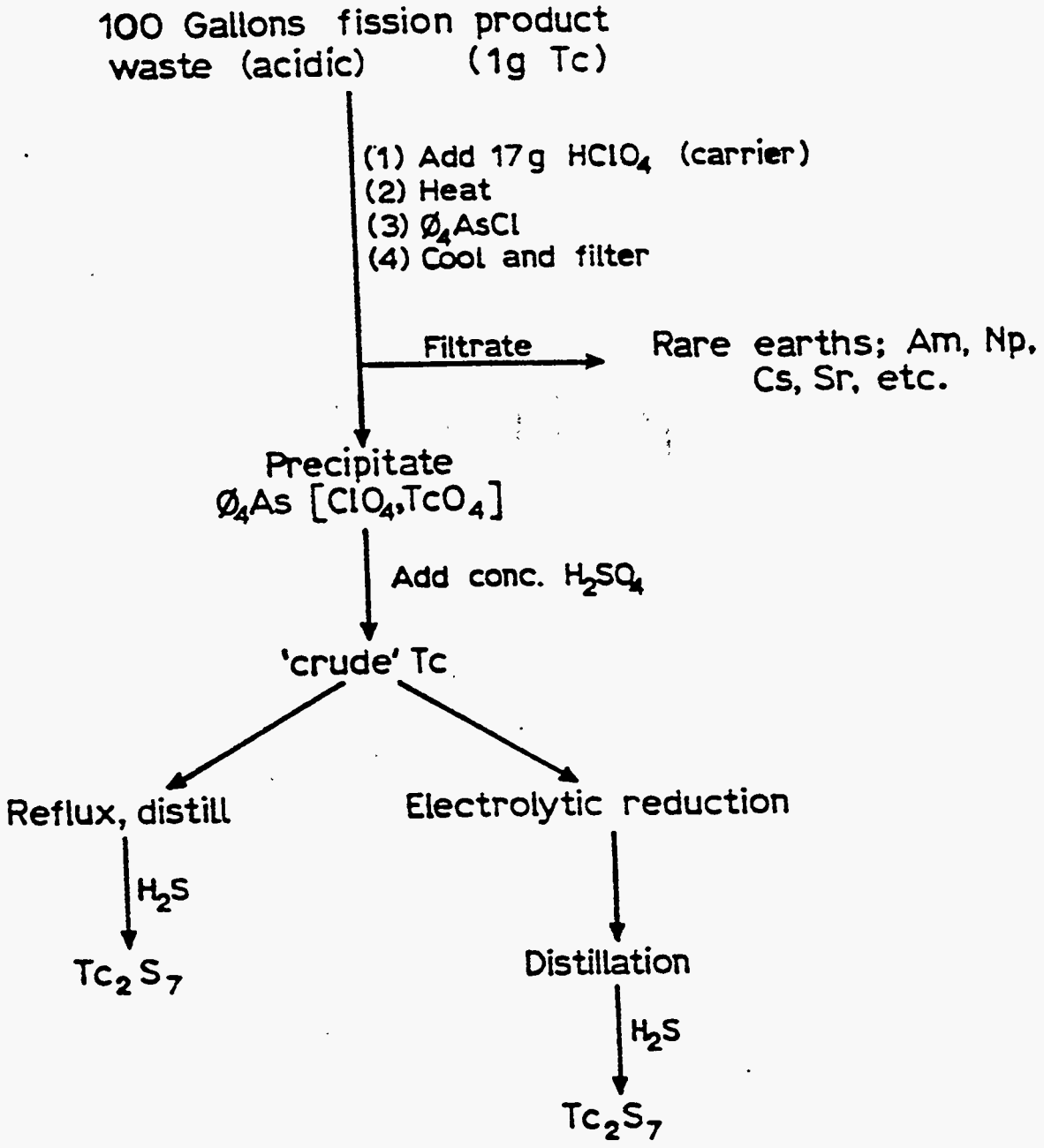

Fig. 3. Hot-cell flow plan for extraction of technetium from fission product waste.

3. EXTRACTION OF RHENIUM

In 1929, Ida and Walter Noddack described the preparation of 1 g of rhenium metal from 660 kg of a Norwegian molybdenite. This constituted the largest single preparation of the metal in the 4 years following the announced discovery of the element by the same authors in 1925.

Prior to World War II, all of the rhenium of commerce was extracted from the molybdenite residues recovered from the Mansfeld copper schists of Germany. Annual production capacity was reported to be 120 kg/year at a cost of ~$2.40/g. If this source has been exploited for rhenium since the close of the war, no mention of it has been found in the literature.

For a number of years, the only known U.S. commercial source of rhenium was a flue dust resulting from the roasting of an Arizona molybdenite. The origin of the rhenium-bearing molybdenite is a copper sulfide ore mined in the vicinity of Miami, Arizona. Over a period of 10 years, ~17 tons of the above mentioned molybdenite roaster flue dust has been processed for its rhenium content at The University of Tennessee. From this material ~240 lb of rhenium has been extracted in the form of potassium perrhenate. The flue dust thus far processed in this operation was found to be of variable composition with the rhenium content varying from 3,000 to 16,000 ppm (0.3 to 1.6%).

The process for the technical preparation of rhenium having its origin in the Mansfeld copper schists of Germany has been described by Feit.[13] A summary of the process used prior to 1940 follows.

Treatment of the Mansfeld copper ore by an unstated metallurgical process gave rise to a complex sulfide slime containing salts of Cu, Mo, Ni, Fe, V, and Re together with minor amounts of other elements. After weathering in air for several months to more than a year, the sludge was leached with water. The leachings were next concentrated by spontaneous evaporation in the open with the consequent precipitation of calcium, copper, and nickel as sulfates.

After separation of the solid sulfates, the leach was further concentrated by heating and then cooled to remove more of the heavy metal sulfates. This process was continued until the leach had a specific gravity of 2. At this point, the solution was treated with a solution of ammonium sulfate to precipitate the insoluble nickel-ammonium salt. Further evaporation of the mother liquor, followed by addition of solid ammonium sulfate, gave on cooling additional nickel-ammonium sulfate together with complex ammonium salts of the heteropoly acids of phosphorus, vanadium, and molybdenum. The ammonium sulfate treatment was continued until only ammonium sulfate separated. The pale yellow liquor remaining from the above series of concentrations and precipitations gave on treatment with potassium chloride an impure potassium perrhenate. Solution of the latter in hot water, followed by filtration to remove a flocculent precipitate, gave a colorless filtrate from which nearly pure potassium perrhenate separated on cooling.

In some respects, the process in use at The University of Tennessee[14] for the extraction of rhenium is similar to that described by Feit. The overall process, however, is much simpler and less time-consuming than the German method.

The flue dust from which the rhenium is extracted is obtained from the Miami Copper Company of Miami, Arizona.[15] The original ore, mined primarily for its copper content, contains copper as the sulfide together with a small amount of molybdenite. Associated with the latter is rhenium, presumably as the sulfide. After crushing and grinding the ore, the sulfides are concentrated by flotation. A second flotation operation serves to separate the copper and molybdenum sulfides, the rhenium following along with the molybdenum.

Roasting of the molybdenite converts the molybdenum to molybdenum (VI) oxide, MoO_3, and the rhenium to rhenium (VII) oxide, Re_2O_7. The conversion, however, is not 100% complete, and, as a result, there is collected at one stage of the operation a product described as "molybdenite roaster flue dust." This product contains unaltered molybdenite, water-soluble complex molybdenum compounds of an undetermined composition, and rhenium (VII) oxide or soluble perrhenates, together with minor amounts of other constituents. On exposure to moist air, the flue dust frequently absorbs water. The moist product or its water solution, as might be expected, is acidic.

Extraction of the rhenium from the flue dust is carried out in a large "Ceratherm-500" vacuum filter equipped with a "Filterstone" porous plate. The upper bowl of 100-gal capacity is separated from the 50-gal lower bowl by the 2-in.-thick porous filter plate. With air passing up through the porous plate, 200 lb of water, or washings from a previous extract, is placed in the upper bowl of the digester and 200 lb of flue dust added. The digestion is carried out for 1 h or until all solids are uniformly dispersed. With the air stream cut off, a vacuum is applied to the lower bowl to separate the soluble fraction containing the rhenium from the insoluble fraction that consists largely of molybdenite. The filtrate is then transferred to a storage tank where it is allowed to remain for several hours in order to allow any fine particles of molybdenite to settle. In the meantime the molybdenite cake remaining on the porous plate is digested with two separate 100-lb batches of fresh water. The washings are combined for use in digesting fresh flue dust.

The supernatant liquid from the initial extraction is transferred to a second digester, similar to the flue dust digester but on a smaller scale. With air passing through the solution, 1 lb of finely ground potassium chloride is added per 1.5 gal of extract. The air stirring is continued for 30 min to 1 h to insure complete solution of the potassium chloride and precipitation of the potassium perrhenate. On completion of the digestion, a vacuum is applied to the lower receiver to separate the insoluble potassium perrhenate from the soluble portion.

Two beneficial effects result from the above processing operations. In the initial digestion, there is a noticeable rise in temperature on solution of the flue dust in water. Secondly, on treating the extract with solid potassium chloride, the digestion mixture is cooled, thereby rendering the potassium perrhenate less soluble. The processing equipment used in the extraction and precipitation operations is represented in Fig. 4. A flow diagram of the process is shown in Fig. 5.

4. CONCLUSION

Chemical processes of technetium and rhenium separation described above, coupled with the sensitive neutron activation analysis, are expected to form the basis for efficient initial extraction of naturally occurring technetium.

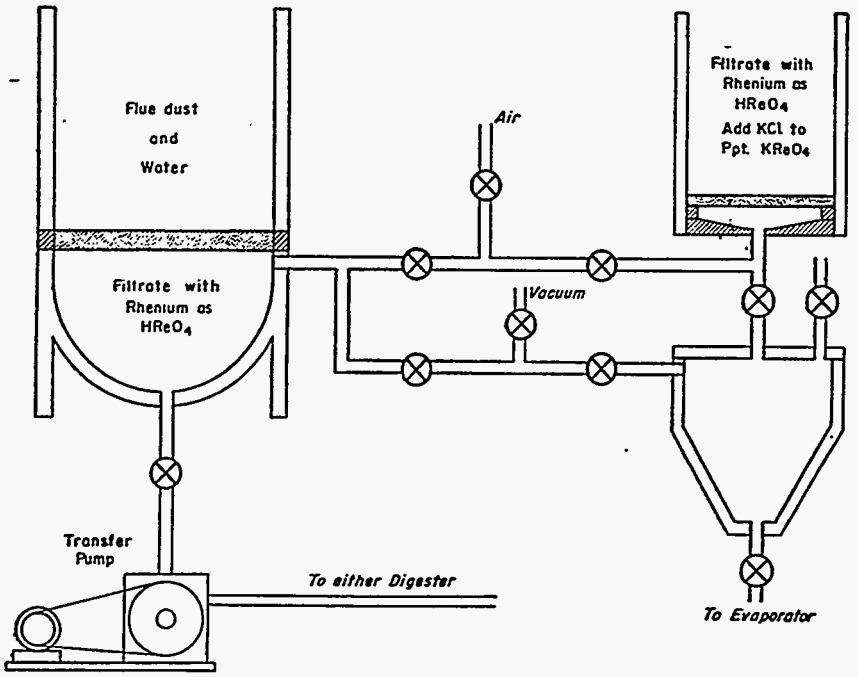

Fig. 4. Extraction of rhenium.

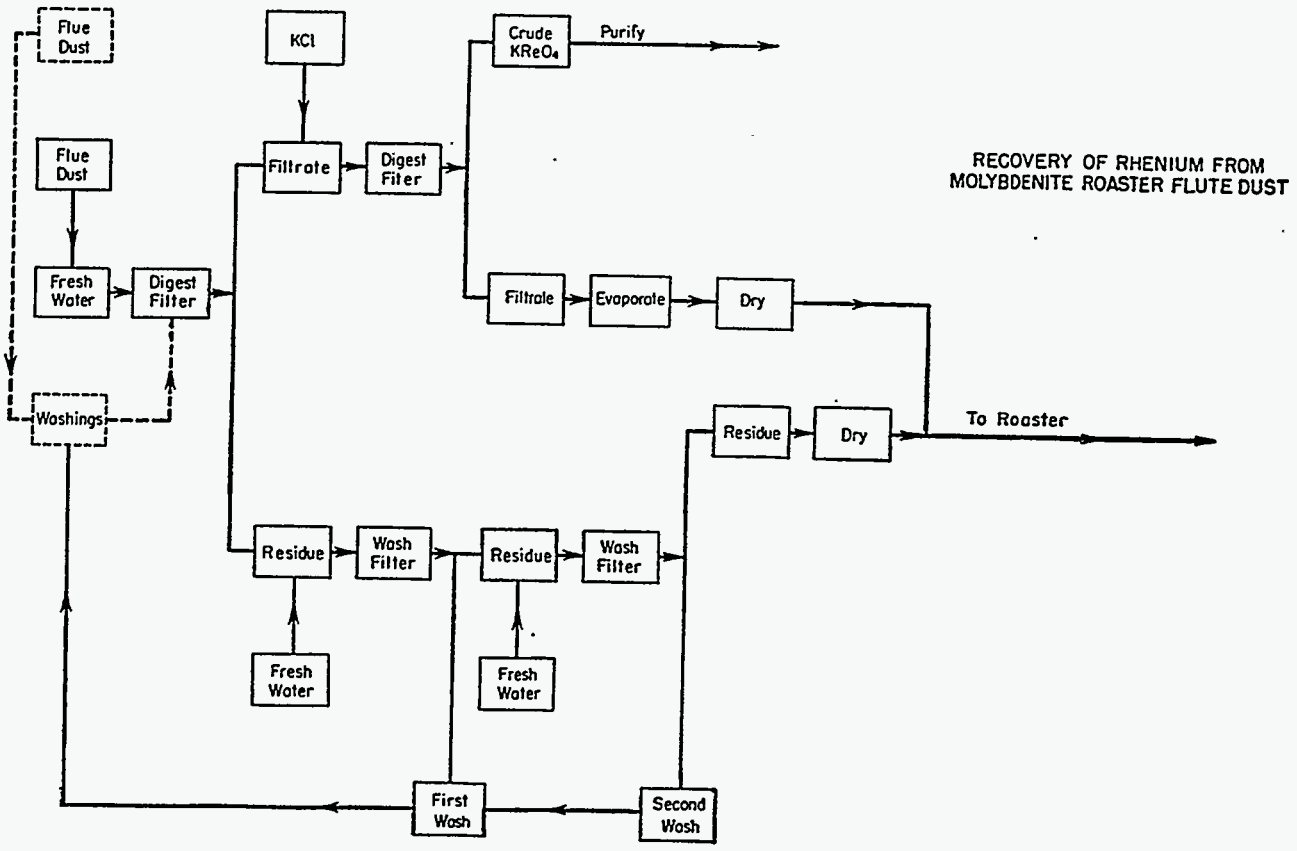

Fig. 5. Extraction of rhenium–flow diagram.

5. REFERENCES

1. W. Noddack, I. Tacke, and O. Berg, "Two new elements of the manganese group," *Proceedings of the Berlin Academy of Sciences,* Mathematics-Physics Section, pp. 400–409 (Session of June 11, 1925).

2. C. Perrier and E. Segré, "Some chemical properties of element 43," *J. Chem. Phys.,* **5**, 712 (September 1937).

3. C. Perrier and E. Segré, "Some chemical properties of element 43," **II**, *J. Chem. Phys.,* 7, 155 (March 1939).

4. G. T. Seaborg and E. Segré, "Nuclear isomerism in element 43," *Phys. Rev.*, **55**, 808 (1939).

5. L. E. Glendenin, CC-1050, p. 9 (November 1943).

6. R. P. Schuman, *Note on a new 43 activity*, CC-3434 (Feb. 7, 1946).

7. E. E. Motta, Q. V. Larson, and G. E. Boyd, *Studies in the tracer chemistry of element 43*, MonC-99 (Apr. 1, 1947).

8. E. E. Motta, G. E. Boyd, and A. R. Brosi, "Production and isotopic assignment of a 90-day activity in element 43," *Phys. Rev.*, **71**, 210 (Feb. 1, 1947).

9. G. W. Parker, J. Reed, and J. W. Ruch, *Isolation of milligram amounts of element 43 from uranium fission*, AECD-2043,Clinton National Laboratory (Jan. 9, 1948).

10. D. Timma, Clinton National Laboratories, unpublished correspondence (September 1946).

11. W. F. Peed, B. G. Saunders, and L. E. Burkhart, *X-ray spectrum of element 43*, Report H-7, 360.7, Clinton Engineer Works, Tennessee Eastman Corp. (Jan. 8, 1947). See *Phys. Rev.*, **73**, 347 (1948).

12. G. W. Parker and W. J. Martin, Oak Ridge National Laboratory Declassified Report, ORNL-1116, p. 26 (January 1952).

13. W. Feit, *Z. angew. Chem.*, **43**, 459 (1930).

14. A. D. Melaven and J. A. Bacon (to University of Tennessee Research Corp.), U.S. Patent 2,414,965 (January 1947).

15. B. W. Gonser, ed., *Rhenium*, papers presented at the Symposium on Rhenium of the Electrothermics and Metallurgy Division of the Electrochemical Society, Chicago, Illinois, May 3–4, 1960, Elsevier Publishing Company, New York (1962).

ULTRA-COLD ANTINEUTRONS (UC$\overline{n}$)

R. Golub
Hahn Meitner Institut
Glienickerst., 100
14109, Berlin

May 11, 1996

Abstract

We discuss the possibility of using Ultra-cold neutrons (UCN) for the search for $n-\overline{n}$ oscillations. It is usually thought that the strong absorption of an $\overline{n}$ on the walls of a UCN container and the phase shift associated with the difference in the interaction of n and $\overline{n}$ with the walls will mean that the effective coherence time will be essentially one collision time. However in the presence of a relatively small magnetic field the time dependent phase difference between n and $\overline{n}$ due to their opposite magnetic moments will tend to cancel the phase shift due to wall collisions for one spin state. In addition using realistic parameters for the interaction of $\overline{n}$ with the walls we show that the absorption of $\overline{n}$, while large, is not so great as might be expected especially for low energy UC$\overline{n}$. Averaged over the entire UCN phase space the effective coherence time is expected to be about 10 collision times. This is particulary interesting for experiments using neutron guides as discussed by Steve Lamoreaux at this conference.

1. Introduction

This talk is based on an original idea of Yoshiki [1] and is the result of a collaboration over several years [2]. As the probability of observing an $\overline{n}$ grows as t^2 it is natural to think of using the long storage time of Ultra-cold Neutrons (UCN)[3] as the basis of a sensitive search for $n-\overline{n}$ oscillations. However it is immediately obvious that the approach is limited and most workers in the field have concluded that the difference between the n and $\overline{n}$ interactions with the walls of the containing vessels will result in the effective coherence time for the measurement being essentially one collision time [4]. This is due to the relative phase shift between n and $\overline{n}$ as well as to the strong absorption of $\overline{n}$ on the walls.

The work summarized in this talk was undertaken to study these questions in some detail. First we show that there is a smooth transition to the normal semi-classical free space description for particles in quantized eigenstates in a box. In the case of strongly absorbing walls the effective eigenstates are decaying. However in the region between the walls wave packets will not decay and one obtains the expected semi-classical limit where the particles propagate freely between wall collisions which are describable in terms of the ordinary complex reflection amplitude.

Second we calculate the reflection coefficient for UC$\overline{n}$ starting from a reasonable model for the $\overline{n}$ - nucleus interaction potential.

Then we go on to show that in the presence of an applied field the Larmor precession phase tends to cancel the $n-\overline{n}$ phase difference for one spin state and we estimate the effects this will have on the ability to search for $n-\overline{n}$ oscillations in various geometries using UCN. Averaged over a reasonably large phase space the effective coherence time of the experiment can approach about 10 collision times.

2. Semi-classical treatment of a particle in a box with absorbing walls

It is expected that the lifetime of UC$\overline{n}$ stored in a container will be much less than that of UCN due to the strong absorption (annihilation) of the former in the walls. Thus the potential of the walls $\left(\widetilde{V}\right)$ will have a significant imaginary part (in what follows we use ~ to indicate a complex quantity) and the states will be decaying with time. The energy of a given state will be complex. In the space between the walls $\left(\widetilde{V}=0\right)$ we have

$$\frac{2m}{\hbar^2}\widetilde{E} \equiv \frac{2m}{\hbar^2}\left(E-i\Gamma\right) = \widetilde{k}^2 \equiv \left(k-i\gamma\right)^2 = k^2-\gamma^2-2ik\gamma \tag{2.1}$$

so that

$$\frac{\Gamma}{\hbar} = v_g\gamma = \frac{-v_g}{2a}\ln\rho \tag{2.2}$$

where the last step follows from the usual boundary conditions at the walls[2]. A wave packet formed out of $\widetilde{k}$ states will have the form

$$\sim \int dk B\left(k\right) e^{-\Gamma t} e^{i\left(kx-\omega t\right)} e^{\gamma x} \tag{2.3}$$

and the peak of the wave packet will move with $\left(x=v_g t\right)$ so that

$$e^{-\Gamma t}e^{\gamma x} = 1 \tag{2.4}$$

because of (2.2). Thus the wave packet will move without attenuation until it strikes the wall, the reflection coefficient following from the usual boundary condition on the $\widetilde{k}$ eigenstates.

3. Search for $n-\overline{n}$ oscillations using UCN

3.1. $n-\overline{n}$ oscillations in a magnetic field

As is well known a magnetic field splits the degeneracy between $n-\overline{n}$ so that their states have a time dependent relative phase which results in the $\overline{n}$ amplitude reaching a limit and returning to zero as time goes on. For times such that $\omega_L t \ll 1$ the evolution of the $\overline{n}$ amplitude is the same as for a free particle.

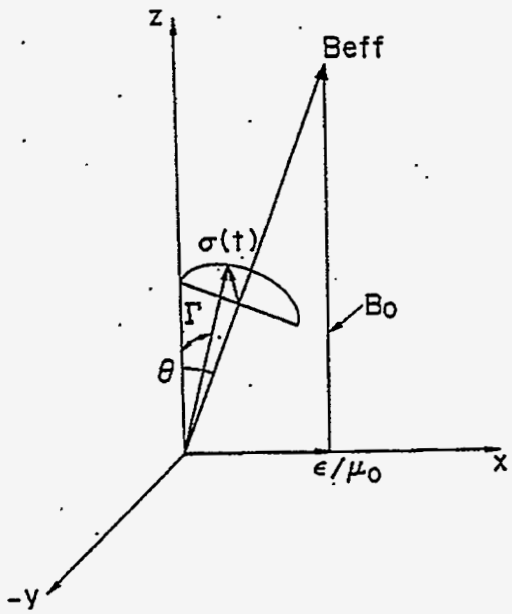

Fig.1. Effective field for $n-\overline{n}$ oscillations. ϵ is the ΔB=2 $n-\overline{n}$ interaction. The system vector precesses around B_{eff}.

The situation can be visualized in diagrams like fig. 1) which shows the motion of the isotopic spin $\sigma_z = +(-)$ corresponds to $n\,(\overline{n})$ under the influence of a magnetic field and ϵ, the $\Delta B = 2$, $n-\overline{n}$ interaction responsible for the oscillations. The probability of observing an $\overline{n}$ is given by

$$P_{n\overline{n}}(t) = |\beta|^2 = \sin^2 \Gamma/2 = \sin^2\theta \sin^2 \omega_L t/2 \qquad (3.1)$$

where $\beta\,(t)$ is the amplitude for finding $\overline{n}$ after time t. If the magnetic field is periodically reversed in fig. 1), the center of rotation, θ, in fig. 2) will move to the position $-\theta$. If this is done at times separated by π/ω_L there will be a continuous increase of $\overline{n}$ amplitude comparable to that in zero magnetic field. A detailed discussion [2] shows that the results are very close to those attained with an optimum sinusoidally modulated [5] field, which has been suggested as a method to reduce the magnetic field sensitivity.

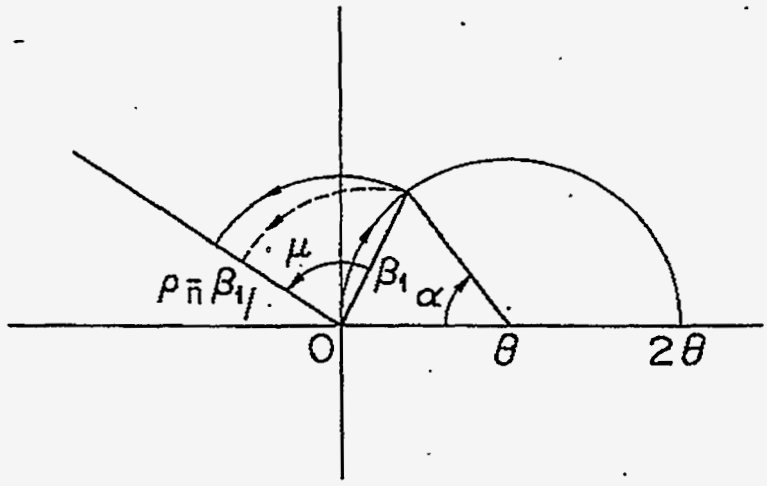

Fig. 2. Collision of an $n - \overline{n}$ system with a wall seen in a plane perpendicular to B_{eff}. α is the Larmor precession angle in the magnetic field during the time between collisions. μ is the relative phase shift due to the collision.

3.2. Wall collisions in the presence of a magnetic field

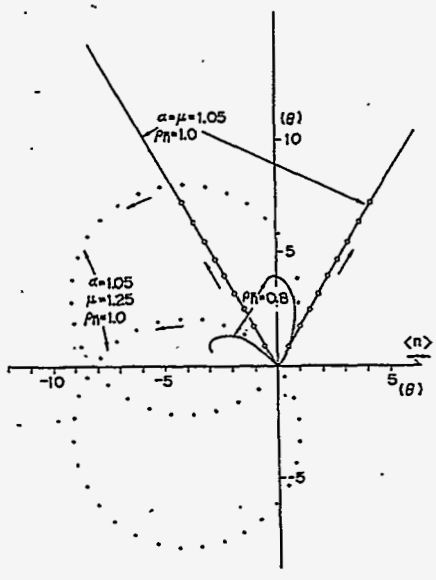

Fig. 3. Build up of $\overline{n}$ amplitude for various conditions. Successive collisions are assumed to be the same. For $\rho_{\overline{n}} = 1, \mu \neq \alpha$ the locus is two circles, for $\mu = \alpha$ the circles degenerate into straight lines (resonance), for $\rho_{\overline{n}} < 1$ the system approaches an equilibrium point.

Fig 2) shows the motion of the system in a plane perpendicular to the effective field. After a collision the system point precesses about the field direction labelled by θ through an angle $\alpha = \omega_L t$ until the next wall collision. The collision produces a sudden jump in the phase of β by an amount $\mu = \phi_n - \phi_{\overline{n}}$ and a reduction in its amplitude by $\rho_{\overline{n}}$ the reflection amplitude for $\overline{n}$ for the conditions of the collision. It

is easy to see that for $\mu = \alpha$, $\rho = 1$ the system will jump back and forth between two lines, receding further from the origin as time goes on. Thus under these conditions the build up of $\overline{n}$ amplitude is very close to that in free space. For $\rho < 1$ the trajectory is more complicated reaching an equilibrium point at some distance from the origin (Fig.3).

3.3. Reflection coefficient for UC$\overline{n}$

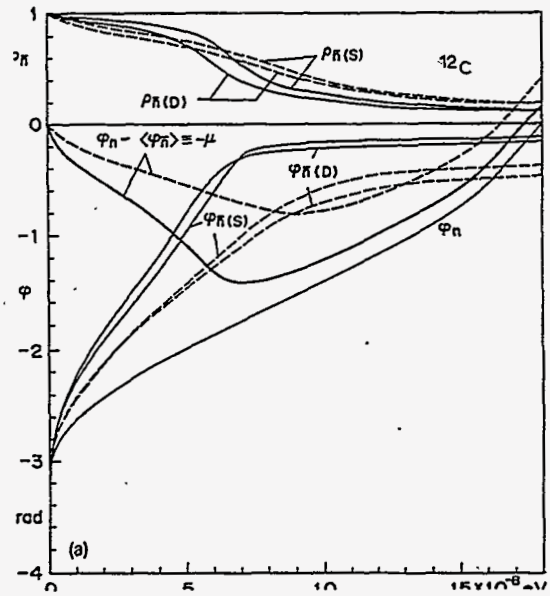

Fig. 4. Reflectivity $\rho_{\overline{n}}$, and relative phase change $\varphi_n - \varphi_{\overline{n}}$ due to a collision on ^{12}C. See text for an explanation of the different curves.

We took the optical potential for $\overline{n}$ to be that determined for $\overline{p}$ atoms by Wong *et al* [6]. We carried out calculations for two shapes of potential, a square well and a modified fermi distribution (diffuse potential). In addition Wong *et al* give two possible fits to the data which they call S and D. Fig 4) shows our results for the UC$\overline{n}$ reflectivity and relative phase shift μ as a function of the kinetic energy perpendicular to the surface for ^{12}C. We see that the two models, S and D, give essentially the same results for $\overline{n}$ reflection but the results for the square well and Fermi shapes are somewhat different (solid and dashed lines).

3.4. Probability of $n - \overline{n}$ oscillations in a UCN storage vessel

We consider a UCN storage vessel in a magnetic field in the presence of $n - \overline{n}$ oscillations. As the $\overline{n}$ probability builds up there will be a loss $(1 - \rho_{\overline{n}}^2)$ of $\overline{n}$ at each wall collision. These losses are due to annihilation in the walls and each $\overline{n}$ lost will result in a signal. We assume that the storage vessel is surrounded with suitable detectors so as to allow the detection of these events. The probability of detecting an $\overline{n}$ in N collisions is

$$P_N = P_{N-1} + |\beta_N|^2 \left(1 - \rho_{\overline{n}}^2\right) \tag{3.2}$$

where β_N is the $\overline{n}$ amplitude before the N^{th} collision.

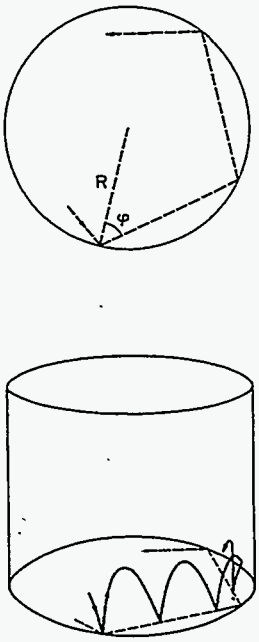

Fig. 5. Typical trajectory in a cylindrical storage vessel under the influence of gravity.

Calculations have been made for two geometries, assuming specular reflections in both cases. The first case was a spherical container in the absence of gravity and the second was a cylindrical container taking the effects of gravity into account. A typical trajectory for the second case is shown in fig. 5). The results of the calculations for this case are shown in fig. 6) using the parameters for ^{12}C. We have plotted the total annihilation probability for $\overline{n}$ in 100 seconds. We see there is some influence of the shape chosen for the $\overline{n}$ nucleus interaction potential. The results shown represent an integration over the usual UCN phase space to allow the use of conventional UCN intensity calculations. For comparison a quasi-free (beam) experiment using *mev* neutrons and a flight time of 0.12 sec would have an $\overline{n}$ probability of 2.5×10^{-18} per neutron. However the much greater throughput of beam experiments as compared to current UCN sources mean that a UCN experiment is not nearly competitive. However the situation may change in the near future with the introduction of the next generation of UCN sources [3].

In addition, as suggested by Lamoreaux (these proceedings), the technique described here may allow a guide to be used for a beam experiment, the effects of the wall collisions being partially compensated by the magnetic field.

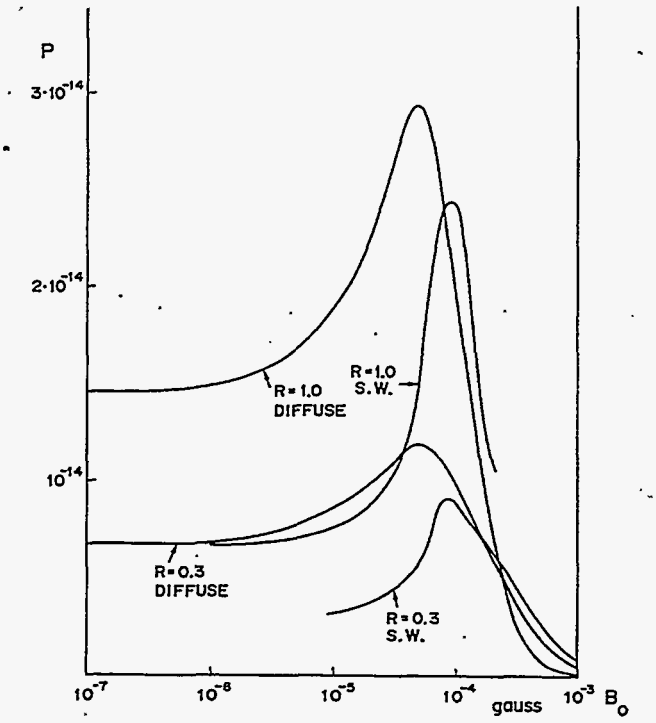

Fig. 6. Probability of detecting an $\overline{n}$ after 100 s storage time as function of applied magnetic field and for different $\overline{n}$-nucleus potentials. R is the cylinder radius in meters, $\epsilon = 10^{-23}$ ev.

References

[1] H. Yoshiki, KEK Reprint 80-10, Tsukuba, Japan (1980) and Proceedings of ICANS-IV, KEK, Japan

[2] R. Golub and H. Yoshiki, Nuc. Phys. **A501**, 869 (1989);
R. Golub, H. Yoshiki and R. Gähler, Nuc. Inst. Meth., **A284**, 16 (1989)
H. Yoshiki and R. Golub, Nuc. Phys. **A536**, 648 (1991)

[3] R. Golub, D.J. Richardson and S.K. Lamoreaux, *Ultra Cold Neutrons*, Adam Hilger, (1991)

[4] M. Baldo-Cellini, in G.L. Greene, ed. *Investigations of Fundamental Interactions with Cold Neutron Beams*, Nat. Bureau of Standards, Special Pub. 711, Gaithersburg, Md. (1985)

[5] U.P. Trower and N. Zorhe, Phys. Rev. **D25**, 3088 (1982)

[6] C.Y. Wong *et al* Phys. Rev. **C29**, 574, (1984)

Ultracold Neutrons in Superfluid ^{4}He and $n - \bar{n}$ Oscillations: Complementarity of Cold Neutron Technology

S.K. Lamoreaux

Physics Department, University of Washington, Box 35160, Seattle, WA 98195-1560

Abstract

Both a proposed new technique to measure the neutron electric dipole moment (EDM) and a proposed new neutron-antineutron oscillation experiment require a high flux of "supermoderated" neutrons (to temperatures less than 15K). The complementarity between these experiments will be outlined in regard to a universal source. Some ideas from ultracold neutron work will be suggested as possible improvements for the new neutron-antineutron experiment.

1 Introduction

We have proposed a new technique to measure the neutron electric dipole moment (EDM) which might lead to a factor of 2000 improvement over the current experimental limits. This technique, fully described in Ref. [1], is based on the production, storage and detection of ultracold neutrons (UCN) produced and stored in a superfluid ^{4}He bath. Polarized ^{3}He is introduced to the bath to serve as a UCN polarizer, spin precession analyzer, and magnetometer. Recent progress is described in Ref. [2]. (See Refs. [3] and [4] for additional commentary). These ideas have also been applied to measurement of the neutron lifetime through use of UCN contained in a magnetic trap filled with superfluid ^{4}He, as described in Refs. [5] and [6].

2 Production of UCN in Superfluid ^{4}He

The production of UCN by the inelastic scattering of 8.9 Å neutrons in superfluid ^{4}He (SHe), the so-called "superthermal" source invented by Golub and Pendlebury, is discussed in Ref. [7]. The basic idea is that the free-neutron dispersion curve crossed the Landau-Feynman dispersion curve for elementary excitation in SHe at 8.9 Å, corresponding to a temperature of about 11K, as shown in Fig. 1. Neutrons of this wavelength which enter a bath of SHe can create a phonon, and in so doing, come nearly to rest; the UCN so produced will be trapped within the bath, up to energy equal to the effective neutron potential of the containment vessel, typically 200 neV and corresponding to neutron velocities of about 5m/s, the practical definition of UCN. SHe is particularly suitable for neutron storage; ^{4}He is the most tightly bound nucleus so neutron absorption is impossible, and the effective potential of SHe is 20neV, much less than useful wall materials.

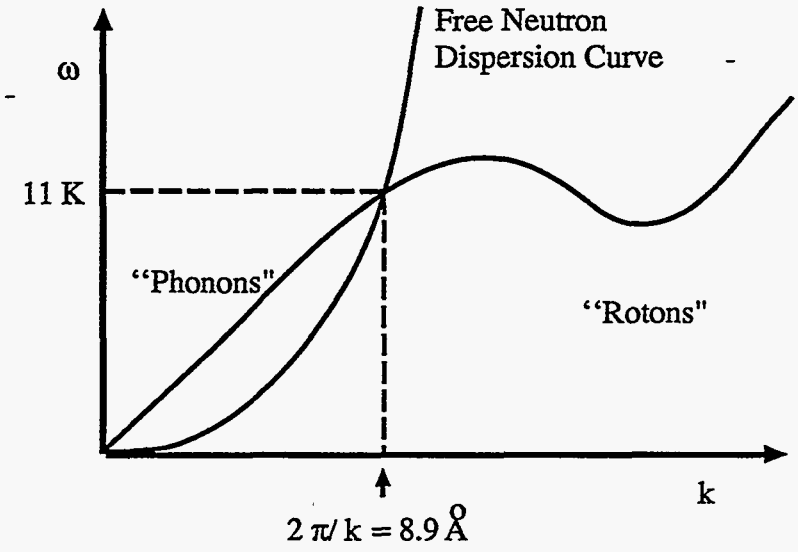

Figure 1: Free neutron and superfluid He excitation dispersion curves.

The inverse scattering process, that is, absorption of a phonon from the bath or "upscattering" to a higher energy out of the UCN range, is suppressed by the Boltzmann factor, $\exp(-11/T)$ where T is the bath temperature. Thus, the production of UCN can be aptly compared to the spontaneous emission of light from a collection of atoms. The crossing of the dispersion curves can be though of as a quasi-two-level system. Neutrons entering the bath can be thought of as an excited atom; the higher energy state decays through spontaneous emission of a phonon, while the inverse process, requiring non-negligible energy in comparison to the system temperature, simply does not occur with any significant rate.

UCN will be lost from the system through beta-decay, wall absorption, or upscattering, giving a loss rate of

$$\tau^{-1} = \tau_\beta^{-1} + \tau_w^{-1} + \tau_{up}^{-1} + \ldots \tag{1}$$

The mean-free-path for an 8.9 Å neutron in SHe is about 100m so for all practical purposes we can assume the neutron flux through the bath is a constant. The production rate, equal to the downscattering rate, is (see Ref. [8])

$$P = 7.2 \frac{d^2\Phi}{d\lambda d\Omega} \frac{1}{\lambda_u^3} \delta\Omega \mathrm{cm}^{-3}\mathrm{s}^{-1} \tag{2}$$

where λ_u is the shortest wavelength UCN which can be contained, $\delta\Omega$ is the solid angle viewed by the SHe bath, and the differential flux is specified at 8.9 Å.

The steady-state density is achieved when the loss rate is equal to the production rate, that is,

$$\rho = P\tau. \tag{3}$$

If we take the expected flux at the proposed long-pulse spallation source, with a solid angle of 0.03 str (a 20 cm hole 1 m from the cold moderator), with $\lambda_u = 500$ Å, we find a density of 260,000 cm^{-3}, which is three orders of magnitude higher than any proposed or existing source, where we have assumed beta decay dominates the losses. Location of the SHe bath so close to the source is really only feasible at a spallation source where the expected radiation flux will be at least an order of magnitude lower than at a reactor.

It is tempting to consider applying some of the ideas of the EDM and lifetime experiments to a neutron-antineutron experiment, but unfortunately, one cannot look for oscillations with UCN stored in the superfluid bath because of the differing potential for the neutrons vs. antineutrons. One could also imagine accumulating UCN in such a bath, then letting them fall freely through up to 20 m, but the counting rate isn't high enough to be competitive with a free beam experiment. See Dr. Golub's contribution to these proceedings for some ideas in regard to oscillation experiment with stored UCN.

3 Supercold Moderation (SCM)

To improve the neutron-antineutron oscillation time limit, it has been proposed that colder neutrons could be used, thereby increasing the free flight time. Such a colder neutron moderator would also be useful for UCN generation as described above.

The basic idea of neutron moderation is that a neutron collides with a stationary H atom, and in so doing, loses about half of its kinetic energy on average. D or C atoms can also be used, with some reduction of direct kinetic energy loss efficiency, but lower neutron loss through nuclear absorption.

At present, the practical limiting temperature for neutron moderation is about 30-40K; this limit is independent of the moderation temperature T_m (for constant density) for $T_m < 20$K. This is because the atoms that the moderator comprises are bound to a lattice; if the incident neutron energy is much less than the energy associated with vibrations in the lattice, the effective H atom mass approaches infinity, and on scattering, the neutron loses no kinetic energy. Not surprisingly, the neutron energy (or neutron temperature) where moderation become ineffective corresponds roughly to lattice binding and vibrational energies of atoms in liquids and solids. In fact, there is little interest in colder neutrons in regard to general neutron scattering studies, for the goal of such work is, to a large degree, associated with studying such vibrations, and the longer wavelengths either do not couple efficiently or provide no additional information; hence, there has been no motivation to develop a general source of colder neutrons, what we call here a Supercold Moderator (SCM).

It has been proposed that either CH_4 or CD_4, cooled to 4K, would serve as a SCM because of the myriad of low-energy internal states of the molecule;

for the energies of interest for SCM, the rotational states are relevant. Unfortunately, at low temperatures, these rotations become hindered by the molecular field in the solid, and at about 20K, there is a second-order phase transition associated with the molecular orientation, and the rotation becomes effectively completely hindered. In fact, it is well-known that solid or liquid methane has no special moderation properties, other than its higher H-atom concentration compared to either solid or liquid hydrogen.

So at first glance it appears completely hopeless to achieve a high neutron flux at temperatures below 20K. However, there appears to be one possibility; that is to use solid methane (possibly deuterated) doped with approximately 20% krypton. It has been shown that in the case of such high doping, the internal molecular field becomes suppressed, and the rotations once again become free; see Ref. 9 for a discussion of measurements and a review of the field. The doping material must be spherically symmetric, hence the choice of a noble gas, and should match the size of the methane molecule; Kr is the most suitable choice. The question of the nuclear properties will be addressed later.

If the rotations are truly free, we can estimate the scattering cross section and energy loss by use of the Teller-Sachs mass tensor approximation[10]. Here it is assumed that the neutron energy is much higher than the rotational level spacings (1 meV, or $T = 10$K for CH_4) and that the momentum transfer on collision is large, in which case the molecules can be treated as classical rigid rotators. Under this approximation, assuming the methane temperature is 0 K, the scattering cross section for ordinary methane becomes

$$\frac{d\sigma}{d\theta} \approx \sigma_s(1 + 0.77\cos\theta) \tag{4}$$

where σ_s is the free proton (or deuteron) scattering cross section, and the energy of the scattered neutrons is described by

$$E(\theta) = E_0(0.59 + 0.41\cos\theta) \tag{5}$$

(the average effective mass of the protons bound in the molecule is $2.4m_n$). (For deuterated methane, the two factors in (5) become 0.71 and 0.29, respectively, while in (4), $0.77 \rightarrow 0.2$ and the total cross section for the deuterium nucleus must be used.) The density of solid methane is 2×10^{22} molecules/cm^3, and the H atom density, which is relevant for calculating the nuclear absorption, is four times that. The scattering mean free path, taking $\sigma_s = 20$ barns, is 2.5 cm, while nuclear absorption length for a 10K neutron is about 7 cm (for deuterated methane, these lengths are 15 cm and 4000 cm).

The foregoing estimates are actually better for deuterate methane because its higher moment of inertia implies a closer rotational level spacing. 10K is the limit of accuracy for normal methane.

We consider the effect of the dopant as a perturbation on the above estimates, with the exception of the dopant nuclear absorption which can be

large. The implication is that enriched ^{84}Kr (57% natural abundance) would have to be used, otherwise the absorption will be too high. In the case of 20% doping of deuterated methane by this isotope, for 10K neutrons, the absorption length is 90 cm. There is also the issue of activation of the ^{84}Kr which, on neutron capture, yields an isotope with a 10 year half-life. Perhaps another noble gas or compound would be equally effective; a more complete study of these points is necessary.

The solid doped methane is best thought of as a secondary moderator, placed some distance from a liquid cold source. Otherwise the radiation damage level will be excessive; in addition there is the usual problems with heat removal from a solid. A reasonable geometry is depicted in Fig. 2. The thickness of the secondary moderator should be twice the mean free scattering length, or 5 cm in the case of methane, or 30 cm in the case of deuterated methane. If UCN are to be extracted directly from the secondary moderator, deuterated methane should be used (with 20% Kr doping, the absorption length for very cold neutrons (VCN) with velocity 50m/s is 9 cm; VCN of this velocity are converted to UCN by the potential drop associated with a vertical rise). Otherwise, it would appear that ordinary solid methane is best. One might expect a factor of 2-3 increase in the effective flux at 8.9 Å by use of the secondary moderator as shown in Fig. 2b. In this case, the radiation heating effects are minimal, and in fact the layer of solid methane can serve as an intermediate heat shield. The increase in complexity required for inclusion of this moderator is minimal.

To be useful for the neutron oscillation experiment, the solid moderator should be located as close as possible to the reactor or spallation target cold source. There is no reason to have the entire cold source of solid methane, as the hot neutrons must scatter several times before reaching a temperature where the doped solid is warranted. With the use of deuterated, doped, solid methane, it should be possible to moderate cold neutrons to 4-5K with high efficiency. The extra distance from the core or target can ease design limitations.

4 Antineutron Annihilation Targets

We have considered a number of low nuclear absorption materials for use in UCN storage containers; the requirements here are the same as those required in the annihilation target.

The ILL oscillation experiment made use of a grafoil target; the non-negligible nuclear absorption in carbon led to a background gamma rate of a few MHz. For the new proposed experiment, the background rate would be of order 10^{10}Hz; clearly, this is a problem. However, carbon is not the best choice of annihilation target. For example, a self-supporting block of compressed cold, solid helium in a suitably clean vacuum environment would give essentially zero background. Fabrication of such a target is complicated;

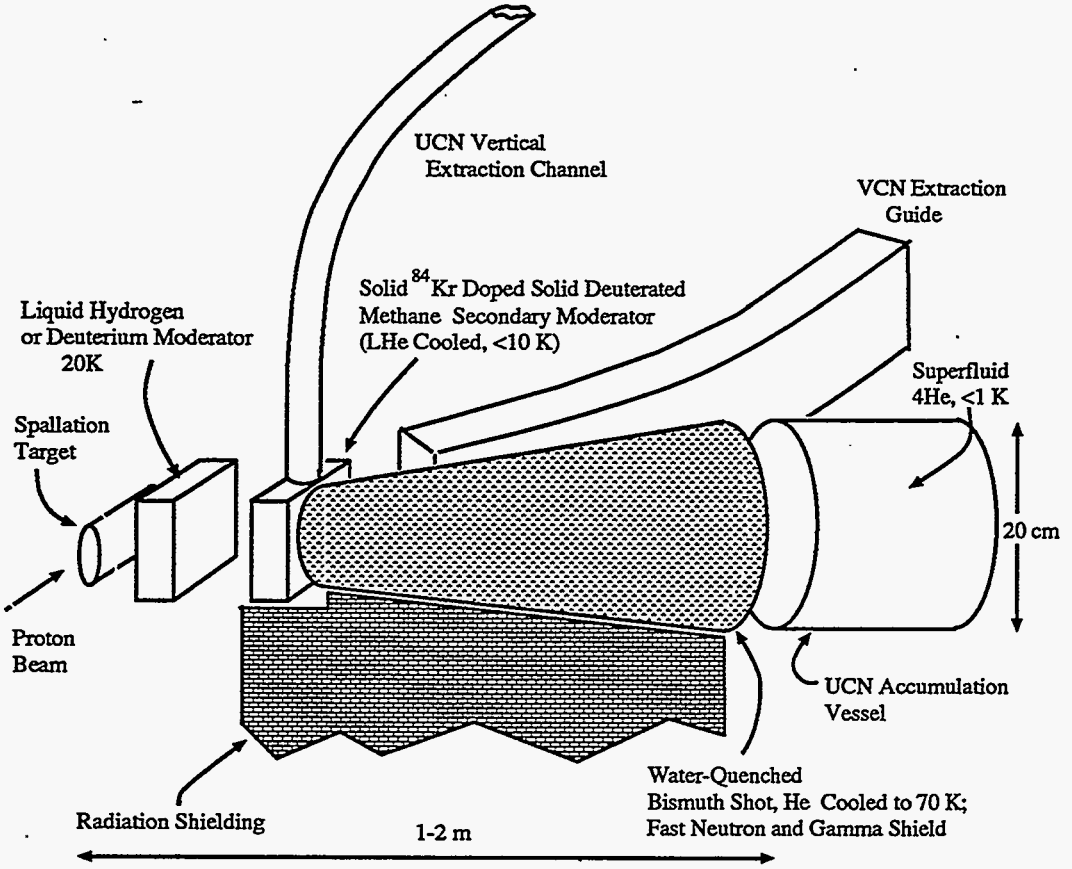

(a)

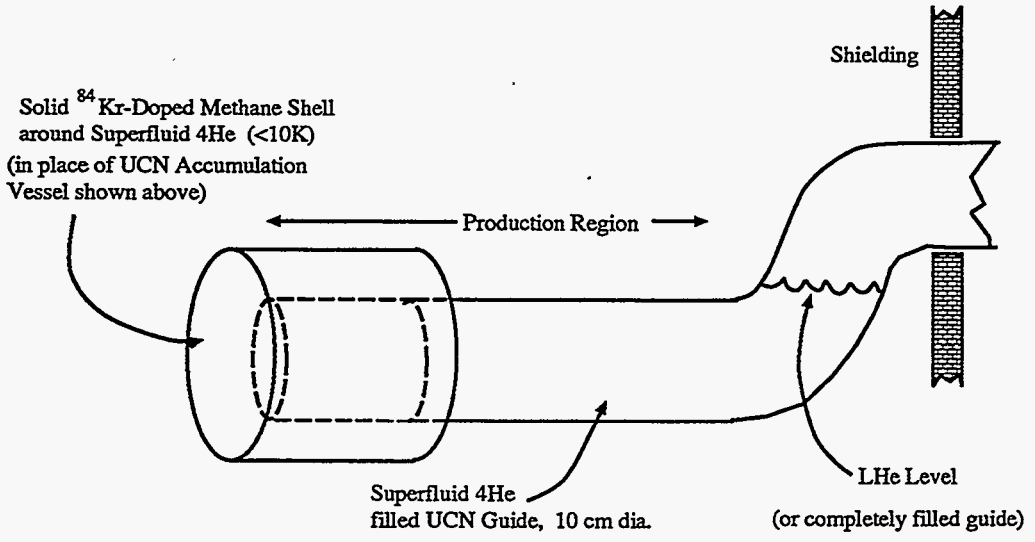

(b) Alternative UCN LHe Source Design

Figure 2: a. Supercold moderation near the cold neutron source, and UCN superthermal source with solid angle 0.03 str; b. Supercold moderator located at the superthermal source. The choice of moderator thickness at the front of the accumulation vessel is critical; loss of 8.9Å neutrons in the direct flux must be balanced against "inscattering".

however, there are other possible materials such as solid oxygen which has a cross section 20 times lower than carbon. Manipulation of a block of solid oxygen would not involve too many technical difficulties.

5 Neutron-Antineutron Oscillations in Neutron Guides?

As described by Dr. Golub in this conference, there are some tricks to eliminate the effects of the differing material potentials for neutrons vs. antineutrons. The basic idea is to apply a static magnetic field to the UCN storage container which undoes the relative neutron-antineutron phase shift which occurs on reflection from the wall. Unfortunately, this tuning away of the wall phase shift begins to wash out after a few (5-10) reflections from the walls.

Interestingly, one expects about this number of reflections for a neutron propagating in a typical neutron guide of lengths of order 50 m, and cross section dimensions of order 20 cm. A primary feature of a guide is the elimination of the effects of gravity on the cold neutron propagation which will be a particular problem if a SCM is used with a free flight experiment. Another major advantage of a guide is that the effective cross sectional area is constant; this means that the detector size is of order of one meter, instead of several meters. The smaller detector will have less background from cosmic rays; furthermore, the guide could be slightly bent, thereby reducing background from the neutron source.

A useful and cheap material to coat the guides is chemical vapor deposited diamond-like films. Such films have been prepared at the University of Washington, and their critical angle is about equal to that of ^{58}Ni.

To set the background magnetic field, the difference in the antineutron and neutron guide potential must be fairly well known. Also, Monte Carlo calculations for the optimum field, based on the spectral characteristics of the neutrons, must be performed. With a proper choice of guide material and background cancellation field, a loss in efficiency of less than a factor of five over a free flight experiment appears possible. Given the reduction in detector size and associated reduction in background rate, the net loss in sensitivity would be negligible.

6 Conclusion

We have described a possible moderation scheme which might give an increase in 11 K neutrons for UCN production in superfluid helium; this moderation scheme would also give a high flux of 4-10 K neutrons for an improved neutron-antineutron oscillation experiment. This moderation scheme is based on solid methane doped with krypton, in which case the hindrance

of the rotational states associated with the second order phase transition at about 20K is eliminated.

We have also described low background annihilation targets and discussed the possibility of an oscillation experiment using guided neutrons. Both can lead to a substantial decrease in background events; furthermore, a guide is of more general use for future experimental work. One could imagine an entire neutron scattering facility subsequently developed around a guide initially built for an oscillation study; in the case of the proposed project with its anticipated intensity, this facility would be the world's best.

References

[1] R. Golub and S.K. Lamoreaux, Phys. Rep. **237**, 1 (1994).

[2] S.K. Lamoreaux, J. Neutron Research, to be published (1996).

[3] S.K. Lamoreaux, in *Proceedings of the XVth Moriond Workshop* (Edition Frontiers, Gif-sur-Yvette, France, 1995).

[4] S.K. Lamoreaux, in *Proceedings of the XIth Moriond Workshop* (Editions Frontiers, Gif-sur-Yvette, France, 1991).

[5] J.M. Doyle and S.K. Lamoreaux, Europhys. Lett. **26**, 253 (1994).

[6] J.M. Doyle, in *Proceedings of the XVth Moriond Workshop* (Editions Frontiers, Gif-sur-Yvette, France, 1995).

[7] R. Golub, D.J. Richardson, and S.K. Lamoreaux, *Ultracold Neutrons* (Adam-Hilger, Bristol, 1991).

[8] S.K. Lamoreaux and R. Golub, JETP Letters **58**, 844 (1993).

[9] S. Grondey, M. Pragen r, W. Press, and A. Heidemann, Jour. Chem. Phys. **86**, 6465 (1987).

[10] R.G. Sachs and E. Teller, Phys. Rev. **60**, 18 (1941).

The Superthermal UCN Production Machine

Hajimé Yoshiki

Department of Engineering, Ibaraki University, Hitachi, 316, Japan
KEK, National Laboratory for High Energy Physics,Tsukuba, 305, Japan

It was not until 1992 that the production of ultracold neutrons (UCN) by means of superthermal method predicted by Golub and Pendlebury [1] was verified quantitatively by changing incident cold neutron wavelengths to observe the maximum of UCN production[2]at a certain wavelength. At this wavelength the dispersion curve of the superfluid liquid helium and the energy momentum curve of a free neutron crosses and the energy and momentum of incident neutron can be converted entirely to those of a produced phonon (Fig.1), leaving the neutron with an infinitesimal energy, a UCN. The value obtained was 8.78±0.06Å, in contrast to the value hitherto often quoted number of 8.9Å for 1.1K liquid, and it fits exactly to our particular liquid temperature of 0.45K(Fig.2)[3]. What we have learned here is that the calculation by Cohen and Feynman is correct and we can now calculate the rate of UCN production per unit time. This was referred to by the previous speaker[4] and the resultant **UCN intensity** is overwhelming, compared to the Turbine[5], or Boltzmann methods. It must be emphasized that 1) this method allows cold neutrons to come from whole 4π–directions to produce UCNs, unlike the Turbine, where rather fine beam collimation of cold neutron is necessary; 2) the produced UCNs are automatically trapped in the superfluid helium vessel, whereas the parent cold neutrons can penetrate freely through the wall, resulting in the build-up of UCN density in time in the vessel. In other methods the UCN transfer to an experimental volume, like a Ramsey Chamber, is necessary and the balancing between inflow and outflow of UCNs to and from it occurs quickly. Golub predicted that required temperatures would be below 0.8K, where the production of UCN creating phonons (down-scattering) would not be surpassed by phonons reabsorbed by UCN (up-scattering). This statement is experimentally demonstrated as shown in Fig.3 [2]. The attenuation coefficient at 0.45K is mainly attributed to a vertical duct open downward on the storage vessel (so called gravity acceleration tube) which was adopted to detect UCN with good efficiency. Fig.4 shows a handmade UCN detector[6].

The task how to keep the 15 litres of liquid helium stable at a low temperature of 0.45K was solved by a new **heat-exchanger** between the

purified (He^3-free) superfluid liquid heilium and the liquid He^3 coolant. The heat exchanger is made of oxgen-free copper block having 29 fins in 5mm pitch, each of which has 3 mm thickness and 20 mm depth (Fig. 5). The fins are vertical because they minimize 1) the He^3 bubble formation on the surface of the fins and 2) the resistance to the viscous gas flow upward formed by the everporated He^3. The delicate fabrication of the fins without resorting to soldering was possible by electrodischarge cutting in KEK(Fig.6) The improvement in cooling capacity gained in this way was enormous as Fig.7 shows. Little He^3 is needed. The liquefied He^3 fills only one and half centimeter deep from the bottom and not only the latent heat of evaporation of the liquid but the sensible heat of the gas passing through the gaps of the fins contributes much to the cooling.

In 1987, we calculated the heat that would be produced in the liquid helium, if it was exposed to a cold neutron field of 3×10^{12} /cm^2/s [7]. If such situation is realized it would produce 5000 UCN/cm^3/s (defined UCN energy upper limit=2×10^{-7}eV) , a strongest UCN source up till now. However the final estimate of the heat to be removed from the liquid amounts to 3000 mW under a certain number of assumptions. They include that irradiated part of the vessel is a steel cylinder of 50 cm in length, 10 cm in diameter and 0.1 mm in wall thickness. Table 1 gives the answer to the problem by combining a new set of circulation pumps for He^3 and a new heat exchanger which has four times as many number of fins as before. The proposed set of circulation pumps for He^3, which were purchased in 1994, is five times larger in displacement than before. From the existing data of Fig. 7 we can extrapolate that this combination is enough to stand 3 x10^{12}cold neutrons/cm^2/s [7]which is to **produce 2 x 10^7 UCN/s** in the aforementioned part of the liquid. Such irradiation will be accomplished most conveniently and most realistically by use of a spallation source, and *not* by a reactor. We will come to this point later.

In regard to the experimental setup in ref.2, remarks are not more than in the article except two points. One is the characteristics of the velocity selector. It is a pair of disks, 380mm in diameter with a 30mm wide window, 8 meters apart, rotating at a speed of 20 rps by a pair of step-motors whose speed and phase are precisely controlled by an electronic pulse generator(Fig.8). It is the **relative phase** of these disks that determines the speed of neutrons. Each phase signal is measured by a clock which ticks at a rate of 10 μs and locks each other at a predetermined value after changing one of the discs' rotation speeds by 0.04%. It turned out that the time jitter of the relative phase is less than 0.2% at 9Å. The λ determined by the relative phase was systematically corrected for the λ^{-5} dependence of the flux. The correction was not more than 0.6% in contrast to the 25% of the earlier experiment[8], where a short single rotor with

a synchronous motor was used. The other remark is the quantity of He^3 remaining after separation by means of heat-flush through a superleak[9,10]. Commercial helium contains 0.16 ppm of He^3 in He^4. By mass spectrograph we did not detect He^3 at all and the sensitivity of this spectrometer gave an upper limit of 1.3×10^{-8}(1σ c.l.) in He^3/He^4 ratio for our superleak[11]. Ref.2 gave an improvement in this ratio by a factor 5 to 3×10^{-9} but it was never the real ratio of the remnant He^3 because we had an escape duct (the gravity acceleration tube) for UCN which was open always, becoming the main source of limited life time of UCN in the storage vessel. McClintock discusses that the ratio can be as low as 10^{-12} by a single heat flush[10]. The absorption cross section of He^3 for 9Å neutron is 25000 barns[12] and the normalized cross section will be 0.3 mb at most, which renders negligible effects on UCN production studies. The construction and operation of a cryostat dubbed Mark3000 are described in ref.13.

The **two main objectives** for getting a strong UCN source are a more precise determination of the neutron lifetime and the search for the electric dipole moment of neutron, a manifestation of the time irreversibility. As for neutron lifetime, there is a proposal with superthermal source and magnetic confinement [14], and we are planning a similar device [15] incorporated in Cooling Tower II (see below). We will look into the latter more specifically in this talk. The search for the electric dipole moment of free neutron has been carried out by two groups[16,17,18], whose latest upper limit for this quantity is $\sim 1.2 \times 10^{-25}$e.cm. In order to go a step further it would be necessary 1) to have UCN more in number and 2) to control systematic errors more in precision, such as magnetic field in its stability and uniformity, or problem of dark current when a strong electric field is applied. Since we are to produce UCN by the low-temperature engineering, the logical solution for 2) would be to take advantage of this orientation. In Fig.9 we show the e.d.m. measurement machine integrated with refrigeration parts, which now is dubbed **Mark3001.** Cooling Tower I does the He^3 refrigeration, Cooling Tower II supplies liquid heilium to superconducting shield and solenoid, and furnishes a space for gravity acceleration and UCN detection. The part where the e.d.m. is measured is conventional in layout[18] except that the shields have to be coaxial by technical reasons and the chamber is filled with 0.5K purified liquid helium in place of vacuum. The Ramsey Block, a cylindrical object 3 m long and 0.8 m in diameter is a vacuum chamber. It contains three layers of high-permeability magnetic shield at room temperature. Coaxially toward the center, a **superconducting magnetic shield** and a **superconducting solenoid** exist, which are enclosed in a double layered cylinder containing liquid helium to

keep them at 4.2K. Those are all made out of aluminum except for the superconducting material. We are aiming at a magnetic field whose instability in space and time will be in the order of 10 ngauss. Fig.10-14, show how those elements are made and look like. Explanations are given in figure captions.

Preliminary measurement was done for the three layer **high-permeability** (μ=10^5) shield at room temperature, which turned out 0.1 mgauss at the center of the shield in ambient magnetic field, satisfying the designed attenuation[19]. As for superconducting shield, lead foil of 0.1 mm thick, 80 mm wide has been used for the shield material. This was wound on the aforementioned aluminum bobbin, which was fabricated with an accuracy of one hundredth of a millimeter near Ramsey Chamber, in 8 mm pitch so that ten turns would make a 1 mm thick shield. A model experiment was done to see the validity of our approach. A cup made out of the same lead foil and wound in the same way was made and submerged in liquid helium in a cryostat. Given an external field by means of a solenoid wound on the outer wall of cryostat, the axial magnetic field at the center of the cup was measured by SQUID to see if the attenuation as a function of the depth varies as theory. For a semi-infinite superconducting cylinder, the theory says that the attenuation is proportional to exp(-*kz*/*R*) where *z* is the depth from the end of the cylinder, *R*, its radius, and *k*=3.83 for the axial field. Our data produced *k*=3.71± 0.14 (Fig. 15)[19]. This shows that our approach is justifiable and the superconducting shield will be working as designed. By combining the high-permeability magnetic shield and the superconducting shield, we expect that our aim of 10 ngauss stability is going to be accomplished. The system is being assembled and is ready for test this summer.

In Table 2, we present the achievement in past and the prospect in future of the electric dipole measurement of neutron. The intensity of UCN depends on the intensity of parent cold neutrons and it can change orders of magnitude whether one use a cold neutron *beam*, or a *field* of cold neutrons (neutron bath created by spallation source). This is because of the difference in solid angle as discussed before. The number (5000 cm^{-3}) is conservative even taking into account the diffusion of UCN into the whole vessel out of the region they are created (50 cm long, 10 cm wide, see above and ref.7), resulting in dilution in density. We therefore belive that we will not face the paucity of UCN but rather the problem of the systematic errors, we have been discussing in measuring the edm. As for $N-\bar{N}$ Oscillation experiment, this vast quantity of UCN could even open a way to look at the $\bar{N}$ amplitude in the random-walk in the $N-\bar{N}$ plane (Fig.16), not only in the coherence mode as reported by Golub (the Bootstrap Method) in this workshop[20].

The issues on **neutron spallation sources** with particle accelerators have been discussed by many neutron laboratories (JHP,LANL, ORNL, Savannah River,

Jülich, Wien etc). The main advantage of spallation source is that it is pulsed and has a high peak intensity, suited for neutron spectroscopy very well. We should not however overlook another big advantage in spallation source. It is the dedicatablity of a source (or sources) to a paricular experiment (or experiments). By the **dedicatability** we mean that each experimenter is able to easily adjust his beam specifications at his own. This is impossible in case of a reactor. If a cold neutron source or a superthermal source are to be installed near the core of a reactor, it would need a very precise evaluation of flux distributions in planning. Once the reactor is on, it is virtually impossible to move these equipments and the relations among different experiments are fixed. On the other hand, a proton beam can be tailored to orders by experimenters. It can be controlled in current, space and time. The primary beam can be even fanned out. By owning one's own spallation target, the experimenter can design his own neutron source(s) or beam(s), taking no attention to other groups. The serious contradictions among different types of experiments, whether a high time resolution or a high intensity, will be solved by designing a target station in each case. For instance the Superthermal UCN production need no time resolution but a little proton current (~10μA) *adjustable* in intensity or able to be even *shut off* if it is not wished. The experimenters will benefit much from the mobility and the dedicatability of the spallation source in this way[7,21] and this is one of the essential advantages in working with spallation sources.

The author thanks ORNL and Prof. Yu. Kamyshkov for the invitation to this workshop. The works in Japan mentioned in this talk have been supported by Monbusho under Grant-in-Aid for Scientific Research on Priority Areas (UCN,No.04244106).

REFERENCES

[1] R.Golub and J.M.Pendlebury, Phys. Ltrs.62A(1977)337

[2] H.Yoshiki,K.Sakai,M.Ogura,T.Kawai,Y.Masuda,T.Nakajima,T.Takayama, S.Tanaka and A.Yamaguchi, Phys. Rev. Ltrs. 68 (1992) 1323

[3] H.Yoshiki, to be published.

[4] S.K.Lamoreaux, in this Workshop.

[5] the latest information can be found in the paper by Kitagaki *et al*

submitted to Int. Symp. on Advance in Neutron Optics and Related Facilities (1996), KUR, Osaka, Japan.

[6] H.Yoshiki, H.Yamaguchi andS.Ishimoto, Nucl. Inst. &Meth. in Phys.Rsrch. **A343**(1994)573

[7] H.Yoshiki, S.Ishimoto and M.Utsuro, Z.Phys.B - Condensed Matter **67** (1987) 161

[8] H.S.Sommers, J.G.Dash and L.Goldstein, Phys.Rev. **97** (1955) 855

[9] M.Atkins and P.V.E.McClintock, Cryogenics. December(1976)733

[10] P.V.E.McClintock, Cryogenics.April(1978)201;

[11] H.Yoshiki, K.Morimoto, N.Kudo, Y.Kiyanagi, **27aP1**, Bulletin of the 35th Annual Meeting of Jap. Phys.Soc.(1980)237

[12] L.D.P.King and L.Goldstein, Phys.Rev.**75**(1949)1366

[13] H.Yoshiki, K.Sakai, T.Kawai and S.Goto'o, Cryogenics.**34**(1994)277

[14] J.M.Doyle and S.K.Lamoreaux, Europhys. Lett. **26** (1994) 253

[15] N.Inoue, to be published

[16] K.F.Smith, N.Crampin, J.M.Pendlebury, D.J.Richardson, D.Shiers, K.Green, A.I.Kilvington, J.Moir, H.B. Prosper, D.Thompson, N.F.Ramsey, B.R.Heckel, S.K.Lamoreaux, P.Ageron, W.Mampe and A.Steyerl, Phys. Lett.**234**(1990)191

[17] I.S.Altarev, Yu.V.Borisov, N.V.Borovikova, S.N.Ivanov, E.A. Kolomensky, M.S.Lasakov, V.M.Lobashev, V.A.Nazarenko, A.N.Pirozhkov, A.P.Serebrov, Yu.V. Sobolev, E.V. Shulgina and A.I.Yegorov, Phys. Letters **B276**(1992)242

[18] J.M.Pendlebury, K.F.Smith, R.Golub,J.Byrne, T.J.L.McComb, T.J.Sumner, S.M.Burnett, A.R.Taylor, B. Heckel, N.F.Ramsey, K.Green, J.Morse, A.I. Kilvington, C.A.Baker, S.A.Clark, W.Mampe, P.Ageron and P.C.Miranda, Physics Letters **136B** (1984) 327

[19] E.Gravador, H.Yoshiki and F.Huang, to be published

[20] R.Golub, H.Yoshiki and R.Gähler, Nucl. Inst. & Meth. in Phys. Rsrch **A284** (1989)16

[21] H.Yoshiki, Proceedings of ICANS-IV, *KEK* (1981) 758;
R.Golub, K.Böning and H.Weber, Realisierungstudie zur Spallations-Neutronenquelle (Teil III), Jülich & Karlsruhe (1981)5;
M.Utsuro and H.Yoshiki, Proceedings of the Meeting on BSF Future Prospects-II, *KEK* (1983)223;
H.Yoshiki, KENS Report-V, *KEK* (Editors; Y.Ishikawa, N.Niimura, M.Misawa) (1984)215;
R.Golub, NBS Special Publication 711(Editor, G.Greene) (1986) 143;
H.Yoshiki, KEK Report 88-3 (1988) 163;
T.Kawai et al, KEK Report 89-13(1983) 91(specially Fig.10);
K.Hosoyama, KEK Report 89-13(1989) 107

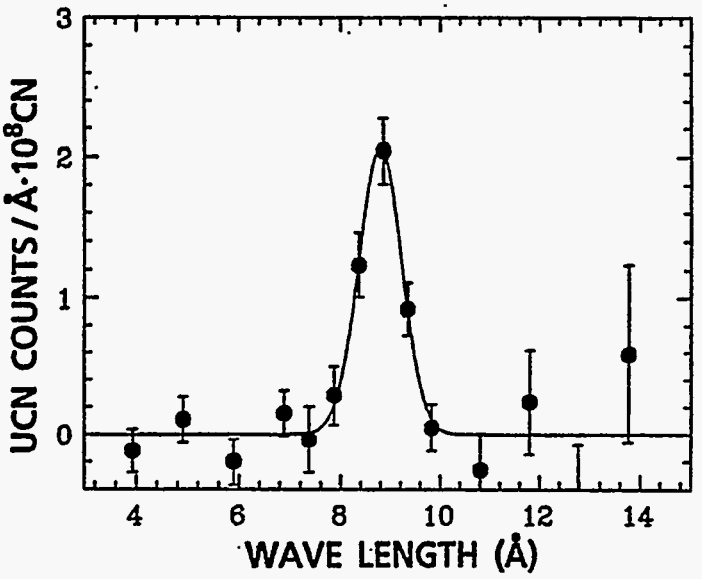

Fig.1 Superthermal UCN counts in the experiment as described in ref.2 *vs* cold neutron wavelength.

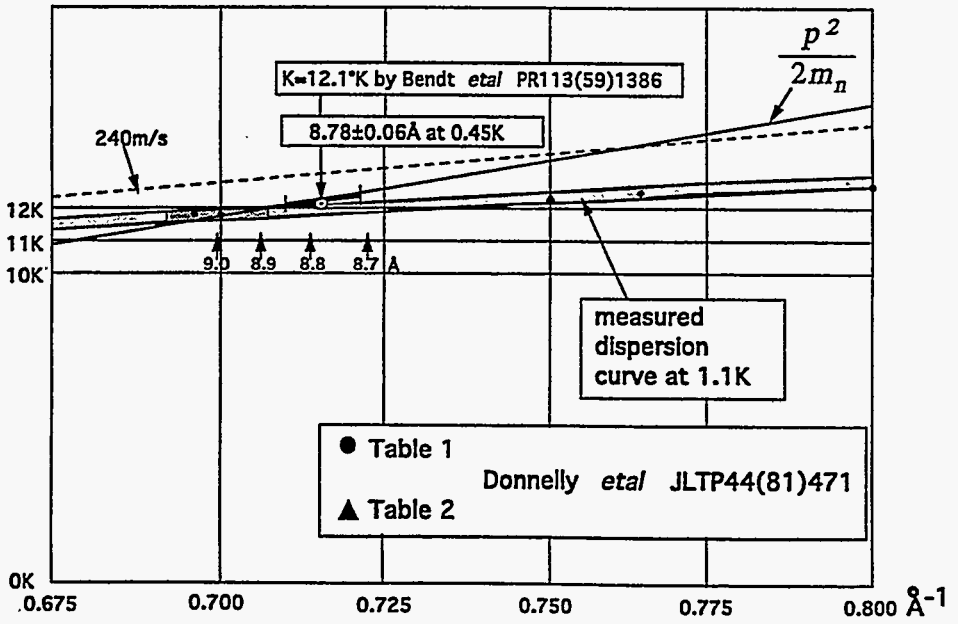

Fig.2 Measured dispersion relation of superfluid liquid helium at 0.45K.

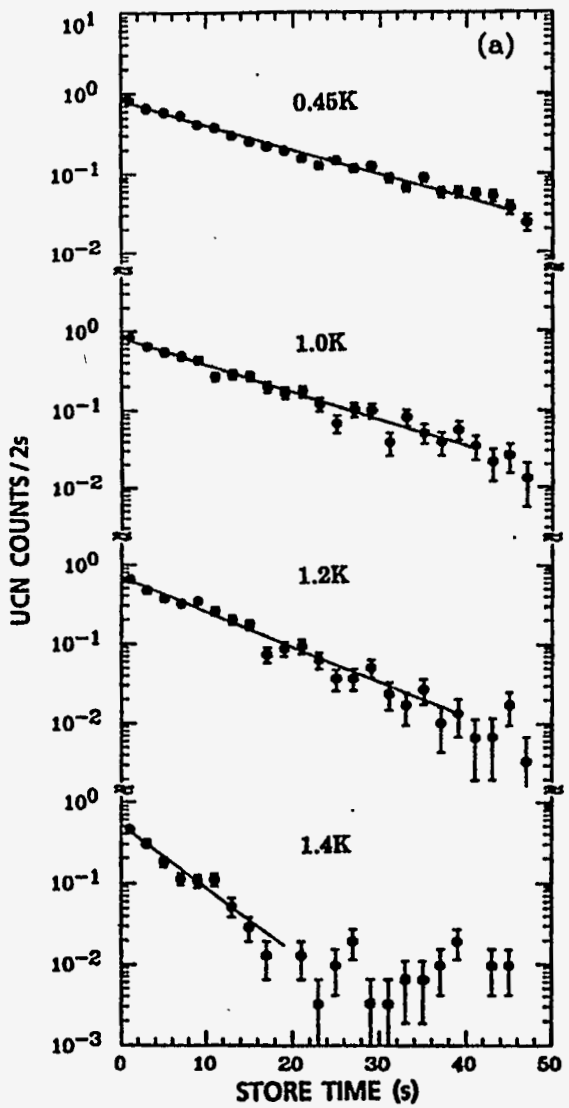

Fig.3 Distribution of arrival time of UCN at the counter, determining the storage lifetime of the UCN in the vessel at different temperatures.

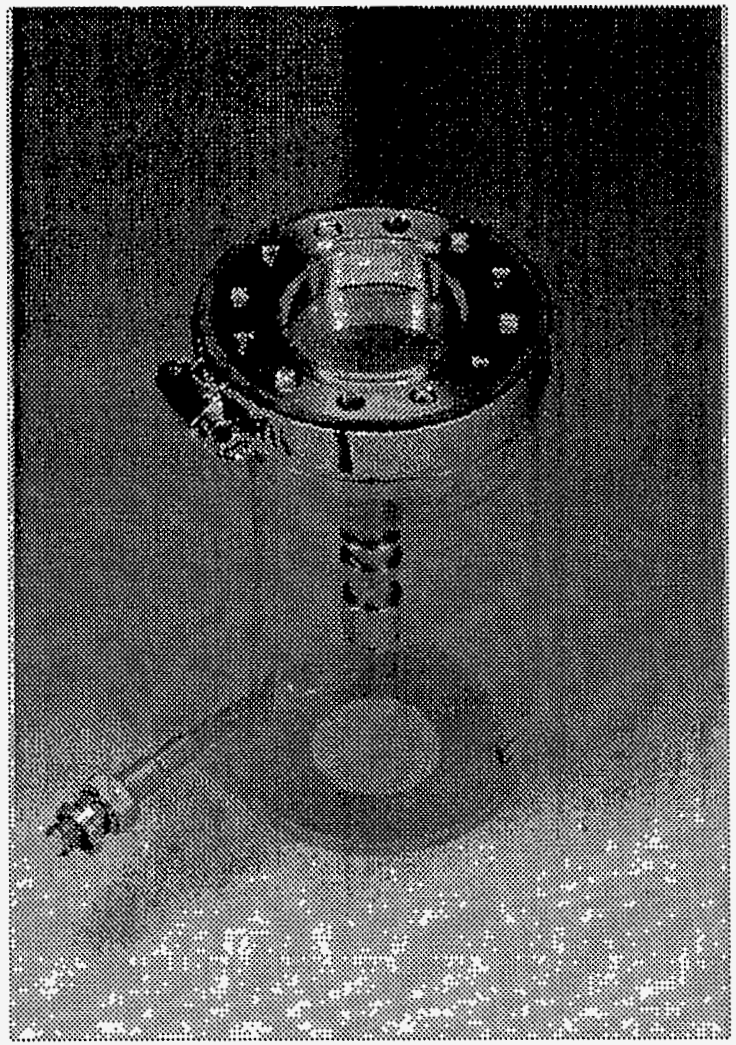

Fig.4 Handmade flat-type He^3 proportional counter with 60μm thick aluminum window (ref.6). Results in ref.2 are all derived from this counter.

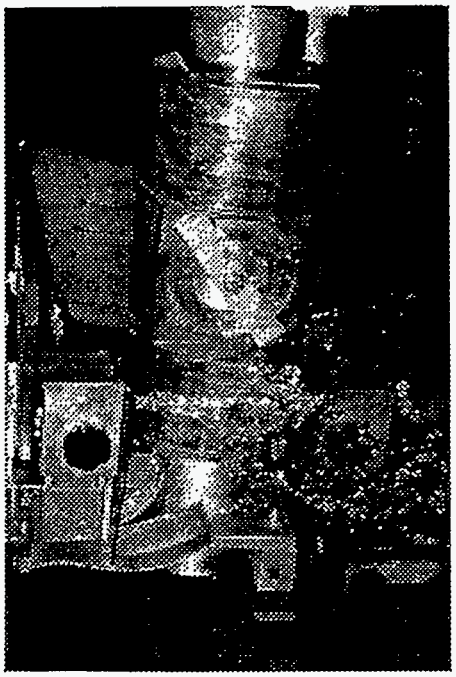

Fig.6 Fabrication of He^3 pot fins by electrodischarge cutting.

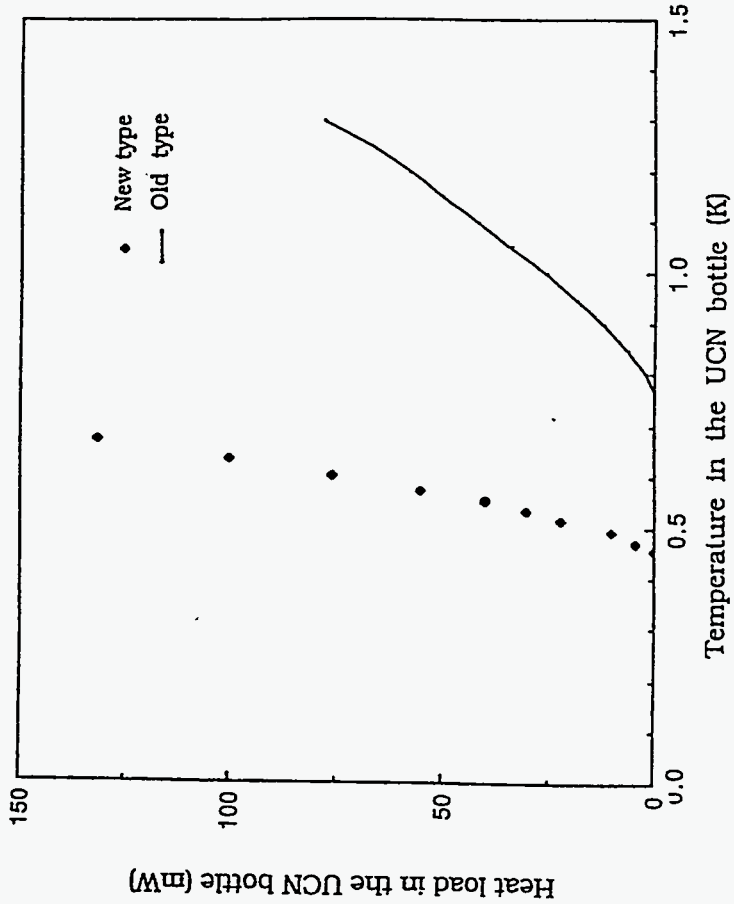

Fig.7 Cooling performance of two types of heat exchanger. "New" stands for the He^3 pot with 29 fins.

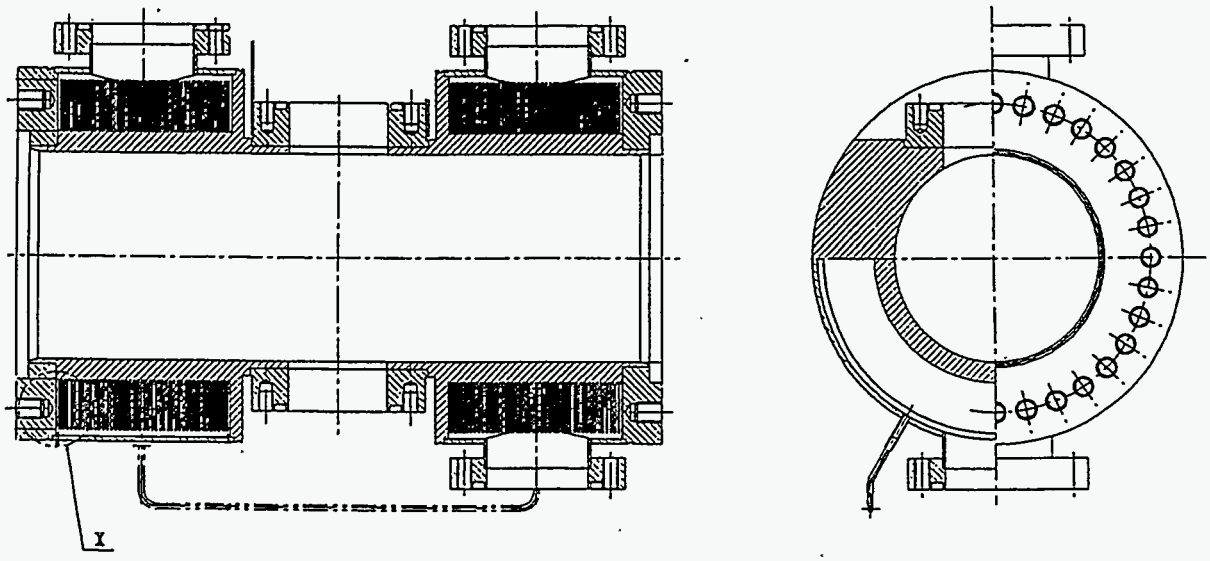

Fig.5 Heat exchanger. He^3 is liquefied, stored and evaporated where fins are (ref.5) and cools liquid He^4 in the center. Also called He^3 pot.

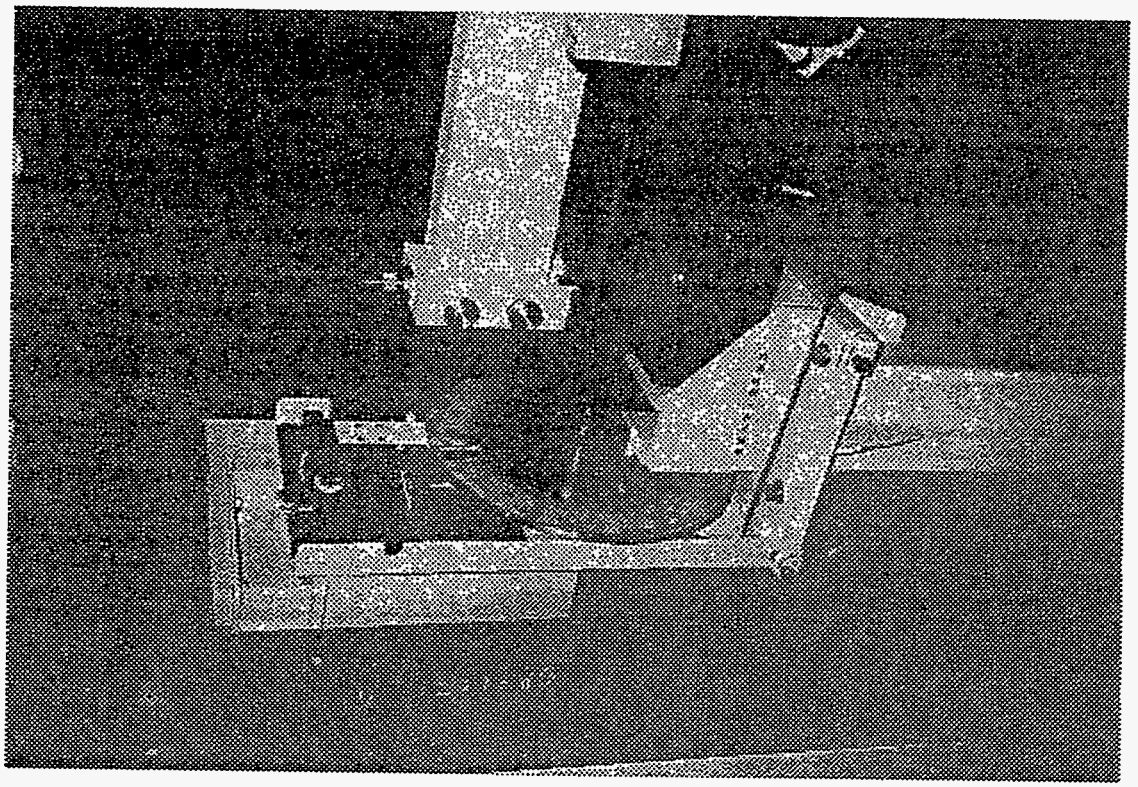

Fig.8 One of the paired discs of the cold neutron velocity selector.

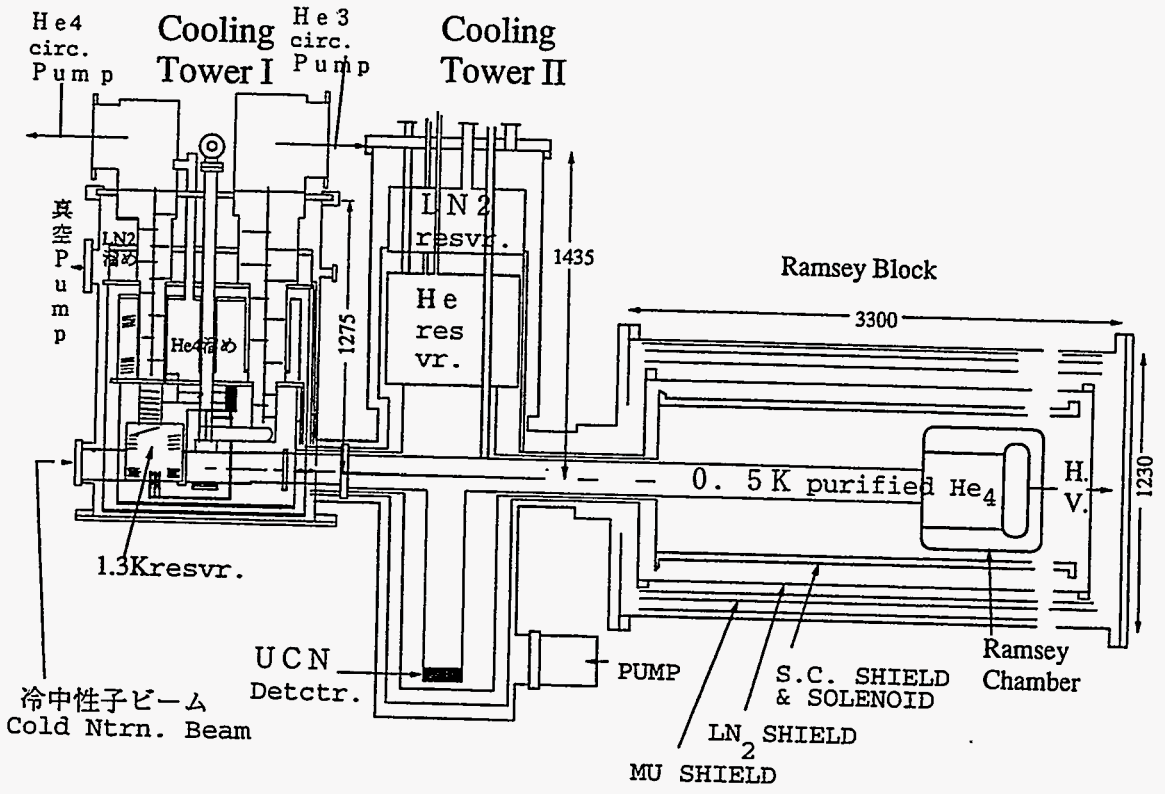

Fig.9 EDM measurement machine. A pipe extends to the left of the figure to be bathed in a cold neutron field of $10^{12}/cm^2/s$ or to receive a cold neutron beam of any strength. Cooling Tower I cools all the purified superfluid liquid helium down to 0.5K by He^3 coolant. Cooling Tower II supplies liquid helium to superconductiong shield and solenoid in Ramsey Block. It also provides space for UCN detection.

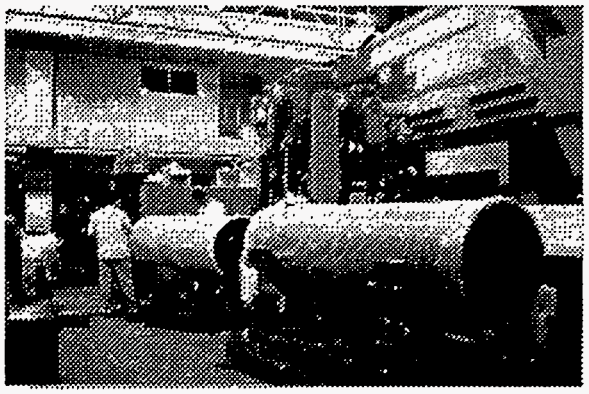

Fig.10 Cylinders in Ramsey Block are being assembled. The 10,000 m^3/hr He^3 circulation pump is seen in the background.

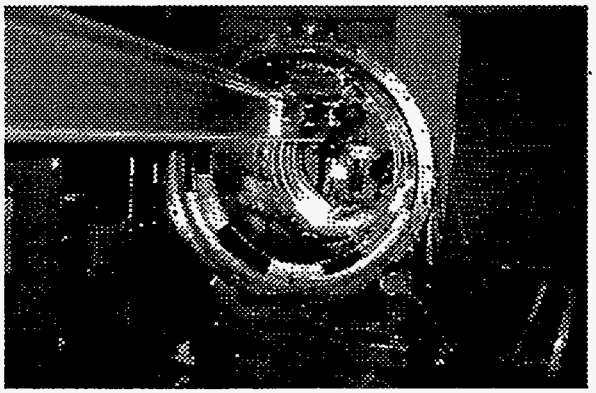

Fig.11 Three layers of high-permeability magnetic shield at room temperature are being housed into the outer jacket of Ramsey Block.

Fig.12 Completed superconducting magnetic shield.

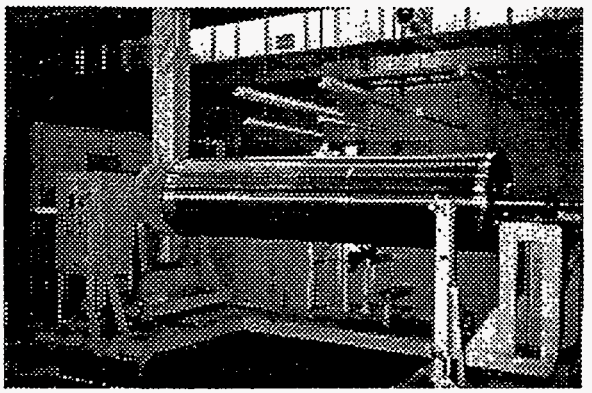

Fig.13 Almost completed superconducting solenoid.

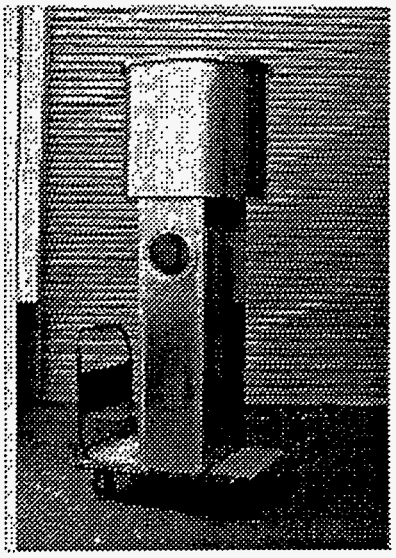

Fig.14 Aluminum thermal shield (77K) in Cooling Tower II.

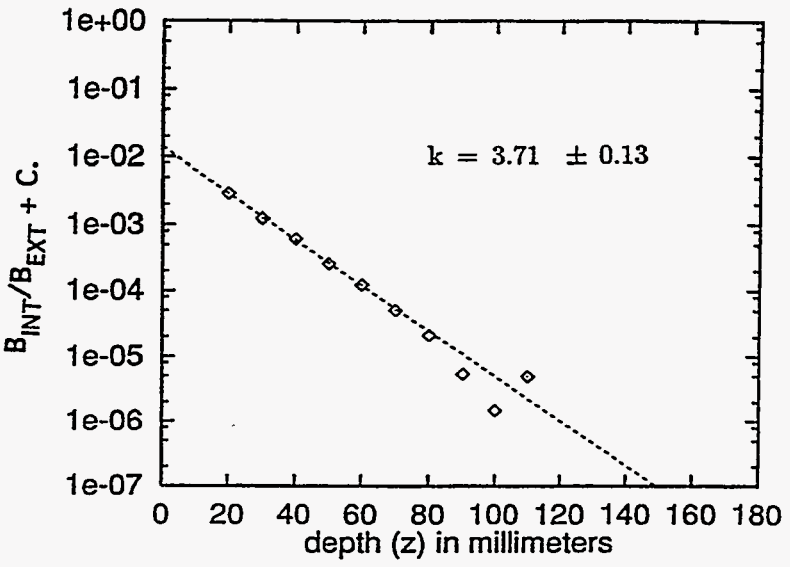

Fig.15 Attenuation of magnetic field with depth by superconducting magnetic shield.

	Mark3000 (P.R.L.68(1992)1323)	Mark3001
He^3 Circulation Pump	2,000 m^3/hr (550 *l*/s)	10,000 m^3/hr (2300 *l*/s)
Heat Exchanger		
# of Fins	29	116
Total Fin Area	5450 cm^2	21800 cm^2
Cooling Power at 0.5K	150 mW(measured)	3000 mW enough to stand 3 x 10^{12} cold neutrons /cm^2/s = 5 x 10^3 UCN/cm^3/ sec (Z.Phys.B-CM67(1987)161)

Table 1 Combination of a larger set of He^3 circulation pumps and an enlarged heat exchanger, which meets the required heat removal .

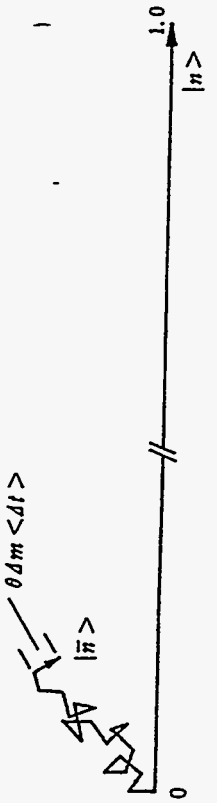

Fig.16 Random walk of $\bar{N}$ amplitude in N-$\bar{N}$ plane. $<\Delta t>$ is the time interval between wall collisions, Δm is the mass difference of two orthogonal N-$\bar{N}$ complex systems.

	type	chamb. volume	UCN CM^{-3}	stored UCN	values	system. error	statis-tical e.	upper limits
DONE								
ILL (PREVIOUS,89)	R.T. BEAM	5*l*	40	$2\cdot10^5$	$-3.3 \pm 3.9 \pm 1.9$ 10^{-26}e.cm			$<1.2\ 10^{-25}$
GATCHINA(91)	R.T.	20*l*	10	$2\cdot10^5$	$+2.6 \pm 1.6 \pm 4.2$			$<1.2\ 10^{-25}$
KEK/JAERI(91)	HeIII BEAM	15*l*	5	$8\cdot10^4$	NO ATTEMPT MADE FOR EDM			
FORECAST								
ILL (PRESENT)	R.T. BEAM	20*l*	50	$1\cdot10^6$	X	2.0	1.0	$<5\ 10^{-26}$
ILL/KEK(3001)	HeIII BEAM	20*l*	350	$7\cdot10^6$	X	1.0	0.2	$<2\ 10^{-26}$
spallation s./KEK	HeIII BATH	20*l*	5000	$1\cdot10^8$	X	X'	<0.1	$<X''\ 10^{-27}$

BATH=cold neutron bath

Table 2 Numbers associated with EDM measurement in tha past and the future.

NUCLEON INSTABILITY SEARCH WITH SUPER-KAMIOKANDE

James Stone

Department of Physics, Boston University, Boston, Massachusetts 02215

ABSTRACT

This manuscript presents an overview of the current experimental situation regarding the search for nucleon decay. The Super-Kamiokande project is described and its expected sensitivity for improving measurements of the nucleon lifetime are discussed.

1. Introduction

For the past few decades, several experiments in the field of particle astrophysics have been performed using large detectors and deep underground facilities. Many of these experiments have already produced significant results and at the same time have posed new questions to be investigated. The Super-Kamiokande project represents the next generation of large deep underground detectors. The significantly increased fiducial mass and the improved resolution of the detector will allow for measurements with increased sensitivity for nucleon decay, solar neutrinos, atmospheric neutrinos, and supernovae neutrinos. In this manuscript, an overview of the project, a review of the current experimental situation and the expectations of Super-Kamiokande for a nucleon decay search are presented.

2. The Super-Kamiokande Experiment

Super-Kamiokande is a 50,000 tonne ring-imaging water Cherenkov detector currently in operation at a depth of 2700 meters water equivalent (mwe) in the Kamioka Mozumi mine in Japan. A schematic representation of the detector is shown in Figure 1. It consists of a stainless steel tank in the shape of a right circular cylinder, 39 m diameter and 41 m height, filled with purified water. The detector is optically segmented into an inner volume (34 m diameter, 36 m height) and an outer (anti-coincidence) region of 2.5 m thickness on top, bottom, and sides of the inner volume. The inner detector is viewed by 11,146 photomultiplier tubes (PMTs) of 50 cm diameter, uniformly distributed on the inner boundary giving 40% photocathode coverage. This extraordinary photocathode coverage and time resolution (2.5 ns at 1 p.e.) allows the detector to attain an energy threshold of 5 MeV and a vertex resolution of 10 cm for processes such as $p \rightarrow e^{+}\pi^{0}$. For through-going muons, the PMT configuration yields an angular resolution of ~1°. The total mass of water inside the inner detector PMT surface is 32,000 tons. The fiducial mass for the proton decay search, defined to be 2 m inside the PMT plane, is 22,000 tons allowing for partial lifetime sensitivities of $> 10^{34}$ years for several modes.

The outer annulus of the detector is an anti-coincidence region used to tag entering muons and low energy components as well as to attenuate low energy gammas and neutrons which cause background in the sensitive volume. This outer detector region is viewed by 1890 PMTs of 20 cm diameter with wavelength shifter plates in the style of IMB-3. The walls of the anti-coincidence region are made reflective to enhance light collection. The PMTs are mounted facing outwards on the same super-structure as the 50 cm PMTs of the inner volume. Also, an optical barrier is mounted on the same structure to separate the inner and outer regions.

2.1 Comparison With Other Experiments

The largest water Cherenkov detector (3300 tonne fiducial mass) previously built was the Irvine-Michigan-Brookhaven (IMB) detector located in the Morton Salt Company Fairport Mine in Ohio. IMB operated successfully from September 1982 until April 1991, placing significant constraints on the nucleon lifetime into 45 possible decay modes. In addition, important results were published on atmospheric neutrinos, neutrino oscillations, neutron-antineutron oscillations, and monopole catalysis of nucleon decay. A highlight of IMB was the first detection of neutrinos from a supernova, SN1987A.

Another large water Cherenkov detector (1040 tons fiducial mass) is the Kamiokande experiment in Japan which commenced operation in July 1983 and continues even now. In addition to the same physics addressed by IMB, the large photocathode coverage of Kamiokande allowed for triggering on low energy events (7.5 MeV) which resulted in the first direct, real-time observation of neutrinos from the Sun. The observation of neutrinos from SN1987A, simultaneous with IMB, provided the first test of standard supernova theory with regards to neutrino production during collapse.

In Table I, the physical and performance parameters of Super-Kamiokande are listed in comparison with those of Kamiokande-III and IMB-3. With 7 times larger fiducial mass and 10 times the photocathode coverage of IMB, Super-Kamiokande will explore nucleon lifetimes to $>10^{34}$ years with a few years of running. The increased discrimination of showering and non-showering events will greatly improve studies of particular nucleon decay modes and the atmospheric neutrino spectrum. It should be noted that energy and position resolutions of Super-Kamiokande are significantly improved, an essential feature for the elimination of background and the detection of low energy interactions. These features will allow Super-Kamiokande to have sensitivity for detection of solar, atmospheric, and supernova neutrinos above a threshold of 5 MeV.

3. Nucleon Decay

Nucleon instability, expected at some level in many extensions of the standard model, still offers a unique probe in searches for the ultimate theory of interactions. The lifetime of the proton depends on the scale of grand unification as determined by the convergence of the three fundamental running coupling constants at a single point at very high energy. Recent measurements of these coupling constants at LEP[1, 2] have resulted in much better predictions of the proton lifetime than was previously possible. These lifetimes are within the reach of a detector the size and resolution of Super-Kamiokande.

Super-Kamiokande is the largest nucleon decay detector ever constructed. In terms of its sensitive mass (22,000 metric tons) it is larger than the sum of the fiducial masses of all previous detectors (NUSEX, Soudan I, IMB, Kamiokande, Soudan II, Frèjus, and KGF. Super-Kamiokande will not only have seven times the fiducial volume of IMB, it will also have ten times the light collection capability. This will result in a substantially higher efficiency for low-light level decay modes. When coupled with lower background rates from atmospheric neutrinos (due to better energy and track resolution), this will lead to at least an order-of-magnitude increase in nucleon decay detection sensitivity for most decay modes. It is this ten-fold improvement that will allow Super-Kamiokande to test unification theories that predict proton decay in the range $10^{33\text{-}35}$ years.

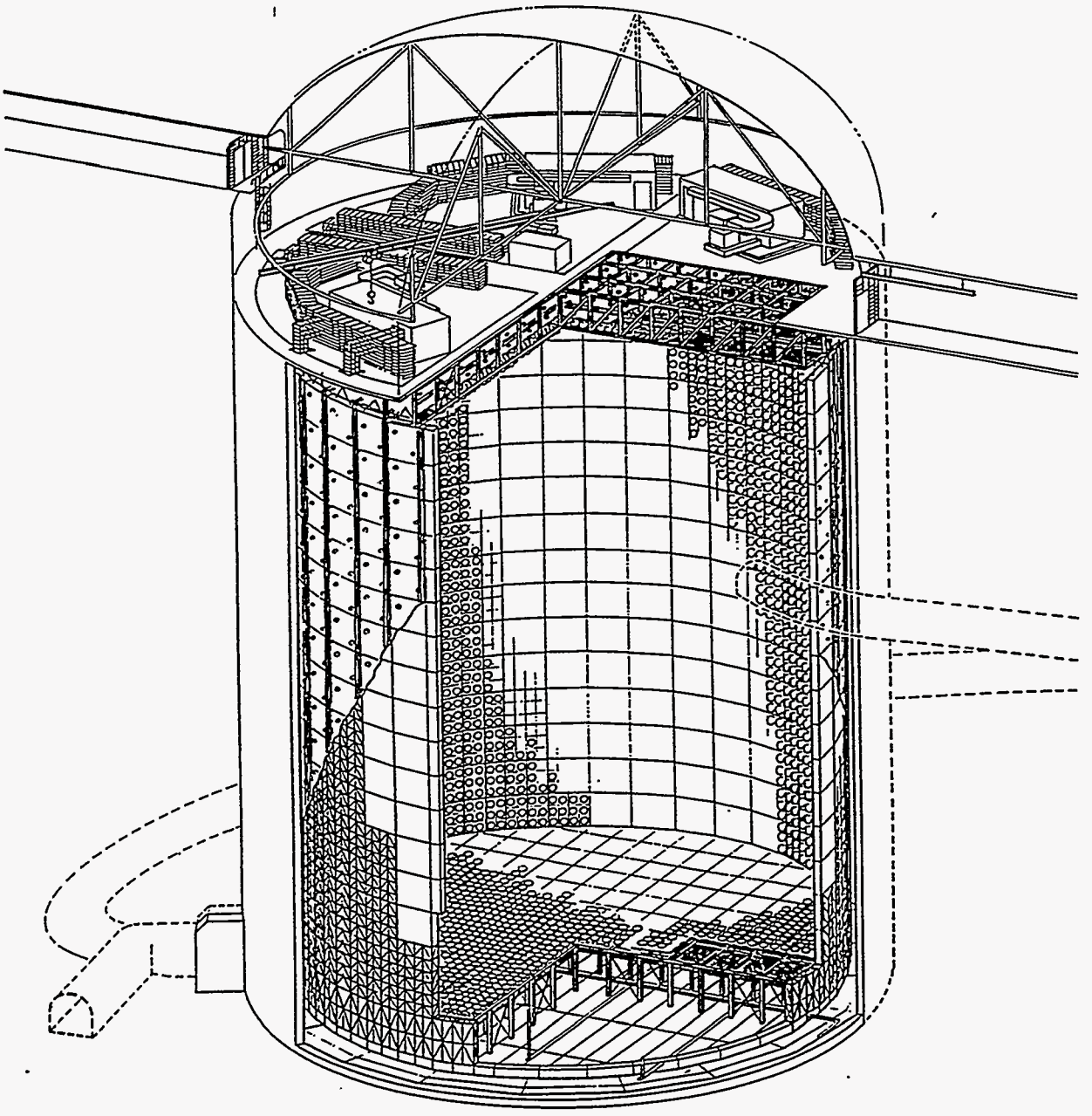

Figure 1. Schematic representation of the Super-Kamiokande detector.

Table I: Comparison of the Physical and Performance Parameters of Large Water Cherenkov Detectors

PARAMETERS	KAMIOKANDE III	IMB-3	SUPER-KAMIOKANDE
DEPTH	2700 mwe	1800 mwe	2700 mwe
TOTAL SIZE	16 mh x 19 mϕ	17 x 18 x 23 m^3	41 mh x 39 mϕ
TOTAL MASS	4500 tonnes	10,000 tonnes	50,000 tonnes
FIDUCIAL MASS (Solar ν)	1040 tonnes 680 tonnes	3300 tonnes NONE	22,000 tonnes 32,000 tonnes
NUMBER of PMTs	948 (20" ϕ)	2048 (8" ϕ + WLS)	11,146 (20" ϕ) 1,890 (8" ϕ + WLS)
PMT TIMING RESOLUTION	4 ns @ 1 pe	7 ns @ 1 pe	2.5 ns @ 1 pe
PHOTO-CATHODE COVERAGE	20%	4%	40%
ANTI-COUNTER	~1.5 m (Side Only)	None	2.5 m (All Sides)
THRESHOLDS: Trigger Analysis	 5.2 MeV 7.5 Mev	 ~15 MeV ~20 MeV	 4 - 5 MeV 5 MeV
ENERGY RESOLUTION	4%	$3/\sqrt{E} \pm 7\%$	2.5%
POSITION RESOLUTION	15 cm	35 cm	10 cm
ANGULAR RESOLUTION	2.7°	5°	~1°
e/μ SEPARATION	98 ± 1%	92%	99%
μ DECAY DETECTION	88 ± 1%	80 ± 4%	95%

3.1 The Standard Model Framework

In the Standard Model, interactions between the elementary fermions are mediated by three forces: electromagnetism, the weak force, and the strong force. These forces arise from fundamental local gauge symmetries of nature, as represented in the form of the covariant derivative:

$$D_\mu = \delta_\mu - ig_1\frac{Y}{2}B_\mu - ig_2\frac{\tau^j}{2}W^j_\mu - ig_3\frac{\lambda^a}{2}G^a_\mu$$

Each of the three gauge terms is characterized by a (multi-component) vector field (B, W, or G); an internal symmetry structure (with generators Y for U(1), τ for SU(2) , and λ for SU(3)); and a scalar coupling constant (g_1, g_2, and g_3).

The vector fields correspond to spin-one bosons (one for each degree of freedom in the internal space) which mediate the interactions between the fundamental fermions (i.e., quarks and leptons). Parity violation in weak interactions is introduced by having the SU(2) term act only on left-handed fermions (arranged in doublets) and not on right-handed fermions (arranged in singlets) and also by assuming a different Y for the left- and right-handed states. Parity conservation is restored in electromagnetic interactions when the W^0 and B fields mix to form the γ and Z fields. It is this framework of electroweak mixing that has served as a blueprint for more extensively unified models which predict nucleon instability.

Nucleon instability is a natural consequence of models which attempt to extend the Standard Model to unify the strong and electroweak forces. In almost all models, the Higgs mechanism is invoked to give the intermediate vector bosons of the theory (which can mediate proton decay) a very large mass. In supersymmetric (SUSY) models, the Higgs particles can themselves mediate nucleon instability, giving in general, different favored decay modes. Thus, discovery of proton decay could provide experimental evidence for an operable Higgs mechanism and help fill the experimental void that exists in support of this central feature of electroweak unification and the Standard Model.

The success in explaining much of the character of low-energy particle interactions by describing them in terms of local gauge symmetries (each with its own gauge coupling parameter and vector boson multiplet) leads naturally to the question of why these specific separate symmetries are the ones nature has selected to be respected. Perhaps they are part of a larger local gauge symmetry. Supporting such an hypothesis is the fact that the individual coupling constants of the Standard Model have an energy dependence, governed by the renormalization group equations, which causes them to evolve in such a way as to converge somewhere in the energy region of 10^{15} GeV.

There are good theoretical reasons to believe that protons might decay into lighter particles. Firstly, there is no *fundamental gauged* symmetry in the Standard Model associated with either baryon number or lepton number which would lead to their conservation, thus ensuring proton stability. Secondly, the observed baryon asymmetry of the universe (i.e., more matter than anti-matter) implies that baryon number is not conserved at some level, if one makes the assumption that the Big Bang baryon number of the universe was zero. Thirdly, in many SUSY theories there are scalar Higgs particles which can mediate proton decay; thus the proton lifetime may be measurably short, even if the GUT energy scale is so high as to virtually exclude vector-boson mediated decay.

Under SU(5) it was possible to make a relatively accurate prediction of the proton lifetime and branching ratios[3]. The proton mean lifetime was predicted to be $10^{29 \pm 2}$ years with the dominant branching ratio being to the lightest lepton and meson, $e^+\pi^0$. This prediction was ruled out by the first results from IMB in 1983. Current results from IMB set a lower limit on this decay lifetime divided by branching ratio of 8.4×10^{32} years. The

possibility of grand unification gains credence in light of recent LEP experiments which have allowed for new determinations of M_Z, α_s and $\sin^2 \theta_W$ leading to much more precise measurements of electroweak and strong coupling constants at the M_Z scale. As shown by Amaldi *et al.*[1, 2], the LEP measurements have allowed for more conclusive extrapolations to high energies in search of the unification scale. It was found that in a non-supersymmetric Standard Model with only one Higgs doublet, the convergence of coupling constants at a single point is excluded by more than eight standard deviations. With additional Higgs doublets unification can be obtained; however, this unification is at a scale conflicting with the experimental limits on the nucleon lifetime.

The results from LEP, coupled with limits on nucleon stability, demonstrate that the idea of a single-point unification of the coupling constants is too simple-minded and stands in need of correction. Either there is no desert between the electroweak and GUT mass scale or GUT is broken in several steps. Since 1986 other GUT models have produced a broad range of possible nucleon lifetimes. Nevertheless, the recent precise LEP measurements now confine the nucleon decay lifetime range for many models to a region just above and close to the current experimental limits.

The inconsistency of the minimal SU(5) model with the observed values of $\sin^2 \theta_W$ and the lower limit on proton lifetime brings forward some new features related to the probing of grand unification through proton decay. To begin with, this inconsistency must not, of course, be interpreted as evidence against the basic idea of grand unification. This is because, as pointed out by several authors[1, 2, 4, 5, 6] beginning in the 1980s (in fact prior to the recent observations), some well-motivated extensions of minimal SU(5) lead to values of $\sin^2 \theta_W$ and τ_p which are higher than those of minimal SU(5), both in accord with the recent data.

In the supersymmetric extension of the Standard Model with a minimal Higgs sector of two doublets, a single convergence point is obtained in the extrapolations of the running coupling constants measured at LEP by fitting both the unification scale M_{GUT} and the SUSY breaking scale M_{SUSY} . For the fitted value of $M_{GUT} = 10^{15.8 \pm 0.3 \pm 0.1}$ GeV, the nucleon lifetime was estimated to be $10^{34.5 \pm 1.2}$ years, if the decay is dominated by gauge boson exchange. This is within the 10^{34} year sensitivity of Super-Kamiokande, though the entire "vector-boson-only" range is not completely covered.

3.2 Current Experimental Status

Although candidate nucleon decay events have been observed, no experiment has yet found evidence for nucleon decay above the expected neutrino backgrounds. The recent generation of detectors has included two types: fine-grain tracking calorimeters and very large water Cherenkov detectors. For nearly every decay mode examined, these detectors (IMB and Kamiokande) have placed the most stringent limits on the nucleon lifetime. This section provides a brief summary of the current status; more detailed reviews of the recent results can be found in Refs. 7 and 8.

The decay mode that has received the most attention, both theoretical and experimental, is $p \rightarrow e^+\pi^0$. The most recently published result from IMB on this decay mode[9] was based on data through 1988 covering 376 days of IMB-3 live time. It set a partial lifetime limit for $p \rightarrow e^+\pi^0$ of 5.5×10^{32} years at 90% confidence level when data from the IMB-1 detector are included. Since then an additional 448 days of data in IMB-3 have been accumulated. Analysis of this sample indicates that there is no $p \rightarrow e^+\pi^0$ decay candidate. These accumulated data in IMB restrict the proton's lifetime into this decay mode to be at least 8.4×10^{32} years. Neither the Kamiokande nor the Frèjus experiments

have observed a candidate for this mode. Thus, a combined lower limit on the partial lifetime based on the world's data is ~1.2 x 10^{33} years.

Supersymmetric unified theories tend to favor the decay mode $p \rightarrow \nu K^+$. Kaons resulting from proton disintegration would decay at rest either to $\nu\mu^+$ (63%) or $\pi^0\pi^+$ (21.2%). For the kaon decay into $\nu\mu^+$, four candidates with compatible muon energy were found in a subset of the IMB-3 data. Without subtracting background, these four events imply a lower limit to the partial proton lifetime of $\tau_B \geq 1.0 \times 10^{31}$ years. The $K^+ \rightarrow \pi^0\pi^+$ channel, though with a small branching ratio, produces more light due to the two γs from the π^0 decay; the presence of the π^+ is inferred by detection of the delayed μ^+ decay. Two events were found to be compatible with this decay mode in IMB-3 data; however, each event had a collapsed Cherenkov ring indicating the presence of a recoil proton as expected from a neutrino interaction. Thus, with no $p \rightarrow \nu K^+$, $K^+ \rightarrow \pi^0\pi^+$ candidates the proton's partial lifetime becomes $\tau_B \geq 8.3 \times 10^{31}$ years. The current Kamiokande lower bound for the $p \rightarrow \nu K^+$ decay mode is 1.0×10^{32} (5 candidates), and the Frèjus limit is 0.15×10^{31} with 1 candidate. These candidates are all compatible with expected neutrino background so there is no evidence for supersymmetric nucleon decay.

A general analysis that works for all nucleon decay modes begins by noting that a nucleon that decays does so nearly at rest. The daughter particles should have a total energy of about 1 GeV and should be emitted to balance their momentum. However, a particle's energy that is visible in a detector, especially a Cherenkov detector, is often less than its total energy. The total visible energy is the quantity of interest for each event. A parameter known as anisotropy, defined as the normalized average direction of the flow of visible energy in each event, is used to estimate the degree of momentum imbalance in the event; the anisotropy should be near zero for a well-balanced back-to-back event and near 1 for an event with a single visible track. Detailed simulations of the particle's interactions in the detector and the detector's response are required to determine the range of parameters possible for each nucleon decay mode of interest. The results of this analysis for IMB-3 are presented in Table II. Results for a variety of modes from IMB-1 & 2 are found in Refs. 10 and 11.

For some decay modes it is possible to make a more discriminating selection of nucleon decay candidates by deducing the invariant mass and residual momentum of the particles in the event. This is possible for those events with widely separated tracks because then each track's momentum can be unambiguously measured. Table III shows results, based on a subset of the IMB-3 data, using this analysis for some selected decay modes. The candidates are located among the wide angle 2 prong events that constitute a small fraction (~3%) of the data sample. For the selected events, invariant masses and residual momenta are calculated assuming all possible particle hypotheses for each track. This analysis usually has slightly poorer efficiency due to the stringent requirements on the track identification; however, in reducing the measured (and expected) neutrino background, it often produces better limits on the nucleon's partial lifetime.

There is currently no compelling experimental evidence for nucleon decay above expected neutrino backgrounds into any mode tested so far. On the other hand, many of the decay modes in question remain background free or nearly background free. Therefore there is a clear need for a much larger detector with improved resolution to continue the search. The preceding section showed that there are sound theoretical reasons to expect that the proton is not absolutely stable. Current unified theories predict the exciting possibility that the proton's lifetime may be well within the discovery potential of Super-Kamiokande.

Table II. Selected nucleon decay partial lifetime lower limits (90% c.l.) set by IMB using visible energy and anisotropy cuts.

Mode	τ/Br ,IMB-3 ($\times 10^{31}$ yr)
$p \to e^+k^0$ ($K^0_S \to \pi^0\pi^0$)	11
$p \to e^+k^0$ ($K^0_L \to \pi^0\pi^0\pi^0$)	6.1
$p \to e^+\eta$ ($\eta \to$ *neutrals*)	16
$p \to e^+\eta$ ($\eta \to$ *charged*)	2.9
$p \to e^+\rho$	3.0
$p \to e^+\omega$ ($\omega \to \pi^+\pi^-\pi^0$)	11
$p \to e^+\omega$ ($\omega \to \pi^0\gamma$)	1.8
$p \to e^+\gamma$	20
$p \to \mu^+\pi^0$	16
$p \to \mu^+K^0$ ($K^0_L \to \pi^0\pi^0\pi^0$)	11
$p \to \mu^+K^0$ ($K^0_S \to \pi^+\pi^-$)	7.6
$p \to \mu^+K^0$ ($K^0_S \to \pi^0\pi^0$)	0.4
$p \to \mu^+\eta$ ($\eta \to$ *neutrals*)	13
$p \to \mu^+\eta$ ($\eta \to$ *charged*)	1.4
$p \to \mu^+\mu^+\mu^-$	17
$p \to e^+e^+e^-$	31
$n \to \nu K^0$	1.4
$n \to \nu\omega$ ($\omega \to \pi^+\pi^-\pi^0$)	1.8
$n \to \nu\omega$ ($\omega \to \pi^0\gamma$)	0.5

Table III. Nucleon decay partial lifetime lower limits obtained with the invariant mass analysis from IMB-3.

Mode	# of Cand.	# of Bkgd	τ/Br IMB-3 ($\times 10^{31}$ yr)
$p \to \mu^+\gamma$	0	0.2	25
$n \to e^+\pi^-$	0	0.4	4.8
$n \to \mu^+\pi^-$	2	0.7	4.6
$p \to \mu^+\omega$	1	0.6	1.6
$p \to \mu^+\rho$	3	1.5	4.1

3.2 Sensitivity of Super-Kamiokande

In their searches for nucleon decay over the last decade the two largest detectors have collected data corresponding to a total exposure of about 17.7 kt-yr (kiloton-years): 11.5 kt-yr for IMB and 6.2 kt-yr for Kamiokande. According to analysis of the total IMB sample plus a 3.76 kt-yr sample of Kamiokande data, no candidate for a $p \rightarrow e^+\pi^0$ decay was found; this yields a lower bound on the proton lifetime/branching ratio of ~1.1 x 10^{33} years. In 5 years of running, Super-Kamiokande will achieve an exposure of 110 kt-yr. This will correspond to a sensitivity to ~10^{34} years for the decay modes which give clear signals above the atmospheric neutrino background.

IMB-3 observed atmospheric neutrino interactions in contained events at a rate of 121 ± 4 (stat) kt-yr^{-1}; Kamiokande II in fully contained events of 87 ± 6 (stat) kt-yr^{-1}. Our Monte Carlo estimates that the events observed in IMB-3 constitute 69 ± 7% (syst) of all the atmospheric neutrino interactions which produce particles detectable by the water Cherenkov technique. This leads to an estimate of 176 detectable interactions occurring in water per kt-yr. This estimate is free of uncertainties in the neutrino fluxes and total cross sections, but is subject to an uncertainty of ~10% in the IMB-3 experimental event-saving efficiency estimate.

It can be conservatively estimated that the neutrino background for $p \rightarrow e^+\pi^0$ is less than 0.1 event per year (90% c.l.) of Super-Kamiokande livetime. Assuming an overall event-saving efficiency of 60% one can get a lower bound on τ_B = 1 x 10^{34} years if no candidate is found after 5 years of livetime or 1.9 times lower if one candidate is found. Table IV shows the current lifetime limits for several representative 2-body decay modes. Included in both tables are estimates of the sensitivity which could be reached by Super-Kamiokande after several years of operation.

Table IV. IMB proton decay lifetime lower limits for some representative two-body modes compared with that expected for Super-Kamiokande.

Decay Mode	IMB (x 10^{31} yr)	Super-Kamiokande (x 10^{31} yr)
$p \rightarrow e^+\pi^0$	84	1000
$p \rightarrow e^+\eta^0$	20	600
$p \rightarrow e^+\omega^0$	11	90
$p \rightarrow e^+\rho^0$	3.2	90
$p \rightarrow e^+K^0$	11	100
$p \rightarrow \mu^+\pi^0$	27	1000
$p \rightarrow \mu^+\eta^0$	13	600
$p \rightarrow \mu^+K^0$	11	300
$p \rightarrow \mu^+\rho^0$	4.1	90
$p \rightarrow \mu^+\omega^0$	4.2	90
$p \rightarrow \nu\,\rho^+$	1.4	60
$p \rightarrow \nu\,K^+$	5.7	100

4. Conclusion

Recent developments in the quest for grand unification are encouraging for experimental searches for nucleon instability. Unification is expected in an energy region which implies a nucleon lifetime close to the values being currently probed. Theory, however, does not provide us with any definite guideline about a preferred decay mode. Depending on the unification model, the dominant decays may lead to a lepton and a pion or to a neutrino and a kaon. It is clear that the relatively small coverage of light sensors in IMB restricted the quality of the results for those decay modes where a better Cherenkov image of a massive particle with low velocity would be vital. Even if a pion is produced at relatively high energy, as in two-body decay modes, the nuclear interactions inside the oxygen nucleus and during its passage through water decrease its final light output. Some decay modes, e.g. $p \rightarrow e^+\pi^0$, are still easily selected from the background. We expect less than 0.1 background events/yr for $p \rightarrow e^+\pi^0$ decay. In order to probe the broadest possible range of expected nucleon partial decay rates for the background-free modes, the increase in the fiducial volume and detection livetime represented by Super-Kamiokande is vital. However, for most decay channels an effective background rejection becomes of major importance. It should be noted that very few decay modes have zero candidates. Due to the soft spectrum of atmospheric neutrinos, many recoiling protons, as well as many charged pions, remained invisible with the IMB detector light sensitivity. The observation of images from particles just above their Cherenkov thresholds will greatly reduce the number of events considered as candidate nucleon decays. Better energy resolution will also improve signal to background ratio. The invariant mass analysis would be more effective in selecting the potential nucleon decay candidates from the continuous neutrino interaction background. An improved energy resolution is essential for identifying monoenergetic muons of 236 MeV/c momentum that unambiguously signal a decay of a kaon resulting from any (p or n) $\rightarrow$ lepton + K^+ decay. A unique identification of kaons is particularly interesting because they are very unlikely products of the soft atmospheric neutrino interactions. Super-Kamiokande has better energy resolution than IMB or Kamiokande due to its increased light collection and ability to calibrate efficiently from low-energy electrons. Hence, there are strong theoretical and experimental motivations for extending the nucleon decay searches begun in the 1980's by IMB and Kamiokande.

6. References

1. U. Amaldi, W. de Boer and H. Furstenau, *Phys. Lett.* **260B**, (1990).
2. U. Amaldi *et al.*, *Phys. Lett.* **281B**, (1992).
3. See, for example, P. Langacker, *Phys. Rep.* **72** (1981).
4. See, for example, J.C. Pati and A. Salam, *Proc. First Grand Unification Workshop*, New Hampshire (1981); T. Rozzo and G. Senjanovic, *Phys. Rev.* **D25**, 235 (1982); F. del Aguilla and L. Ibanez, *Nucl. Phys.* **B177**, 60 (1981); M. Fukugita, T. Yanagida and M. Yoshimura, *Phys. Lett.* **106B**, 183 (1981).
5. U. Amaldi *et al.*, *Phys. Rev.* **D36**, 1385 (1987) and W. Marciano, *Proc. Eighth Grand Unification Workshop*, Syracuse, World Scientific, pp. 185--199 (1987).
6. P. Langacker and M Lou, *Phys. Rev.* **D44**, 817 (1991); J. Ellis, S. Kelley and D.V. Nanopoulos, *Phys. Rev.* **D44**, 817 (1991).
7. Review of Particle Properties, *Phys. Rev.* **D45**, (1992).
8. R. Barloutaud, TAUP '92, *Nucl. Phys. B (Proc. Suppl.)* **28A**, 437 (1992).
9. R. Becker - Szendy *et al.*, *Phys. Rev.* **D42**, 2974 (1990).
10. T.J. Haines *et al.*, *Phys. Rev. Lett.* **57**, 1986 (1986).
11. S. Seidel *et al.*, *Phys. Rev. Lett.* **61**, 2522 (1988).

1995-96 RESULTS FOR THE AMANDA NEUTRINO OBSERVATORY

AMANDA Collaboration
presented by Francis Halzen
Physics Department, University of Wisconsin, Madison, WI 53706

Abstract

At the AMANDA South Pole site, four new holes were drilled to depths ~2050 to 2180 m and instrumented with 86 PMTs at depths ~1520 to 2000 m. 79 of the PMTs are working, with 4 ns timing resolution and noise rates ~300 to 600 Hz. Various diagnostic devices were deployed and are working. An observed factor $\sim 10^2$ increase in scattering length and a sharpening of the distribution of arrival times of laser pulses relative to measurements at 800–1000 m showed that bubbles are absent at depths $z \geq 1500$ m. Absorption lengths are ~100 to 200 m at wavelengths in the blue and UV to 337 nm. Muon coincidences are seen between the SPASE air shower array and the AMANDA PMTs at 800–1000 m and 1500–1900 m. The muon track rate is ~30 Hz for 8/3 triggers and ~10 Hz for 10/3 triggers. The present array is the nucleus for a future expanded array.

1. Introduction

The deep Antarctic ice is the purest, most transparent of all natural solids. As a site for a high-energy neutrino observatory it has a number of advantages over deep sea water. It consists of compressed pure H_2O snow with the lowest contamination by aerosols and volcanic dust of any place on earth, and it contains neither bioluminescent organisms nor radioactive ^{40}K. Before the AMANDA collaboration began to measure the optical properties of ice at the South Pole, one could have listed a number of potential drawbacks:

- no one had ever drilled a hole deeper than 349 m at South Pole;
- the depth at which air bubbles completely transform into solid crystals of air hydrate clathrate was not known;
- the absorption length of light in ice was thought (on the basis of laboratory data) to be shorter than in sea water;
- the effects of dust, traces of marine salt, traces of natural acids, and birefringence of polycrystalline ice on scattering of light in ice at South Pole had not been studied.

These issues have now been addressed.

2. Results from the AMANDA-A Array at 800 to 1000 m

The successful deployment of the four-string AMANDA-A array with PMTs at 800 to 1000 m was the first step toward demonstrating that the South Pole ice is a

suitable site for a high-energy neutrino observatory.[1] With a hot-water drill, four holes ~60 cm in diameter were created during the 1992-93 season and instrumented with PMTs spaced at 10 m intervals from 810 to 1000 m. To measure optical properties, a dye laser in a laboratory very close to the holes was used to send nanosecond pulses down any of 80 optical fibers to emitting balls located near each PMT. From the distributions of arrival times at neighboring PMTs, it was possible to determine separately the absorption length, λ_a, and effective scattering length, $\lambda_e \equiv \lambda_s/(1 - \langle\cos\theta\rangle)$, at wavelengths from 410 to 610 nm. Here $\langle\cos\theta\rangle$ is the mean cosine of the scattering angle. Because $\lambda_e \ll \lambda_a$, the data fitted an expression for three-dimensional diffusion with absorption. Three major results were obtained:[2,3]

- In contrast to laboratory ice, for which λ_a was reported[4,5] to be < 25 m at all wavelengths and $\lambda_a = 8$ m at the wavelength for maximum quantum efficiency of a PMT, we found values of λ_a exceeding 100 m at wavelengths less than $\sim$ 480 nm and values exceeding 200 m at wavelengths less than ~420 m.

- We found that, independent of wavelength, λ_e increased monotonically from ~40 cm at 820 m to ~80 cm at 1000 m. We interpreted this result as evidence for scattering by bubbles with size much larger than the wavelength of light, with the size and number density of bubbles decreasing with depth.

- We found that the absorption coefficient ($\alpha \equiv 1/\lambda_a$) increases with depth, from which we concluded that absorption is given by the sum of an intrinsic contribution and a contribution due to dust, with adust proportional to dust concentration and decreasing with wavelength.[6]

3. Predictions of Depth-Dependence of Scattering by Bubbles and Dust

For the South Pole ice temperature of $-50°$ C, at pressures corresponding to depths greater than ~400 m, the air trapped in bubbles is unstable against a phase transformation into the air hydrate solid phase, but the rate of transformation is controlled by the slow diffusion of water molecules through the growing shell of air hydrate inside a bubble wall. When the activation energy for diffusion through the hydrate and the age of South Pole ice as a function of depth were taken into account, it was possible to fit data on bubbles in Byrd Station and Vostok Station ice cores and AMANDA data on λ_e as function of depth at 800-1000 m, and to predict that λ_e would grow to ~10 m at 1450 m and to ~100 m at 1520 m.[7]

Measurements of dust concentration as a function of depth in a number of ice cores are consistent with the hypothesis that insoluble dust strongly correlates with global climate. For example, for Vostok cores, the dust concentration shows peaks at depths corresponding to ice ages at ~17,000 yr BP and ~150,000 yr BP and at an intermediate cold period at ~60,000 yr BP. Although corresponding data do not exist for the South Pole ice, we were able to develop a model of age vs. depth for that location and thus to predict that there will be peaks in absorption due to dust at depths of ~1050, 1720, and 2400 m.[8] Whether peaks in the scattering due to dust

will show up at those same depths depends on the magnitude of contributions to scattering that may not depend much on depth.

The conclusion of these studies was that PMTs should be placed in new holes at depths no shallower than 1500 m and extending as deep as drilling equipment will permit.

4. Technical Aspects of the AMANDA-B 1995-96 Drilling Season

New drilling equipment, operating at a power of ~1.9 MW, used water emerging at 75° C to drill at a rate up to ~1 cm/s. It required a time of no more than 4 days to melt a 60 cm diameter cylinder of ice to a depth of 2000 m. Due to a late start and several problems associated with commissioning the new equipment, only four holes were drilled, of which one reached a depth of 2180 m. It took typically 8 hours to remove the drill and water-recycling pump from a completed hole. The rate of refreeze was ~ 6 cm decrease in diameter per day, which easily allowed time to mount PMTs and other devices on cables, to lower the cables to bottom, and to route the upper ends of the cables into the AMANDA building in time to monitor the entire refreezing process.

The diagnostic devices included four inclinometers to measure shear vs. time, thermistors to measure temperature vs depth, and pressure gauges to follow the refreezing. The measurements of temperature at three depths, together with previous measurements, confirmed the validity of a model of temperature vs. depth. At the greatest depth, the temperature of the ice was ~ −31° C, about 20° warmer than at the surface. During refreeze, the pressure reached a maximum of ~460 atm.

73 of the 80 PMTs on the coaxial cables survived the deployment and refreezing, and all of the six PMTs in the bottom 100 m of a prototype twisted-pair cable are working. With a total of 173 operating PMTs, the overall success rate is greater than 90% for phototube deployment on AMANDA-A and B. No PMTs have failed since refreezing of the ice. The mean time to failure is inferred to be >150 years per PMT.

With no local amplification, the analog signals are preserved, though broadened, in transmission along a 2 km coaxial cable, with a standard deviation of better than 4 ns in timing resolution. Of this, ~2.5 ns is due to the resolution of the optical fiber itself.

The noise rates of the 8-inch Hamamatsu PMTs are in the remarkably low range of 350 to 600 Hz. The twisted-pair cable has a significantly shorter rise time than the coaxial cable and requires front-end amplifier gains of only 30 instead of ~100. A great advantage of the twisted-pair cable is that a single cable can supply 36 optical modules instead of only 20.

At the surface, the new ADCs and new amplifiers are working as well as hoped. A newly installed trigger logic to search for gamma-ray bursts and supernovas at timescales of both milliseconds and seconds is operating with 64 optical modules at 0.8 to 1 km depth and with 79 optical modules at 1.5 to 1.9 km. Data are being taken by our Bartol colleagues with two radio receivers at depths of ~150 m and ~280 m, their aim being an initial evaluation of a method of detecting Cherenkov radiation at radio frequencies by ultrahigh energy cascades in the ice.

The YAG laser in the surface laboratory provides tunable pulses at 410 to 610 nm with only ~10 dB loss down the optical fibers. A pulsed nitrogen laser (337 nm) at a depth of 1820 m, held at a temperature of 24° C, is operating flawlessly. Pulsed blue LED beacons with filters for 450 and 380 nm emission are operating at various depths. DC lamps at 350 nm, 380 nm, and broadband are also operating.

5. Physics Results

5.1. Scattering

The burning issue — whether the bubbles are still present at depths 1500 to 2000 m — is now settled. We found λ_e to be two orders of magnitude greater at $z \geq 1500$ m than at 800–1000 m. We also found that λ_e should be expressed as a function of the pulse amplitude at the detector: at the single photoelectron level, λ_e is in the range 25–30 m; with a 2 p.e. cut, it grows to 50–60 m (which is greater than the interstring spacing), and for a 3 p.e. cut, it is 75–90 m. This enables us to use a few high-amplitude hits to anchor an event. The value of λ_e shows no strong dependence on either wavelength or depth. Because λ_e is comparable to the spacing between neighboring optical modules, many of the photons from one emitter have undergone none or few scatters before reaching a PMT. Thus, the analytic expression for diffusion with absorption is inapplicable, because the photons are not in the diffusion regime. Our present approach is to use Monte Carlo modeling and statistical techniques to find the best values of λ_a and λ_e for each combination of emitter, receiver, and wavelength. We will certainly know more about a possible dependence of scattering on depth and wavelength in a few months.

An example of a possible contribution to scattering that would be independent of depth is submicron liquid acid droplets that precipitated onto the snow as the nuclei of snowflakes. The concentration of acid in the ice is estimated to be an order of magnitude greater than the concentration of dust, and chemical measurements in ice cores from other sites have showed that the acid concentration does not depend on depth (and therefore on climate).[9] Much, perhaps all, of the acid collects in the linear boundaries between three adjacent ice crystals. Veins of concentrated acid have a higher refractive index than that of ice and can scatter light. The intensity of this scattered light might dominate over the scattering due to dust and might thus obscure a local peak at 1700 m.

5.2. Absorption

The large absorption length of ice in the blue and UV wavelength regimes is confirmed by the AMANDA-B data. At 337 nm, λ_a is of order 100 m, which is astonishing in view of the fact that λ_a is only a few meters for lake water and ocean water, and was reported to be only ~5 m for laboratory ice. The measurement at 337 nm is particularly important because it provides the first datum at a wavelength shortward of 410 nm and helps to pin down the absorption spectrum in the region where it is expected to start rising. At longer wavelengths in the blue, values of λ_a significantly longer than 100 m are being inferred from the data. A search for a peak

in absorption due to an increase in dust concentration expected at ~1700 m is in progress.

Comparison of the data on λ_a at 1500 to 2000 m with data at wavelengths 410 to 610 nm and at depths 810 to 1000 m suggests that the concentration of absorbing dust is greater at the greater depths. This is consistent with our observation[3,6] that, at short wavelengths where λ_a is most sensitive to dust, λ_a is constant at depths 800–900 m and decreases at depths 900–1000 m. Our interpretation is that the ice at 800–900 m was formed in the post-glacial Holocene period (<13,000 yr BP) where the dust concentration has been remarkably low, and that the ice at 900–1000 m was formed near the end of the most recent ice age, with a peak in the dust concentration ~17,000 yr BP. Assuming the correctness of our age vs. dust model and using the Vostok data on dust concentration vs. depth as a guide, we estimate that the South Pole ice at depths of 1500–2000 m contains 4 to 20 times as much absorbing (mineral) dust as at depths <900 m. The liquid acids, whose concentration is roughly independent of depth, do not contribute to absorption.

Despite the larger concentration of dust at 1500–2000 m, the absorption lengths and scattering lengths are quite acceptably long, allowing us to move forward with plans for an expansion of the AMANDA array.

5.3. Muons

We now have a large collection of well-defined muon tracks. The rate is ~30 Hz for 8/3 triggers (at least 8 PMTs on at least 3 strings), and is ~10 Hz for 10/3 triggers, as expected from a Monte Carlo model. We see coincidences of tracks of energetic muons between the surface SPASE array, AMANDA-A, and AMANDA-B. We are presently studying pattern recognition and muon track reconstruction, with the goal of seeing upward-going neutrino candidates. The long tails of the timing distributions for muon tracks can be greatly narrowed by cutting on two photoelectrons, leading to much longer effective scattering lengths than the 25–30 m values measured for single p.e. signals.

6. Conclusions

By any measure the 1995-96 AMANDA expedition has been a great success. The large values of λ_a mean that experiments that require large transparent volumes without the need for tracking are already very effective. These include searches for neutrinos accompanying gamma-ray bursts and accompanying supernova explosions. The values of scattering length $\lambda_e \approx 25$ to 30 m are acceptably long, provided that the spacing of PMTs is optimized.

We estimate that, by operating the present type of hot-water drilling equipment in duplicate, with enough personnel to operate in shifts without undue fatigue, we can deploy 16 new strings of PMTs per year over a period of several years in succession, building upon AMANDA-A and B. An intermediate step in the expansion should be to drill one hole to bedrock at a depth of ~2900 m and to check the predicted optical, thermal, and mechanical properties of the ice in the unexplored region below 2100 m.

Acknowledgments

We are indebted to the Polar Ice Coring Office and to Bruce Koci for the successful drilling operations, and to the National Science Foundation (USA), the U. S. institutions U. C. Berkeley, U. C. Irvine, and U. of Wisconsin, the Swedish National Research Council, the K. A. Wallenberg Foundation and the Swedish Polar Research Secretariat, and the German Electron Synchrotron Institute DESY for their support.

List of AMANDA Collaborators:

Physics Department, University of California at Berkeley, Berkeley, CA, USA:
D. M. Lowder, P. B. Price, and A. Richards

Lawrence Berkeley National Laboratory, Berkeley, CA, USA:
D. Nygren

Physics Department, University of California at Irvine, Irvine, CA, USA:
S. W. Barwick, P. Mock, R. Porrata, and E. Schneider

Physics Department, University of Wisconsin, Madison, WI, USA:
K. Engel, L. Gray, F. Halzen, J. Jacobsen, V. Kandhadai, I. Liubarsky, R. Morse, and S. Tilav

Physics Department, Stockholm University, Stockholm, Sweden:
P. Askebjer, L. Bergstræm, A. Bouchta, E. Dahlberg, B. Erlandsson, A. Goobar, P. O. Hulth, S. Johansson, Q. Sun, and C. Walck

Physics Department, University of Uppsala, Uppsala, Sweden:
S. Carius, A. Hallgren, and H. Rubinstein

DESY/Zeuthen, Germany:
H. Heukenkamp, A. Karle, T. Thon, C. Spiering, O. Streicher, and R. Wischnewski

Bartol Research Institute, University of Delaware, Newark, DE, USA:
T. C. Miller

References

[1]See papers by P. C. Mock et al. and by L. Gray et al. in *Proc. 24th International Cosmic Ray Conf.*, Rome, (1995).

[2]P. Askebjer et al., Science **267** (1995).

[3]P. Askebjer et al., *Wavelength Dependence of Light Scattering and Absorption in Deep Ice at the South Pole*, submitted to Science (1996).

[4]T. C. Grenfell and D. K. Perovich, J. Geophys. Res. **86**, 7447 (1981).

[5]D. K. Perovich and J. W. Govoni, Geoph. Res. Lett. **18**, 1233 (1991).

[6]AMANDA Collaboration, *Optical Properties of Deep Ice at the South Pole: Absorption*, to be submitted to Applied Optics (1996).

[7]P. B. Price, Science **267**, 1802 (1995).

[8]AMANDA Collaboration, J. Glaciology **41**, 445 (1995).

[9]M. R. Legrand, C. Lorius, N. I. Barkov, and V. N. Petrov, Atmospheric Environment **22**, 317 (1988).

BARYON INSTABILITY SEARCH: PRESENT STATUS AND FUTURE PERSPECTIVES

L. Moscoso
Direction des Sciences de la Matière, DAPNIA/SPP
CEA/Saclay, F-91191 Gif-Sur-Yvette, France

ABSTRACT

Nucleon decay appears as a consequence of models trying to explain the baryon-antibaryon asymmetry. This has motivated 15 years ago many underground experiments devoted to the search of proton and neutron decay. A very large number of decay channels have been investigated and no evidence has been found yielding lower limits on lifetime which rule out the minimal SU(5) Grand Unified Theory predictions and put severe constraints on more complicated models.

Next generation experiments like Super-Kamiokande, which is starting to take data now, ICARUS, whose a 600 ton prototype is under construction, will be sensitive to more complicated models predicting larger lifetimes.

1. Introduction

During its early story the Universe was dominated by radiations and baryon-antibaryon pairs were continuously created and annihilated. The annihilation rate decreased with the expanding Universe because the probability that nucleons and antinucleons could find each other decreased. So, it is natural to ask what is the mechanism which allows the observed asymmetry between baryons and antibaryons at least at the galactic scale.

The hypothesis that the large asymmetry observed today is the relic of a small statistical fluctuation at the epoch when $N_N \approx N_{\overline{N}} \approx N_\gamma$ is excluded [1] because the present ratio N_N/N_γ is of the order of 10^{-10} and the present number of nucleons in the Galaxy is $\approx 10^{69}$ ($10^{12} M_\odot$). So, the number of nucleons and antinucleons was 10^{79} before 10^{-6} s after the bang in the same co-moving volume allowing only a 10^{-40} relative statistical fluctuation which would be 30 orders of magnitude lower than what observed.

In 1967 A. D. Sakharov [2] suggested that the simultaneous effects of B-violating interactions, C and CP violation, and departure from thermal equilibrium could produce a small baryon-antibaryon asymmetry which, after baryon-antibaryon annihilations, would produce the asymmetry observed today with a nucleon density $N_N/N_\gamma \approx 10^{-10}$.

Models allowing B-violating interactions have been developed in the framework of Grand Unified Theories (GUT) that unify strong and electroweak interactions. In

these models quarks, antiquarks, and leptons are members of the same representations and, thus, there exist gauge bosons that allow B-violating transitions between quarks and antiquarks or leptons. Unlike what happens at low energy the cross section for B-violating scattering of fermions was not suppressed relative to other interactions when the temperature was greater than the mass of the gauge boson.

A fundamental consequence is that, if some mechanisms violating the baryon conservation exist, one can expect that the nucleon is unstable. The simplest model is the minimal SU(5) GUT [3] which predicts a proton lifetime between 10^{28} and 10^{31} years. Its supersymmetric extension [4] predicts that the dominant channel in proton decay is $p \to \overline{\nu}_\mu K^+$. As it will discussed below the first model is excluded by experiments searching for nucleon decay. Moreover it has been demonstrated that these models cannot explain the present baryon-antibaryon asymmetry [1].

Different schemes have been proposed [5] like dinucleon decays in nuclei ($NN \to Nl^+ + \cdots$), virtual meson exchanges ($pn \to l^+\overline{\nu}_l$) and models violating $B - L$ ($N \to l +$ mesons). The possible decay modes are summarized in table 1 for channels which may be detected in underground experiments.

Table 1. Schematic description of different visible nucleon decay modes for different ΔB and $\Delta(B-L)$ values. M represents a "mesonic" system of particles (i.e. a system with $B = L = 0$).

	$\Delta(B-L)=0$	$\Delta(B-L)=2$
$\Delta B = 1$	$N \to \overline{l}M$ $N \to \overline{l}\overline{l}l$ $NN \to l^+N$	$N \to lM$ $N \to ll\overline{l}$ $NN \to l^-N$
$\Delta B = 2$	$pp \to l^+l^+$ $pn \to l^+\overline{\nu}$	$NN \to MM$ $pn \to l^+\nu$ $nn \to l^+l^-$

2. The experiments

Among seven experiments [6–12] devoted to the nucleon decay searches listed in table 2, three were Čerenkov devices and four were ionization tracking calorimeters.

Table 2. Major characteristics of different underground experiments.

Experiment	technique	Total mass (Tons)	Fiducial mass (Tons)	Depth (m.w.e.)
IMB	Water Č	6900	3000	1600
HPW	Water Č	700	150	1500
KAMIOKANDE	Water Č	4500	1000	2700
KGF	Tracking cal.	140	60	7600
NUSEX	Tracking cal.	150	100	5100
Fréjus	Tracking cal.	912	550	4700
Soudan II	Tracking cal.	963	800	2100

The principle of the search of nucleon decay candidates is based on the selection of fully-contained events with energy-momentum balance compatible with the nucleon decay hypothesis. For this purpose only events with the primary vertex inside the fiducial volume and with all secondary tracks stopping inside the detector are selected. The energy of each track is estimated. The final selection consists in rejecting all events but those for which the sum of energies of all detected secondary particles (visible energy) and the sum of their momenta (visible momentum) are compatible with what is expected for the nucleon decay hypothesis.

3. Experimental method

The method used to estimate the nucleon lifetime consists in searching for a signal and in correcting it to take into account of the background contamination and of the detection efficiency.

3.1. Efficiency estimate

In order to calculate the detection efficiency a Monte Carlo simulation is used. Nucleon decays are generated inside the nuclei. The secondary particles are propagated in the nuclear matter by taking into account nuclear effects such as elastic scattering, charge exchange interactions and absorption. Effects due to the reinteraction inside the nucleus involving nucleons which are off their mass shell and due to the Fermi motion of the nuclear matter are also taken into account.

Particles leaving the nuclei are tracked in the detector and their interactions with the detector matter are simulated. The detector response is treated with the same

algorithm as real data.

The analysis of simulated events allows to define the selection cuts on the visible energy and on the visible momentum. The overall detection efficiency is calculated as the ratio of the number of accepted events to the number of simulated events.

3.2. Background calculation

It is well known that the main source of background is atmospheric neutrinos interactions in the detector. In principle these events are characterized by a $E_{\rm vis} - \mid \vec{P}_{\rm vis} \mid$ balance, where $E_{\rm vis}$ and $\mid \vec{P}_{\rm vis} \mid$ are the visible energy and momentum and M_N is the nucleon mass, incompatible with the nucleon decay hypothesis. Nevertheless, nuclear effects and Fermi motion of the target nucleon may degrade the energy-momentum balance in such a way that several neutrino interactions may simulate nucleon decays. In order to calculate this contamination a Monte Carlo technique is used to simulate the νN interactions. The detector response to secondary particles is simulated as described for the efficiency calculations. The contamination of each nucleon decay channel is then estimated by taking into account the number of events which are selected by using the same topological and kinematical selection criteria as for nucleon decay events. The contamination is given by $N_B = N_{\rm sel} S_{\rm exp}/S_{\rm MC}$ where $N_{\rm sel}$ is the number of selected events, $S_{\rm exp}$ and $S_{\rm MC}$ are the exposures (in kt$\cdot y$) used respectively for the real data and for the simulated atmospheric neutrinos interactions.

3.3. Calculation of the nucleon lifetime

A large number of decay channels has been investigated by different experiments [6–12]. For all channels no significant excess of events has been found and, thus, lower limits on the nucleon lifetime have been estimated for each channel.

The method of this calculation is based on the search of the upper limit at 90% of confidence level on the signal S_0 by taking into account othe number of selected candidates, the estimated background and corrections for the efficiency and for branching fractions of mesons in the final state.

The branching fraction of each nucleon decay studied is unknown. So, only limits on the ratio of the nucleon lifetime τ_N to the branching fraction BR are given. Its expression is:

$$\frac{\tau_N}{BR} = \frac{N_N M T}{S_0}$$

where N_N is the number of protons or neutrons per mass unit, M is the mass of the fiducial volume and T is the operating time.

4. Present status

A very large number of decay channels has been explored by underground experiments up to 1994. Since this date no new results have been published in this field.

All results are reported in the "Review of Particle Properties" published in 1994 [13] and are summarized in table 3.

Table 3. Ranges of nucleon lifetime lower limits for different type of decay channels.

	$\Delta(B-L)=0$	
$\Delta B=1$	$N \to \bar{l}M$	$10^{31}-10^{33}y$
	$N \to \bar{l}\bar{l}l$	$6\cdot10^{30}-6\cdot10^{32}y$
	$NN \to l^+N$	$2\cdot10^{31}-10^{32}y$
$\Delta B=2$	$pN \to l^+\bar{l}$	$1.6\cdot10^{30}-5.8\cdot10^{30}y$
	$\Delta(B-L)=2$	
$\Delta B=1$	$N \to lM$	$5\cdot10^{30}-5.5\cdot10^{31}y$
	$N \to l\bar{l}\bar{l}$	$5\cdot10^{30}-7.4\cdot10^{31}y$
$\Delta B=2$	$NN \to MM$	$5\cdot10^{29}-3.4\cdot10^{30}y$
	$NN \to l\bar{l}$	$9\cdot10^{29}-5.8\cdot10^{30}y$

Clearly limits obtained for channels characterized by $\Delta B=1$ with $\Delta(B-L)=0$ are sufficiently constraining to rule out the minimal SU(5) GUT. Othe model which benefit of larger degrees of freedom, like the supersymmetric extension of SU(5) and models capable to explain the $B-\overline{B}$ asymmetry are also well constrained but not completely ruled out. The lower lifetime limit for the dominant SuSy channel, $p \to K^+\overline{\nu}_\mu$, is 10^{32} years.

In order to reach more severe constraints more massive detectors are under construction or in project.

5. Future perspectives

The Super-Kamiokande detector has started to operate in March, 1996 [14]. The total mass is 50 000 tons and the fiducial mass will probably be 30 000 tons. The Čerenkov light is collected by 11 146 PMTs with 20" photocathode diameter. The total photocathode area is 40% of the total walls area doubling the light collection efficiency compared to the Kamiokande detector.

Lifetime limits will be improved by a factor 5-20 and the limit of 10^{34} years will be reached for $p \to e^+\pi^0$.

Afterwards, the ICARUS project [15, 16] will achieve a significant improvement on the background rejection. Its 5 000 tons version will explore the region between 10^{33} and 10^{34} years in 5 years equivalent running time. A 600 tons prototype is under construction [16, 17]. This detector will be able to reach lifetime limits comparable to what obtained by the present experiments and will improve by an order of magnitude the limits for exotic channels.

Looking futher in the future, the only way to explore lifetimes above 10^{34} years is to use a detector containing 10^{35} to 10^{36} nucleons which corresponds to several hundreds of ktons. With the present technologies only a Čerenkov detector can be considered with several 100 000 PMTs for a cost of several 100 M$. It is clear that, due to financial and technological considerations, this kind of project could be realized only by a very large international collaboration and could be integrated in a larger programme like the cubic kilometer detector.

6. Conclusions

The different underground experiments have accumulated more than 15 kt·y of total sensitivity and no evidence of nucleon decay has been found in any decay channels studied.

In order to improve significantly the sensitivity to nucleon decay, progresses must be achieved in increasing the detector masses and in improving the background rejection.

It has been shown by the Kamiokande collaboration [8] that no significant background contamination can be expected below 100 kt·y for several decay channels. This means that the Super-Kamiokande experiment will yield a major improvement for decay channel like $p \to e^+\pi^0$. Moreover, the ICARUS project will allow a further improvement on the background rejection yielding to a considerable increase of the sensitivity to decay channels which still suffer frm a large background contamination.

To reach a sensitivity to lifetimes above 10^{34} years requires a detector with a mass greater than that of Super-Kamiokande by at least an order of magnitude which represents several 100 kton. The only way to realize such a huge detector is to go to a worldwide collaboration.

REFERENCES

1. E. W. Kolb and M. S. Turner, Annu. Rev. Nucl. Part. Sci. **33** (1983) 645.
2. A. D. Sakharov, Zh. Eksp. Teor. Fiz. Pis'ma **5** (1967) 32 (JETP Lett. **5** (1967) 24).

3. J. C. Pati and A. Salam, Phys. Rev. **D 8** (1973) 1240; Phys. Rev. Lett. **31** (1973) 661;
   H. Georgi and S. L. Glashow, Phys. Rev. Lett. **32** (1974) 438;
   H. Georgi, H. R. Quinn and S. Weinberg, Phys. Rev. Lett. **33** (1974) 451.
4. J. Wess abd B. Zumino, Nucl. Phys. **B 70** (1974) 39; Phys. Lett. **B 49** (1974) 52.
5. R. N. Mohapatra and R. E. Marshak, Phys. Rev. Lett. 44 (1980) 1316;
   C. B. Dover et al., Phys. Rev. **D 24** (1981) 2886;
   L. Arnellos and W. J. Marciano, Phys. Rev. Lett. **48** (1982) 1708; R. N. Mohapatra and G. Senjanovic, Phys. Rev. Lett. **49** (1982) 7;
   J. C. Pati, A. Salam and U. Sarkar, Phys. Lett. **B 133** (1983) 330;
   J. C. Pati, Phys. Rev. **D 29** (1984) 1549;
   M. N. V. Murphy and K. V. L. Sarma, Phys. Rev. **D 29** (1984) 1975.
6. M. R. Krishnaswamy at al., Nuovo Cimento **9C** (1986) 167.
7. IMB Collaboration, S. Seidel et al., Phys. Rev. Lett. **61** (1988) 2522.
8. Kamiokande Collaboration, K. S. Hirata et al., Phys. Lett. **B 220** (1989) 308.
9. NUSEX Collaboration, G. Battistoni et al.,Phys. Lett. **B 133** (1983) 454.
10. Fréjus Collaboration, Ch. Berger et al., Nucl. Phys. **B 313** (1989) 509;
    Ch. Berger et al., Z. Phys. **C 50** (1991) 385.
11. HPW Collaboration, T. J. Phillips et al., Phys. Lett.**B 224** (1989) 348.
12. Soudan II Collaboration, J. L. Thron et al., Nucl. Instr. and Meth. **283** (1989) 642.
13. L. Montanet et al. (Particle Data Group) Phys. Rev. **D 50** (1994) 1173.
14. Y. Totsuka, "Kamiokande and Super-Kamiokande", invited talks in the *IV International Workshop on Theoretical and Phenomenological Aspects of Underground Physics-TAUP 95*, Toledo, Spain, September, 1995 and the *II Recontres du Vietnam*, Ho Chi Minh City, October,1995, ICRR-Report-359-96-10.
15. Proposal by the ICARUS Collaboration, P. Cennini et al., "ICARUS II a Second-Generation Proton Decay Experiment and Neutrino Observatory at the Gran Sasso Laboratory", LNGS-94/99 I&II.
16. F. Mauri, "ICARUS Experiment", Report at this Workshop.
17. Addendum to proposal LNGS-94/99 I&II by the ICARUS Collaboration, P. Cennini et al., "A first 600 Ton ICARUS Detector Installed at the Gran Sasso Laboratory", LNGS-95/10.

BARYON INSTABILITY WORKSHOP SUMMARY TALK

Barry C. Barish
High Energy Physics, California Institute of Technology, Pasadena, CA 91125 USA

ABSTRACT

This workshop reviewed both the theoretical and experimental status of our understanding of baryon instability. New projects that are being implemented, and various ideas for proposed future initiatives were presented. In this summary talk I review the present situation and future prospects from an experimentalist's perspective.

1. Introduction

In 1967, Sakharov conjectured that in order to explain the origin of the matter-antimatter asymmetry in the Universe, three conditions are required:

1) baryon non-conserving interactions
2) CP violation
3) thermal non-equilibrium of these interactions

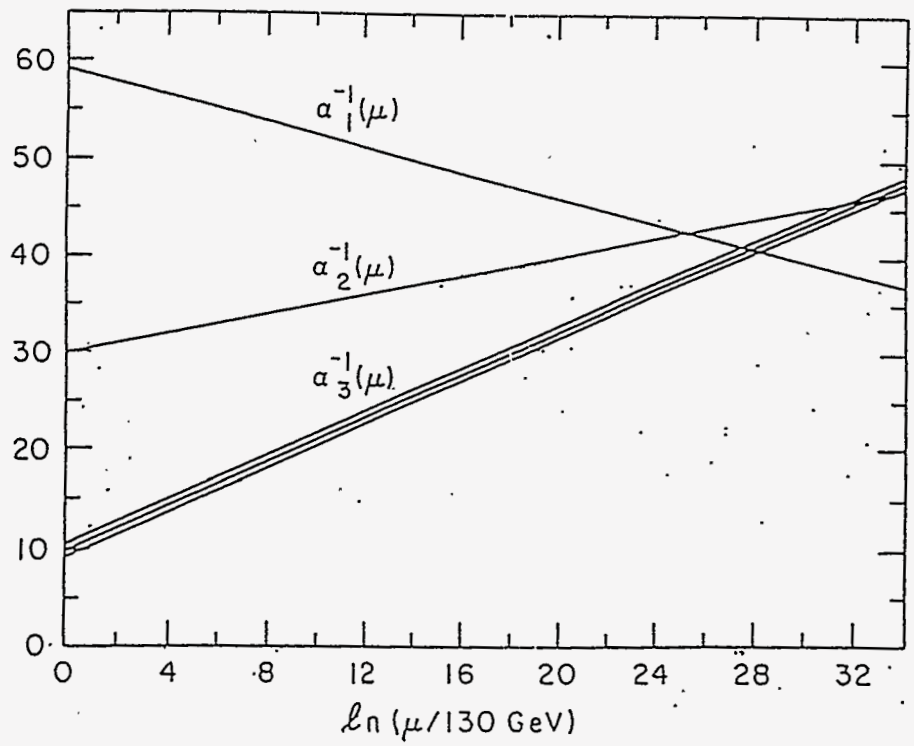

Figure 1. Grand Unification (almost)

This motivation, coupled with the specific predictions of SU(5) Grand Unified Theories motivated a generation of experiments searching for the consequences of baryon instability. The main prediction was the existence of nucleon decay modes and branching ratios at detectable rates. In particular, large proton decay experiments, IMB and Kamiokande, were built to search for such decays, especially the decay mode $p \rightarrow e^+ \pi^\circ$, which was predicted to have a branching ratio of between 9% and 38%. This mode has a particularly clear experimental signature using Cerenkov techniques and the experiments resulted in setting limits well below the predicted level.

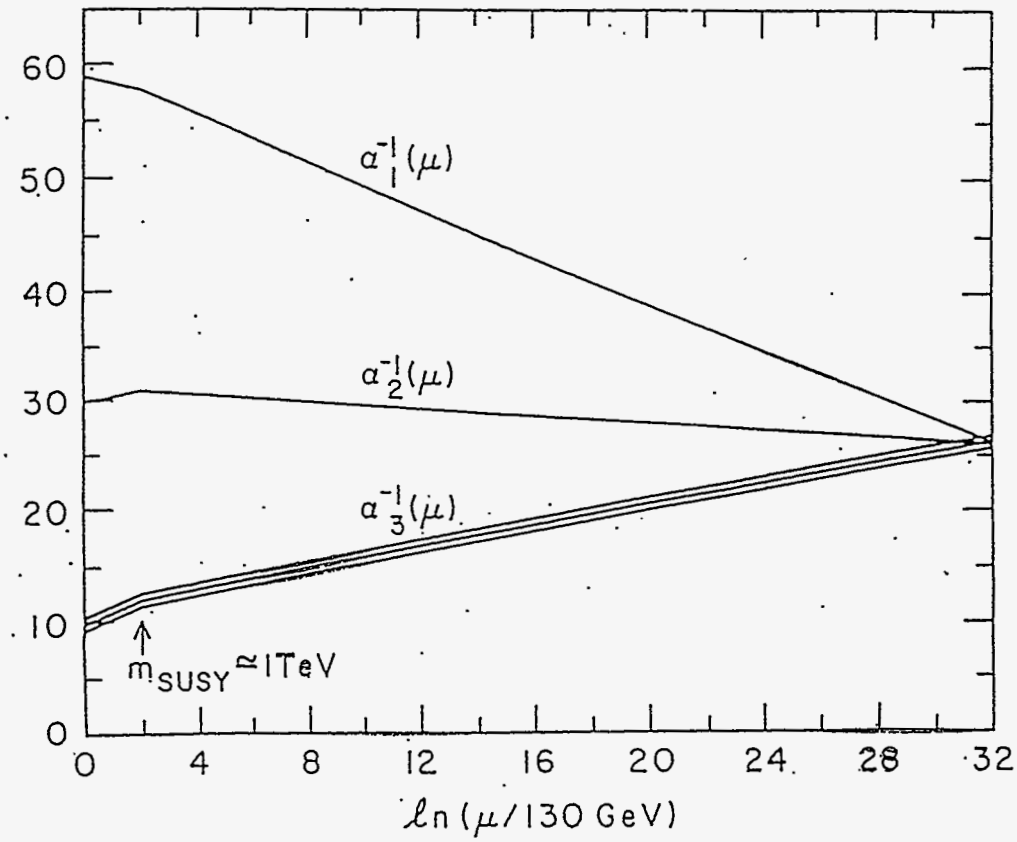

Figure 2. Evidence for SUSY?

This result rules out the simplest Grand Unified Model SU(5) and motivates us to make both more generalized searches of possible decay modes, and to develop sensitivity to longer proton lifetime. Predictions of other models of Grand Unification are generally less specific and usually predict longer lifetime.

Over the past decade or so, while the experiments yielded negative limits for proton decay over a broad range of decay channels, theoretical alternatives to SU(5) have emerged. Figure 1 shows that, although the general convergence of the electromagnetic weak and strong forces appears to occur at a large mass ($\approx 10^{16}$ GeV), in detail they do not cross at one point. If this very long extrapolation is taken seriously, some other physics between present energies ($\sim 10^2$ Gev) and the Grand Unification point ($\gtrsim 10^{16}$ Gev) might be indicated.

Table 1. Current Experimental Limits - Nucleon Lifetime Limits.

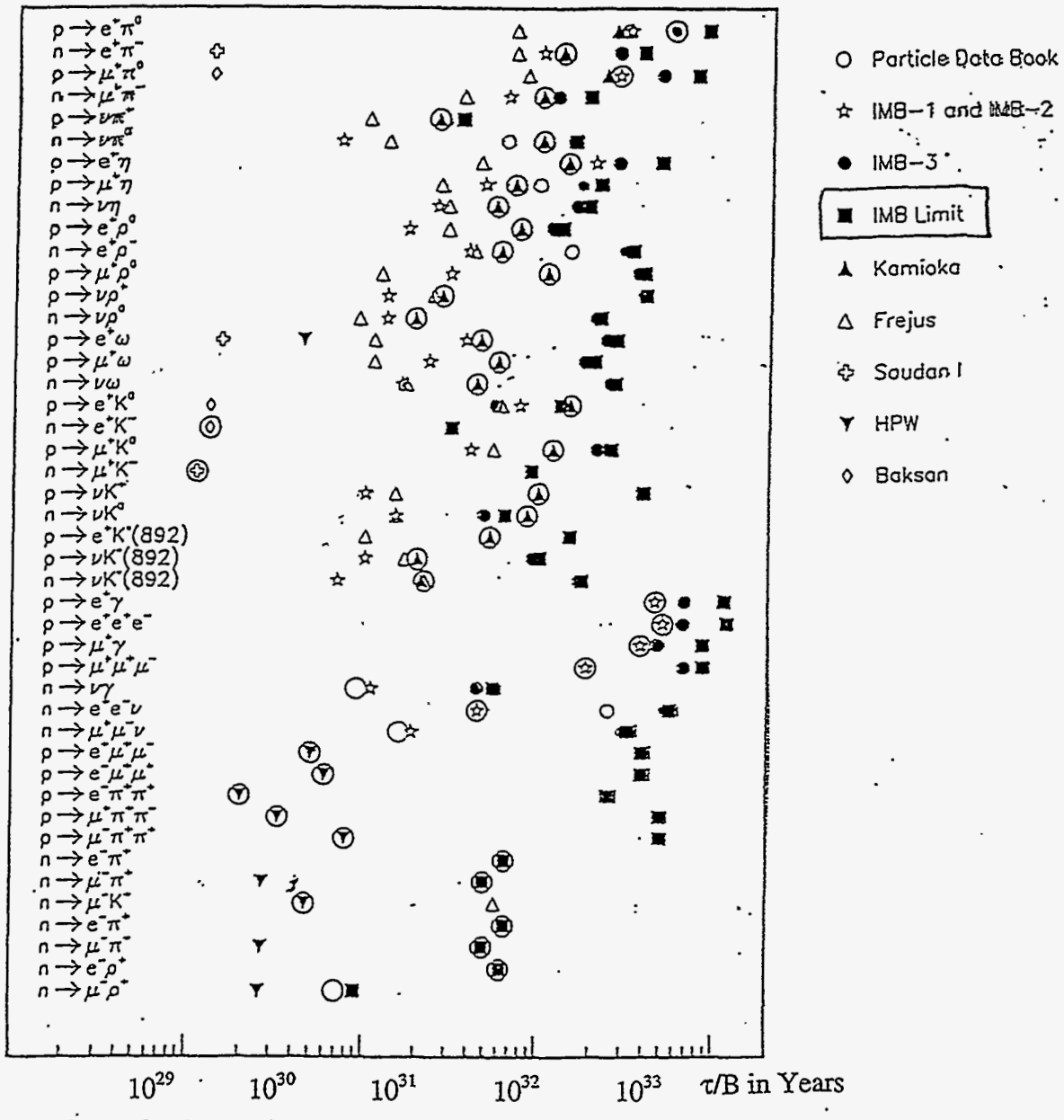

A favored solution that can help this unification to occur at a point is supersymmetry. Figure 2 illustrates how insertion of a SUSY mass scale could fix this problem. Is this evidence for SUSY? Although that would be too strong a statement, it certainly implies that Grand Unified Supersymmetric Theories and their consequences should be considered seriously. This model and a variety of other Grand Unification alternatives have been discussed in this workshop and they lead to a large variation of predictions regarding baryon instability. This means that a new generation of proton decay experiments should not only have greater sensitivity, but also be sensitive to a broad range of possible decay channels.

In general, there are two complementary approaches to observing the consequences of baryon instabilities:

1) decay of protons (or bound neutrons) $\Delta B = 1$
2) neutron-antineutron oscillations $\Delta B = 2$

The first generation of experiments focused primarily on large proton decay experiments. This was logical because they were to a large extent motivated by SU(5) and it should be emphasized that the minimal SU(5) model predicted specific decay and rate for $p \rightarrow e^+ \pi^\circ$, perhaps at detectable rates but no $n\bar{n}$ oscillations. A more general set of theories predict proton decay, but some possibly at undetectable rates, and some predict $n\bar{n}$ oscillations. It is therefore plausible that, in addition, to the next generation proton decay experiments, a complementary project at a significantly increased sensitivity should be pursued for $n\bar{n}$ oscillations. That question coupled with the prospects of doing an experiment on $n\bar{n}$ oscillations at several orders of magnitude improved sensitivity (at ORNL or elsewhere) has motivated this workshop.

Table 2. Soudan 2 Proton Decay Limits - Exclusive Channels.

mode	exposure (kt-yr)	τ/B@90%CL (yr)
$n \rightarrow e^+ e^- \bar{\nu}$	(1.0)	5.0×10^{31}
$n \rightarrow \eta \bar{\nu}$	(1.0)	1.6×10^{31}
$n \rightarrow \pi^0 \bar{\nu}$	(1.0)	3.2×10^{31}
$p \rightarrow K^+ \bar{\nu}$	(0.5)	4.5×10^{30}
$n \rightarrow e^- K^+$	(0.5)	7.5×10^{30}
$n \rightarrow \mu^- K^+$	(0.5)	6.5×10^{30}

Regarding the approach and value of oscillation studies, it is worth recalling that strangeness non-conservation has been observed and studied in $K^\circ \rightarrow \bar{K}^\circ$ transitions, beauty non-conservation in $B^\circ \rightarrow \bar{B}^\circ$ transitions, and likewise, Baryon non-conservation can be probed in $n \rightarrow \bar{n}$ transitions. In this case, $n\bar{n}$ oscillations probe new physics at a mass scale of ~ 10^5-10^6 GeV. This $n\bar{n}$ oscillation process, which represents $\Delta B = 2$ transitions can be studied two different ways:

1) reactors (free moving neutrons)
2) intra-nuclear transitions

2. Review of Proton Decay Status

The major proton decay experiments have been of two types:

1) Cerenkov detectors (e.g. IMB, Kamiokande)
2) Fine Grain Sampling (e.g. NUSEX, Frejus, Soudan 2)

After more than a decade of searches in a large number of channels, none of these experiments report any evidence for proton decay. The limits are $\Gamma(e^+\pi^0) \geq 10^{33}$ yrs, well beyond the minimal SU(5) prediction, and $\Gamma(\bar{\nu}K^+) \gtrsim 10^{32}$ years in the favored supersymmetric mode. A summary of all results is shown in Table 1.

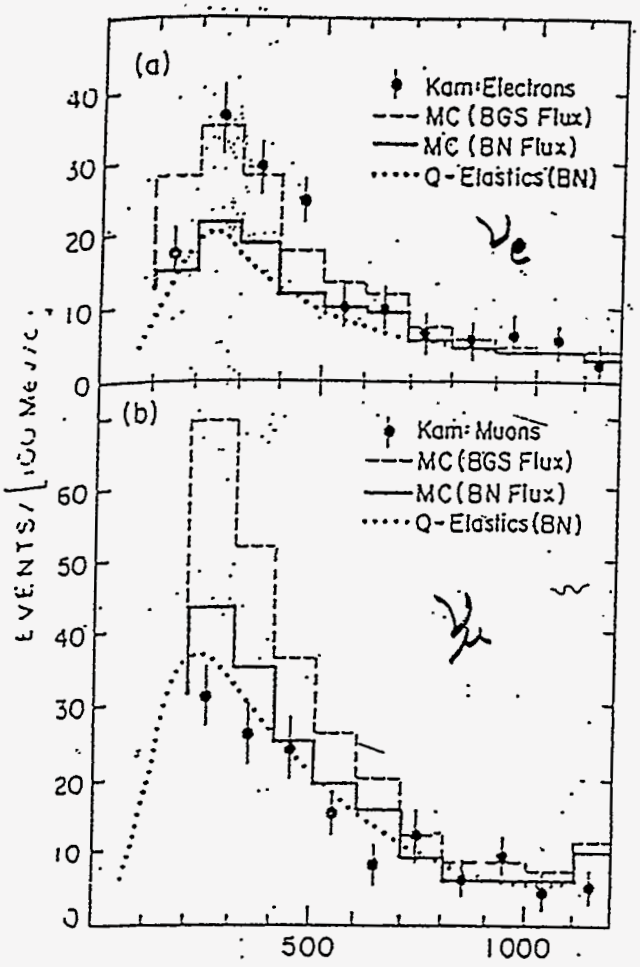

Figure 3. Momentum {Me V/c}.

The only ongoing search is in the Soudan 2 detector, which is aimed at checking Kamiokande limits with lower backgrounds for candidates in some modes. In particular, there is low background for multi-track events, ionization information gives information on the track direction and recoil proton, and neutron detection gives added rejection of ν interactions. Results on several exclusive channels are given in Table 2 for present

running and the projected improvement is projected to be to reach an integrated 5 kiloton years by the year 2000.

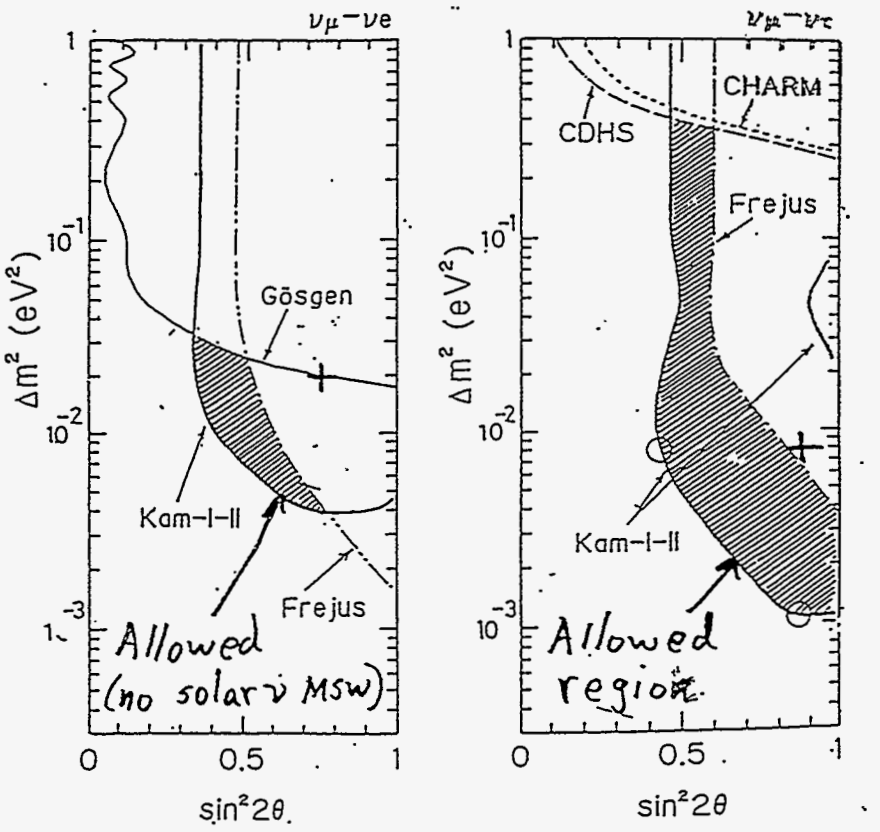

Figure 4. Kamiokande Lower Limits And Allowed Oscillation Parameters.

The only result from experimental data in proton decay experiments that has been suggested as a possible indication of proton decay comes from a different possible interpretation of the atmospheric neutrino anomaly. For several years, there has been evidence for an anomaly in this data which is usually interpreted (if the effect is real!) as an indication of neutrino oscillations. An alternative interpretation of the anomaly as being due to proton decay events in the sample has been put forward by Mann, et.al.[1]

Briefly, the effect is the following: a flux of neutrinos are created near the top of the atmosphere from the interaction and subsequent cascade of primary cosmic rays, in the subsequent cascade, many pions are produced which emit muon neutrinos in their primary decay ($\pi \rightarrow \mu\ \nu_\mu$); this creates a flux of muon neutrinos on the earth; in addition, the decay of the muon from this decay yields both another muon and electron neutrino ($\mu \rightarrow e\ \nu_\mu\ \nu_e$); from the combination of π and μ decay it is easy to see that we should find approximately two ν_μ's for every ν_e; the experimental data, however, indicates a substantially smaller ratio.

The data for this anomaly from the Kamiokande experiment is shown in Figure 3. Also shown are the results of a flux estimates based on modeling the hadronic cascade, but it should be noted that while one model (denoted BGS) indicates a deficit of muon

neutrinos, the other (denoted by BN) actually indicates an excess of electron neutrinos. This radical difference in the predictions is a result of different extrapolations from accelerator data to the small x region where no data exists.

For the usual and favored explanation explaining the anomaly in terms of a muon deficit, an interpretation as being a result of neutrino oscillations is shown in Figure 4. The shaded regions show oscillation solutions for $\nu_\mu \rightarrow \nu_e$ and for $\nu_\mu = \nu_\tau$. Both of these result in the disappearance of ν_μ 's consistent with the experimental observations.

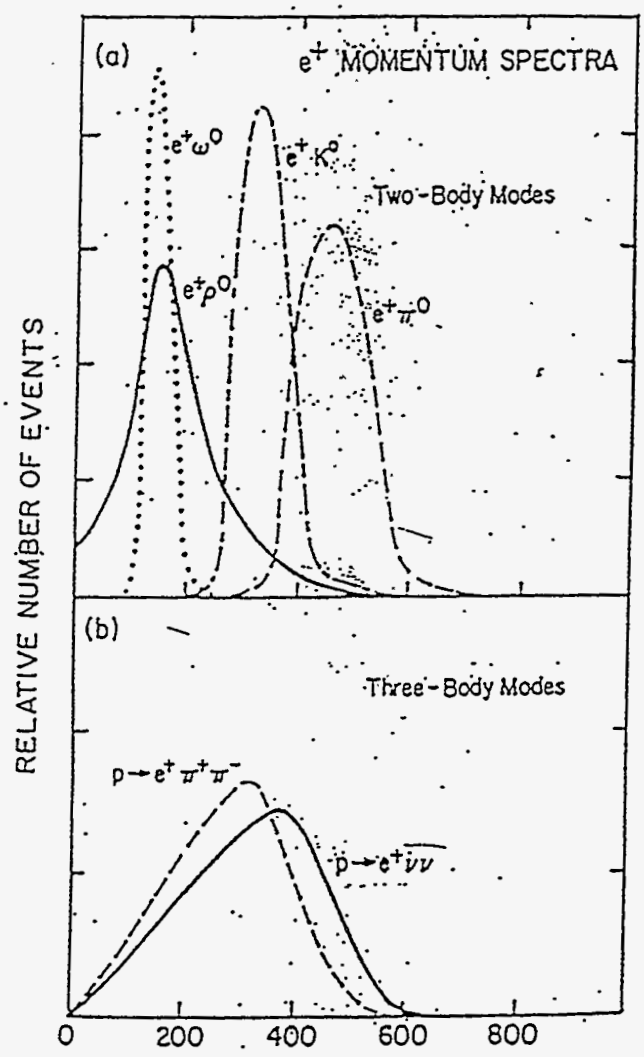

Figure 5. Relative Number of Events/Positive Momentum {Me V/c}.

An alternate interpretation, in terms of proton decay, would be that there is not deficit of muon neutrinos, but rather an excess of ν_e events, which are actually due to proton decay events in the data. Possible two body and three body decay momentum distributions for positrons is shown in Figure 5, where the decay $p \rightarrow e^+ \nu\nu$ shape has then been used to explain the effect, as shown in Figure 6. If this excess is due to proton decay, the rate is $\Gamma = 4.0 \, ^{+\ 1.9}_{-\ 1.0} \, 10^{31}$ years.

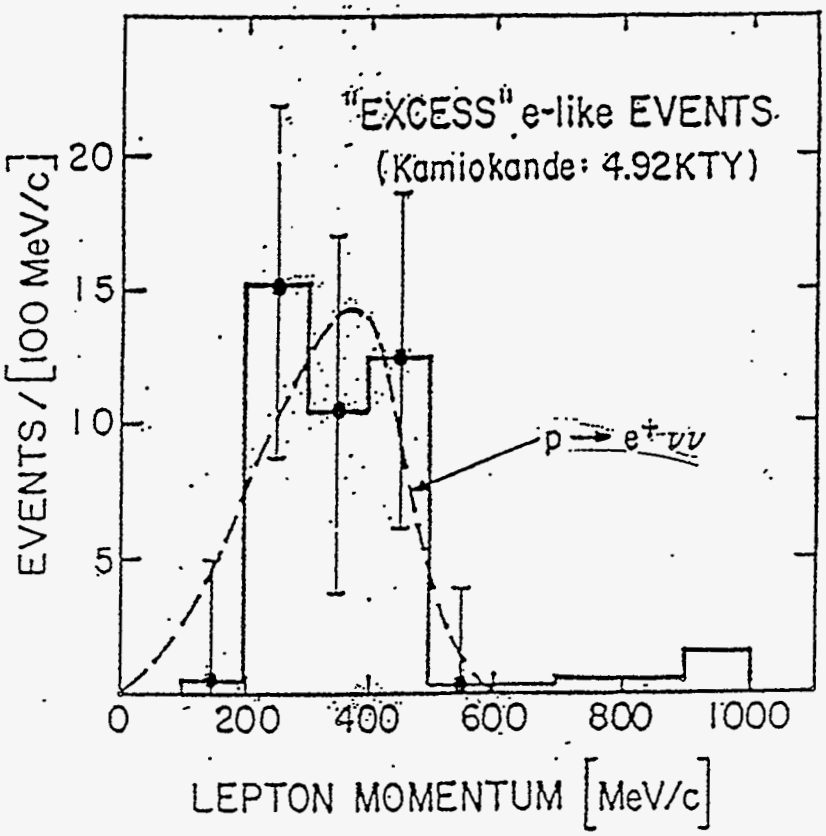

Figure 6. Events {100 Me V/c}/Lepton Momentum {Me V/c}.

More detailed analysis of this anomaly, including an independent flux estimate using satellite data at high altitude on muon rates and angular distributions with respect to the zenith for higher energy neutrinos strongly support the interpretation as a muon deficit and therefore the neutrino oscillation hypothesis, of course, assuming the effect is real.

However, this example should be taken in the spirit that it illustrates the importance for future proton decay experiments to have the ability to measure such decay channels and to separate them from background. For example, at least one model[2] based on SU(4) of Color, unifying quarks and leptons, has $\Delta(B-L) = -2$ and a dominance of $p \rightarrow e^+ \nu\nu$ over alternate channels, $p \rightarrow \mu\nu\nu$, etc.

3. The Next Generation Proton Decay Experiments

For future experimentation in proton decay experiments there will be two large new complementary detectors. At the Gran Sasso in Italy, the ICARUS detector is a long drift imaging liquid argon detector that will have reconstruction ability that will allow low background studies of many difficult channels, while the SuperKamiokande detector with its enormous volume will have significantly improved sensitivity based on its volume for the channels that are not background limited. The ICARUS detector is still in its developmental stage and it will be several years before a full size operational detector will exist. In contrast, the SuperKamiokande detector is being turned on as this workshop goes on and it should produce significant new results in the very near future.

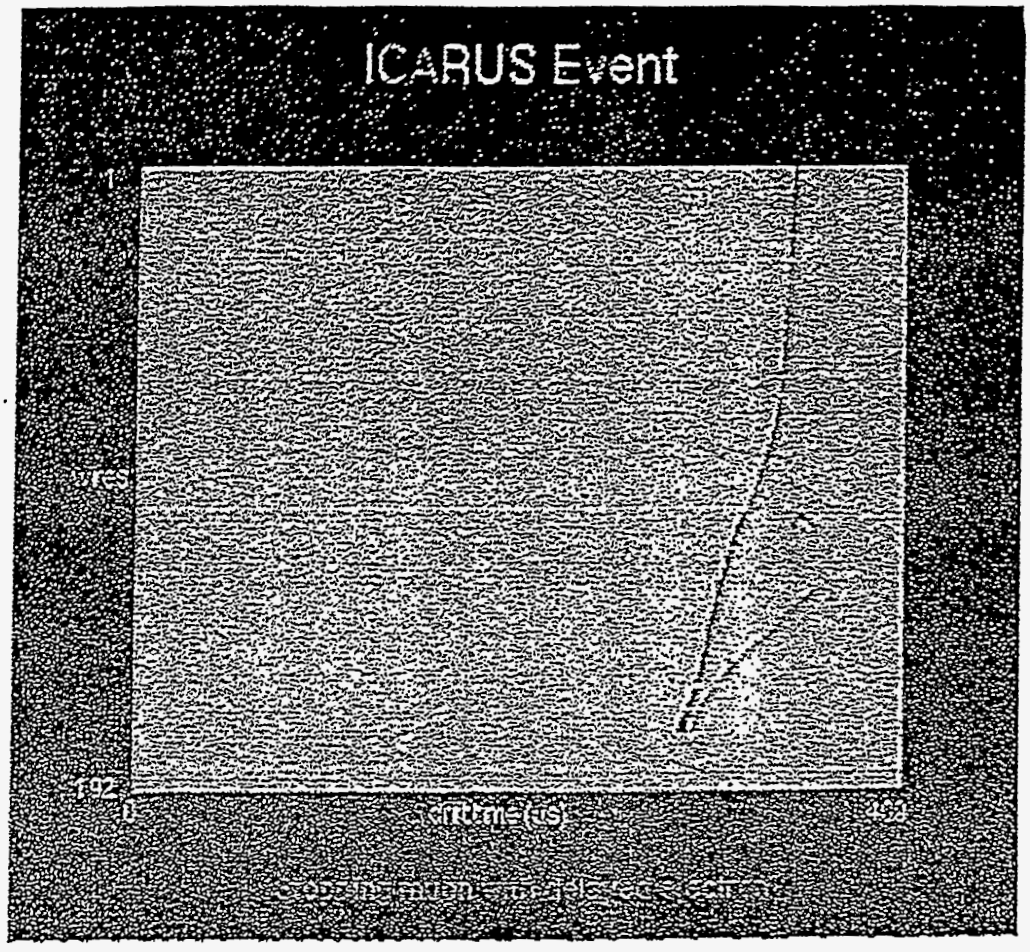

Figure 7. Icarus Muon Decay.

Figure 7 shows an example of an observed muon decay in a small (~ 3 ton) ICARUS prototype chamber that has been built and tested at CERN. The powerful reconstruction capability of such an imaging chamber is evident. Simulations of searches in many exotic decay modes indicate that a substantial improvement over present limits can be achieved with such a detector. Figure 8 shows the projected improvement that can be obtained in an extended run for a variety of decay channels.

I note in order to illustrate of the power of such a detector the analysis of its projected ability in the channel $p \rightarrow e^+ \nu \nu$ that I discussed above as an alternative explanation of the atmospheric neutrino results. Present detectors cannot distinguish proton decay in this channel from neutrino interactions. For that mode, they propose to use as selection criteria: 1) one isolated electron shown, and 2) a reconstructed energy 150 MeV < E_{tot} < 450 MeV. With those criteria, they estimate a reconstruction efficiency of ~ 75% for 25 events/module/year and most importantly, with a signal/background of 5/1. So, such channels for proton decay will be identifiable for the first time in the ICARUS detector.

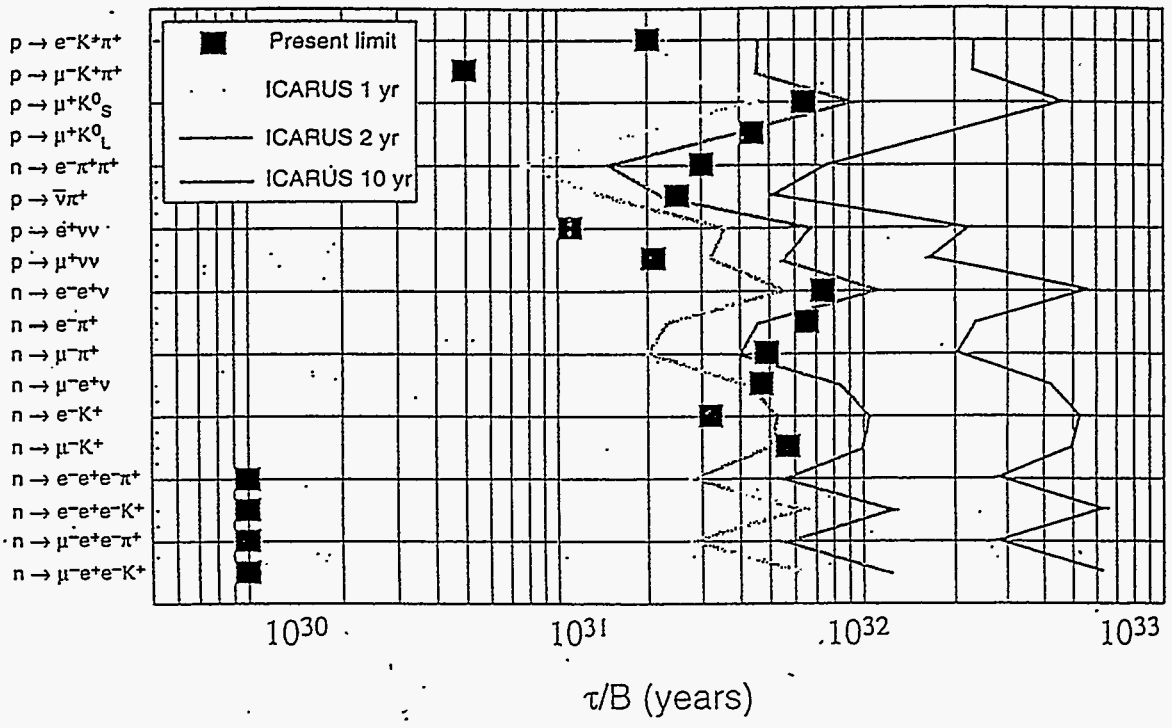

Figure 8. ICARUS 600 Ton Limits For Exotic Decay Modes.

Figure 9 shows the structure of the enormous SuperKamiokande detector, which is presently beginning operations. The major parameters of this detector, in comparison to IMB and Kamiokande are given in Table 3. The new detector is not only much larger than last generation H_2O $\check{C}$ detectors, but also has superior resolution, phototube coverage, background shielding, etc. The projected improvements for a large number of decay channel are shown in Figure 10 and an indication of the sensitivity as compared to various Grand Unification Schemes is shown in Figure 11.

Table 3. Physical Parameters of Large Water Cerenkov Detectors.

PARAMETERS	KAMIOKANDE III	IMB-3	SUPER KAMIOKANDE
TOTAL MASS	4500 tonnes	8000 tonnes	50,000 tonnes
FIDUCIAL MASS			
p-decay	1040 tonnes	3300 tonnes	22,000 tonnes
Solar ν	680 tonnes	None	22,000 tonnes
Supernova	2140 tonnes	6800 tonnes	32,000 tonnes
DEPTH	2700 mwe	1570 mwe	2700 mwe
TOTAL SIZE	16 mh × 19 mϕ	22 × 17 × 18 m^3	41 mh × 39 mϕ
# PMTs	948 @ 50 cm	2048 @ 20 cm + WLS	11,200 @ 50 cm + 2,200 @ 20 cm
PHOTO-CATHODE COVERAGE	20% ~5 pe/MeV	4% ~1 pe/MeV	40% ~7 pe/MeV
PMT TIMING RESOLUTION	4ns @ 1 pe	11 ns @ 1 pe	2.5 ns @ 1 pe
ANTI-COUNTER	~1.5 m	None	2.5 m All Sides

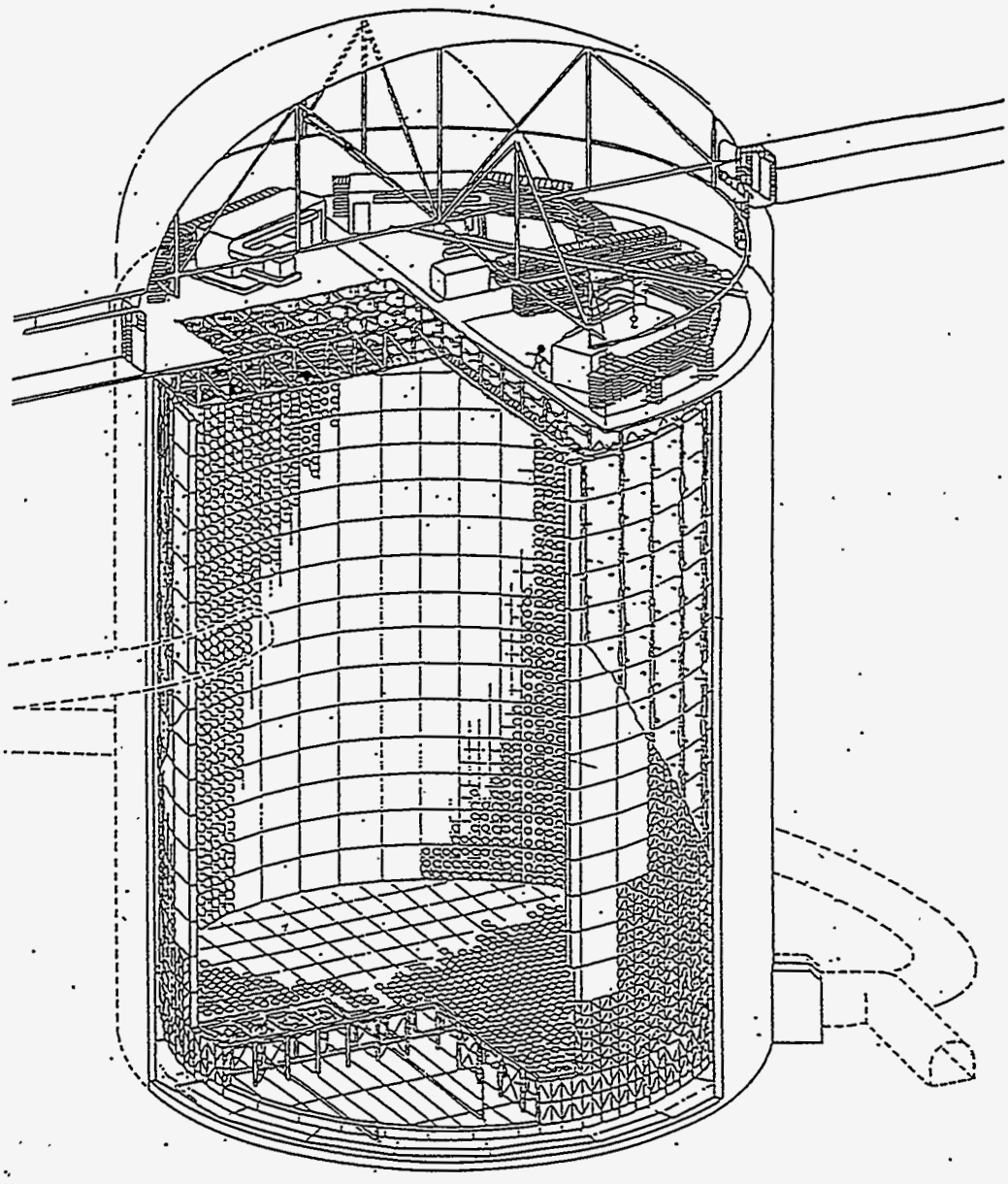

Figure 9. Super K.

The improved sensitivity and reconstruction capability for SuperKamiokande has been studied for various decay channels. In particular, the favored supersymmetric channel $p \rightarrow \overline{\nu}_{\mu} K^+ \rightarrow \pi^+ \pi^\circ$ will be searched for as was done in IMB (B.R. = 21.2%), and also in the dominant $K^+ \rightarrow \overline{\nu}_{\mu} K^+ \rightarrow \mu^+ \nu$ channel through observation of the ^{16}O excited state and rapid decay of a 6 MeV ray, which can be detected. This will potentially further improve the sensitivity of this important channel.

4. Review of $n\bar{n}$ Status

Neutron - anti-neutron oscillations are $\Delta B = 2$, $\Delta L = 0$ transitions which would be suppressed in SU(5). In other Grand Unification schemes, however, those transitions are possible. There are two approaches experimentally: 1) $n\bar{n}$ oscillations in a nucleus; and 2) free neutron - anti-neutron oscillations.

For the case of $n\bar{n}$ oscillations in a nucleus, data from the large proton decay detectors has been used to set limits for these transitions.

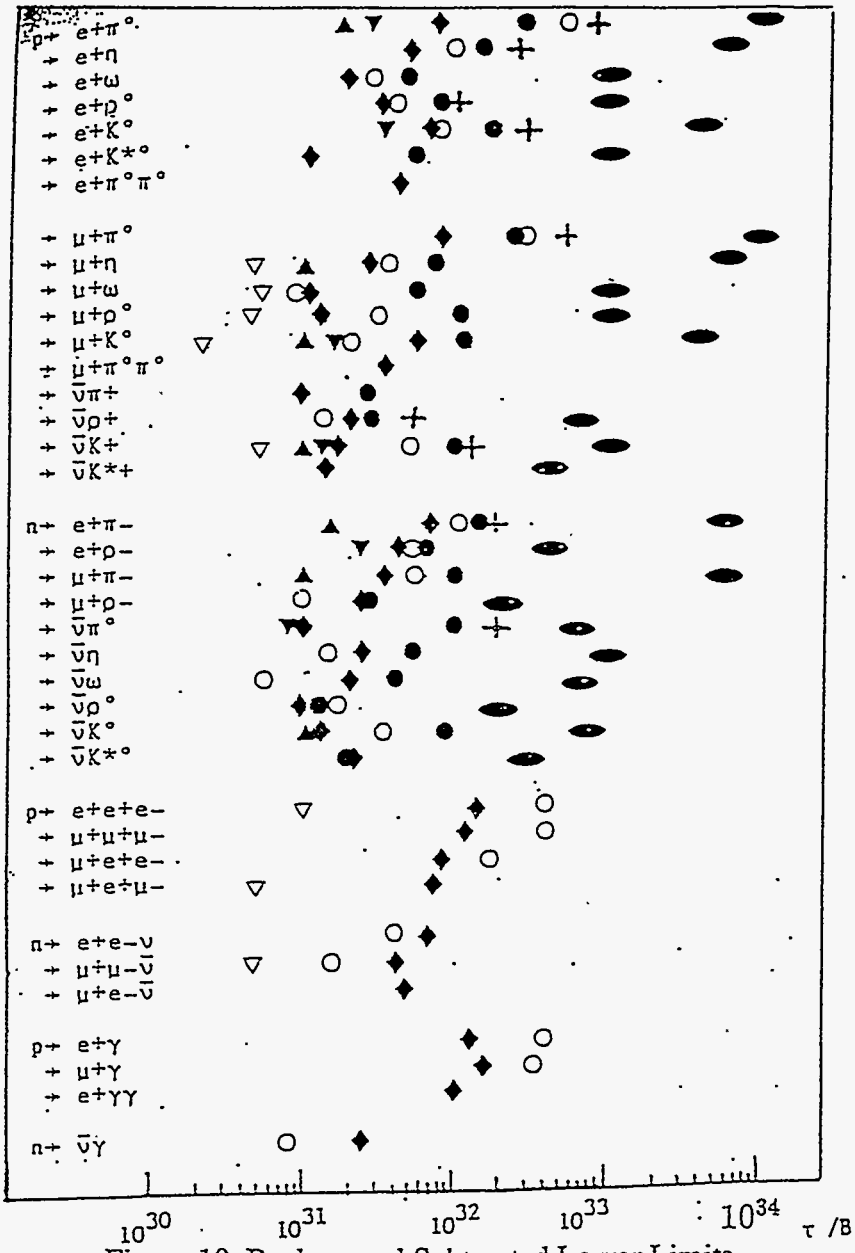

Figure 10. Background Subtracted Lower Limits.

SUPER K

Present Limits and Sensitivity of Super-Kamiokande
Compared to Various Grand Unification Schemes

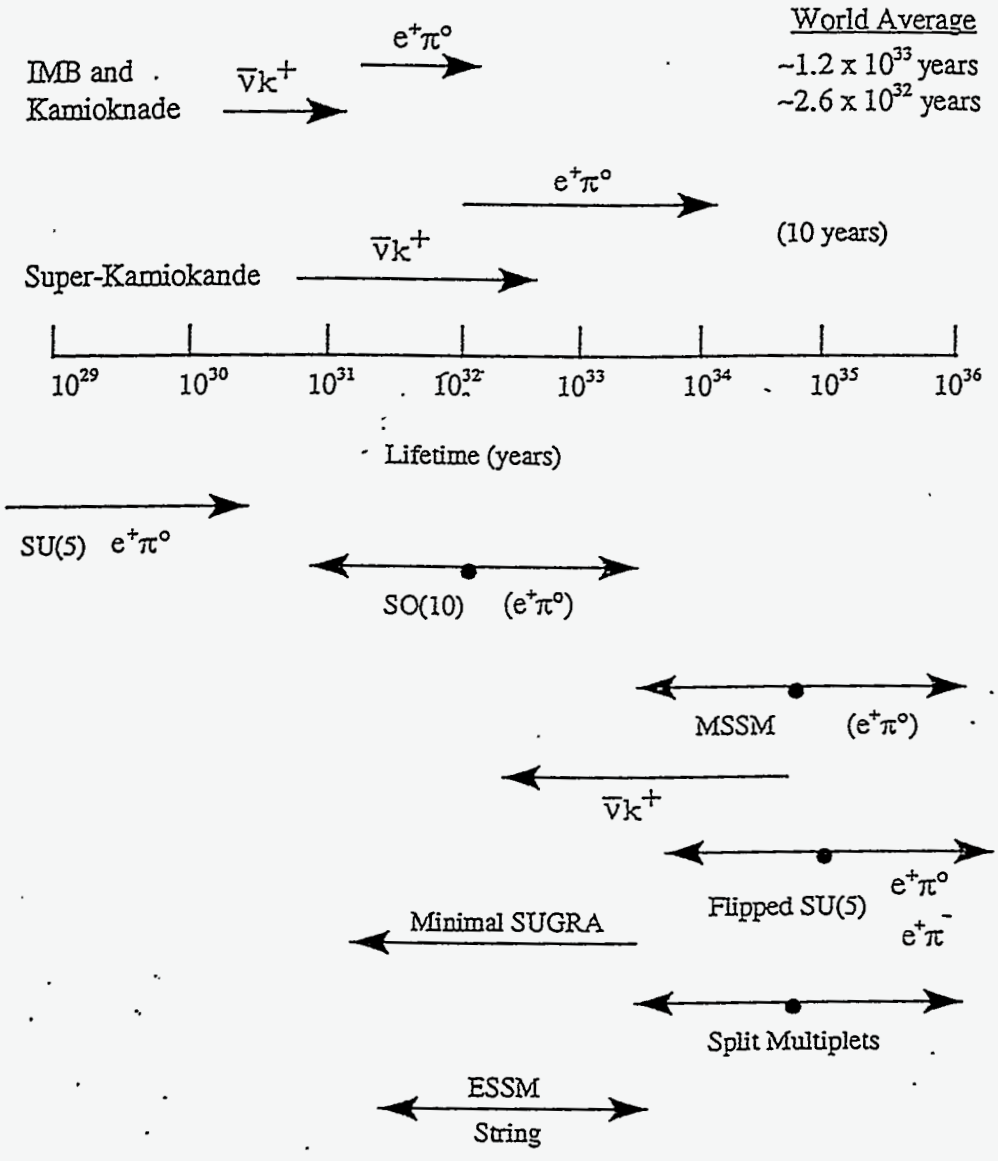

Figure 11. Super K Present Limits and Sensitivity.

For Kamiokande,[3] the process would take place on ^{16}O where one expects a total multiplicity of ~ 5.1 (4.1), charged multiplicity ~ 3.2 (2.6) and mean value of charged pion momentum spectrum <p> ~ 350 MeV/c (300 MeV/c), where the numbers in parenthesis indicate the modification due to nuclear effects.

Table 4.

Detector	Events Observed	T $n\bar{n}$ 90% CL	τ $n\bar{n}$ 90% CL
Kamiokande (^{16}O)	0	4.3 10^{31} yr	1.2 10^{8} sec
Frejus (^{56}Fe)	0	6.5 10^{31} yr	1.2 10^{8} sec

The search is performed with fully contained events, which have multiple rings due to the multiplicity, and selected kinematics consistent with this process are imposed. The requirements are:

- ring multiplicity ≥ 3
- large energy release including at least one μ - e decay observed
- large invariant mass $1200 < M_t < 2200$ MeV/c^2
- small residual momentum $P_t < 600$ MeV/c

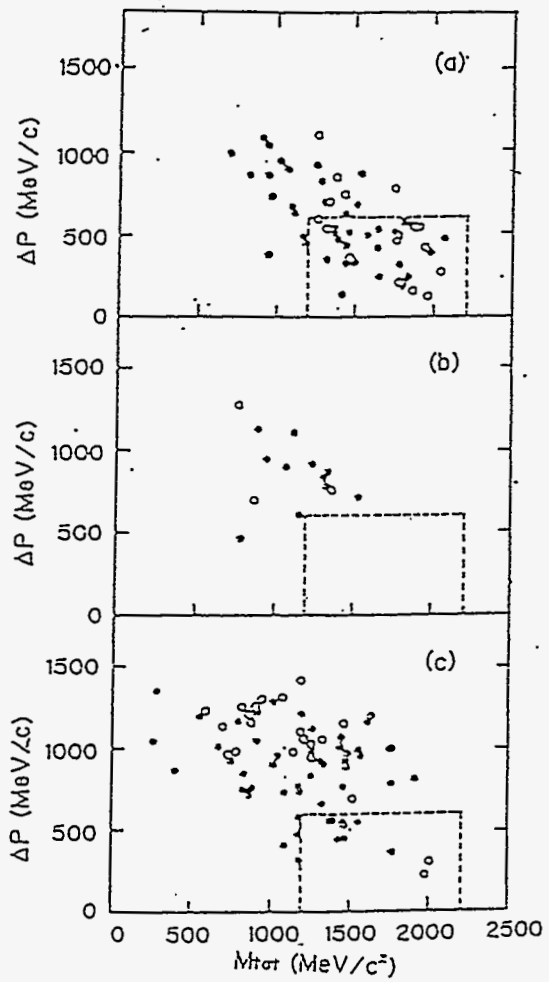

Figure 12. Kamiokande $n\bar{n}$ Analysis.

A sample of data from 474 days of running with 141 fully contained events (44 multiple rings) has been analyzed. Figure 12 shows the data (b), and Monte Carlo expectations for both $n\bar{n}$ oscillations (a) and cosmic ray background (c). There are no data events in the allowed kinematic region indicated with dashed lines.

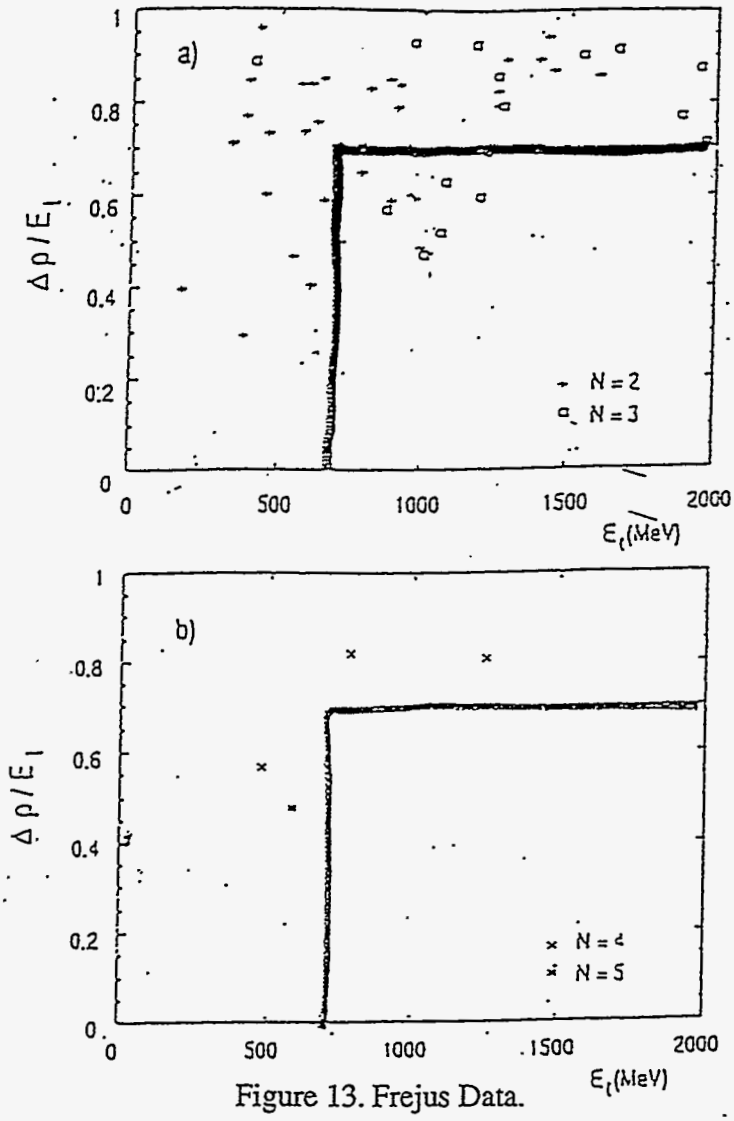

Figure 13. Frejus Data.

A similar analysis in Frejus[4] with 1600 days of running and 142 fully contained events for ^{56}Fe also shows no events as indicated in Figure 13 for multiplicity equal to at least 4.

The results given both as an observed lifetime and through model calculations of Dover,[5] *et. al.* are shown in Table 4.

The search for neutron - anti-neutron oscillations using free neutrons has been carried out over the past decade by ILL at Grenoble. This search used a high flux cold neutron beam (~ 1.3 x 10^{11} n/sec), for an integrated running period (~ 1 year). The flight time of the neutrons (υ = 600 m/sec) was > 0.1 sec. The experiment was in vacuum with a reduced B-field to satisfy the "quasi-free condition".

- In triggering with estimated $\varepsilon = 77\%$ the rate is reduced 1 MHz $\rightarrow$ 4 Hz
- The total data sample is then T = 2.4 10^7 seconds $\Rightarrow$ 6.8 10^7 events
- Kinematic conditions are applied (vertex condition, visible energy, etc.) $\Rightarrow$ 12,000 events
- These are hand scanned $\Rightarrow$ 335
- These are reconstructed $\Rightarrow$ 0

The final result yields no candidacy leading to a result $\tau_{n\bar{n}} \geq 0.86\ 10^8$ sec (90% C.L.).

5. The Future for $n\bar{n}$ Experiments

At this workshop we have heard about future prospects for developing a new experimental facility with free neutrons at ORNL (or possibly elsewhere), as well as the projected capability of SuperKamiokande with bound neutrons.

The free neutron possibilities at ORNL include the HFIR or future spallation sources. The possible gains (relative to ILL Grenoble experiment) that could be realized in such a new experiment are impressive, as tabulated below:

Table 5. Possible Discovery Potential Gain at Upgraded HFIR Reactor Relative to ILL-Grenoble Experiment

Gain	Factor
Reactor power (100 MW v 57 MW)	x 1.75
Larger area detector	x 3.3
Large acceptance elliptical focusing reflector	x 50
Cold neutron moderators	
Larger cold source area	x 16
3 years running	x 3
TOTAL	x 10^4

The key elements for realizing this large improvement are to implement a close focusing reflector on a cold neutron source as shown in Figure 18. The second element introduced, however, is the necessity to handle the higher intensity both in terms of data rate in the detector and having sufficient rejection for the data analysis. Further Monte Carlo studies are needed in this area to determine the requirements this imposes on a detector.

Assuming these improvements can be realized, the sensitivity would approach $\tau_{n\bar{n}} = 10^{10}$ sec, which is well beyond that reachable by SuperKamiokande with bound neutrons (see Figure 18).

The "quasi-free" neutron propagation region is shown in Figure 14 and the simulated intensity distribution on target in Figure 15. The beam is cold ($\langle E \rangle \sim 2\ 10^{-3}$ eV ; $\upsilon \sim 600$ m/sec) and with a divergence $\delta_{div} \sim 5.7$ mrad.

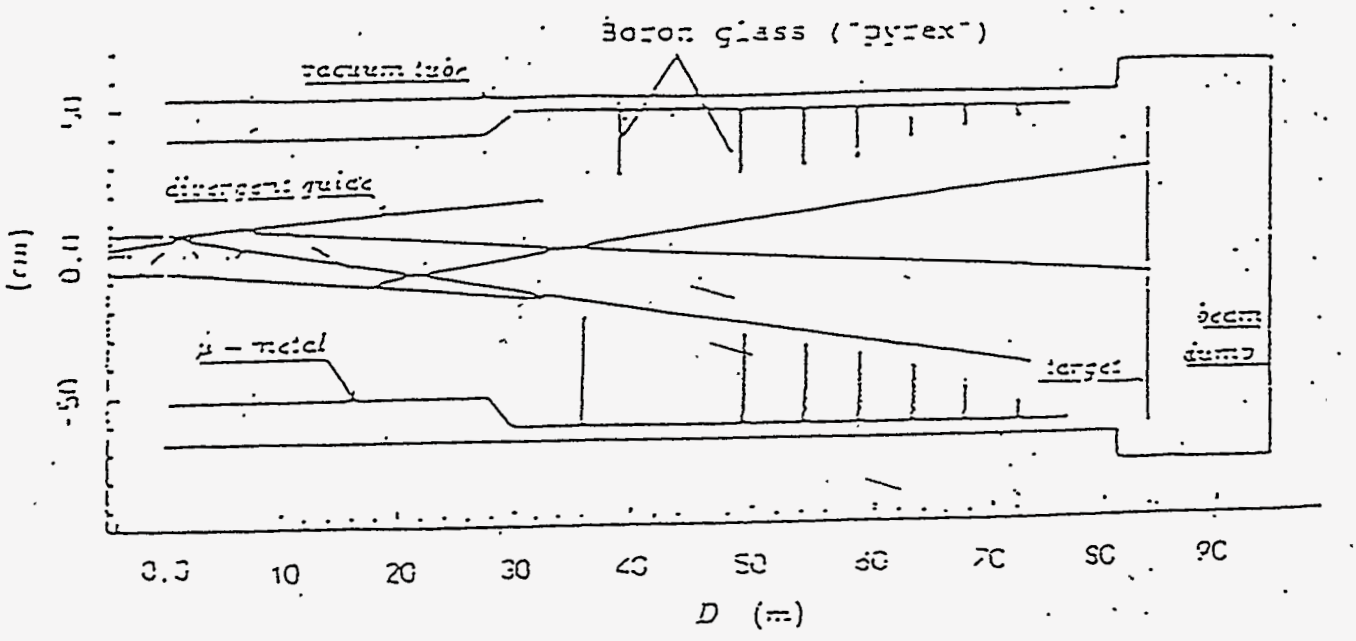

Figure 14. The $n\bar{n}$ Experimental "Quasi-Free" Neutron.

The neutrons are drifted for L ~ 60 m, giving a drift time t ~ 0.1 sec. In order to capture the neutrons and direct them onto the target a divergent guide (neutron horn) shown in Figure 15 is used. It is 33 m long with a taper of 3 mrad. This horn reduced the beam divergence to $\delta_{div} \lesssim 2$ mrad. In addition, the flight region is shielded with a combination of passive and active magnetic shielding which reduces the field from $B_{init} = 510^{-5}$ T $\rightarrow$ B ~ 10nT.

The neutron beam is incident on a graphite target, which is surrounded by a $\Omega = 0.94 \times 4\pi$ solid angle detector with streamer tubes and scintillator for detectors. Figure 16 shows the target and detector with a typical recorded event.

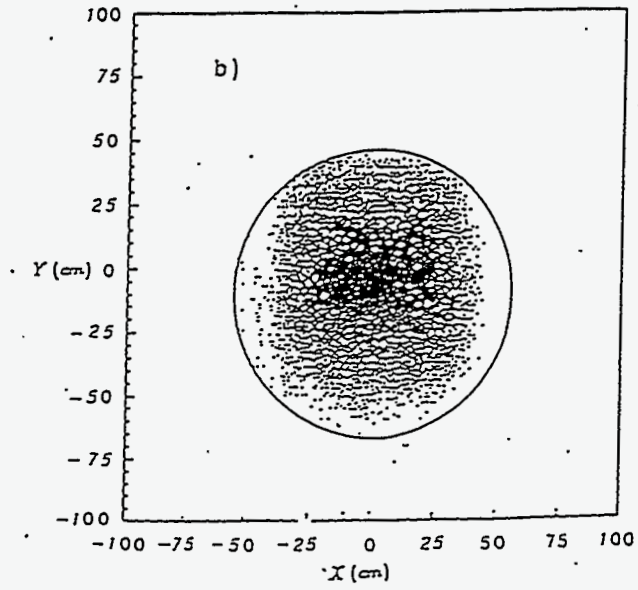

Figure 15. Simulated intensity distribution of the neutron beam.

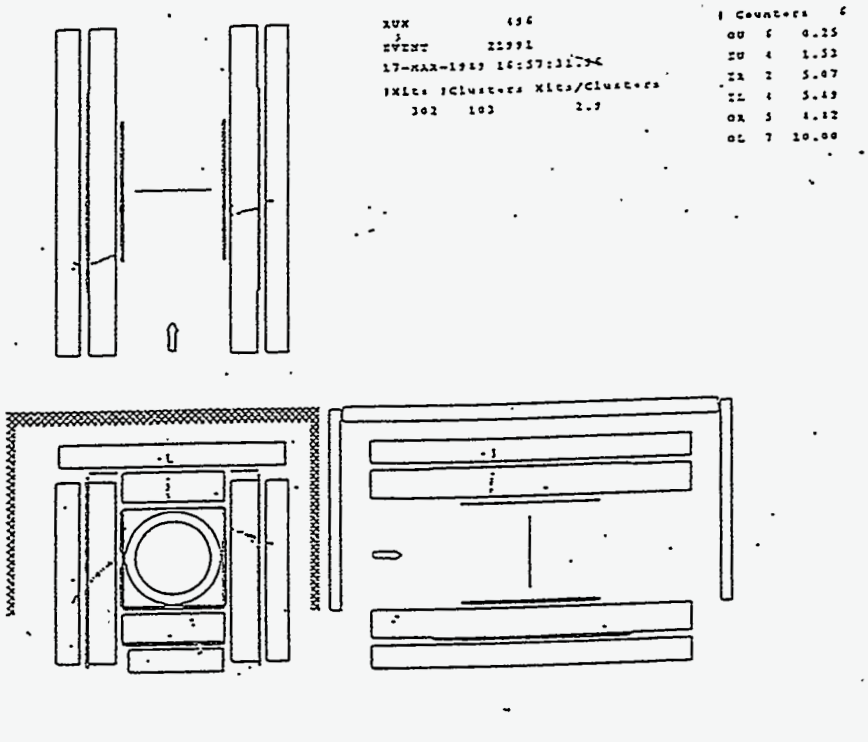

Figure 16. A Typical Recorded Event.

The triggering and analysis have the difficult job of reducing a ~ 1 MHz trigger rate to an analyzable sample. This is done in steps:

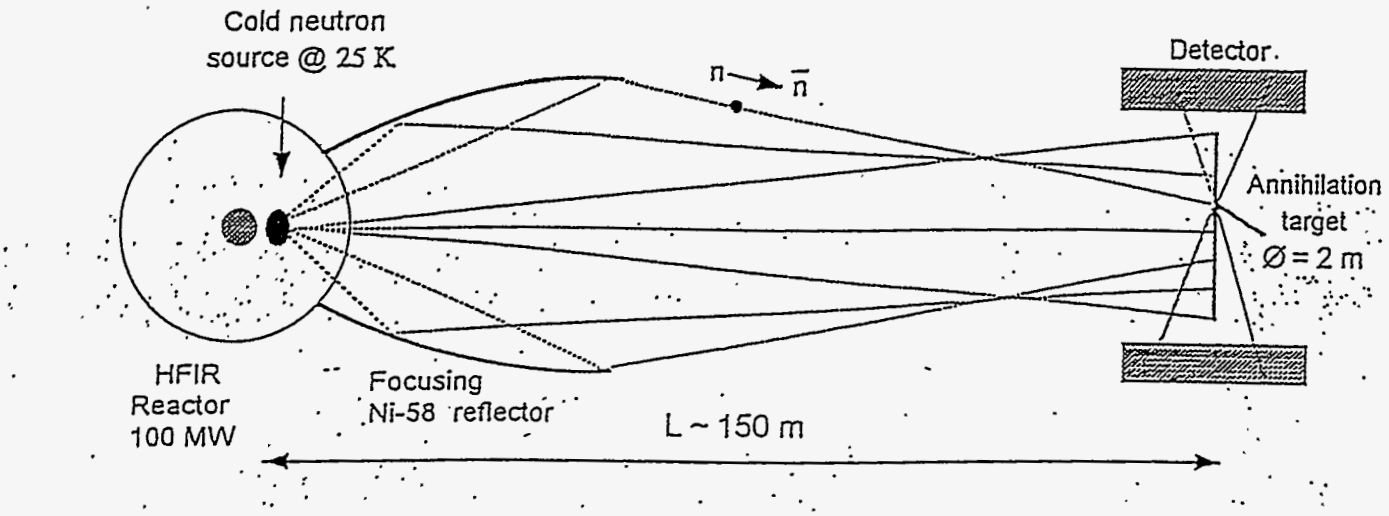

Figure 17. Conceptual Layout of $n\bar{n}$ -Search Experiment.

This large gain would make an $n\bar{n}$ oscillation experiment truly complementary to proton decay experiments. Although only some models of Grand Unification yield $n\bar{n}$ oscillations, those possibilities can be explored beyond the capability in proton decay experiments.

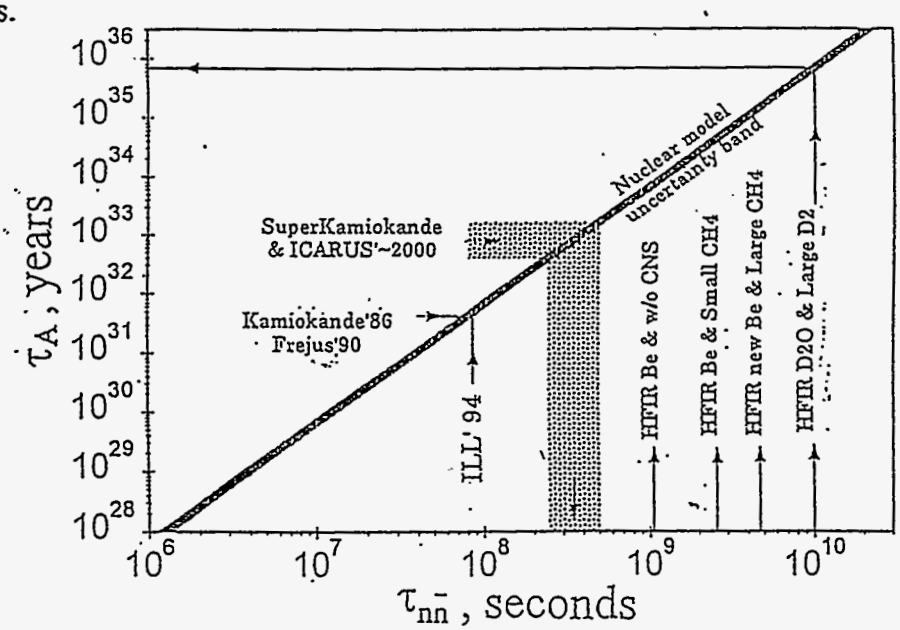

Figure 18. Range of Neutron - Anti-Neutron Transition.

6. Conclusions

In anticipation of a new round of proton decay experiments, we have assessed at this workshop both the theoretical and experimental status of our knowledge of baryon instability. We have seen that the next generation of experiments being developed can improve our sensitivity to observe baryon instability in a large variety of models, or to the possibilities. However, it will not be possible to rule out some theories that yield very low rates.

Complementary studies of $n\bar{n}$ oscillations appear to offer an alternate approach for $\Delta B = 2$ transitions that could be very sensitive in the next generation of experiments. Further study possibly leading to a new experiment seems well justified.

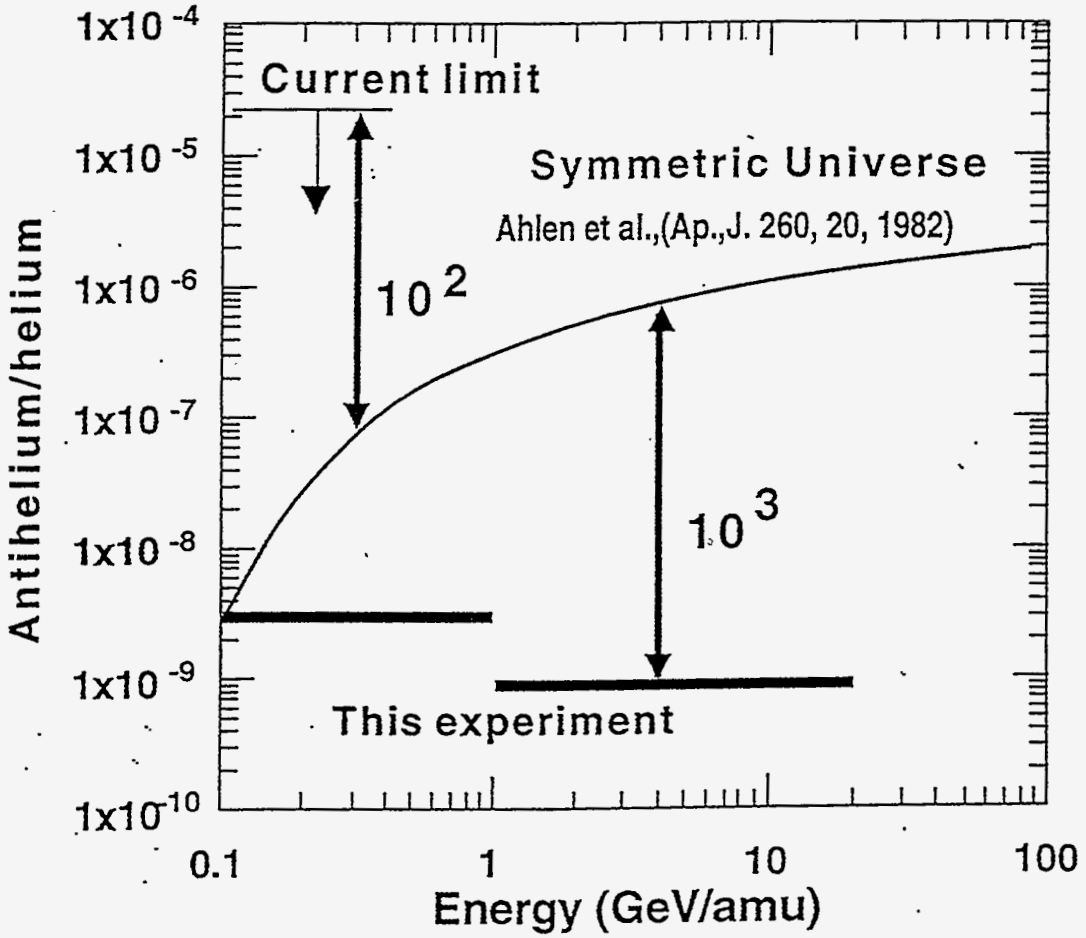

Figure 19. The Current Limit Is Not Sensitive.

We also heard at this meeting of some longer range projects (under ice or the ocean), complementary information form ultracold neutrons and electric dipole moment studies and some new ideas (gaseous p-decay detector, long-lived isotopes, etc.). Hopefully, some of these will develop into operational experiments.

Finally, we were presented with an ambitious search for antimatter in space (AMS). This experiment, which will first fly on the space shuttle, then be implemented on the space station involves a large aperture permanent magnet spectrometer with high field, large acceptance and modern instrumentation. AMS will improve our experimental sensitivity by $\lesssim 10^3$ (see Figure 19). Despite the fact that it remains a long shot to discover galaxies of antimatter, this project represents a very large step experimentally and will put a sophisticated instrument in space that will make many other observations.

7. References

1. Mann, *et. al.*, Phys. Lett. **B291** (1992).
2. Pati and Salam, PRL, **31**, 661 (1973).
3. M. Takita, *et. al.*, Phys. Rev. **D34**, 902-904 (1986).
4. C. Berger, *et. al.*, Phys. Lett. **B240**, 237 (1990).
5. C.B. Dover, *et. al.*, Phys. Rev. **D27**, 1090 (1983).

List of Participants

Steve Ahlen
Physics Department
Boston University
590 Commonwealth Avenue
Boston, MA 02215
ahlen@buphyc.bu.edu

Wanda Alberico
Department of Theoretical Physics
University of Torino
Via Pietro Giuria 1
I-10125, Torino, Italy
alberico@to.infn.it

Frank T. Avignone
Dept. of Physics and Astronomy
University of South Carolina
Columbia, SC 29209
waters@psc.psc.sc.edu

James B. Ball
Building 4500N, MS 6240
Oak Ridge National Laboratory
Oak Ridge, TN 37831-6240
balljb@ornl.gov

Barry C. Barish
HEP 256-48
California Institute of Technology
Pasadena, CA 91125
barish@cithe502.cithep.caltech.edu

William M. Bugg
Department of Physics
University of Tennessee
Knoxville, TN 37996-1200
bugg@slacvm.slac.stanford.edu

Lali Chatterjee
Department of Physics
University of Tennessee/ORNL
Knoxville, TN 37996-1200
lalichat@utkux.utcc.utk.edu

William Chinowsky
National Science Foundation
4201 Wilson Boulevard
Arlington, VA 22230
wchinows@nsf.gov

David B. Cline
Physics Department
University of California, Los Angeles
4-107 Knudsen
Los Angeles, CA 90095-1547
dcline@physics.ucla.edu

Andrew G. Cohen
Physics Department
Boston University
590 Commonwealth Ave.
Boston, MA 02215
cohen@buphyc.bu.edu

Hans Cohn
Department of Physics
University of Tennessee
Knoxville, TN 37996-1200
hcohn@utkux.utcc.utk.edu

George Condo
Department of Physics
University of Tennessee
Knoxville, TN 37996-1200
condo@utkux.utcc.utk.edu

Michael V. Danilov
ITEP
B. Cheremushkinskaya 25
Moscow, 117259, Russia
f15dan@dsyibm.desy.de

Pavel V. Degtyarenko
High Energy Nuclear Physics
ITEP
25 B. Cheremushkinskaya ul.
Moscow, Russia
pavel@cebaf.gov

Alexandre Dolgov
ITEP
B. Cheremushkinskaya 25
Moscow, 117259, Russia
dolgov@vxitep.itep.ru

Yuri Efremenko
Building 6003, MS 6372
Oak Ridge National Laboratory
Oak Ridge, TN 37831-6372
efremenk@utkux.utcc.utk.edu

Jerry Garrett
Physics Division, MS 6368
Oak Ridge National Laboratory
Oak Ridge, TN 37831-6368
garrettjd@ornl.gov

Daniele Gibin
Department of Physics
University of Padova
via F. Marzolo 8
I-35131 Padova, Italy
gibin@padova.infn.it

Maurice Goldhaber
Physics Department, 510F
Brookhaven National Laboratory
Upton, NY 11973
goldhab1@bnl.gov

Robert Golub
Fakultat fur Physik
Technische Universitat Berlin
D-1000 Berlin, Germany
cfl@hmi.de

Elena Golubeva
Institute for Nuclear Research, RAS
60th October Anniversary prospect 7a
117312 Moscow, Russia
golubeva@al20.inr.troitsk.ru

Francis Halzen
Dept. of Physics
University of Wisconsin
1150 University Ave.
Madison,WI 53706
halzen@phenxh.physics.wisc.edu

P. K. Kabir
Physics Bldg 319
University of Virginia
McCormick Rd
Charlottesville, VA 22901
kabir@athena.phys.virginia.edu

Yuri Kamyshkov
Building 6003, MS 6372
Oak Ridge National Laboratory
Oak Ridge, TN 37831-6372
kamyshkov@orph01.phy.ornl.gov

H. Klapdor-Kleingrothaus
Max-Planck Institute fuer Kernphysik
Postfach 103980
6900 Heidelberg, Germany
klapdor@enull.mpi-hd.mpg.de

L. A. Kondratyuk
ITEP
B. Cheremushkinskaya 25
Moscow 117259, Russia
kondratyuk@vxitep.itep.ru

Irina Krivosheina
Radiophysical Research Institute
ul. Kudminskaya 2, kv. 130
Nizjny Novgorod, Russia
irina@nirfi.sci-nnov.ru

Vadim Kuzmin
Institute for Nuclear Research, RAS
117312 Moscow, Russia
kuzmin@ms2.inr.ac.ru

Steve Lamoreaux
Physics, Box 351560
University of Washington
Seattle, WA 98195-1560
lamore@dirac.phys.washington.edu

Paul Langacker
Dept. of Physics
University of Pennsylvania
Philadelphia, PA 19104
pgl@langacker.hep.upenn.edu

Richard A. Lillie
Building 6025, MS 6364
Oak Ridge National Laboratory
Oak Ridge, TN 37831-6364
arl@ornl.gov

Valentin Lubimov
ITEP
B. Cheremushkinskaya 25
Moscow 117259, Russia
lubimov@dice2.desy.de

T. Lucas
Engineering Technology
Y-12 Facility
9204-1, MS 8045
Oak Ridge, TN 37831-8045
a9t.ornl.gov

Anthony Mann
Physics Department
Tufts University
Medord, MA 02155
mann@tuhep.phy.tufts.edu

Fulvio Mauri
INFN - Sezione di Pavia
via A. Bassi 6
I-27 200 Pavia, Italy
mauri@axppv0.pv.infn.it

Luke Mo
Department of Physics
Virginia Polytechnic Inst. & State Univ.
Blacksburg, VA 24061-0435
eptech@vtvm1.cc.vt.edu

Rabindra Mohapatra
Dept. of Physics & Astronomy
University of Maryland
College Park, MD 20742
rmohapatra@umdhep.umd.edu

Luciano Moscoso
DAPNIA/SPP
CEA-Saclay
F-91191 Gif-sur-Yvette Cedex, France
moscoso@hep.saclay.cea.fr

Pran Nath
Dept. of Physics
Northeastern University
360 Huntington Ave.
Boston, MA 02115
nath@neu.edu

Valery Nozik
ITEP
B. Cheremushkinskaya 25
Moscow, 117259, Russia
nosik@vxitep.itep.r

Felix Obenshain
Physics Department
University of Tennessee
Knoxville, TN 37996-1200
obenshain@orph01.phy.ornl.gov

George W. Parker
Chemical Technology Division
Oak Ridge National Laboratory
Oak Ridge, TN 37831
xng@ornl.gov

Jogish C. Pati
Dept. of Physics & Astronomy
University of Maryland
College Park,MD 20740
pati@umdhep.umd.edu

Frank Plasil
Building 6003, MS 6372
Oak Ridge National Laboratory
Oak Ridge, TN 37831-6372
PlasilF@ornl.gov

Jean-Marc Richard
Institut des Sciences Nucleaires
Universite de Grenoble
53 avenue des Martyrs
38026 Grenoble Cedex, France
jmrichar@isnnx2.in2p3.fr

Thomas A. Romanowski
Division of High Energy Physics, E221
Department of Energy
19901 Germantown Road
Germantown, MD 20874-1290
Tom.Romanowski@mailgw.er.doe.gov

Rencheng Shang
Dept of Physics
Tsinghua University
Beijing, China 100084
src-dmp@mail tsinghua edu.cn

Konstatine Shmakov
MS-43
Stanford Linear Accelerator Center
P.O. Box 4349
Stanford, CA 94309
shmakov@slacvx.slac.stanford.edu

James Stone
Physics Department
Boston University
590 Commonwealth Avenue
Boston, MA 02215
stone@buphyc.bu.edu

Lawrence R. Sulak
Physics Department, Room 255
Boston University
590 Commonwealth Ave.
Boston, MA 02215
sulak@buphyc.bu.edu

Bennie F.L. Ward
Department of Physics
University of Tennessee
Knoxville, TN 37996-1200
bflw@slacvm.slac.stanford.edu

Achim W. Weidemann
MS 94
Stanford Linear Accelerator Facility
P.O. Box 4349
Stanford, CA 934309
achim@slac.stanford.edu

Colin West
FEDC, MS 8218
Oak Ridge National Laboratory
Oak Ridge, TN 37831-8218
col@ornl.gov

Cheuk-Yin Wong
Physics Division
Oak Ridge National Laboratory
Oak Ridge, TN 37831-6373
wong@ornl.gov

H. Yoshiki
National Lab. for High Energy Physics
Oho-machi, Tsukuba-shi
Ibaraki-ken, 305, Japan
hyoshiki@kekvax.kek.jp

Glenn Young
Building 6003, MS 6372
Oak Ridge National Laboratory
Oak Ridge, TN 37831-6372
young@orph01.phy.ornl.gov

Olga Zeldovich
ITEP
B. Cheremushkinskaya 25
Moscow, 117259, Russia
zeldovich@vxitep.itep.ru